THE SEDIMENTOLOGY OF DIAMONDIFEROUS DEFLATION DEPOSITS WITHIN THE SPERRGEBIET, NAMIBIA

by

Ian Bedford Corbett

Thesis submitted in fulfilment of the requirements for the degree of Doctor of Philosophy in Geology

University of Cape Town

August, 1989

ACKNOWLEDGMENTS

I would like to thank Mr. J.B. Hawthorne, Dr. C.R. Clement and Mr. K.R. Hazell, for allowing me to undertake this study. I am indebted to the management of CDM (Pty) Ltd. for providing the logistical support for this project, and in particular, to the Security Department for providing the helicopter flights from which this project has benefitted greatly. I would also like to thank Anglo American Corporation of South Africa for providing a bursary whilst I was resident at the University of Cape Town writing-up, and De Beers for providing the funds to have the manuscript printed.

I am extremely grateful to my supervisor, Prof. W.E.L. Minter for helpful discussions, and for his thorough reading and constructive criticism of the manuscript.

Numerous people have willingly shared their experience and provided advice during the course of this project, and thanks are expressed to Mr. R.S. Liddle, Dr. J. Rogers, Dr. H. Swart, Dr. G. Schneider, Prof. C.L. Merry, Dr. Q.B. Hendey, Mr. J. Pether, Dr. M. Pickford, Dr. A. Scholtz and Dr. A. Channing. The expertise of Mr. A. Von Johannides, of ISM, in using VULCAN is gratefully acknowledged. Special thanks go to my good friend John Ward, whose enthusiasm and encouragement is an example to us all.

I would also like to thank Mrs S. Chadwick and Prof. B. Schneider for translating parts of Kaiser (1926), and the CDM Geological and Draughting Departments, together with Mrs. M. Michalowsky and Mr. B. Griffin and his staff at De Beers Marine (Pty) Ltd., for help with producing the manuscript.

Finally, words cannot convey the appreciation I feel for my wife Ali, to whom the completion of this project owes so much. Her dedication and encouragement has made her a tower of strength, and her assistance in the field has been enormous.

THE SEDIMENTOLOGY OF DIAMONDIFEROUS DEFLATION DEPOSITS WITHIN THE SPERRGEBIET, NAMIBIA

ABSTRACT

In this thesis the processes that produced diamond placer deposits within closed endoreic basins along the west coast of Namibia are addressed. These deposits, first discovered in 1908, and documented by Kaiser in 1926, occur in an area of wind deflation between latitudes 26 and 28 degrees South. Salt rock weathering and aeolian abrasion has eroded elongated depressions that are upto 120 m deep, that happen to be parallel with the dominant wind flow from the south and south-southeast, which governs aeolian processes in the coastal tract.

The velocity of winds from the south and south-southeast frequently averages 50 to 60 km/hour between October and March, and gusts at 80 to 90 km/hour. At these velocities, grains exceeding -1 phi (2 mm) in diameter are commonly entrained into the saltation load above stone pavement surfaces, making this an extremely active aeolian environment.

Sand entering the aeolian system as a result of the deflation of coastal point-sources remains within wind-aligned, 1 to 2 km-wide linear zones delineated by barchan dune trains. The pattern of secondary helical vortices in the planetary boundary layer is believed to maintain these zones, where sandflow is up to 13 times greater than in adjacent areas. In such "aeolian transport corridors", saltation bombardment of the bed beneath the high sandflow creates optimal conditions for the propagation of bedload creep transport by saltation grain impact. Granule ripples maintained on the stoss slopes of 25 to 30 m high barchan dunes within the corridors probably migrate at about the same rate as the dunes, which move 30 to 60 m per year.

Under these conditions loose grains on the bed, including garnets and diamonds between 0 and -2 phi (1.0 to 4.0 mm) in diameter, are rapidly sorted by size, density and shape. As stone pavement surfaces are reworked, creep erosion ripples, with an upwind-facing concave crest comprised of very coarse sand and granules. The segregation of garnet grains along the crests of these bedforms indicates that like-sized particles move predominantly as kinematic waves.

This study has established that sandstorm events contribute 20 to 50 percent of the annual sandflow transported towards the Namib Sand Sea. For the period February to May, 1987, about 7 to 8 tonnes of sand per metre width was transported along the aeolian transport corridor generated at Bakers Bay. Some 23 percent of this material moved along the corridor in two to three days of very high sandflow. This measurement contradicts previous estimates, based upon wind data analysis that failed to take cognizance of interaction between the aeolian system and the marine environment which ultimately determines sediment input to the deflation basin.

Stone pavement bed configurations are determined by the spatial distribution of sandflow through the deflation basin. In areas of moderate sandflow, surfaces stabilised against deflation are characterised by regularly spaced, east-west oriented rows of pebbles with their long axes preferentially oriented transverse to the southerly surface-wind flow. Beneath aeolian transport corridors, the dense packing arrangements of granules and small pebbles comprising the creep bedload protect the substrate from deflation. The most stable configuration is attained when particles develop an imbricate shape-fabric, with their upper surfaces inclined into the saltation load derived from the south. The long axes of these particles are commonly aligned parallel with the prevailing wind. The presence of cumulate soil textures has been noted beneath surfaces stabilised in this way.

Raindrop impact during high velocity northerly winds is able to destroy the stable bed configurations created by creep processes. The exposure of the underlying substrate to rainsplash erosion, and deflation as the surfaces dry out, probably results in surface lowering prior to rearrangement of the bed into a stable configuration by creep.

Dendritic tributary networks generated by surface run-off during heavy rainfall generally occur at the northern ends of endoreic basins, and feed streams which flow south into ponded water bodies at the base-level of the ephemeral systems, which are sometimes below sea-level. Although stream transport is highly ephemeral, sediment dispersal is rapid during these events, and coarse-grained aeolian deposits on the floor of endoreic basins are commonly reworked. A repetitive cycle of transport is therefore observed, whereby aeolian processes essentially transport material to the

north, and ephemeral streams redistribute material to the south.

Cyclical reworking of sediments by aeolian and ephemeral stream processes is reflected by computerised analysis of diamond dispersal in endoreic basins. The patterns produced also illustrate the extent to which diamonds have been transported into successive basins to the north. This transport has primarily occurred by creep, but experiments using garnet grains with a similar size distribution show that the entrainment of some diamonds into saltation probably also occurred. East-west oriented obstacles transverse to the creep-migration direction provided sites for aeolian heavy mineral segregation, which can be examined using kinematic wave theory.

Analysis of the Cenozoic stratigraphic record reveals a similar pattern of sedimentation to that which has previously been defined in the Kuiseb River area further north. Suggested new correlations include the assignment of the Blaubok and Gemsboktal gravels to the Lower to Middle Miocene, together with the Kalkrücken sandstone and the Strauchpfütz carbonate. The aeolian Fiskus Sandstone Beds, which were formerly believed to be Lower Miocene, were probably deposited between the Latest Miocene and the Early Pleistocene. Their deposition in a tidally-flooded pan environment, at about 25 m above sea-level, suggests that tentative correlation with the 30 m Pleistocene transgression is possible. This implies that minimal crustal warping of the Plio-Pleistocene beach elevations along the west coast has occurred, contrary to previous concepts.

Dateable stratigraphic units broadly constrain the duration of the phases of regional development that are identified. Middle Eocene (Upper Buntfeldschuh Formation) to Lower Miocene (Rooilepel sandstone) aeolian deposits, which are correlated with the Tsondab Sandstone Formation of the Central Namib, provide evidence of an early arid phase, which may represent a proto-Namib. This phase was terminated during the Lower Miocene, when widespread alluvial activity led to the deposition of the Grillental Beds, Kalkrücken sandstone, Gemsboktal and Blaubok gravels, and the Arries Drift Gravel Formation. A regionally extensive pedogenic hardpan calcrete formed during the early Late Miocene, prior to the Namib Desert Phase, which is represented by the aeolian Fiskus Sandstone Beds and the Annental sandstone.

The silcrete-capped topographic residuals occurring within the

study area, which probably correlate with the African palaeo-surface, might have been associated with the initiation of aridification on the west coast during the Late Cretaceous to Early Tertiary. The preservation of the Grillental Beds and the Rooilepel sandstone in depressions below the elevation of the silcrete show that the silcrete had been incised prior to the Lower Miocene. This reduces the time span represented by the African erosion cycle.

The extent and location of sand seas within the region has varied with time. Periods of sand sea expansion occurred during marine regressions, when it is thought that aeolian accretion occurred along the former western coastal margins of ergs, as sea-level was lowered, and the dynamic aeolian tract was displaced to the west. However, it is likely that sand seas contracted during transgression, when areas which were formerly within the depositional basin came to lie within the new limit of the deflation basin. As shown by the Fiskus Sandstone Beds, this resulted in the development of regional bounding surfaces caused by aeolian erosion.

The previous model of endoreic basin placer formation invoked progressive deflation and surface lowering of a pre-existing diamondiferous sediment pile. Had such a body existed, it is likely that erosion during the Lower Miocene alluvial phase would have redeposited the material to the west on the continental shelf, which was exposed by regression at the time. In the new model proposed here, the Bogenfels Basin is identified as the site of a major south-facing re-entrant embayment, in which marine placer bodies were deposited during transgressions. Non-active (palaeo) yardangs along the embayment's western edge prove that the area has been traversed by an aeolian transport corridor during regressions. Former marine placer bodies would then have been subjected to reworking by the aeolian system, and the occurrence of optimal conditions for creep transport would have resulted in diamond input to the endoreic basin system represented by the Daheimtal-Idatal conduit. Subsequent cyclical reworking of the diamondiferous sediments by the aeolian and ephemeral stream systems, coupled with continued transport of the diamonds to the north into successive basins, would have led to the formation of the placer bodies.

CONTENTS

page

LIST OF FIGURES

TABLES

1. INTRODUCTION

1.1. LOCATION OF STUDY AREA

The study area lies within a 150 km long coastal belt ranging from 0 to 15 km wide between 26°30'S and 27°40'S on the Atlantic coast of Namibia (South West Africa) (Figure 1.1). This area lies wholly within Diamond Area Number 1, which was proclaimed after extensive diamond placer deposits had been discovered there in 1908 by August Stauch. Numerous mining companies operated within the region between 1908 and 1919, after which Sir Ernest Oppenheimer formed the CDM (Pty) Ltd. (CDM).

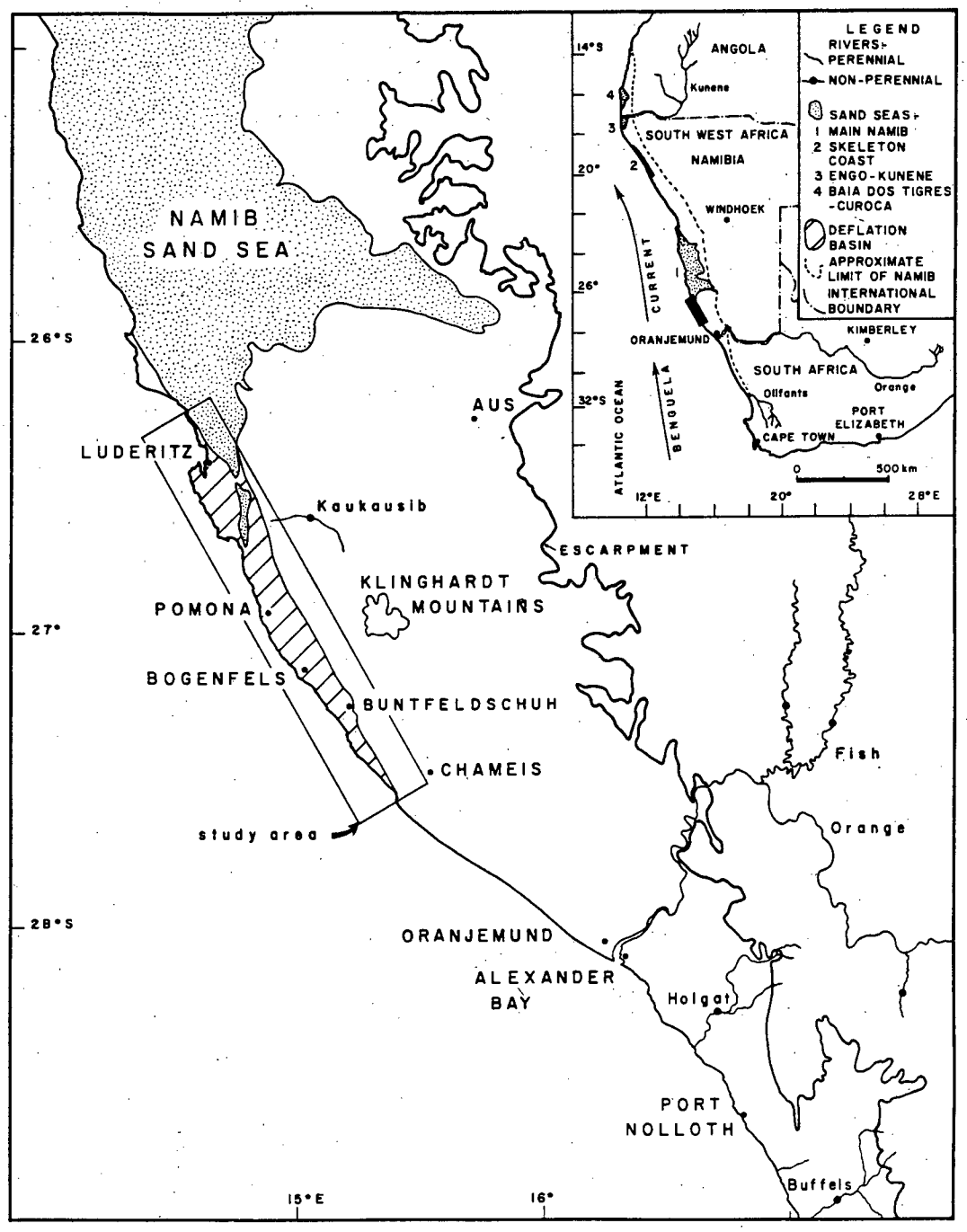

Figure 1.1. Locality plan showing location of the study area.

1.2. GENERAL PHYSIOGRAPHY OF THE REGION

1.2.1. REGIONAL CLIMATE

The Namib is a coastal desert located on the western margin of the southern African sub-continent. The desert is bounded on the west by the Atlantic Ocean, and on the east by the Great Escarpment. The Namib extends approximately from the Olifants River in Cape Province (South Africa) to the Carunjamba River in the Moçamedes District of Angola.

The study area is situated in the winter rainfall region of the Namib's extreme-arid core which extends from about 18°S to 29°S (Meigs, 1966). Being a coastal desert, this belt remains cool throughout the year. The annual rainfall is less than 10 mm for 50 percent of the available records between 15°S and 33°S (Van Zinderen Bakker, 1975), and rainfall when it occurs is ephemeral. Cold surface sea water, and the Benguela Current, provide ideal conditions for advective fog formation, which is an important moisture source within the desert's coastal zone. Pietruszka and Seely (1985) have shown that the fog is a more reliable moisture source than the sporadic rainfall, and conclude that it may have been an important factor in the evolution of the unusual biota of this desert. The coastal fog belt is also thought to be geologically significant, because it is closely associated with the development of gypsum crusts (Watson, 1985). It is also likely to be an important factor in controlling salt weathering.

The South Atlantic Anticyclone, situated off-shore at about 30°S, acts as a barrier to the passage of extra-tropical storms from the south-west. This stable air mass is capped by an inversion, which prevents convective precipitation. The Benguela Current, together with coastal upwelling, introduce cold South Atlantic bottom water to the coast. This further enhances aridification which is also made possible by the divergence of the South-East Trade winds along the coast (Meigs, 1953, 1966; Schulze, 1972; Van Zinderen Bakker, 1975).

The Namib's surface-wind regime is distinctly zonal. A coastal high-energy tract is dominated by a southerly wind component that is governed by the South Atlantic Anticyclone. A more complex and variable inland wind regime, influenced by the atmospheric circulation pattern of the continental interior, occurs to the east of this zone (Rogers, 1977; Ward, 1984; Lancaster, 1985).

This study is principally concerned with the sediment dynamics of the coastal high-energy tract in an area that has been described as one of the windiest in the world by Rogers (1977). The south-north velocity gradient of the southerly wind flow peaks at Pomona (within the study area being considered here) and diminishes to the north and south (Rogers, 1977). This gradient is fundamental to understanding the development of the Namib Sand Sea, and is a major factor in controlling the spatial relationship of the regional geomorphology.

1.2.2. REGIONAL GEOMORPHOLOGY

Three contrasting geomorphic units exist within the study area. The first is a depositional basin containing the present-day Namib Sand Sea. The second is a deflation basin, which lies south (upwind) of the sand sea and is dominated by rugged, south to north trending troughs and ridges closely related to trends in the basement lithology and structure. The third unit comprises gently undulating plains, largely devoid of significant relief, which lie to the east of the deflation basin, and extend eastwards to the base of the Great Escarpment. The transition from the deflation basin to these eastern plains delineates the eastern margin of the study area. The detailed geomorphology of the deflation basin and the southern part of the depositional basin is discussed in section 2.

1.3. OBJECTIVES

The first objective of this study is to examine the present-day sediments and sediment dispersal system(s) operating within the deflation basin of the main Namib Sand Sea. Although much of the area was mined between 1908 and 1931, some areas remain undisturbed. Extraordinarily rich diamond placer deposits contained within the Idatal and Hexenkessel valley systems near Pomona have been completely mined-out, but original prospecting data is on record. The diamond concentrates can be regarded as extremely robust tracers within the sedimentary system, and provide valuable insight into present-day sediment dynamics. The diamond concentration data, coupled with observations of the natural physical processes over a four year period, provides a unique opportunity to describe sediment dispersal within a hyper-arid

sedimentary environment.

The second objective is to interpret the palaeo-dynamics of the aeolian sediment dispersal system that prevailed in the region during the Cenozoic Era. To do this, features preserved in the regional stratigraphy are compared with the present-day aeolian system. A third objective is to refine our understanding of the stratigraphic history in the Southern Namib, which will improve our knowledge of the regional stratigraphy of the Namib.

This work forms part of an on-going, comprehensive regional study of sedimentary deposits within Diamond Area Number 1 being undertaken by CDM. Employment as a field geologist stationed at Bogenfels over the past 4 years has provided me the priviledged opportunity of witnessing the present-day sediment dynamics of one of the world's major deflation basins on an almost daily basis. Emphasis is thus placed upon recording field observations regarding this dynamic sedimentary system.

To fully appreciate the variation of sediment dispersal systems operating within the region through time, it has been necessary to test and revise field relationships exhibited by the various Cenozoic deposits scattered throughout the region. Emphasis has been placed upon the collation of field evidence. The difficulties of dealing with poorly preserved exposures strewn over an enormous area coupled with the total destruction of others by the highly erosive aeolian system is readily appreciated. There is no doubt, however, that an even greater problem is the scant fossil record preserved within the sediments throughout much of the Namib, which renders lateral correlation extremely difficult. Ironically, despite the poor preservation of the Cenozoic sediments within the study region, the fossil record is more complete than elsewhere, and radiometric dating of volcanic bodies provides additional age definition.

The testing of field relationships and increased resolution of sea-level movement influencing the West Coast has raised potential problems with earlier interpretations. Revision of the earlier Southern Namib stratigraphic frameworks by Kaiser (1926), Greenman (1966) and Stocken (1978) is therefore proposed. This has enabled Ward and Corbett (in press) to correlate key events influencing the development of the Southern and Central Namib given by Ward et al. (1983) and Ward (1984) more accurately.

Ideas presented here provide a platform from which studies of the Namib can continue. There is no doubt that better refinement of age relationships is necessary. It is hoped that further progress will be made in this respect as this work is tested and extended over a wider region. The next phase of this project will be detailed facies analysis of available exposures. This work has commenced, and will no doubt continue in to the future in what must surely be one of the world's most exciting sedimentary environments.

1.4. PREVIOUS WORK

After the discovery of diamonds in the region in 1908, numerous papers broadly outlined the nature of the deposits (Ashmore, 1911; Krause, 1910; Lotz, 1909, 1913; Merensky, 1909; Wagner, 1910, 1914). The placer deposits were found along valley floors, and diamonds were consistently associated with "gravel waves" banked up by the wind (eg. Merensky, 1909; Krause, 1910; and Wagner, 1914).

Although most early authors commented upon the high-energy winds and the possibility of wind-action being responsible for the transport of material through the area, no detailed accounts were given. The only previous work to investigate sediment dynamics of the region is that edited by Kaiser (1926). This excellent collection of papers, published in German, is undoubtedly a major contribution to studies of arid zone sedimentology. It outlined the essential character of the sediment dispersal system and also defined many of the regional stratigraphic relationships. Kaiser concluded that interaction of aeolian and ephemeral stream systems caused deflation of earlier deposits and created the diamond placer bodies within endoreic basins. This study extends investigation of the aeolian system, and previously unrecognised processes are defined.

The declaration of the "Sperrgebiet" (meaning forbidden area) by the German government in 1911 instigated the policy of restricted access to the region. Subsequent publications concerning the Cenozoic geology have therefore primarily dealt with the preserved marine and alluvial deposits in isolation of the regional stratigraphic framework. Of particular significance are the only onshore marine Cretaceous sediments on the southern part of the West Coast (Haughton, 1930a and b; Klinger, 1977), and the extensive preservation of Eocene marine deposits in the vicinity of

Bogenfels (Böhm, 1926; Beetz, 1926; Haughton, 1930b; Siesser, 1977; Siesser and Salmon, 1979). The other notable aspect of the geology is the preservation of the only known Lower Miocene vertebrate fossils in southern Africa, which are contained in widely scattered alluvial sequences (Stromer, 1926; Hopwood, 1929; Heissig, 1971; Hamilton and Van Couvering, 1977; Corvinus and Hendey, 1978; Hendey, 1978; Pickford, 1987). These Eocene and Miocene sequences provide important age constraints for the stratigraphic framework.

The concept that the diamonds were redistributed from an inland source, transported to the coast by fluvial systems, and distributed along the coast by ocean currents is attributed to Lotz (1909) and Range (1909) according to Krause (1910). This model has remained unchallenged since its inception.

In this study an integrated approach is used to examine the variation of the aeolian sediment dispersal system during the Cenozoic. Based upon knowledge of the present-day aeolian system, new data defining the dynamics of the palaeo-aeolian system(s) is presented. This leads to the proposal of a new model to explain diamond placer formation within endoreic basins.

1.5. METHODOLOGY

1.5.1. GENERAL APPROACH

Explanation of the sediment dispersal pattern described above requires detailed knowledge of:

1) present-day sediment dynamics;
2) the variation of sediment dispersal systems operating within the region through time.

This work thus consists of two parts. The initial section considers the present-day sediment dynamics, whilst the second deals with the stratigraphy and palaeo-dynamics of the aeolian dispersal system within the region. The present-day sediment dynamics is considered first because the appreciation of the aeolian sediment dispersal system currently operating greatly aids the interpretation of the palaeo-dynamics of the earlier aeolian sand bodies for which ample field evidence exists.

1.5.2. METHODS USED TO MONITOR PRESENT-DAY SEDIMENT DYNAMICS

Surface-Wind Recorders

Aeolian transport and deposition is controlled by the surface-wind regime. Four Lamprecht anemometers were deployed to monitor the surface wind flow. The configuration shown in Figure 1.2 was

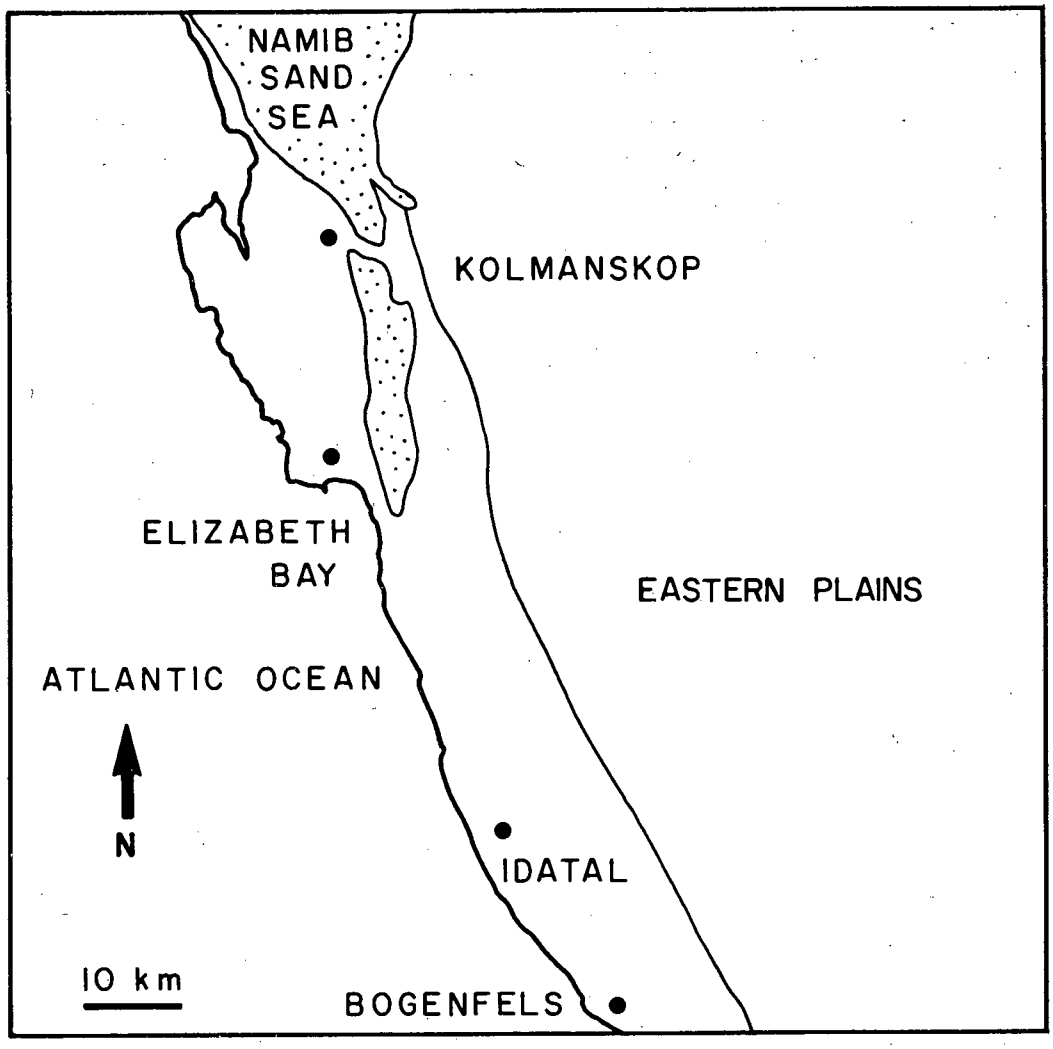

Figure 1.2. Map showing the location of the four anemometers deployed during this study.

selected so as to record changes in the pattern of wind flow that occurrs when the surface-wind blows onshore and interacts with the regional topography. It was also intended to monitor the south-north velocity gradient described previously. Monthly records of hourly data were obtained, providing values for surface wind speed (km/hr) and direction (16 principal compass points aligned with true north). Unfortunately, mechanical problems due to the sandy and salty conditions, and inaccurate

clock mechanisms negated three of the records. It is planned to replace the Lamprecht instruments with more accurate electronic wind recorders to overcome these difficulties. A 2.5 year record was obtained at Bogenfels. It is planned to continue the monitoring programme in the future, to obtain better resolution of the aeolian current system.

Measurement of Sandflow and Bed Form Movement

Three types of sand trap were used to monitor the regional sandflow (Figure 1.3):

1) a venturi-compensated trap (VST) based on a design by Illenberger and Rust (198?), with an aperture 1.7 cm wide and 47 cm high;
2) a perspex sand trap (PST) based on a design by Horikawa and Shen (1960), cited in Goudie (1981), with a 16 cm high, 1 cm wide aperture;
3) a 183 cm high, compartmentalised version of the PST design.

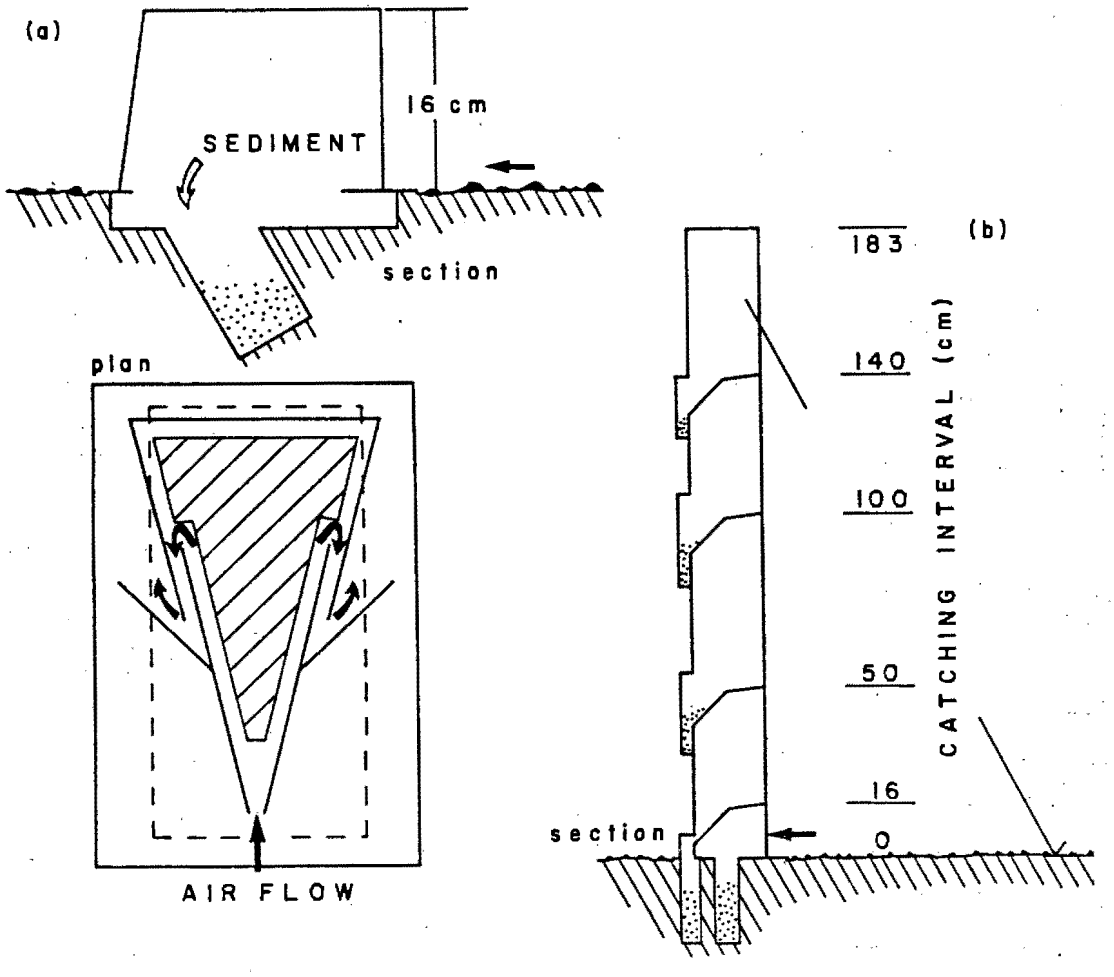

Figure 1.3. (a) Perspex sand trap design (PST) based on a design by Horikawa and Shen (1960). (b) Section through the 1.83 m high version of small sand trap showing catching intervals.

It was necessary to modify this experiment during the study, as the understanding of the aeolian sediment dispersal system within the study area improved. All traps used were oriented to catch sandflow from the south, because previous workers have shown that the southerly wind regime is dominant (Kaiser, 1926; Rogers, 1977; Lancaster, 1985). This conclusion was confirmed by personal observation.

Initially, the VST device was deployed at the wind recorder site north of Bogenfels beach. This operated from February 1986 to early December 1986. Subsequently, three PST devices were built and deployed at three sites (Figure 1.4). These provided an

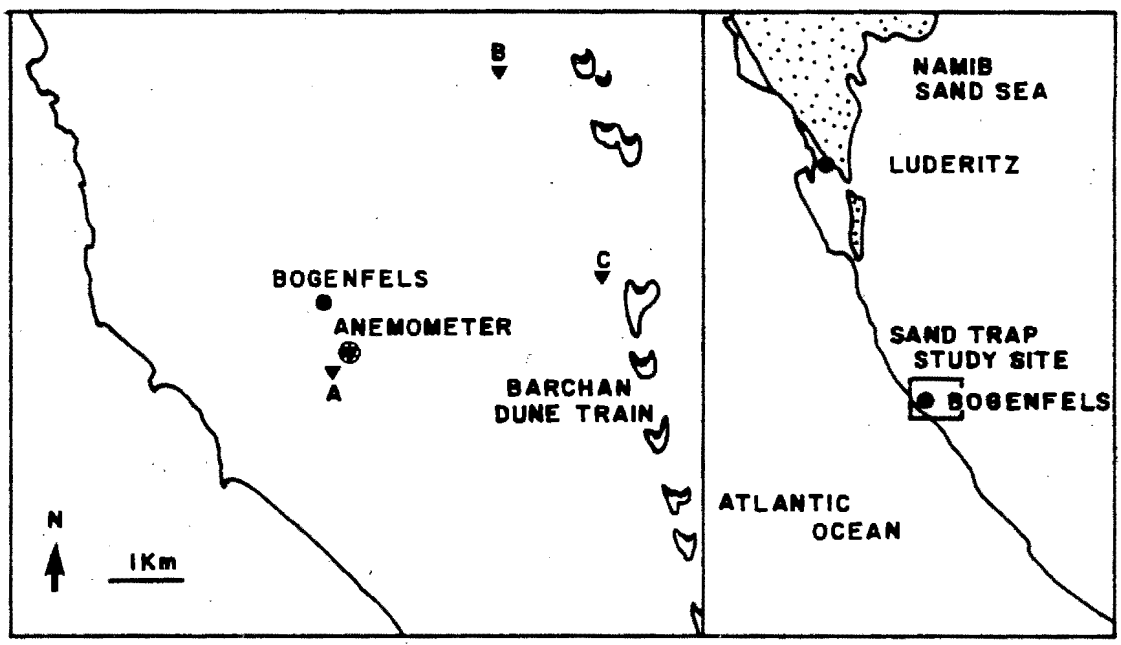

Figure 1.4. Map showing the position of sandtraps deployed near Bogenfels.

east-west transect across the study area. All four traps operated contemporaneously from 22/01/87 to 22/09/87. The PST device at site C was replaced on 08/07/87 with an identical trap extended to a height of 1.83 m, and compartmentalized to catch at the following intervals: 0-16; 16-50; 50-100; 100-140; and 140-183 cm (Figure 1.5). The VST device, repositioned at site C in early December 1986, is being maintained as a permanent station, but the PST devices are no longer operating.

Figure 1.5. Sand trap site C. The venturi-compensated trap is seen in the foreground, and the compartmentalised, 1.83 m high perspex sand trap can be seen in the background. The barchan dunes on the horizon are about 28 m high, their crests have been slightly reversed by a northerly wind. Southerly wind flow is from top right to bottom left.

To verify the direction of net aeolian bedform migration, and to ensure that the bedforms were actually migrating, their movement was monitored. The migration of barchan dunes to the north has previously been demonstrated by Kaiser (1926) and Endrody-Younga (1981) but the relative rate of movement of aeolian barchan dunes and granule ripples had not been measured. The stoss slope skirt of two barchan dunes located south-south-east of sand trap site C were staked at their most southerly point (Figure 1.6a). Measurements were made periodically from the stake to the southern-most point of the stoss slope skirt in the line of dune movement. In addition, four aeolian granule ridges in different geographical settings were staked (Figure 1.6b). The movement of these bedforms was monitored by stretching a piece of cotton taut between the two stakes and measuring the distance to the new crest position. Unfortunately one site was destroyed before the experiment was concluded.

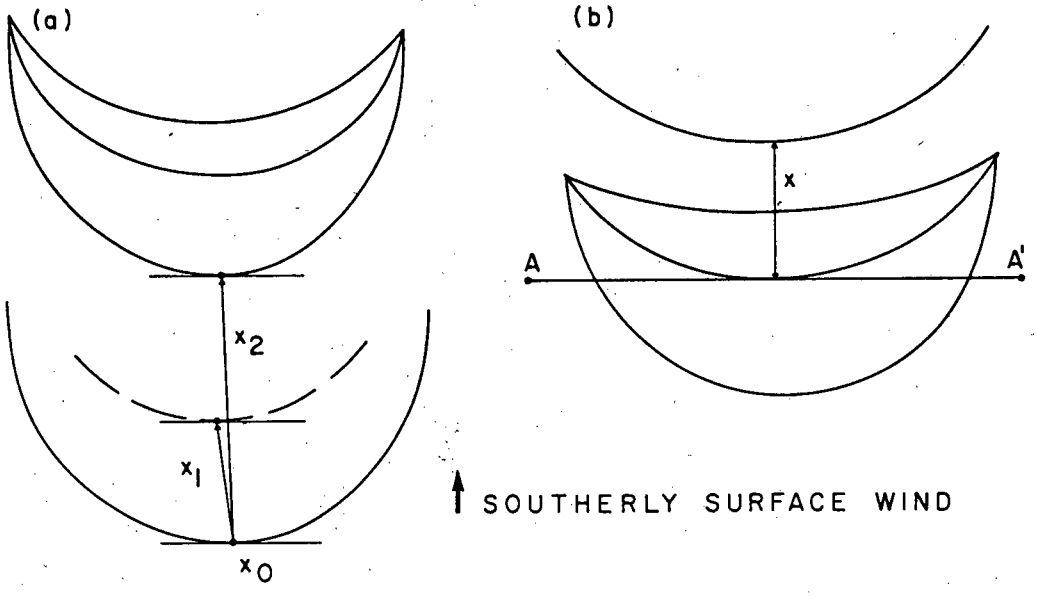

Figure 1.6. Methods of bedform migration measurement. (a) Staking of the stoss slope of a barchan dune. (b) Staking of a granule ripple, and measurement of the crestal migration.

Surface Creep Tracers

As the study progressed, the importance of transport by aeolian surface creep in the present-day sediment dispersal system was confirmed. Tracers were then used to test the ability of the saltation load to move particles across the bed by surface creep.

Personal experience showed that garnet is seldom present in concentrates from the study region. Therefore it was decided that this would be an ideal resistant mineral and also because its specific gravity is similar to that of diamond. Garnet grains of 1 mm to 3 mm diameter from Meob Bay were selected because they are well-rounded due to transport in the aeolian environment. This eliminated potential problems which might have arisen due to irregular particle shapes.

The garnet concentrate was laid in a 1 m long line, perpendicular to the prevailing southerly wind direction on 31/07/87, on the stone pavement surface a few metres to the east of sand trap site C (Figure 1.7a). The stone pavement surface to the north of the release site was then sampled on 05/01/88, and 23/11/88 in two lines parallel with the southerly wind flow (Figure 1.7b). The stone pavement surface within each 25 by 25 cm block sampled was swept, and the underlying 1 to 2 cm of the bed was also scraped up. Each sample was then sieved to obtain the +1 mm to -4 mm fraction from which the garnets were hand-sorted, and the total population weighed. The size distribution of the garnet population in each sample taken on 05/01/88 was then determined using a quarter-phi nest of sieves.

Sediment Peels and Casts

Sections cut through granule ripples, granule ridges and sand sheets provide excellent opportunities for the study of their three-dimensional internal geometry. After fog-wetting or light rain increases the cohesiveness of the sediments vertical sections can be cut. Artificial wetting was not as effective because of the low porosity-permeability characteristics of the silt carapace beneath the surficial sediment. This tended to promote surface run-off by preventing infiltration into the bed.

To overcome the destruction of sections by wind-action, and allow observations to be made without having to endure intense aeolian saltation, sediment peels were made using a technique devised by Buck (1986). The technique relies upon the differential infiltration of cellulose acetate, dissolved in acetone, into the section in response to variation of the grain size, sorting, and packing of the sediment. These parameters are related to the

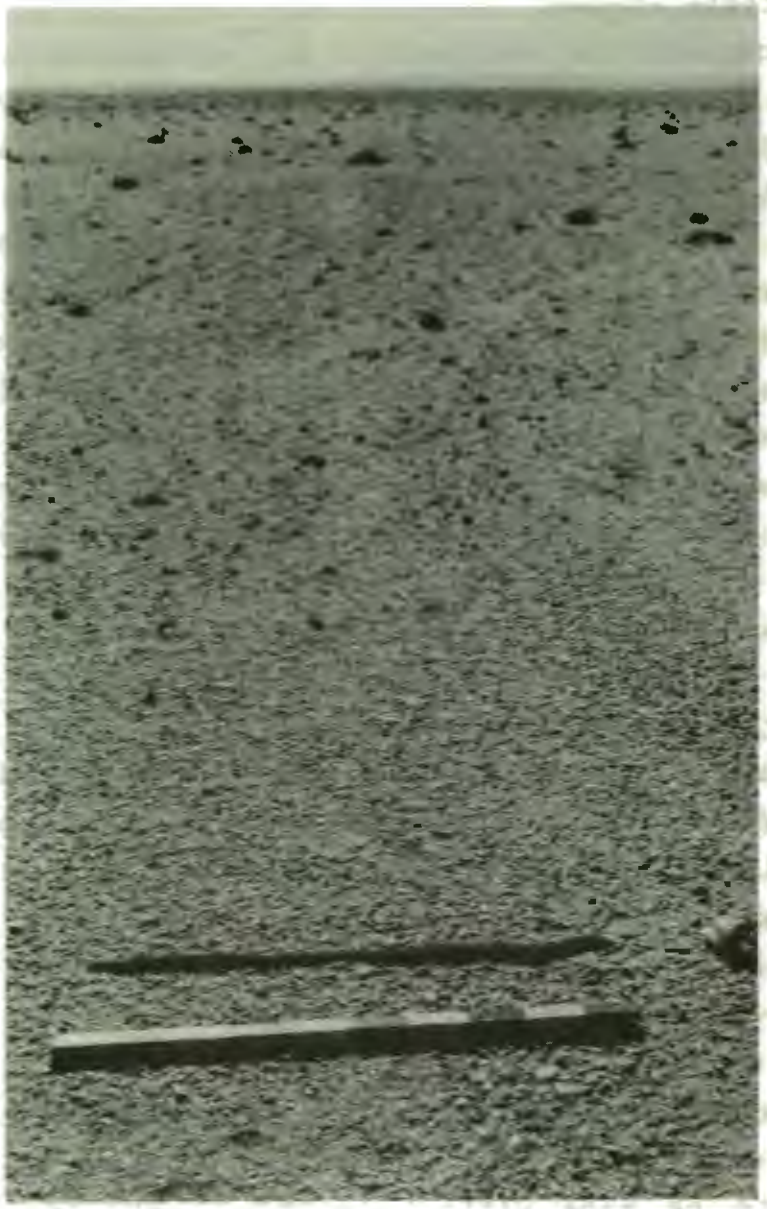

Figure 1.7. (a) Release site of the garnet creep tracers on 31/07/87. Southerly wind flow from bottom to top of frame. Scale 1 m. (b) Orientation of sample lines used to monitor the redistribution of the garnet by aeolian processes.

sedimentary structures present, and their location within the bedform.

The surface of stone pavements represents part of a dynamic sedimentary system. They are subjected to pervasive modification in response to the collision impact of saltating grains, and variation in the weather pattern. Apart from the difficulty of obtaining accurate measurements from an unconsolidated sediment surface under hostile conditions, it is desirable to create a permanent record of particular bed configurations for comparative purposes. A technique devised during this study to obtain accurate plaster casts of complex sediment surfaces is described in Appendix 1.

Grain Size Analysis

The grain size distribution of sediment samples has been determined using a 0.5 phi nest of sieves. A standard sieving time of 15 minutes was used for each sample. Grain size distributions were plotted as cumulative plots and the mean grain size, sorting, skewness, and kurtosis calculated using the graphic formulae of Folk and Ward (1957).

Samples collected using sand traps were analysed to examine the grain size distribution of the saltation load. A major consideration has been to examine the ability of the saltation load to propagate surface creep transport. In examining the grain size variation with time and height above the sediment surface it has been important to obtain an idea of the maximum size of particles transported by aeolian saltation. Samples were therefore split to obtain a dry sand sample of about 100gm where possible. When the original sample weight was less than this, the whole sample was used. This large sample size permitted better definition of the coarse tail of the distribution, which I consider to be an important factor in determining the potential for surface creep. Each sample was washed to remove organic matter, and dried in an oven at 100°C prior to sieving.

Granule ripples and granule ridges have been sampled at numerous localities. Field observation shows that grain size varies widely depending upon the location of the sample on the bedform. To overcome this, all samples were taken from bedform crests. The main objective of this sampling was to establish the grain size of material in the surface creep population. Dried samples were

therefore sieved to remove material smaller than 1 phi prior to sieving in a half-phi nest of sieves.

Samples were collected from the stone pavement at sand trap site C, and from the immediate vicinity of the aeolian barchan dune due east of this site. The main objective was again to establish the grain size of the surface creep population, and to investigate surface creep in the vicinity of the barchan dune. The samples were dried and then sieved to remove the material smaller than 1 phi prior to analysis in the half-phi nest of sieves.

Visual Observation and Photography

Between November 1983 and July 1987 I was stationed in a field camp at Bogenfels by CDM (Pty) Ltd. This afforded me the unusual opportunity of observing present-day sediment dynamics within the deflation basin on an almost daily basis and to record short-lived changes within the system. These changes have been recorded on film, and I am indebted to the Management, Security Department, and helicopter pilot of CDM (Pty) Ltd for permitting me to use the company helicopter to obtain aerial photographs to do this. It has greatly aided my appreciation of the present-day sediment dynamics.

The deflation basin is an incredibly dynamic sedimentary environment which responds rapidly to a change in conditions, but evidence of this response vanishes almost as quickly. Comparative photography of specific sites is a valuable approach to the study of changes within a sedimentary system. The technique was particularly useful for monitoring changes within ephemeral stream channels and where ponded water bodies formed after rain. Several sites were demarcated and photographed on a regular basis, creating a complete record of events over several months.

1.5.3. METHODS USED TO STUDY REGIONAL STRATIGRAPHY AND PALAEOGEOGRAPHY

Regional mapping has been undertaken using aerial photographs from Job 591 (1965), supplied by the Surveyor General, at a scale of 1:25 000. Interpretation has been checked extensively on the ground. Vertical sections have been recorded where possible, and detailed facies analysis of key exposures has been undertaken. This work will continue in the future. An unfortunate feature of the region, related to the unbelievably erosive sedimentary

region, related to the unbelievably erosive sedimentary environment, is the paucity of good sections through sedimentary sequences. This severely hampers detailed examination of the sequences, and makes facies analysis particularly difficult.

Laboratory work has been kept to a minimum, although it will play an increasingly important role as more detailed investigation of specific aspects is undertaken in future. Thin-section examination of some sediments has been used to assess their nature, and for comparing different sandstones. X-ray fluorescence (XRF) and X-ray diffraction (XRD) techniques have been used to identify the principle chemical and mineralogical constituents of specific samples. XRF analyses were undertaken by staff of the Anglo American Research Laboratories, and XRD analyses were kindly undertaken by Dr G. Schneider in the South West African Geological Survey, Windhoek.

2.GEOMORPHIC ELEMENTS

2.1. INTRODUCTION

Numerous geomorphic elements comprise the main deflation basin. It is impossible to locate all of these on one plan, however, the location of some of the larger-scale elements are shown in Figure 2.1.

2.2. DURICRUSTED RESIDUALS

2.2.1. SILCRETE TOPOGRAPHIC RESIDUALS

Three types of duricrust occur within the study area (Figure 2.1). The silcrete is the oldest because it underlies both the ferricrete and the calcrete. The calcrete is the youngest because it overlies the ferricrete at the Buntfeldschuh and Chalcedon Tafelberg.

The silcrete capped table mountain landscape is a prominent geomorphic feature of the Southern Namib (Kaiser, 1926; Beetz, 1926. Scattered residuals are widely distributed to the north of the Orange River, but are absent north of the Grillental. The best examples occur around Pomona (Figure 2.2). Concave slopes mantled with angular silcrete debris are capped by a sub-horizontal to gently undulating silcrete horizon up to 3 m thick (Chalcedon Tafelberg Silcrete Formation, sensu SACS, 1980). The close proximity of scattered remnants between 100 to 160 masl. around Pomona indicate that the silcrete probably formed a more extensive horizon of gently undulating relief. X-ray diffraction analyses confirm that in many instances the silcrete is underlain by a kaolinized weathering profile (Figure 2.3). Examination of thin-sections show that the development of the silcrete diminishes with depth through the profile. The relationship with the kaolinized profile supports correlation with the African palaeo-surface (sensu Partridge and Maud, 1987). In the study area, the minimum age for the silcrete is 37 My. based upon a radiometric age for overlying phonolite at Swartkopp (Stocken, 1978 - see Figure 2.1 for location). The silcrete is therefore an important, dateable, stratigraphic marker horizon, whose palaeoclimatic implications are addressed in section 7.2.1.

Weathering and slope processes gradually reduce the extent of the resistant silcrete cap (Figure 2.4) and ultimately, residuals are completely destroyed. The only evidence of their former presence

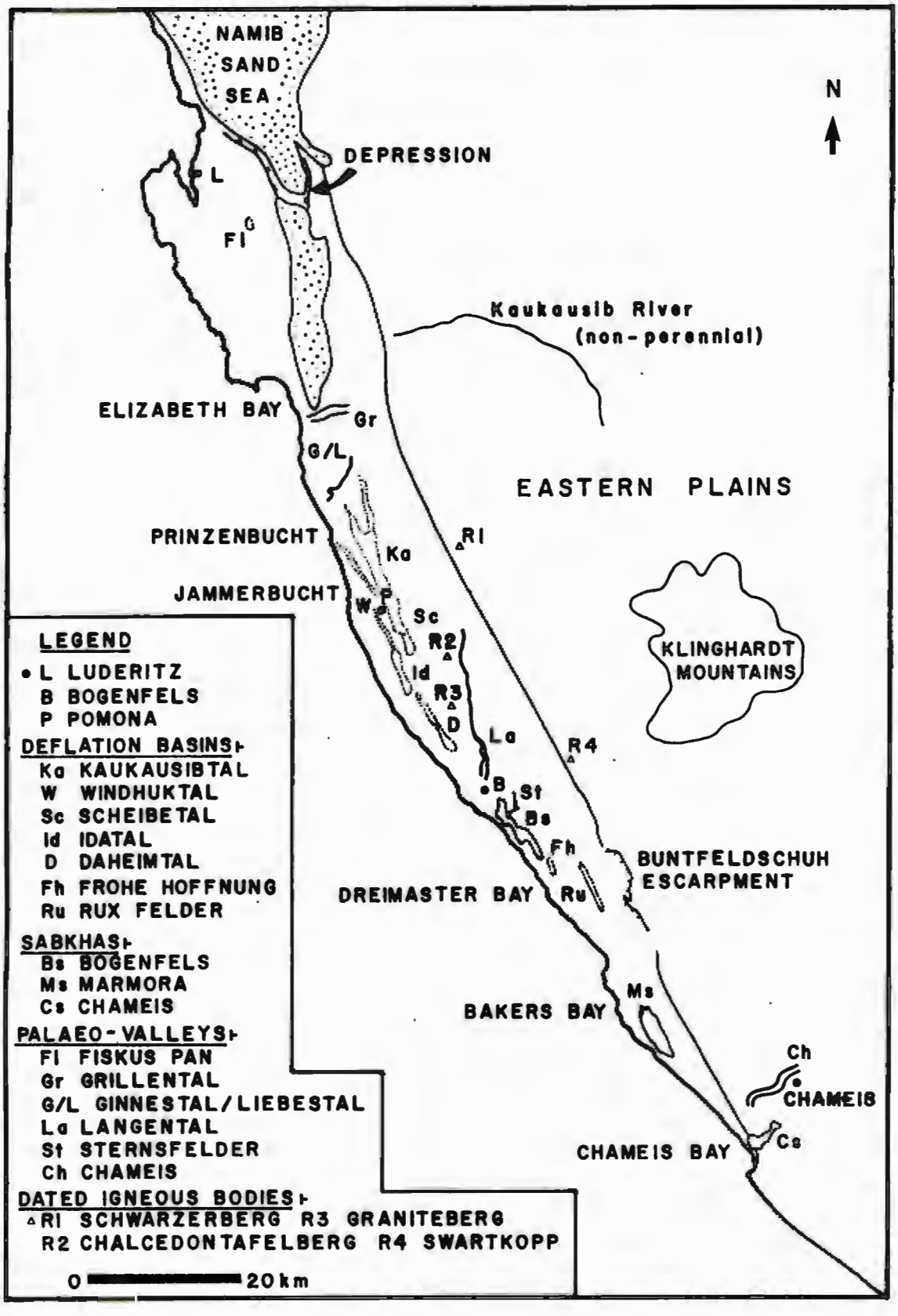

Figure 2.1. Map illustrating the main geomorphological features of the study area.

Figure 2.2. Oblique aerial view of the silcrete capped residual "Tafelberg Nord" (arrowed), at an elevation of 155 masl. Topographic inversion of about 60 m has occurred at this point. Note the yardang field formed in Bogenfels Formation Dolomite at top left of frame.

Figure 2.3. Mottled zone of a deeply kaolinised weathering profile beneath a silcrete cap, located about 15 km north of Chameis (Lat. 27°29'30"S; Long. 15°34'E). Gypsum veining developed after the kaolinisation, and is probably much younger. Scale 1m in 10 cm divisions.

is then a few silcrete clasts incorporated into a stone pavement. Valley floors are now up to 120 m below the silcrete horizon, for example at Idatal (Figure 2.5). This proves that substantial topographic inversion occurred after silcrete formation (Kaiser, 1926). Where neighbouring residuals are separated by Bogenfels Formation dolomite, valley floors frequently show evidence of severe aeolian corrasion (Figure 2.6). It is thus likely that much of the erosion after the initial incision of the silcrete has been by aeolian processes.

2.2.2. FERRICRETE PROFILE DEVELOPMENT

A 10 to 15 m thick ferricrete is present at Kakaoberg, towards the southern end of the Buntfeldschuh escarpment (Figure 2.7). The aeolian Kakaoberg Sandstone Member of the Upper Buntfeldschuh Formation (see section 7.3.3) is the host sediment, and there was a return to aeolian sedimentation after the ferricrete had formed.

A mottled, reddened zone occurs at the base of the profile, in which the relict aeolian primary sedimentary structure can still be seen (Figure 2.8). Above this, a grey/brown gleyed horizon underlies the deep brown to red pisolitic ferricrete (Figure 2.9). Chalcedonic pedotubules are a feature of the deposit, and evidence of burrowing is also present. The ferricrete must be younger than the underlying Upper Palaeocene to Lower Eocene marine sediments. At the southern end of Kakaoberg the ferricrete is overlain by an extensive pedogenic hardpan calcrete. A similar sequence of sediments is present at Chalcedon Tafelberg. Scree obscures the contacts of the sedimentary units, but loose blocks of ferricrete have been observed.

The development of similar ferricrete presently occurs along the Zululand coast of Natal (Maud, pers. comm., 1987). This suggests that when the ferricrete formed the palaeoclimate was warmer than today.

2.2.3. PEDOGENIC HARDPAN CALCRETE

Silcrete residuals such as Elfertberg, the Katchen Plateau (Lat. 27°15′S; Long. 15°39′45"E) and Rundekuppe (Lat. 27°10′S; Long. 15°21′30"E) are commonly overlain by a mature pedogenic hardpan calcrete (see Figure 4.24). The calcrete has developed in a wide variety of host materials. In the Pomona area, and to the east of

Figure 2.4. Latter stages in the destruction of a silcrete capped residual. Note the collection of loose silcrete blocks forming the cap, and covering the concave slopes. Man (arrowed) for scale standing on the scour-remnant ridge in the lee of the residual.

Figure 2.5. View north from the Idatal floor, near Stauchslager, towards the silcrete residual capping Elfertberg, elevation 124 masl. Topographic inversion has left the Idatal floor about 100 m below the silcrete. Note the planed bedrock in the middleground, and the small delta deposited at the earlier site of a ponded water body.

Figure 2.6. Severely fluted, small dolomite yardang on the deflation basin floor between silcrete capped residuals near Tafelberg Nord, illustrating the highly erosive nature of the southerly wind regime, which flows from bottom right to top left in the frame. Person for scale.

Figure 2.7. View south from the Buntfeldschuh escarpment showing the ferricrete profile capping Kakaoberg, which stands about 100 m above the floor of the deflation basin. Pebble bands within the Upper Palaeocene to Lower Eocene, marine, Lower Buntfeldschuh Formation, can be seen in the foreground.

Figure 2.8. The basal mottled zone of the ferricrete profile. Note the relict aeolian bedding which can be seen on either side of the altered zone. Scale about 11.5 cm.

Figure 2.9. Pisolitic, hardpan capping the ferricrete profile. Part of the gleyed horizon within the profile can be seen at the base of the frame. Scale about 11.5 cm long.

the deflation basin, the calcrete exploited fractures in the silcrete, and envelopes rounded silcrete clasts (Figure 2.10). It therefore follows the underlying relief provided by the silcrete. At other localities, erosion has removed the silcrete, and the calcrete has subsequently developed in the kaolinized deep weathering profile. In other places, Cenozoic aeolian and alluvial sediments provide the host material.

The calcrete forming extensive plains to the east of the deflation basin, probably developed at about 12 Ma (see section 7.2.6). It is an important stratigraphic marker horizon throughout the Southern and Central Namib due to its widespread preservation (Ward, 1984). The abrupt termination of the calcrete about 120 m above the deflation basin floor at Buntfeldschuh (Figure 2.11), along the eastern margin of the deflation basin, indicates that it probably extended further to the west, possibly beyond the present coastline.

Figure 2.10. Rounded clasts of silcrete (S) enclosed by the younger pedogenic hardpan calcrete at Rundekuppe, east of Pomona. Note the polished and fluted surface produced by aeolian corrasion. Scale 1 m in 10 cm divisions.

Figure 2.11. Oblique aerial view to the east, showing the termination of the pedogenic hardpan calcrete along the Buntfeldschuh escarpment, approximately 120 m above the deflation basin floor. Note the extensive, gently undulating plain to the east of the deflation basin margin.

2.3. ENDOREIC BASINS

2.3.1. DESCRIPTION OF MORPHOLOGY

A south-north oriented trough up to 5 km wide (Figure 2.12) prompted Kaiser (1926) to term the deflation basin the "Trough Namib". The trough extends from Bogenfels to the Grillental along the regional strike of the miogeosynclinal Bogenfels Formation, forming part of the Gariep Province (Figure 2.13). When not covered by Cenozoic sediments, the deflation basin floor consists either of refoliated granitoid gneiss or the gently folded volcano-sedimentary pile of the Pan African Gariep Geosyncline (Martin, 1965; Kroner, 1974a; Davis and Coward, 1982) which was deposited between about 920 Ma and 550 Ma (Tankard et al., 1982). North of Bogenfels, folds and thrusts affecting shale, arkose, quartzite, dolomite, and a basal conglomerate of the miogeosynclinal Bogenfels Formation, verge eastward and trend north-south (Kaiser, 1926; Kroner, 1974a; Davis and Coward, 1982). The anticlines are cored by refoliated Namaqua basement (Martin, 1965). Significantly, this structural trend is not only coincidentally sub-parallel to the present coastline but is also sub-parallel to the prevailing southerly surface-wind flow. Both to the north of the Grillental, and within a narrow coastal belt up to 4 km wide along the western margin of the main trough, refoliated gneisses form the deflation basin floor. The relief is noticeably more subdued in these areas (Figure 2.14), apparently reflecting the absence of marked lithological variation.

The main trough extending north from Bogenfels consists of smaller, south-north oriented basins separated by topographic highs. The surface airflow is funnelled through the resulting complex topography. The basins are essentially endoreic, with no alluvial outlet to the coast, and minimal alluvial interaction is possible between them (Kaiser, 1926). Although these features are formed in both miogeosynclinal and eugeosynclinal deposits of the Gariep Group, the best examples occur where sandstones and conglomerates of the Bogenfels Formation are exposed (Figure 2.15). The Idatal (Figure 2.16) provides a classic example of an endoreic basin. In plan, the basins are triangular depressions bounded to the east and west by steep bedrock walls. The base-level is usually situated towards the southern end, near the widest point. From here, a south-facing slope rises, and gradually tapers to an apex

Figure 2.12. Landsat image of the Southern Namib deflation basin and eastern plains, showing the position of the main south-north oriented trough (T) located along the strike of the clastic metasediments of the Bogenfels Formation.

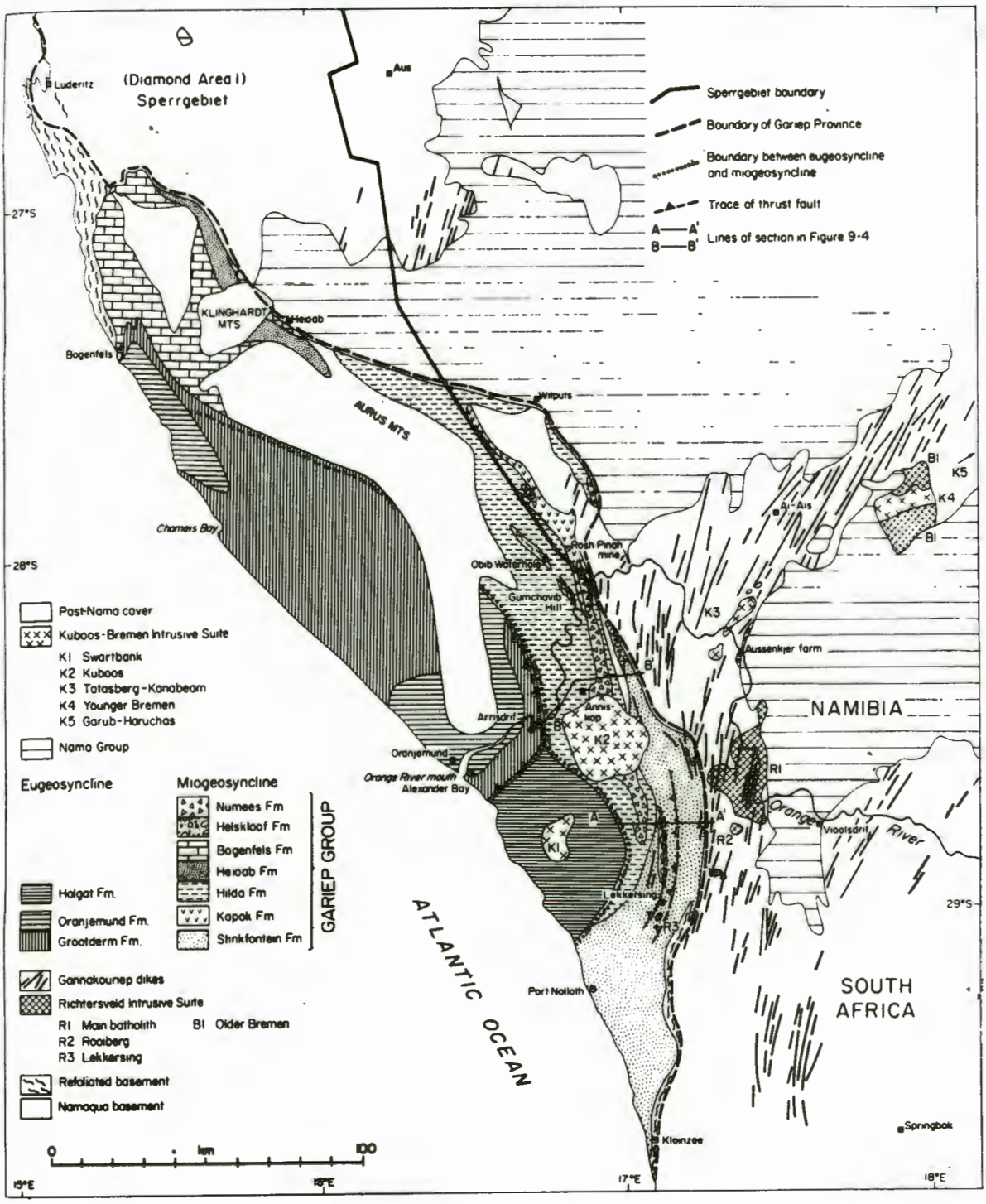

Figure 2.13. Geologic map of the Gariep Province to show the distribution of the Gariep Group. After Tankard et al. (1982, Fig. 9-1).

Figure 2.14. Oblique aerial view to the west across the gneiss platform, north of the Grillental, showing the gently undulating relief. Southerly wind flow from top left to bottom right.

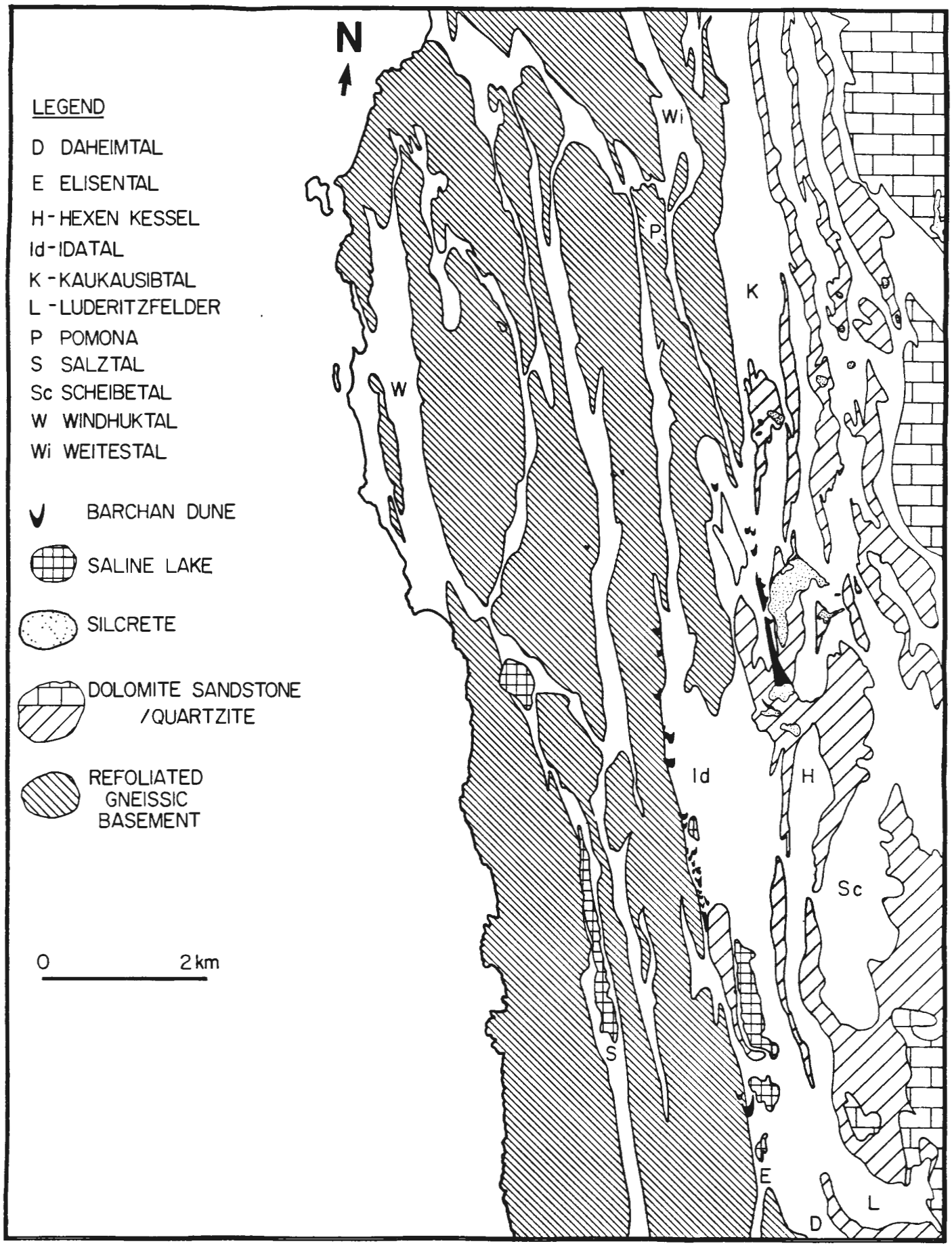

Figure 2.15. Map showing the relationship between the main endoreic basins within the Pomona area, and the distribution of Bogenfels Formation sandstones.

Figure 2.16. Oblique aerial view to the north, up the Idatal towards Elfertberg (E), standing about 120 m above the basin floor. Note the sharply defined east and west margins to the basin and the relatively flat floor, where halite (H) has crystallised in shallow pans.

in the north. The base-level elevation can be below the water table, as in the case of the Idatal, where it is about 1 mbsl. At their southern end, the basin floor either drops abruptly to base-level from a surrounding bedrock rim, or, if the previous basin runs into the succeeding one, a less severe step occurs.

When resistant quartzites form the limbs of folds, the erosion of weathering products leaves south-north trending ridges subdividing broad depressions (Figure 2.17). Kaiser (1926) termed these features "isoclinal valleys". The Windhuktal (Figure 2.18) is an example of a "synclinal valley". This feature resulted from the erosion of Bogenfels Formation clastics from a syncline between two north-south trending gneissic anticlinal cores (Kaiser, 1926).

Evidence of differential erosion due to lithological variation is seen along the western margin of the Idatal. A "hanging valley" has developed at the contact between the dolomite flooring an extension of the Elisental, and the Basal Clastic Member flooring the main Idatal basin (Figure 2.19). Coupled with the change in relief where gneiss floors the deflation basin, this supports the hypothesis that the distribution of endoreic basins is governed by differential weathering of variable bedrock lithologies, and the

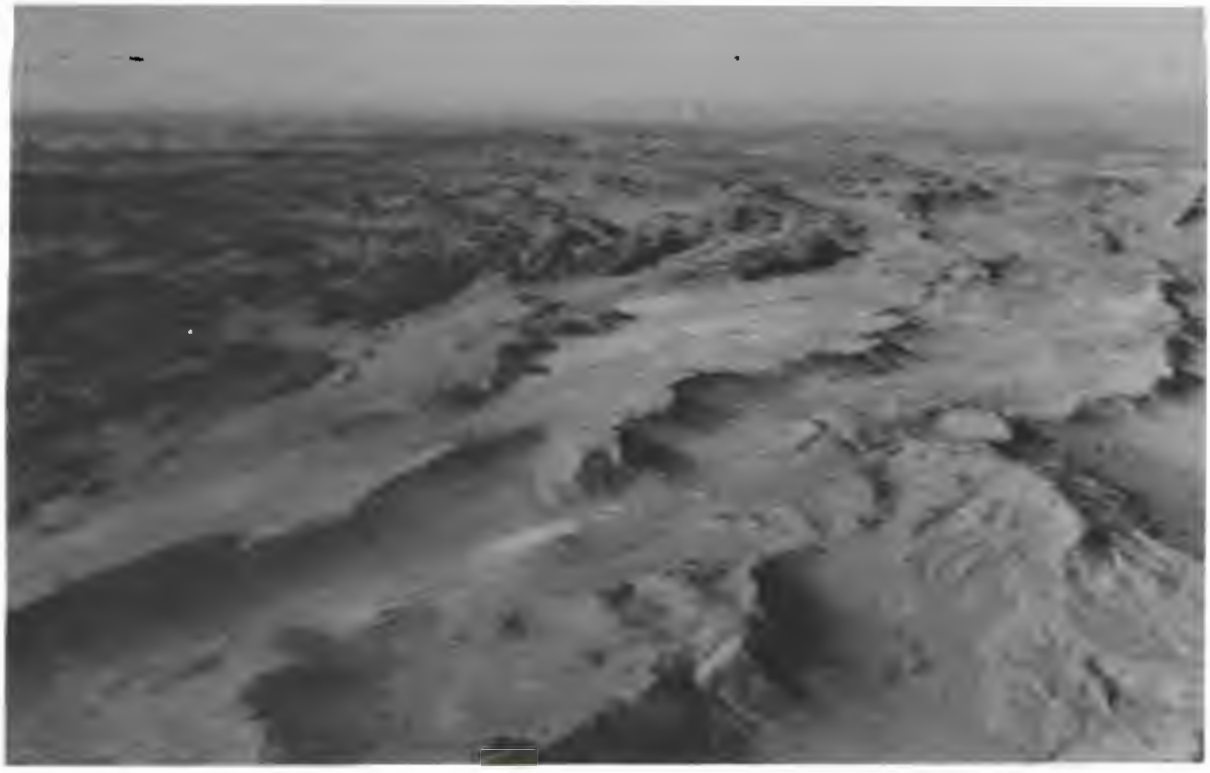

Figure 2.17. Oblique aerial view to the south-east across the eastern part of the Kaukausibtal area, illustrating the development of endoreic basins by resistant Bogenfels Formation quartzite ridges forming the limbs of folds. Note the yardang field formed of Bogenfels Formation Dolomite in the top left corner, which stands above the surrounding basin.

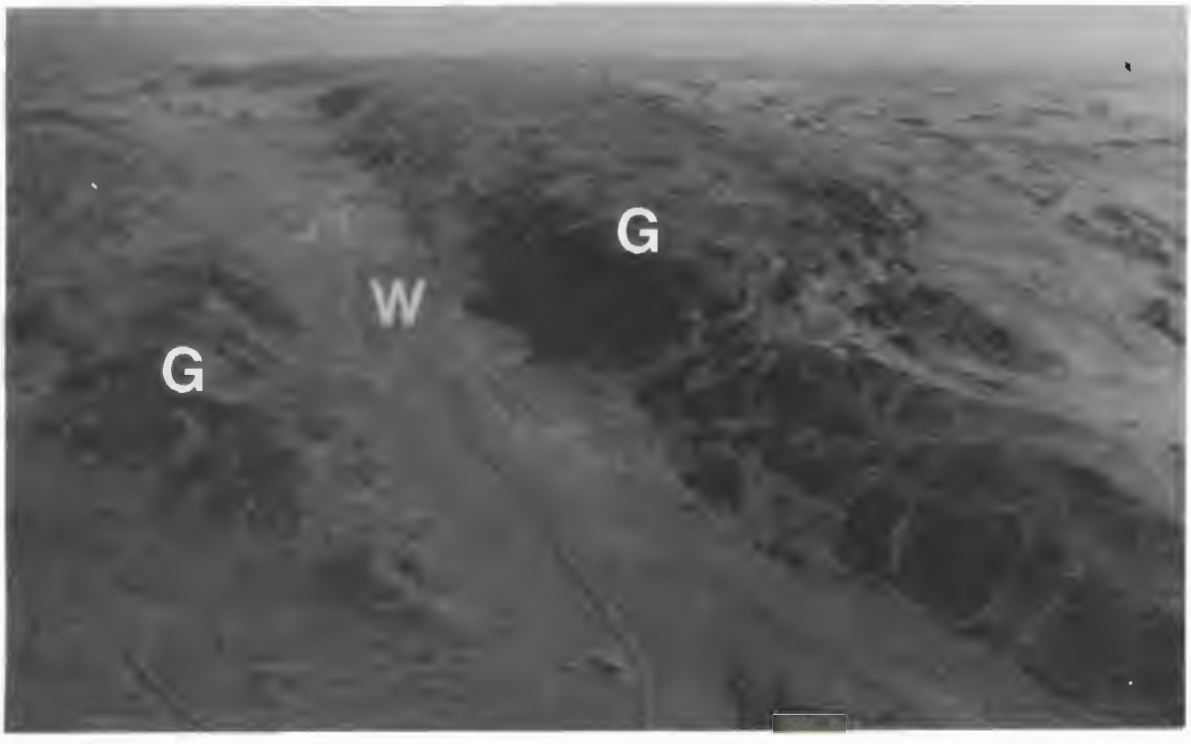

Figure 2.18. Oblique aerial view to the north up the Windhuktal (W) formed by the erosion of Bogenfels Formation clastics from a syncline bordered by relatively resistant anticlinal cores of gneiss (G), which form steep south-north oriented basin margins about 50 to 60 m high.

Figure 2.19. View west across the Idatal from Stauchslager, showing a wedge-shaped cliff of Bogenfels Formation Dolomite about 15 m high descending abruptly to Idatal base-level. Note the quartz rubble in the foreground eroded from Bogenfels Formation clastics.

north-south structural trend (Kaiser, 1926). Undoubtedly, sediment transport and erosion are also important factors.

The southern end of the Windhuktal endoreic basin is floored by partially cemented, locally derived alluvial infill which was probably deposited during the Pleistocene. The basin floor progressively descends northwards towards base-level in a series of abrupt, concave steps which are a few metres high (Figure 2.20). In plan, the V-shaped steps open northwards, apparently resulting from ephemeral stream-head retreat. Aeolian deflation of ephemeral stream deposits covering the basin floor (section 5.3) leads to its progressive lowering. Cavernous weathering of the gneiss along the basin margins is associated with fluting due to aeolian corrasion (Figure 2.21). Significantly, cavitation of this type is a common feature of salt weathering (Wellman and Wilson, 1965; Cooke, 1981).

Kaiser (1926) attributed endoreic basin development to differential chemical weathering plus aeolian deflation and corrasion. Observations from this study strongly suggest that it is salt weathering, in conjunction with the high-energy aeolian regime, which explains these features. In the Namib's humid coastal zone, advective fog is an important source of salts (Goudie, 1972; Watson, 1981; Cooke, 1981), which includes sulphate, an important agent in rock breakdown (Goudie, Cooke and Evans, 1970). In addition, the groundwater throughout most of the Southern Namib is highly saline, with values of 2000 to 11000 mg/l of chlorine in basins such as Luderitzfelder, Scheibetal and Windhuktal (Kaiser, 1926). Salts are progressively concentrated during the evaporation of ponded water bodies (measured by Kaiser, 1926) within depressions collecting water from spring discharge or surface run-off. This occurs very effectively within endoreic basins such as the Idatal (Figure 2.22). Consequently, the floors of endoreic basins provide ideal sites at which salt weathering can proceed. Sperling and Cooke (1984) have shown that the rate of salt weathering differs according to lithology. Of the specimens they tested, dolostone was the most durable due to its low porosity/water absorption capacity, and saturation coefficient. Weathering rates for York and Hollington Stone (fine-grained arkosic and quartz sandstone respectively) increased with daily immersion in saturated salt solution. The variation of the results was attributed to differing macro- and micro-porosity /

Figure 2.20. View south down Windhuktal, showing the stepped profile (arrowed), about 3m high, cut into Bogenfels Formation clastics by a combination of ephemeral stream-head retreat and deflation.

Figure 2.21. View north along the western, gneissic margin of Windhuktal, showing cavernous weathering features (C), and the fluted surface of the gneiss (F) produced by aeolian corrasion. Note also the resistant quartz vein (Q), standing proud of the fluted gneiss surface. Scale 1 m in 10 cm divisions.

permeability characteristics of the sandstones, which controls the quantity of salt absorbed. The sandstone samples principally underwent granular disintegration, and it was concluded that salt crystal growth pressure is more effective in rock weathering than is hydration.

The observed distribution of endoreic basins supports the conclusion that differential salt weathering has played an important role in the evolution of deflation basin geomorphology within the Southern Namib. Whilst granitoid gneiss is affected (Figure 2.23), the sandstones of the Bogenfels Formation appear to be more susceptible, and the erosion rate is consequently faster. Salt weathering potentially proceeds most rapidly where aeolian erosion perpetually creates a fresh bedrock surface for it to act upon. This is observed to be the case on the floor of the Idatal.

The desiccation of Bogenfels Formation sandstone after wetting by ephemeral rainfall, or a particularly heavy fog, leads to salt concentration near the rock surface, and salt efflorescence. Dome-shaped surface irregularities, with walls a few sand grains thick, lift from the sandstone surface, probably as a result of salt crystallization pressure. The domes form delicate sandstone surface roughness elements, about a centimetre high, which protrude into the saltation layer. Granular disintegration of the sandstone by salt weathering renders the sandstone domes prone to erosion by the saltation load, and they are rapidly removed. The basin floor is thus fractionally lowered. The Bogenfels Formation dolomite should be less suceptible to salt weathering, which probably explains why it forms topographic highs surrounded by depressions eroded into clastic lithologies. This further supports the hypothesis that salt weathering is an important factor in the geomorphological development of the region.

To what extent the presence of the deep kaolinized weathering profile affected regional geomorphological development subsequent to the incision of the protective silcrete cap is pure conjecture. It is possible that variation of the profile's development in different host lithologies partially accounts for the initial formation of depressions during the incision of the silcrete. Subsequent salt weathering, aeolian corrasion and deflation, and ephemeral stream processes probably exploited this to create the endoreic basins. The kaolinized profile might also have influenced

Figure 2.22. Halite crystallisation in shallow pans on the sandstone floor of the Idatal.

Figure 2.23. Cavernous weathering of granitoid gneiss south of Kolmanskop, near Luderitz, which probably results from salt weathering. Scale 1 m long in 10 cm divisions.

the development of early coastal basins, such as that at Bogenfels, where the bedrock is phyllite.

2.4. WIND-ALIGNED, STREAMLINED LANDFORMS

2.4.1. YARDANGS

Under the influence of the highly abrasive aeolian dispersal system, it is not surprising that yardangs are present within the deflation basin (Kaiser, 1926; Rogers, 1977; McCauley et al., 1977). These landforms are principally developed in dolomite of the Bogenfels Formation, and the distribution of this lithology is an important factor in determining their spatial distribution. They generally occur in groups, forming a yardang field (Figure 2.24). Kaiser (1926) first drew attention to their similarity to aeolian landforms described by Bosworth (1922), and noted their resemblance to inverted boat hulls (Figure 2.25). Examination of yardangs formed in bedded dolomites indicates that the tectonic structure is an important factor in determining their development, and their dimensions are highly variable.

Southern Namib yardangs are particularly interesting because of their development in crystalline rock, which is rarely observed in other deserts on earth (McCauley et al., 1977). McCauley et al. (1977) consider that yardangs indicate undersaturated sandflow conditions. This suggests that the erosional power of the Southern Namib aeolian regime is exceptionally high within the deflation basin. This conclusion is confirmed by the examination of aeolian ventifacts formed from weathered blocks at the base of some of the landforms (Figure 2.26a and b). The spikes and blades of this ventifact provide striking evidence that the erosional power of the southerly surface-wind regime far exceeds that of any other wind direction influencing the deflation basin at the present time. Further observations concerning the distribution and development of yardangs are given in section 7.4.3.

2.4.2. LARGE-SCALE SCOUR-REMNANT RIDGES

Wind-aligned, streamlined landforms similar to yardangs have developed in other lithologies of the volcano-sedimentary Gariep Group in the lee of topographic highs formed by resistant rock types. Streamlined, bedrock tails of triangular plan-form, with their apex pointing north have a well-defined ridge along their

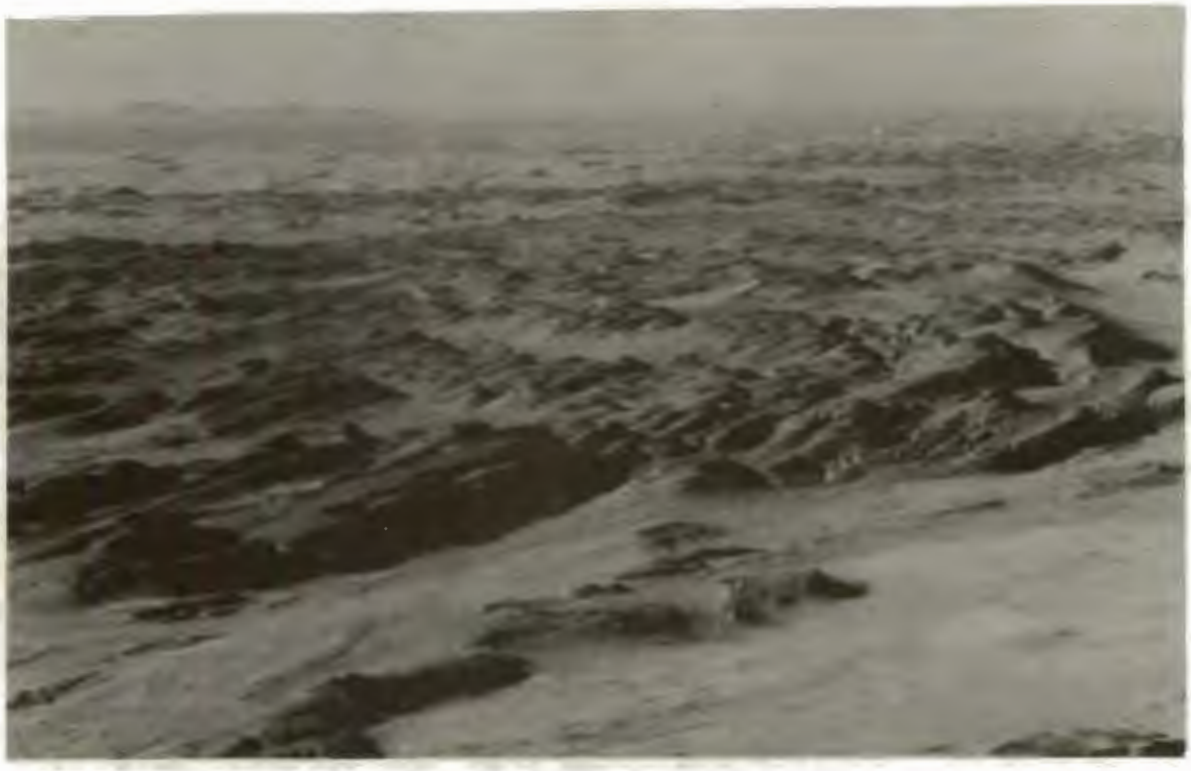

Figure 2.24 Oblique aerial view of the main dolomite yardang field due east of Pomona. Note how abruptly the ground surface drops at the contact with the Bogenfels Formation clastics in the foreground. Southerly wind flow from right to left.

Figure 2.25. Yardangs of bedded dolomite west of Bogenfels. Note the influence of the variable dip direction on the development of landforms, and the planed dolomite in the foreground. The largest yardang is about 20 m high. Vegetation is particularly dense in the troughs between the landforms. Southerly wind flow from right to left.

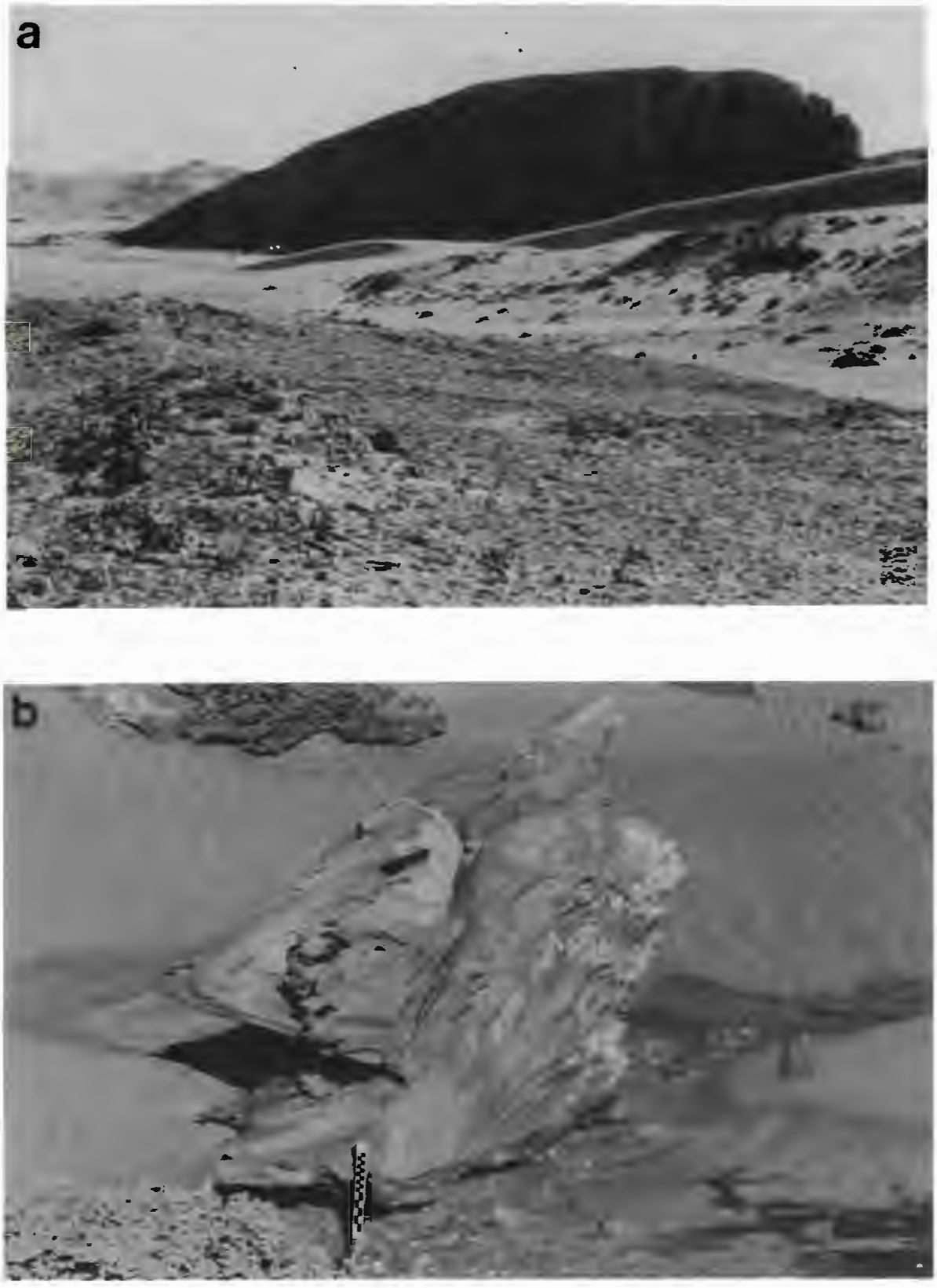

Figure 2.26. (a) Approximately 26 m high dolomite yardang east of Bakers Bay. (b) An example of the amazing spikes and blades developed on the south face of loose blocks of dolomite at the foot of the yardang. Southerly wind flow from left to right. Scale bar 10 cm long.

long axis, which is parallel to the southerly surface-wind regime (Figure 2.27). These features resemble much smaller-scale obstacle marks termed scour-remnant ridges by Allen (1982).

The resistant hills at the upwind end of the landform approximate to the case of domical hills discussed by Greeley (1986), and act as bluff bodies in the planetary boundary layer. Modelling of the flow pattern around such objects of low height-to-width ratio by Iversen and Greeley (1978) demonstrate that a horseshoe vortex is shed from their flanks (Figure 2.28). Together with the availability of saltation and suspension load, this probably determines the form of scour in the lee of the obstacle. As a result, the scour-remnant ridge is likely to approximate to the form of the vortex.

The example in the lee of Schwarzerberg, a nephelinite dated radiometrically at 30 Ma (Spriggs, 1988), is seen as supporting evidence for the concept that the position of the eastern margin of the deflation basin has not remained constant throughout time (see section 7.4.2 for detailed discussion).

Scour-remnant ridges in the lee of silcrete capped residuals occurring to the east of Pomona, provide further evidence that aeolian corrasion and deflation have, and still do, significantly influence the geomorphological evolution of the deflation basin.

2.5. SMALL-SCALE EVIDENCE OF AEOLIAN CORRASION

Harger (1914) first drew attention to the wonderfully intricate aeolian ventifacts formed by the corrasion of Precambrian and Cambrian crystalline rock flooring the deflation basin. These small-scale features provide further testimony to the erosive nature of the aeolian regime. In some instances, the cavitation of leeward faces of obstacles (Figure 2.29) provides evidence for the role of vorticity (sensu Whitney, 1978, 1983). The detailed treatment of ventifact formation is beyond the scope of this study. It is, however, important to illustrate some of the ventifacts observed, in order to demonstrate the dominant influence of the southerly surface-wind regime over aeolian corrasion (Figure 2.30).

No rock type has been located which can withstand the erosive force of the aeolian regime within the deflation basin of the Southern Namib. The debate as to whether aeolian corrasion results primarily from windbourne dust or the impact of the coarser-grained

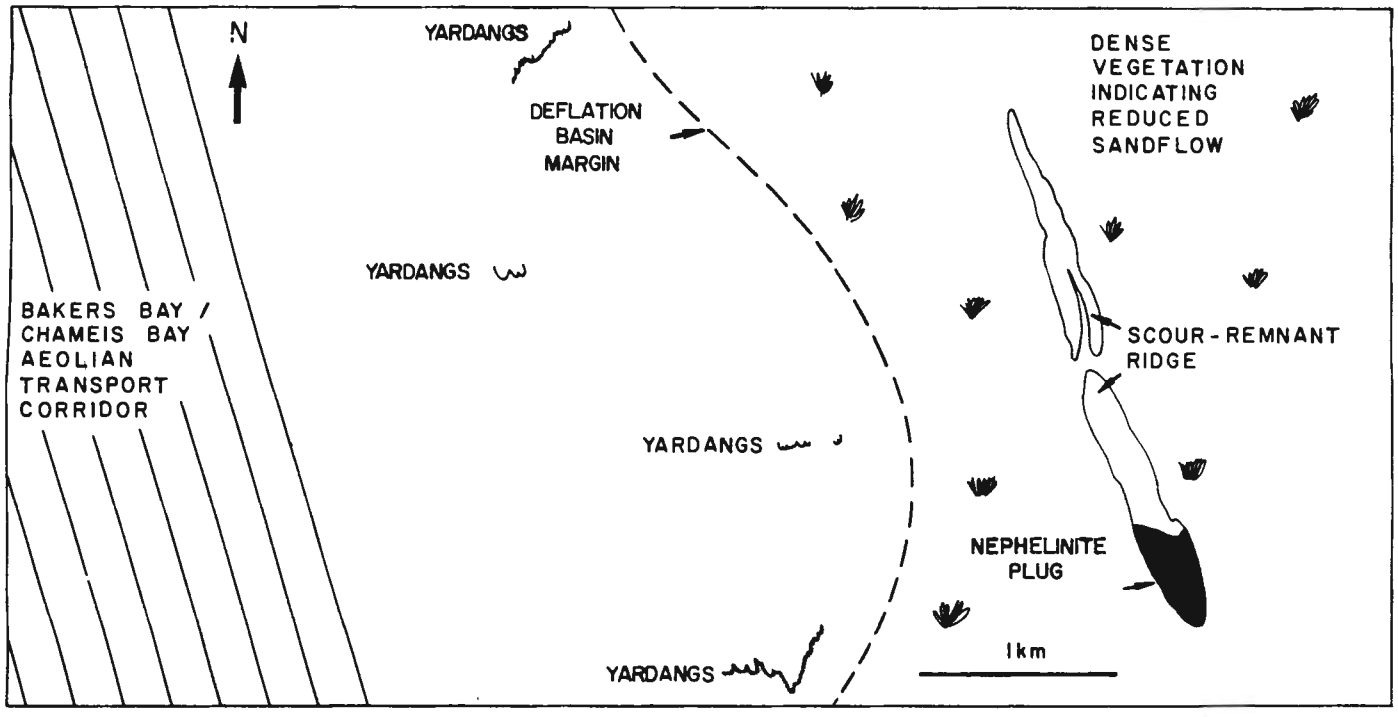

Figure 2.27. Scour-remnant ridge in the lee of a resistant nephelinite plug forming a topographic high at Schwarzerberg.

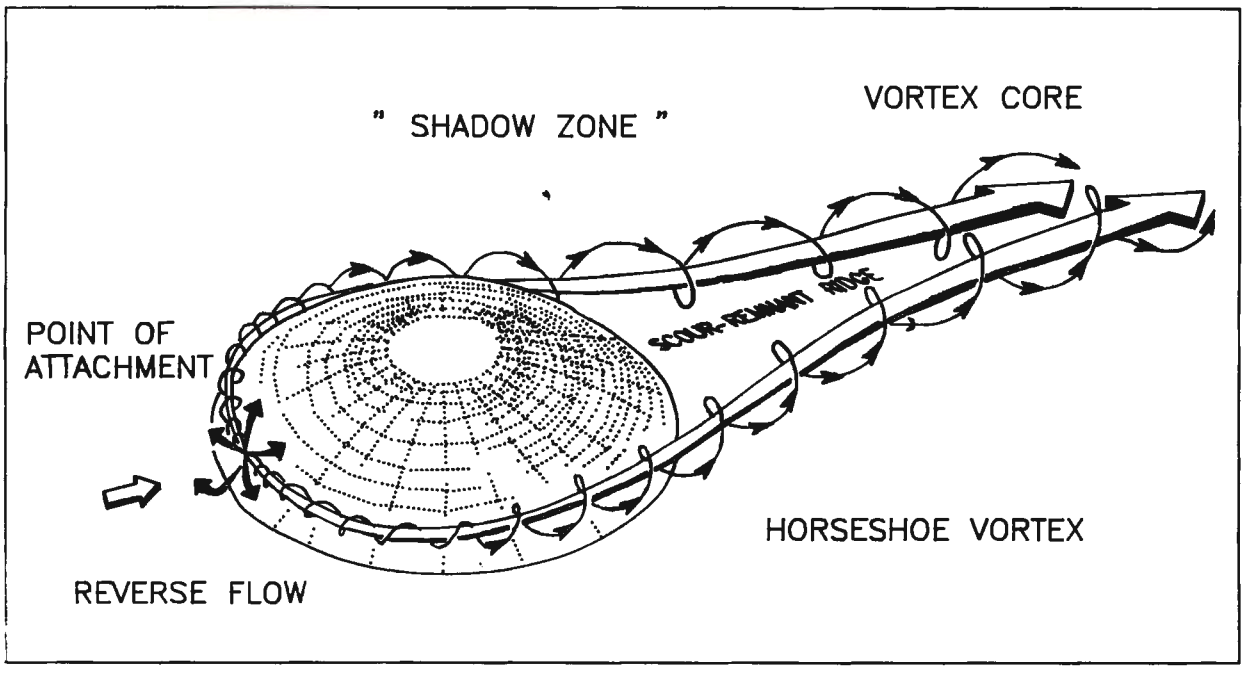

Figure 2.28. Sketch showing the form of the horshoe vortex shed by domical bluff bodies in the planetary boundary layer. After Greeley (1986, Fig. 6).

Figure 2.29. Unusual quartz ventifact on the floor of the Idatal exhibiting greater erosion on the northern, lee face, than on the southerly, windward one. Scale graduated in cm.

saltation load will undoubtedly continue. One of my most graphic memories of the Southern Namib, during a sandstorm, however, will always be the musical cacophony of sound that fills the air during high-velocity saltation collisions on the delicate quartz veins protruding above polished dolomite pavements planed by aeolian corrasion.

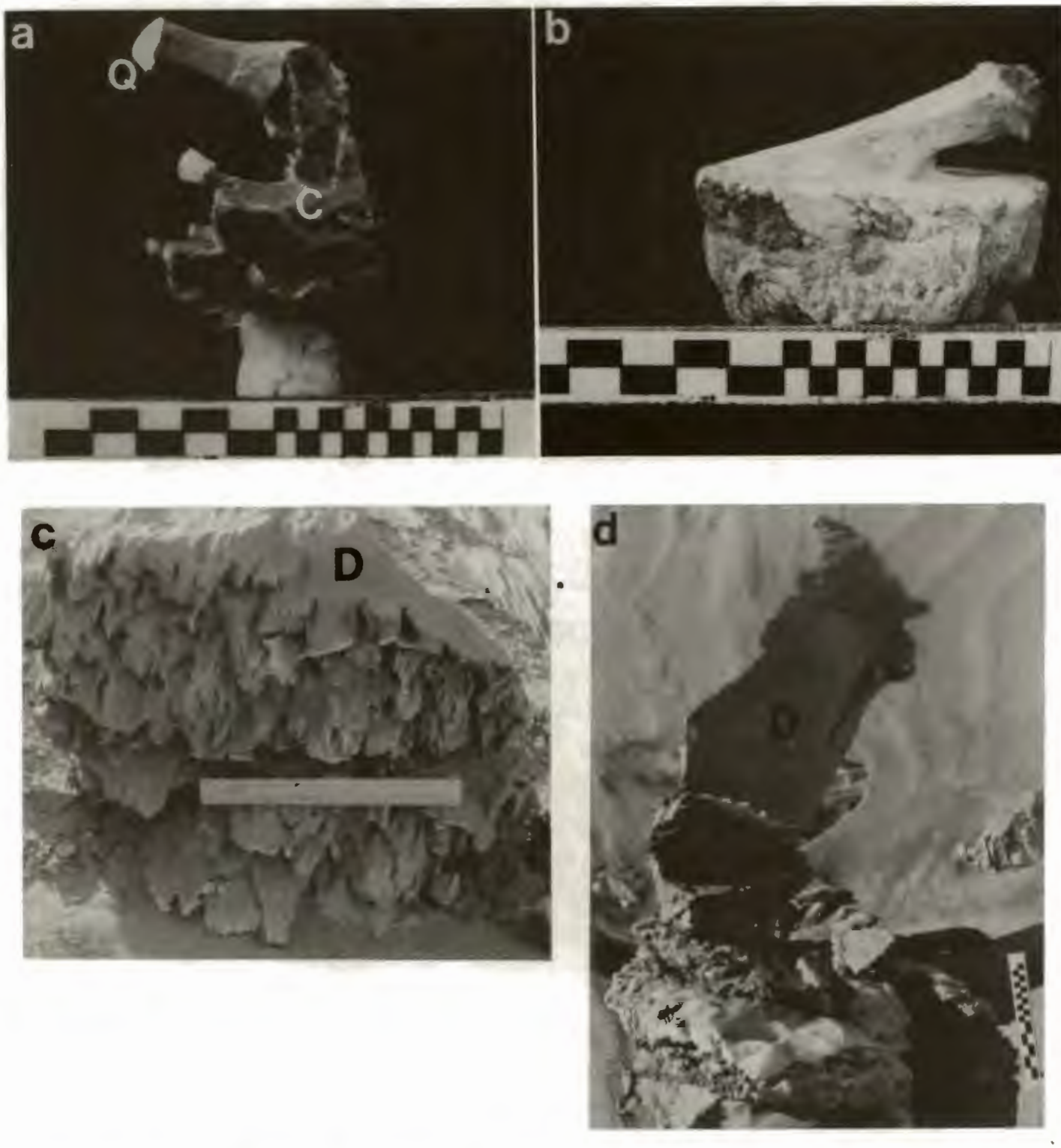

Figure 2.30. Examples of differential aeolian corrasion. (a) pedogenic hardpan calcrete (C) and quartz clasts (Q), southerly wind flow from left to right. (b) Pan carbonate and chalcedonic vug infill, southerly wind flow from right to left. (c) dolomite (D) and thin quartz veins, southerly wind from bottom to top of frame, scale 30 cm long. (d) dolomite (D) criss-crossed by quartz veins, southerly wind flow from right to left. Scale bar 10 cm long in frames a, b, and d.

2.6. COASTAL MORPHOLOGY

2.6.1. THE PLAN-FORM OF COASTAL EMBAYMENTS

The morphology of the present-day exposed Atlantic coastline of the Southern Namib is remarkably constant over much of its length. It is characterised by long stretches of relatively straight, steeply sloping beaches, or rugged, gullied cliffs. Embayments are comparatively rare, and widely dispersed. Kaiser (1926) observed that the coastal morphology is intimately related to the regional basement lithology and its tectonic structure, and to the geomorphological evolution of the deflation basin.

Swell waves generated in the Southern Ocean, approach the coastline obliquely from the south-west (Swart, 1983). The offshore current, generated by high-energy plunging breakers, prevents sand deposition on exposed beaches, and maintains the northward littoral drift (Swart, pers. comm., 1988). Exposed beaches tend to straighten minor irregularities in the coastline (Figure 2.31). Where waves encounter rocky headlands, log-spiral embayments commonly form.

2.6.2. RELATIONSHIP BETWEEN EMBAYMENT FORMATION AND DEFLATION BASIN GEOMORPHOLOGY

Along the present coastline, log-spiral embayments specifically result from marine transgression across former endoreic south-north oriented basins (Kaiser, 1926; Hallam, 1964; Rogers, 1977). The best example is currently provided by Prinzenbucht (Figure 2.32) at the northern end of Windhuktal. Marine transgression over the basin's former western margin, which continues submerged to the north-northwest, has created a rocky headland and a small island to the north. Sand deposition by waves diffracting around the headland and island, into the shadow zone protected from direct wave approach, subsequently connected the former island to the mainland (Kaiser, 1926). The protection of the beach from direct wave approach due to the embayment shape and Albatross Island reduces the wave energy and wave height. Therefore, the beach profile is flatter than that of the exposed coast and substantial sand deposition occurs.

Elizabeth Bay, a south-facing re-entrant (Figure 2.33), provides an example of the second form of coastal embayment. In this instance the bay defines the position of a transgressed basin.

Figure 2.31. Oblique aerial view to the south west, showing the arcuate crescent of the 4 m Beach at Bogenfels (arrowed), and the comparatively straight, present-day beach beyond it. Southerly wind flow from left to right.

Figure 2.32. Oblique aerial view of the log-spiral embayment at Prinzenbucht, with Albatross Island in the distance. Note the wedge-shaped area of aeolian compound transverse dunes in the backshore area, deposited by the southerly wind which blows from left to right. Also of interest, is the curved outline of the palaeo-channel "Liebestal" (L) in the foreground, which cuts across the regional north-south structural trend.

This type of embayment also forms where the shoreline cuts across the regional strike, exposing less resistant rock types to marine erosion (Kaiser, 1926; Rogers, 1977). At Bogenfels, phyllites were preferentially eroded and a very large re-entrant developed.

Figure 2.33. Oblique aerial view of Elizabeth Bay, a south-facing re-entrant embayment. Note the small barchan dunes migrating across the sand-sheet surface in the foreground. The larger slip-faces are about 10 m high. Wind streaks on the surface of the coastal sabkha (arrowed) are aligned with the southerly wind which blows from top left to bottom right.

2.7. DISTRIBUTION OF AEOLIAN DEPOSITS

2.7.1. INTRODUCTION

Landsat images have proved to be a valuable tool in studies of aeolian dune form and distribution, and provide very useful information about wind regimes on a regional scale (Fryberger and Dean, 1979). A detailed map showing the distribution of aeolian dune forms within the deflation basin and the southern part of the Namib Sand Sea has been prepared using Landsat image numbers 51273-08183, 51264-08235, and 51241-08171 (Figure 2.34).

The map includes information about areas outside the immediate study area, which is pertinent to understanding the nature of the regional wind regime discussed in section 3.1.

2.7.2. WIND STREAKS

Wind Streaks East of the Deflation Basin

East-west oriented streaks cutting across the principle drainage tracts descending from the Great Escarpment, occur 60 km inland of the southern end of the deflation basin (Figure 2.34, F10, O13). Similarly oriented features also occur about 70 km east of Luderitz. Between these localities, wind streaks occur along the Great Escarpment, some 100 km east of the coastline.

Wind Streaks in the Deflation Basin Environs

South-north oriented wind streaks entirely dominate a belt extending about 60 km to the east of the coastline (Figure 2.34, L7, O9). The streaks become more pronounced closer to the coast, and are best developed within a coast-parallel belt upto 15 km wide. This approximately corresponds to the areal extent of the deflation basin. The streaks are particularly pronounced along the transition zone between the deflation basin and the eastern plains.

2.7.3. CRESCENTIC DUNES

Barchan Dune Trains

Simple and compound barchan dunes occur within the deflation basin. The barchan dunes migrate in discreet dune trains (Figure 2.35, O7, K5) across firm substrates formed by stone pavement, bedrock, or the wet sediment of coastal pans. The dunes are propagated at log-spiral and south-facing embayments (Kaiser, 1926; Hallam, 1964; O'Brien, 1972; Rogers, 1977), and essentially remain

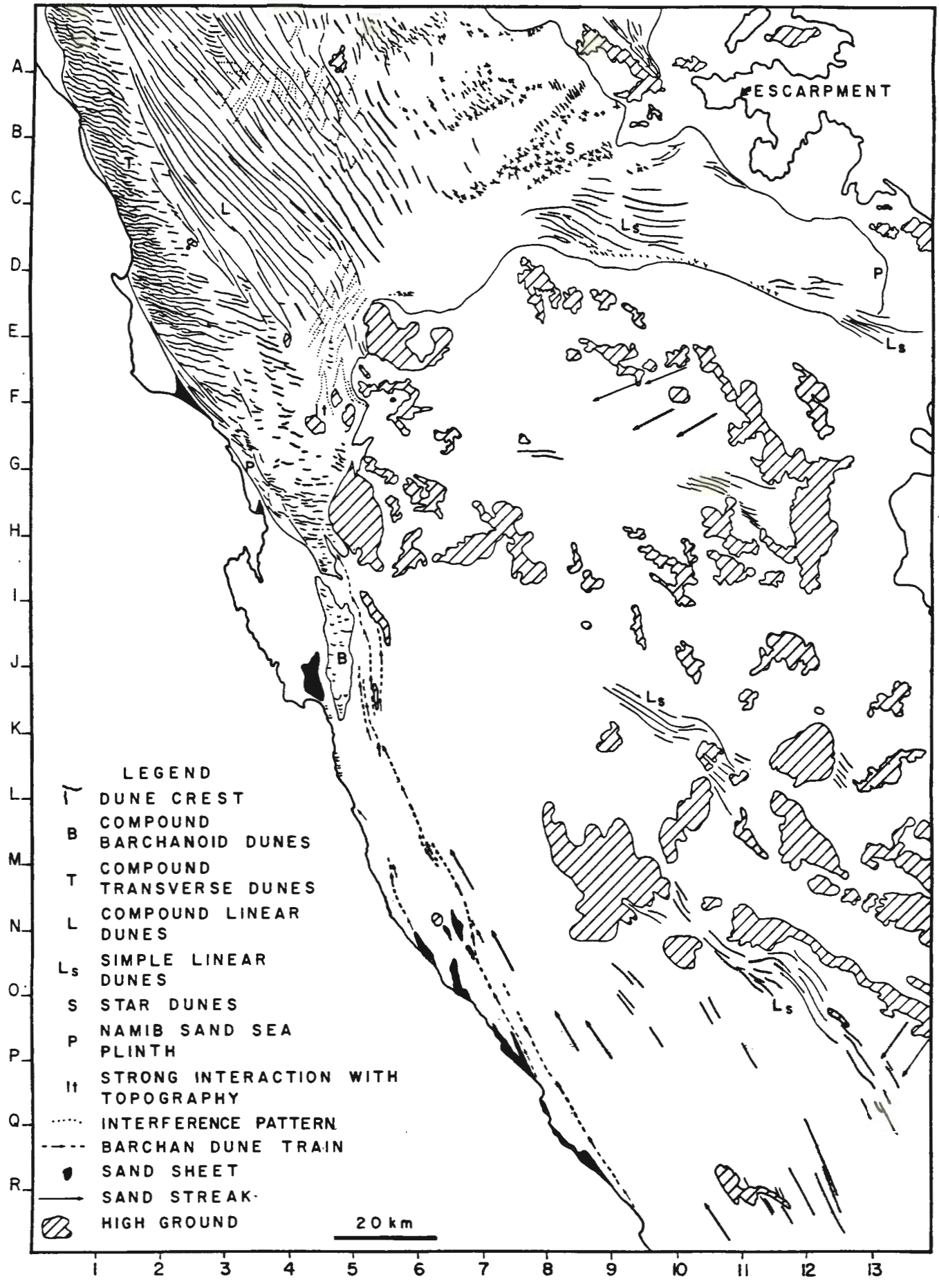

Figure 2.34. Map showing the distribution of aeolian deposits within the southern end of the Namib Sand Sea, the deflation basin, and the surrounding environs. Prepared from Landsat images 51273-08183, 51264-08235, and 51241-08171.

within the same train until they reach the Namib Sand Sea which is as much as 100 km to the north.

Compound Barchanoid Dunes

Compound barchans occur at the southern limit of the Namib Sand Sea (Figure 2.34, J5; 2.36) (Fryberger and Dean, 1979; Lancaster, 1983). Barchanoid draas are also present, up which smaller barchans are migrating. (Figure 2.37).

Compound Transverse Dunes

Within the Namib Sand Sea a coastal belt about 10 to 12 km wide is dominated by large, compound transverse dunes (Figure 2.34, E3; 2.39) (Fryberger and Dean, 1979; Lancaster, 1983). This belt is bordered on the west by the sand sea plinth, and to the east by linear dunes (Fryberger and Dean, 1979; Lancaster, 1983).

A second area of crescentic dunes is shown at the top of Figure 2.34 (A3). Immediately south of this area, evidence of an interference pattern formed by south-south-west to north-north-east oriented streaks cutting across linear dune forms is seen (A4).

Star Dunes

Star dunes occur along the eastern margin of the Namib Sand Sea at the southern end of the depositional basin (Figure 2.34, B9), where complex topography occurs (Fryberger and Dean, 1979; Lancaster, 1983).

2.7.4. LINEAR DUNE FORMS

Simple Linear Dunes

Linear dune forms are not confined to the Namib Sand Sea. Extensive areas south-south-east of the main sand body are covered by simple linear dunes (Figure 2.34, O11). Evidence of topographic interaction with surface-wind flow is clearly shown by their variable orientation.

Compound Linear Dunes

Linear dunes within the Namib Sand Sea exhibit a greater complexity of form than those further south (Figure 2.34, C4). The most southerly, and westerly example of linear dune development is provided by the Namib Sand Sea plinth. Compound linear dunes

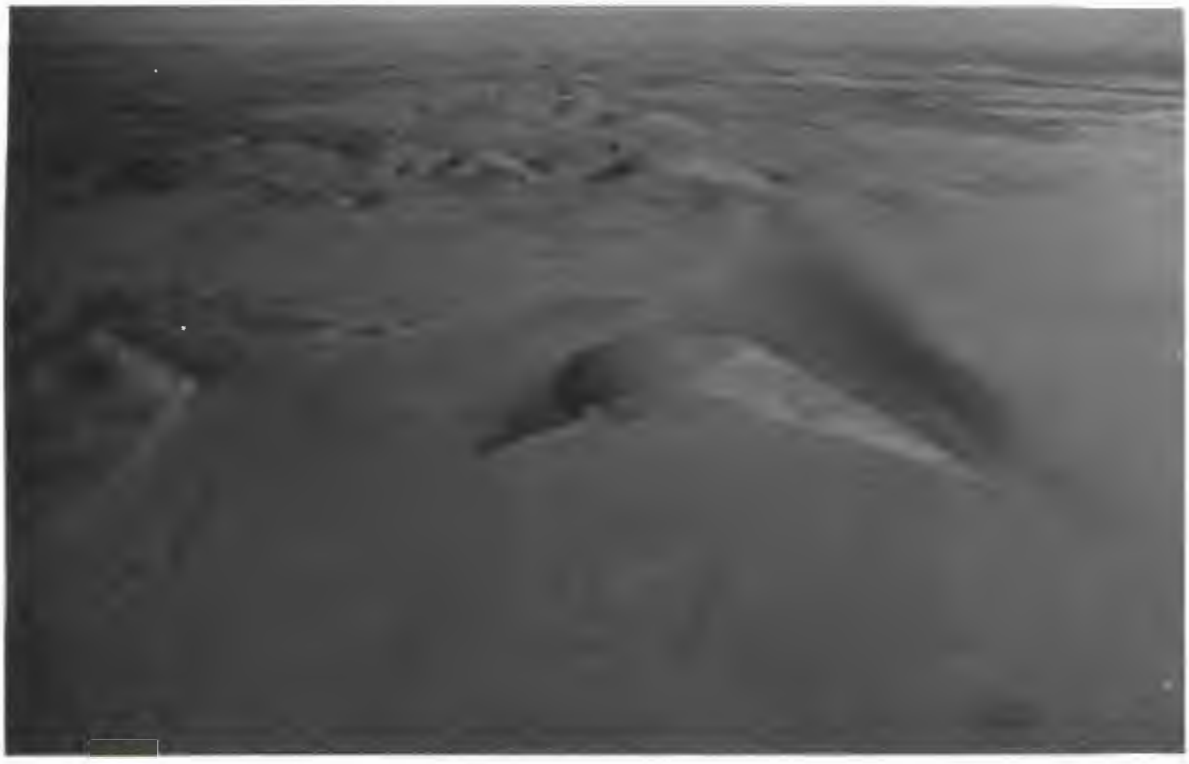

Figure 2.35. Oblique aerial view to the south down the Bakers Bay barchan dune train, traversing exposed bedrock and stone pavement, approximately 4 km east of Bogenfels. The barchan in the foreground is about 28 m high. Note the wind streaks on the bed which are aligned with the southerly wind which blows from top to bottom of the frame.

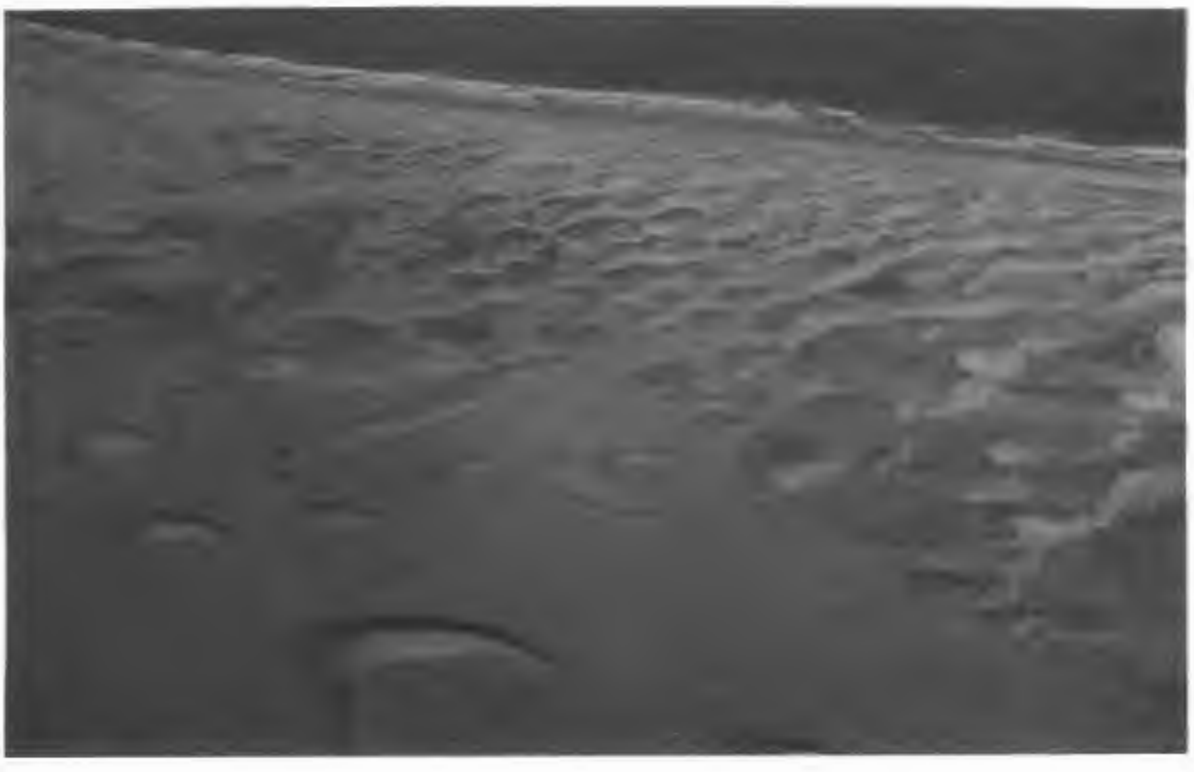

Figure 2.36. Oblique aerial view of compound transverse dunes migrating across a saturated lagoonal area at the western end of Grillental. The southerly wind blows from left to right.

Figure 2.37. Oblique aerial view south, showing the large barchanoid draas at the southern end of the Namib Sand Sea. Note the small barchans (mid-frame) migrating up the stoss slope of the draa in the foreground. The southerly wind blows from the top to the bottom of the frame.

Figure 2.38. Oblique aerial view of laterally extensive slip-faces of compound transverse dunes on the western margin of the Namib Sand Sea, to the north of Luderitz. The southerly wind blows from right to left.

(Figure 2.39) are primarily located towards the centre of the southern end of the Namib Sand Sea (Fryberger and Dean, 1979; Lancaster, 1983), but they also occur at coastal sites.

2.7.5. SAND SHEETS

Sand sheets mainly occur in coastal locations (Figure 2.34, E3, J4, N6, P7, Q8), where they commonly develop at the sites of log-spiral and south-facing embayments. Inland occurrences are not as common. Vegetated sand sheets tend to form in bedrock depressions, or where the zone of active sandflow is diverted by topographic interaction with the surface-wind flow (Figure 2.34).

Sand sheet formation is more common to the east of the deflation basin margin, which is itself marked by the accumulation of sand to form wind streaks.

2.7.6. STONE PAVEMENT

Stone pavements are essentially confined to depressions, and have formed from a wide variety of host deposits. The preservation of marine transgressive horizons in the Bogenfels-Buntfeldschuh Basin (Figure 2.40), has resulted in the development of stone pavements capping clastic shoreline deposits, which previously have been documented (Beetz, 1926; Böhm, 1926; Weissermel, 1926). Much of the evidence for Upper Eocene marine deposition has been removed during mining, but arcuate shorelines are still preserved in the vicinity of Bogenfels (Figure 2.41). They are delineated by surficial concentrations of well-rounded agate, chalcedony, jasper and chrysoprase clasts forming stone pavements which clearly differ from those of locally derived quartz and quartzite cobbles. Occasionally, fragments of marine shell, tabulate coral, and sharks teeth occur within stone pavements (Figure 2.42a and b), confirming the presence of an underlying marine deposit.

Along the eastern margin of the Bogenfels-Buntfeldschuh Basin and within the Grillental, alluvial braidplain deposits covering an enormous area (section 7.1 to 7.2) form the host deposit from which extensive stone pavements have developed. Where erosion has occurred, such as within the main trough extending north from Bogenfels (see Figure 2.12), the floors of endoreic basins are covered by a thin veneer (about 1 to 30 cm deep) of locally derived weathering and erosion products. Stone pavements of this type are

usually dominated by angular quartz clasts.

Figure 2.39. Oblique aerial view of compound linear dunes in the Namib Sand Sea, slightly to the north of Luderitz. The southerly wind blows from top right to bottom left of the frame.

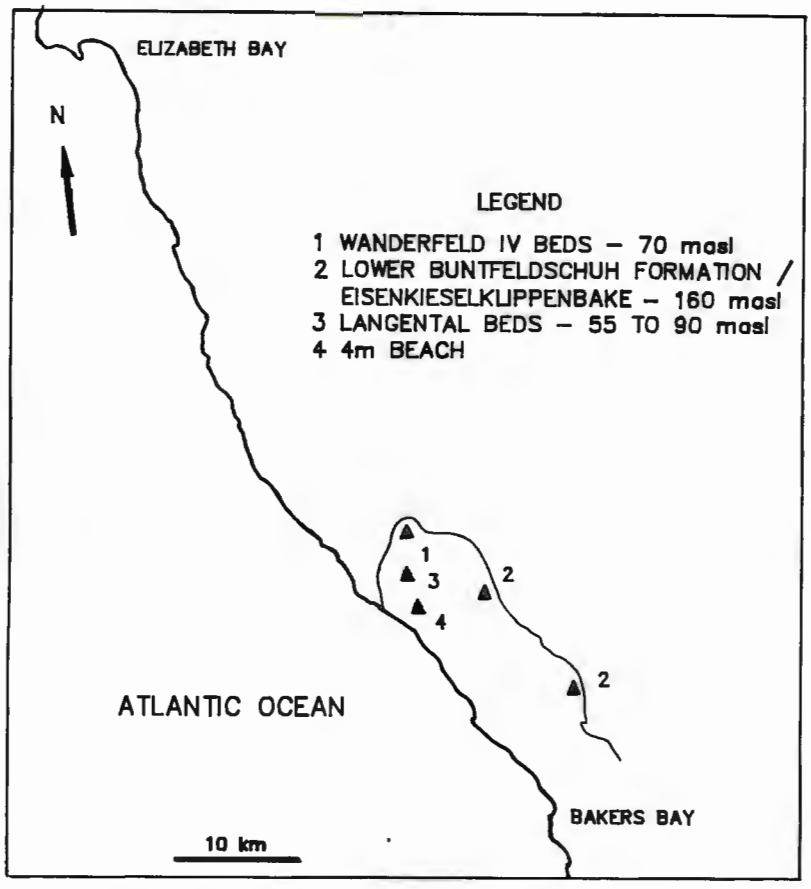

Figure 2.40. Map showing the position of the Bogenfels -Buntfeldschuh Basin, and the distribution of transgressive marine deposits within it.

Figure 2.41. The preserved Upper Eocene marine shoreline at about 65 masl (Lat. 27°25'10"S; Long. 15°26'10"E). Exotic marine clasts forming a stone pavement are surrounded by a crescent of quartz and quartzite cobbles. Scale (arrowed) 1 m long.

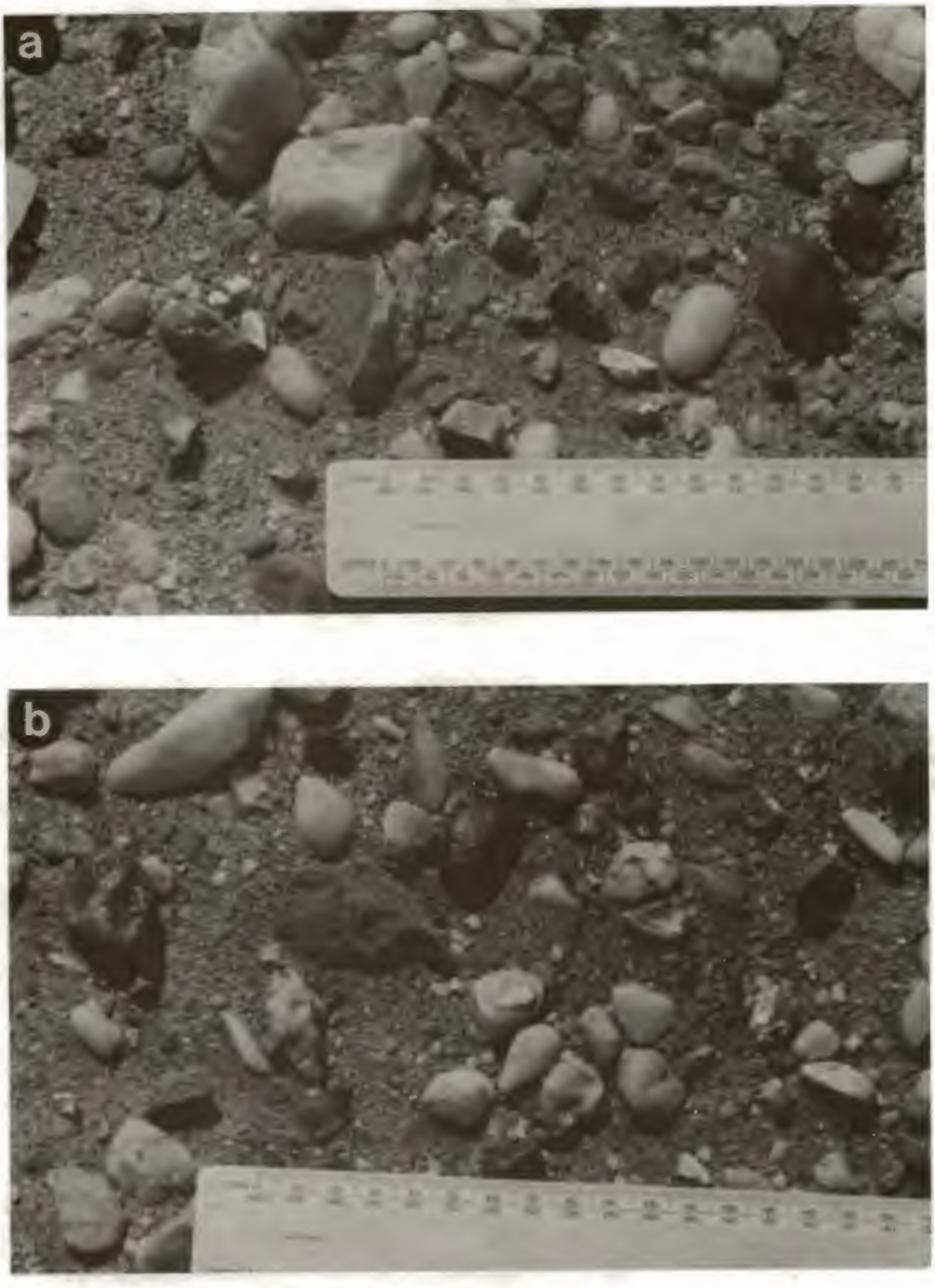

Figure 2.42. (a) Fragments of Ostrea sp. incorporated in the stone pavement overlying the Upper Eocene marine sediments at about 55 masl. (b) Fragment of tabulate coral, probably Diplochaetetes sp. (Weissermel, 1926), incorporated into a stone pavement overlying Upper Eocene marine sediments at about 55 masl. Scale in cm.

3. THE AIRFLOW SYSTEM

3.1. INTRODUCTION

The detailed examination of the surface-wind regime has been confined to the 15 km wide, coast-parallel belt in which the main deflation basin of the Namib Sand Sea is situated. The regional surface-wind regime must be broadly defined if the dynamics of the aeolian system is to be comprehensively established.

3.2. REGIONAL SURFACE-WIND REGIME

The regional pattern of surface-wind flow can effectively be described by mapping the distribution and orientation of aeolian dune forms (Fryberger and Dean, 1979; Lancaster, 1983) and wind streaks from Landsat images (see Figure 2.35).

Wind streaks to the south and east of the Namib Sand Sea define an essentially two-component surface-wind system, exhibiting a distinct spatial zonation. Wind streaks further than 60 km inland of the Atlantic coast are oriented east-west, and provide evidence for the strong influence of the easterly wind component. Streaks exhibiting this orientation frequently occur along the edge of the Great Escarpment, from where they descend westwards, cutting across the drainage tracts on alluvial surfaces.

During the winter months a thin red line is often observed on the horizon to the east of the Klinghardt Mountains in the late afternoon. The depth of the red zone increases rapidly as sand and dust are transported westwards by high-energy easterly winds. Personal experience over the past four years has shown that these events are seldom experienced at ground-level at the coast. The easterly winds are therefore probably passing over the top of the sea breeze, which are governed by the South Atlantic Anticyclone.

Star dunes along the eastern margin of the southern end of the Namib Sand Sea, have also been attributed to the influence of easterly winds occurring either as katabatic winds, or "berg winds" (from April to August) when regional pressure gradients are normal to the coast (Fryberger and Dean, 1979; Lancaster, 1983). These dunes are often located to the west of gaps between topographic highs, where abnormally high surface-wind speeds are probably experienced due to the turbulent wakes and vortices shed from the complex topography.

During frequent trips 100 km inland of the coast along the

Orange River in September 1986, a sharp daily contrast was observed between the inland and coastal surface-wind regimes. When the interior was either calm or influenced by easterly winds, the southerly wind regime remained dominant at the coast. In particular, when an easterly wind influenced the interior, a distinct boundary was crossed 20 to 40 km east of Oranjemund in the late afternoon. At this boundary the temperature dropped, the wind suddenly switched from easterly to southerly, and the aeolian transport direction changed accordingly. A similar boundary has regularly been observed at Bogenfels during the past 4 years. During sandstorms governed by the southerly surface-wind regime, aeolian dust in suspension creates hazy conditions within the coastal tract. A sharp, steeply dipping boundary about 10 to 15 km inland of the coast separates this dust column from comparatively clear air containing minimal aeolian dust in suspension.

A belt of linear dune forms, about 40 km wide, lies immediately to the west of the east-west oriented streaks. This belt extends from about 15 km north-north-east of Oranjemund to the north of the Klinghardt Mountains (see Figure 2.34). The western margin of this linear dune belt is approximately 25 km inland of the coast near Chameis, and about 12 km inland at the south end of the Namib Sand Sea. The linear dune systems are principally aligned north-north-west. To the east of the deflation basin, curved crestal alignment around topography provides evidence of topographic interaction with the southerly wind component. This supports the concept that the southerly wind component is principally responsible for maintaining the linear dune system of the Namib Sand Sea (Lancaster, 1983; Ward, 1984).

Within the Namib Sand Sea, linear dunes are located in the central belt of low to moderate wind-energy, where a complex bimodal wind regime operates (Fryberger and Dean, 1979; Lancaster, 1983; Ward, 1984). It is likely that a similar surface-wind regime influences the linear dunes to the south of the Namib Sand Sea.

West of the linear dune belt, wind streaks are all aligned to the north and the dune types change from a linear to crescentic form. In the study area, simple and compound barchan dunes migrate in trains from south to north, under the influence of a strong, unimodal, southerly surface-wind regime (Kaiser, 1926; O'Brien, 1972; Rogers, 1977; Lancaster, 1983). Personal observation,

(section 4.2.5) confirms that these dunes are periodically affected by high-energy northerly and easterly surface-winds (Kaiser, 1926).

The regional surface-wind pattern of the Central Namib has been mapped in greater detail than the Southern Namib. Data shows that the surface-wind regime can be divided into coast-parallel belts whose characteristics change from west to east (Ward, 1984; Lancaster, 1985). Inland of the coastal belt, the wind regime changes from high-energy southerly unimodal to a bimodal regime. This primarily consists of a southerly and easterly component, with a minor northerly component. The wind-energy of this belt is reduced relative to the coastal zone (Ward, 1984; Lancaster, 1985). Although sandflow conditions south-east of the Namib Sand Sea differ relative to the Central Namib, and the scale and complexity of linear dune systems is reduced, the distribution of aeolian bedforms is broadly similar in both areas. Thus the spatial zonation of the surface-wind regime probably extends along the length of the coast. Attempts have been made to define this variation in the Southern Namib (Rogers, 1977), but there is a definite need for tighter control, with more monitoring stations.

Another regional velocity gradient is exhibited by the unimodal surface-wind flow within the coastal tract. The wind velocity progressively increases from south to north as the deflation basin is approached, and peaks in the central to northern part of the basin (Rogers, 1977; Lancaster, 1983, 1985). It then diminishes northwards, before increasing again in the vicinity of Toscannini. At the present time, this gradient is best illustrated by the distribution of major centres of oceanic upwelling, which is directly related to wind stress on the ocean surface (eg. Kamstra, 1985; Jury, 1985). The largest upwelling cell along the west coast occurs off Luderitz (Shannon, 1985).

The regional distribution of aeolian bedforms thus delineates three broadly coast-parallel zones (Figure 3.1). These are:

1) a coastal zone dominated by a high-energy southerly surface wind regime extending approximately 15 km east of the shoreline;

2) an intermediate zone between 20 and 60 km inland, where the wind-energy of a complex bimodal surface wind regime is reduced relative to the coastal zone;

3) an inland zone extending from about 60 km east of the coast to the escarpment, in which aeolian bedforms are strongly influenced by easterly winds.

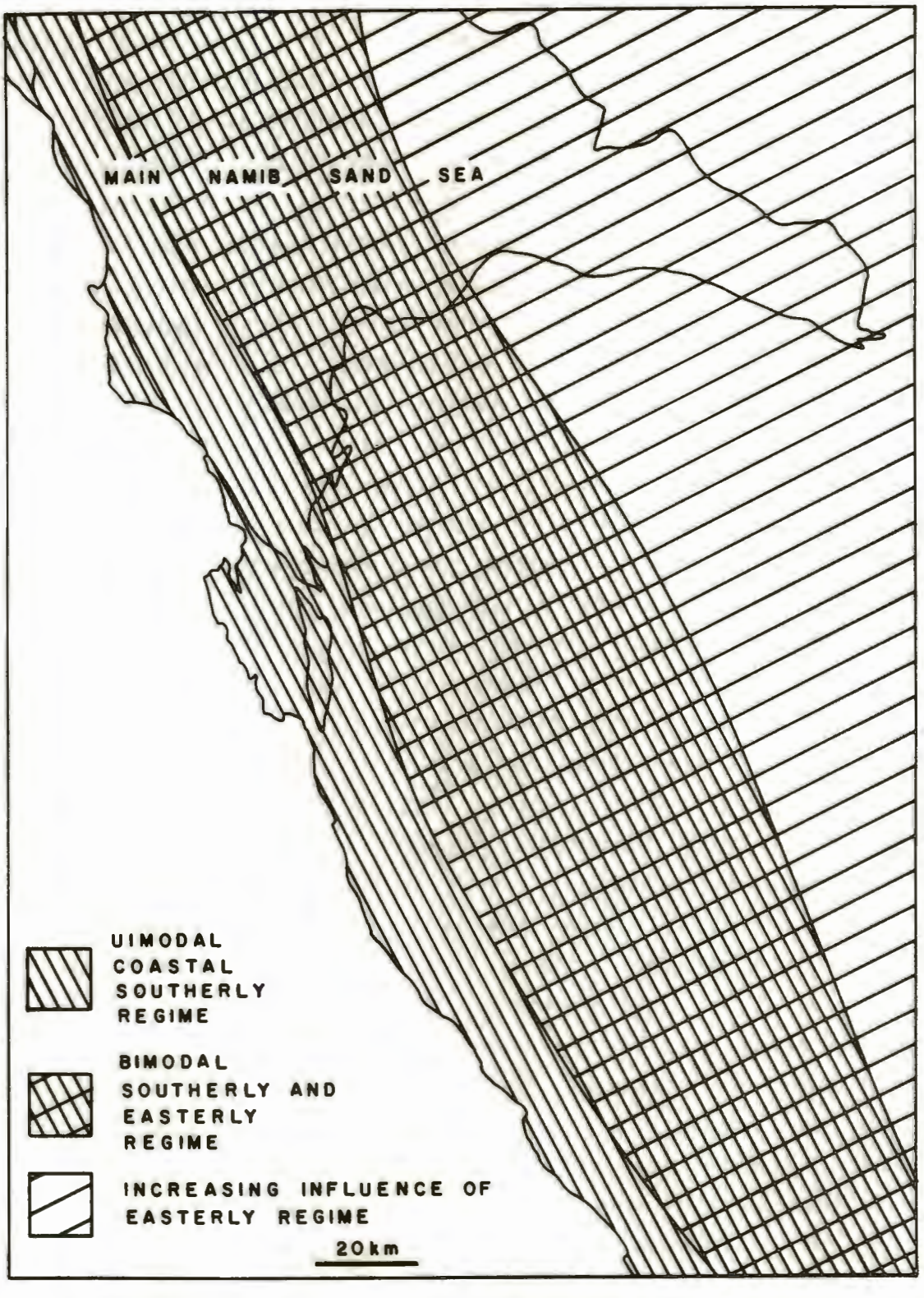

Figure 3.1. Map illustrating the regional variation of surface-wind direction based upon the analysis of aeolian bedforms using Landsat images 51273-08183, 51264-08235, and 51241-08171.

3.3 SURFACE AIRFLOW THROUGH THE DEFLATION BASIN

3.3.1. PRESENTATION OF RESULTS

Wind roses summarizing hourly anemometer data from Bogenfels during 1987 (Figure 3.2) confirm the narrow unimodal nature of the southerly surface-wind regime from October to March previously recorded in the deflation basin (Kaiser, 1926; Rogers, 1977). These data also illustrate the marked seasonal variation of the surface-wind regime (Table 3.1).

Table 3.1. Summary of percentage observations for the principle wind directions recorded at Bogenfels during 1987, illustrating the seasonal variation of the surface-wind regime.

QUARTER	WIND DIRECTION		
	SE - S	SSW - SW	NE - NW
JAN - MAR	90,2	6,7	1,0
APR - JUN	62,6	12.4	20,8
JUL - SEP	62,9	6,3	23,5
OCT - DEC	91,1	3,4	2,5

The wind regime is characteristically narrow unimodal between October to March (summer) when the energy of the southerly surface-wind regime peaks. Depending upon the incidence of northerly winds, a weakly bimodal regime occurs between April to September (winter). Seasonal variation and short-term fluctuation of the surface-wind direction and velocity is more clearly illustrated by histograms compiled from the same quarterly data used for the wind roses (Figure 3.3). Presentation of the data in this form shows the diurnal peaks in surface-wind velocity, and the rapid changes in wind direction of short duration.

3.3.2. AIRFLOW DURING THE SUMMER

During the summer (October to March), the surface-wind regime is characterised by persistent high-energy southerly wind conditions. The longest period during the year 1987 lasted about 4 weeks, prior to its termination by a brief northerly wind reversal which lasted a couple of days. Wind reversals during the summer mostly occur at night or in the early morning (Table 3.2). The northerly winds are normally of low-energy, prior to the resumption of the southerly wind system by mid-day. Summer wind reversals are usually signalled by fluctuating wind direction for a few hours and an abrupt reduction of wind velocity, prior to a rapid switch to a northerly

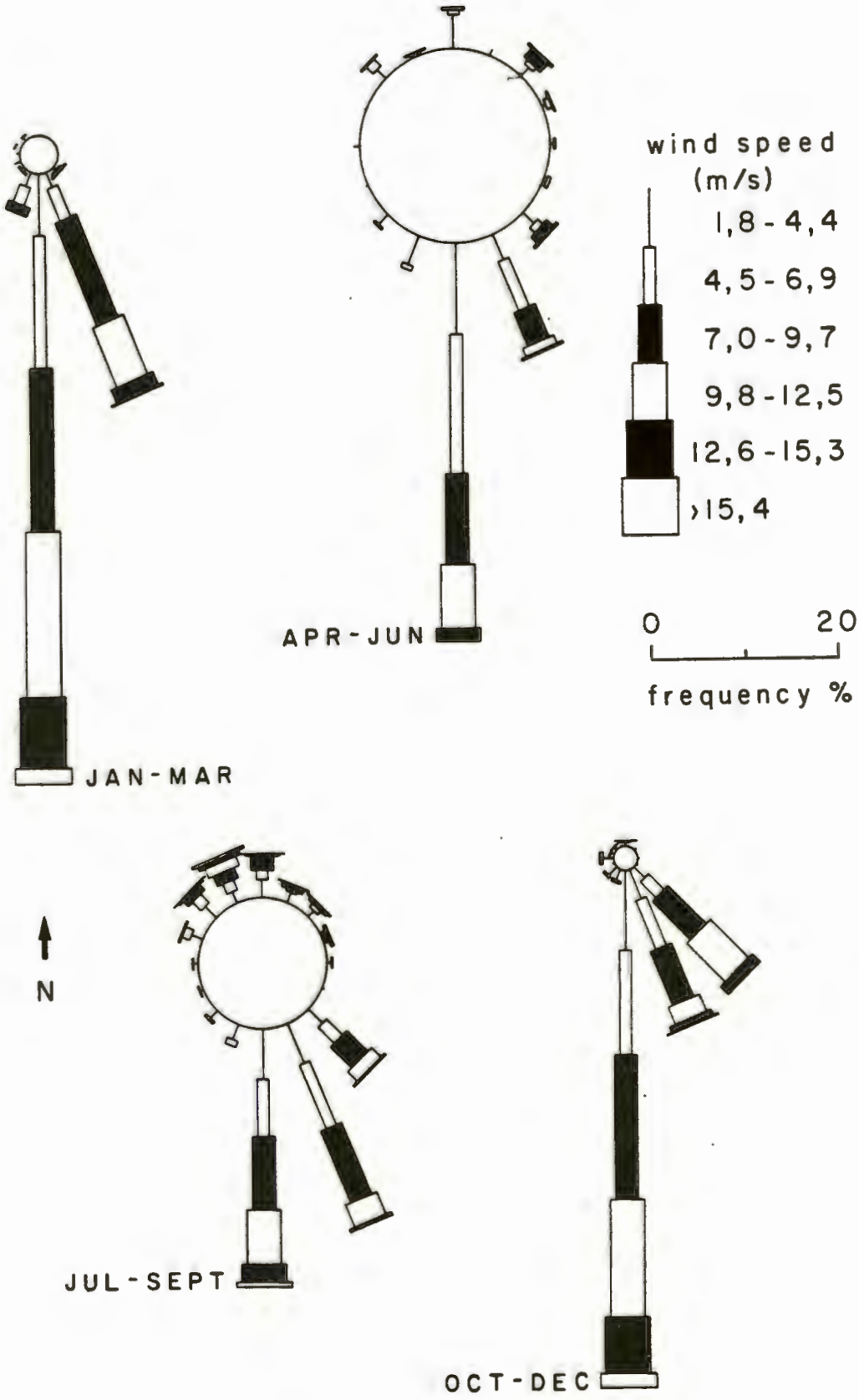

Figure 3.2. 16-point wind roses summarising hourly averaged surface-wind data recorded at Bogenfels during 1987. Distinct seasonal variation in the percentage of calms, surface-wind energy, and unimodality are seen.

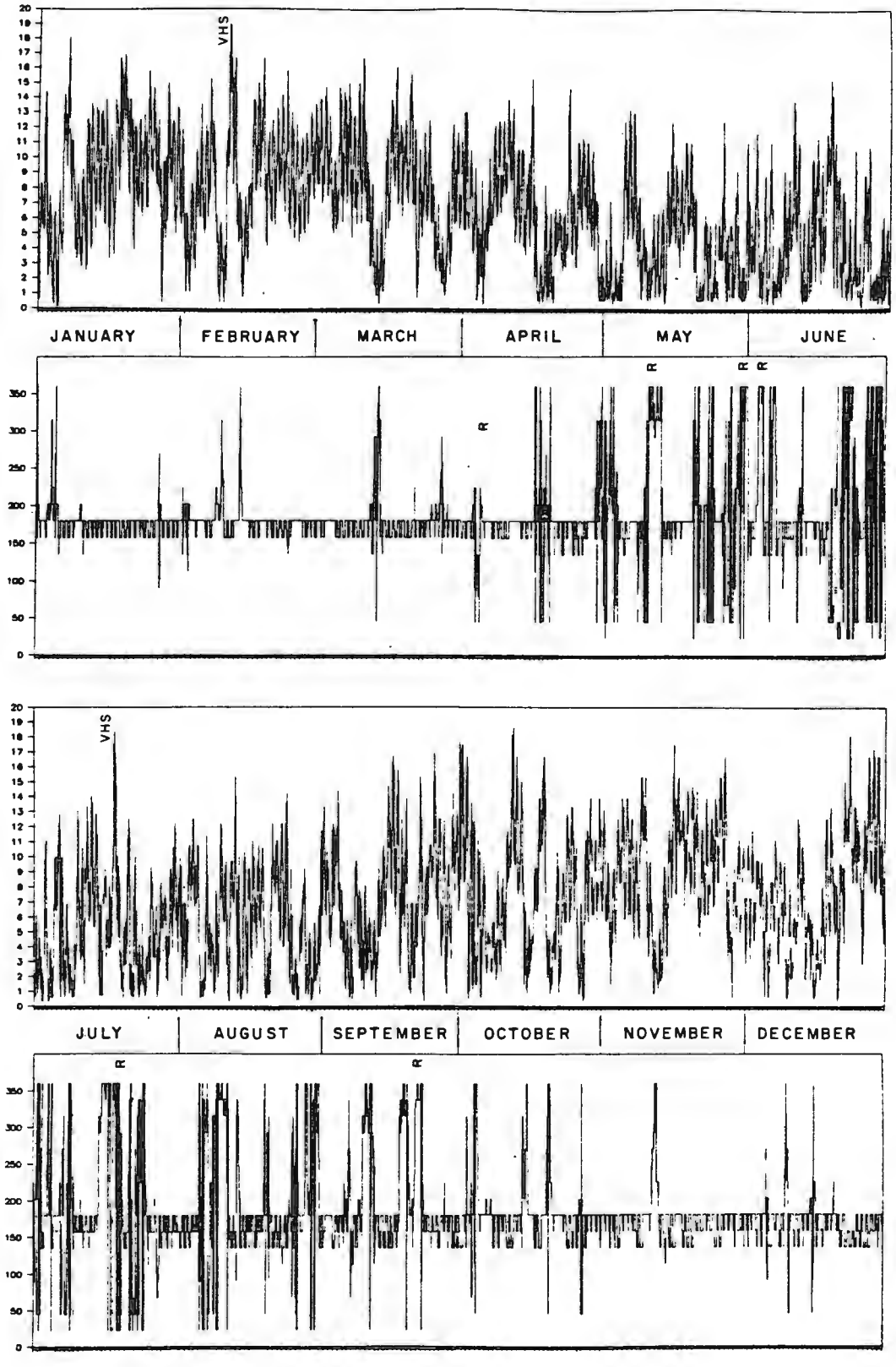

Figure 3.3. Histograms summarising the data for 1987. The upper graph of each six monthly set shows the variation of wind velocity, and the lower graph shows the variation of wind direction relative to true north. Peaks in the lower graph thus show the occurrence of northerly quadrant wind reversals, which are more frequent between April and September. The distribution of rainfall events (R) is marked, together with the occurrence of very high sandflow (VHS).

wind in a matter of minutes. The subsequent wind velocity increase at the onset of the next period of southerly wind is rapid.

Table 3.2. Percentage frequency of northerly winds with time for the period 01/10/87 to 31/12/87.

TIME INTERVAL	DIRECTION				
	NW	NNW	N	NNE	NE
1-4	1,8	0	16,1	0	10,7
5-8	10,7	0	19,6	0	1,8
9-12	14,3	0	8,9	0	0
13-16	0	0	0	0	0
17-20	1,8	0	0	0	0
21-24	8,9	0	3,6	0	1,8

TOTAL HOURS OF WIND REVERSAL = 56 hours

Southerly surface-wind energy peaks between December to February (Kaiser, 1926; Rogers, 1977), when wind velocities between 15.4 and 18.0 m/sec occur most frequently. The average wind velocity sustained by the system is substantially greater over this period than during the winter months (Figure 3.4).

The southerly surface-wind system is strongly diurnal (Kaiser, 1926; Rogers, 1977). Although wind speeds less than or equal to 4.4 m/sec can occur at any time of day, they are rare between 09.00hrs to 20.00hrs. The highest velocity winds generally occur during this time interval. Wind velocities between 9.8 m/sec and 18.0 m/sec are most frequent between 09.00hrs and 16.00hrs. Very high-velocity southerly winds exceeding 18.1 m/sec generally occupy a narrow time range between 13.00hrs to 16.00hrs. These winds are occasionally maintained between 17.00hrs to 20.00hrs. During periods of persistent high-energy southerly surface-winds, high velocities are periodically maintained throughout the night. The wind direction also exhibits a weak diurnal variation, with south-easterly winds occuring most frequently during the early morning, after which south-south-easterly to southerly winds dominate throughout the rest of the day.

Gusting could not be measured with the Lamprecht wind recorders used in this study. Wind velocities greatly exceeding 18.1 m/sec have, however, been recorded during particularly high wind-energy conditions by using a hand-held anemometer 1,5 m above the ground. Short-term gusts lasting a few seconds to a few minutes, regularly attain velocities of 20 to 25 m/sec during strong southerly winds.

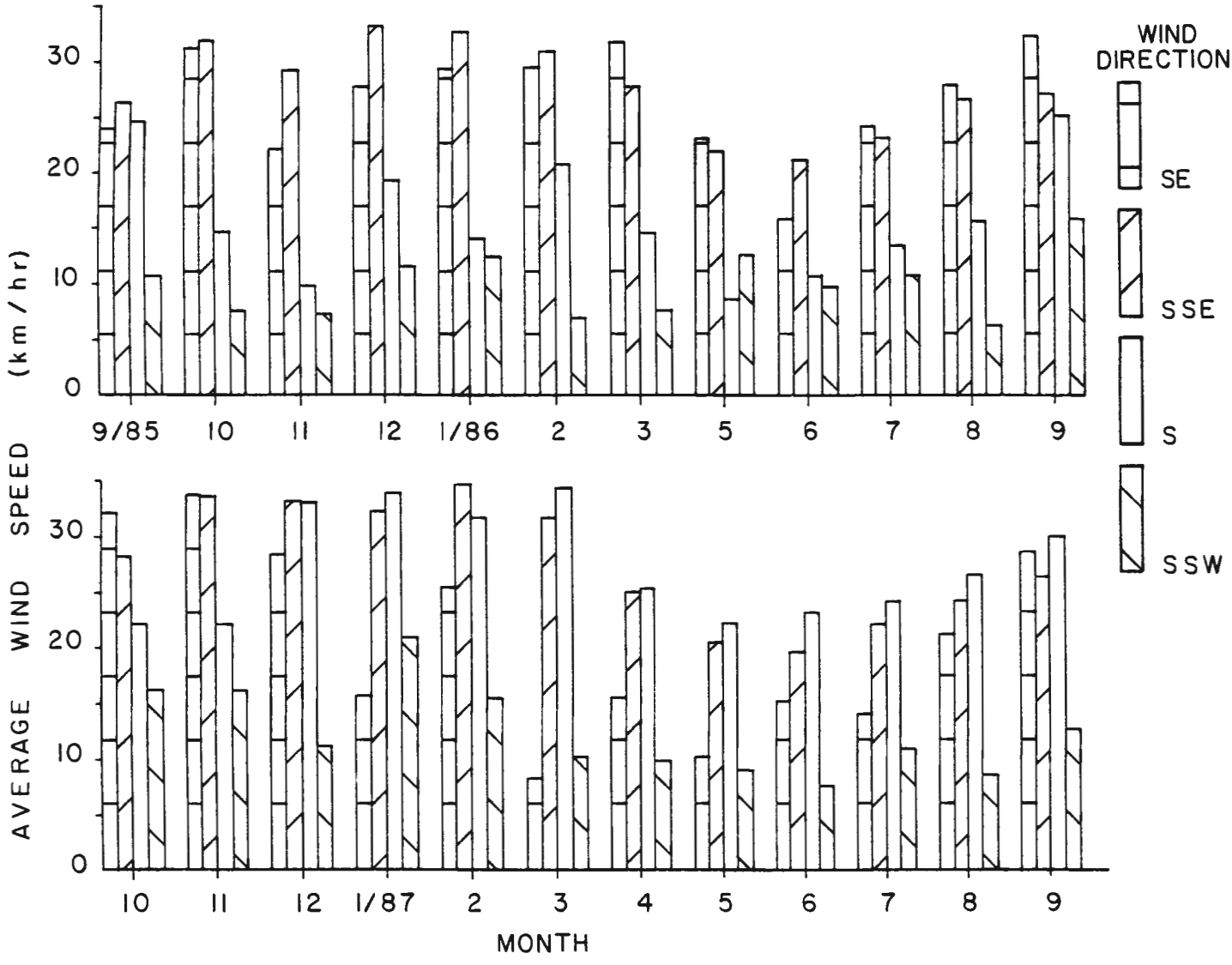

Figure 3.4. Monthly variation of the average wind speed at Bogenfels. Data for April 1986 was lost due to recorder problems.

3.3.3. AIRFLOW DURING THE WINTER

Marked differences characterise the summmer and winter surface-wind regimes of the Southern Namib (Kaiser, 1926; Rogers, 1977). This is also the case in the Central Namib (Ward, 1984). The unimodal pattern of wind flow is maintained throughout the year, but it is less pronounced in winter due to the increased incidence of northerly wind reversals, and the decline of southerly wind-energy. Although wind reversals remain episodic, the interval separating them is shorter, and at times their distribution appears rhythmical. In contrast to wind reversals during the summer months, those during winter are occasionally very high-energy and maintained over a number of days (Table 3.3). Sustained periods of southerly wind domination therefore occur less frequently during the winter, and are of a shorter duration.

Table 3.3. Percentage frequency of northerly winds with time for the period 01/07/87 to 30/09/87.

TIME INTERVAL	DIRECTION				
	NW	NNW	N	NNE	NE
0-4	1,0	4,6	7,5	4,6	3,3
5-8	3,5	3,1	9,1	3,5	3,5
9-12	4,8	4,4	3,3	1,2	2,1
13-16	5,4	3,5	1,2	0,2	0
17-20	4,1	5,4	1,7	0,2	0,6
21-24	2,5	4,4	6,2	3,1	2,1

TOTAL HOURS OF WIND REVERSAL = 518 hours

The southerly surface-wind energy reaches a minimum between May and June (Figure 3.3), and wind velocities exceeding 15.3 m/sec were entirely absent from April to June during 1987. Wind velocity maxima remain confined to between 09.00hrs to 20.00hrs during the winter. From July to September during 1987, wind velocities greater than or equal to 18.1 m/sec were restricted to between 12.00hrs to 16.00hrs. With the general reduction of southerly wind-energy, there is an increase in the frequency of southerly wind velocities between 0 and 9,7 m/sec during the winter. The frequency of south-easterly winds rises between July to September. This reflects the gradual increase in southerly wind-energy as summer approaches.

The Bogenfels anemometer was carefully positioned away from pronounced topography to permit the influence of surface-winds from any direction to be recorded. Easterly winds are seldom experienced in the coastal zone. Coupled with the observations during sandstorms, this is interpreted as evidence that the sea breeze wedges in under the easterly winds.

3.3.4. FACTORS GOVERNING ATMOSPHERIC CIRCULATION OVER THE SOUTHERN NAMIB

The coastal surface-wind regime approximates to a uni-directional current system for much of the year. This system is governed by the South Atlantic Anticyclone, which is centred at about 30°S 5°E offshore during the summer, shifting to about 26°S 10°E during winter (Schell, 1968; Van Loon, 1972).

In summer, strong continental heating creates a heat low in the interior of the sub-continent (Tyson, 1969), which produces a very steep zonal gradient along the west coast. The energy of the southerly wind regime is extremely high under these conditions, as

demonstrated by the increase of the average wind speed during summer by about 10 km/hr relative to that of winter. Because the continental interior is warmest between 09.00 to 20.00hrs the zonal pressure gradient is likely to be steepest over this time interval. This probably accounts for the diurnal variation in the energy of the southerly wind regime, and might also relate to the slight diurnal shift in wind direction prevalent during the early morning.

The seasonal variation of the southerly surface-wind energy and the periodicity and energy of northerly wind reversals are important aspects of the aeolian current system. The increased frequency of northerly wind reversals during the winter is significant, but more important is the attainment of very high velocities, which occasionally persist for a few days. According to Nelson and Hutchings (1983) the major reversals reflect the passage of cyclonic systems south of the continent. In winter, the South Atlantic Anticyclone shifts north, permitting these perturbations, which are commonly accompanied by cold fronts, to impinge on the southern tip of Africa (Kamstra, 1985), rather than passing to the south of the continent. The main reversal is commonly preceeded by the southward passage of comparatively weak coastal lows which develop near Luderitz and migrate southwards in sympathy with the westward progression of cold front (Taljaard, Schmidt and Van Loon, 1961, cited in Shannon, 1985) causing rapid fluctuation of the wind direction. The passage of coastal lows is frequently accompanied by rain, and the deflation basin therefore lies within the winter rainfall region of the west coast. The significance of this aspect with respect to the sediment dynamics will be discussed in Section 5.

4. PRESENT-DAY AEOLIAN SEDIMENT DISPERSAL

4.1. REVIEW OF AEOLIAN TRANSPORT PROCESSES

4.1.1. INTRODUCTION

Bagnold (1954) has established the physical basis for three modes of aeolian transport. Namely, suspension, saltation and creep (Figure 4.1).

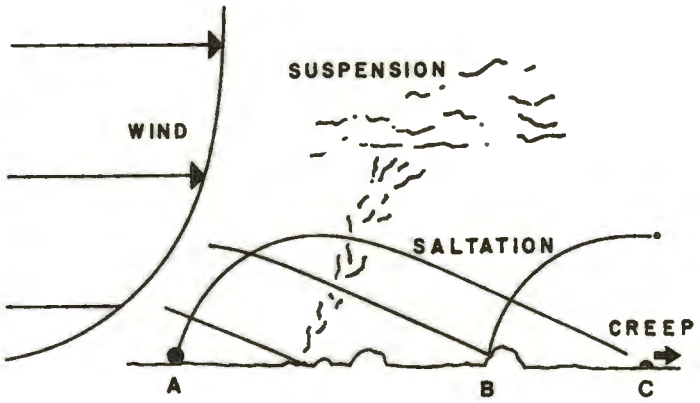

Figure 4.1. Sketch illustrating the three modes of aeolian transport: surface shear stress entrains grain (A) into saltation and carries it downwind back to the bed, where it rebounds back into flight (B). This action potentially displaces other grains, some of which are thrown into the air, thus leading to additional saltation. The force of saltation impact might be sufficient to push larger grains resting on the bed downwind slightly (C), resulting in aeolian creep. (Modified from Greeley and Iversen, 1985)

It has been shown that particles less than 0,08 mm in diameter are susceptible to suspension once airbourne (Bagnold, 1954). For the purposes of this study, the dynamics of the suspended load is not considered in any greater detail. The principle aim is to establish the present-day dynamics of both the saltation and creep loads.

Particles greater than 0,08 mm diameter rising above the bed are accelerated by the wind during their transport in a series of convex up, flat trajectories described as saltation. On impact, some of their kinetic energy is transferred to the bed and the pervasive rearrangement of grains alters the bed configuration. Saltating grains are thus capable of moving a grain six times their size or about 200 times their own weight, by creep transport (Bagnold, 1954). Detailed knowledge of saltation load dynamics is therefore required before the dynamics of the creep load can be fully understood.

4.1.2. SALTATION OVER A LOOSE GRANULAR BED

There is a minimum friction velocity (u_{*t}) at which the air flow has sufficient energy to entrain sediment particles from the bed thereby initiating saltation. This is given by:

$$u_{*t} = A(p_p g D_p / p)^{\frac{1}{2}}$$

where p = fluid density, p_p = particle density, D_p = particle diameter, g = acceleration due to gravity, and A = a dimensionless coefficient (Bagnold, 1954). In fully developed turbulent flow, Bagnold (1954) assumed that A is dependent upon the friction Reynolds Number (R_*), given by:

$$R_* = u_* D_p / v$$

where u_* = surface friction velocity and v = kinematic viscosity.

Iversen et al. (1976, cited in Greeley and Iversen, 1985) have shown that when $R_* < 5$, A increases rapidly with decreasing R_*. The bed is then described as aerodynamically smooth. Particles small enough to lie wholly within the viscous sublayer are unaffected by turbulent fluctuations in the flow above, and cannot be entrained. For this reason, particles less than or equal to 0,03 mm diameter cannot be entrained by aerodynamic forces alone (Bagnold, 1954). If $R_* > 70$, the diameter of particles on the bed sufficiently exceeds the thickness of the viscous sublayer that it ceases to exist. The surface is then aerodynamically rough, and the velocity profile above the bed is independent of viscosity.

Chepil (1945c) has shown experimentally that the sediment transport capacity of wind acting on a loose, granular soil, is dependent on air density, flow velocity, and air viscosity. For a 10°C air temperature reduction, the increase in the air density results in a 2.5 to 4% increase in wind force. For a 10mm of mercury increase in atmospheric pressure, the air density increases by 1.3%, which also increases the wind force. The erosive force of the wind is not altered by more than 3% by varying the humidity, and the erosive power of dry air exceeds that of moist air. Although the rate of soil movement varied with air density, Chepil considered that drag velocity and wind gustiness were the governing factors. Under suitable conditions, however, the experiments

suggest that the air density could be a significant factor, and that particle entrainment could begin at slightly lower values of u_{*t}. Once saltation is initiated, it continues at wind strengths below the threshold friction velocity, provided that saltating grains continue to collide with the bed (Bagnold, 1954).

For a one-dimensional flow situation, the velocity in the vertical direction (y) is zero and the velocity in the flow direction (x) is a function only of height above the bed (Bagnold, 1954). Provided the flow is fully turbulent, the boundary layer has a logarithmic velocity profile given by:

$$u/u_* = 1/k \ln(y/y_o)$$

where y_o= roughness height (approximately 1/30 of the bed particle diameter) and k= von Kármáns constant. The profile, however, is considerably altered by the presence of saltating particles (Bagnold (1954) (Figure 4.2).

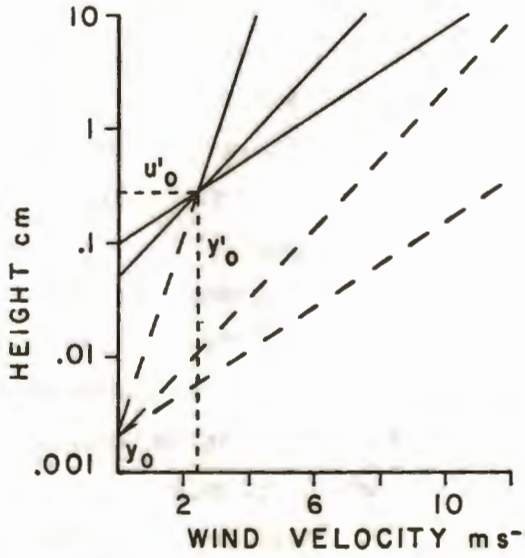

Figure 4.2.Sketch showing the influence of the saltation load on a wind velocity profile. (Modified from Bagnold, 1954, Fig.18)

If no saltation occurs, height-velocity lines converge at a focus, y_o, the roughness height, where the velocity is zero. During saltation, the height-velocity lines converge at a greater height, y'_o, where velocity u'_o is not zero. The velocity, y'_o, is prevented from rising above the impact threshold velocity by the extra drag imposed on the flow by the saltating grains even if wind velocity is increased, and saltation effectively increases the roughness height of the bed (Bagnold, 1954).

At the threshold of movement, the forces acting on a particle on the bed are assumed to be at equilibrium about the pivot point (p) (Figure 4.3). Increasing the wind velocity causes the particle to lift from the surface. There is mounting evidence that lift forces, due to the steep velocity gradient near the ground, are important at the threshold of motion. Chepil (1945) considered that particle spin is an important factor. Recent measurements seem to confirm this, since trajectory heights exceed those predicted by consideration of drag forces alone (White and Schulz, 1977).

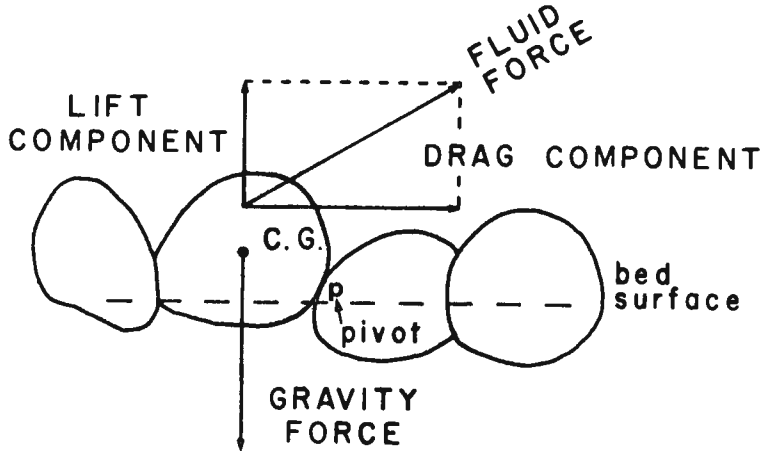

Figure 4.3. Summary of the forces acting on a particle on a bed of similar grains. (After Middleton and Southard, 1984).

The characteristic trajectory shape (Figure 4.4) first described by Gilbert (1914, cited in Bagnold, 1954) has been observed in detail (Bagnold, 1954; Chepil, 1945a). This shows that the horizontal saltation path length is typically about eight times the trajectory height. Trajectory measurements at a friction velocity of 38 cm/sec show that the average particle lift-off angle is about 50° (range 20° to 100°), and the average impact angle is about 14° (range 4° to 28° (White and Schulz (1977). Particle lift-off velocity averaged about 69 cm/sec whilst the impact velocity averaged 161 cm/sec at a friction velocity of 38cm/sec (White and Schulz (1977)°. This indicates that saltation impact has the potential to significantly alter the bed configuration.

Particle concentration and transport rate over a moderately well-sorted sand bed decline exponentially with height above the

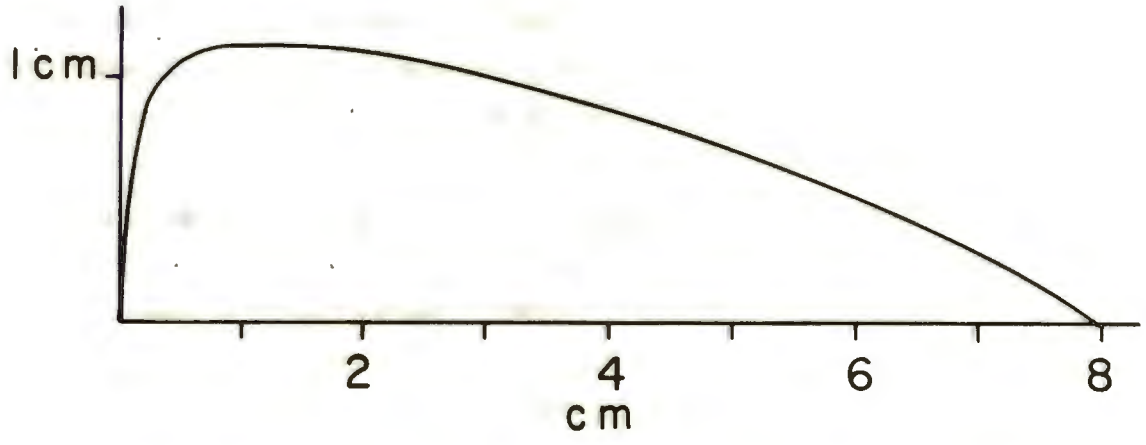

Figure 4.4. Typical path of a medium sand grain saltating in air. (After Maegley, 1976, cited in Middleton and Southard, 1894). Note vertical exaggeration.

bed (Zingg, 1953, cited in Middleton and Southard, 1984; Williams, 1964). The rate of change of concentration with height is only slightly affected by changes in wind strength, whereas the variation of particle shape exerts a greater influence (Williams, op. cit.). Zingg (op. cit.) also found that the mean height of grain rise varies both with grain size and shear velocity. Experimental evidence shows that variation in the wind strength has the greatest effect on the transport rate and that interestingly, this is more pronounced for spherical grains than for angular ones (Williams, 1964; Willetts, 1983). Spherical particles also travel along higher trajectories than platy grains, and the path length of platy grains exceeds those of spherical ones under similar conditions (Willetts, 1983). Willetts (1983) has postulated that these differences relate to differing modes of entrainment. Angular particles appear to be predominantly entrained by aerodynamic forces, whilst collision dislodgement by saltating particles ejects more spherical than platy grains from a bed at higher wind velocities. The transport rate of platy grains is greater at low wind speeds (Williams, 1964; Willets, 1983), which suggests that particle shape influences the threshold friction velocity (Williams, 1964).

4.1.3. SALTATION OVER IMMOBILE SURFACES

The nature of saltation over an immobile surface differs from

that over a loose granular surface. On collision with a loose sand bed, the kinetic energy of a grain is largely dissipated. In contrast, when a saltating particle strikes an immovable object, such as a quartz pebble, the retention of a larger proportion of its kinetic energy results in a far greater rebound height above the bed. In addition, the average lift-off velocity of a grain is greater, and its trajectory path length increases considerably (Bagnold, 1954). Grains rebounding into the air accelerate downwind, towards a velocity approaching that of the wind (Bagnold, 1954). The saltation particle velocity reaches a maximum just before impact with the bed, with the grains attaining about 50 to 70 % of the free-stream wind velocity (Greeley, Williams and Marshall, 1983). Since the wind velocity increases with height above the bed, the increase in rebound height potentially means that the saltating grains impact with the bed at faster velocities.

4.1.4. SUBSTRATE INFLUENCE ON POTENTIAL SANDFLOW

Saltation across a loose, granular surface proceeds at one definite rate, which is dependent upon the character of the sand for a given wind strength (Bagnold, 1954). Under these conditions, the sandflow effectively reaches saturation level because the intensity of saltation adjusts itself to wind strength (eg. Bagnold, 1954).

Over an immobile surface, for the same wind strength, the rate of sandflow does not maintain saturation level, and the sandflow rate across the surface is potentially higher (Bagnold, 1954). Sandflow is then dependent upon the availability of sand. This increases the complexity of the pattern of sandflow, and the application of theoretical models of sandflow based solely upon anemometer data becomes more difficult.

4.2. PRESENT-DAY SEDIMENT DISPERSAL BY AEOLIAN SALTATION

4.2.1. INTRODUCTION

The presence of barchan dune trains within the deflation basin has been known for some time. They are propagated at log-spiral and south-facing embayments (Kaiser, 1926; Hallam, 1964; Rogers, 1977). The significance of these features in terms of sandflow through the deflation basin has not, however, previously been investigated.

The laterally extensive, planar stone pavement about 3 km due

east of Bogenfels, which is traversed by barchans of the Bakers Bay dune train, provides an excellent site to observe saltation transport in action. Initial observations indicated that the saltation load does not always travel across the stone pavement during high-energy southerly winds. Instead, pulses of saltation transport occur, with peak movement closely associated with very high-velocity gusts of wind. Looking south, into the wind, gusts which entrain sediment at the south end of the stone pavement snake northwards prior to redepositing the sand as the energy of the gust declines, or the saltation capacity of the wind is exceeded.

Saltation bombardment is particularly intense during gusts of 18 to 25 m/sec, and grain impact is excruciatingly painful on any exposed flesh. Grains impacting on hands raised 2.5 to 3 m into the air collide with incredible force, and despite wearing a ski-mask and goggles, one's face cannot withstand the pain of impacts 1.3 to 1.5 m above the ground for long. Such conditions are relatively common within this high-energy aeolian environment.

The dynamics of the aeolian creep bedload is governed by the dynamics of the saltation load. It has therefore been important to determine:

1) the spatial distribution of sandflow;
2) the temporal variation of the actual sandflow rate through the deflation basin;
3) the spatial variation of the grain size in the saltation load.

Both the spatial distribution, and the sandflow rate, are probably more variable within the deflation basin than the Namib Sand Sea due to the undersaturated nature of the sandflow within the former high-energy system. This results from the combined influence of the following factors:

1) the spatial zonation of the high-energy coastal wind regime;
2) the spatial variation of sediment dispersal by the system;
3) the temporal variation of sediment dispersal by the system;
4) the variable nature of the substrate over which saltation occurs;
5) the distribution of vegetation.

4.2.2. SPATIAL VARIATION OF SANDFLOW RATE AND GRAIN SIZE

Sand Trap Results

The total sandflow measured by the venturi-compensated sand trap (VST) whilst deployed at site A, north of Bogenfels beach (Figure 4.5) from 04/02/86 to 02/12/86, was about 1.7 tonnes/m width (tmw). Reasoning that sandflow close to the main Bakers Bay barchan dune train would be higher, this sand trap was moved to site C (Figure 4.5), and a smaller perspex sand trap (PST) was placed alongside for comparison. The estimated total sandflow measured by the VST catching between 0 and 47 cm above the ground surface was 1.24 tmw for the initial 16 day period from 02/12/86 to 18/12/86. The estimated sandflow based upon the PST device, catching from 0 to 16 cm above the ground surface, was 1.05 tmw over the same period. In 16 days, the sandflow at site C almost equalled that which passed the VST at site A in 10 months.

To examine the spatial distribution of sandflow more closely, two more PST devices were deployed, in a traverse across the south-south-easterly to southerly surface-wind flow, as shown in Figure 4.5. These traps operated simultaneously between 22/01/87 to 28/05/87, and the VST has now operated continuously at site C since 02/12/86.

The spatial variation of measured sandflow based upon PST device data per catching period is very pronounced (Figure 4.6). For identical catching periods, the total sandflow at site C of about 7.1 tmw was 11.6 times greater than at site A, where the total sandflow was about 0.63 tmw, and 13 times that at site B where the total sandflow was about 0.57 tmw. The sandflow at all sites declined rapidly during March, and was subsequently only measureable at site C. The results at site C for the PST and VST devices compare favourably, and estimates for the total sandflow of 7.1 and 7.9 tmw were obtained respectively.

PST device results for sites A, B, and C were reduced to show the sandflow rate in tmw / 24 hours for each catching period (Figure 4.6). A pattern can be seen, showing a rhythmical alternation between periods of higher and lower sandflow. Immediately after a peak in sandflow, the rate tended to decrease. The interval separating peaks in sandflow appears to increase from February onwards in response to the decline in the southerly surface-wind energy. The sandflow rate declines dramatically from March onwards.

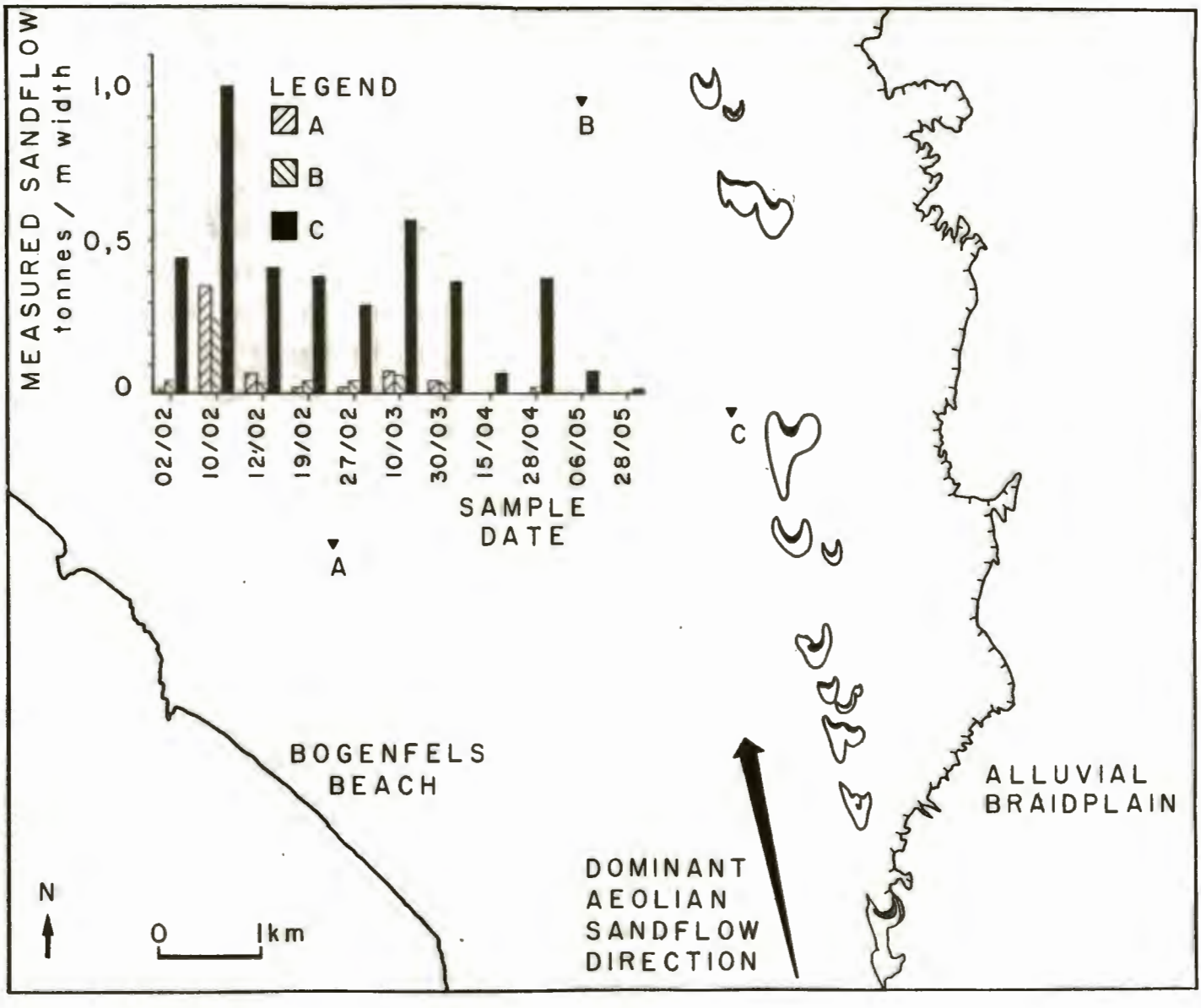

Figure 4.5. Map showing the location of sand trap sites A, B, and C, and the variation of sandflow per trapping period recorded at each site between 22/01/87 and 28/05/87.

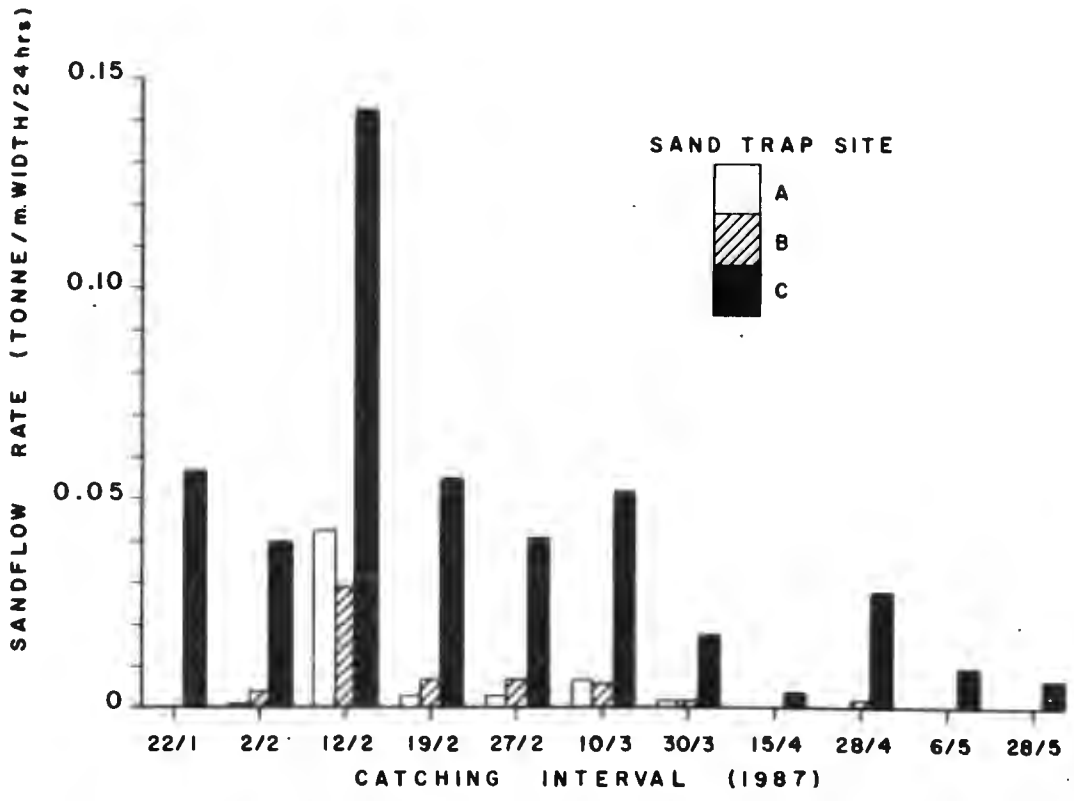

Figure 4.6. Variation of sandflow rate per trapping period at sites A, B, and C.

The sandflow was only maintained at a measurable level at site C after March. The cyclical variation of the sandflow rate proves that the peaks of the measured sandflow are not a manifestation of variable trapping period length. PST device data for site C between 02/12/86 to 12/02/87, when the southerly wind-energy peaks, were also reduced to a value of sandflow rate per 24 hours. Wind roses for each catching period were constructed from Bogenfels anemometer data (Figure 4.7). Distinct peaks and troughs defining the cyclical nature of the sandflow rate are again evident, and the alternation of high and low sandflow rates is clearly defined. Despite tha maintenance of high-energy southerly surface-winds, high sandflow conditions were followed by a period of reduced sandflow. Furthermore, high sandflow rates were not always associated with the highest-energy winds (eg. 18/12/86 to 29/12/86).

The sandflow rate gradually declined at site C from the end of December 1986. The cyclical nature remained evident, but the sandflow was subsequently maintained at a slightly lower level

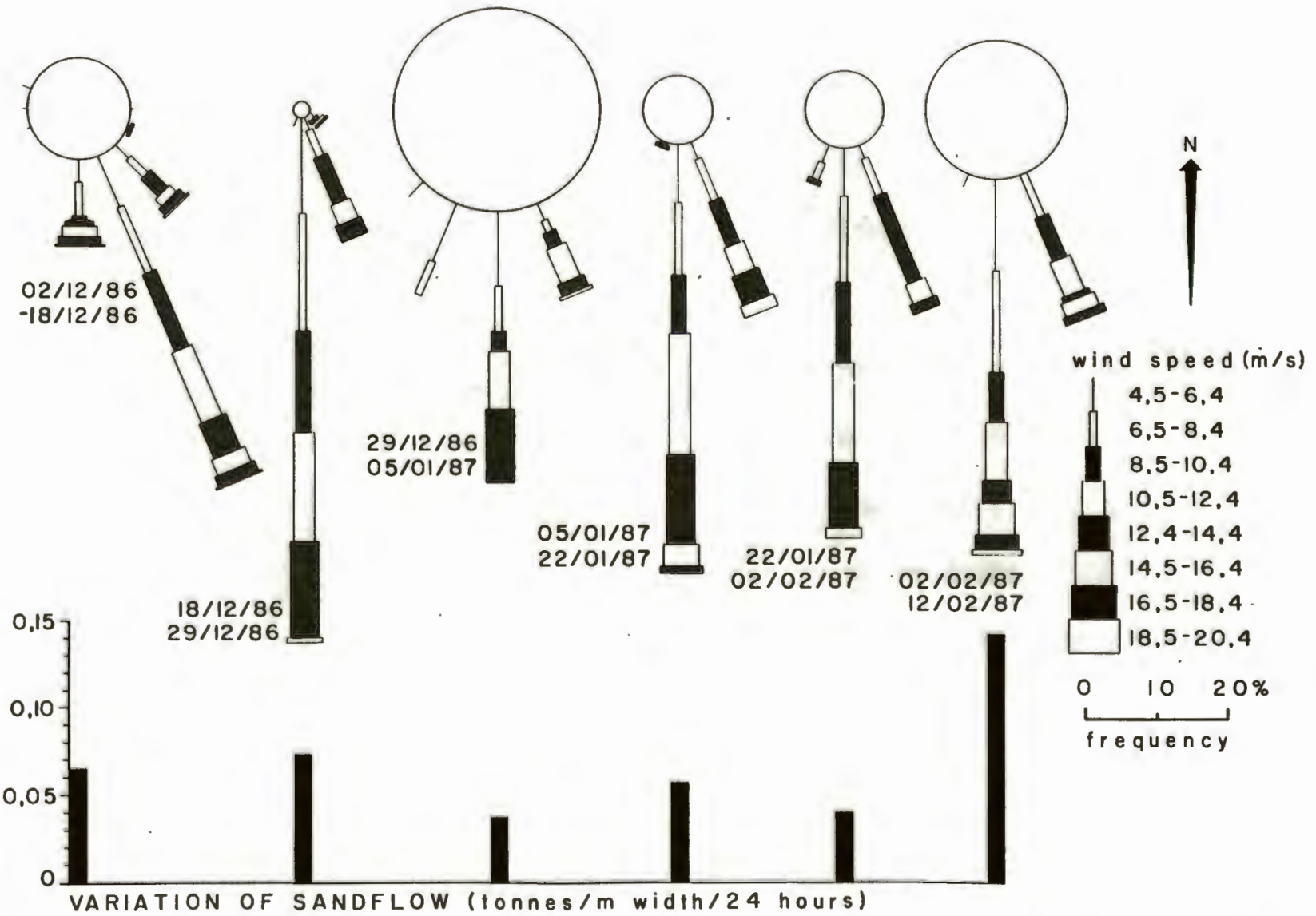

Figure 4.7. Variation of the sandflow rate between 02/12/86 and 12/02/87. Wind roses provide insight into the surface-wind conditions prevailing throughout each trapping period. Note that the highest energy winds occurring between 18/12/86 and 29/12/86 did not coincide with the period of maximum sandflow.

until a major sandflow event occurred on the 10/2/87. This event lasted until 12/2/87, and was one of the most impressive very high sandflow events witnessed during the study period.

The Definition of Aeolian Transport Corridors

The sand trap results demonstrate the existence of a zone near the Bakers Bay barchan dune train, about 4km east of Bogenfels, in which both the sandflow rate and the total sandflow are very high with respect to the rest of the sand trap traverse. The western margin of the zone, as defined by sand trap results from sites B and C, is no greater than 1200 m from the barchan dune train (Figure 4.8), at which point the sandflow diminishes dramatically. Although the high sandflow zone's eastern margin was not defined using sand traps, personal observation indicates that it lies a similar distance to the east of the dune train. The zone is therefore between 1 to 2km wide, and approximately parallel to the southerly surface-wind. At Bakers Bay, acknowledged to be the starting point of the barchan dune train (Kaiser, 1926; Hallam, 1964; O'Brien, 1972; Rogers, 1977), the width of the high sandflow zone is about 1 km (see Figure 4.15). The narrow width of the zone of high sandflow thus appears to be maintained, and hardly increases at all on reaching Bogenfels, approximately 25 km north (ie. downwind) of the sediment input point. The saltation load derived from the Bakers Bay log-spiral beach therefore does not fan-out downwind, as perhaps might be anticipated. Instead, it mostly remains within a sharply bounded, wind parallel zone along which barchan dunes migrate. It is proposed that zones of this type be termed an "aeolian transport corridor".

Proposed Mechanism for Aeolian Transport Corridor Maintenance

Although topographic interaction with the surface-wind regime undoubtedly influences the sandflow passing some localities (Figure 4.9a and b), complex topography does not influence the sandflow in the vicinity of any of the sandtrap sites. To the south of trap sites B and C, the barchan dune train migrates across a gently undulating alluvial surface, prior to dropping down a small (5 to 20 m) scarp slope onto the sub-horizontal stone pavement on which sand trap site C was located.

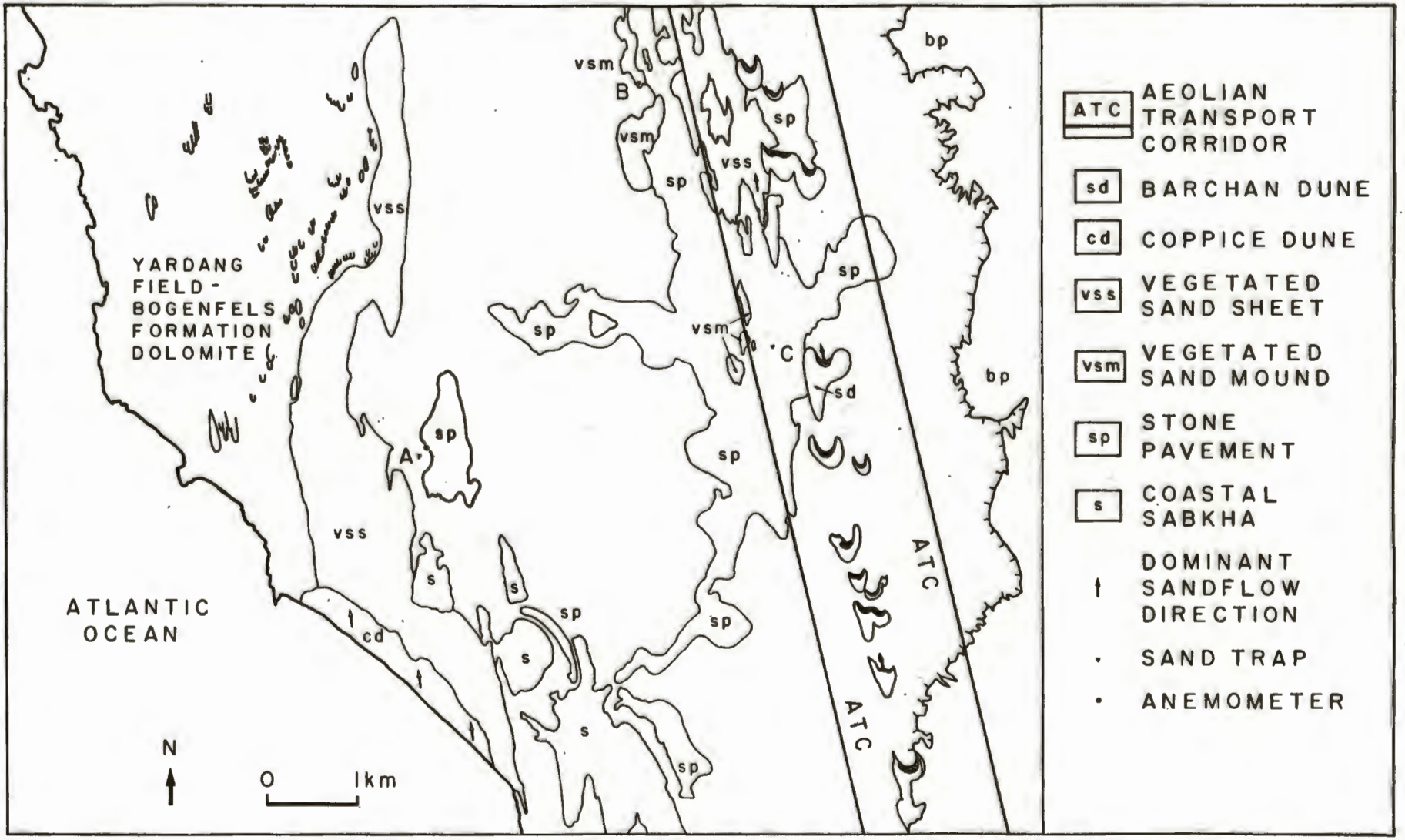

Figure 4.8. Map showing the position and orientation of the aeolian transport corridor defined by sand trap results.

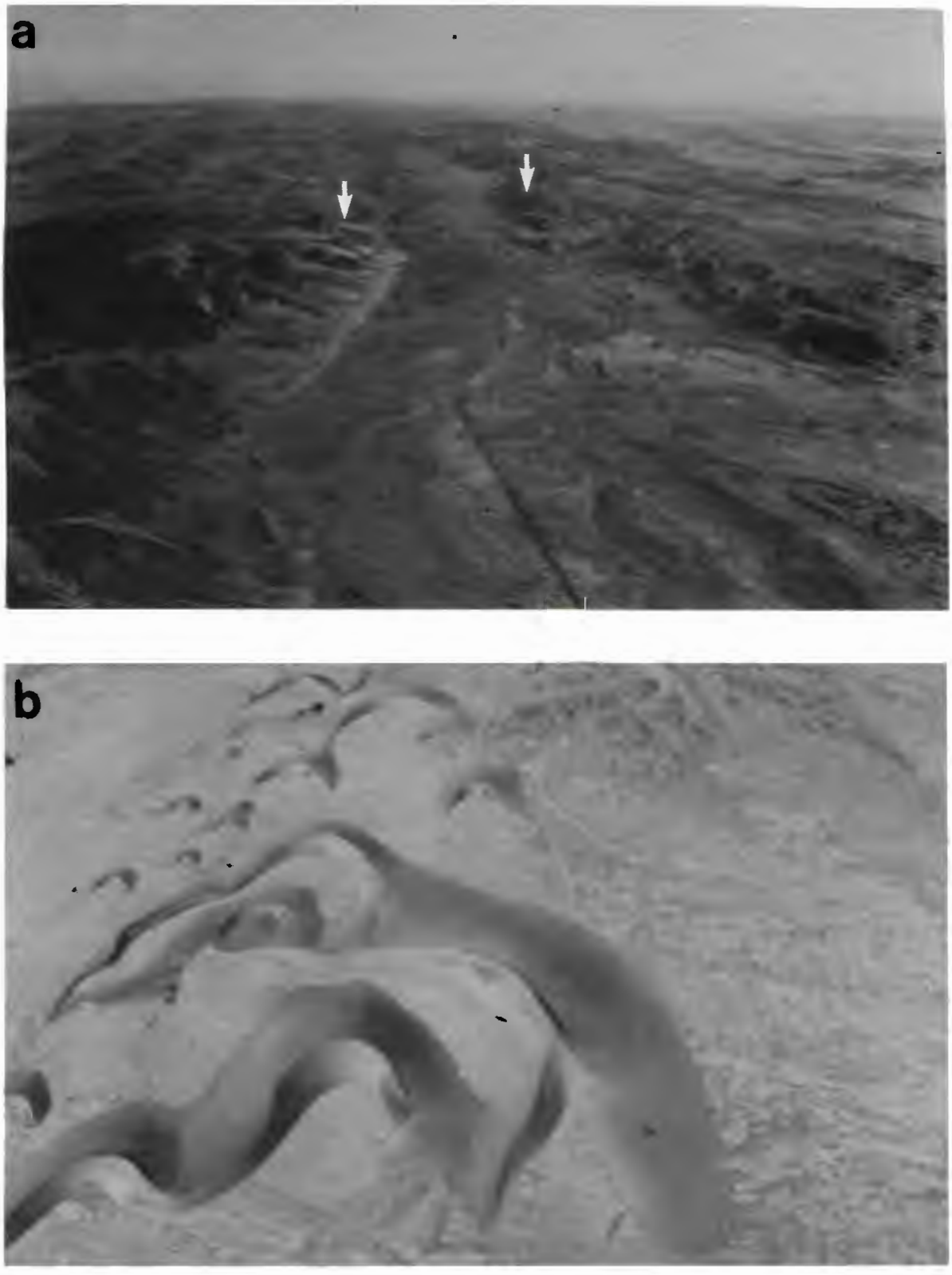

Figure 4.9. (a) Oblique aerial view of the barchan dune train on the western margin of the Idatal basin. Note how the dunes dissipate at the constriction of the basin margins (arrowed). This is probably the result of the acceleration of wind flow as it is funnelled by the constriction. Southerly wind blows from bottom to top of frame. (b) Compound barchans about 30 m high on the floor of the east-west oriented Grillental trough. The surface-wind flow probably decelerates across the trough, resulting in the development of larger dune forms. Note the smaller barchans migrating down the southern edge of the trough in the background. Southerly wind blows from top to bottom.

Where cold, southerly surface-winds flowing over the cold Atlantic Ocean surface arrive at the relatively warm land surface, considerable thermal contrast occurs. This provides conditions suitable for the development of thermal instability within the atmospheric boundary layer. Provided that sufficient shear occurs, this instability can result in the development of longitudinal spiral vortices (eg. Jeffreys, 1928; Phillips and Walker, 1932). The transverse instability of wind flow in the planetary boundary layer resulting from secondary flow of this form is widely acknowledged to be important in the maintenance of linear dune systems (Hanna, 1969; Mabbutt et al., 1969; Glennie, 1970; Folk, 1971). It has also been shown to govern the distribution of dust and pollutants within the planetary boundary layer (Brown, 1983). Hence the presence of linear dune systems throughout the Southern Namib strongly suggests the development of secondary flow within the atmospheric boundary layer of the region. Further evidence of the presence of secondary flow within the planetary boundary layer is occasionally provided by the presence of cloud streets above the deflation basin.

The crestal spacing of linear dune systems south-east of the deflation basin is about 250 to 500 m, whilst at the southern end of the linear dune systems within the Namib Sand Sea, it is about 2 km. This variation, if it is governed by longitudinal spiral vortices, is possibly explained by the close proximity of the escarpment in the south, because it forms an orographic barrier against which the anticyclonic wind system is possibly compressed.

The crestal spacing of the linear dune systems at the southern end of the Namib Sand Sea approximately equals the width of the Bakers Bay aeolian transport corridor. It is therefore proposed that these zones of high sandflow might correspond to the conceptual model of Allen (1982:2 Fig.1-2d), for secondary flow in a system where there is insufficient sediment supply to cover the bed (Figure 4.10). The sharply defined margins of the aeolian transport corridor on the bed are interpreted as the position at which the longitudinal reattachment lines of adjacent longitudinal vortex cells diverge. It is postulated that the sandflow travelling

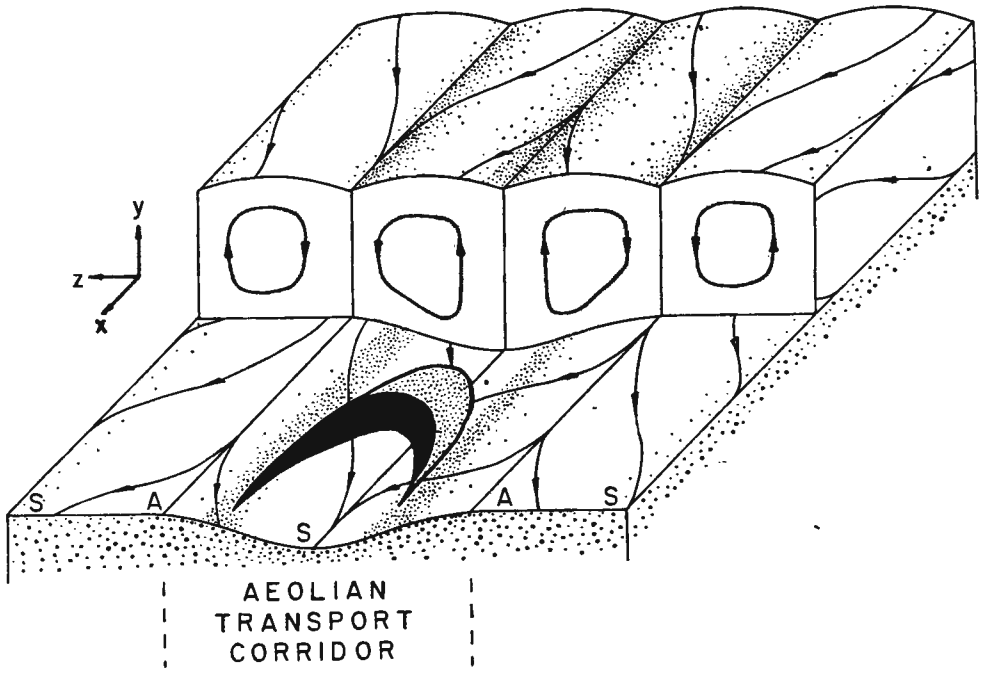

Figure 4.10. Diagram of the pattern of the longitudinal secondary flow vortex cells which possibly maintain the aeolian transport corridor. The flow associated with neighbouring vortex cells reattaches with the bed (A) and diverges towards the point of its separation from the bed (S). Flow converges along the separation line, and confines the sandflow to the aeolian transport corridor. Neighbouring cells are thus starved of sandflow.

along the aeolian transport corridor is effectively swept in towards the barchan dune train from this boundary. Theoretically, the maximum areal concentration of sandflow within the aeolian transport corridor should therefore occur along the separation line of the adjacent longitudinal vortex cells, which is probably indicated by the position of the barchan dune train. Longitudinal, wind-parallel secondary flow vortex cells thus provide a potential mechanism for the maintenance of aeolian transport corridors which is independent of topography.

Further evidence supporting this concept of aeolian transport corridor maintenance is present in the Grillental, where the sandflow emerges from the complex deflation basin topography. Four barchan dune trains develop, and subsequently descend into the valley which runs perpendicular to the southerly surface-wind flow (Figure 4.11a). The east-west crestal separation of the dune trains is about 2 to 2.5 km, the estimated width of the aeolian transport

corridor at Bogenfels. The regular spacing of these bed forms can therefore also be interpreted on the basis that secondary flow occurs within the planetary boundary layer (Figure 4.11b).

The definition of aeolian transport corridors has important implications for the interpretation of aeolian bedload creep dynamics, which is driven by saltation collision within the Southern Namib. Sediment input to the aeolian current system is restricted to log-spiral and re-entrant embayments. The maintenance of aeolian transport corridors by longitudinal vortex cells, confines the sandflow entering the system at these points to a narrow zone, which is approximately aligned with the southerly to south-south-easterly surface-wind flow. Neighbouring vortex cells, into which there is minimal sediment input therefore experience significantly reduced sandflow rates.

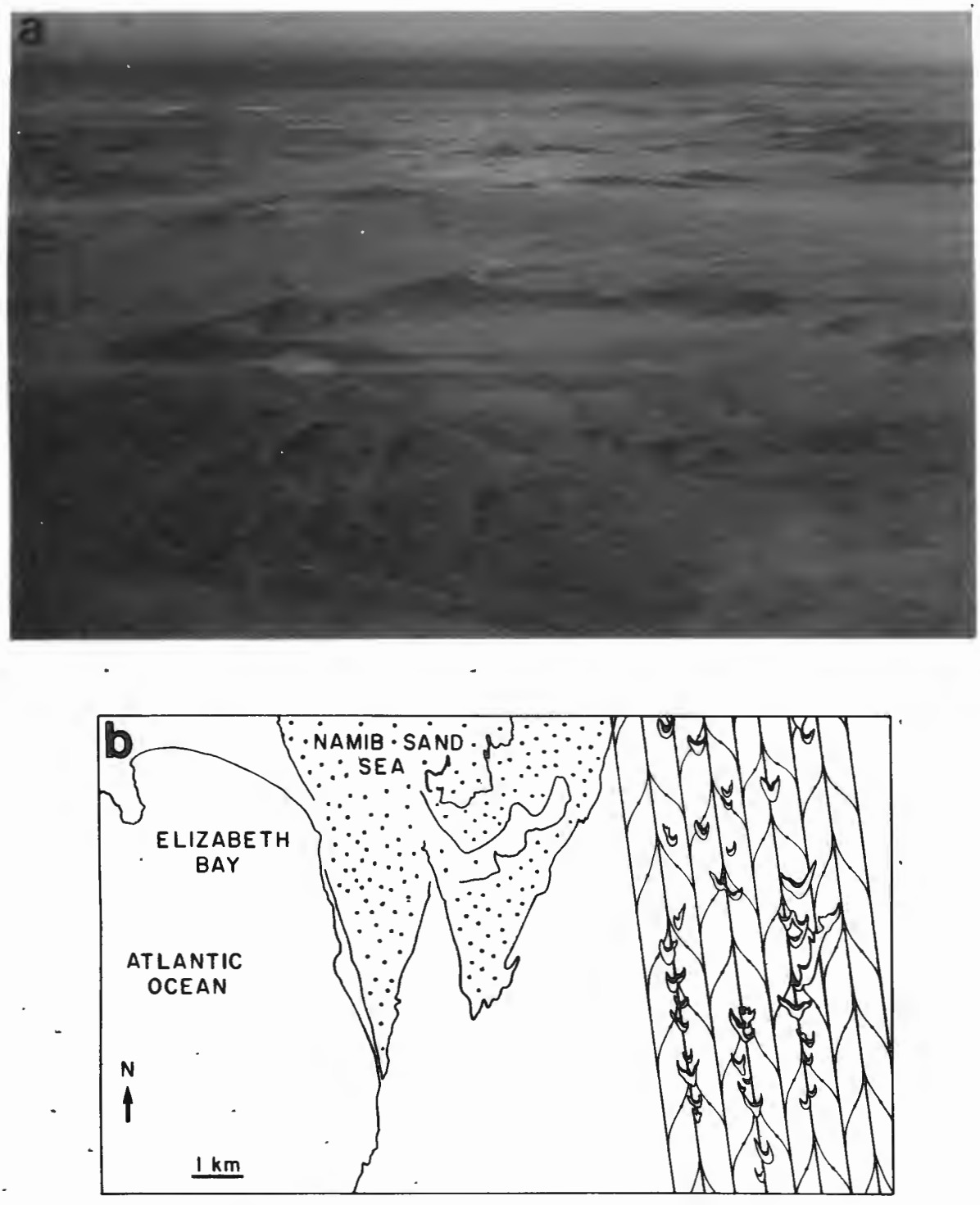

Figure 4.11 (a) Oblique aerial view to the west showing barchan dune trains descending into the Grillental trough. Dunes in foreground about 30 m high. Southerly wind blows from left to right.
(b) Interpretation of the barchan dune trains in (a) using the concept of longitudinal secondary vortex cells in the planetary boundary layer. Only the pattern of secondary flow on the bed is shown for clarity. In this case, the sediment input occurs over a wide enough east-west window to maintain the sandflow along three aeolian transport corridors.

4.2.3. SPATIAL AND TEMPORAL VARIATION OF SALTATION LOAD GRAIN SIZE

Presentation of Results

Care was taken to avoid placing the sand traps in the lee of vegetation, which complicates the pattern of sandflow. To minimize the influence of substrate on the sandflow, trap sites A and C were located on a stone pavement, and trap B on a sand mound with a surface armour of granules and pebbles. The grain size distributions of the trapped sandflow exhibit distinct variation (Figure 4.12).

Mean Grain Size Variation

The mean grain size at each PST device site along the traverse remained fairly constant over the entire trapping period. Collectively, each sample set showed the same relationship. The mean grain size at site C, within the aeolian transport corridor, was always significantly coarser than at site A or B. The finest mean grain sizes were recorded at site B. This spatial variation was most pronounced during the high sandflow event between 10/2/87 and 12/2/87.

At site C, the sample trapped primarily on 10/2/87, during peak sandflow, exhibited a reduction in mean grain size relative to samples trapped prior to this event. Subsequently, it then increased slightly in the sample collected between the late afternoon of 10/2/87 to 12/2/87, after the peak in sandflow had begun to decline. At site A, the mean grain size increased significantly for the duration of peak sandflow, and subsequently declined again after the main event. At site B, immediately west of the aeolian transport corridor, both sets of samples showed a reduction of mean grain size. After the high sandflow event, the mean grain size at site C fined slightly, and coarsened slightly at sites A and B approximately regaining its value prior to the sandflow peak.

Variation of Sorting

The sorting of the sand trap samples also showed a reasonably consistent relationship between the data sets, which was only interrupted during high sandflow events. Samples from site C were generally the least sorted. The worst sorting was exhibited at all

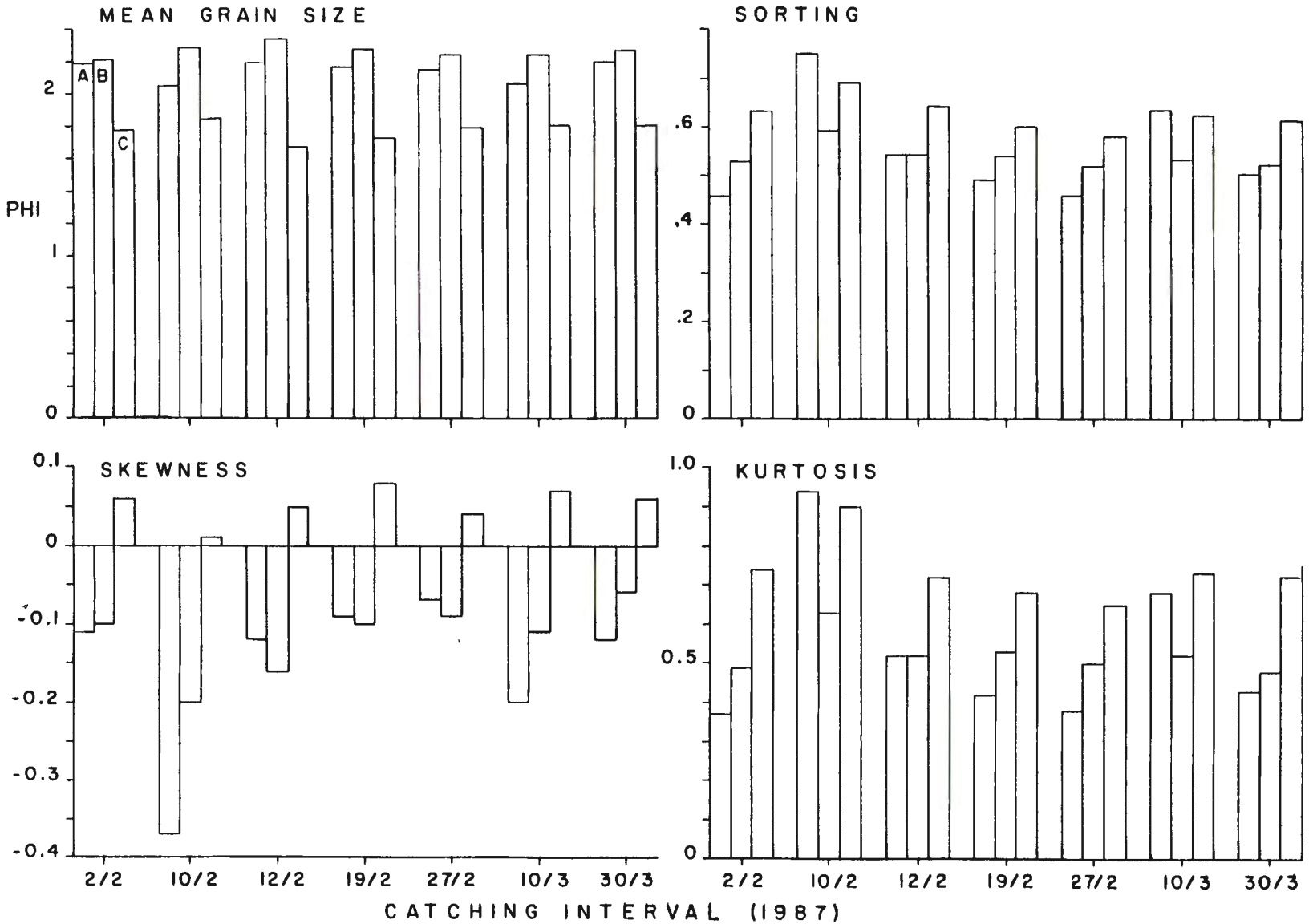

Figure 4.12. Characteristics of grain size distributions for some of the sediment trapped at sites A, B and C between early February and the end of March, 1987.

sites during the peak in high sandflow conditions on 10/2/87 (Figure 4.12). The sorting increased straight after the main event as the wind-energy diminished. The decrease in sorting was most marked at sites A and C during this event. A further reduction in sorting was recorded at site A, and to a lesser extent at site C, on 10/3/87. This also coincided with conditions of relatively high sandflow through the deflation basin. Optimium sorting consistently occurred during catching periods when sandflow was relatively low.

Variation of Skewness and Kurtosis

Values for skewness undoubtedly show the greatest variation across the traverse (Figure 4.12). All samples from the aeolian transport corridor (site C) exhibit positive values, whilst samples from both sites A and B were consistently negatively skewed.

At sites A and B, the distribution was most negatively skewed during the peak sandflow conditions on 10/2/87, when the positive skewness of the sample distribution at site C was also reduced. These changes were accompanied by a marked increase in kurtosis; sites A and C became conspicuously leptokurtic. A smaller negative peak is shown for samples from sites A and B collected on 10/3/87 which were also collected during high sandflow conditions.

Comparison of VST Samples with PST Samples from Site C

The grain size characteristics of samples collected with the venturi-compensated sand trap over a catching interval of 0 to 47 cm above the ground surface at site C, are summarized for comparison with those from site A (Figure 4.13a). The data sets were not collected simultaneously. Although comparatively few data sets are available for site A some obvious differences are apparent with respect to site C. The most noticeable of these are the poorer sorting, the negative skewness and larger values of kurtosis found at site A relative to site C, which shows a similar trend to PST samples.

VST device data for site C spans a year. The mean grain size data exhibits an overall trend. Finer-grained material is associated with the summer months, when the sandflow and wind-energy both peak, and the mean grain size is coarser for the winter months. The PST data for site C also exhibits this trend (Figure 4.13b).

VST and PST data indicate that the sandflow is better sorted

during the winter months, when values for kurtosis decline, than during the summer. The skewness of the VST data seem to show this apparent seasonal trend most strongly. The values shift from being positive during the summer months to slightly negatively skewed during the winter months.

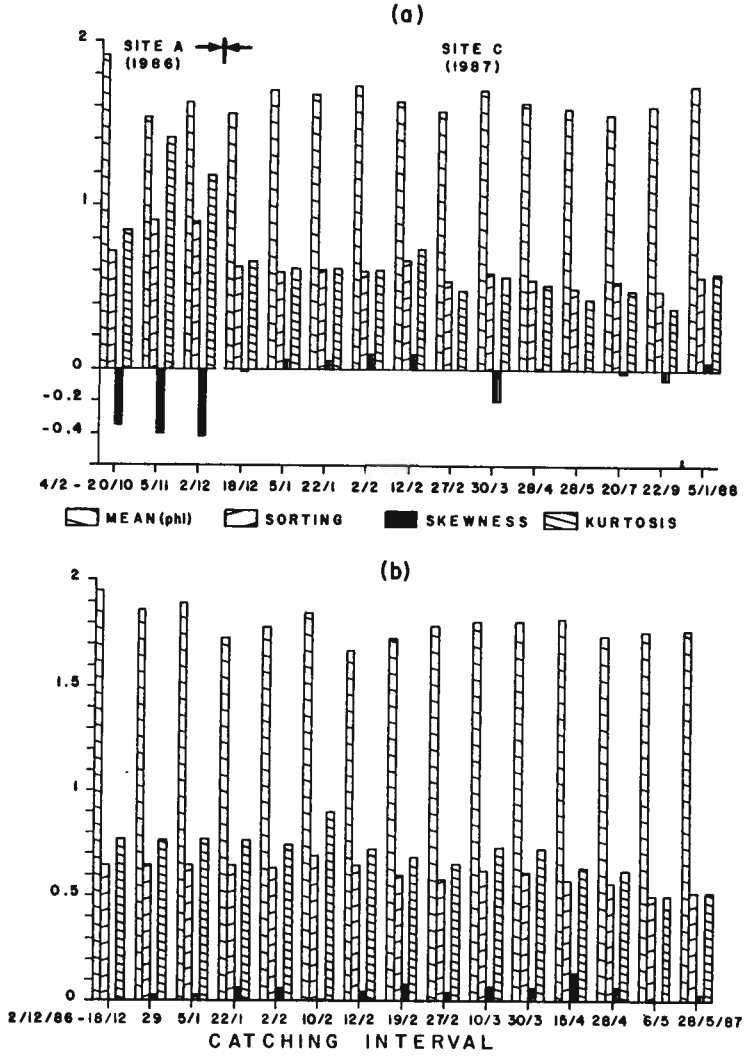

Figure 4.13. (a) Grain size statistics for VST samples from sites A and C. (b) Summary of grain size statistics for PST samples from site C, showing the seasonal variation of parameters.

Influence of Beach Dynamics on Sandflow Grain Size

Restriction of sediment input to the aeolian system to localised embayments is governed by the deflation basin geomorphology, which influences the coastal morphology, and the nearshore sediment dynamics along the Atlantic coast (Kaiser, 1926; Hallam, 1964; Rogers, 1977). This is well illustrated at Bakers Bay. Transgression across a former endoreic basin has created rocky headlands and islands along the strike of remaining land-based resistant bedrock ridges, and the formation of a log-spiral embayment (Figure 4.14 and 15). Swell waves generated in the Southern Ocean, and local wind-generated surface waves, approach the Atlantic coastline obliquely, approximately from the south-west (Swart, 1983). The high-energy, plunging breakers, maintain the steep beach profile along the exposed coastline. A strong offshore current is developed in response to nearshore wave dynamics, which results in the seaward transport of the sand fraction, and offshore bar formation (pers. comm. Swart, 1988). Therefore, the steep, exposed beaches are almost entirely composed of material coarser than 0 phi (Figure 4.16). The rocky headland at Bakers Bay creates a shadow zone to the north, which is protected from direct wave approach. The waves are therefore diffracted around the promontary. The wave energy is transmitted along the wave fronts within the shadow zone, where wave height and energy both diminish. This results in the development of a residual nearshore current and the reduction of the beach slope and the grain size of beach sediment within the embayment. Within Bakers Bay, the offshore islands also cause wave diffraction, which further modifies the nearshore sediment dynamics. The gently sloping beach, dominated by fine to coarse sand, therefore extends along a greater length of the embayment (sample sites F to C) than would otherwise be possible. Beyond the shadow zone caused by the offshore islands, there is an abrupt return to exposed coast conditions; the beach profile steepens and the size of the sediment increases at sample sites A and B once more.

Small barchan and dome-shaped dunes develop at the spring-tide mark and in the backshore area of the embayment (Figure 4.17a), where high-energy southerly winds deflate the beach (Figure 4.17b) (Kaiser, 1926; Rogers, 1977). From here, the sand is rapidly introduced to the aeolian transport corridor.

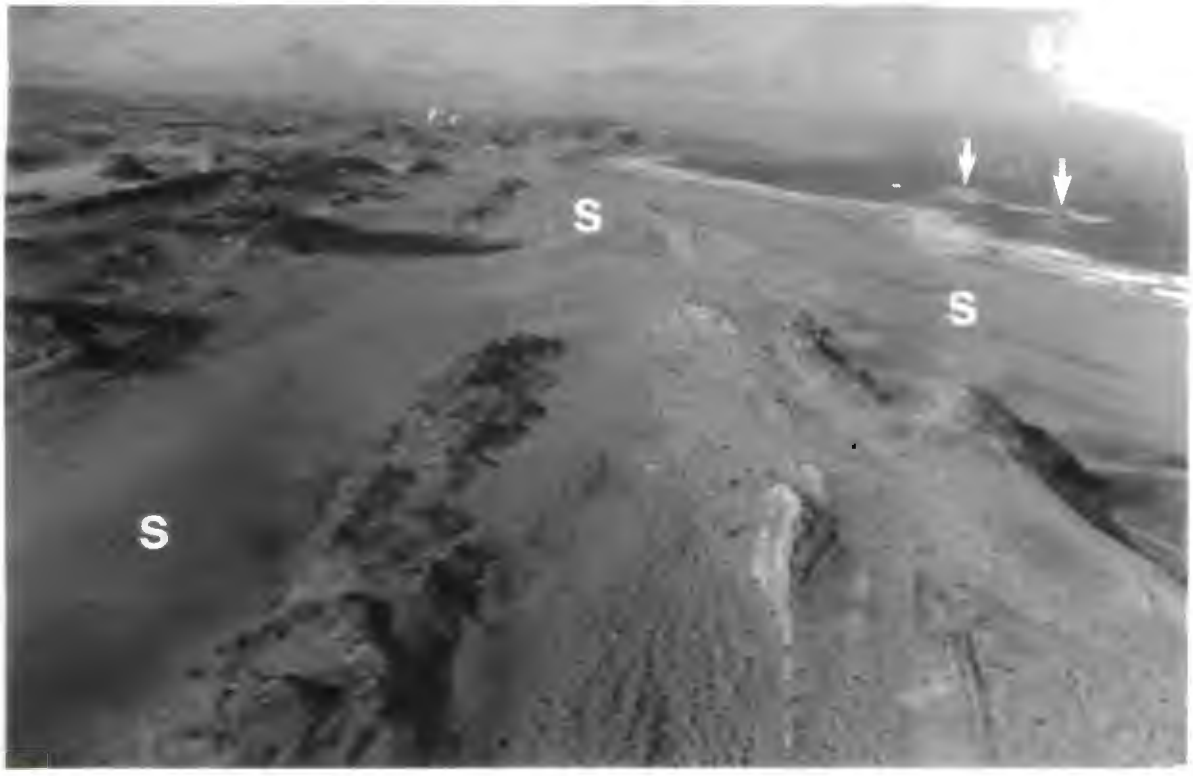

Figure 4.14. Aerial view to the south, showing the log-spiral embayment at Bakers Bay. Note the north-south strike of the resistant bedrock ridges in the foreground. Similar ridges are responsible for the presence of the offshore islands (arrowed). The extensive backshore sand sheet (S) is clearly visible. The southerly wind blows from top to bottom of the frame.

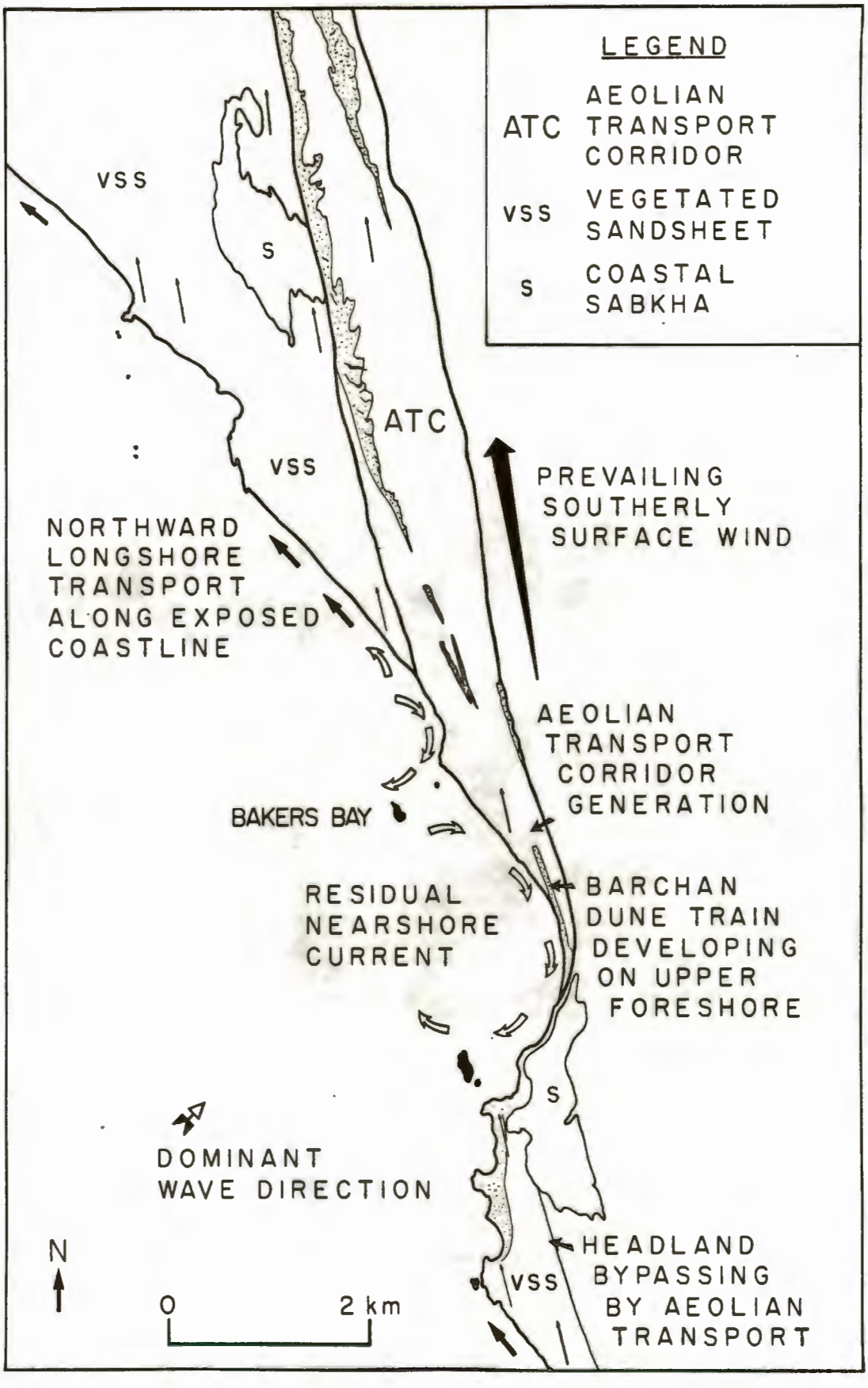

Figure 4.15. Sketch illustrating the postulated nearshore current systems within the Bakers Bay log-spiral embayment, and the position of the point at which the aeolian transport corridor is generated.

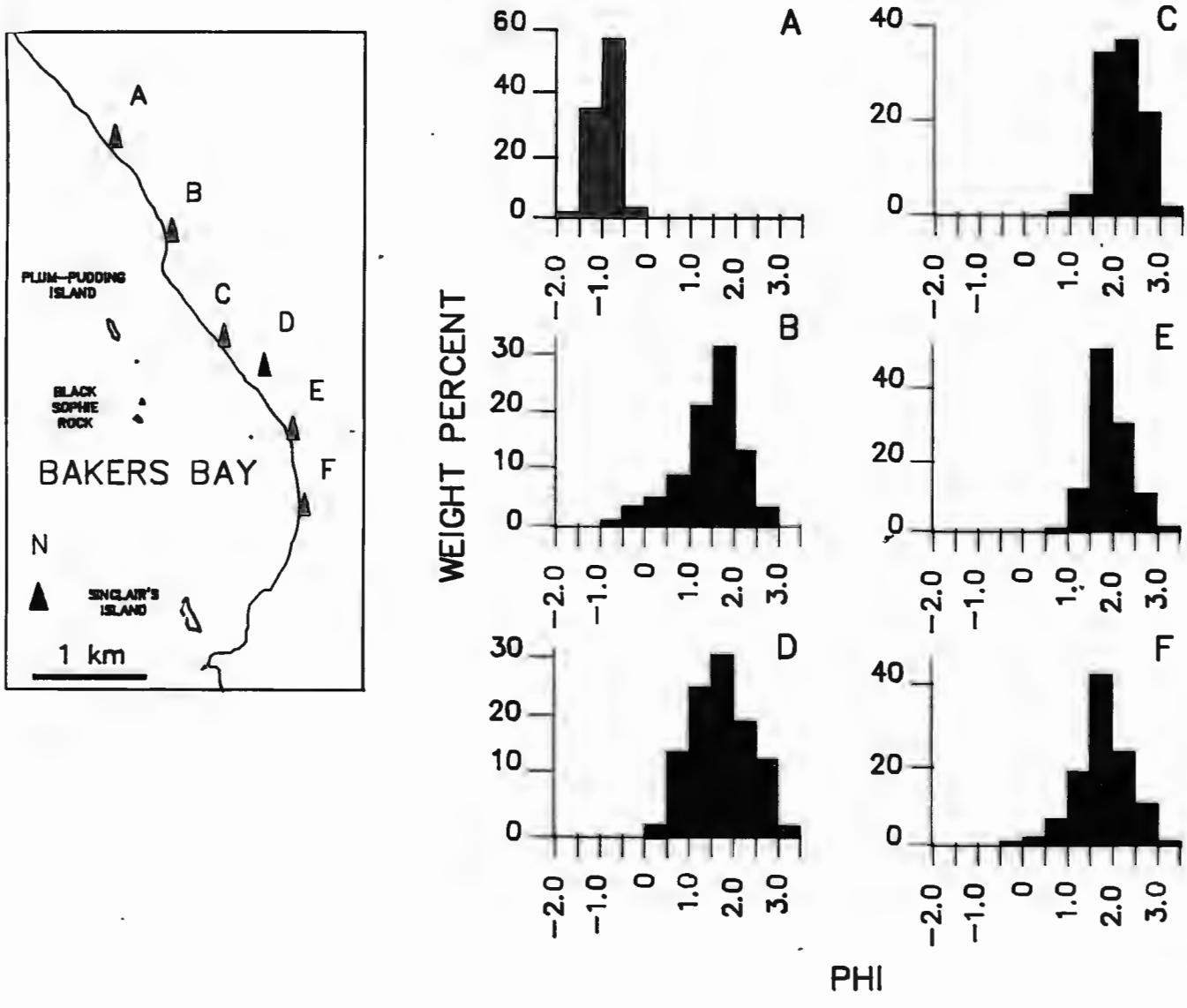

Figure 4.16. Grain size variation of beach sediment within the Bakers Bay log-spiral embayment, and along the exposed coastline. Sample D is from a barchan dune crest in the backshore area.

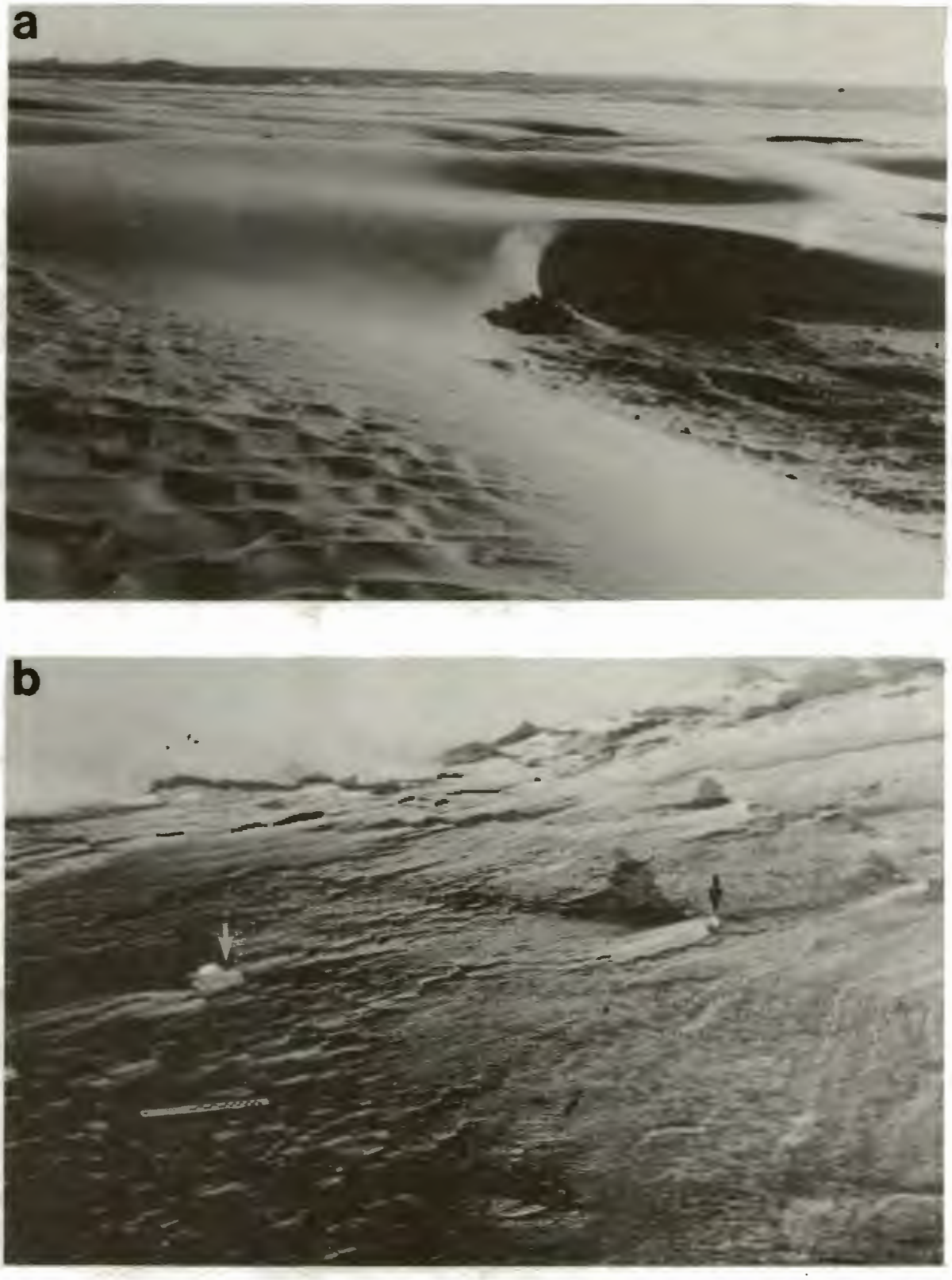

Figure 4.17. (a) Barchans about 1 to 2 m high in the backshore area of Bakers Bay. Note the sand driving over the beach during deflation. Southerly wind blowing from top to bottom of the frame. (b) Scour-remnant ridges in the lee of shells (arrowed) in damp beach sand, providing evidence of active beach deflation. Southerly wind blowing from right to left. Scale 10 cm.

Material that is too coarse to be transported by saltation moves north from the beach as the creep bedload, and is incorporated into granule ripple streets on the extensive sand sheet developed in the backshore area.

Where exposed coastal conditions prevail once more, the sediment comprising the beach coarsens as the beach profile steepens. This drastically reduces the amount of material available for beach deflation, and the sandflow off the beach declines abruptly, as shown by sand trap results from site A to the north of the exposed beach at Bogenfels. Coppice dunes develop in the backshore area, and aeolian current shadows are deposited in the lee of vegetation on the sand sheet surface. The establishment of vegetation occurs abruptly, and appears to delineate the boundary with the aeolian transport corridor where the sandflow rate is much greater. The vegetation apparently does not influence the width of the aeolian transport corridor. The reduction of aeolian sandflow due to change in the marine nearshore environment appears to allow the vegetation to grow. Within aeolian transport corridors, vegetation is frequently restricted to localized areas offering protection from the high-energy saltation load (Figure 4.18). To the north of the exposed beach at Bogenfels, the measured sandflow rate is very low relative to that within the aeolian transport corridor, and consequently the backshore area is vegetated.

Because of the relationship between nearshore sediment dynamics and sediment input to the aeolian system, it is to be expected that seasonal beach dynamics will be reflected by sandflow through the deflation basin. The measurement of CDM beach and nearshore profiles over a 6 year period provides evidence that a distinct seasonal variation of the beach profile is related to variation of wave energy, and the arrival at the coast of storms generated in the Southern Ocean (Swart, 1983). In the vicinity of the seawall, constructed for mining purposes, the period of maximum shoreline recession occurs between June and August (end of winter), and the maximum rate of progradation occurs between December and February (end of summer) (Swart, 1983). Analysis of beach profiles beyond the influence of mining activity confirm that beach progradation occurs between October and March, and that beach recession tends to occur between May and August.

Figure 4.18. A woody succulent takes advantage of the flow separation bubble in the lee of a large silcrete boulder. Note the vegetation defines the expected form of an aeolian current shadow, which is neatly maintained by the high-energy saltation load. Southerly wind flow from left to right. Scale 1 m.

The reduction of saltation load mean grain size during the summer, despite the peak in wind-energy, probably reflects the seasonal variation in the grain size of beach sediment. In an extensive review of available wave data for the west coast, De Decker (1986) concludes that waves arriving from the south-western quadrant are more prevalent during the winter, when the wave height also increases. As a consequence, the northward littoral drift intensifies over this period. Because the wave energy and storm activity are at a minimum during the summer months, the deposition of finer-grained material on beaches probably occurs. During the winter, when wave energy and storm activity increase, a progressive coarsening of beach sediment is likely to accompany shoreline recession. Hence the sand input to the aeolian system during the winter is possibly coarser-grained than it is during the summer. A larger threshold friction velocity is then required to entrain particles from the beach (eg. Bagnold, 1954). The sandflow rate therefore declines substantially in response to the general reduction of southerly surface-wind energy. Beach samples were not taken to test this hypothesis, but the variation of sediment grain size on beaches due to variable wave energy has been recorded at numerous locations elsewhere (eg. King, 1953). This hypothesis provides a possible explanation for the observed seasonal variation of the saltation load grain size. The same combination of factors possibly explains the change from positively skewed sandflow in the summer to negatively skewed sandflow during the winter months.

As a result of beach progradation between October and March, the area of exposed beach at the generation point of aeolian transport corridors increases. This expansion of the beach surface area potentially coincides with the period when the umimodality of the southerly wind regime is most pronounced and surface-wind velocities peak. Optimal conditions then prevail for the deflation of beaches and the transport of the saltation load through the deflation basin.

The diurnal variation of wind speed and the tidal cycle are also potential factors influencing the rate of beach deflation. This theoretically reaches a maximum when low tide coincides with the peak in surface-wind energy between 09.00hrs to 17.00hrs. Active beach deflation leads to a lowering of the surface, which alters the beach profile. This is likely to limit the deflation process,

because watertables remain close to the sediment surface despite the seasonal increase in beach width (Horikawa et al., 1983). In addition to the increased threshold wind velocity required to entrain damp beach sand (Svasek and Terwindt, 1974), the bonding of beach sand by dissolved salts as the sediment dries, creating a surficial crust, also reduces the deflation rate (Nickling and Ecclestone, 1981).

Episodic short-term variation in the amount of beach deflation results during storm events and high tides, when waves reach higher levels on the shoreline. The newly deflated sediment is then prevented from entering the aeolian transport corridor by wave erosion, which reintroduces it to the marine environment (Figure 4.19a). This results in the alternation of aeolian horizons interbedded with beach lamination (Figure 4.19b). It would be difficult to fully appreciate the significance of a small exposure with these structures preserved in the rock record.

The sandflow rate is therefore highly variable because of the interaction of many factors, of which surface-wind velocity is but one. This probably explains why peaks in the fluctuating sandflow rate and saltation load grain size do not always correspond with the highest-energy wind conditions. These peaks are more likely to be controlled by the sediment input to the aeolian system.

Influence of Stone Pavements on Sandflow Rate

Sand storage within stone pavements is a particularly important aspect of saltation load dynamics in deflation basin environments (Bagnold, 1954). During long periods of sustained high-energy southerly winds, the rate at which sandflow moves into, and progressively along, aeolian transport corridors is determined by the surface-wind energy and sediment supply. The diurnal fluctuation of wind speed profoundly influences this rate, thereby aiding the progressive accumulation of sand stored in the interstices of stone pavements, vegetated sand sheets and aeolian current shadows of various dimensions.

Provided that sediment is available, the sandflow rate will peak during high-energy conditions, especially when high-velocity gusting also occurs. In summer, peak wind velocities are restricted from 13.00hrs to 16.00hrs, and high-energy conditions prevail from 09.00hrs to 20.00hrs on a daily basis. Observations confirm that

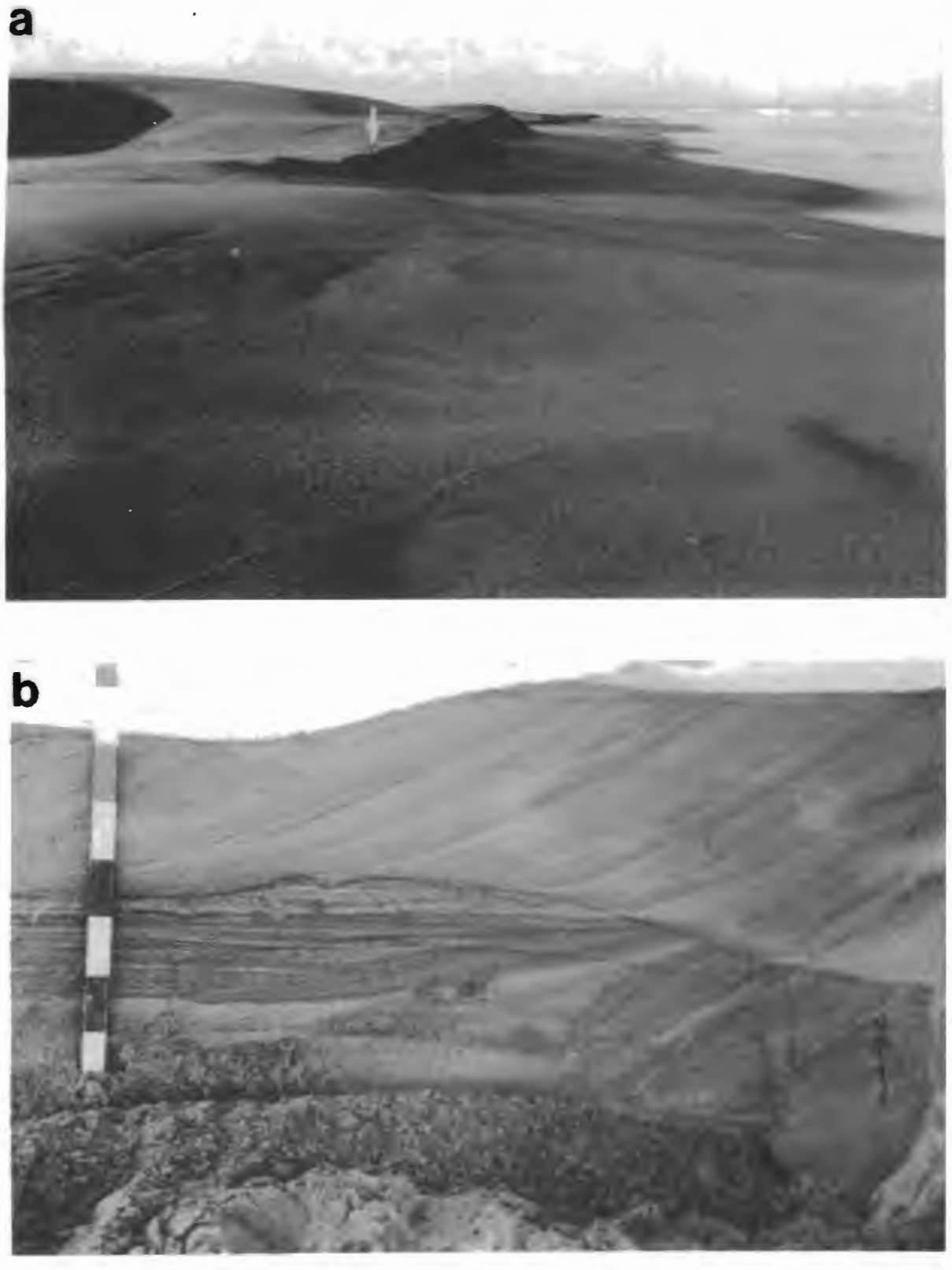

Figure 4.19. (a) Wave erosion of small barchans in the backshore area of Bakers Bay on 29/07/87. Wave energy and storm activity is greatest at about this time of the year. Southerly wind flow from top to bottom. Scale 1 m (arrowed). (b) Longitudinal section through an eroded barchan flank showing bottomsets of the aeolian dune overlying low-angle beach lamination. Southerly wind flow from right to left. In the rock record, these structures could represent the input point to a major aeolian system. Scale in 10 cm divisions.

sandflow usually commences between 09.00hrs to 11.00hrs during the summer, with a significant increase from 12.00hrs to 13.00hrs (Kaiser, 1926). Sandflow conditions are then usually maintained until about 17.00hrs to 18.00hrs when the surface-wind velocity starts to decline. Sandflow therefore moves in daily pulses. The saltation load is progressively entrained as peak wind-energy is approached, and re-deposited as wind-energy drops in the evening. The quantity of sand stored in the system varies in response to fluctuations in the velocity of the surface-wind, and the influence of low-energy wind reversals which interrupt the northward sandflow.

The Occurrence of Very High Sandflow Events

The very high sandflow conditions between 10/2/87 and 12/2/87 produced an abrupt peak in the record of both sandflow rate and total sandflow. This peak should have been more pronounced because observation showed that the majority of sandflow occurred on 10/02/87, and not over the entire trapping period from 02/02/87 to 12/02/87. The build-up to this sandflow event probably reflects the optimum conditions for sandstorm development in the Southern Namib deflation basin (Figure 4.20). A remarkably abrupt peak in southerly surface-wind velocity is sandwiched between two minor wind reversals, which possibly indicate the passage of coastal lows. The wind velocity almost continuously exceeded the threshold for sand movement over a loose granular bed during the persistent, high-energy southerly surface-winds on either side of the reversals. This was followed by an extremely abrupt peak of southerly wind-energy. The wind direction veered from northerly to southerly, and the wind velocity rose sharply from an hourly averaged figure of about 2 m/sec (7 km/hr) to about 19 m/sec (68 km/hr). This was accompanied by very high-energy gusting in excess of 19 m/sec.

The brief, northerly wind reversals prior to the main event, were insufficient to destabilize the equilibrium of the aeolian system with the southerly surface-wind regime. They did, however, disrupt the northward sandflow. This created conditions conducive to the storage of the saltation load within the aeolian system. The pulse of very high-energy southerly wind suddenly entrained this material, resulting in a rapid increase in the sandflow rate.

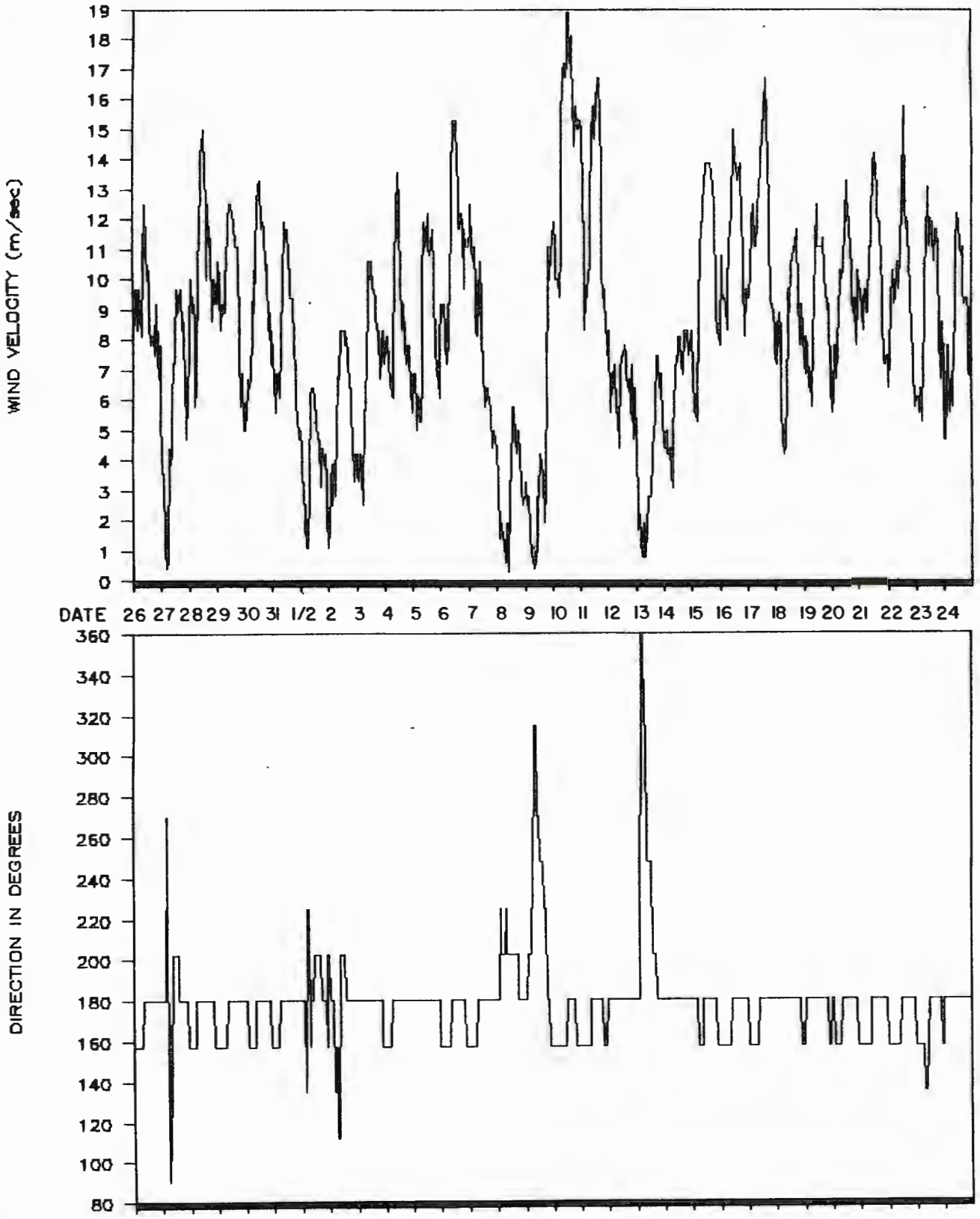

Figure 4.20. Summary of surface-wind velocity and directional variation around the time of the very high sandflow event on 10/02/87.

The increase in beach deflation at Bakers Bay, and the entrainment of material from temporary storage sites during the event accounts for the reduction of the mean grain size at site C. The greater frequency of saltation collision with the bed potentially entrains coarse-grained material into saltation. This probably accounts for the marked shift towards more negatively skewed distributions, and the reduction in the sorting during sandstorms. After the event, fine-grained material continues to migrate past the trap site 25 km down wind of the sediment input point, but the transport of coarser-grained sediment is greatly reduced, and the grain size distribution at site C subsequently became more positively skewed. The increase in the mean grain size of the sandflow passing site C immediately after the high sandflow event possibly illustrates the speed with which the finer-grained saltation load moves through the system. It may also reflect the vertical stratification of saltation load grain size above the bed under very high-energy conditions. The self-limiting nature of beach deflation might also have been activated during rapid deflation, with the result that the input of new material to the system was reduced. Theoretically, increased wave erosion along the coast during very high-energy onshore winds (eg. Shephard and La Fond, 1940; King, 1953) possibly also limits the deflation of beach material by reducing the beach width exposed to the wind.

Variation of the grain size distribution at sand trap site A probably reflects the entrainment of material stored in aeolian coppice dunes in the backshore area, and as aeolian current shadows on the Bogenfels sand sheet. The plan form of these features varies in response to changes of wind direction and wind velocity, because the vegetation acts as a permeable barrier to the wind flow. Under very high-energy conditions, the adjustment of these bedforms to the new conditions potentially supplies an abnormally large quantity of material to the aeolian system. This provides a better explanation than increased beach deflation along the exposed coastline, where beaches are likely to remain too coarse-grained to provide suitable material for deflation. A similar explanation is suggested to explain the variation of samples from site B, just outside the aeolian transport corridor. This sandflow was probably derived from the vegetated sand sheets in the backshore area of exposed stretches of the coastline between Bakers Bay and

Bogenfels. Ordinarily, these trap the sediment which is deflated off the beaches by aeolian processes.

Very high sandflow was maintained until the wind-energy declined. By the time this occurred, the storage reservoir of saltation load had probably been substantially depleted. During the next cycle, the storage reservoir of aeolian sand in the system is progressively built-up.

Two sandstorm events were witnessed during the period from 02/12/86 to 05/01/88. The first, on 16/12/86 accounted for about 9% and the second from 10/02/87 to 12/02/87 for about 14% of the total sandflow measured between 2/12/86 to 05/01/88. A third event is suspected to have occurred in early January 1987, which would account for a further 11%. Thus at least 23% of the sandflow between 02/12/86 and 05/01/88 along the main aeolian transport corridor east of Bogenfels, took place over 2 to 3 days. The infrequent, very high sandflow events are therefore quantitatively extremely important to the sediment dynamics of the deflation basin, which ultimately controls the sediment dynamics of the depositional basin.

The significance of the event on 10/02/87 is even greater when the data from sites A and B is examined. PST data shows that this event accounted for about 19.7% (site A) and 50% (site B) of the total sandflow measured at these sites between 22/01/87 to 08/07/87. Consequently, the peak in sandflow was more pronounced at these sites than at site C within the aeolian transport corridor. This proves that high sandflow conditions are not confined to major aeolian transport corridors during these events. Enormous pulses of sediment throughput thus occur throughout the deflation basin, as sand is entrained from temporary storage sites and effectively flushed into the depositional basin. The increased sandflow increases the frequency of saltation collisions with the bed, which potentially increases the entrainment of coarse material from temporary storage sites into saltation. This is probably reflected in the reduction of sorting observed at all stations on 10/02/87, and the increased negative skewness of the samples. These events are therefore crucial to the dispersal of the aeolian saltation load from its source to the depositional basin. This contradicts the conclusion of Lancaster (1985), who stated that "There is no evidence that infrequent high magnitude "sand storm" events play a

significant role in the Namib". The empirical data presented here proves that they must be very significant events, but their true importance is unlikely to be established by theoretical models of potential sandflow. This is because the quantity of sandflow through the deflation basin is not solely a function of the surface wind velocity, which theoretical models assume to be the case. This empirical study proves that the quantity of sandflow is governed by the complex interaction of:

1) the surface-wind regime;
2) the distribution of coastal sediment supply points;
3) the variation of the quantity of material available for deflation at these points;
4) the distribution of aeolian transport corridors;
5) the quantity of sand stored within the aeolian system.

Grain size analysis of samples from site C, within the aeolian transport corridor, proves that the sandflow within these narrow, wind-aligned zones, is coarser-grained than elsewhere within the deflation basin. Combined with the substantially higher sandflow rate, this makes them potential zones in which optimal conditions for aeolian bedload creep and corrasion exist.

4.2.4. VERTICAL VARIATION OF SANDFLOW AND SANDFLOW GRAIN SIZE

Introduction

The sand trap samples obtained from 0 to 16 cm and 0 to 47 cm above the ground surface were disappointing in one respect. Holding a plastic bag open to the southerly wind at head height during peak sandflow conditions proved that coarser material is transported as part of the saltation load. Unfortunately, it was not until a paper by Sharp (1964) was located that it was realised that it was necessary to have a taller sand trap, and there was only time to monitor the trap for two periods. This allowed the distribution of grain size with increasing height above the bed, and the vertical distribution of the sandflow to be examined.

Results and Interpretation

A compartmentalized sand trap was located on the stone pavement at site C, within the aeolian transport corridor, next to the venturi-compensated trap. The first catching period from 08/07/87

to 20/07/87 caught a surprise catch. A very high-energy, northerly wind reversal occurred, which resulted in very high sandflow from the north. Although the event was not witnessed, a flaw in the design of the PST device allowed material to be caught. Importantly, it could be proved that this flaw did not significantly affect the previous PST device results, because they correlate well with those from the VST which was ONLY able to trap the sandflow associated with the southerly surface-winds. The examination of surface-wind data also showed that wind reversals during the period from 2/12/86 to 28/05/87 were low-energy, and that wind velocities associated with them were insufficient to significantly entrain sand. The second trapping period ran from 20/7/87 to 22/9/87.

The two samples demonstrate that the concentration of the saltation load above a stone pavement surface varies significantly with height (Figure 4.21). Between 40 to 50% of the total sandflow was found to travel in the first 16 cm above the bed. About 30% of the sandflow was trapped at between 16 to 50 cm, and a further 10 to 20% between 50 to 100 cm. Above this, the amount of material travelling in saltation diminished greatly.

Although a major southerly sandflow event was not sampled, the two data sets were used to produce a correction factor for converting the sandflow figures for the PST and VST devices to a figure for the total sandflow passing a 1,83 m high column. It is planned to deploy a further sand trap, which will monitor the vertical distribution of the sandflow over a longer period.

The saltation load grain size also varies greatly with height above the stone pavement surface (Figure 4.22). The major variation is the marked increase in the grain size of the material travelling above 1 m above the bed. The coarsest grains were trapped in the compartment 1.4 to 1.83 m above the bed, in which there was a concomitant increase in the percentage of material finer than 3 phi. One quartz grain that was trapped was slightly smaller than 2.8 mm diameter, and weighed 0.042 gm. It is probable that if the trap had operated for longer, considerably larger grains would have been caught, because observations by myself and other geologists in the area show that quartz grains of about 0.5 mm diameter are occasionally entrained into saltation. Grains of this size possibly travel at heights exceeding 1.83 m above the bed. This is based

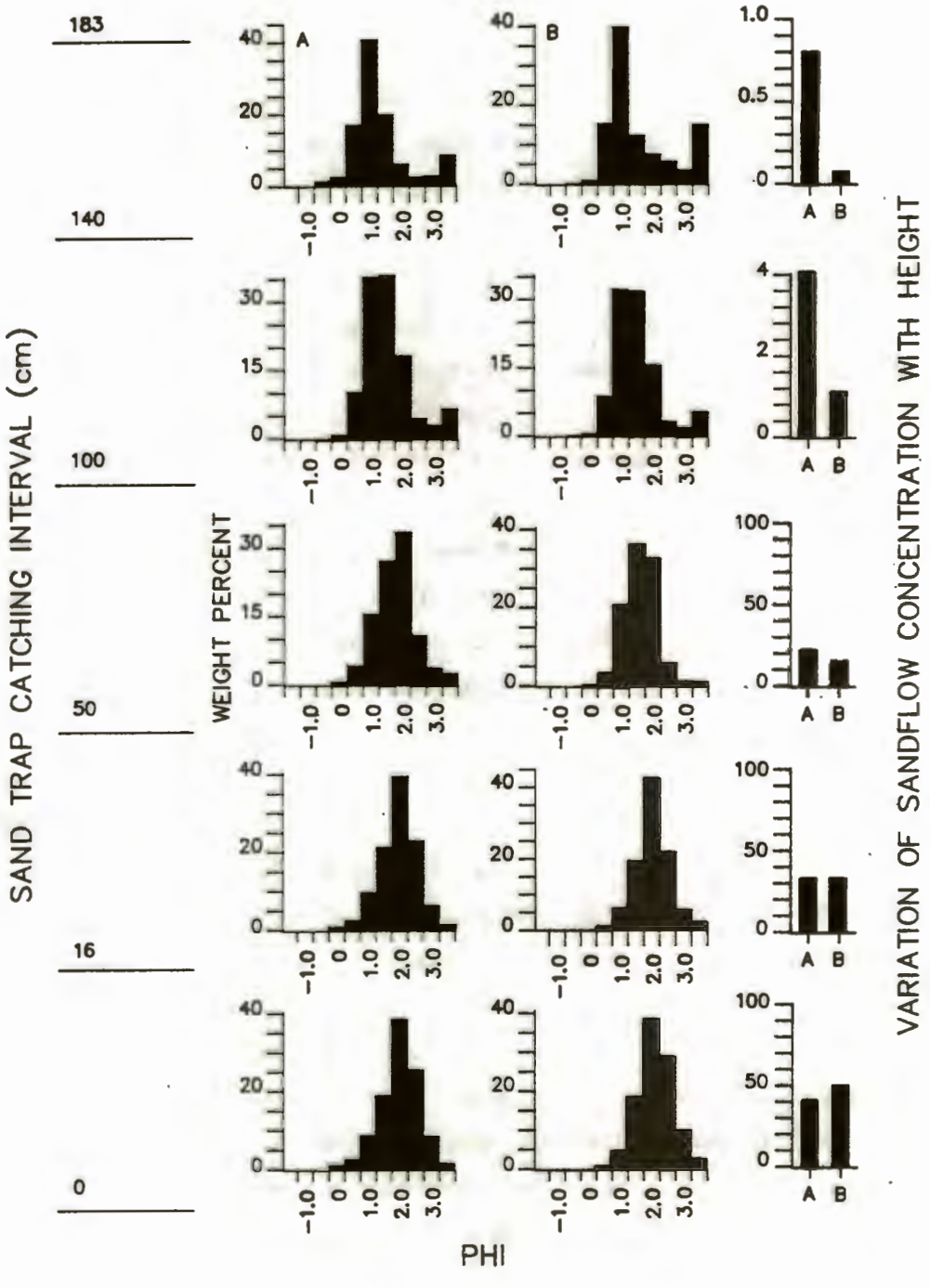

Figure 4.21. Graphs illustrating the variation of saltation load grain size and concentration with height above the stone pavement surface. The data in (a) are from the material trapped during the major wind reversal on 18/07/87, and that in B represents sandflow driven by the southerly wind between 20/07/87 and 22/09/87.

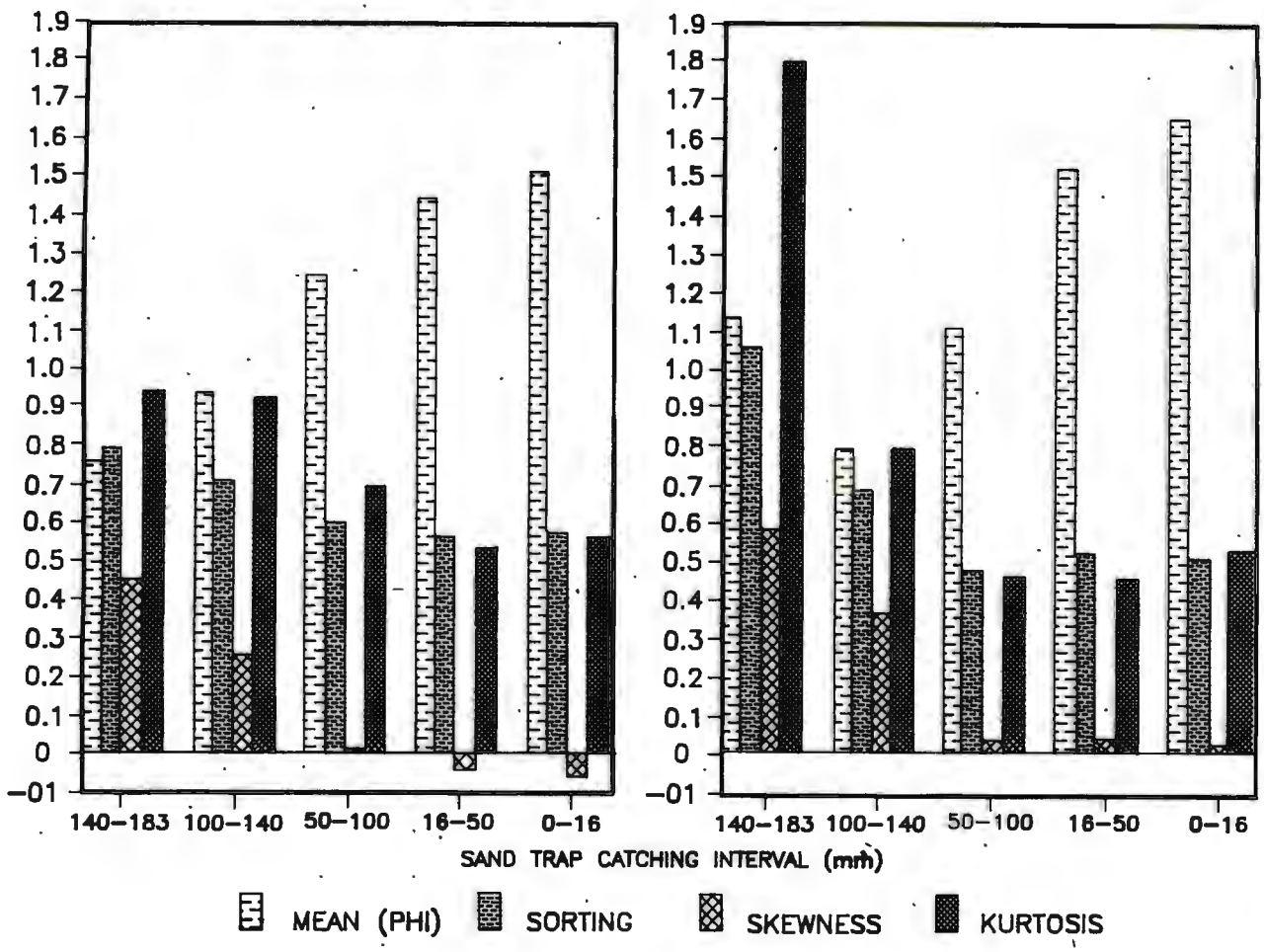

Figure 4.22. Variation of the grain size characteristics of sandflow travelling between different height intervals above the stone pavement surface at sand trap site C.

upon observations during high sandflow conditions at site C, which show that large grains impact on hands stretched 2.5 to 3 m into the wind flow. According to Greeley, Williams and Marshall (1983), saltation particle velocities reach a maximum just before impact, and grains travelling along higher trajectories attain greater velocities. Although these authors found that on average, grains only attain 50 to 70% of the freestream wind velocity, large grains following high trajectories in the Southern Namib are regularly influenced by freestream velocities of 60 to 90 km/hr. Consequently, the grains are potentially capable of attaining substantial forward velocities during saltation, and strike the bed with considerable force. Although there are comparatively few of them, they are therefore likely to exert a considerable influence on the modification of the bed configuration. Because the frequency of saltation impact with the bed, and the grain size of the

sandflow, are both greater within aeolian transport corridors, the entrainment of large grains into saltation is likely to be more frequent within these zones. Coupled with the increased height of trajectory paths due to transport across hard, immobile surfaces of bedrock or stone pavement, the saltation load within aeolian transport corridors should be most effective in promoting aeolian creep transport and in rearranging the bed configuration.

The increase in the percentage of material finer than 3 phi (fine to very fine sand) first becomes noticeable between 1.0 and 1.4 m above the bed. This material is interpreted as representing the suspended load. Hence at some point between 1.0 to 1.4 m above the bed, suspension begins to be an important transport mode.

4.2.5. SANDFLOW DURING NORTHERLY WIND REVERSALS

Introduction

The surface-wind regime of the deflation basin south of the Namib Sand Sea is strongly unimodal. In terms of both the frequency and the wind-energy, southerly to south-south-easterly winds dominate the aeolian sediment dispersal system. Provided that the wind regime remains stable and undisturbed, the aeolian dispersal system establishes equilibrium with the prevailing wind conditions, and aeolian sand is stored in the system. Some of the material is stored within the interstices between roughness elements on stone pavement surfaces, and an enormous amount of sediment is stored as aeolian current shadows in the lee of roughness elements or vegetation. Shadow dunes formed in the lee of topographic highs such as the duricrusted residuals near Pomona (Figure 4.23) provide excellent sites for sand accumulation, and ridges oblique to wind flow provide additional storage sites. This vast reservoir of sand is only subjected to comparatively minor modification by variation of the southerly surface-wind direction and energy. It is, however, fully exposed to the influence of high-energy northerly wind reversals.

Observations

Sustained, high-energy wind reversals rarely occur in the Southern Namib. Two were experienced over the four year observation period, although low-energy reversals were comparatively frequent during the winter months. The first major reversal witnessed

occurred on 21/05/1985. Like the second, which occurred from the 18 to 19/07/87, it was accompanied by rain (see section 4.4.8).

During the first major reversal, sandflow was exceptionally high. Intense sandflow crossed the stone pavement within the aeolian transport corridor at Bogenfels during gusts of 70 to 80 km/hr, and a great deal of material hurtled through the air at heights in excess of 1.5 m above the bed. Barchans of the Bakers Bay dune train were subjected to severe modification by the northerly wind, as the surface-wind accelerated up the former slip-face. At the crests of the 25 to 30 m high dunes, wind speeds in excess of 90 km/hr were measured. The rain-dampened dune flanks were eroded by the north wind (Figure 4.24), as the high-velocity northerly wind hugged the dune surface and converged towards the centre of the normal stoss slope. On the dune flanks, the saltation load did not rise much above knee height. A slip-face about 2 m high developed to the south of the former crest position (due to the southerly wind), as sediment was carried up the former slip-face and over the dune by the north wind. An incredibly powerful eddy occurred in its lee due to flow separation over the crest. Dune sand was swept up by the backflow at the base of the separation bubble. Some of the material was incorporated into the plume of aeolian sand which extended some metres downwind of the reversed crest. The rest was taken back down to the bed by the flow within the separation bubble. This was an incredibly unpleasant position, and detailed observation was impossible. Upon the cessation of the event, aeolian current shadows in the lee of vegetation had been completely reversed to face south, and the dune had been greatly modified. Of particular interest was the development of parabolic bedforms on the dune flanks (Figure 4.25). During the second reversal on 19/7/87, the modification of the dunes was less pronounced, but aeolian current shadows in the lee of vegetation on the stone pavement were entirely reversed.

High-energy northerly winds are potentially capable of reintroducing huge quantities of aeolian sand back into the aeolian dispersal system from southerly wind storage sites. Under these circumstances, unusually high sandflow conditions occur throughout the deflation basin, and are not restricted to aeolian transport corridors. To some extent, this was demonstrated by the unintentional sand trap results for 20/7/87. Unfortunately no

Figure 4.23. Oblique aerial view of the silcrete residual Elfertberg (E), with a large shadow dune formed in its lee. Southerly wind flow is approximately from top to bottom.

Figure 4.24. A barchan dune, about 30 m high, being modified during a northerly wind reversal on 21/05/85. Note the plume of sand extending to the south from the reversed crest, and the large eddy formed by flow separation over the crest.

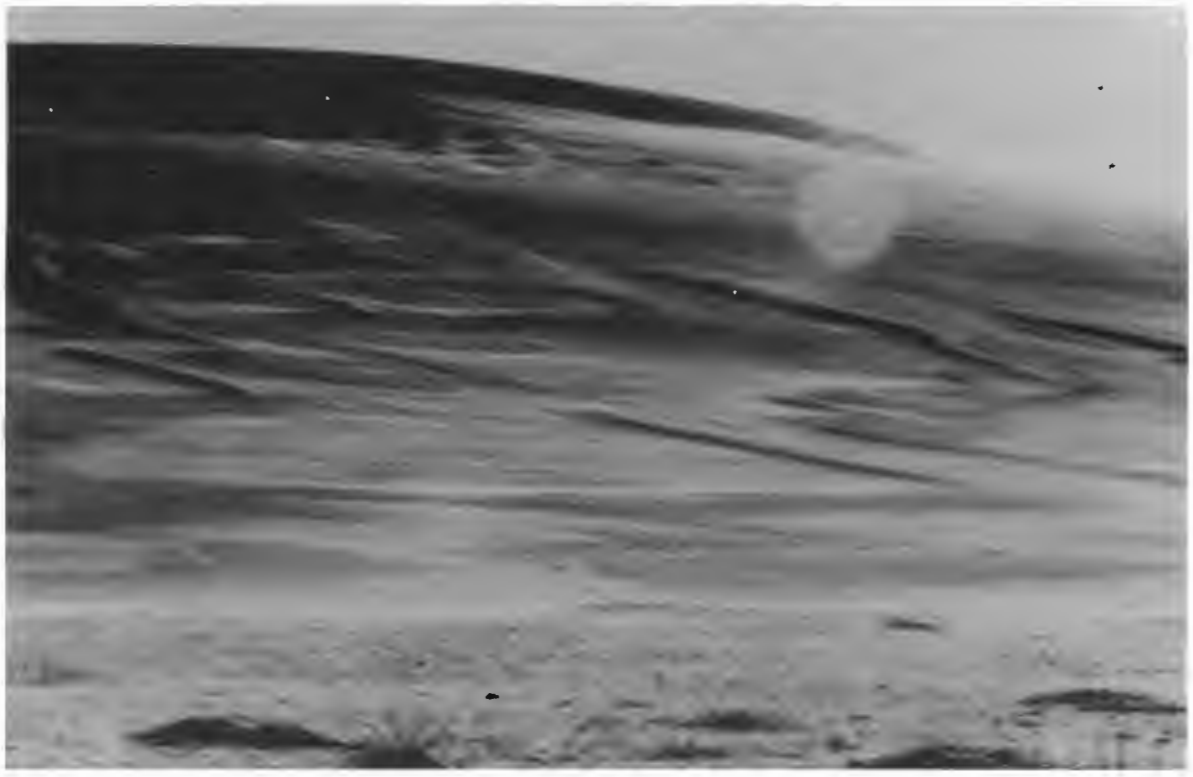

Figure 4.25. Parabolic bedforms about 20 to 30 cm high on the eroded flank of a barchan dune. Note the scoured depression in the lee of the reversed crest, and the uneven nature of the sand surface, which provides evidence of the erosive power of the eddy within the separation bubble. The final height of the reversed slip-face was about 3m. The dune was about 25 to 30 m high after the reversal had modified it.

estimate of sandflow from the material trapped was possible, but this was the first time that the PST devices at sites A and B caught appreciable quantities of saltation load.

4.2.6. CONCEPTUAL MODEL OF SANDFLOW THROUGH THE DEFLATION BASIN

Sandflow Governed by the Southerly Surface-Wind Flow

It has been shown that the Bakers Bay barchan dune train defines the position of the maximum areal concentration of sandflow within an aeolian transport corridor. Other dune trains can therefore be used to identify similar aeolian transport corridors within the present-day deflation basin. On this basis, three major aeolian transport corridors are currently active. These originate at Chameis Bay, Bakers Bay and Prinzenbucht respectively (Figure 4.26). A fourth, smaller aeolian transport corridor, commences in the vicinity of Van Reenan Bay. It has previously been determined that these barchan dune trains originate at either log-spiral or south-facing embayments (Kaiser, 1926; Hallam, 1964; O'Brien, 1972; Rogers, 1977). Their full implications with respect to the aeolian sediment dynamics of the deflation basin have not, however, previously been realised.

According to empirical sand trap data from this study, the sandflow within aeolian transport corridors greatly exceeds that occurring elsewhere within the deflation basin. This is the first time that such zones have been defined within an aeolian deflation basin. The secondary flow pattern which is postulated to be maintaining them has previously been found to influence the distribution of finer-grained particles such as dust and pollutants within the atmosphere (eg. Brown, 1983). The delineation of four of these high sandflow zones therefore has important implications for the study of the aeolian bedload creep dynamics. Theoretically, optimal conditions for bedload creep transport occur within aeolian transport corridors. The bedload transport rate within these linear zones should therefore be higher than elsewhere within the deflation basin.

During persistent southerly surface-wind conditions, the aeolian sediment dispersal system establishes equilibrium with the prevailing wind conditions. Provided that abrupt peaks in the wind velocity do not occur, the saltation load is progressively stored

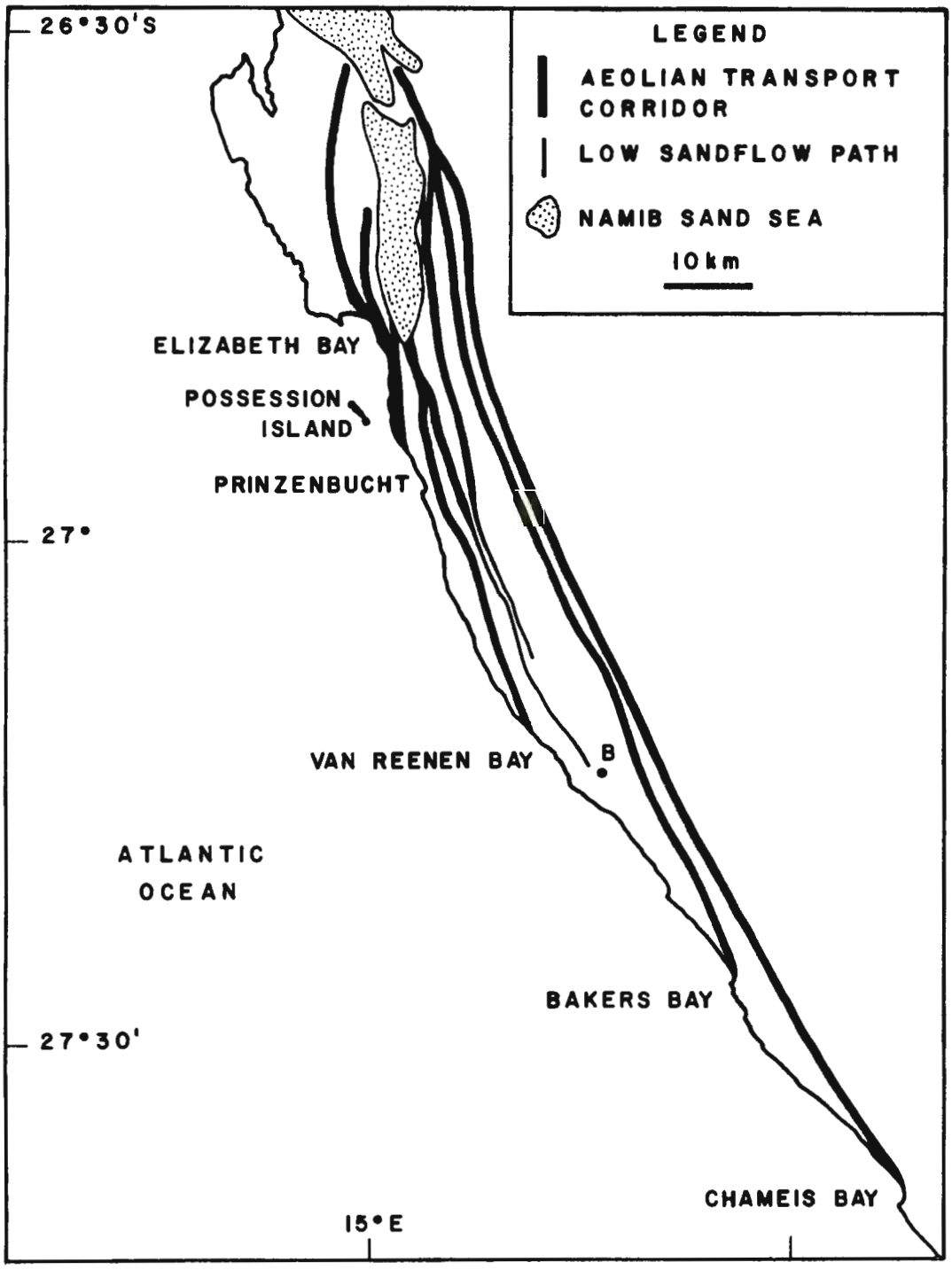

Figure 4.26. Conceptualised distribution of sandflow through the present-day deflation basin, from coastal point sources, via aeolian transport corridors into the Namib Sand Sea.

within the system.

The position of aeolian transport corridors is primarily governed by the coastal morphology. This controls the distribution of embayments in which the marine deposition of material suitable for aeolian deflation occurs. Sea-level movement, resulting in changes in the coastal morphology, will theoretically modify the deflation basin sediment dynamics by altering the sites of sediment input to the aeolian system. This important concept, arising from this study, has implications for the interpretation of palaeo-aeolian system dynamics within the Namib.

Sandflow Governed by Northerly Wind Reversals

During persistent southerly wind conditions, the aeolian system moves towards a state of equilibrium, and a vast storage reservoir of aeolian sand accumulates. The brief, high-energy pulse of a major wind reversal disrupts this equilibrium, and basin-wide, high sandflow conditions occur as the stored material is entrained. This reintroduces large quantities of aeolian sand back into the aeolian system from the temporary storage sites. Provided that the northerly wind reversal is of sufficient energy and duration, the aeolian system will move towards equilibrium with it. During the subsequent return to southerly wind conditions, high sandflow conditions are again probable on a basin-wide scale, as the aeolian system re-establishes equilibrium with the prevailing southerly wind regime. This brief alternation of the sandflow direction in response to northerly wind reversals may, therefore, ultimately result in a brief peak in the sandflow entering the Namib Sand Sea. Reversals are thus considered to be significant events in terms of deflation basin sediment dyanamics. The collection of a substantial, empirical data base for sandflow through the system would be required to fully confirm this hypothesis.

Overall Movement of Sandflow

The barchans of the Bakers Bay aeolian transport corridor vary in height from about 26 m (measured during this study) to 33 m (Kaiser, 1926). Based upon extensive observations by Bagnold (1954), this is close to the maximum size for solitary dune forms of this type. Kaiser (op. cit.) monitored a 33 m high barchan, which advanced 136 m to the north over 34 months. This is equal to

a migration rate of about 48 m/year. This figure is in reasonable agreement with my own observations which give a rate of about 37 m between 15/10/86 to 05/01/88, and the estimate of 30 to 56 m/year by Endrody-Younga (1981), for comparable barchans in the Grillental area.

Measurements during this study showed that although some reversal in the dune migration direction does occur in response to northerly wind reversals, the dominant direction of migration is northward.

4.3 SEDIMENT DISPERSAL BY AEOLIAN BEDLOAD CREEP

4.3.1. INTRODUCTION

Comparatively few studies of the aeolian creep process have been made. The basic concept that saltation impact propels larger grains over the bed is well established (eg. Bagnold, 1954). More recently, Willets and Rice (1986) have experimentally examined the mechanics of the collision process.

It has not been possible to study the process of aeolian creep in detail under controlled conditions during this study. It is very difficult to observe what is happening under field conditions, when it is barely possible to see the ground surface, let alone attempt time lapse photography. The main aim during this study has therefore been to examine whether creep occurs or not, and if so, to examine the possible implications for sediment dispersal within the deflation basin. The modification of the bed configuration by creep has also been examined. This is discussed in section 4.4.

4.3.2. EVIDENCE OF CREEP, AND ITS INFLUENCE ON THE BEDLOAD

The Transport of Garnet Creep Tracers by Aeolian Processes

Between 27/07/87 to 05/01/88 a 26 m high barchan, comprised mainly of medium- to coarse-grained quartz sand, migrated 13.2 m to the north within the Bakers Bay aeolian transport corridor. Over the same time period, bedload creep tracers of very coarse sand to granule sized garnet grains released about 200 m west of the measured dune, migrated only about 1.5 m (Figure 4.27). By the time the bed was sampled again on 23/11/88, the main concentration of garnet grains was located between 2 to 3 m north of the starting position. This indicates that a garnet creep bedload advances about 8 or 9 times more slowly than a barchan at this point within the aeolian transport corridor.

Evidence of Size-Sorting During Creep

Initially, the entire 1 m long line of garnet grains laid perpendicular to the southerly surface-wind flow moved forward en masse (Figure 4.28). As the experiment proceeded, some of the garnet grains continued to migrate to the north, whilst others remained behind. The stone pavement surface over which the garnet grains were being transported was first sampled on 05/01/88, and subsequently on 23/11/88. The garnet creep tracers were recovered from surficial stone pavement samples of 0 to 2 cm depth, taken in a line parallel to the southerly wind regime. Grain size distributions for the garnet creep tracers illustrate the progressive decrease in mean particle size to the north of the starting point (Figure 4.29). The smallest garnet grains have evidently advanced a greater distance. This is evidence of aeolian size-sorting by creep. If a quarter phi sieve size class contained less than 10% of a sample's total garnet population, it was assumed to represent the migration limit of that grain size. The rate of advance for that grain size relative to the barchan dune was then calculated.

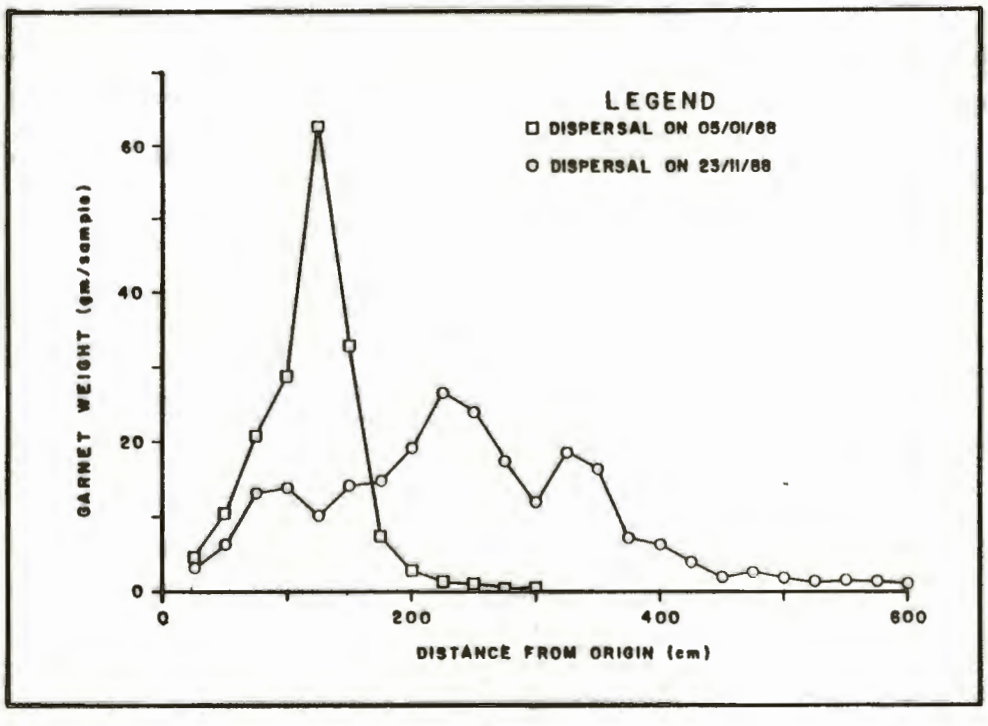

Figure 4.27. Graph showing the amount of creep transport undergone by garnet bedload creep tracers between 27/07/87 and 23/11/88.

phi decreased abruptly (Table 4.1). This data is

Table 4.1. Variation in the rate of creep transport for different size fractions of garnet relative to the rate of a barchan dune between 15/10/87 to 5/01/88. Measurements were taken within the Bakers Bay aeolian transport corridor to the east of Bogenfels.

GRAIN SIZE (PHI)	ADVANCE (m)	RATE SLOWER THAN DUNE
-1.5 TO -1.0	0.75	17.3
-1.0 TO -.75	1.50	8.6
-.75 TO -.50	7.50	1.7
-.50 TO -.25	9.00	1.4

interpreted as evidence for a change in the entrainment potential of the garnet grains, with grains smaller than -0.75 phi (1.68 mm) being more susceptible to transport by both saltation and creep. A cut-off of 3m from the origin was employed to limit those samples used for defining the statistical parameters of the garnet grain size distribution (Figure 4.29). Beyond this distance, the sample size as at 05/01/88 was found to be too small to adequately define the distribution. Small sample size possibly explains the sharp reduction of the mean grain size and other parameters at 200 cm from the origin. The sorting of the garnet grains comprising the samples also increased to the north, confirming the subtle influence of aeolian size-sorting. The values of skewness for the distributions also systematically changes to the north. Near the origin, the samples were strongly coarsely skewed, with the change to finely skewed distributions occurring about 120 cm to the north. The coarse tails of the intial samples are interpreted as the result of the progressive sorting of the original material. The coarser, slower moving garnet grains were left behind by the smaller faster moving ones. This probably accounts for the segregation of the garnet grains into three distinct peaks when the surface was re-sampled on 23/11/88. The change from negative to positively skewed distributions, for samples taken on 05/01/88, approximately corresponds to the point at which the rate of garnet movement slower than a barchan dune decreased abruptly. The mean grain size of the garnet at this point was found to be -0.75 phi. This is interpreted as support for the idea that the entrainment potential of garnet grains less than or equal to this size is much

Figure 4.28. Dispersal of the garnet bedload creep tracers by aeolian processes. By 05/01/88 the initial line of garnet grains had been transported about 1 to 1.5 m to the north across the stone pavement. The original starting point is marked by a pile of stones near the scale. Southerly wind flow from bottom to top, scale 1 m.

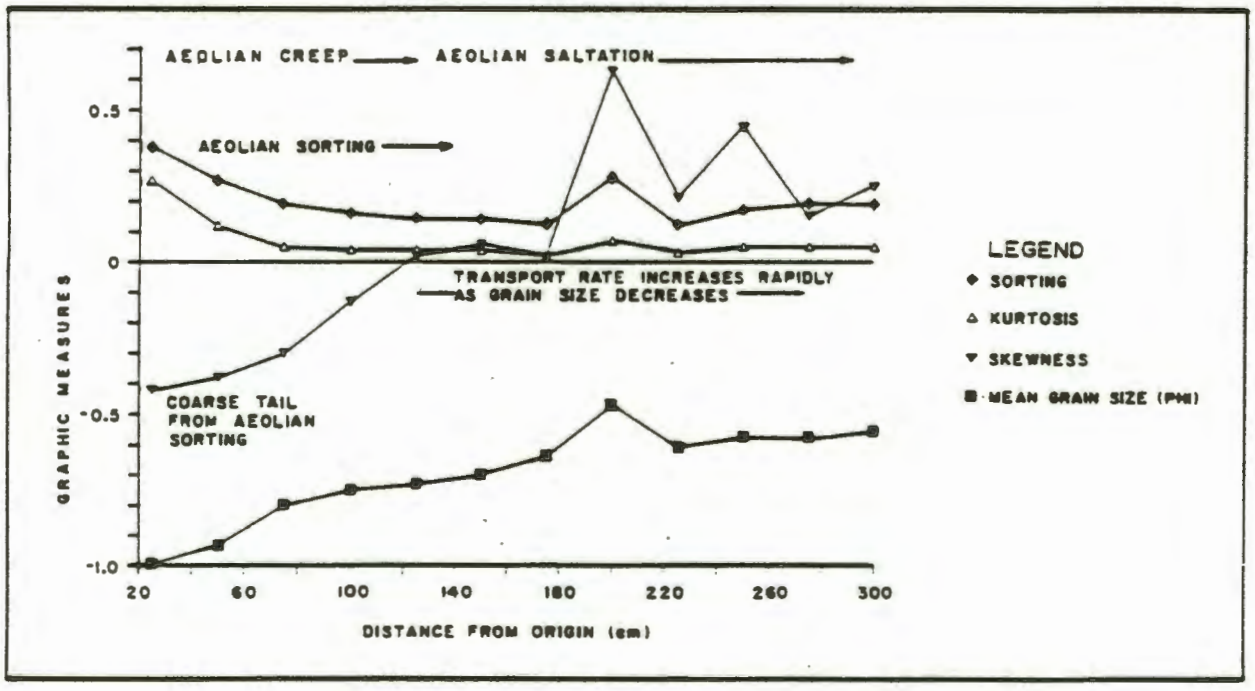

Figure 4.29. Graphs showing the variation of garnet grain size over the first 3 m of the stone pavement surface to the north of the release line on 05/01/87. The size of the garnet tracers decreases progressively to the north of the starting line, providing evidence for aeolian size-sorting.

greater than for larger grains. The transport of garnet grains smaller than -0.75 phi is probably maintained during comparatively low sandflow conditions, when the force of saltation collisions is relatively small. As the garnet grain size increases, so too does the dependence upon the collision of large saltating grains to entrain the grains into creep or saltation. A small percentage of the saltation population is comprised of quartz grains coarser than -1.0 phi, and observations indicate that this material is mainly active during infrequent high sandflow events. The probability of

garnet grains coarser than -0.75 phi being entrained into transport is therefore reduced because these grains, which are denser than quartz grains, are probably transported primarily by creep driven by relatively rare large, high-velocity particles in saltation.

4.3.3. AEOLIAN SIZE-SORTING WITHIN AEOLIAN TRANSPORT CORRIDORS

Sample Collection

Surficial samples were collected from the windward slope of a 28 m high barchan dune and the surrounding stone pavement (Figure 4.30) within the Bakers Bay aeolian transport corridor east of Bogenfels. The sand to small pebble fraction of each sample was sieved, to examine whether the variable transport rates of the aeolian saltation and creep loads modify the grain size of the material composing the bed.

Presentation of Results

The grain size distributions of a selection of the samples collected are shown in Figure 4.31. A very coarse-grained lag deposit was present at the base of the barchan's stoss slope (sample K). This lag was separated from the underlying stone pavement by cross-stratified toesets of aeolian dune sand, marking the former dune position. Grain size analysis of this material revealed a weakly bi-modal distribution, with a minor population of quartz granules and small pebbles (Figure 4.32), but the majority of the material is very coarse quartz sand (1 to -0.5 phi).

About 48 m up the stoss slope (sample L) granule ripples ascend in a wind-aligned street towards the slip-face (Figure 4.33), but they do not reach it. Samples L to O demonstrate that the granule ripples in the centre of the street are coarser-grained than those above and below on the stoss slope. There is a tendency for the grain size to decrease up the stoss slope, but granules are still present near the crest at sites N to O.

Grain size distributions for newly exposed stone pavement along the windward base of the dune (samples F, G, and I) do not exhibit the same bimodal form as those from the stone pavement to the west of the barchan. Pronounced peaks in the distribution of sample F, suggest a tri-modal deposit. Very coarse sand forms the largest proportion of the sample, with smaller peaks of medium to coarse

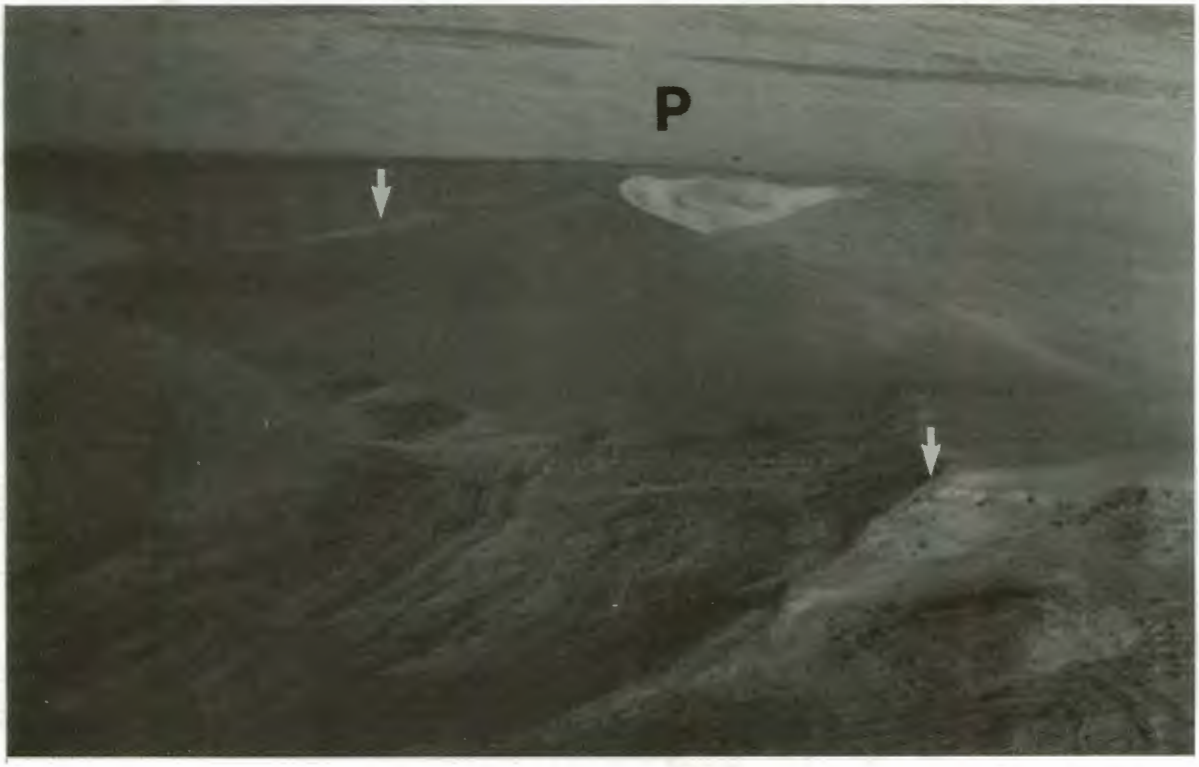

Figure 4.30. Oblique aerial view west, across the 28 m high barchan dune and the stone pavement (P) which were sampled. Note the granule ripple street on the dune's stoss slope (arrowed), the large ripples on the eastern flank of the dune, and the granule ripples and encroachment deposit along its skirt. North pointing, white, quartz granule streaks in the lee of a flow transverse, downwind-facing bedrock step (arrowed), prove that aeolian creep transport is predominantly to the north.

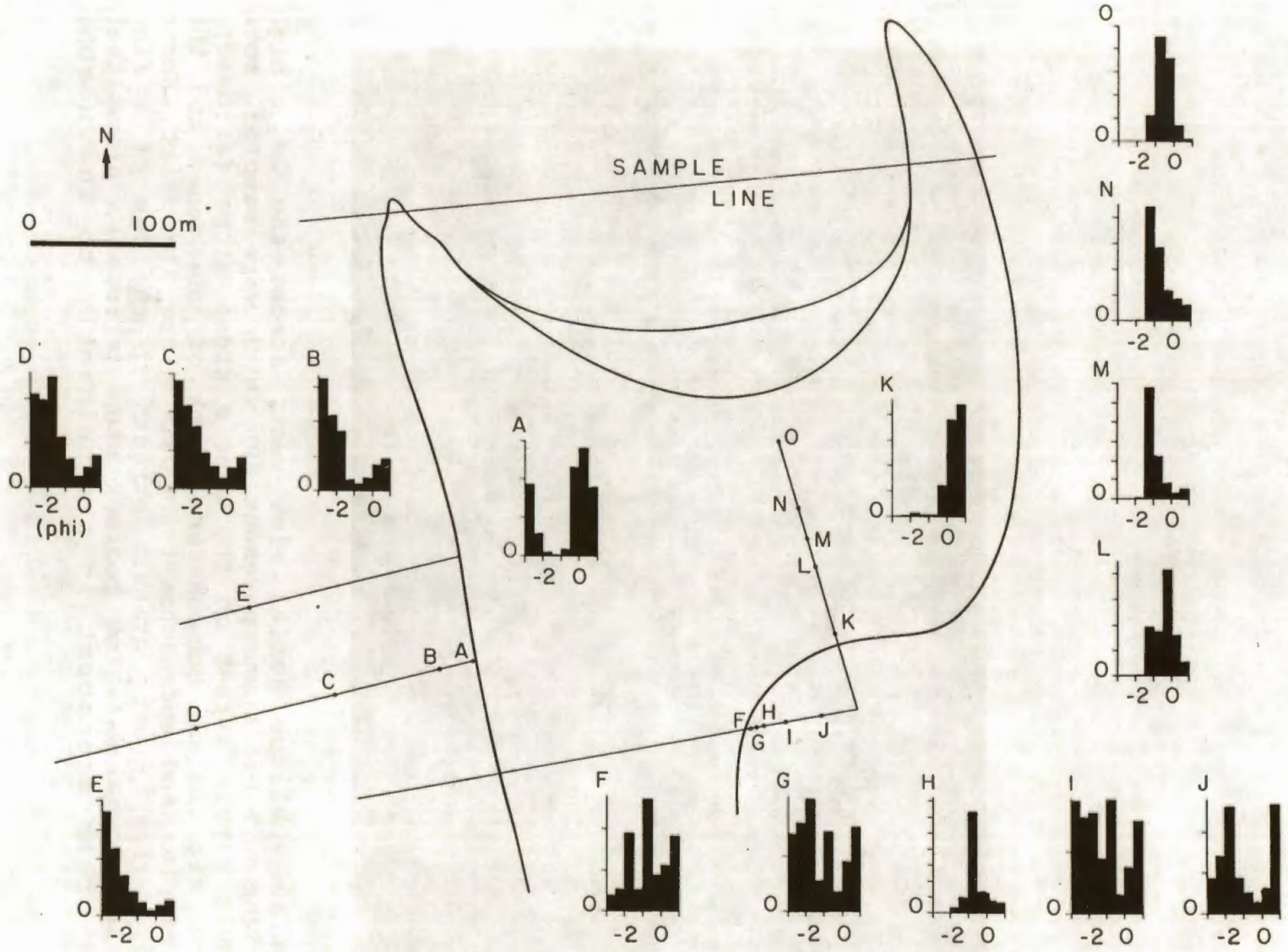

Figure 4.31. Grain size distributions of samples from a 28 m high barchan dune and stone pavement within the Bakers Bay aeolian transport corridor, near sand trap site C. The vertical axes of all graphs are in units of 10 percent

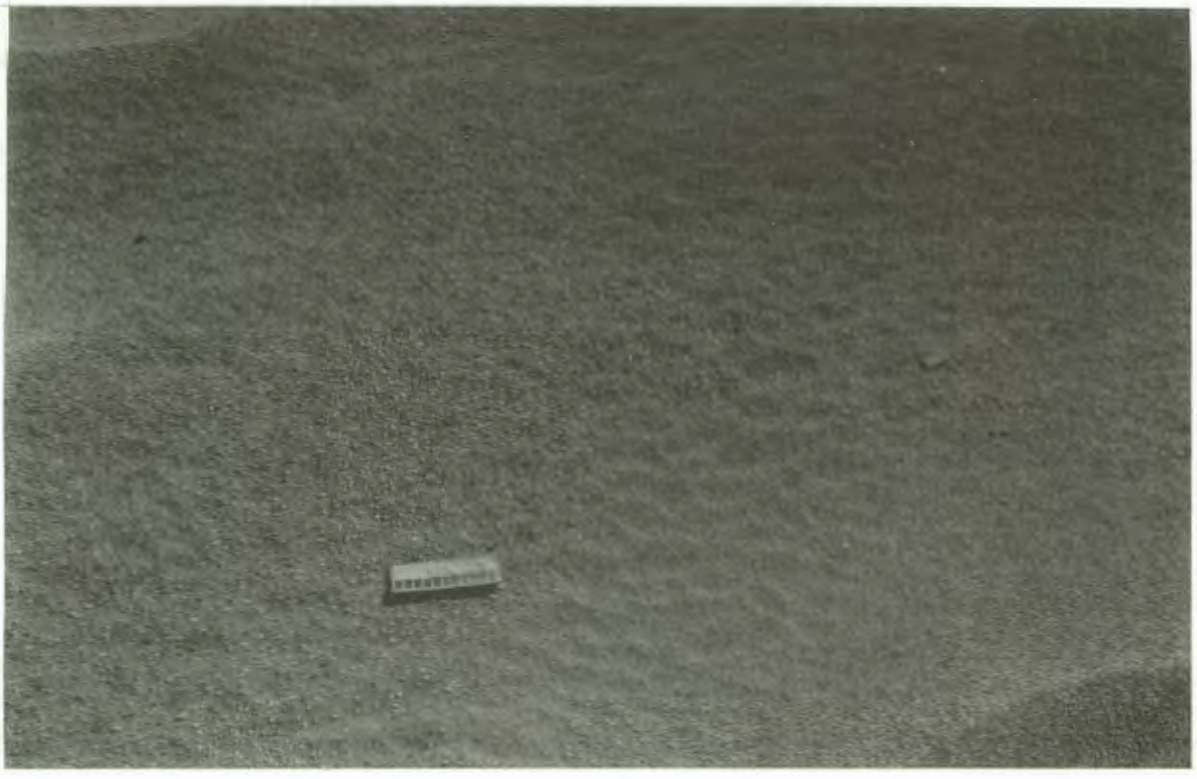

Figure 4.32. Skirt of Barchan stoss slope (sample K), showing very coarse-grained lag deposit overlying toesets, which develops as the barchan migrates to the north. Scale 11.5 cm long.

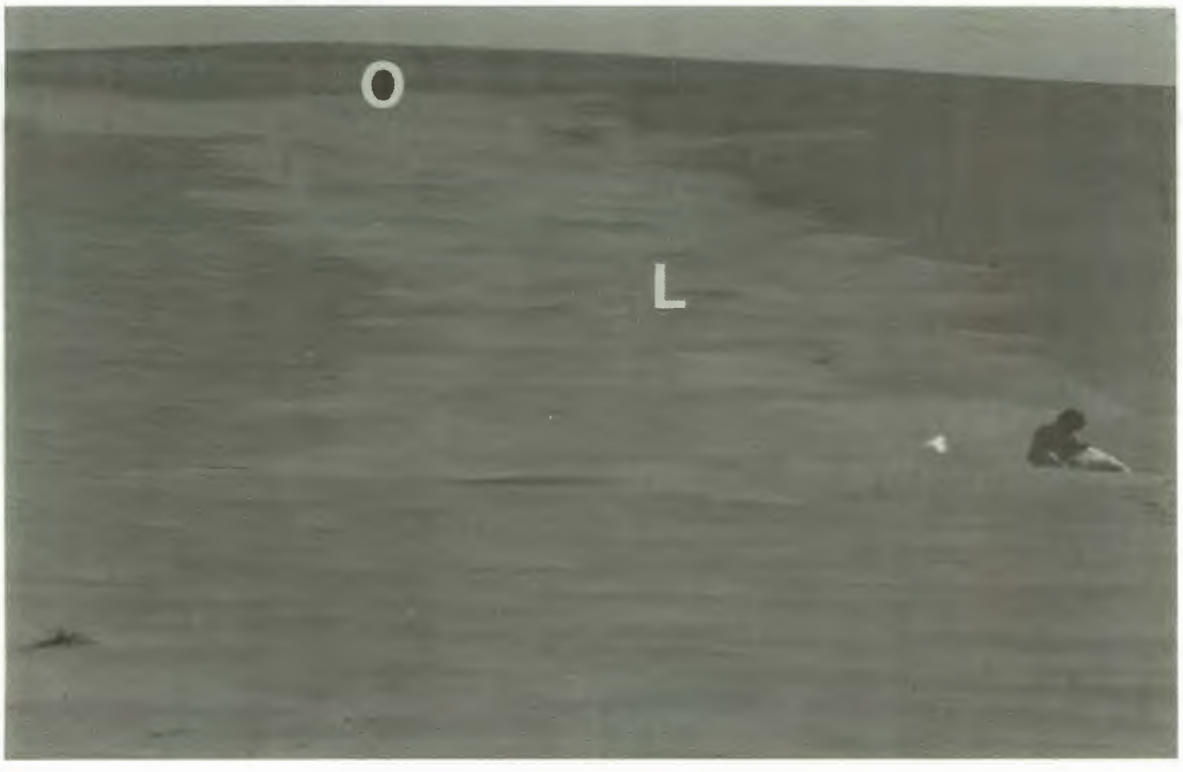

Figure 4.33. Granule ripple street ascending the stoss slope of the 28 m high barchan (samples L to O). Note that the ripples do not commence at the base of the slope, and that they do not reach the crest. Person sitting for scale.

quartz sand and granules. Coarser fractions dominate sample G, where a pronounced peak in the quartz granule to small pebble range occurs. This reflects the start of granule ripple development at this point. The progressive increase in the percentage of the granule and small pebble fractions, together with the emergence of immobile clasts because of deflation are important factors in the stabilisation of the bed (Figure 4.34).

Granule ripples at sample site H, near the dune skirt, are well-sorted, and material finer than 0 phi has largely been removed. Material of 0 to -2 phi is thus concentrated at the surface by aeolian size-sorting. The continued introduction of sediment between 0 to -2 phi by aeolian creep from the south blankets the bed, forming an encroachment deposit along the upwind margin of the dune skirt. No encroachment deposit was present at site I, which is relatively poorly sorted. Deflation of the sand which remains after the passage of the barchan had left pebbles, introduced by alluvial and weathering processes, forming roughness elements on the stone pavement where large quantities of aeolian sand is temporarily stored.

With increased duration of exposure to the influence of the southerly surface-wind, grain size distributions become noticeably more bimodal. Sample J shows that as the coarse to very coarse sand fractions are removed by aeolian processes, there is a relative increase in the granule to small pebble fractions along the dune skirt. An encroachment deposit is formed in response to the accumulation of creep bedload at the base of the barchan stoss slope (Figure 4.35).

Although the surficial concentration of the coarser-grained material on the bed progressively increases upwind of the barchan, after its passage over the surface, the amount of sand fraction remains significant. The sand is either stored as current shadows in the lee of vegetation, or large roughness elements (clasts) on the bed, or in the interstices between the roughness elements. In contrast, samples from the stone pavement west of the dune train do not contain a significant sand fraction.

The grain size distributions of the stone pavement samples (B to E) are distinctly bimodal, and more strongly skewed towards the coarser fractions. Along the western margin of the dune skirt (sample A), the sand fraction remains significant due to very

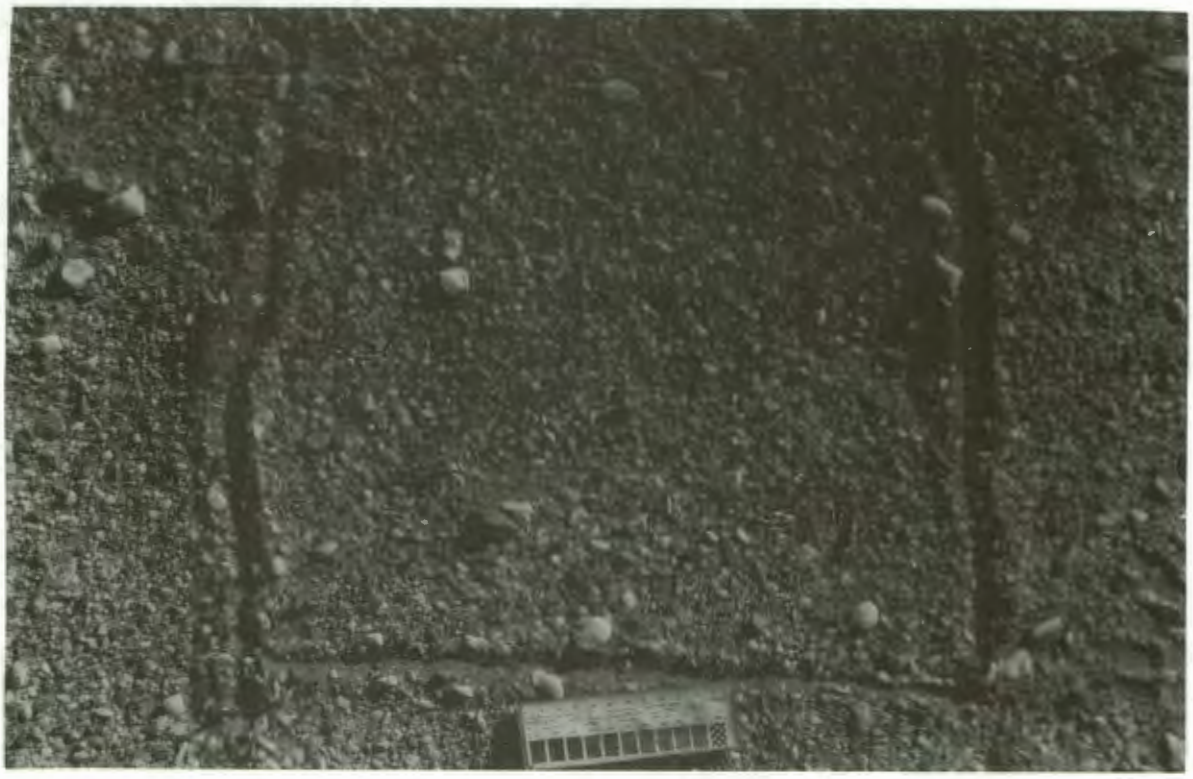

Figure 4.34. Stone pavement surface development is accomplished by the concentration of the granule and small pebble creep bedload on the surface, and the emergence of immobile roughness elements. Scale 11.5 cm.

Figure 4.35. View south from barchan crest, showing the street of granule ripples on the stoss slope, and the encroachment deposit (E) along the dune skirt.

coarse to coarse sand ripples migrating across the stone pavement surface with the barchan (Figure 4.36). Moving west, there is a rapid transformation, as the granule and pebble fractions become dominant, and the sand fraction becomes subordinate (samples B to E). There is a visible increase in the percentage of quartz granules on the bed, until this eventually becomes the dominant component (sample D) (Figure 4.37). In other cases (samples C and B), the small to medium pebble fraction is the major component.

Interpretation

Upwind of the barchan skirt the newly exposed bed containing a large proportion of dune material is reworked by aeolian processes. This grain size distribution is progressively modified by the removal of material by aeolian processes, as predicted by experiments and observations by Bagnold (1954).

Initially, the grain size distribution of material upwind of the advancing dune exhibits three peaks (sample F). The medium to coarse and coarse sand fractions represent the material transported both by saltation and creep, whilst the granule fraction predominantly migrates by creep. The variable rate of removal, which is dependent on grain size for a uni-density sediment, results in the pervasive alteration of the grain size distribution of material resting upon the bed. The granule and pebble fractions therefore accumulate on the bed, as the finer-grained material is selectively removed.

The barchan dune migration rate of about 30 to 50 m/year means that the bed immediately in their path is continuously in a state of flux, because it is alternately covered and exposed by the migrating dunes. As the removal of material progresses along the upwind margin of the dune skirt, well-sorted very coarse sand and granules accumulate to form granule ripples oriented transverse to the southerly wind flow. Theoretically, this position within the aeolian transport corridor corresponds to the point at which the areal concentration of sandflow peaks. The collision bombardment of the creep grains by the saltation load should therefore be most frequent here, so that entrainment of the coarse material into creep, and possibly saltation is potentially greater.

According to Willetts and Rice (1986), the creep rate increases up an inclined plane. However, the vigour with which saltation is

Figure 4.36. Small, very coarse sand ripples of the barchan skirt migrating across the stone pavement surface on the western margin of the dune. Southerly wind blows from bottom to top of frame. Scale 11.5 cm.

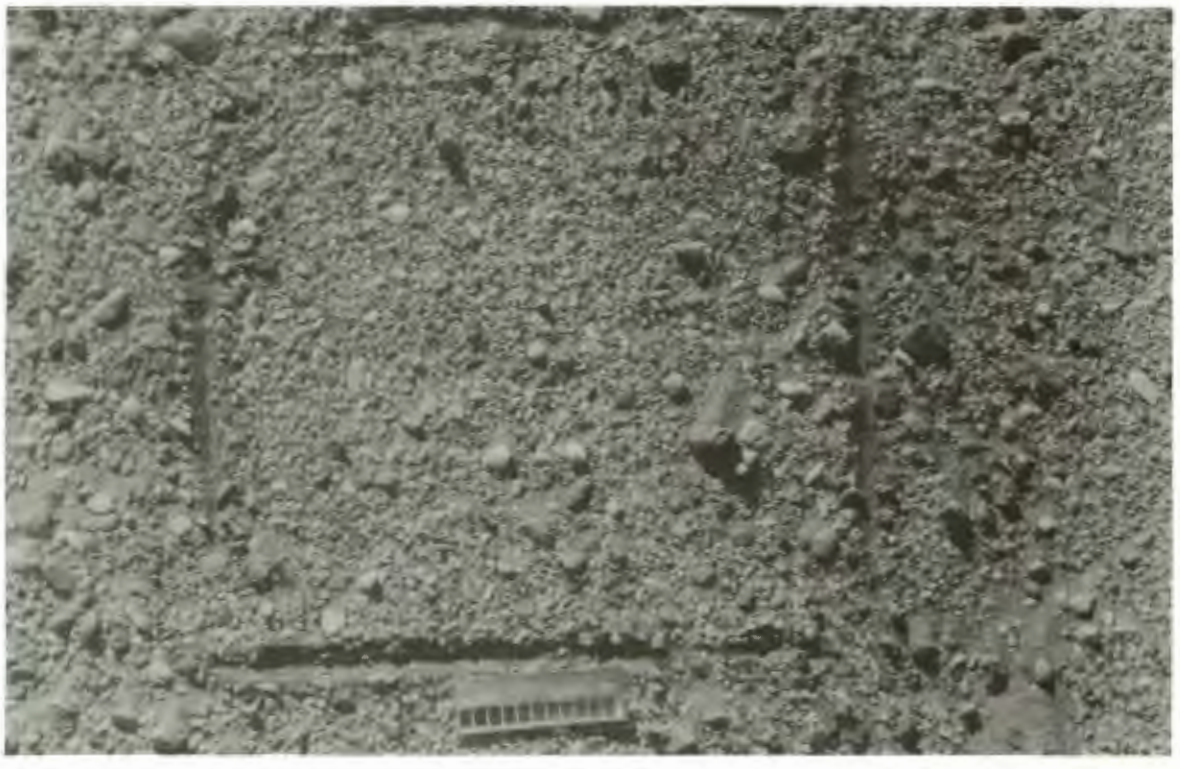

Figure 4.37. Stone pavement west of the barchan dune train comprised mainly of quartz granules and small pebbles between widely scattered immobile roughness elements. Note the sand storage within aeolian current shadows in the lee of roughness elements. Southerly wind flow from bottom to top. Scale 11.5 cm.

propagated declines because of the slope of the bed, which alters the magnitude of the vertical and horizontal components of saltation collision momentum. Thus a combination of the increased concentration of sandflow, and the changes in saltation grain momentum imposed by the stoss slope, possibly explains why creep transports some of the granule fraction up the barchan stoss slope, but not completely to the dune crest. In order to maintain the granule ripple street, some granules at the base of the barchan are required to be advancing faster than the dune. About 48 m up the stoss slope granule ripples about 30 to 40 cm high form. The height of the bedforms increases up-slope until they are about 50 cm high. From this point on, the grain size of the material declines progressively, until about 140 m up the stoss slope, there is a rapid reduction of granule ripple size, and the bedforms are only 5 to 10 cm high. Further up, they die-out, and rippled dune sand separates them from the slip-face. The point where this occurs conceivably indicates the limit to which granules can be readily transported by creep, since they appear to be absent nearer the crest. Aeolian size sorting is therefore occurring on the stoss slope. This is possibly the result of a number of factors:

1) reduction in the concentration of the saltation load with increasing height up the stoss slope;
2) the increased dissipation of saltation grain kinetic energy on a sandy substrate resulting in reduced saltation trajectory height and path length;
3) a change in the incident angle of the saltation load relative to the sediment surface and alteration of the direction of the resultant impact force;
4) alteration of the surface wind flow across the dune.

When the creep bedload encroaches onto the dune, observations indicate that the smaller grain sizes migrate up the slope at a faster rate. On the stoss slope of barchans to the north of the Grillental, ripples composed of very coarse sand also diminish as they approach the crest. On examples north of the Grillental, a small percentage of the coarse grains on the dune surface were observed advancing towards the crest. On reaching this point, they were incorporated into avalanche tongues, which cut back into the crestal area of the dune (Figure 4.38). The coarse material associated with an individual barchan dune therefore appears to be

Figure 4.38. Avalanche tongues cutting back into a barchan slip-face, and transporting very coarse sand grains from the top of the stoss slope onto the slip-face. Scale 1 m.

recycled as the dune advances (Figure 4.39).

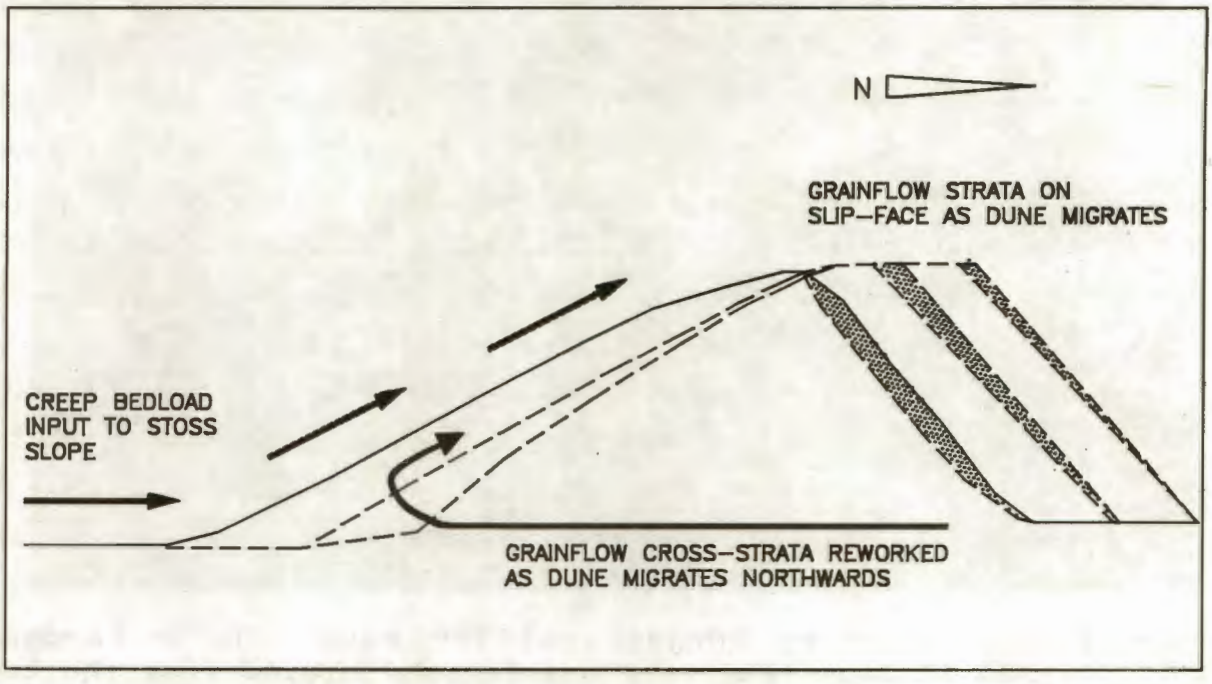

Figure 4.39. Sketch illustrating the cycle of reworking to which the coarse grained material associated with the dune is subjected.

Some granules will be deposited on the bed as the dune advances. Thus to maintain the granule ripple street, some granules in the creep bedload must migrate at a similar rate to the dune, which is very fast compared to the garnet creep tracer migration rate measured about 200 m west of the sampled dune. These observations confirm that aeolian transport corridors are probably optimal sites for creep transport. Not only do the corridors represent zones of high sandflow, they are also linear, wind-aligned zones along which the creep transport rate is very high. On the basis that the areal concentration of sandflow probably diminishes away from the dune train, it is suspected that the creep transport rate varies laterally across aeolian transport corridors (Figure 4.40).

Conditions affecting the stone pavement to the west of the barchan dune train differ, because the bed is not traversed by barchan dunes. It is thus a more stable environment, in which aeolian processes governed by the southerly surface-wind flow operate uninterruptedly over comparatively long periods of time.

The population of garnet creep tracers released on the sampled stone pavement, near sand trap site C, within the aeolian transport corridor proved that material is rapidly redistributed by creep, resulting in size-sorting of the sediment. The comparison of stone pavement samples (sites B to E), with those of granule ripples from the barchan's stoss slope (samples L to O), and other granule ripple samples from the study area, demonstrate an interesting correlation. The peaks of the well-sorted granule ripple distributions coincide with the troughs in the bi-modal stone pavement distributions (Figure 4.41). As confirmed by the garnet creep tracers, particles between -2.5 and -0.5 phi are transported northwards by creep. The absence of this range of grain size is therefore interpreted as evidence for progressive aeolian modification of the bed between immobile roughness elements. Thus from a wider starting distribution, the grain size of the sediment comprising the stone pavement surface has gradually increased through time. The continued input of creep bedload from the south over a long time period has probably further altered the grain size distribution.

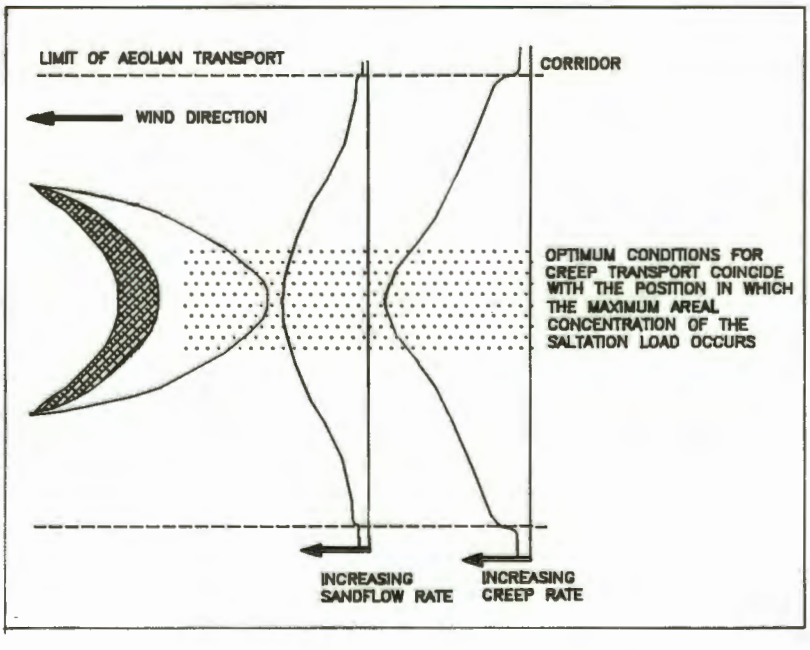

Figure 4.40. Sketch illustrating the conceptual lateral variation of the creep transport rate across aeolian transport corridors.

This significantly influences the way in which the stone pavement environment is interpreted. Within the Southern Namib deflation basin, and more specifically within aeolian transport corridors, stone pavement surfaces are not entirely composed of clasts which are immobile in the aeolian dispersal system. They in fact represent a dynamic substrate which changes continuously, in response to variable sandflow conditions, which act in conjunction with other processes to modify the bed configuration. This is discussed more fully in section 4.4.

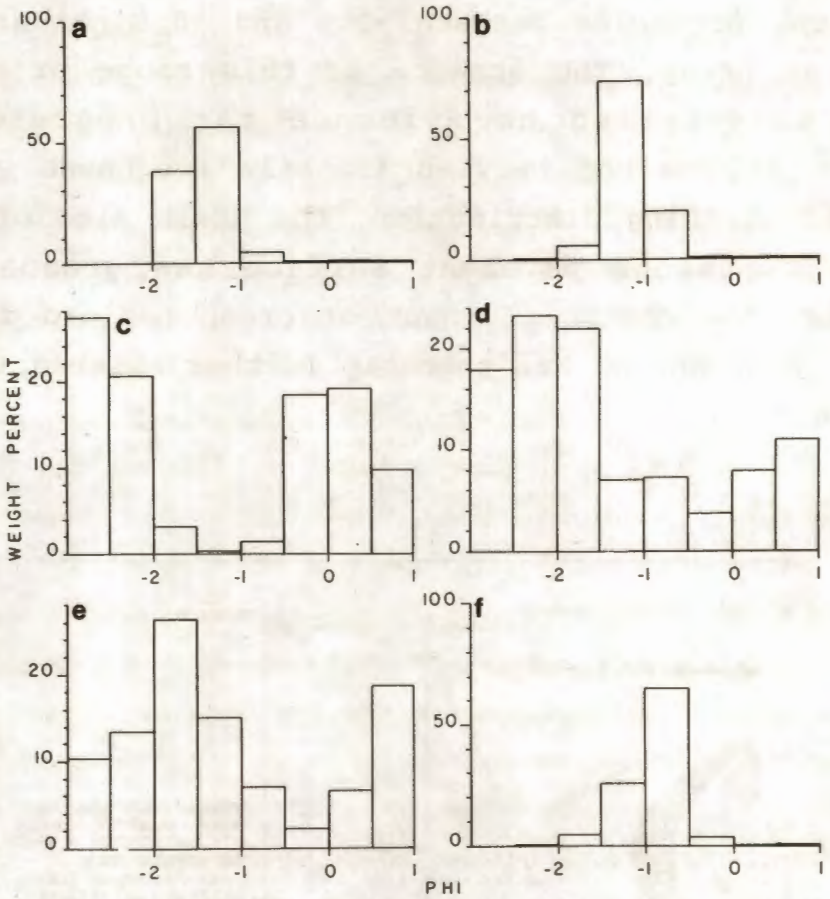

Figure 4.41. Comparison of stone pavement grain size distributions with granule ripple crest grain size distributions. Note the coincidence of the bi-modal trough with the ripple peak. (a, b, and f) granule ripples, (c, d, and e) stone pavement within the Bakers Bay aeolian transport corridor.

4.3.4. GRANULE RIPPLE MORPHOLOGY AND DYNAMICS

Introduction

The granule ripples examined, which have previously been described as "gravel waves" by earlier geologists working in the Southern Namib deflation basin (eg. Merensky, 1909; Krause, 1910; Wagner, 1914), are analagous to those described by Sharp (1963), and to the pebble ridges of Bagnold (1954).

External Granule Ripple Morphology

A stoss slope covered with coarse-grained material, leads up to a crest, delineated by a concentration of quartz granules and small pebbles. These form a slight step which drops abruptly down to the lee face, which is predominantly composed of medium to coarse quartz sand (Figure 4.42).

In general, the stoss slope is longer than the lee face. Well-rounded granules and small pebbles, predominantly of quartz, cover the entire stoss slope surface. The blade-shaped particles commonly exhibit a preferred orientation, with their long axes approximately parallel to the southerly surface-wind direction. Many granules are disc-shaped. These particles frequently exhibit an imbricate shape-fabric, with the upper surfaces inclined into the southerly surface-wind (Figure 4.43).

During periods of reduced southerly wind-energy, the lee face of granule ripples are usually composed of sand, with granules scattered across the surface. Evidence of deflation is often seen on fog-dampened lee faces (Figure 4.44). The eroded material is transported along the lee face at a slight angle to the prevailing southerly wind direction. Once the lee face dries out, small sand ripples migrate along the lee face. The orientation of small, scour-remnant ridges (terminology of Allen, 1982), formed in the lee of granules exposed on the lee face by deflation, define the pattern of flow over the ripple crests.

Internal Granule Ripple Structure

Longitudinal sections through granule ripples, cut parallel to the southerly surface-wind flow, reveals that they are comprised entirely of concave, north-dipping foresets (Figure 4.45). Tightly packed, wedge-shaped concentrations of quartz granules are sandwiched between the quantitatively more significant foresets of

Figure 4.42. Granule ripples migrating to the north across the floor of the Grillental. Note the white, quartz granule covered stoss slope and the sandy lee face. Southerly wind flow from right to left. Person for scale.

Figure 4.43. Granules and small pebbles on the stoss slope of a granule ripple north of Bakers Bay. Note the close packing, imbricate shape-fabric (arrowed) and the alignment of particle long axes with the southerly wind flow (A). The lee face can be seen in the bottom left corner. Scale 11.5 cm long.

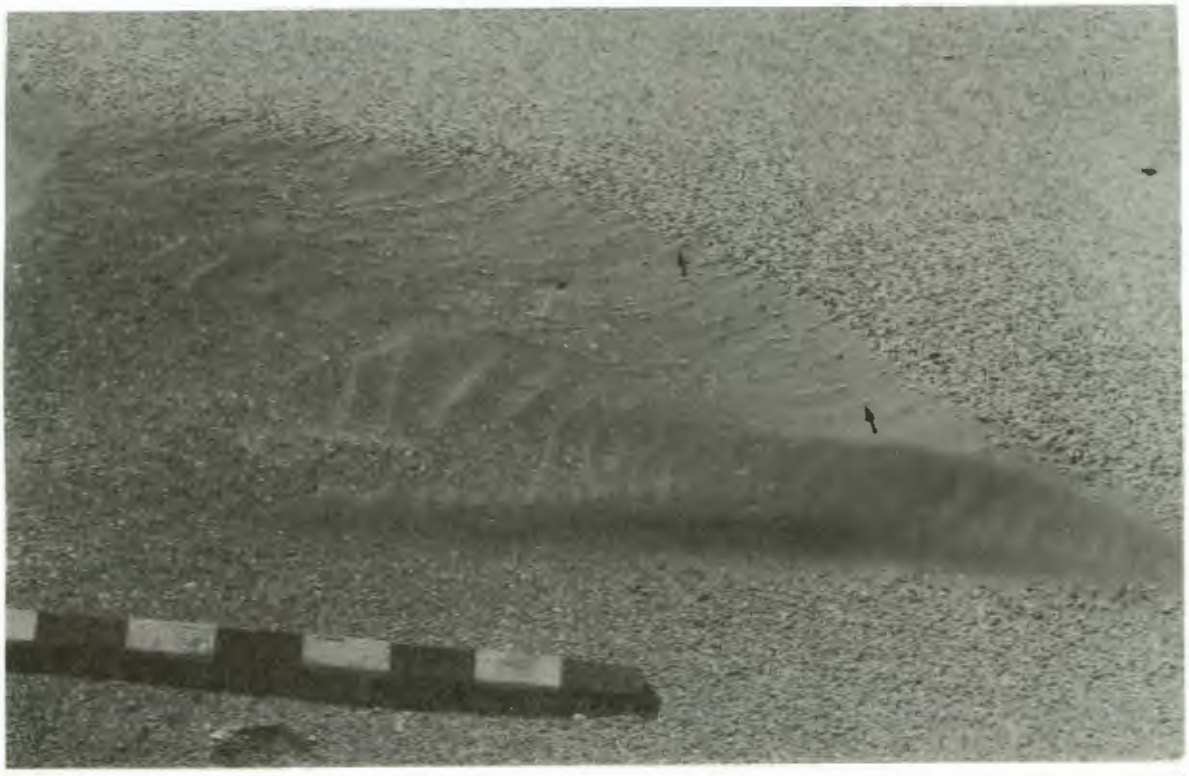

Figure 4.44. Scour-remnant ridges (arrowed), formed in the lee of granules exposed by deflation of the lee face of a granule ripple. The orientation of the ridges defines the pattern of surface-wind flow across the bedform. Scale 0.75 m long.

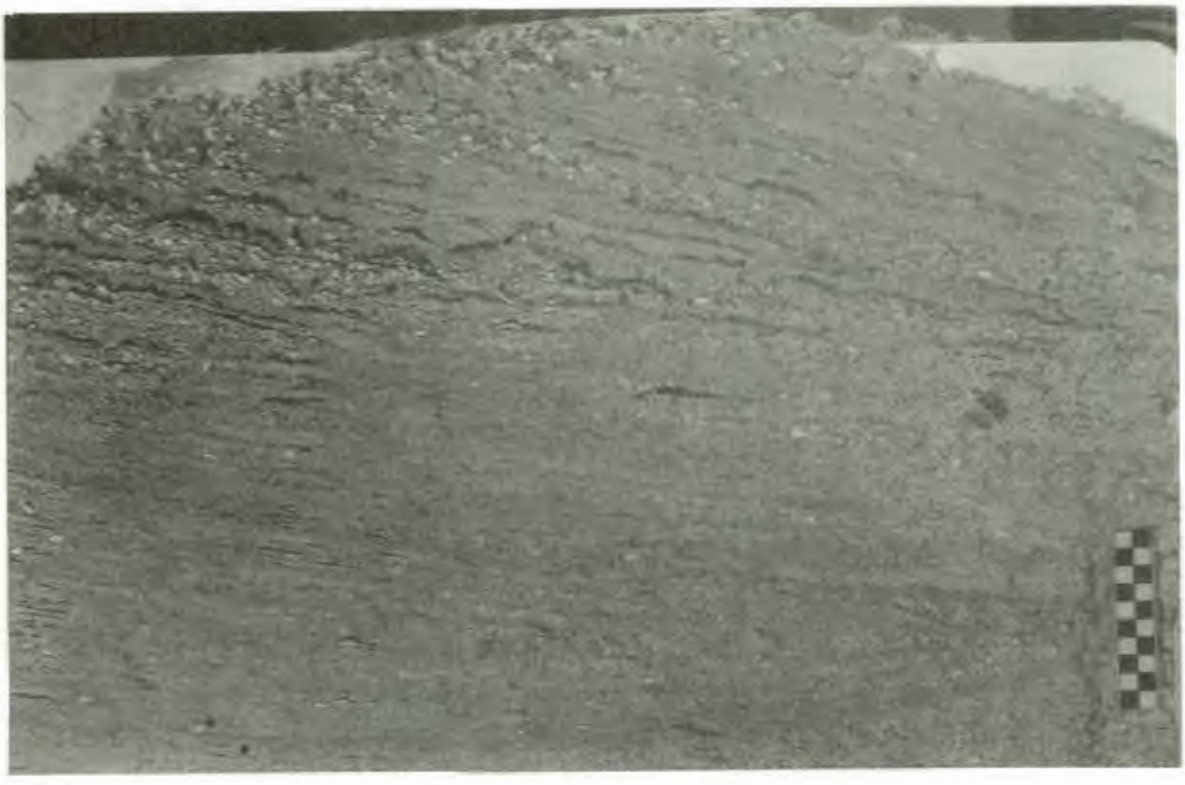

Figure 4.45. Longitudinal section through gently inclined, north-dipping foresets of a granule ripple. Note the white wedges of quartz granules interspersed between sandy foresets. Scale in cm.

finely laminated sand, which contain few granules. Sections transverse to the southerly surface-wind flow, provide oblique sections through the north-dipping foresets, which are represented by laterally continuous, sharply bounded sets of low-angle strata (Figure 4.46).

Although the stoss slope is covered by tightly packed, coarse-grained material, the underlying deposit reflects the internal structure, and alternating bands of sand and granules (Figure 4.47) correspond to the foresets observed in longitudinal sections.

Interpretation

The uniformity of foreset orientation proves that the granule ripples are migrating to the north under the influence of the southerly wind regime. The absence of steeply dipping foresets in transverse sections indicates that easterly and westerly winds have little influence on these bedforms.

The sand foresets are probably the combined result of grainfall deposition on the lee face, and translatent strata (sensu Hunter, 1977), resulting from sand ripple migration over their surface. The relative abundance of foresets composed of sand, in both longitudinal and transverse sections, strongly suggests that its deposition on the lee face contributes to the maintenance of these bedforms. During low- to moderate-energy southerly wind conditions, the deposition of fine-grained material possibly results in lee face migration. During high sandflow conditions, granules have been observed to advance up the stoss slope by creep, and to continue over the crest onto the surface of the lee face. If sufficient fine-grained sediment is added to the lee face prior to the next high sandflow event, the creep bedload crossing the former crest position, possibly tumbles onto the new sandy surface, advancing the crestal portion of the granule ripple slightly to the north. Although the coarse component of granule ripples can probably be entrained into saltation, in this high-energy aeolian environment, bedload creep appears most likely to account for their migration. Sharp (1963) interpreted the same mechanism for similar features in the Kelso Dunefield and within Coachella Valley. The imbricate shape-fabric of granules on the stoss slope of these bedforms is

Figure 4.46. Transverse section through the granule ripple in Fig. 4.45. Note the low-angle stratification, and concentrations of white granules along bedding planes. Scale in cm.

Figure 4.47. Cellulose acetate peel showing the stratification of the stoss slope deposits underlying the granules covering the surface. Crest of ripple is at the left end. Scale in cm.

of granules on the stoss slope of these bedforms is probably best explained by the bedload creep process (see section 4.4 for detailed discussion). Grain size analyses of crestal material from granule ripples in a wide variety of settings within the deflation basin indicates that sediment between -2.5 to -0.75 phi is transported by bedload creep in the present-day aeolian sediment dispersal system. Many of the early mining areas were characterised by the presence of granule ripples. It is likely that mining has therefore removed examples of these bedforms which were coarser-grained than those examined in this study.

Granule Ripple Migration During Southerly Surface-Wind Conditions

The rate of barchan dune migration within the Bakers Bay aeolian transport corridor compared to that of granule ripples lying outside the corridor exhibits great variation. A barchan advanced 36.6 m between 15/10/86 to 5/1/88. Of four granule ripples measured over the same period, the maximum northward advance was between 0.12 and 0.17 m, with two sites showing negligible resultant movement, despite an initial advance of 0.05 to 0.10 m, because winter wind reversals almost returned the bedforms to their starting positions. The migration rate of the granule ripples to the north, is therefore potentially 200 (or more) times slower than for very large barchan dunes within the Bakers Bay aeolian transport corridor.

The examination of the rate of granule ripple advance between 15/10/86 and 12/03/87 (Table 4.2) shows that the greatest migration rates coincide with the occurrence of very high sandflow events. The frequency of saltation collision with

Table 4.2. Summary of the rate of granule ripple advance in relation to the incidence of high sandflow events driven by the southerly surface-wind flow.

DATE	SITE 1 (cm)	SITE 2 (cm)	SITE 3 (cm)	SITE 4 (cm)	SITE 5 (cm)	SITE 6 (cm)	HIGH SANDFLOW EVENTS
15/10/86	0.0	0.0	0.0	0.0	0.0	0.0	
01/12/86	2.8	2.0	1.0	2.0	0.6	2.4	
18/12/86	10.9	9.6	2.4	3.8	3.4	2.0	16/12/86
30/12/86	1.3	0.2	0.4	0.0	0.0	0.0	
04/02/87	2.5	1.7	0.2	-0.2	-0.2	-1.2	
12/03/87	3.5	6.5	2.5	4.0	4.7	3.0	10/02/87

the bed increases during these events, and the probability of impact by large saltating grains probably also increases. This confirms that optimal conditions for creep should exist within aeolian transport corridors, where the sandflow rate is consistently high.

Granule Ripple Migration During Northerly Wind Reversals

In areas outside aeolian transport corridors granule ripple advance to the south, during brief high-energy wind reversals can exceed the total northward advance achieved under southerly wind conditions over a much longer time period (Table 4.3). The rapid bedform migration rates during wind reversals is also a response to the abnormally high sandflow conditions experienced by these areas during these wind conditions. This underlines the importance of aeolian saltation in promoting the migration of these bedforms, be it by entrainment of the granule population into saltation or creep.

Table 4.3. Summary of monitored granule ripple movement outside aeolian transport corridors over one year illustrating the influence of wind reversals on bedform migration.

DATE	SITE 1 (m)	SITE 2 (m)	SITE 4 (m)	SITE 5 (m)	SITE 6 (m)	NOTES
15/10/86	0.0	0.0	0.0	0.0	0.0	start of observations
12/03/87	23.0	20.0	9.5	8.5	6.0	end of summer
05/01/88	12.0	17.0	0.0	0.0	0.0	influence of reversals

Modification of Granule Ripple Morphology by Northerly Winds

Rain during a reversal on 22/9/87 allowed sections to be cut through granule ripples (Figure 4.48). Longitudinal sections through the bedforms were dominated by gently inclined, concave, north-dipping foresets. The lower surface of individual cross-bedded sets were formed by convex downward bounding surfaces. Sections through the granule ripple crests demonstrated the effects of wind reversal, which transformed the normally sandy lee faces during southerly wind conditions, into the stoss slopes of reversed bedforms (Figure 4.49).

Figure 4.48. Longitudinal section through granule ripples to the east of Bakers Bay. Note the reversed crests, and that the former sandy lee face has been modified by the northerly wind reversal and is now covered by quartz granules. Cross-bedded sets are separated by convex downward erosion planes. Scale 10 cm.

Figure 4.49. Quartz granule wedges forming a granule ripple crest as a result of a wind reversal. Note the alternation of coarse- and fine-grained material at the crest, which indicates that more than one reversal occurred. Few granules are preserved within the sequence. Southerly wind flow from left to right. Scale 10 cm.

Aeolian erosion of the former, sandy lee face, results in the development of a granule lag resting upon an erosion plane. The lag is subjected to bombardment by the saltation load, and the material is transported by creep up the new stoss slope, to form a coarse-grained wedge at the crest of the bedform. If the reversal is of sufficient duration, the new crest will migrate over the former stoss slope. During the winter, frequent reversals create granule wedges in the crestal area, which are separated by fine sand and silt laminae deposited during southerly wind flow. These coarse-grained wedges become incorporated into the lee face aligned for the southerly wind, when this regime becomes dominant once more. This sensitivity to changes in the wind regime, make these bedforms useful indicators of palaeo-wind conditions in the rock record. In this example, the granule wedges formed during wind reversals were not incorporated in the sequence, which was mainly comprised of concave, sandy bottomsets. This could perhaps be misinterpreted as the grouped bottomsets of very small aeolian dune forms in the rock record.

Transverse sections cut through the same bedforms exhibited low-angle stratification. Again, this is interpreted as oblique sections through the foresets observed in longitudinal sections (Figure 4.50). In the transverse sections, the variation of the dip direction probably reflects the variable plan-form of granule ripple lee faces, and lateral shifts in the points of deposition and erosion along the lee face of the bedforms.

The internal structure of sequences deposited by granule ripples at Elizabeth Bay (Figure 4.51) differs considerably from those described above. The Elizabeth Bay examples are from a sand sheet, and exhibit an internal structure closely resembling the "type-b" interdune deposit of Fryberger, Ahlbrandt and Andrews (1979).

Figure 4.50. Transverse section through granule ripples in Fig. 4.48, showing low-angle stratification. Despite the concentration of granules on the bed there are very few granules in the section. Southerly wind flow out of page. Scale 10 cm.

Figure 4.51. Longitudinal section through granule ripples comprising the Elizabeth Bay sand sheet. Also note the underlying Fiskus Sandstone Beds. Southerly wind flow from right to left. Scale in cm.

4.3.5. ENCROACHMENT DEPOSITS

Encroachment Deposit Morphology

Bagnold (1954) proposed the term encroachment deposit to describe accumulations of aeolian sediment on the upwind side of obstacles oriented transverse to the dominant transport direction. The progressive approach of the creep bedload leads to the vertical aggradation of the bed on the upwind side of the obstacle. The orientation of these deposits thus provide further evidence for the dominant influence of the southerly surface-wind regime on the aeolian sediment dispersal system. In longitudinal section, the differences in the structure, as compared with granule ripples, become obvious (Figure 4.52). In contrast to granule ripples, encroachment deposits are comprised of low-angle stratification, which approximately mimics the underlying topography.

Due to the nature of encroachment deposits, they probably form slowly. The surfaces upon which they occur therefore represent relatively stable substrates, on which aeolian processes have operated uninterruptedly over a long period of time.

The creep bedload commonly exhibits a very well-developed imbricate shape-fabric (Figure 4.53). This shape-fabric is therefore likely to be a very stable bed configuration. As Kaiser (1926) observed, the long axes of grains forming these deposits are commonly aligned parallel to the southerly wind direction. Kaiser also noted that many surficial grains exhibit evidence of aeolian corrasion, and creep bedload particles commonly exhibit the form of small ventifacts. Seeing this, Kaiser attributed the orientation and imbrication of the grains to aeolian corrasion. This does not appear to be the case. It is more likely that the imbricate shape-fabric displayed by the surficial grains of encroachment deposits are the result of creep processes (see section 4.4.).

Sites Conducive to Encroachment Deposit Formation

Encroachment deposits develop on a variety of scales, depending upon the dimensions of the obstacle. Rough bedrock topography, especially where the Bogenfels Basal Clastic Member forms the floor of endoreic basins, is a feature of the deflation basin. Frequently, this leads to the existence of small-scale walls, positive and negative steps, and cavities, which are oriented transverse to the southerly surface-wind flow. As Kaiser (1926)

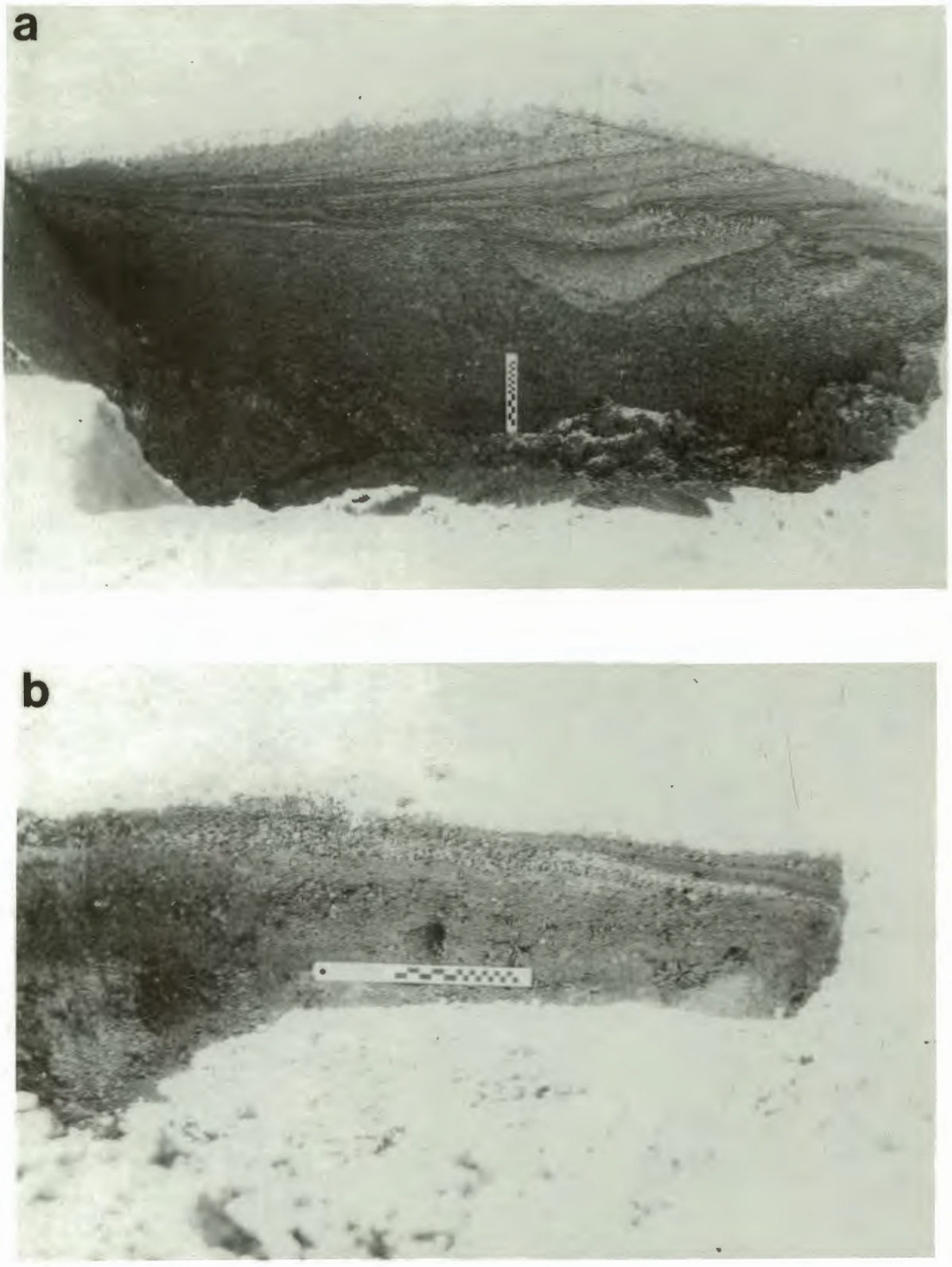

Figure 4.52. (a) Longitudinal section through a granule ripple, showing the north-dipping foresets. Southerly wind flow from right to left. Scale 10 cm long, is approximately vertical.
(b) Longitudinal section through an encroachment deposit showing the absence of north-dipping foresets. Note the domination of the internal structure by low-angle stratification, which mimics the underlying bedrock topography. Southerly wind from right to left. Graduated part of 10 cm long scale is approximately horizontal.

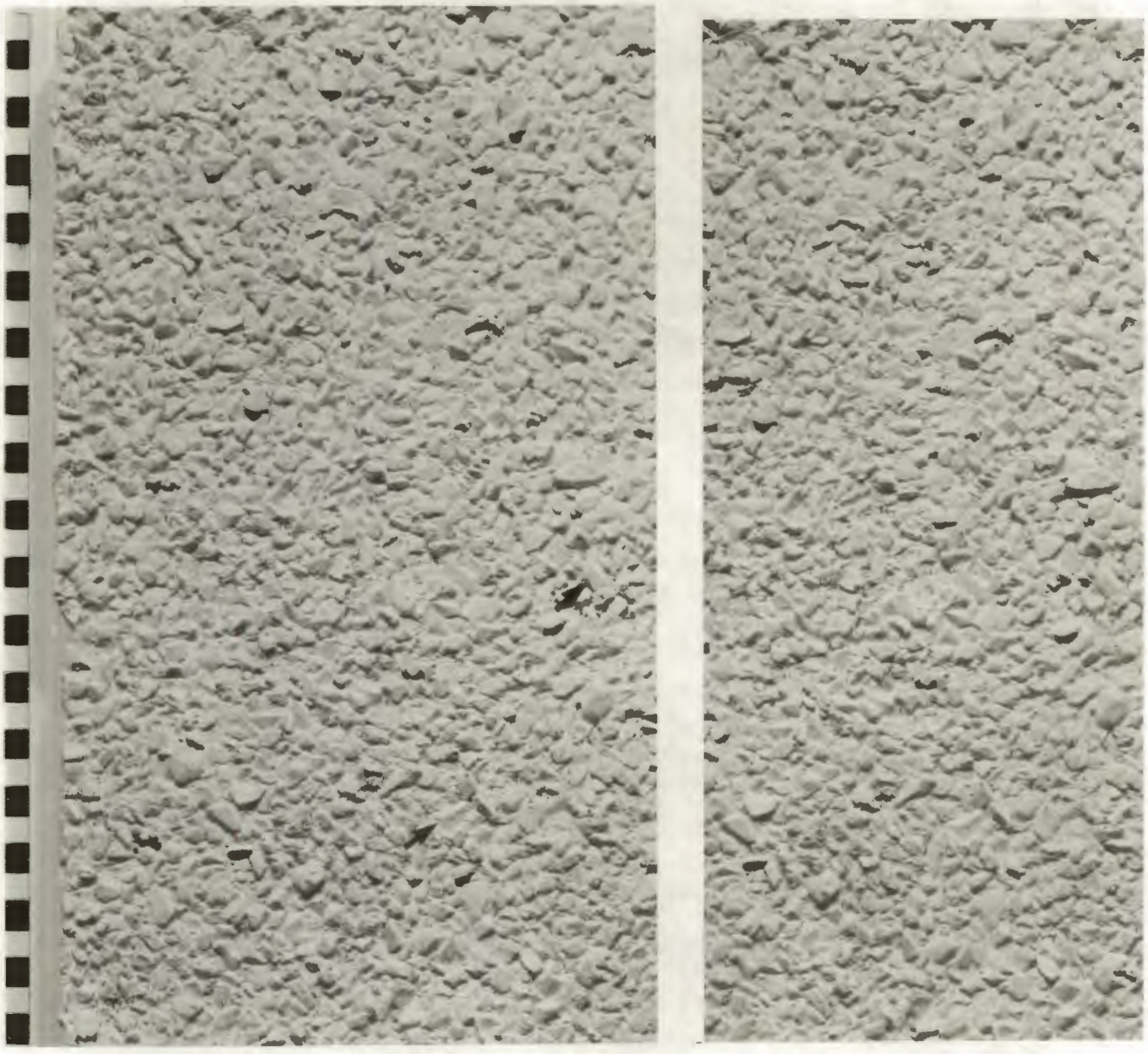

Figure 4.53. Stereo-pair of a plaster cast of an encroachment deposit taken at the south end of the Idatal. Note the imbricate shape-fabric exhibited by the clasts. Some clasts (arrowed) also show evidence of facetting by aeolian corrasion, and are small ventifacts. Southerly surface-wind flow from bottom to top of frame, scale in cm.

Figure 4.54. Oblique aerial view of the south-facing slope at the northern end of an endoreic basin about 2 km east of Bakers Bay. Granule ripples (arrowed) are migrating to the north, up the south-facing slope, towards the encroachment deposit of white quartz granules (E). Granule ripples are also migrating to the north from the northern margin of this deposit. Note the very clear, wind-aligned, streaks of creep particles on the bed. Southerly wind flow from bottom right to top left.

observed, these form effective obstacles to the migration of the creep bedload, and thus provide sites at which encroachment deposits form. Historically (Wagner, 1914; Kaiser, 1926), encroachment deposits on the upwind side of dykes oriented transverse to the southerly surface-wind have been recognised as potential sites for placer development (section 6.1).

On a basin-scale, the south-facing slopes at the northern end of the endoreic basins appear to form obstacles to the migration of the creep bedload. This situation was identified as being conducive to placer deposit formation during the initial phases of mining (Wagner, 1914; Kaiser, 1926). The creep bedload is transported up the south-facing slopes by collision impact of the sandflow driven by the southerly surface-wind regime. Many of the examples which were formerly present, have long since been mined-out but in some places, the deposits on south-facing slopes remain intact. The development of encroachment deposits is indicated by the presence of brilliant white patches of quartz granules on the darker aeolian sands (Figure 4.54). There is a need for detailed examination of the influence of bed slope on the incidence of creep for granules, before the mechanism of encroachment deposit formation can be fully described. Some of the possible causal factors are briefly discussed in section 4.4.4.

4.3.6. INTERPRETATION OF AEOLIAN CREEP TRANSPORT USING KINEMATIC WAVE THEORY

Definition of a Kinematic Wave

As defined by Langbein and Leopold (1968), "a kinematic wave is a group of moving objects in a zone along a flow path through which the objects pass. These concentrations may be characterised by a simple relationship between the speed of the moving objects and their spacing as a result of interaction between them". This introduction to kinematic wave theory is based upon work by Lighthill and Whitham (1955a and b) describing flood movement in long rivers and traffic flow along long crowded roads respectively. Analogies can be drawn between the creep bedload and the movement of traffic along a road. Consequently, this introduction to kinematic wave theory is largely based upon Lighthill and Whitham (1955b).

Lighthill and Whitham (1955b) show that the movement of cars

along a single-lane road can be expressed using a flow-concentration curve (Figure 4.55A). The flow is defined as the number of cars passing a particular point on the road per unit time, and the concentration is the average number of cars per unit distance of road. When the cars are spaced very far apart, the linear concentration is zero and the curve goes through the origin. Conversely, as the concentration increases, the point is reached where the vehicles are nose to tail and the flow is then zero. The maximum transport rate occurs when the cars are about two car lengths apart. The rising limb of the flow-concentration curve is stable, and the road is in an uncrowded state. The descending limb is, however, unstable and the road is crowded. As traffic flows along a road, local concentrations bounded both front and back by a zone of lower concentration occur. This variation along the road represents a kinematic wave.

Shock Wave Generation

The velocity of the kinematic wave at any point along the road is given by the slope of the flow-concentration curve for that particular point (Figure 4.55A). On the rising limb, a kinematic wave will travel more slowly than the cars on the road, but in the same direction. A tangent drawn on the descending limb has a negative slope and hence, the kinematic wave will travel backwards, towards the approaching traffic flow. When this happens, the wave is termed a "shock" wave. The influence of a shock wave is seen when traffic is denser in front than it is behind (Figure 4.55B). Waves on which the flow is less dense travel forwards faster than those on which flow is more dense. In terms of a distance-time graph, the two waves coalesce to form a shock wave. Oncoming cars entering this wave experience a very rapid reduction of speed.

Shock Wave Propagation by Bottlenecks

If the flow capacity of the road varies along its length, the potential exists for the development of a bottleneck. Under these circumstances, the maximum possible flow past a particular section of road falls below that of the main road. Provided the incoming flow rate to the bottleneck does not exceed its capacity, vehicles will experience only a temporary reduction of speed as they pass through. The wave velocity within the bottleneck will, however, be

reduced (Figure 4.55C).

If as time goes on, the incoming flow exceeds the capacity of the bottleneck, waves then turn back before reaching the centre of the bottleneck. A shock wave consequently forms (Figure 4.55D), which passes back down the road and forces vehicles to pile up upstream of the bottleneck at a rate given by the difference between the incoming flow and the bottleneck capacity. On passing back out of the bottleneck, the shock wave reduces the oncoming flow almost to that of the bottleneck because waves carrying flows less than this have passed through, and waves carrying greater flows have been turned back and absorbed by the shock wave. The vehicles approaching the bottleneck are thus reduced to a crawl (Figure 4.55E). The shock wave will continue to travel upstream until the oncoming flow is reduced below the capacity of the bottleneck. At this point the wave will commence to travel in the downstream direction once more. Provided this condition continues for a sufficient length of time, the wave then passes through the bottleneck, and the shock wave then behaves like an ordinary shock wave in the rear of a traffic hump. The shock wave accompanying the approaching traffic hump, plus the modified bottleneck shockwave then combine.

Lighthill and Whitham also make the point that where several bottlenecks occur in close proximity, the one with the least capacity will define the greatest flow possible under steady conditions. An influx of vehicles exceeding this capacity can only pile up in a continually increasing queue in front of the bottleneck system.

Interpretation of Granule Ripple Develepment According to Kinematic Wave Theory

Bagnold (1935) perceived that larger grains on a bed subjected to aeolian saltation shield those lying immediately downwind from saltation impact by varying degrees, depending upon the variation of grain size. Grains downwind of others are therefore transported more slowly, and in turn, retard the advance of the grains situated immediately upwind. He thus envisaged that there were "among the bigger grains alternate traffic blocks and empty spaces", implying that ballistic ripples can be treated as kinematic waves. This concept is supported by the theoretical modelling of ballistic

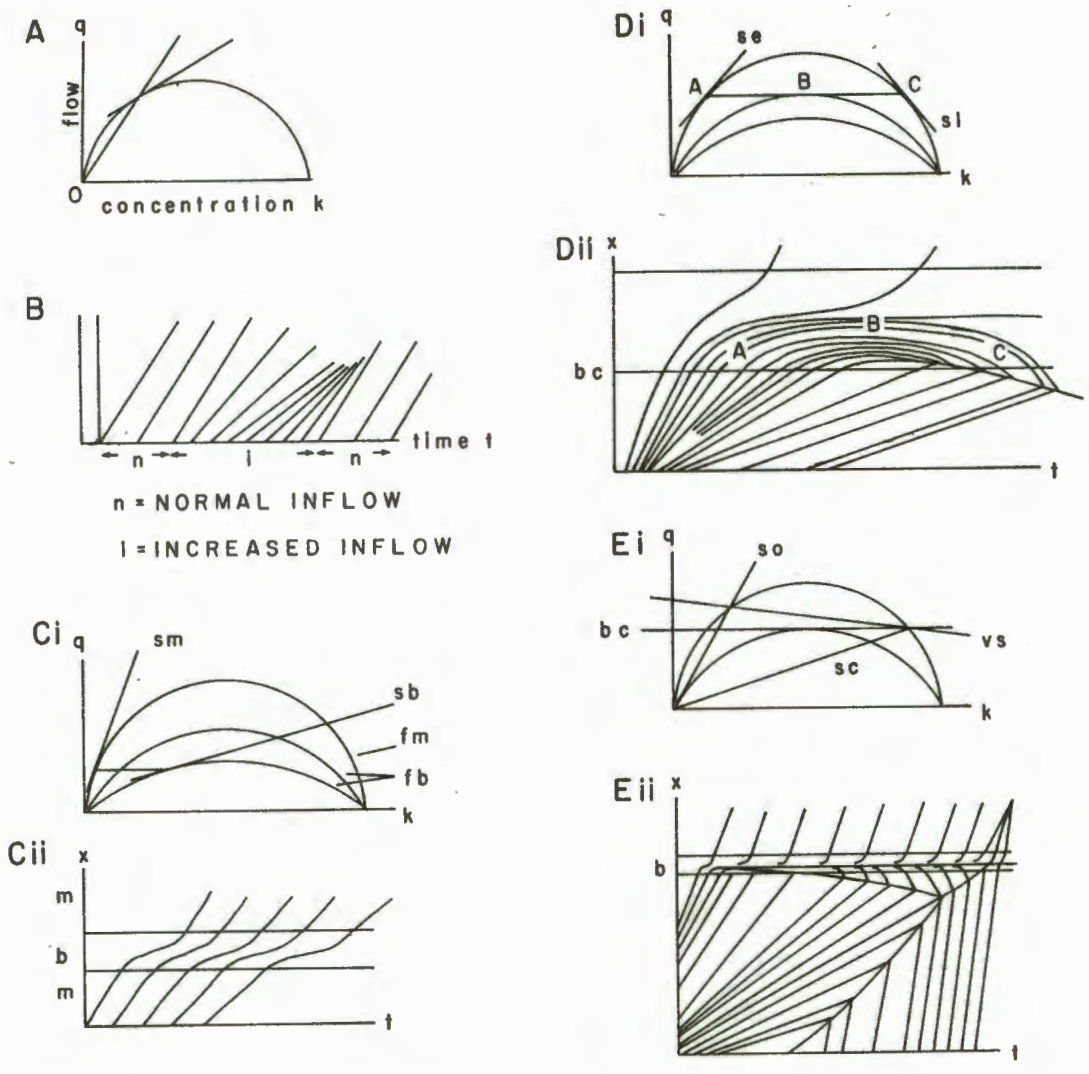

sm = speed of wave in main road

sb = speed of same wave at centre of bottleneck

fm = flow-concentration curve on main road

fb = flow-concentration curves inside bottleneck

se = wave velocity entering bottleneck

sl = wave velocity leaving bottleneck

so = average oncoming speed in flow

sc = average speed in flow behind shock wave

vs = shock velocity

bc = bottleneck capacity

Figure 4.55. (A) flow-concentration curve. (B) the influence of increased and reduced inflow on the passage of cars along a road. (C) (D) (E).

ripples (Müller, 1969).

Observations of granule ripple development on a planar ephemeral stream bed during this study provide further support for the above concept. The initial planar bed was progressively modified into flow transverse ridges of variable amplitude, increasing in height from south to north. Ridge propagation first occurred at the northern end of the planar bed, where granule ripples ultimately developed. Subsequently, modification of the bed progressively occurred to the south (ie. in the upwind direction) (Figure 4.56).

Although it was not measured during this study, visual observation indicates that distinct grain size variation occurs across the bed upwind of the fully developed granule ripples (Figure 4.57). The lee-slope is particularly well-sorted compared to both the stoss slope and trough locations. Within the trough at the base of the stoss slope, the bed is comprised of a wide range of grain sizes. The coarsest particles occur here. Some larger particles are present on the lowermost portion of the stoss slope. Note that smaller grains distinctly occur within the intertices between the larger particles. This corresponds to Bagnold's "traffic blocks and empty spaces". The sorting of the surficial grains improves up the stoss slope (ie. in the downwind direction), with a concomitant decrease in the frequency with which finer-grained material occurs within the interstices between larger particles. Particle concentration in the troughs is much less than on the ridges, where the maximum concentration is visually estimated to occur on the lee-slope.

The ridges at the southern end of the planar bed also represent concentrations of similar particles (Figure 4.58), but these are only a few particle diameters high. These low ridges are also bordered by zones of lower grain concentration in both the upwind and downwind direction, and larger particles occur in the troughs. The lee-slope of the low ridges is hardly discernible, but its position is clearly marked by a flow transverse band of better-sorted granules. Bagnold's "traffic blocks and empty spaces" are again observed on the stoss slopes, and within the troughs.

Langbein and Leopold (1968) investigated the relationship between the speed of discrete non-coherent particles to their spacing in a narrow flume. A shielding effect was observed, whereby upstream particles moved more rapidly and overtook those downstream, after

Figure 4.56. The distribution of aeolian bed forms on the ephemeral stream bed, and the approximate positions of the casts shown in Figure 4.57 (A), 4.58 (B).

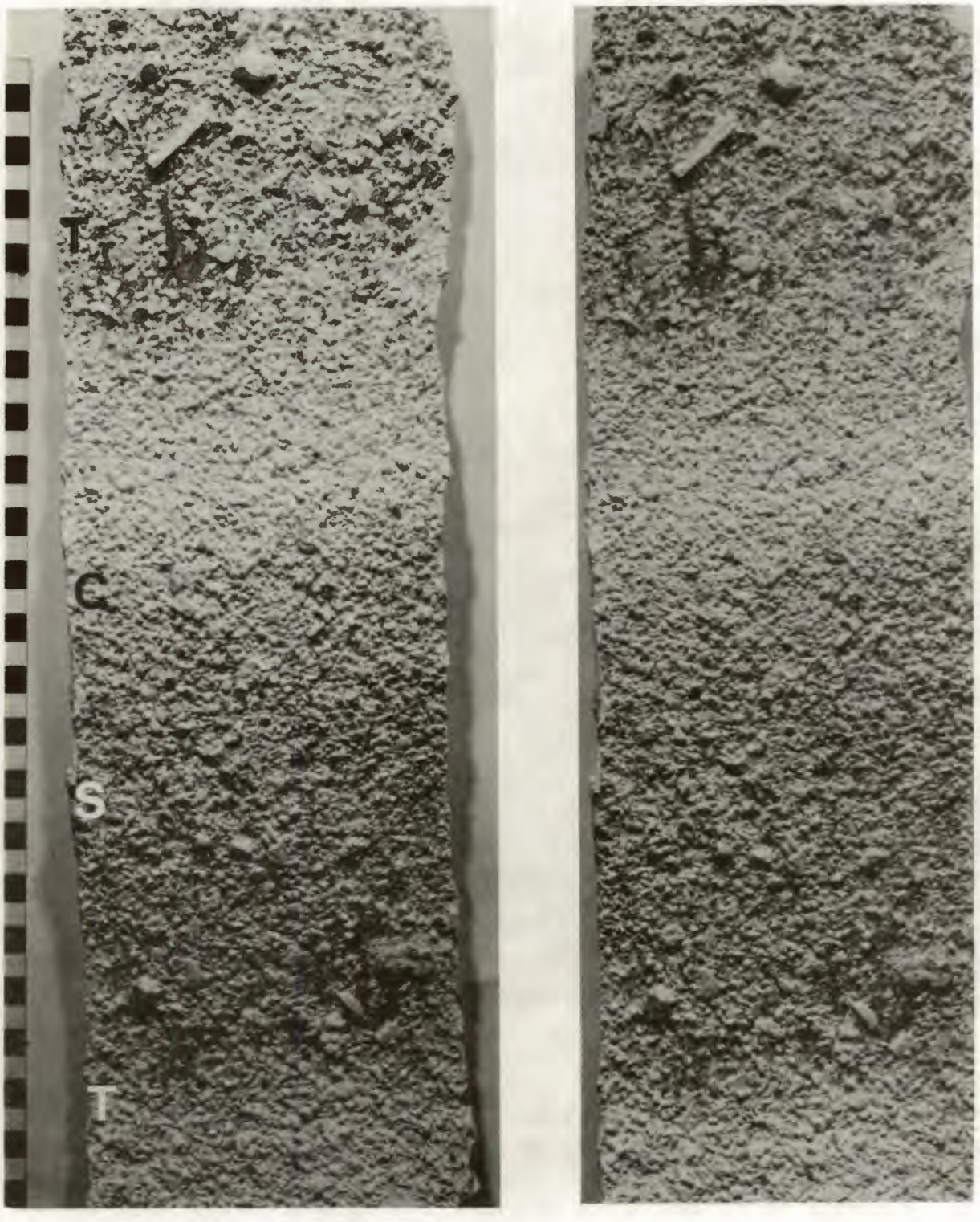

Figure 4.57. Stereo-pair of the ephemeral stream bed which has been modified by aeolian processes to form granule ripples. Once the initial deflation of the surface had removed the fine-grained sediment, aeolian size-shape-density sorting progressively altered the bed. Note the comparatively low density of grains on the floor of the troughs (T), and the well-packed creep population forming the stoss slope (S) and crest (C) of the bedform. Southerly wind flow from bottom to top, scale in cm.

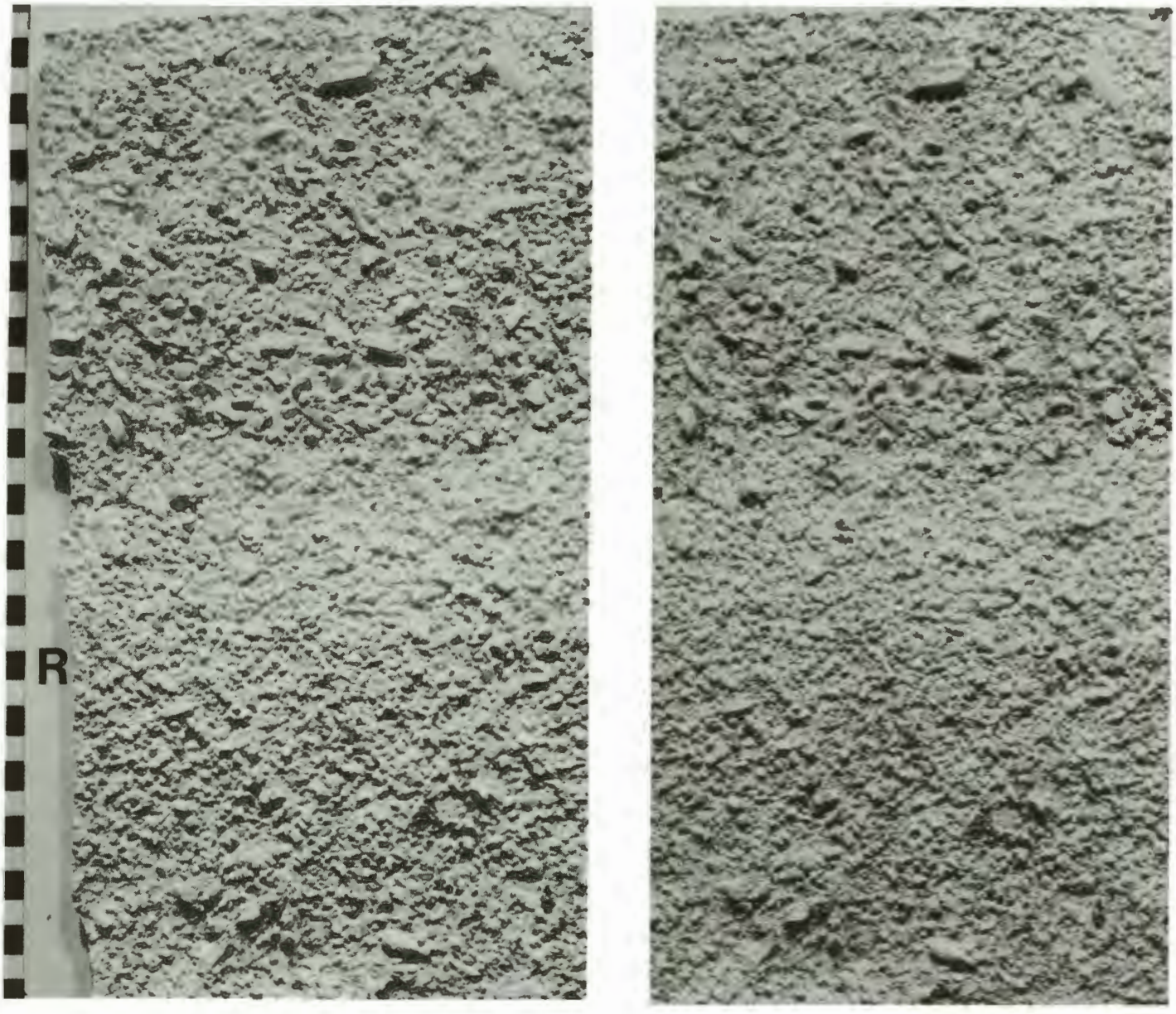

Figure 4.58. Stereo-pair of the southern end of the ephemeral stream bed, showing the embryonic granule ripple bedforms. Note the very low ridge (R) formed of the creep population, which is bordered to the north and south by areas in which the packing density is reduced, and the grain size of the material is larger. Southerly wind from bottom to top, scale in cm.

which the two particles moved as a group. Single beads sometimes left the front of the group and overtook the group ahead. As the rate of feed was increased, the groups of beads increased in size and their average speed decreased. Finally, a blockage occurred and transport ceased completely. This confirmed that kinematic waves can be composed of discrete particles.

Sediment grains on the planar ephemeral stream beds are initially comprised of a heterogeneous size-shape-density mixture of grains. As the garnet tracer experiment demonstrated, the entrainment potential of grains of similar density declines as their grain size increases. Grains transported by saltation were progressively removed by aeolian deflation under the influence of the essentially unidirectional surface-wind regime. As a result, a bed developed which was composed of the creep bedload and grains which are simply too large to be moved. In the aeolian environment, grains which are more readily entrained will theoretically approach those of lesser entrainment potential ahead, which migrate more slowly. Hence the distance separating the grains decreases, and they mutually interfere with each other. The progress of those immediately downwind of other particles is thus likely to be retarded due to particle shielding from direct saltation bombardment. By analogy with Lighthill and Whitham's (1955b) explanation of traffic hump formation, a kinematic shock wave is developed as a response. Hence, as grains enter the "hump", they experience a dramatic reduction of speed. The region of increased concentration spreads backwards according to the theory. This seems to be what happens in the case during the generation of granule ripples, since the main point of concentration is located along the windward slope and crest, and the concentration decreases towards the upwind trough. In the case of the planar stream bed, kinematic shock waves apparently first developed towards its northern end, and subsequently formed from north to south, (ie.in the direction of the oncoming flow). This provides a possible explanation for the progressive modification of the entire bed.

Although detailed experimentation under controlled conditions is required to confirm the above hypothesis concerning the development of the ridges, the aeolian creep bedload transported by a unidirectional surface-wind system appears to withstand examination by kinematic wave theory. After extreme sandflow conditions during

November 1988, the granule ripples at one monitoring site were completely replaced by a planar bed. This is predicted to occur as part of the birth and death cycle of bedforms according to kinematic wave theory (Allen, 1982).

Bottleneck Influence on Encroachment Deposit Formation

It has been shown that discrete, non-coherent particles moving within a unidirectional aeolian transport system behave as kinematic waves. Previous observations supplemented by those made during this study demonstrate that flow-transverse obstacles of various scales are associated with the development of encroachment deposits. The obstacles vary in scale from individual pebbles on a stone pavement surface, to dykes perpendicular to the main axis of an endoreic basin, to the entire south-facing slope at the northern end of basins. All of these obstacles appear to have one effect in common, they locally reduce the transport capacity of the aeolian system. In terms of kinematic wave theory, these obstacles can therefore be viewed as bottlenecks in which kinematic shock waves are generated.

4.3.7. CONCEPTUAL MODEL OF SEDIMENT DISPERSAL BY CREEP

Spatial Variation of Creep Transport

The frequency of saltation bombardment of the bed has been shown to be fundamental in determining the rate of creep transport. The aeolian system operating within the deflation basin is essentially unidirectional for much of the year. This is interrupted only occasionally by brief, northerly wind reversals. Within the present-day deflation basin, consistently high sandflow rates occur only within aeolian transport corridors, which therefore provide optimal sites for aeolian creep. The migration rate of the creep bedload is thus substantially greater within these corridors than elsewhere within the basin (Figure 4.59).

Sandstorms significantly influence the creep bedload population. The basin-wide, high sandflow conditions experienced during these events results in a brief pulse of creep activity. Much of the creep bedload migration within areas lying outside the influence of aeolian transport corridors probably occurs during these events.

In areas outside the influence of aeolian transport corridors, the influence of a brief, high-energy wind reversal is more

pronounced, because of the abnormally high sandflow conditions which are experienced. This can result in zero net migration of the creep bedload. These events also effect the creep bedload within aeolian transport corridors. Within these zones, however, their influence is short-term, and the net transport direction is very definitely to the north.

Variation of the coastal morphology in response to sea-level fluctuation hypothetically influences the position of aeolian transport corridors within the deflation basin. The location of optimal conditions for creep transport will therefore also alter, and areas which were previously influenced by low sandflow conditions may then be subjected to high sandflow. If this occurs, the bedload will migrate more rapidly in response, until the coastal morphology alters once more. A further consequence of this type of system modification will be that the loci for encroachment deposit formation will shift, depending upon the position of the aeolian transport corridors.

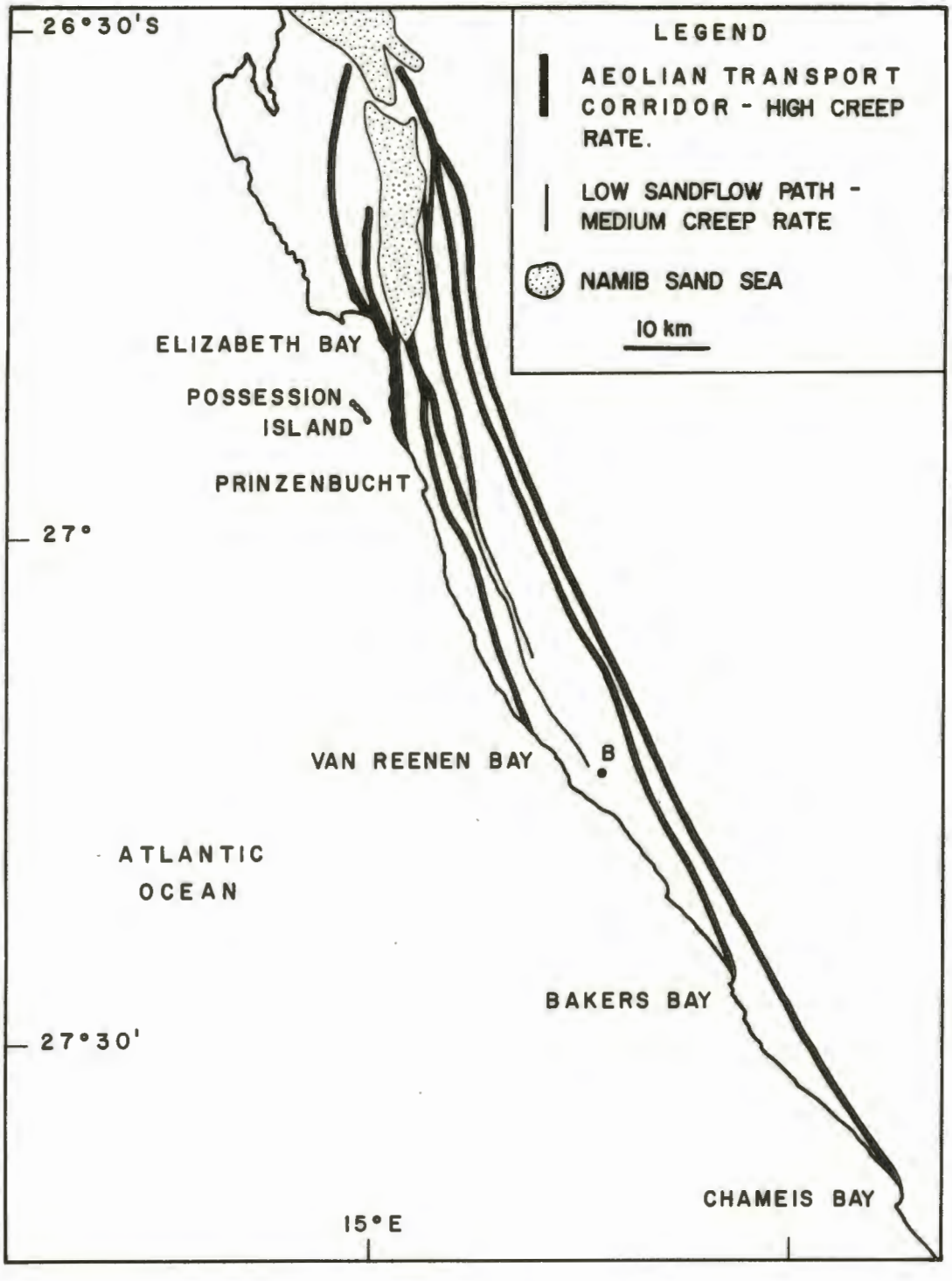

Figure 4.59. Conceptual model of the distribution of aeolian transport corridors through which the creep transport rate is very high relative to the rest of the deflation basin.

4.4. STONE PAVEMENT SURFACE MORPHOLOGY

4.4.1. PREVIOUS CONCEPTS

The Influence of Immovable Roughness Elements on Flow Structure

The nature of near surface flow is greatly complicated by the presence of immobile clasts, which assume variable spatial densities and arrays on stone pavement surfaces during erosion. For a flat bed comprised entirely of small, loose granular particles, R_* is so small that particles lie wholly within the viscous sublayer, and flow is aerodynamically smooth. Immobile roughness elements influence the velocity profile, which becomes dependent on their size, shape and spacing, so that the time averaged velocity in the flow ($\bar{u}$) direction (x) is expressed by:

$$\bar{u} = f(\acute{o}_o, p, u, y, \text{roughness geometry})$$

where ó = boundary shear stress, p = fluid density, u = instantaneous fluid viscosity in the direction x, and y = the cross-stream coordinate direction normal to the boundary (Middleton and Southard, 1984).

When y does not greatly exceed the height of bed roughness elements, the shedding of turbulent wakes affects the velocity profile within the lower part of the inner layer of the turbulent flow, a couple of grain diameters above the bed (Figure 4.60a), and turbulent wakes impinge on the upwind surfaces of succeeding roughness elements (Figure 4.60b) (Taniguchi, Sakamoto and Arie, 1982; Brayshaw, Frostick and Reid, 1983; Middleton and Southard, 1984).

Surface Stabilisation by Immovable Roughness Elements

The rate of deflation declines as non-erodible roughness elements are progressively exposed on the bed by wind erosion, and erosion ceases most rapidly when a high percentage of non-erodible roughness elements are present in the original sediment (Figure 4.61) (Chepil, 1950).

Marshall (1971, cited in Lyles et al., 1974) examined the influence of various densities and arrays of roughness elements on the total drag (ó), the sum of that due to the roughness elements ($\acute{o}_r$) and that due to the intervening planar bed ($\acute{o}_s$):

$$\acute{o} = \acute{o}_r + \acute{o}_s$$

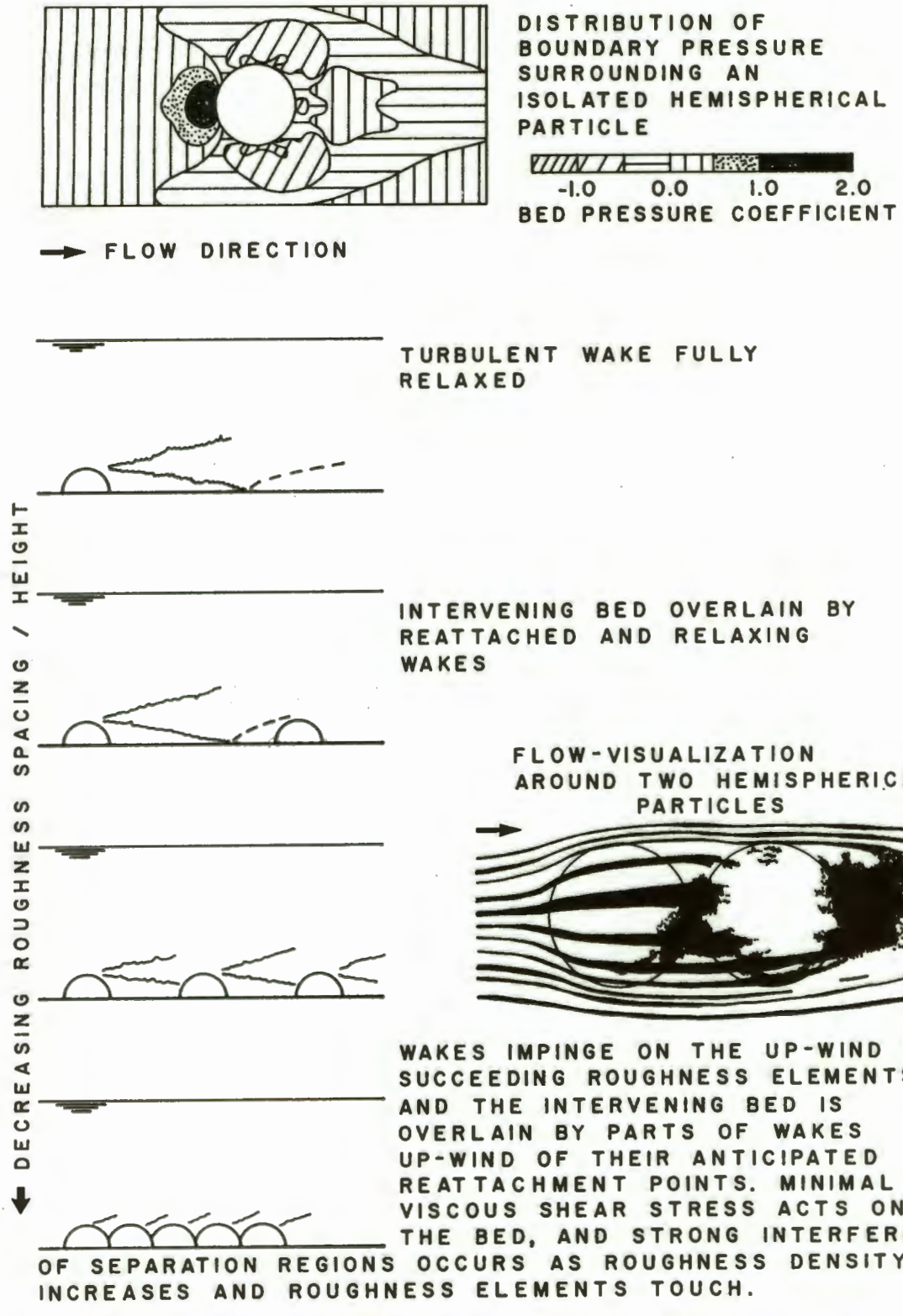

Figure 4.60 (a) Changes in the flow structure as roughness spacing is decreased relative to roughness height (After Middleton and Southard, 1984). (b) Flow-visualization around two in-line hemispherical particles. (After a photograph by Brayshaw, Frostick and Reid, 1983).

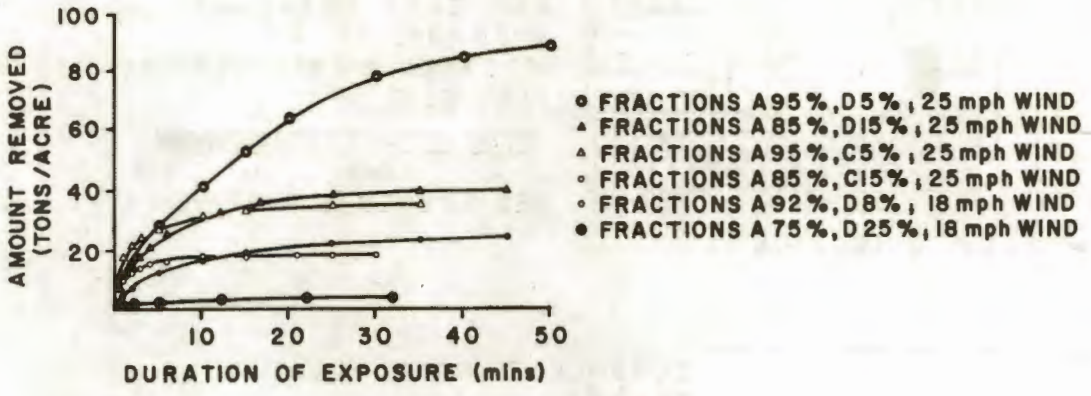

Figure 4.61. Diagram showing the decline in the rate of soil removal with increasing duration of exposure to wind in a wind tunnel. The rate of aeolian removal decreases as the roughness of the bed increases. (After Chepil, 1950)

Lyles et al. (1974) showed how surface stabilization by roughness elements proceeds (Figure 4.62). For a loose granular sand bed, $\acute{o} = \acute{o}_s$, and $\acute{o}_r = 0$. During erosion, the total drag increases due to the exposure of roughness elements. The drag on the bed between roughness elements decreases, whilst that on the roughness elements increases. When $\acute{o}-\acute{o}_r < {}_rt$ (threshold friction velocity), erosion of the intervening planar bed ceases. $\acute{o}_s$ need only be reduced below ${}_rt$ for the particular particle size range of the bed, and does not have to be reduced to zero (Lyles et al., 1974). Maximum surface roughness occurs when roughness element spacing is approximately equal to twice the roughness element height for closely spaced spherical roughness elements, (Greeley and Iversen (1985).

The Theoretical Pattern of Flow Around Roughness Elements

Apart from the influence that the spacing and density of roughness elements have upon the flow velocity profile, there is a further important consideration. This is the pattern of airflow which can be expected to occur around a roughness element. Naturally occurring roughness elements are generally complex shapes, which give rise to a complicated pattern of airflow across them. They can, however, be viewed as acting like bluff objects in a unidirectional flow. Assuming that the roughness elements

approximate to isolated, hemispherical particles on the bed, this gives rise to a specific distribution of bed shear stress (Figure 4.63), which has been modelled in a wind tunnel by Brayshaw, Frostick and Reid (1983).

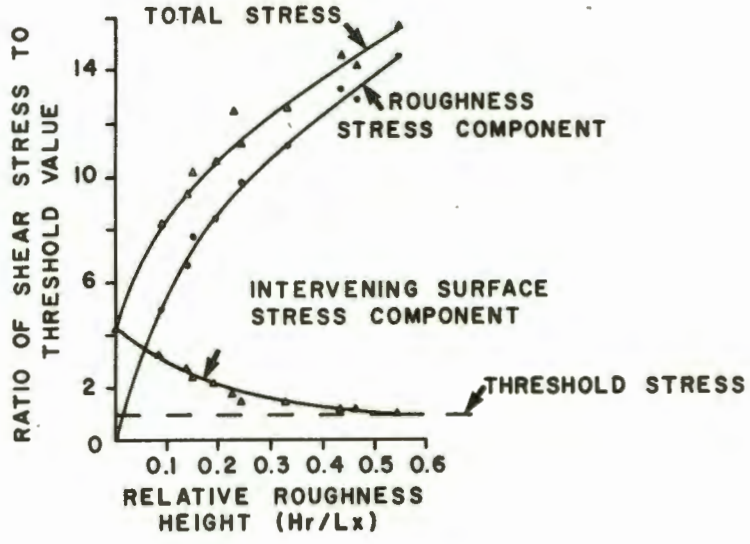

Figure 4.62. Surface shear stress as a function of the ratio of height (Hr) to separation (Lx) of immobile roughness elements on the bed. The roughness increases with Hr/Lx. (After Lyles et al.,1974)

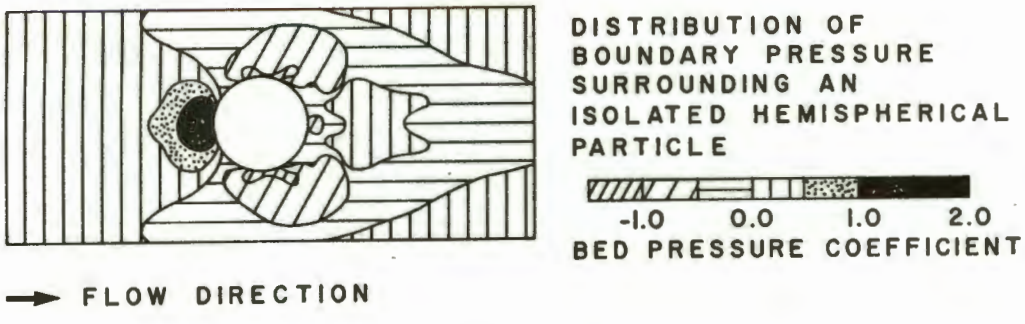

Figure 4.63. Distribution of bed pressure coefficients (Cp) about an isolated, stationary hemispherical particle, given by Cp = (p-po)/0.5 Uo) where p = local bed pressure, po = fluid density, and Uo = the free stream velocity. (After Brayshaw et al., 1983).

4.4.2. NAMIB PAVEMENT MORPHOLOGY ATTRIBUTED TO DEFLATION

Surface Configuration

In some areas of the deflation basin, the roughness elements on stone pavement surfaces exhibit a preferred orientation. Their long axes are approximately aligned transverse to the prevailing southerly surface-wind flow (Figure 4.64), in regularly spaced rows. If the roughness elements are assumed to approximate to isolated cylinders on a horizontal bed, this orientation offers the least resistance to the bed if the clast is rolled across the surface, and fluid drag on the roughness element is also a minimum (Allen, 1982). This suggests that these clasts are subject to periodic transport by rolling.

Mode of Formation

Wherever roughness elements exhibit this preferred orientation, within the coastal high wind-energy tract of the Southern Namib, the bed between them is predominantly sandy. In the Idatal, current crescents occur on the upwind side of roughness elements (Figure 4.65), and evidence of substantial undermining by scour along the base of roughness element windward faces, suggest that instability due to wind scour results in overturning and rolling. This mechanism has been shown to operate in other deserts by Bagnold (1954) and Sharp (1964). Sharp found that blocks placed with their faces oblique to the prevailing wind direction, tilted into the wind more than similar blocks oriented differently, and they were thus less stable. The southerly wind regime probably accounts for most of the wind scour observed in Southern Namib examples, because strong surface-wind from other directions is comparatively rare. Consequently, roughness elements are liable to tilt into the southerly winds, and thus are prone to overturning by rare high-energy northerly wind reversals.

Under highly erosive wind velocities, erosion of a soil bed continues until the height and spacing of the roughness elements protects the intervening bed from bombardment by saltating grains (Chepil, 1950). The drag acting on the intervening bed is then insufficient to entrain sediment by aerodynamic forces alone (Lyles et al., 1974), and deflation ceases. Chepil (op. cit.) found that the angle from the top of one grain to the base of the next varied

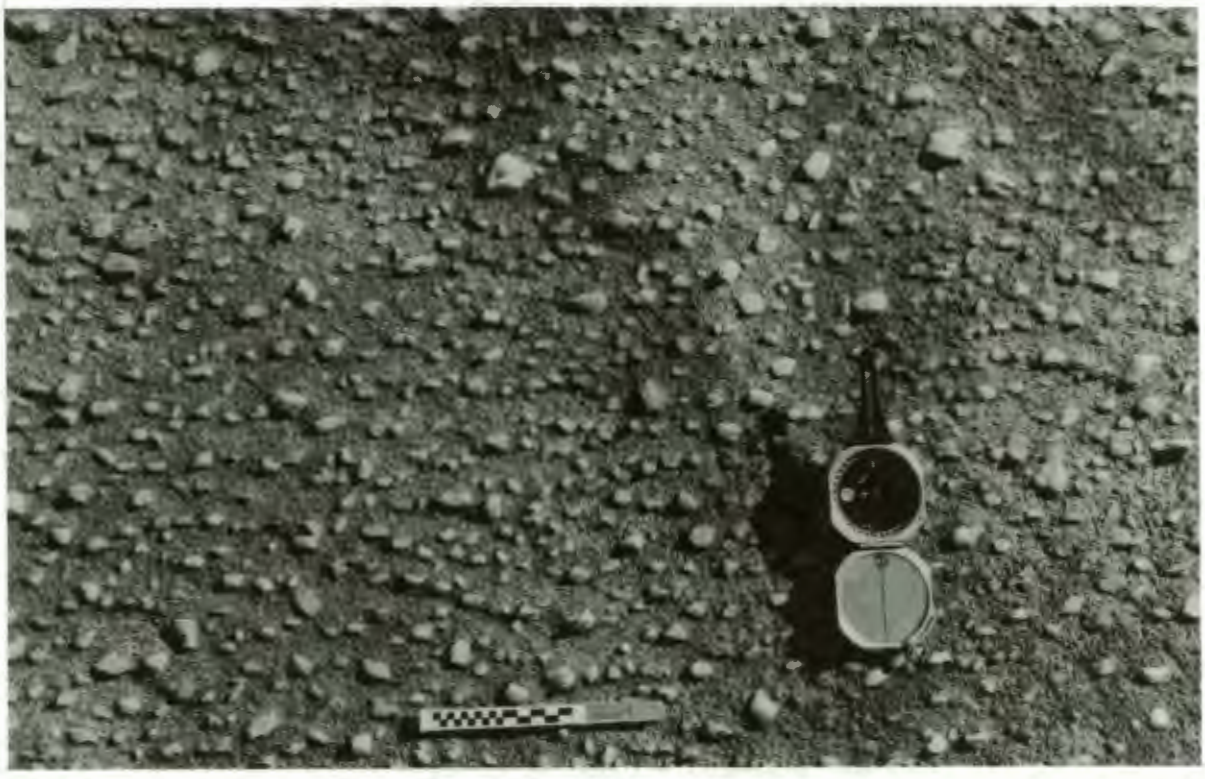

Figure 4.64. Roughness elements on a stone pavement near Frohe Hoffnüng (Lat. 27°33′S; Long. 15°33′30"E), exhibiting a preferred orientation, with their long axes transverse to the southerly wind, which blows from the bottom to top of frame. Note the regular arrangement of the roughness elements in east-west rows. The bed between roughness elements is sandy, and the pitted surface pattern is the result of rainsplash erosion.

Figure 4.65. Stereo-pair of a current crescent on a plaster cast taken in the Idatal. The current crescent is at the base of the windward face of a quartz roughness element preferentially oriented transverse to the southerly wind flow, which is from left to right, and a current shadow has formed in its lee. Note undermining at the base of the leading edge and the support of the roughness element by small, underlying clasts.

between 4° and 12° once the bed had been stabilised and erosion was reduced to a minimum. Measurements of a plaster cast taken in the Idatal, shows that for the larger, oriented clasts, this angle varies from approximately 4° to 7°. The ratio of roughness element spacing (from high point to leading edge of the next downwind clast) to height varied from 8.4:1 to 11.5:1. The similarity of the measured angles with Chepil's data, implies that saltating grains are effectively prohibited from striking the intervening bed. This provides convincing evidence that surfaces of this kind have attained stability principally by aeolian deflation. The regularity of roughness element spacing, which is achieved by rolling, is interpreted as being equal to the separation distance at which wind scour at the base of windward faces by saltation collision and aerodynamic forces is reduced to a minimum. Once this happens, provided that the surface remains undisturbed it is likely that minimal modification of the roughness element positions by aeolian processes will occur.

This surface configuration was not observed on natural stone pavements within the main aeolian transport corridors. The windward surfaces of 50 to 70 year old tailings heaps from mining operations within the Idatal exhibit this type of roughness element orientation and spacing. These tailings heaps are within the aeolian transport corridor which originates at Van Reenan Bay, and illustrate the potential speed with which surface stabilisation can occur.

4.4.3. ROUGHNESS ELEMENT INTERACTION WITH THE CREEP BEDLOAD WITHIN AEOLIAN TRANSPORT CORRIDORS

Clast Types Present on the Stone Pavement Surfaces

Three clast types occur on the stone pavement at sand trap site C, about 200 m west of the Bakers Bay barchan dune train:

1) immobile roughness elements larger than -2.5 phi;
2) coarse-grained bedload creep and saltation load (generally between -2.5 to -0.75 phi);
3) sand fractions representing the saltation load stored within the stone pavement.

Bed Morphology

The surficial spaces between immobile roughness elements are predominantly covered by quartz granules and small pebbles, with occasional clasts of quartzite, phonolite, agate, chalcedony and jasper, derived from earlier deposits. Some clasts on the stone pavement surface have been facetted by aeolian corrasion, to form perfect examples of aeolian ventifacts.

The intervening surface between the roughness elements gently undulates, and horizontal featureless surfaces are rare. As the upwind face of an isolated roughness element is approached, the bed rises fractionally above the surrounding surface. The resulting mound is covered with granules and small pebbles, which exhibit a well-developed imbricate shape-fabric (Figure 4.66), with the clasts inclined into the southerly surface-wind. These congregations are interpreted as particle clusters. In the lee of isolated roughness elements, small aeolian current shadows of medium to coarse sand are deposited, and the surface elevation drops back to that of the surrounding bed.

Where a narrow gap oriented transverse to flow, separates two or more immobile roughness elements, the bed comprised of granules and small pebbles is slightly elevated above the surrounding bed and the clasts are frequently imbricated (Figure 4.67). A downwind-facing step forms some distance north of the gap, where the bed elevation drops abruptly to that of the surrounding bed, and sand is deposited in its lee.

Small, ripple-like bed forms, generally less than 2 cm high are a common feature of the stone pavement surface. A stoss slope about 5 to 10 cm wide is covered by tightly packed, very coarse sand and granules at its base, which exhibit an imbricate shape-fabric. The grain size gradually increases towards the crest, which is generally up to 30 cm in length, where small and medium quartz pebbles accumulate (Figure 4.68). In some cases, there is a clear tendency for clasts on the stoss slope to become preferentially oriented with their long axes parallel to the southerly surface-wind. The crest shape varies from slightly crescentic to relatively straight. The gently sloping lee face, downwind of the crest, is composed of medium to coarse sand, but granules and small pebbles are also commonly scattered on them.

Wherever stone pavement surfaces are disturbed, patches of

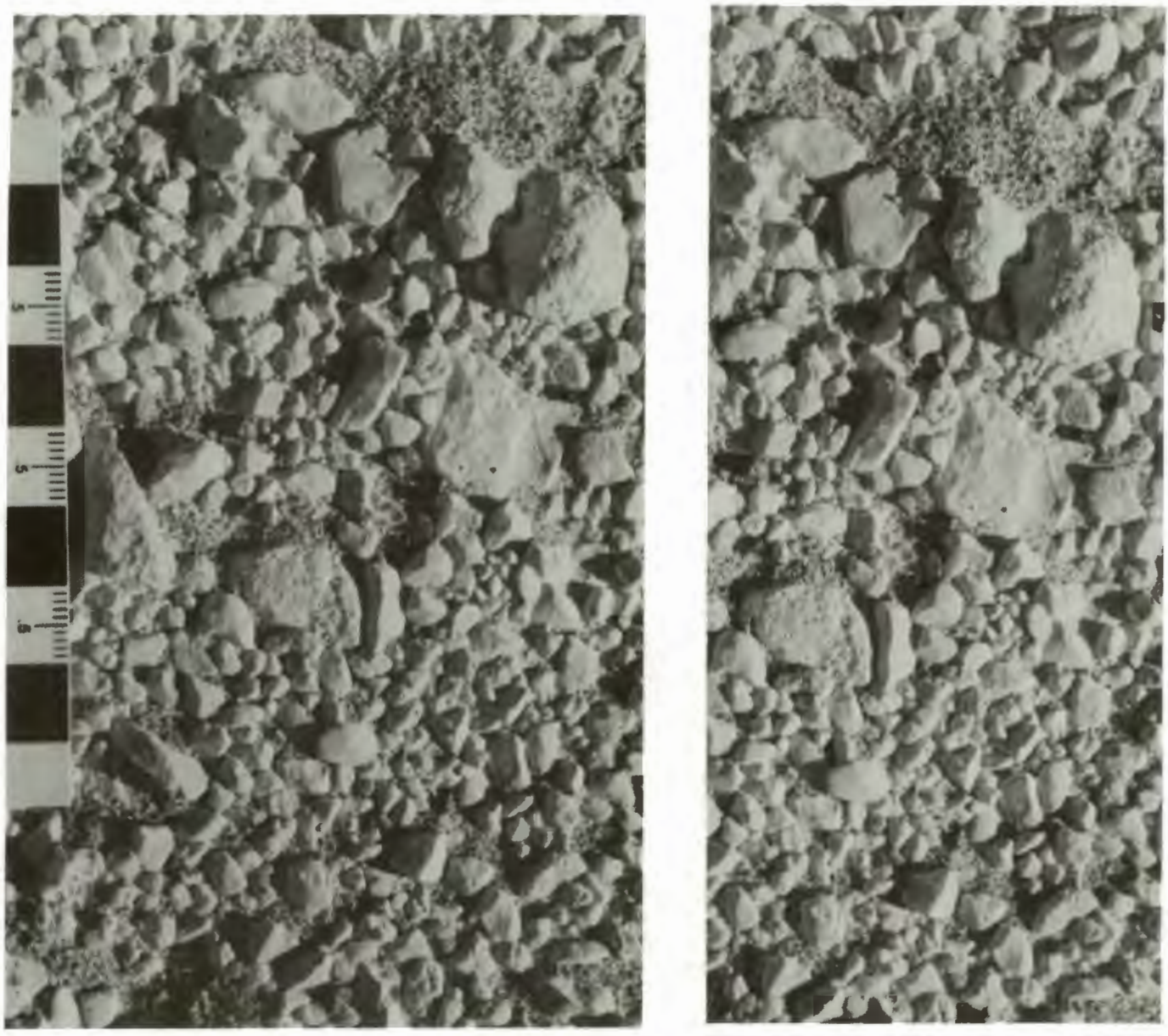

Figure 4.66. Stereo-pair of a small, granule covered mound on the upwind side of an immobile roughness element on the stone pavement near sand trap site C, forming a particle cluster. Note the imbricate shape-fabric of some of the creep bedload, some of which are small ventifacts. Southerly wind flow from bottom to top of frame. Scale in cm.

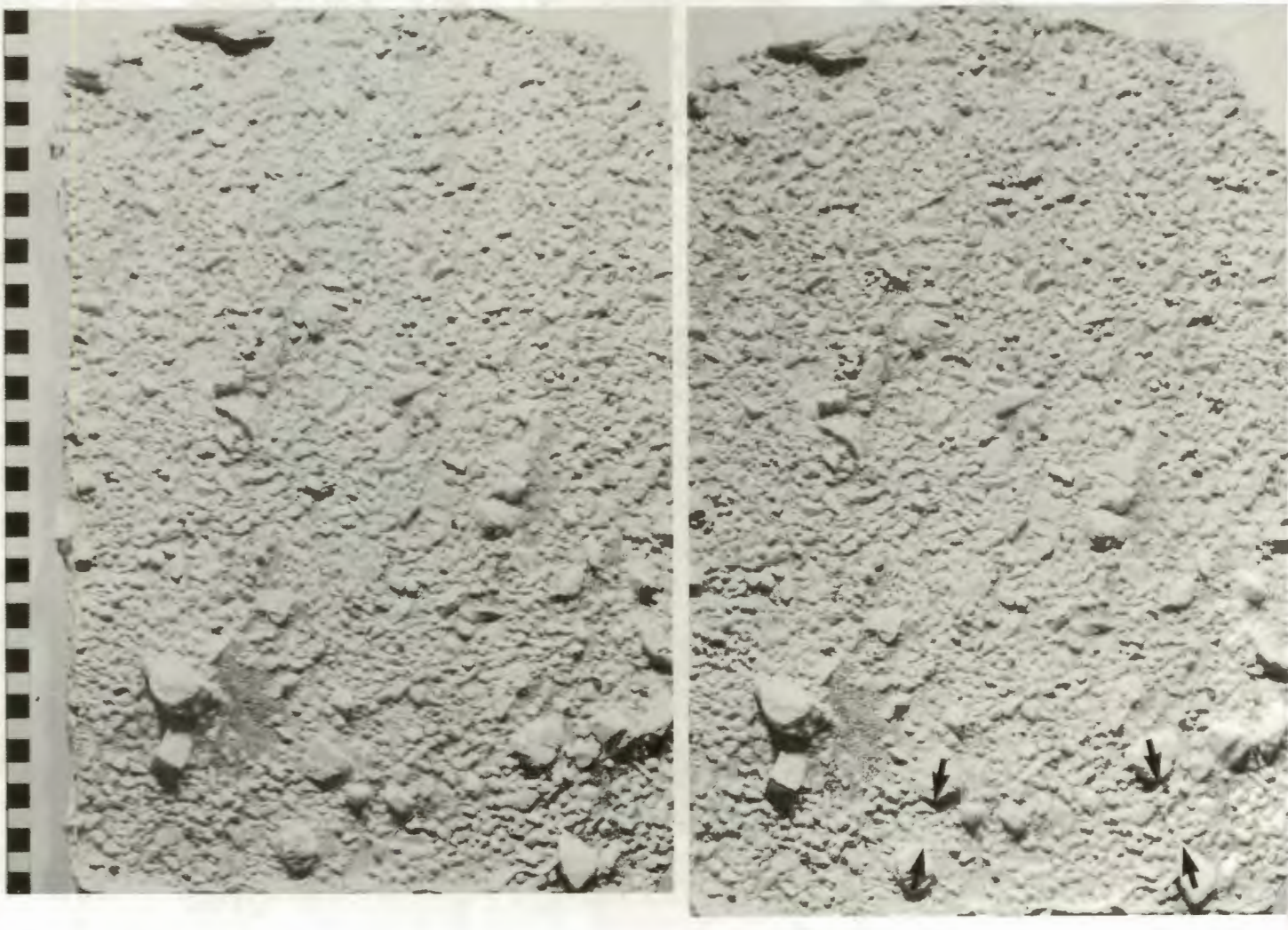

Figure 4.67. Stereo-pair of plaster cast taken on stone pavement at sand trap site C. Particle clusters can be seen in the gaps between neighbouring roughness elements on the bed (arrowed). In addition, further examples of particle clusters on the upwind side of roughness elements can be seen. Examples of small aeolian current shadows can also be seen in the lee of some of the roughness elements. Note that many of the creep bedload particles are imbricated into the southerly wind flow, which blows from left to right. Scale in cm.

Figure 4.68. Straight-crested, small, ripple-like bedform on the stone pavement surface near sand trap site C. Note the increase in grain size of the densely packed creep bedload from the ripple trough towards the crest. The lee face is primarily composed of sand, with granules scattered over it. The southerly wind flow is from left to right. Scale is 11.5 cm long. Also note that many of the grains in the creep bedload exceed the 2 mm diameter circles on the scale.

tightly packed and imbicated granules and small pebbles are found. Abandoned, or infrequently used game trails provide very good examples (Figure 4.69)

Particle Cluster Formation

As shown previously, aeolian size sorting results in the gradual increase of the grain size of the material on stone pavement surfaces. Consequently, bedload creep ultimately becomes the dominant aeolian transport mode with time. Observations during high sandflow conditions, and sand trap results, strongly suggest that the movement of material between -2.5 to -1.0 phi occurs principally by bedload creep. Because the creep bedload is not significantly raised from the bed, the micro-topography of roughness elements assumes a role which has not previously been recognised. They act as obstacles to creep migration. Roughness elements then become potential nuclei for the development of particle clusters on stone pavement surfaces as a result of creep transport to the north. Particle clusters due to selective aeolian transport on the bed of alluvial channels (Dal Cin, 1968; Laronne and Carson, 1976; Reid and Frostick, 1987), show some similarity with those generated by the aeolian current system, in that those formed in either fluid medium exhibit imbrication, with clasts inclined into the flow.

The consideration of experimental studies by Allen (1982) and Brayshaw et al. (1983) lead to the expectation of a localized zone of very high bed pressure along the windward edge of roughness elements, and along part of their margins. Smaller creep particles entering these areas are likely to be unstable, and the powerful vortices which are associated with such zones (eg. Allen, 1982), will probably move these grains along the sidewall. The larger grains are more stable in these locations, and become lodged at the leading edge of the roughness elements. Hence size-density-sorting may occur as bedload particles arrive from the south.

Roughness elements thus create bottlenecks, which retard the advance of the bedload creep. This creates a situation which can be examined using kinematic wave theory (see section 4.3.6).

Figure 4.69. Unused game trail crossing the stone pavement near sand trap site C. Note that the surface is now covered with quartz granules which have been transported into the depression by creep, and exposed by deflation. The streaky appearance of the bed is caused by the distribution of the creep bedload. The streaks are aligned with the southerly wind, which blows from the lower right to upper left corner of the frame. Note also that there are numerous aeolian current shadows in the lee of vegetation and large roughness elements on the bed. These are temporary sites of sand storage within the aeolian system. Scale 11.5 cm.

4.4.4. THE INFLUENCE OF IMBRICATE SHAPE-FABRIC ON BED STABILISATION

Whilst the forward movement of grains forming clusters is retarded, saltation bombardment continues to add additional bedload to particle clusters and bedforms on the stone pavement surface. As a result, the creep bedload particles become densely packed, and an imbricate shape-fabric is developed. Observations under controlled conditions in a wind tunnel are required in order to establish the mechanism for this. It has not been possible during this study, but the consideration of observations from flume experiments possibly provides some insight as to what happens.

According to the experimental results of Brayshaw et al. (1983), an area of very high bed pressure exists along the leading edge of particles on the bed. Hence wind scour can be anticipated to occur, forming small scour hollows. Provided that scouring continues, the grains will ultimately slide into the hollows, and tilt, so that their upper surfaces face into the southerly surface-wind flow. Fahnestock and Hauschild (1962) observed the initiation of an imbricate shape-fabric by a similar mechanism in flume experiments. Scour at the upstream edge of bedload particles obstructed by an obstacle on the bed created small upstream scour hollows. The particles, which were previously rolling with their long axis transverse to flow, subsequently sank into the hollows, and rotated until their long axes were parallel to the flow, and their upper surfaces were tilted upcurrent.

Once this shape-fabric is developed by the aeolian creep bedload forming encroachment deposits or stone pavements, inclined particle surfaces are exposed to the saltation load. Saltation collisions then possibly glance off the imbricate grain surface, because the inclination of the surface possibly alters the horizontal and vertical component of the collision force acting on the stationary grain (Figure 4.70). In addition, once the grains are imbricated, experimental evidence suggests that the pivoting angle is substantially increased relative to those which are not (eg. Li and Komar, 1986). A reduction in the frequency of entrainment into creep may then result, because a smaller proportion of the saltation load is capable of supplying sufficient collision force to overcome the relative increase in the pivotting angle. Therefore surfaces exhibiting this high degree of organization are considered

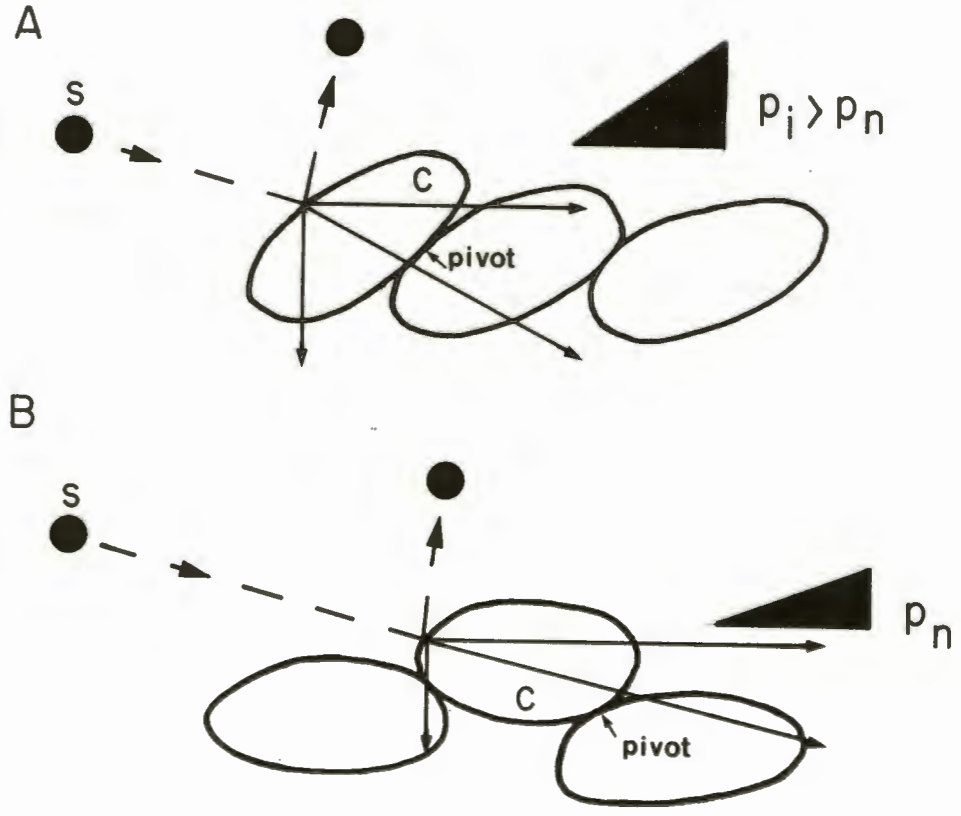

Figure 4.70. Sketch illustrating the suspected role of the imbricate shape-fabric in modifying the direction in which the impact force acts on a grain on the bed. Note schematic representation of the envisaged difference between the pivotting angle of imbricate grains (pi) and non-imbricate grains (pn).

to be stable, and in a relative state of equilibrium with the southerly surface-wind flow. The turbulent wakes shed from upwind, closely packed, similarly sized particles covering the bed, impinge on the inclined surfaces of succeeding particles downwind and not on the intervening bed (eg.Brayshaw, et al., 1983). The density of the grain packing thus prohibits further deflation of the sand fraction which underlies the sediment surface. In the high-energy aeolian environment of the deflation basin, this is therefore one of the most stable bed configurations that a stone pavement surface can attain, and aeolian removal processes are reduced to a minimum.

The garnet creep tracers showed that some creep activity persists across these stable surfaces. It is therefore postulated that grains which are not locked into the imbricate shape-fabric continue to move until they themselves become trapped. Creep transport of the bedload is thus maintained to some extent, and material is progressively transported through the deflation basin. During very high sandflow conditions, when large grains are entrained into saltation, this surface organisation is possibly disrupted due to abnormally large saltation impact forces. Imbricated grains may then be dislodged from the stable surface and reintroduced to the creep population. The vacant space on the pavement is possibly closed-up by the modification of the configuration of surrounding grains, or a new particle introduced from upwind may replace the entrained grain.

The dynamics of the creep bedload moving through the complex micro-topography of stone pavements within the deflation basin appears to resemble the behaviour of unidirectional traffic flow approaching bottlenecks along a road. It thus seems to behave in the manner predicted by kinematic wave theory (see section 4.3.6), as described by Lighthill and Whitham (1955).

Theoretically, provided that the system is not disrupted, the movement of bedload across the stabilized bed will continue until the entire upwind reach of the aeolian transport corridor attains equilibrium with the southerly surface wind regime. If this were to occur, aeolian removal processes would cease completely. In reality, a combination of other aeolian processes, weathering processes and current systems also operate to modify the shape, size and distribution of immobile roughness elements. Viewed on sufficient time-scale, this limits the degree to which the bed can

establish equilibrium.

4.4.5. SURFACE DESTABILISATION BY NORTHERLY WIND REVERSALS

The photography of stone pavement surfaces during high sandflow conditions is difficult, not only due to the sand in saltation, but also because gusting causes camera shake. The garnet creep tracers were photographed on 22/09/87 during a moderate-energy wind reversal.

The stone pavement surfaces are usually in equilibrium with the southerly surface-wind flow. During a northerly wind, the imbricate shape-fabric is not as effective in stabilising the surface grains, and some of the bedload creep population is likely to be dislodged from stable positions on the bed (Figure 4.71). This results in the partial destruction of equilibrium with the southerly surface-wind. Northerly winds are therefore instrumental in reintroducing creep grains to the mobile population, and maintaining transport through the basin.

4.4.6. OTHER PROCESSES REDUCING THE DEGREE OF STABILISATION THAT A STONE PAVEMENT SURFACE CAN ATTAIN

Modification of Roughness Element Shape by Aeolian Processes

Optimal conditions for aeolian corrasion of the roughness elements, protruding into the saltation layer above stone pavement surfaces, theoretically exist within aeolian transport corridors, where the areal concentration of sandflow is a maximum. Observations support this concept, and many roughness elements exhibit evidence of aeolian corrasion. The facets cut into the roughness elements are predictably best developed on south-facing surfaces. The facetted surfaces are either rather flat and fluted (Figure 4.72), or concave-up and smoothly polished (Figure 4.73). On some windward surfaces, a sub-horizontal step can be observed above the ground surface (Figure 4.74). The height at which this step is cut probably indicates the height at which the kinetic-energy flux of the saltation load (sensu Anderson, 1986) diminishes close to the bed.

Ultimately, whatever the form of corrasion initially takes place, given sufficient time, aeolian erosion is likely to plane the roughness element almost level with the surrounding bed

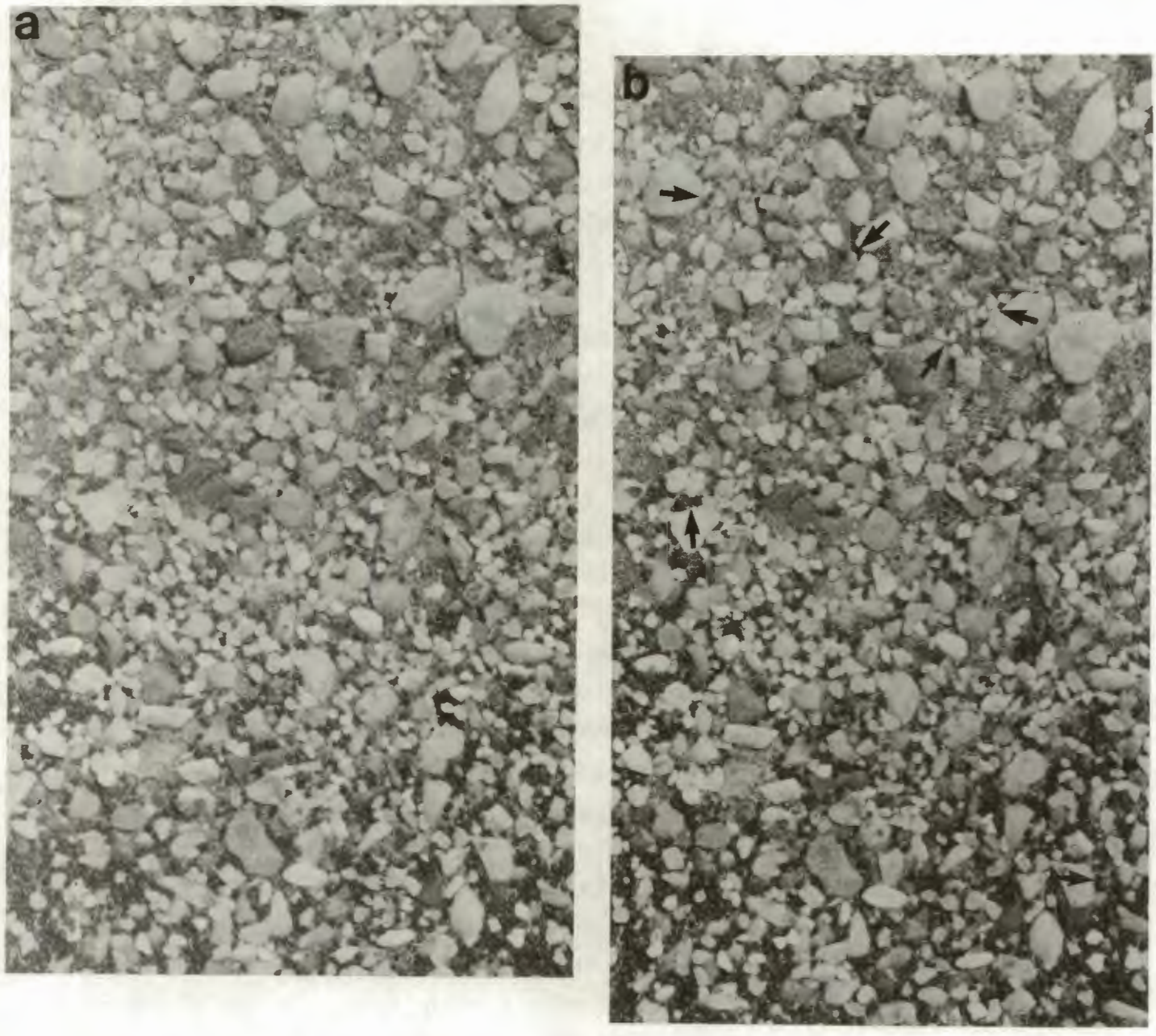

Figure 4.71. Stereo-pair of stone pavement taken during a northerly wind reversal on 22/09/87. (a) was taken about 5 minutes before (b). The arrows highlight the pervasive changes which effected the bed configuration as creep transport proceeded. The dark grains are the garnet bedload creep tracers used in the experiment on the stone pavement near sand trap site C. Note how some of the grains become lodged behind the immobile roughness elements.

Figure 4.72. Cobbles and boulders of silcrete on a stone pavement formed from an alluvial host deposit. The windward faces are severely facetted and fluted. Note the creep bedload covering the surface between the immobile roughness elements. The barchan dune in the top right corner (arrowed) indicates this site's proximity to the centre of the Bakers Bay aeolian transport corridor. The southern end of the main dolomite yardang field, approximately due east of Pomona, can be seen to the north of the stone pavement.

Figure 4.73. Concave-up facetted surface of a phonolite cobble on an alluvial plain at the eastern margin of the Bakers Bay Aeolian transport corridor, approximately due east of Bogenfels. Note the fluting on the upper surface, which appears to be initiated where feldspar phenocrysts are exposed. The silcrete clasts on the upwind side have been polished by aeolian processes. Southerly wind from right to left. Scale 30 cm.

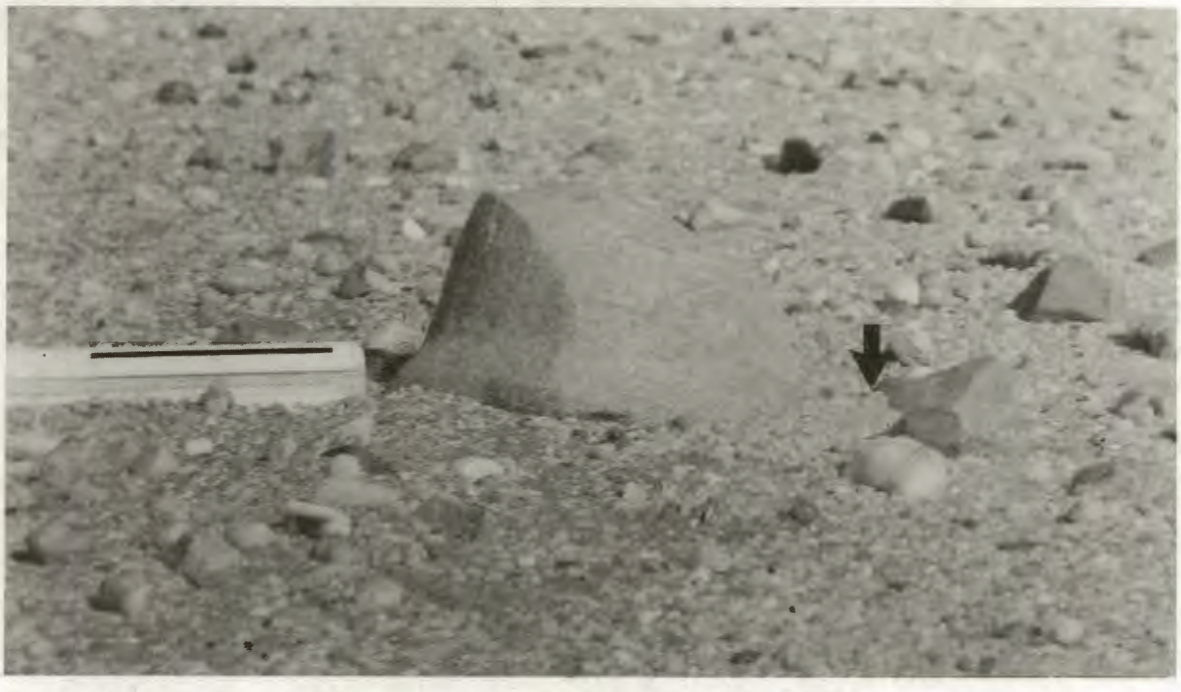

Figure 4.74. Stepped facet cut into a quartzite cobble on a stone pavement surface at the eastern end of the Grillental. The step probably marks the height at which the saltation loads kinetic-energy flux diminishes above the bed. Note the particle cluster on the bed (arrowed). Southerly wind flow from left to right, bar on scale 10 cm.

(Figure 4.75). The achievement of the end-point of modification is probably rarely observed because the surfaces are disturbed by other factors. It is most frequently attained where relatively soft clasts of pan carbonate (calcite, with minor dolomite) and Bogenfels Formation dolomite occur on surfaces.

Initially, aeolian corrasion modifies the pattern of wind flow in the vicinity of the roughness element. This is liable to change the pattern of bed shear stress surrounding the roughness element. The configuration of the creep bedload on the stone pavement must readjust if surface stability is to be maintained. The alteration of cross-sectional profiles is also likely to modify the pattern of vortices shed by the roughness element. Thus the points at which the high-velocity vortices impinge on the downwind bed will vary with time, resulting in further readjustment of the bedload. In addition, as the cross-sectional area of the roughness element protruding above the bed is reduced, the extent of the lee-side shadow zone protected from direct saltation impact during southerly wind flow decreases. Pervasive alteration of the bed configuration over a wide area downwind of the modified roughness element probably then results. This reflects the extensive sphere of influence which roughness elements impart on the downwind bed configuration. Once a roughness element is planed to the approximate elevation of the surrounding stone pavement, its influence is reduced considerably. Provided that the step, marking the upwind margin is sufficiently elevated above the bed, it will act as a barrier to the migration of the creep bedload (Figure 4.76).

The Effects of Salt Weathering

Other weathering and erosion processes influence the spacing and density of roughness elements on stone pavement surfaces situated within aeolian transport corridors, but evidence of them is rapidly destroyed by aeolian corrasion and transport. Stone pavement surfaces beyond the limits of aeolian transport corridors do not exhibit the same degree of surface organisation (Figure 4.77) despite the continued, but reduced, influence of the aeolian dispersal system. A common feature of these surfaces, many of which contain large cobbles and boulders derived from underlying and surrounding alluvial and / or marine deposits, is the splitting and

Figure 4.75. Pedogenic hardpan calcrete nodule with a sub-horizontal step cut into the south face. Had this process continued, the entire clast would eventually have been planed at the elevation of the bed. Note the small knobs and bosses near the top of the windward face, which formed in response to differential corrasion due to the presence of small quartz grains in the calcrete. Scale 10 cm.

Figure 4.76. A roughness element of Bogenfels Formation dolomite planed approximately level with the surrounding bed by aeolian corrasion. Note the small knobs and bosses formed due to small patches of quartz in the dolomite. There is a small step along the windward edge, which forms a slight obstruction to the migration of the creep load. A particle cluster is present along this temporary barrier. This clast lies directly in the path of a 28 m high barchan dune within the Bakers Bay aeolian transport corridor. This accounts for the large quantity of aeolian sand stored on the pavement surface. Scale 11.5 cm.

Figure 4.77. Example of a stone pavement outside the influence of an aeolian transport corridor. Note that the surface does not show the same degree of organisation and that there is much less evidence of the creep bedload between immobile roughness elements. A silcrete clast (S) and a dolomite clast (D) have been split. This is a feature of stone pavements. Quadrant marked in 10 cm divisions, arrow shows the direction of southerly wind flow.

spalling of clasts.

The spalling of successive layers from clast surfaces protruding above the stone pavement surface particularly seems to affect quartzite clasts (Figure 4.78). This form of weathering produces angular, relatively platy fragments as succeeding layers are loosened, reducing the height of the roughness element. Loosened flakes are eroded from the south-facing surfaces by aeolian corrasion, whilst the flakes remain attached to downwind surfaces. The continuation of the weathering process ultimately almost destroys any evidence of the original roughness element. Pebbles, possibly transported to the site by ephemeral surface run-off, or brought to the surface by soil-forming processes, or deflation, subsequently occupy the gap on the stone pavement surface (Figure 4.79).

Splitting (Figure 4.80) affects a wide variety of different rock types, including quartz, quartzite, silcrete, phonolite, dolomite, and pan carbonate. Many of the affected clasts show minimal evidence of planes of weakness, although the presence of bedding planes is frequently exploited. As with examples of splitting from other desert regions (Cooke, 1970), the fracture orientation relative to the stone pavement surface varies widely, and there is no distinct evidence of chemical alteration. The fractures continue below the stone pavement surface, but close with depth in some instances (Figure 4.81a and b). This implies that they have opened at the sediment surface, where the addition of loose granular material progressively infills the opening. Split clasts on stone pavement surfaces also act as nuclei for creep bedload particle clusters. Splits oriented into the southerly surface-wind provide openings into which the creep bedload can migrate (Figure 4.82). This is one mechanism by which grains are introduced to the crack, allowing the split to be maintained. This resembles the process of dirt cracking described by Ollier (1969).

Evidence of salt weathering is widespread throughout the deflation basin, and surface crusts and salt efflorescences prove that salts are present (section 5.3). Frequent fog-wetting in the coastal area of the deflation basin, together with ephemeral rainfall, present suitable conditions for salt crystallization (eg. Goudie, 1972; Watson, 1981) during alternating cycles of wetting and drying. Consequently, salt weathering, which is the mechanism

Figure 4.78. Quartzite boulder on a stone pavement surface overlying Upper Eocene marine deposits near Bogenfels. Note the spalling of the surface. Fragments have been removed from the south face by aeolian corrasion. Southerly wind flow from right to left. Scale in cm.

Figure 4.79. A quartzite cobble which has been almost destroyed by spalling. Note that clasts have migrated into the gap produced on the stone pavement surface, masking the presence of the remains of the original clast beneath the surface. Scale in cm.

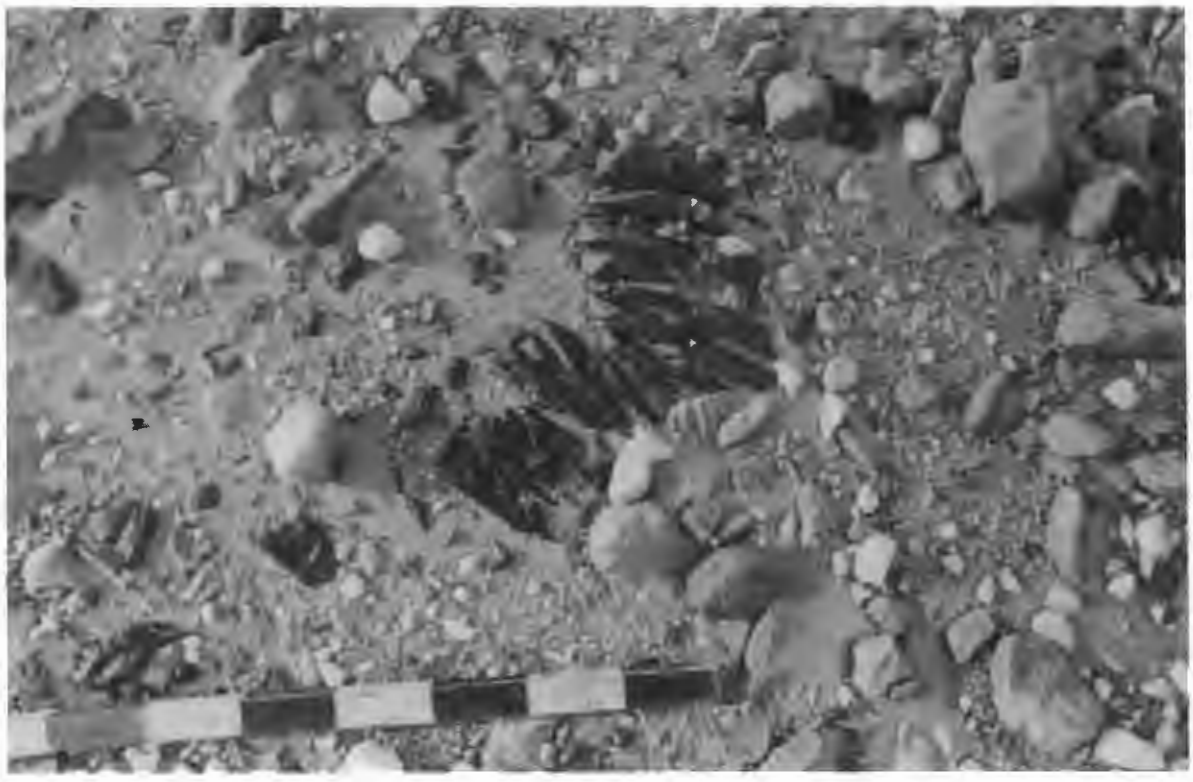

Figure 4.80. Split phonolite boulder on a stone pavement formed from an alluvial host. The fragments are close-fitting, and there is little evidence of planes of weakness. Scale 0.75 m.

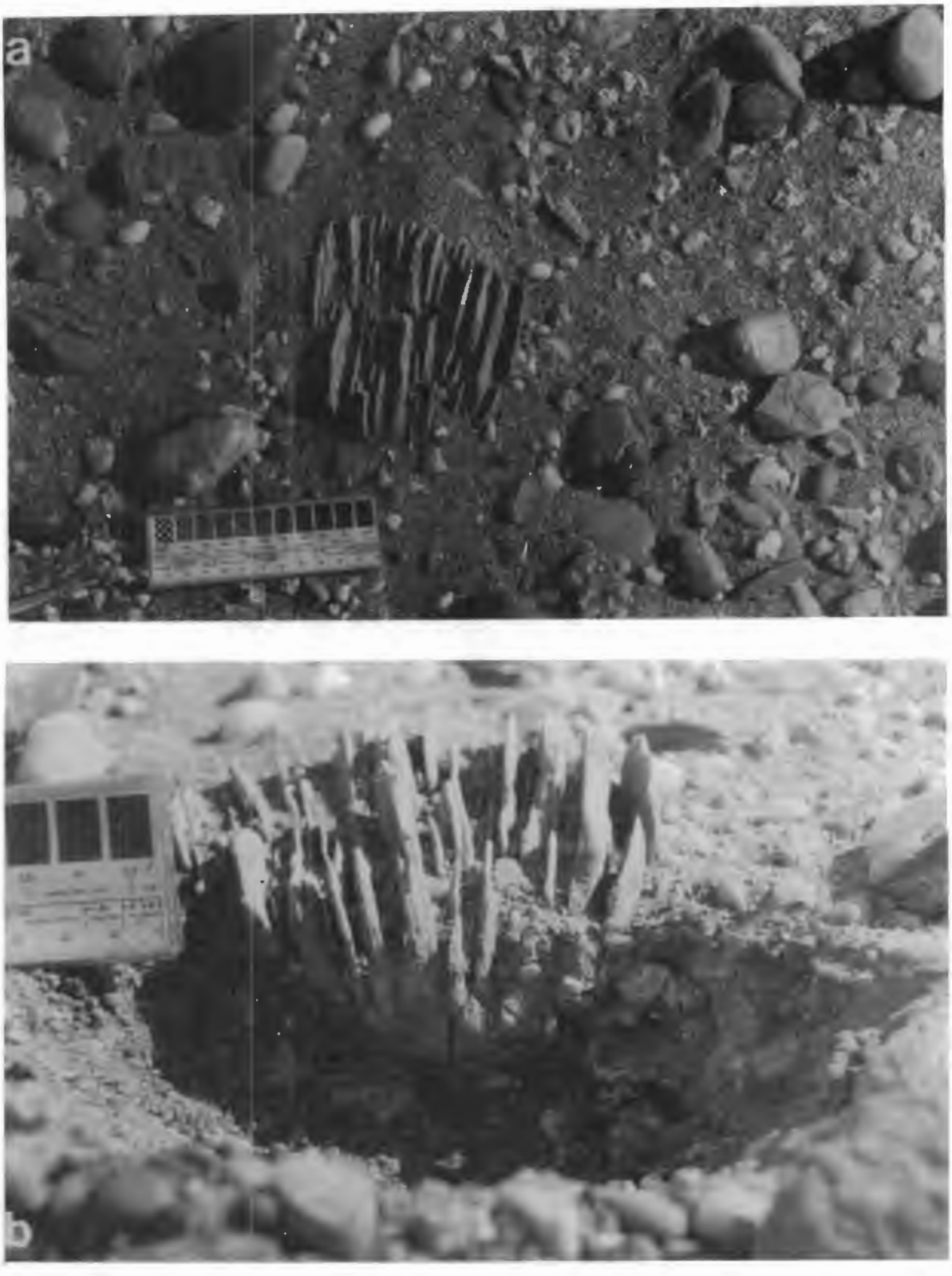

Figure 4.81. (a) Stone pavement surface with a quartzite clast split along bedding planes. The fragments are approximately parallel with the southerly wind which blows from bottom to top. Note the absence of quartz granules of the creep bedload. Scale 11.5cm. (b) Section at the south end of the split clast, showing the closure of the fractures with depth. The gaps between the fragments have been infilled by fine-grained, silty material. It is likely that this accumulates by the infiltration of the fines into the bed after fog or rainfall. Some quartz grains between the split fragments were probably transported there by aeolian creep. Scale in mm.

Figure 4.82. Split and facetted quartzite clast on an alluvial surface in the Grillental. Note that the creep bedload particles have migrated into the south end of the wind-aligned split. This provides a possible mechanism for the maintenance of the split once it is initiated. In this instance it has resulted in the development of a particle cluster on the bed at the leading edge of the roughness element. Quartz granules along the windward edge and eastern side exhibit a poorly developed imbricate shape-fabric. Small particles are probably unstable along the leading edge, and vortices potentially move them to the margins of the roughness element. Also note the aeolian current shadow on the north side of the roughness element. Southerly wind flow from bottom to top. Scale in cm.

proposed to explain this surface phenomenon in other deserts (eg. Cooke, 1970; Goudie and Day, 1980; Cooke, 1981), is invoked to explain the production of split fragments. This provides an alternative to the insolation hypothesis proposed by (Kaiser, 1926).

Cooke (1970), demonstrated that an important effect of splitting is to increase the density of roughness elements on stone pavement surfaces with time. In the Southern Namib deflation basin, the accompanying reduction in the size of the clasts forming roughness elements performs another function. Within this high-energy aeolian sediment dispersal system, the weathered fragments can subsequently be removed to the north by aeolian processes. It is therefore possible that the stone pavement surfaces are lowered because new, unweathered material is theoretically being continuously exposed. In areas outside aeolian transport corridors, this material might remain on the surface for a long period of time, until a change in the coastal morphology alters the position of high sandflow zones.

Slope processes, which probably act in conjunction with ephemeral surface run-off, also redistribute the weathering products in many instances (Figure 4.83).

4.4.7. POSSIBLE EVIDENCE OF CUMULATE SOIL DEVELOPMENT

Introduction

Recently, McFadden et al. (1987) have shown that the presence of a vesicular A horizon in soil profiles within the Cima volcanic field, provide evidence of cumulate soil formation. These authors have suggested that this soil forming process is primarily responsible for maintaining the clasts on the surface of stone pavements. Unfortunately, this information became available late in this study, and only a few observations could be made.

Possible Occurrences of Cumulate Soils within the Deflation Basin

A desiccated soil profile underlies the stone pavement surface in the path of the Bakers Bay barchans which lie within an aeolian transport corridor (Figure 4.84). The A horizon of this soil profile exhibits a vesicular texture. Other examples of a vesicular A horizon have been observed to occur beneath the surface of encroachment deposits within the deflation basin.

Figure 4.83. Split silcrete clast on a slope. Note the redistribution of the dark fragments by slope processes, which probably operate in conjunction with surface run-off. Scale 1 m.

Figure 4.84. Area of cleared stone pavement in the Bakers Bay aeolian transport corridor near sand trap site C. Note the desiccation polygons on the surface of the soil profile comprised of fine sand and silt. The A horizon exhibits a vesicular texture, which suggests that cumulate soil formation was taking place beneath the encroachment deposit which formerly covered the surface. Scale (arrowed) is 11.5 cm.

It is suggested that once the creep population has covered the bed, and the dynamic surface is stabilised by the development of an imbricate shape-fabric, cumulate soil formation proceeds. Fine-grained material may be washed down between the interstices of the stable creep bedload grains on the bed during ephemeral rainfall, or more frequently, by droplets of moisture condensed on the surfaces of the particles from the coastal fog. Thus the soil profile beneath the stable bed vertically aggrades by small increments providing the stable surface is not disturbed. This further prevents the creep bedload population on the surface from becoming embedded in the soil profile, which is maintained by the surficial addition of material. Within the high-energy deflation basin, the surficial build-up of fine-grained material at the surface is also prevented by aeolian corrasion and deflation. It is, however, likely that the process of cumulate soil formation does influence the dynamics of the creep bedload within the region to some extent.

4.4.8. THE EFFECT OF EPHEMERAL RAINFALL ON STONE PAVEMENT SURFACE ORGANISATION

Disruption of the Stone Pavement

Although it has previously been postulated that raindrops influence stone pavement surface configurations (eg. Cooke, 1970), it has not, as far as the author is aware, been observed.

An important feature of the deflation basin climate is that the incidence of heavy rainfall tends to coincide with high-energy wind reversals. Such an event occurred between 18/7/87 to 20/7/87, and is a classic example of the weather pattern associated with the passage of a coastal low moving down the coast in response to the passage of a cyclone south of the continent (Figure 4.85). The atmospheric pressure fluctuated markedly prior to the main event. This resulted in several low-energy wind reversals, typical of the winter months. The atmospheric pressure recorded at Alexander Bay shows a period of deep low pressure between 17/7/87 and 19/7/87, which corresponds with the intense peak in northerly wind-energy which was experienced at Bogenfels, during the main rainfall event.

People witnessing the main period of rainfall stated that it was unusually heavy for the west coast, and that it was accompanied by high-velocity northerly winds. Evidence of this wind reversal was widespread (see section 4.2). Prior to this event, the stone pavement surface exhibited a high degree of surface organization (as decribed above), and had established equilibrium with the southerly surface-wind regime. No evidence of this remained on 20/7/87 (Figure 4.86).

The changes were remarkable. Granules and small pebbles of quartz were reorganized into low ridges resembling ripples, one or two grains high, which were approximately oriented transverse to the northerly wind flow. The surface configuration resembled that observed after an earlier rainfall event in May 1985, which was better developed (Figure 4.87). In addition, granules and small pebbles of quartz could be seen piled up on the sediment surface. Some of these particles were imbricated, but their upper surfaces were inclined to the north (ie. opposite from previous observations), and uneven, deeply eroded pits separated the larger clasts (Figure 4.88). Some particles could be seen standing on their edge on the floor of some of these pits.

Prior to the 20/07/87, the rainfall events which had been

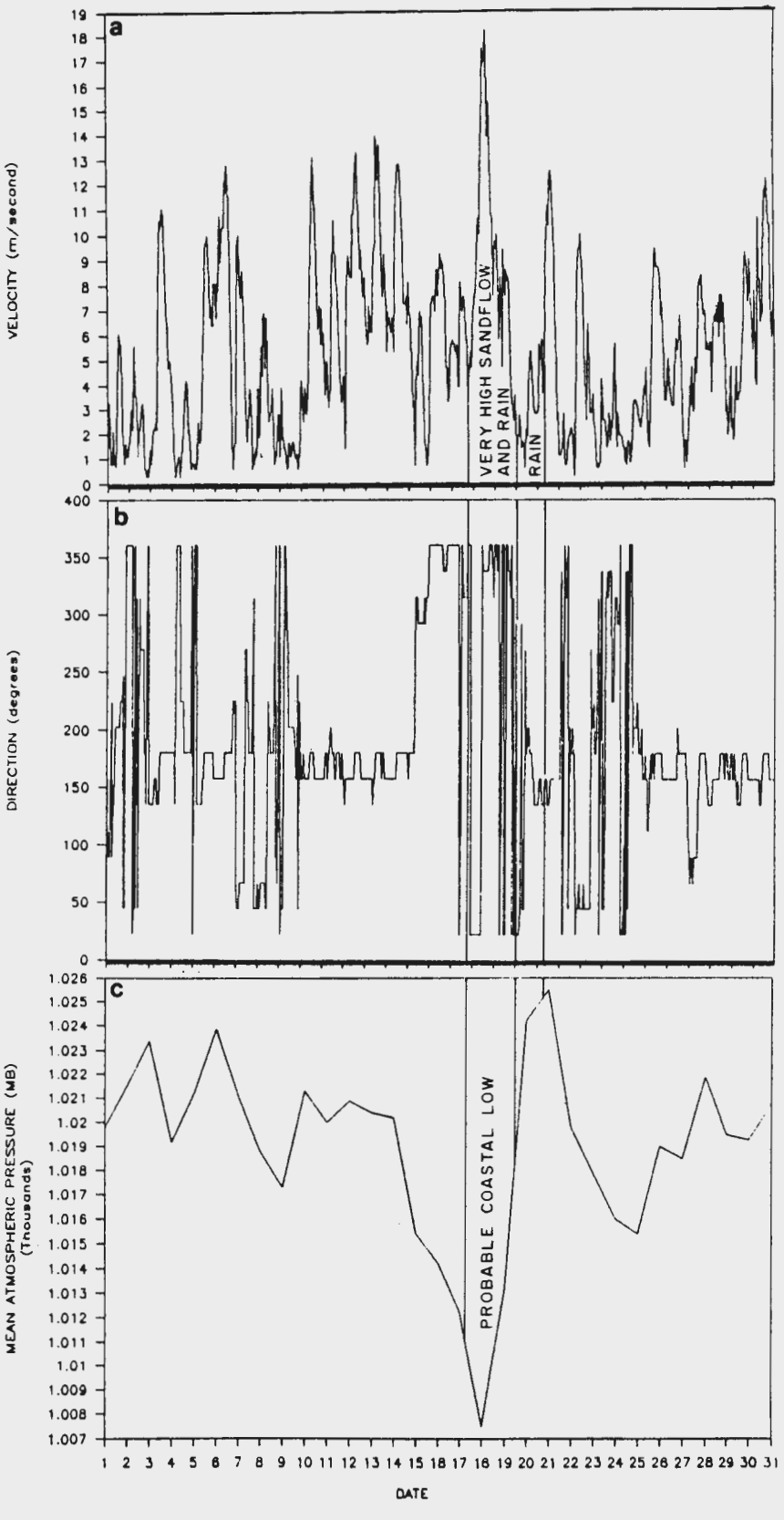

Figure 4.85. Graphs showing the variation of (a) the wind speed (b) the wind direction, and (c) the atmospheric pressure during July 1987. Pressure records are for Alexander Bay. Note that the peak in northerly wind energy clearly corresponds to the sharp reduction of atmospheric pressure, which is interpreted as a coastal low. The duration of the rainfall event is also shown.

Figure 4.86. (a) Aeolian current shadows in the lee of vegetation entirely reversed by the high-energy wind reversal. Note the disorganised, chaotic appearance of the stone pavement near sand trap site C. Northerly wind flow from left to right. (b) The destruction of the imbricate shape-fabric and close packing of the creep bedload by rainsplash erosion. The underlying fine-grained material has been exposed, and eroded by rain-impact. Northerly wind flow from top to bottom. Note that the quartz granules have accumulated in discrete patches. Scale 11.5 cm long.

Figure 4.87. Ridged, sandy surface marking the earlier position of an aeolian current shadow (now reversed), on which rain-impact ripples have formed. Ripple-like, transverse bedforms in the foreground have developed on a previously planar encroachment deposit surface. Northerly wind flow from right to left. Scale 1 m.

observed were not as heavy, and evidence of rainsplash had been limited to rain-impact craters on silt and clay sediment surfaces (Figure 4.89), upon which a similar ripple-like effect had been seen after rain on 04/05/87. The craters in the troughs between the ripple-like features are attributed to raindrop impact. It is suspected that the ridges, a few millimetres high, represent rain-impact ripples (sensu Clifton, 1977). The absence of rain-impact craters on the crests is puzzling. It possibly reflects a tendency for the ridges to be flattened by repeated raindrop impact once they attain a certain height which is related to raindrop size, as described by Allen (1982). The transverse ridges on the surface of aeolian current shadows in May 1985 are also attributed to raindrop impact. Their steeper face was inclined into both the northerly wind and the rain. The surface of the encroachment deposit between the aeolian current shadows was also transformed into a series of ridges as a result of raindrop impact.

Evidence from stone pavements along the margin of Marmora Pan show that the surface break-up of 17 to 20/07/87 recorded above was also due to rain impact. Large quartz roughness elements were found perched on top of sand pedestals about 0.5 to 1 cm high, which were surrounded by sandy depressions with pitted floors (Figure 4.90). Ridges of sand associated with these features were pointing to the south. These are interpreted as scour-remnant ridges in the lee of the roughness elements, which probably resulted from raindrop impacts driven by the northerly wind reversal.

Implications for Aeolian Sediment Dispersal

The combination of heavy rainfall, large droplets and a high-velocity northerly wind is capable of greatly modifying the surface configuration of granules and small pebbles on stone pavements. Sustained surface wetting probably softens the underlying soil carapace composed of silt, which reduces its resistance to rainsplash erosion. As the impact of large raindrops alters the surface configuration, the underlying fine-grained material is then susceptible to rainsplash. The sand and silt is thrown up and erosion hollows are formed. The stone pavement is totally destabilised by this activity.

During the subsequent return to southerly surface-wind conditions, the stone pavement surface dries out. The fine-grained

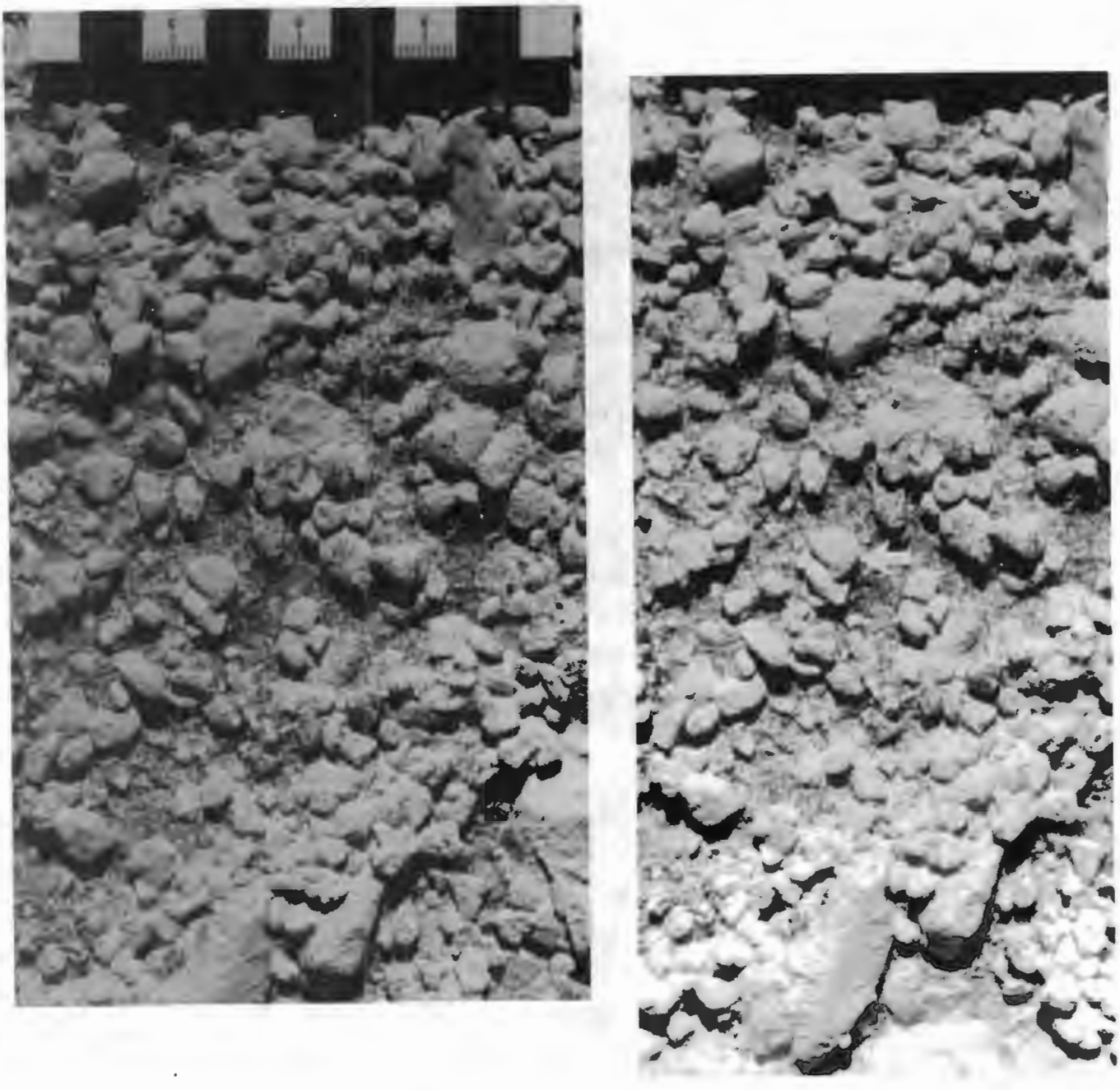

Figure 4.88. Stereo-pair illustrating the depth of the rain-impact hollows eroded into the fine-grained material exposed between the immobile roughness elements and creep bedload. Note the imbrication of clasts (arrowed), which are oriented for a northerly wind flow from top to bottom.

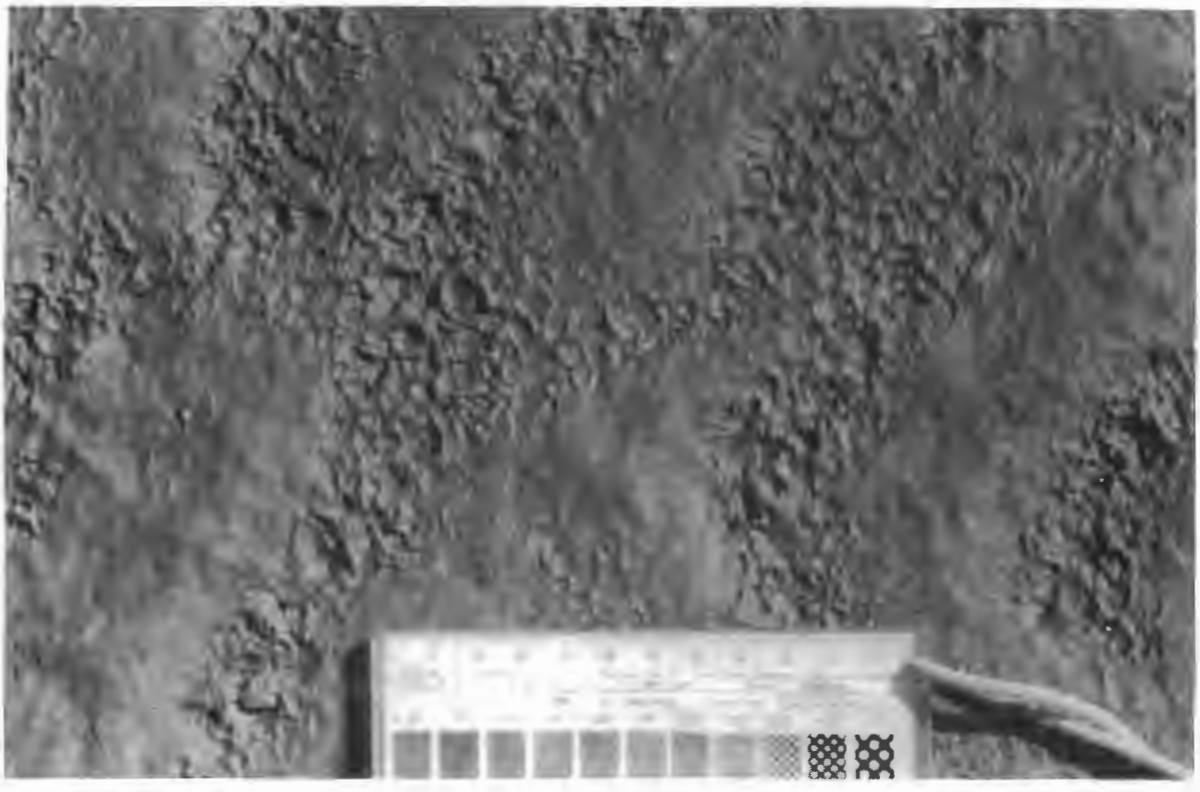

Figure 4.89. Rain-impact ripples formed in silt and clay. Note the rain-impact craters on trough floors. There is minimal evidence for crater formation on the crests. Scale 11.5 cm.

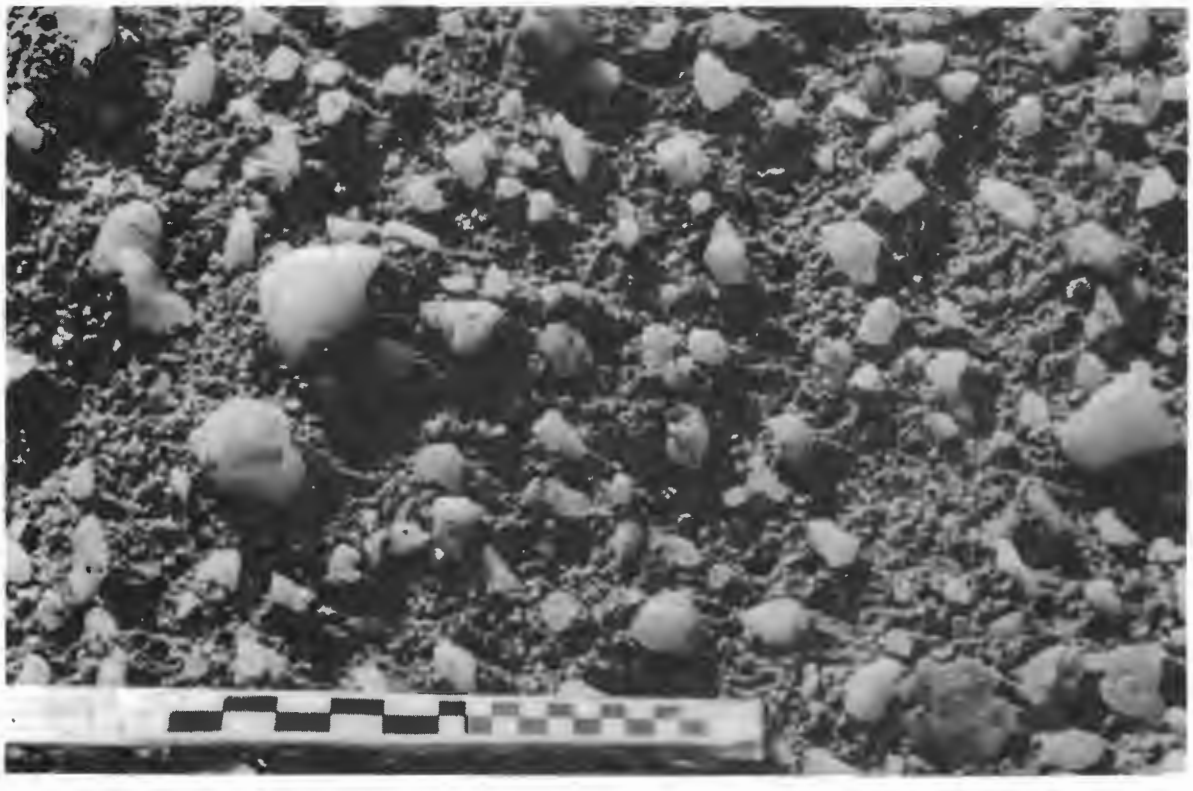

Figure 4.90. South-pointing, fine-grained ridges in the lee of roughness elements raised on pedestals above the surrounding bed, which represent areas which were protected from rainsplash erosion. Northerly wind flow from left to right. Scale 10 cm.

deflation. In places, raindrop erosion exposes new roughness elements which were previously beneath the surface, and changes in the configuration of immobile roughness elements are possible. As deflation proceeds, the pedestals supporting the larger clasts are eroded, and the roughness elements are lowered to the new elevation of the bed. This also changes the surface configuration and provides a potential mechanism for the lowering of stone pavement surfaces.

Because the creep bedload is not in a stable surface configuration, sandflow crossing the stone pavement is probably able to entrain granules and even small pebbles more readily than it can normally. This possibly results in a brief period when creep transport rates are increased.

The evidence of rain-impact modification is very short-lived. Within a few days, the erosion hollows are difficult to locate, and the surface begins to readjust. By early January 1988, the organisation of the creep bedload had advanced considerably, and indications of imbricate shape-fabric development could be seen. Within a year, the stability of the surface has been re-established. Small ripple-like bedforms are present once more, and the imbricate shape-fabric is clearly developed.

When rain-impact occurs on a sand dominated bed, rainsplash is likely to be an important mechanism whereby roughness elements are brought to the surface. Ephemeral stream beds of the type described below are likely to be susceptible to this type of stone pavement development. Examples are found at the southern end of the Idatal, where roughness elements appear to stand noticeably more proud of the intervening sand surface after rain events than they do normally. Surface run-off along with other factors (see below) may also partially account for this.

The evidence presented above shows that within high-energy aeolian environments such as the Southern Namib, the history of stone pavement development can be very complex. The role of raindrop impact erosion in the development and maintenance of stone pavements cannot be overestimated. Coupled with observation of the role played by bedload creep transport, and salt crystallization near the sediment surface in promoting stone pavement formation, it is clear that previous deflation hypotheses (eg. Blake, 1904;

Moulden, 1905; and Free, 1911) are too simplistic. It now appears as though the process of cumulate soil formation must also be considered when studying the development of stone pavements. It is therefore dangerous to assume that one process might explain the development of stone pavements, because the climate and wind conditions under which they occur varies greatly. It is far more likely that numerous processes, some of which might occur only very rarely, interact to create a stone pavement. Depending upon local conditions one process might completely dominate the others. The role of infrequent events, however, in creating and maintaining stone pavements should not be underestimated.

5. SEDIMENT DISPERSAL BY EPHEMERAL SURFACE RUN-OFF

5.1. RUN-OFF GENERATION

Rainfall occurs throughout the year within the deflation basin, but the heaviest rain tends to fall during the winter months (April to July) (Kaiser, 1926). Personal observation shows that surface run-off generation is enhanced by the presence of exposed bedrock and the sub-surface carapace of silt beneath stone pavements. As in other deserts, the sub-surface carapace tends to reduce infiltration of the run-off (eg. Cooke, 1970), as does the bedrock. The best catchments are therefore located in areas in which the areal extent of exposed bedrock and stone pavements is greatest.

5.2. EPHEMERAL STREAM SYSTEM RESPONSE TO RUN-OFF

5.2.1. RUN-OFF RESULTING FROM LIGHT RAINFALL

During light rainfall, the generation of surface run-off is principally restricted to areas of exposed bedrock. Slight depressions form very localised catchments which collect the run-off. This subsequently flows in shallow channels a few centimetres to tens of centimetres wide.

These small streams are highly ephemeral. Their transport capacity is limited and they tend to rework aeolian deposits of sand and granules downslope over short distances. The reworked material is redeposited in a series of small lobes (Figure 5.1), each of which remain active for a short period only, due to infiltration of the run-off. Consequently, the distributary channels frequently switch direction. Where the catchments are slightly larger, or the rainfall persists longer, gullies are rapidly eroded into substrates of aeolian sediment, and the material is redeposited as small alluvial cones at the base of the slope (Figure 5.2).

The main effect of these events on the aeolian system is the re-introduction of sediment from aeolian deposits along the margins of the basins. The resulting alluvial cones are rapidly reworked by the aeolian dispersal system, as the sediments undergo desiccation. A slight increase in the sandflow rate is probably experienced by areas lying downwind (ie. to the north) until the alluvial deposits have been completely reworked or the sediment surface becomes stabilised once more.

Figure 5.1. Aeolian sands partially reworked by a very brief period of surface run-off from a bedrock floored catchment. Note the depositional lobes formed by switching of the main channel. Scale 1 m.

Figure 5.2. Gullies eroded into aeolian sands during a brief period of surface run-off from a bedrock high. Note the alluvial cone deposited at the foot of the slope. Scale 1 m.

5.2.2. RUN-OFF RESULTING FROM HEAVY RAINFALL

Ephemeral Stream System Morphology

During heavy rainfall events, as occurred on 03/12/85, 11/6/86, 4 and 5/6/87 and 17 to 20/7/87, surface run-off is generated over a much wider area. The generation from catchments floored by bedrock probably still exceeds that from catchments floored by other substrates though.

Numerous distributary channels from different catchments form a braided network which rapidly merges into larger channels within the system (Figure 5.3). As the water flows down from the basin margins, aeolian sands choking old channel courses are rapidly eroded down to bedrock (Figure 5.4). The run-off from larger catchments is sufficient to re-activate old channel courses that cross relatively flat stone pavements (Figure 5.5), and large-scale reworking of the stone pavement sediment occurs.

No matter what form the basin takes, there is a tendency for the ephemeral stream systems to focus on subtle topographic depressions which need only be 2 to 3 m deep, at the base-level of the ephemeral stream systems. A centripetal drainage system is therefore developed (Figure 5.6), which terminates at ponded water bodies. Kaiser (1926) termed these sites "gravitational centres", because of the deposition of reworked material around the margins.

The ephemeral stream networks within endoreic basins are entirely controlled by basin morphology (Kaiser, 1926). Typically, the systems consist of dendritic tributary networks which form on the south-facing slopes at the northern ends of basins (Figure 5.7). These slopes act as a natural catchment, which feeds into successively higher order streams, until a main channel flows south into the ponded water body at base-level.

The dendritic tributary networks rework large quantities of aeolian sediment, including creep bedload material (Figure 5.8). Aeolian deposits are also reworked along the margins of the basins, and aeolian granule ripples are eroded in many cases (Figure 5.9). These sediments are then incorporated into deposits on the ephemeral stream bed (Figure 5.10). Provided that the rainfall maintains the run-off for sufficient duration, the reworked aeolian material is transported back towards base-level.

Major rainfall events rarely occur within the hyper-arid deflation basin, but their role in terms of the regional sediment

Figure 5.3. Bedrock floored catchment south-east of Bakers Bay, showing the sandy nature of the material transported between 17-20/07/87. Note how the channels coalesce, and the reworking of aeolian sand from former current shadows (C) which were blocking the channel courses. Scale 1 m.

Figure 5.4. Reactivation of an ephemeral stream channel resulted in the erosion of large quantities of aeolian sand from the channel course. This material was removed from a temporary storage site, and re-introduced to the aeolian system. The channel is about 1 m deep.

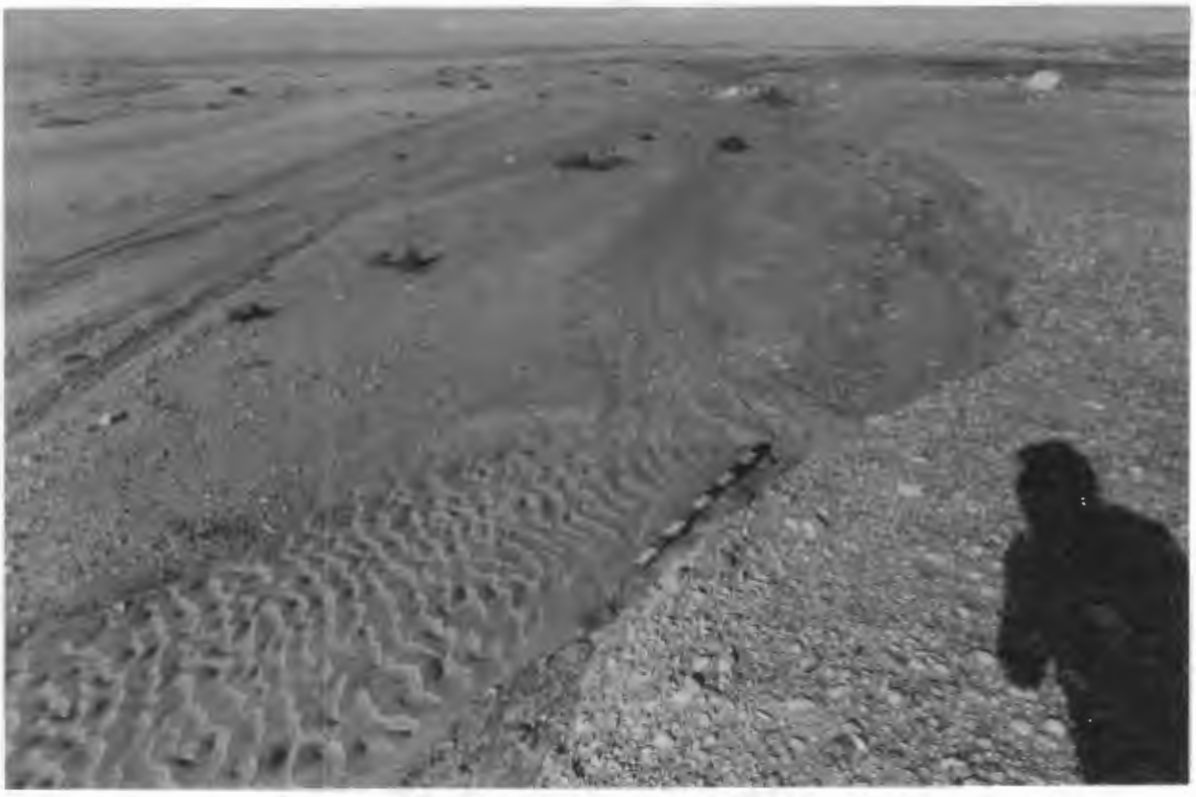

Figure 5.5. An ephemeral stream channel re-incised into a stone pavement about 3 km east of Bogenfels. Note the current ripples of reworked aeolian sand on the channel floor. Scale 1 m.

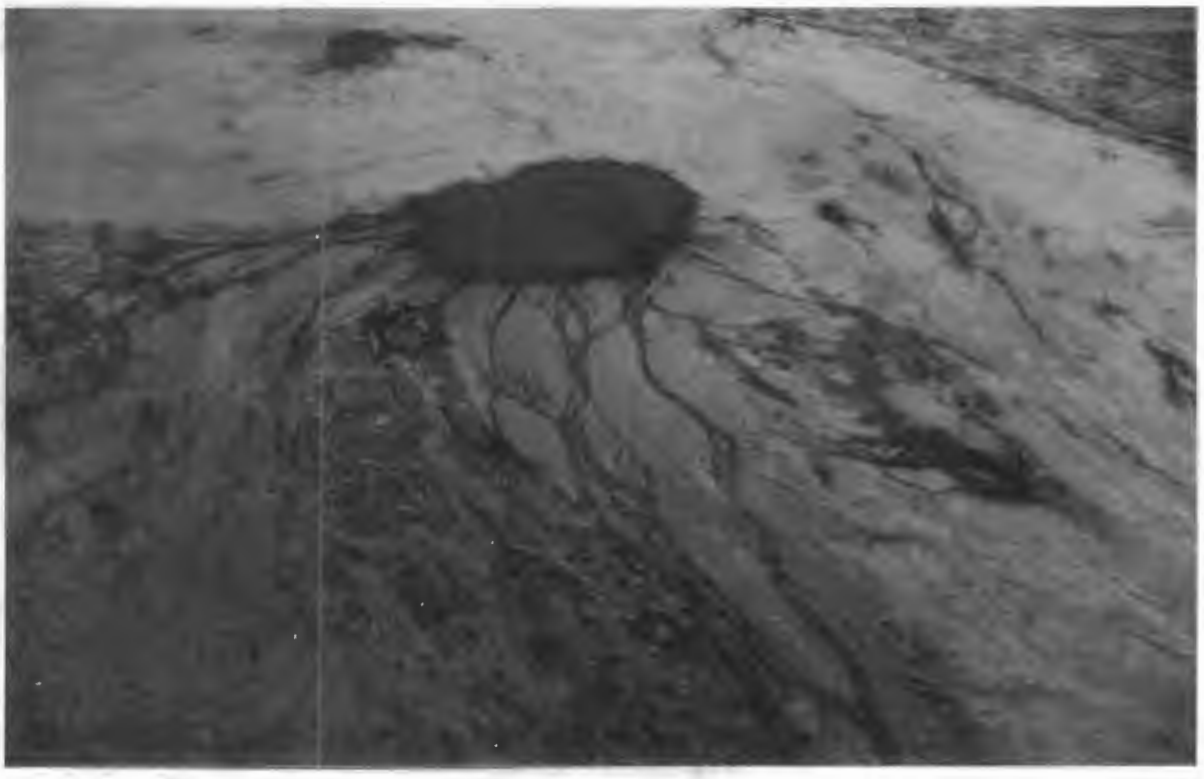

Figure 5.6. Ponded water body at the distal end of numerous ephemeral stream channels flowing into a minor bedrock depression south-east of Bogenfels.

Figure 5.7. Dendritic, ephemeral stream tributary network reworking aeolian sands, and an encroachment deposit of granules on a south-facing slope at the northern end of an endoreic basin. Note that some granule ripples in the background were unaffected by the ephemeral stream activity. Southerly wind flow from right to left. Scale 1 m.

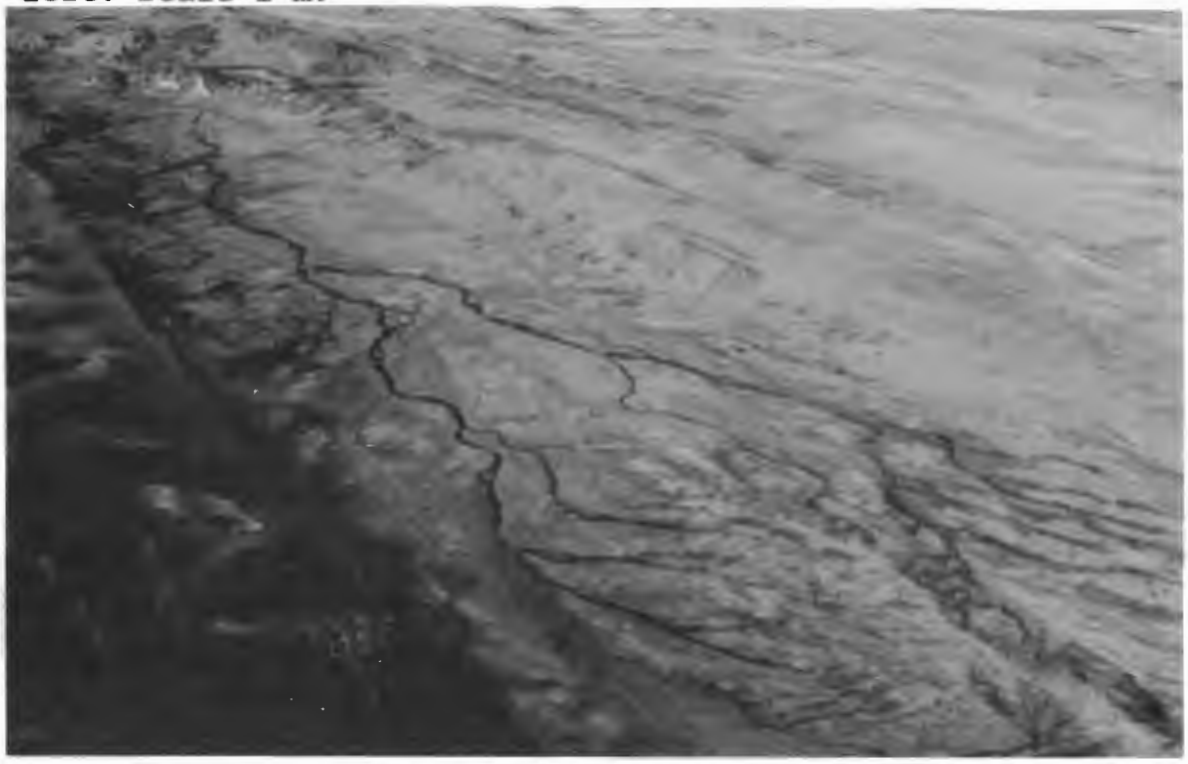

Figure 5.8. Oblique aerial view south, down Rux-Felder, about 3 km west of the Buntfeldschuh escarpment. The ephemeral stream catchment was situated on the south-facing slope at the northern end of the endoreic basin. The tributary network feeds into a main channel, which enters the ponded water body formed at the southern end of the basin. Note the western margin of the Chameis Bay aeolian transport corridor in the bottom left corner. Southerly wind flow from top left to bottom right.

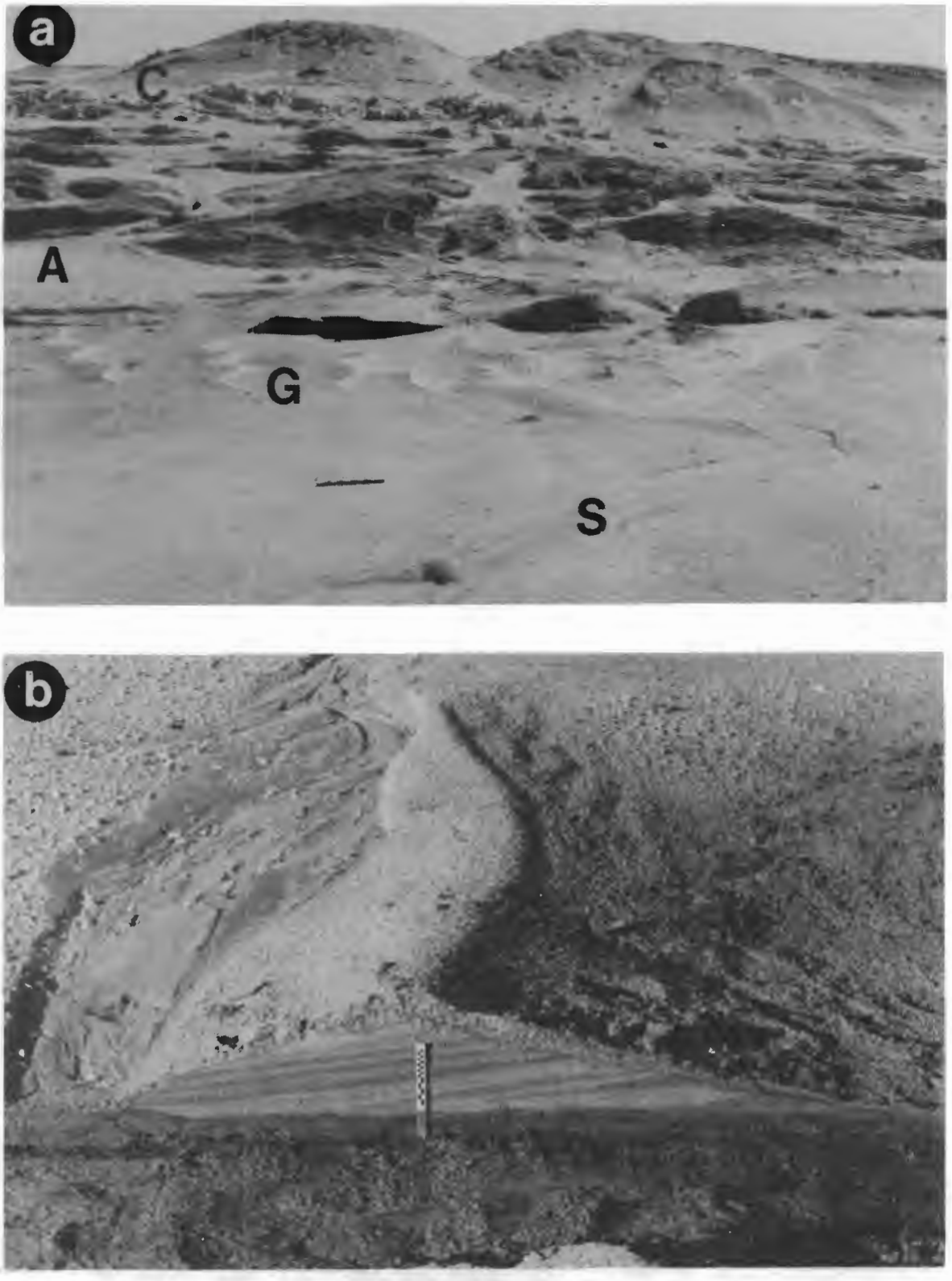

Figure 5.9.(a) Bedrock catchment (C) with an alluvial cone (A) at the base of the slope and an ephemeral stream (S) reworking reversed aeolian granule ripples (G). (b) Longitudinal section through an aeolian granule ripple, showing crestal reversal in response to the northerly wind of 17-20/07/87. A small ephemeral stream channel partially reworked the bed form. Note the very shallow depth of the deposit beneath the granule ripple, which rests on weathered bedrock. Southerly wind flow is from right to left. Scale 10 cm.

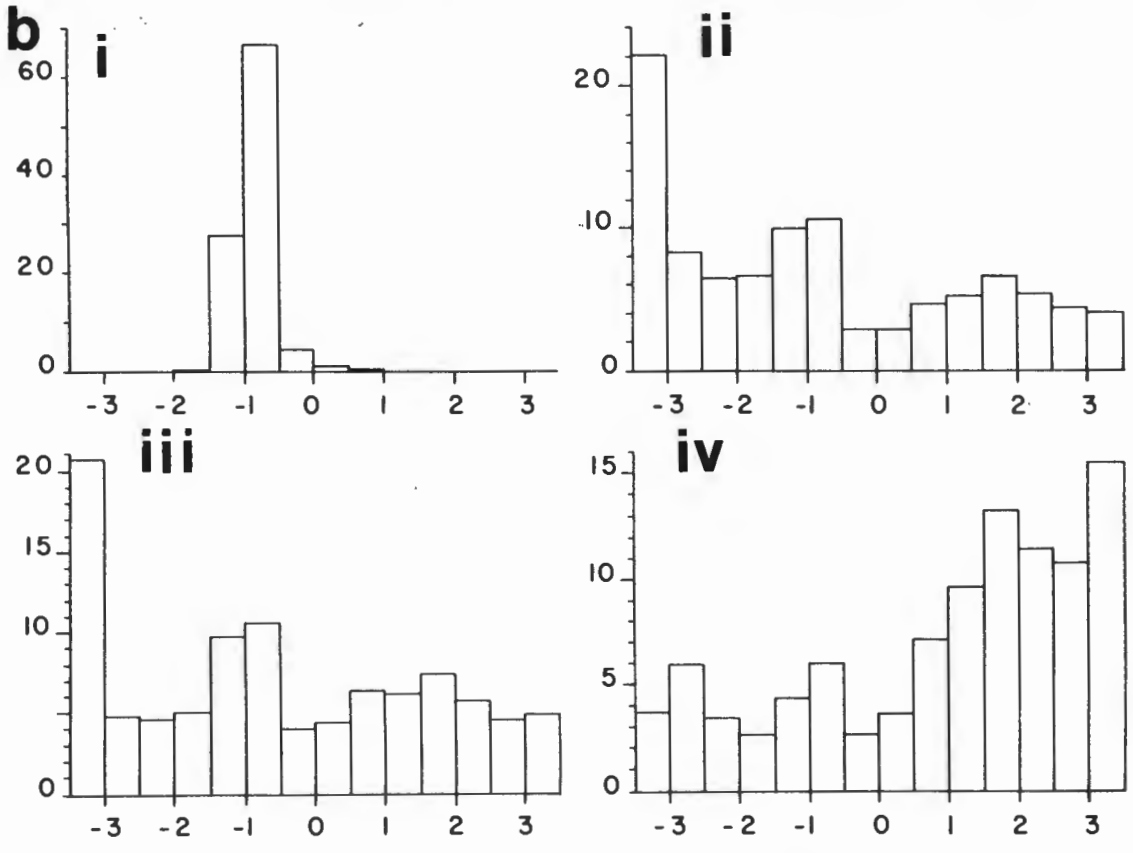

Figure 5.10. (a) Sample locations in the channel shown in Figure 5.9. Scale 1 m. (b) Graphs showing the variation of grain size distributions, (i) granule ripples, (ii) stone pavement south of ephemeral channels, (iii) south channel floor (iv) north channel floor. Sand is more abundant on the floor of the ephemeral stream bed. This probably reflects the reworking of aeolian sands from up-slope, and its deposition during waning flow within the channel, as run-off generation ceased and the remaining flow infiltrated the bed.

dynamics cannot be underestimated. In contrast to aeolian bedload transport, which is comparatively slow, ephemeral stream systems transport large volumes of sediment, including sand and pebbles, in a very short space of time. Like northerly wind reversals, these events disrupt the equilibrium of the aeolian system with the southerly surface-wind flow, and re-release vast quantities of material back into the aeolian sediment dispersal system from temporary storage sites. They therefore have a significant influence upon the sandflow through the deflation basin. It is probable that higher sandflow rates occur downwind (ie. to the north) of areas in which ephemeral stream systems operate, during the subsequent deflation of the deposits.

5.3. AEOLIAN SYSTEM RESPONSE TO EPHEMERAL STREAM EVENTS

5.3.1. EPHEMERAL STREAM BEDS WITH NO SURFACE CARAPACE

As shown above, ephemeral alluvial activity within the deflation basin has two main effects:

1) release of aeolian sand from southerly wind storage sites;
2) redistribution of sediment of various grades from catchments to base-level focal-points of the stream systems.

In all cases, the initial ephemeral stream deposit is not in equilibrium with the southerly surface-wind flow.

Widespread rainfall occurred throughout the Southern Namib on the 4 and 5/04/87, and many ephemeral stream systems flowed. Three sites were subsequently monitored in the Idatal as sub-aerial desiccation proceeded (Figure 5.11). Importantly, all of the ephemeral stream beds examined were intially composed of gravel and sand, because minimal clay or silt is present within the catchment. Consequently, no fine-grained surficial drape was deposited on the stream bed at any of the sites.

Idatal Site 1

Immediately after shallow, channelized ephemeral flow had ceased, flow parallel sand ribbons were present on the rough gravel bed (Figure 5.12). The initial wavelength of these bedforms, which are developed by secondary flow created by the variation of flow transverse roughness on the gravel bed (Karcz, 1966, 1967; Allen, 1966), was about 0.1 to 0.2 m.

Initially, sand partially blanketed the bed, and only the larger

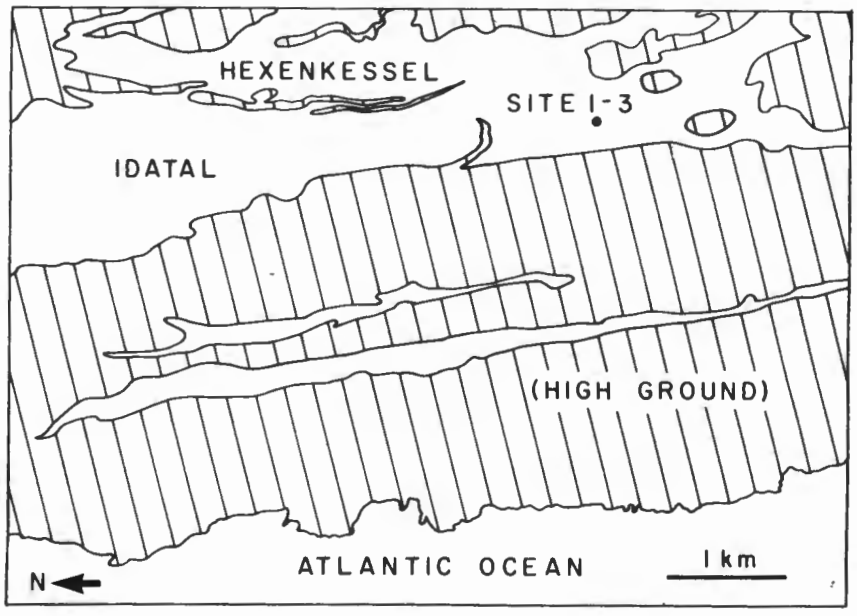

Figure 5.11. Map showing the location of the Idatal comparative photography sites used to monitor post-ephemeral stream flow modification of the stream beds.

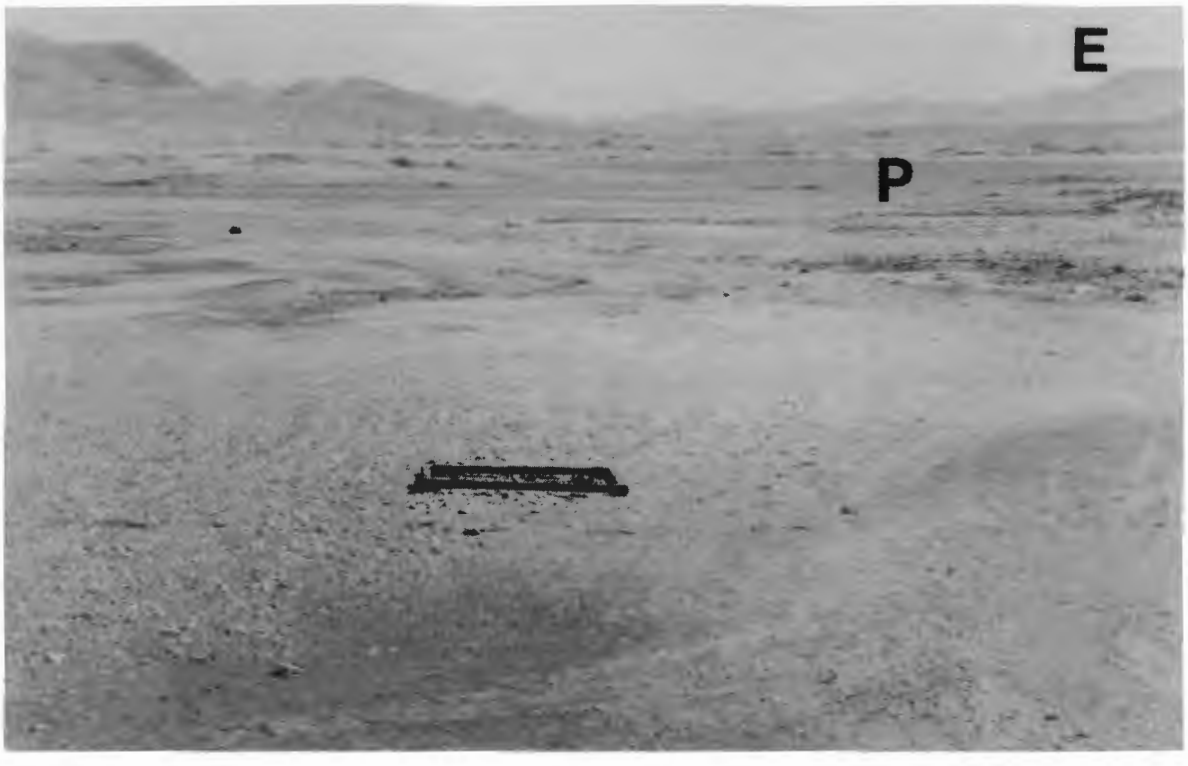

Figure 5.12. View north along the Idatal basin floor. 0.9 m wide quadrat marks the position of Idatal site 1. The ponded water body (P), which persisted for some months, marks the distal end of the ephemeral drainage system. Elfertberg (E) can be seen in the background.

quartz pebbles projected through the surface (Figure 5.13a). As desiccation of the bed proceeded, the micro-relief became more pronounced. The sand ribbons were raised relative to the surrounding bed, and their surfaces became uneven and "crumpled" (Figure 5.13b). As desiccation continued, the surface became more deformed. The surface then began to break up. A thin (few grain thick), surficial crust composed of sand grains was destroyed by the saltation load and aerodynamic forces (Figure 5.13c). Once the initial break-up of the surface crust had occurred, aeolian deflation could proceed more rapidly. Granules and small pebbles released from the ephemeral stream deposit by deflation surrounded small fragments of the crust adhering to the bed. Scour-remnant ridges developed in the lee of these clasts as deflation proceeded under the influence of the southerly surface-wind flow.

Repeated wetting and drying in response to subsequent rain events were punctuated by periods of deflation, which released more clasts from the underlying ephemeral stream deposit. In time, a disordered stone pavement was generated (Figure 5.13d).

Idatal Site 2

At site 2, about 2 m east of site 1, the initial sediment surface was predominantly sandy, and straight crested current ripples covered the bed. Aeolian processes acted more swiftly upon this part of the stream bed, and destroyed the initial bed forms within 11 days of the rainfall (Figure 5.14a). The bed remained sandy for some time, but deflation of the surface gradually exhumed clasts from the stream bed (Figure 5.14b).

There was no evidence of surface crust formation at this site, which suggests that the sediment was possibly being removed too quickly to allow its development. Scour-remnant ridges were formed in the lee of clasts brought to the surface by deflation (Figure 5.14c). The development of these features was also controlled by the southerly surface-wind flow.

After about 5 months of sub-aerial exposure, the bed, which had not experienced any further alluvial activity, was transformed into a well-developed stone pavement (Figure 5.14d). The surface was stabilised by the release of granules and small pebbles from the stream bed by deflation. Rainsplash on the bed between roughness elements during subsequent rain events, possibly added additional

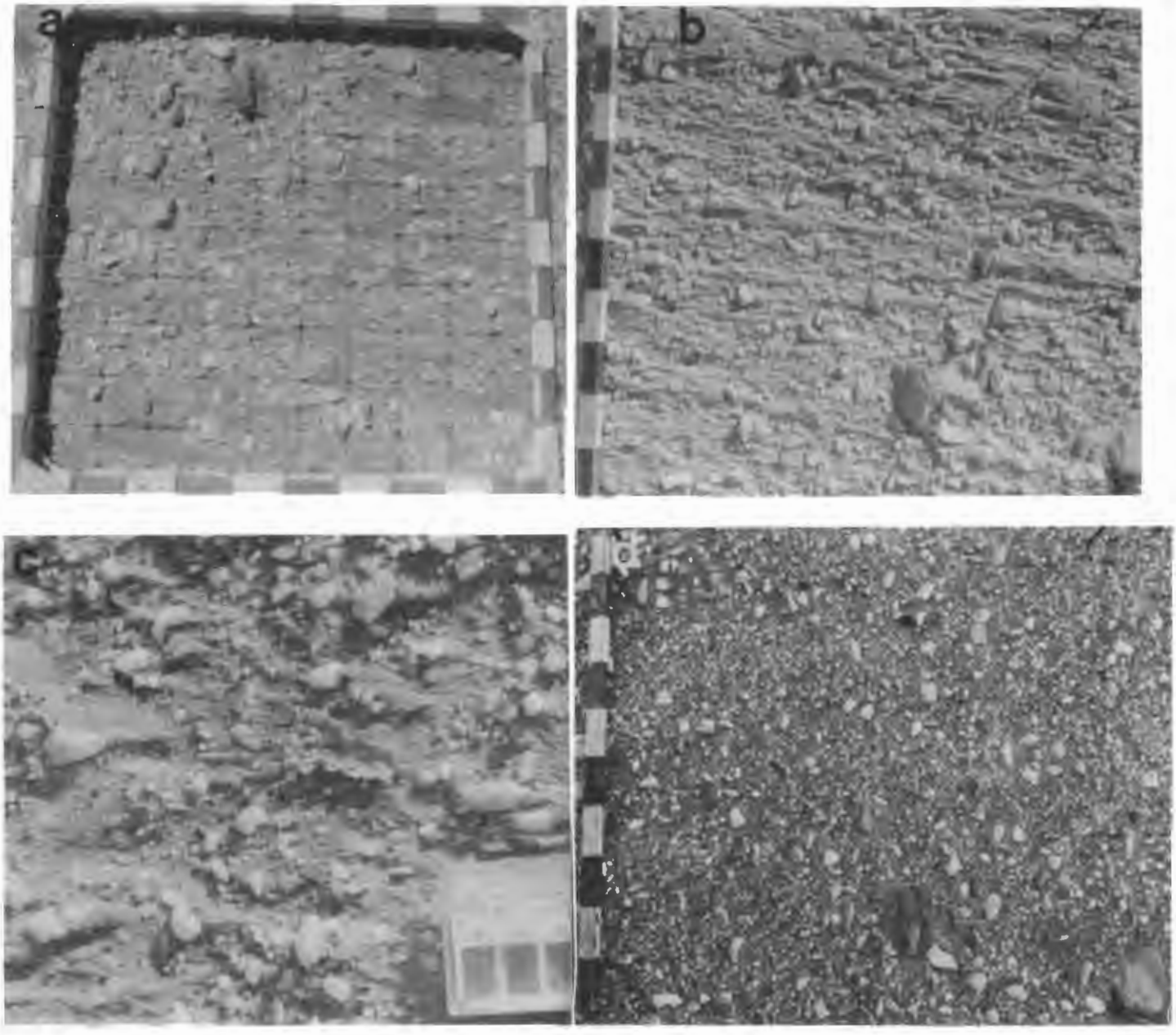

Figure 5.13. Idatal comparative photography site 1. (a) Initial bed configuration on 16/04/87 after rain on 4 and 5/04/87, showing sand ribbons on the gravel stream bed. Quadrat marked in 10 cm units. Arrow points to the north. (b) Initiation of surface deformation on 05/05/87 prior to surface break-up. Sand ribbons are more prominent at surface, with a "crumpled, puffy" appearance. Flow from left to right. Scale in 10 cm divisions. (c) Detail of surface adjacent to site 1 on 05/05/87. Note the thin, surficial crust fragment (C) adhering to the underlying sediment, and the development of scour-remnant ridges on the northern side of clasts exposed on the bed by deflation. Note that the particles show no evidence of organisation on the bed. Scale in mm. (d) Immature stone pavement surface on 22/09/87. Comparison with (b) proves the progressive release of clasts from the stream bed by deflation. Southerly wind flow from left to right. Scale in 10 cm units.

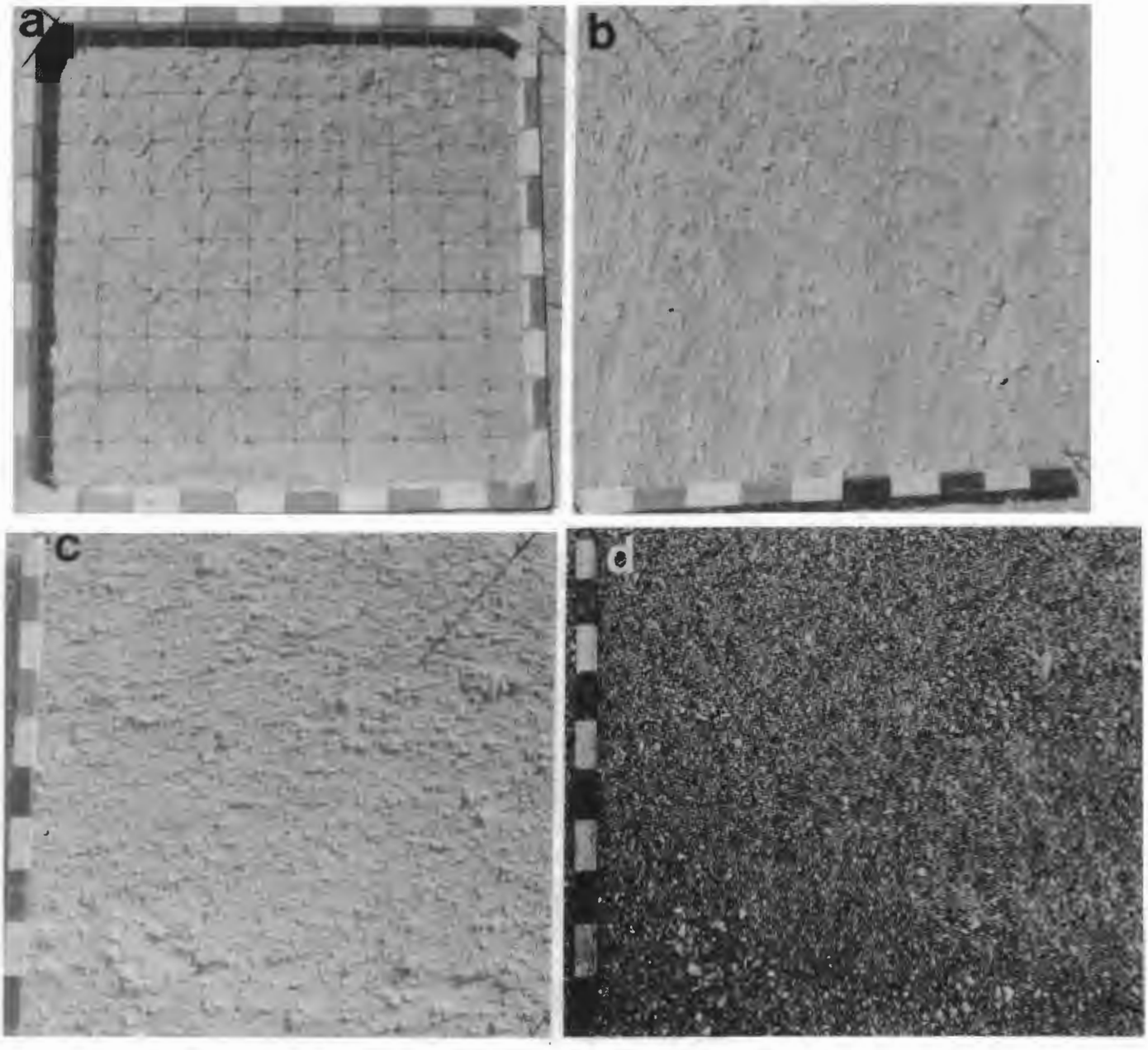

Figure 5.14. Idatal comparative photography site 2. (a) Stream bed on 16/04/87, showing remnants of sandy, long-crested current ripples. Note the scarcity of roughness elements on the surface. Arrow on quadrat points in direction of flow. (b) Stream bed on 23/04/87, exhibiting less evidence of the original current ripples. Note that quartz granules and small pebbles are beginning to appear at the surface. Scour-remnant ridges developed in the lee of the roughness elements provide evidence that deflation by the southerly wind, which flows from the bottom to the top of this frame was responsible. (c) More advanced stage of pavement formation on 05/05/87. Additional roughness elements have emerged at the surface, and scour-remnant ridges have been formed by deflation of the bed. Southerly wind flow from left to right. (d) Complete cover of fine-grained stream bed by roughness elements was achieved by 22/09/87. Note that scour-remnant ridges are no longer visible, and that the bed was effectively stabilised from this point in time. Southerly wind flow from left to right. Scale in all frames in 10 cm divisions.

clasts to the stone pavement surface, by erosion of the sand.

Idatal Site 3

The third site was located in a small depression on the stream bed. This site provided the best demonstration of surface crust formation. The bed was initially covered by current ripples of locally reworked aeolian sand, with a scattering of quartz pebbles over the bed, and within ripple troughs (Figure 5.15a). The location of this site within a small depression meant that sub-aerial desiccation progressed more slowly, and the sediments remained saturated. The bed forms were therefore still intact at the start of observations.

Gradual deformation of the current rippled bed occurred as desiccation proceeded (Figure 5.15b), and salt efflorescence occurred in the ripple troughs. Eventually, the doming of a thin (few grain thick) surficial crust above the underlying bed almost destroyed the initial form of the current ripples (Figure 5.15c and d). These delicate, hollow domes were progressively raised into the saltation layer, and became increasingly susceptible to aeolian erosion. Flaky fragments of the crust remaining on the surface were rapidly destroyed by the wind. This doming effect, and its subsequent destruction by aeolian processes, resembles that affecting the Bogenfels Formation sandstones which form the floor of parts of the Idatal (section 2.2.3). As deflation proceeded, the density of roughness elements exposed at the surface progressively increased (5.16a and b), leading to the eventual stabilisation of the surface.

The extent to which aeolian deflation of ephemeral stream beds proceeds is dependent upon the periodicity of rainfall events, which either saturate the bed, or result in further ephemeral stream deposition. Repeated surface crust development will then occur, before deflation can proceed with the development of a stone pavement. This cycle introduces short-term pulses of aeolian sand back into the aeolian system from temporary storage sites.

A large reservoir of sediment redistributed by ephemeral stream systems is therefore potentially available for deflation as the southerly wind-energy increases after winter rainfall. This sediment input to the aeolian system is probably very significant in areas outside aeolian transport corridors, where sandflow is low

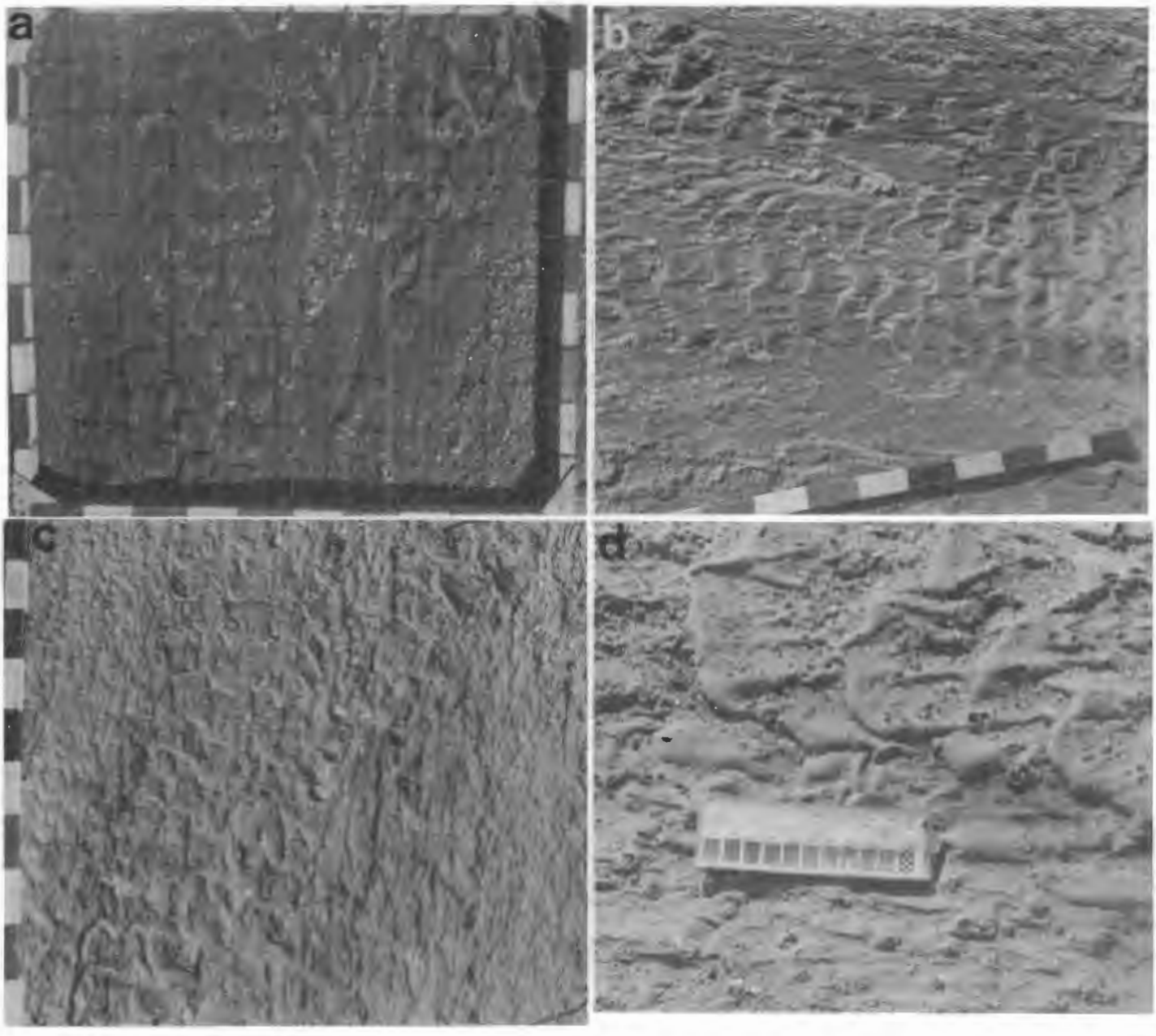

Figure 5.15. Idatal comparative photography site 3. (a) Short- and long-crested current ripples on the predominantly sandy ephemeral stream bed on 16/04/87. Flow from bottom to top of frame. (b) Initiation of surface crust development and surface deformation on 23/04/87. Note the light areas in the ripple troughs, which provided sites for salt efflorescence. (c) Latter stages in surface crust formation on 14/05/87. Note the "puffy" appearance of the domed sediment surface, and the gross deformation of the original bed morphology. (d) Close-up of the bed in (c), to show the hollow nature of the domes. Scale 11.5 cm. Scale in (a) to (c) in 10 cm units.

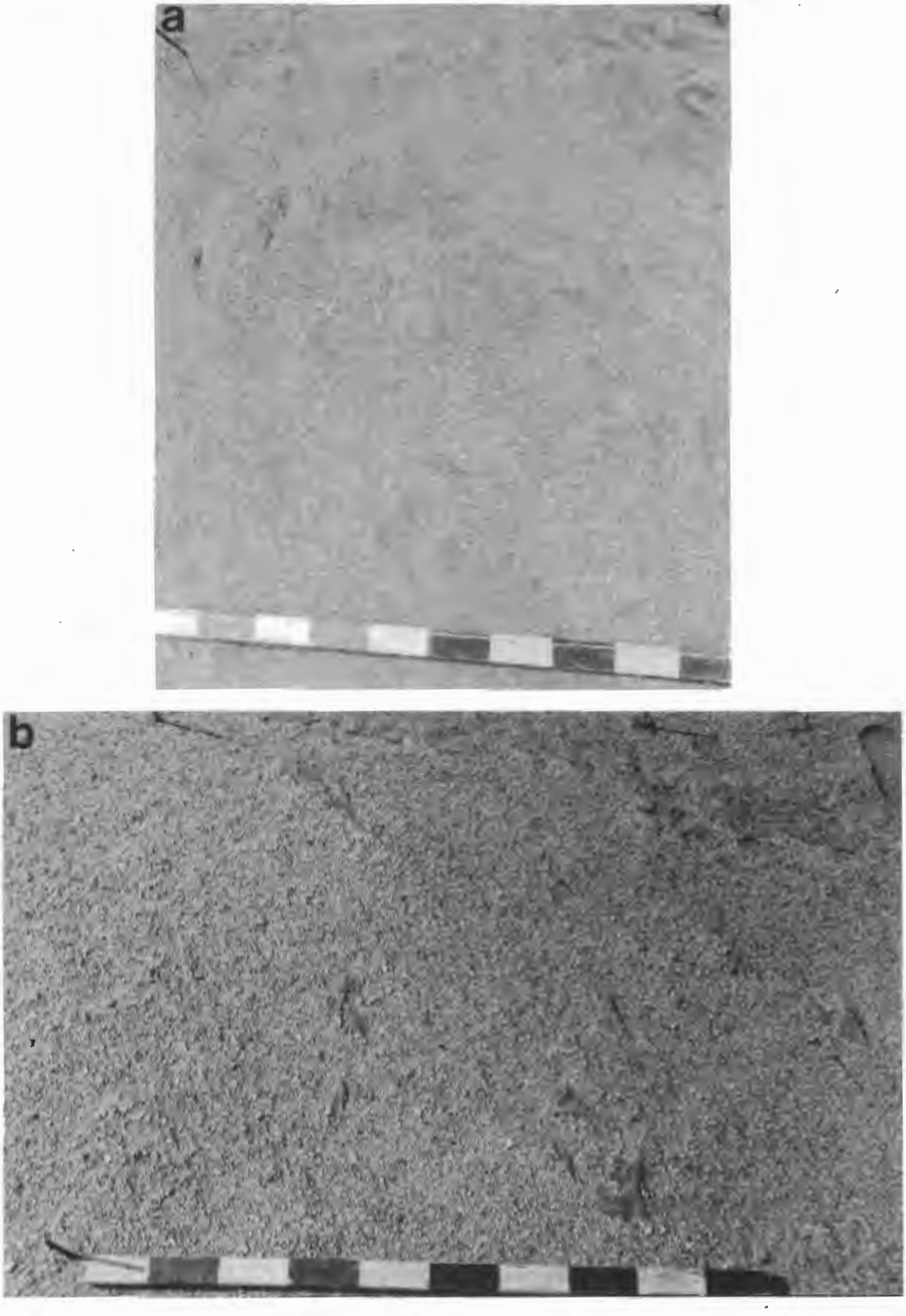

Figure 5.16. Idatal comparative photography site 3. (a) Initial stages of stone pavement development on the ephemeral stream bed on 22/09/87. Periodic rainfall saturated the site a number of times, resulting in the repetition of the cycle of surface crust formation. (b) Stone pavement surface on 05/01/88. Note the increase in the cover by roughness elements on the stone pavement. The bed was not completely stabilised, because the presence of scour-remnant ridges proved that deflation was still active. Southerly wind flow from bottom to top, and scale in 10 cm units.

due to the lack of a sediment source under normal conditions.

Observation of a Ponded Water Body in the Idatal

A ponded water body was also monitored within the Idatal (Figure 5.17a). Wind-generated surface waves propagated in response to the southerly surface-wind progressively reworked aeolian current shadows. These sands were redeposited as tongues of sediment elongated to the north, which were out of equilibrium with repect to the southerly surface-wind regime once the ponded water body dried-out. The aeolian dispersal system then rapidly reworked the sand tongues (Figure 5.17b).

Clays and silts are deposited from suspension in ponded water bodies to form drapes over the former stone pavement surface (Figure 5.18a). A remarkable sequence of events was observed once this drape had been sub-aerially exposed, and desiccation proceeded. Shortly after exposure, steeply dipping clay rims began to develop around the base of clasts protruding through, and resting upon the clay drape (Figure 5.18b). Despite aeolian sandflow across the surface, small domes appeared on the clay drape between the clasts, and the rims subsequently entirely enveloped the quartz clasts (Figure 5.18c). The mounds which developed on the surface acted as roughness elements, and small aeolian current shadows formed in their lee. Once the aeolian saltation load associated with high-energy southerly surface-winds began crossing the exposed bed, the clay drape forming hollow domes was rapidly eroded (Figure 5.18d). The underlying stone pavement was then re-exposed at the surface.

Doming of the clay drape on other parts of the bed resulted in the development of convex-upward desiccation polygons (Figure 5.19). These thin crusts were also rapidly destroyed by the saltation load and aerodynamic forces, and the fine-grained sediment was deflated to the north.

Observations South of Bogenfels Pan

A fifth site, situated to the south of Bogenfels Pan was also monitored. The ephemeral stream bed chosen crosses a flat stone pavement dominated by quartz clasts (Figure 5.20). Ephemeral stream flow partially reworked the stone pavement and also introduced aeolian sand eroded from the catchment.

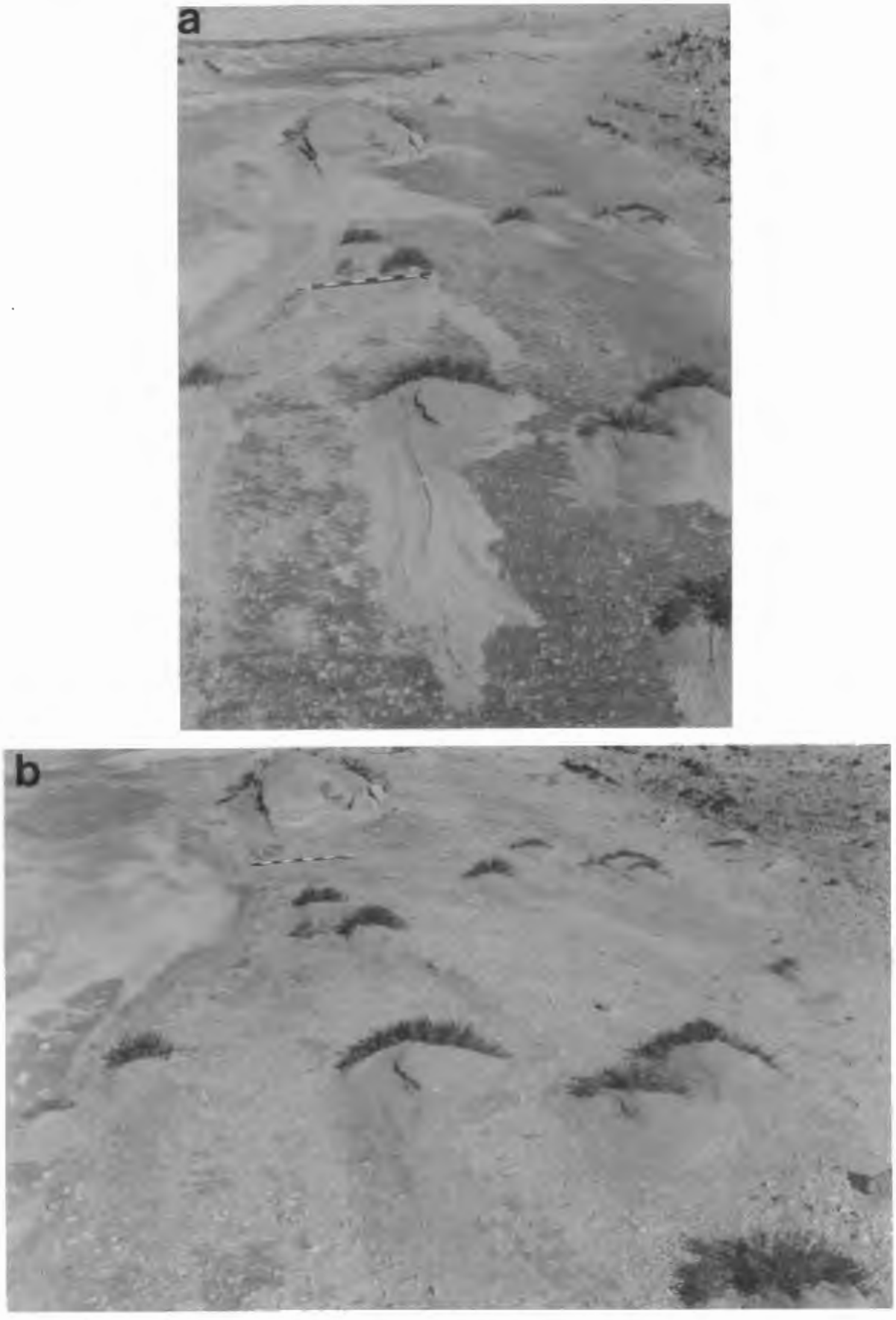

Figure 5.17. Comparative photographs of a ponded water body. (a) Aeolian current shadows in the lee of vegetation, partially reworked by wind-generated surface waves on a ponded water body on 05/05/87. (b) Same area on 14/05/87, showing that once the reworked aeolian sands were dry, they were rapidly reworked by the southerly wind blowing towards the reader in this frame. This reworking introduced a brief pulse of sandflow into the aeolian dispersal system. Scale in 10 cm units.

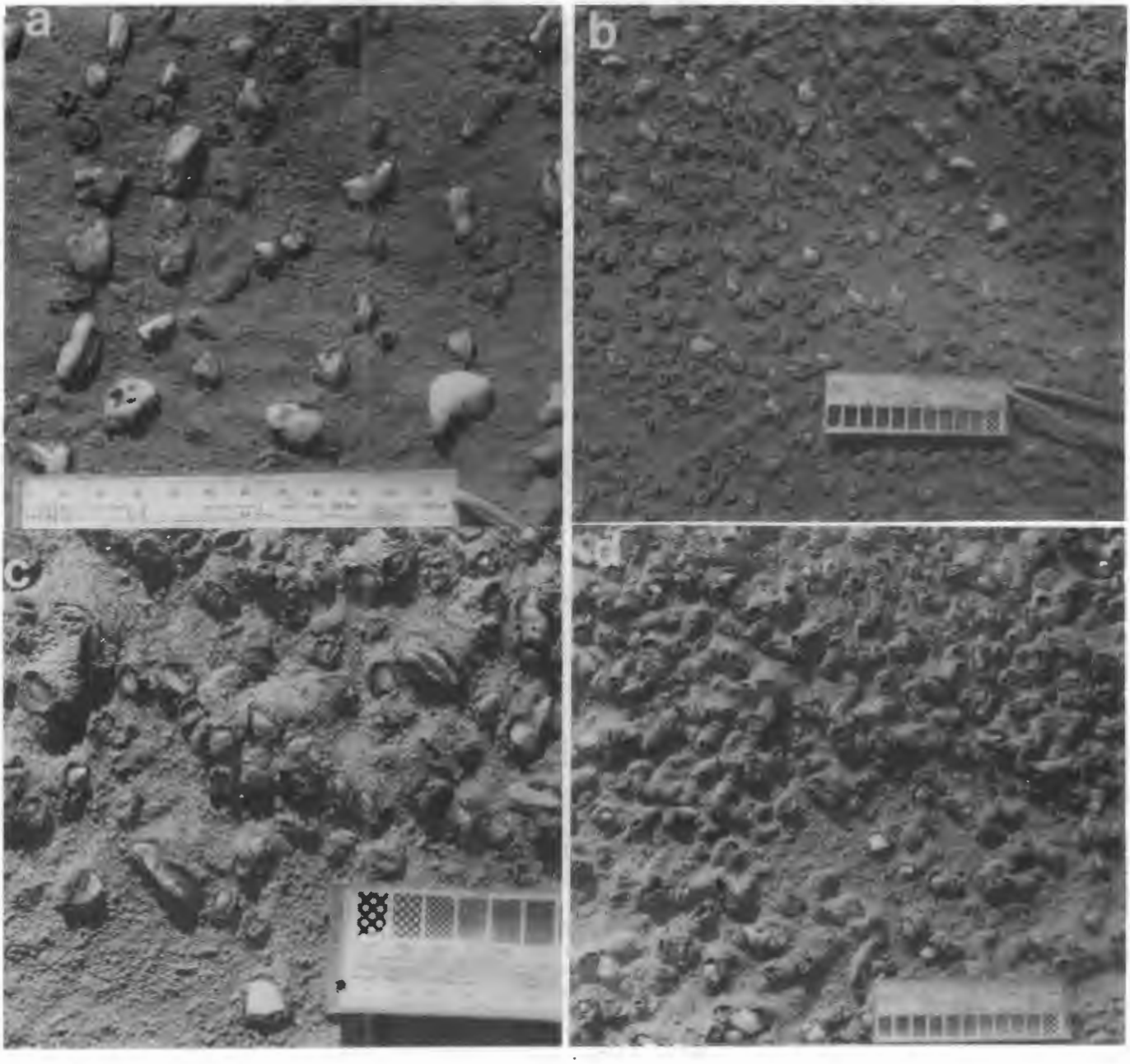

Figure 5.18. Idatal ponded water body comparative photographs. (a) Knobbly clay drape surface deposited from suspension, covering an underlying stone pavement. Note the quartz pebble roughness elements on the surface which acted as sites for salt efflorescence (arrowed). Minimal surface deformation was evident at this point, but steep "curls" of the drape surrounded the base of the roughness elements. (b) Surface deformation on 30/04/87. Note that the drape is now far more knobbly, and that the curls around roughness elements extend considerably higher from the bed. Some clasts are now almost completely enveloped by the domed drape. It is possible that this surface configuration could be misinterpreted in the rock record as clasts having been dropped into the mud from above, forming impact craters. (c) Further curl development by 14/05/87. Many clasts are now entirely submerged, and the domed drapes were acting as roughness elements, with small aeolian current shadows on their northern side. (d) Latter stages of deformation on 25/05/87. More clasts had become submerged beneath the domed drape. The planar, draped bed also became progressively more knobbly. Southerly wind flow from bottom to top and scale in mm in all frames.

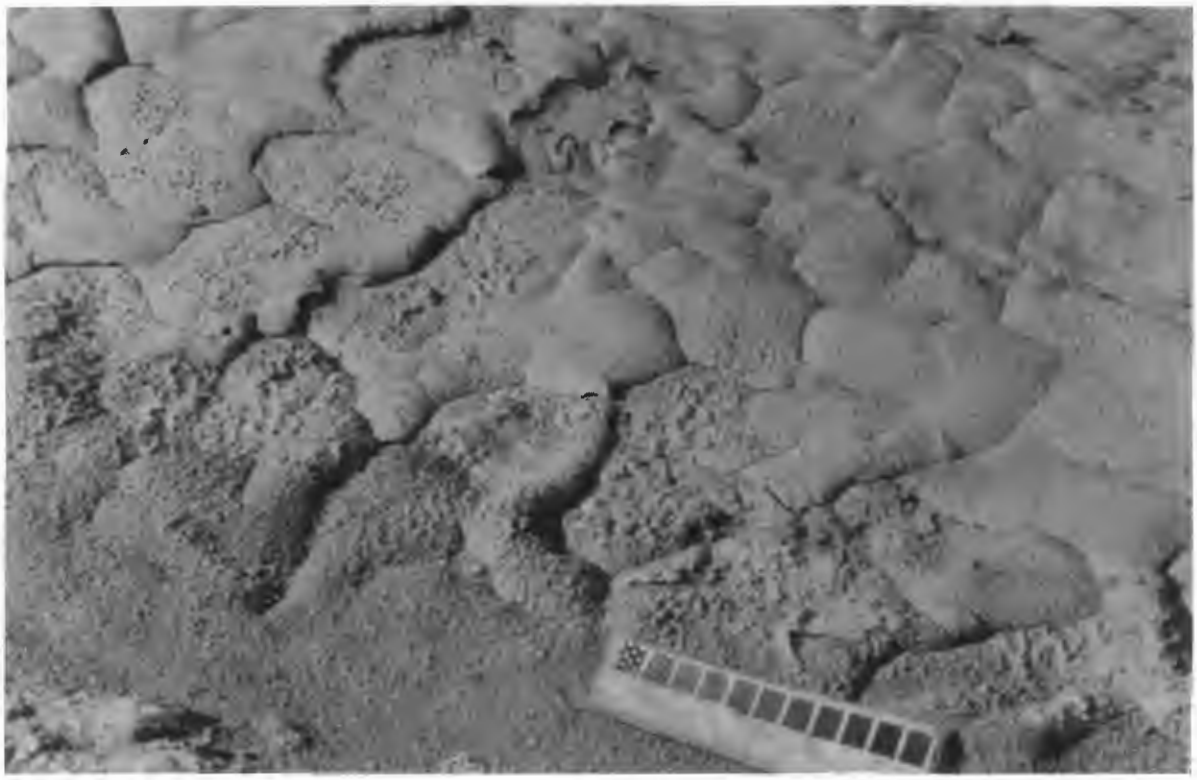

Figure 5.19. Convex-up desiccation polygons formed during the doming of the clay drape covering the floor of the ponded water body in Fig. 5.18. The polygons were hollow, and raised above the underlying sediment surface. Note the remnants of raindrop impact craters, which account for the roughened surface. Scale 11.5 cm.

This site was also influenced by the development of a domed crust, and salt efflorescence occurred at the base of clasts on the ephemeral stream bed during sub-aerial desiccation (Figure 5.21). Split quartzite clasts resting on the bed were also surrounded by salt efflorescence. Observations show that the modification of this surface is progressing far more slowly than at the Idatal sites. Between the 4 and 5/04/87 and the 5/01/88 very little change had been observed (Figure 5.22a and b).

The Formation and Implications of the Surface Crust

The formation of halite crusts, comprised of hopper crystals, on the floor of the Idatal prove that the groundwater is highly saline. Salt efflorescence at the surface also shows that salts concentrate within the surficial sediments during desiccation. As Kaiser (1926) recorded, these salts are probably responsible for the development of the surface crust.

The doming of the bed during the development of the surface crust strongly suggests that the addition of salts to the surface results in expansion of the surficial layer. As a result of salt crystallisation pressure, compressional forces are probably created. This effectively causes the surficial crust to lift from the underlying bed, creating hollow domes. This process breaks up the sediment surface, and promotes deflation by raising the delicate domes into the saltation layer. It is therefore a crucial stage in the initiation of deflation surfaces and the development of stone pavements on sandy ephemeral stream beds within the deflation basin.

In some instances, the salt crust develops to the extent that all aeolian sediment transport ceases. An example of this was observed at the northeastern margin of Bogenfels Pan. After ephemeral stream action had ceased, the material comprising large aeolian granule ripples was bonded together by crystallised salts. The crusts produced are extremely durable, and have reduced the transport of this material by aeolian processes to a minimum.

Within ponded water bodies, the particles of silt and clay are theoretically too small to be entrained from the bed solely by aerodynamic forces. The development of a surface crust, resulting in the projection of domes of the fine-grained sediment into the saltation layer promotes more rapid deflation. The flaky fragments

Figure 5.20. Comparative photography site south of Bogenfels Pan. Note the aeolian deposits in the background which were reworked by the ephemeral stream. Scale 1 m.

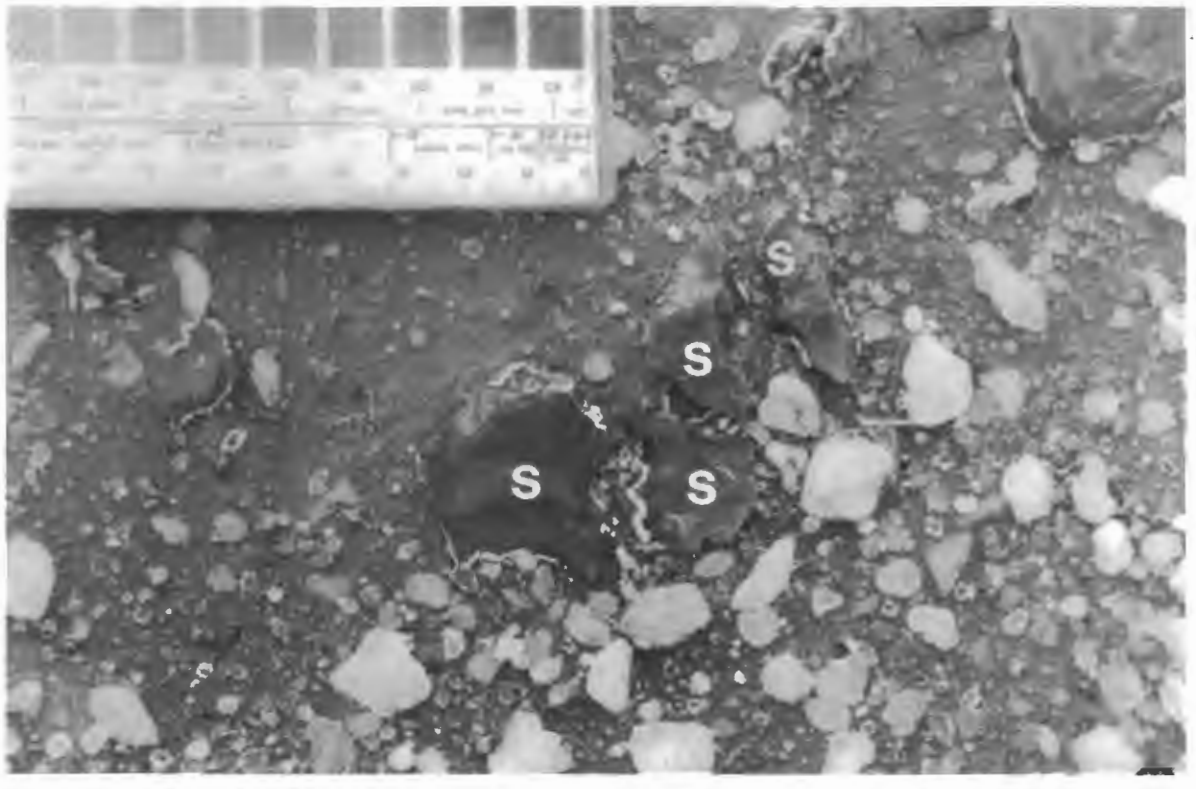

Figure 5.21. Salt efflorescence around the base of roughness elements on the stream bed on 14/04/87, after rainfall on 4 and 5/04/87. Note the split silcrete clast (s), whose fragments have become separated. Scale in mm.

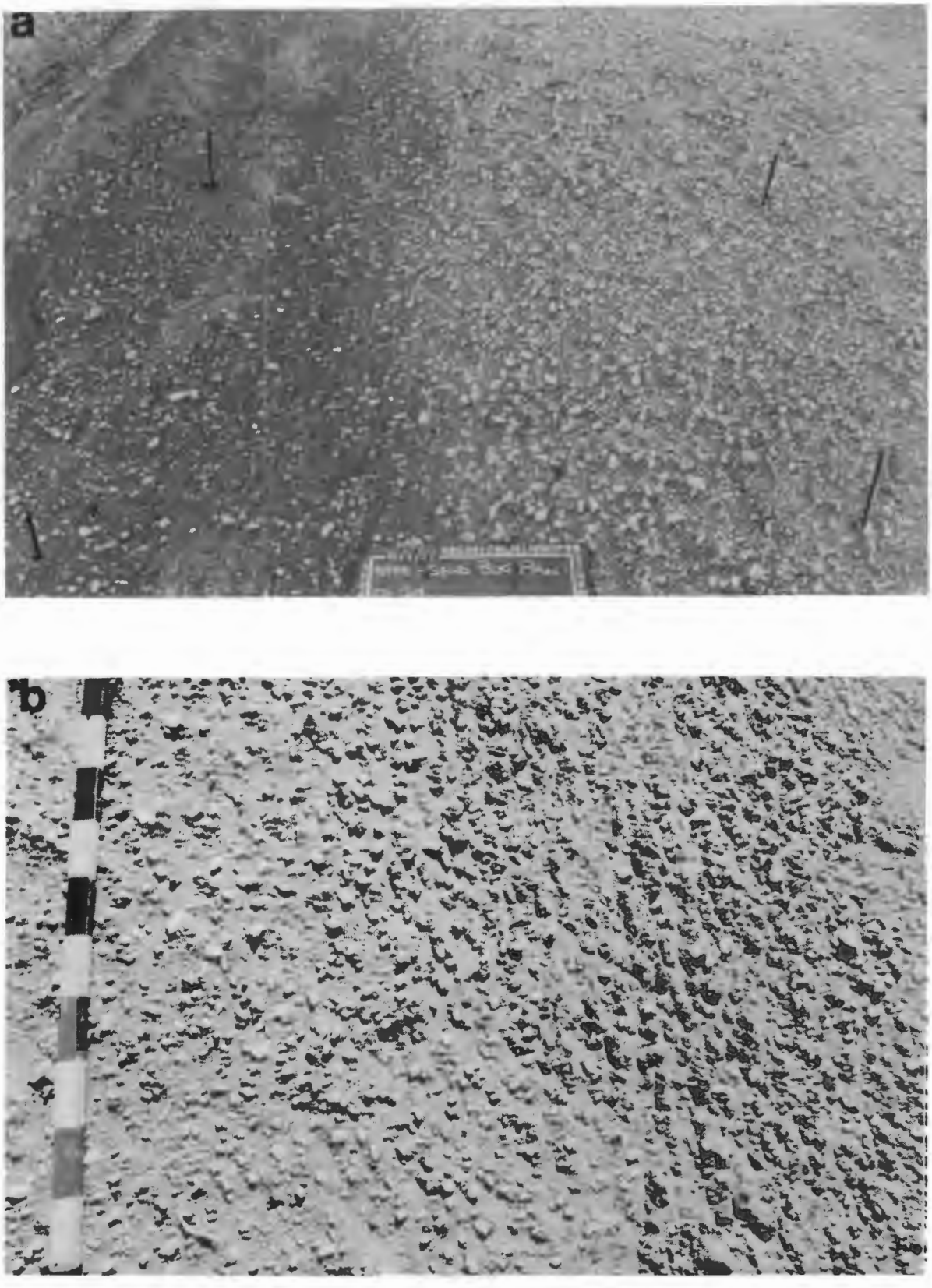

Figure 5.22. (a) Ephemeral stream bed south of Bogenfels Pan on 14/04/87, showing salt crust affecting poorly developed sand ribbons. Steel spikes separated by 1m. (b) Same site on 22/09/87 showing minimal surface modification. Scale 1m. Southerly wind flow from bottom to top in both frames.

remaining on the surface are found to be highly susceptible to entrainment by the wind.

Despite the doming of the surface, the site monitored to the south of Bogenfels Pan remained intact for a substantially longer period of time. This site lies outside the influence of any significant sandflow based upon personal observation. Thus, without aeolian saltation across the surface of ephemeral stream beds covered by a surface crust, deflation proceeds very slowly and the crust effectively stabilises the bed.

The development of salt efflorescence around clasts on the stone pavement surface south of Bogenfels Pan is particularly significant. The reduction of sand-sized particles by salt has been shown to occur experimentally by Goudie, Cooke and Doornkamp (1979). The concentration around roughness elements on stone pavement surfaces suggests that these clasts provide preferential sites for salt accumulation. This supports the idea that salt weathering plays an important role in the splitting and spalling of roughness elements. Repetitive cycles of wetting and drying, resulting from rainfall and fog-wetting, potentially result in the frequent alternation of salt crystallisation and solution. This provides ideal conditions for salt weathering.

The surficial concentration of salts apparently results in the expansion of the surficial sediments. This provides a possible mechanism for initiating the separation of split fragments, and might explain why the splits open faster at the sediment surface.

5.3.2. EPHEMERAL STREAM BEDS WITH A SURFACE CARAPACE

Ephemeral stream activity in the Bogenfels area was observed on 11/06/86 after rainfall on 2 and 3/06/86. Although the example is from a mined area, and the initial bed was not natural, the observation of the processes influencing it are considered to be valid. Ephemeral stream flow was shallow, and sedimentary structures on the bed show that the infiltration of run-off was a significant factor (Figure 5.23). Much of the bedrock upstream of the site examined, consists of weathered phyllite of the Bogenfels Formation. This released large amounts of clay into the ephemeral stream system during the erosion of the channel, and consequently the stream system transported a large suspended load. Infiltration of the run-off, and the reduction of flow allowed the deposition of

extensive clay drapes on the stream bed in the latter stages of the flood event (Figure 5.24). Surface crust formation, and doming of the surficial sediment did not occur during desiccation of the stream bed, and no salt efflorescence was observed. Instead, the clay drape dried to form a resistant surface carapace covering the stream bed.

During high-energy southerly surface-wind flow, the saltation load rapidly eroded wind aligned grooves through the drape, and preferentially attacked the current ripple crests protruding into the saltation layer (Figure 5.25). As corrasion advanced, the removal of the carapace permitted the deflation of the underlying sediment, which was then exposed to aeolian removal processes. Channel bar surfaces were subjected to aeolian size sorting as the finer-grained material was transported away by saltation. The coarser-grained material progressively accumulated into ridges, as creep transport occurred over the entire bed (Figure 5.26a and b). Upstream of the site described above, continued aeolian removal led to the development of granule ripples (Figure 5.27). The morphology of these bedforms and the stages of their development are discussed in section 6.3.1.

Thin clay drapes, deposited on the floor of ponded water bodies from suspension, frequently overlie aeolian deposits in depressions after rain. Raindrop impact is capable of penetrating the clay drape when it is still moist, and animal tracks also break-up the potential surface carapace (Figure 5.28). Both produce defects which are quickly exploited by aeolian processes, which enlarge the holes. The destruction of the carapace increases the rate of deflation of the underlying material.

Particularly thick clay drapes prevent further modification of the underlying sediment by aeolian processes. In these instances, subsequent ephemeral stream activity can lead to these deposits being ripped-up to form loose blocks on the surface, where they are susceptible to aeolian corrasion.

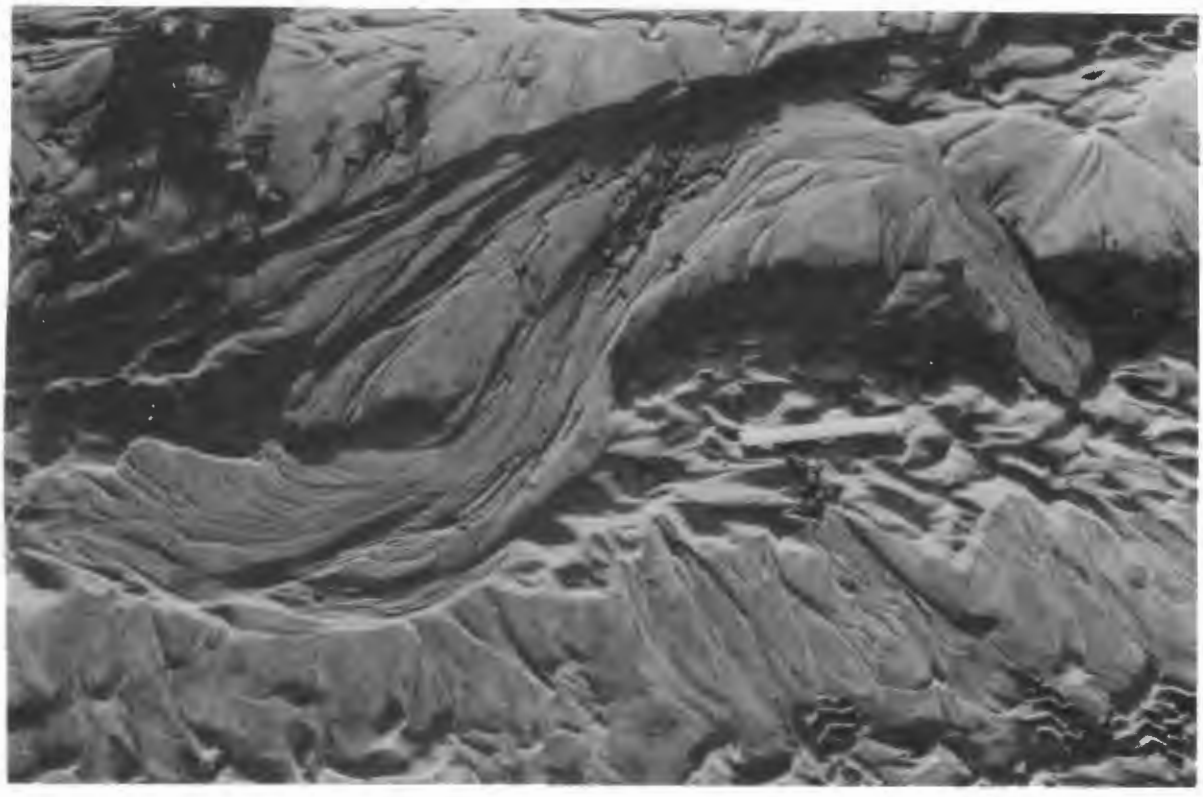

Figure 5.23. Ephemeral stream bed at Bogenfels on 11/06/86, after rain on 2 and 3/06/86, showing late stage modification of the bedforms. As infiltration of the flood water occurred, and surface run-off generation decreased, the depth of flow was drastically reduced. This lead to modification of bar forms as the channels switched direction, forming small delta-like bodies. Flow from top right to bottom left, scale 30 cm long.

Figure 5.24. Clay/silt drape covering the ephemeral stream bed once flow had ceased. Note the break-up of the drape during desiccation. Cracks appeared initially along the crests of the current ripples. Raindrop impact craters can be seen on the drape. Flow from top to bottom, scale 30 cm long.

Figure 5.25. Aeolian erosion of the clay drape covering the ephemeral stream bed on 15/06/86. Note the small grooves on the large area of drape, which are aligned with the southerly wind which blows from bottom to the top of the frame. Once created, these erosion grooves are rapidly enlarged by aeolian processes. Scale in cm.

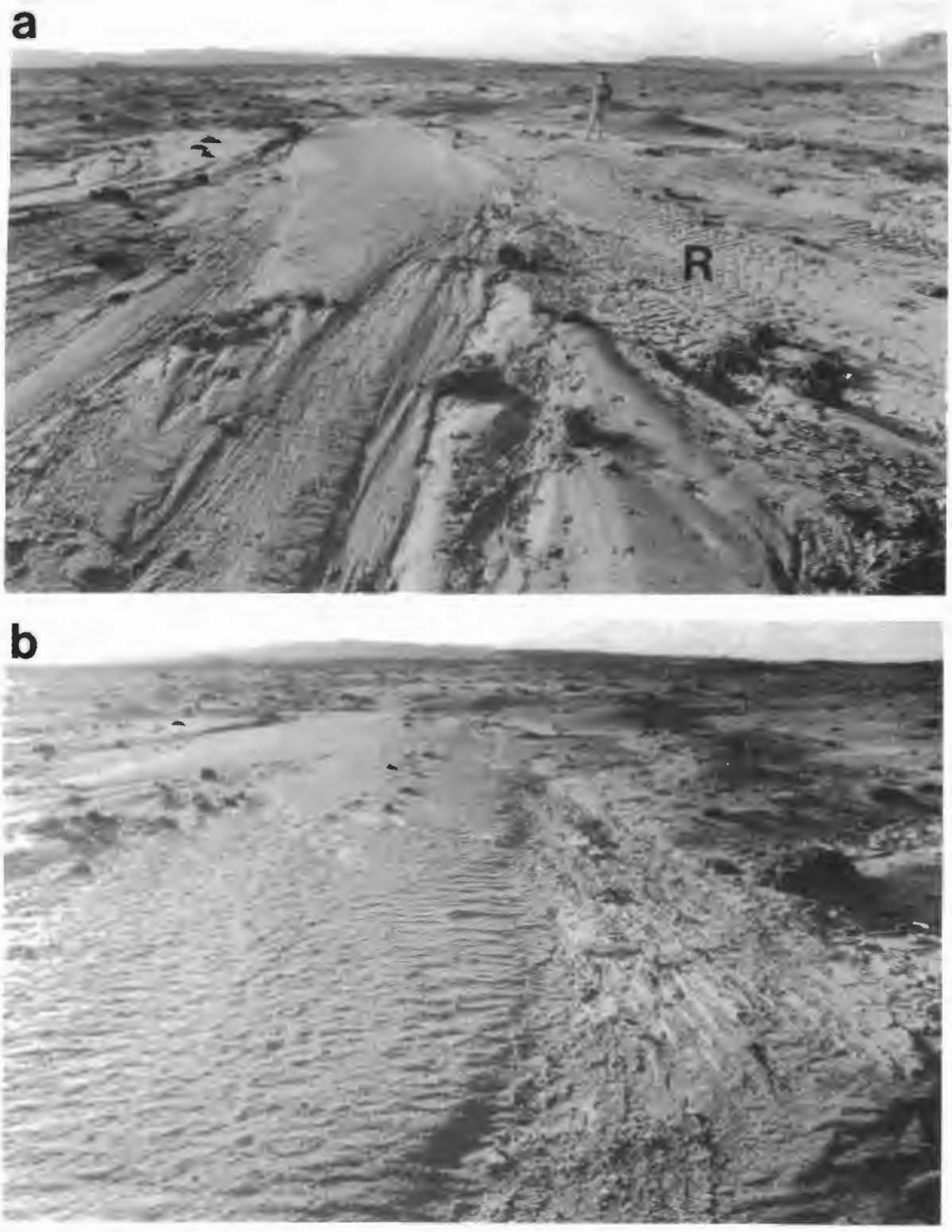

Figure 5.26. Comparative photographs of an ephemeral stream bed at Bogenfels. (a) View north on 11/06/87, after rainfall on 2 and 3/06/87. Note the very shallow nature of the flow, and the large area of bed covered by current ripples (R). Flow towards the reader, person for scale. (b) Enlarged view of the bed covered by current ripples on 19/06/86, after the break-up of the original surface carapace formed by the clay/silt drape. Aeolian processes rapidly began to deflate the fine-grained material exposed on the bed once the carapace had been destroyed. Aeolian removal processes continued to operate, and aeolian size sorting of the material took place. This led to the generation of a large creep bedload population, which subsequently began to form granule ripples. The carapace continued to be eroded in other places on the bed. Southerly wind flow from bottom to top, scale 30 cm.

Figure 5.27. View south, showing the development of granule ripples on an initially planar, ephemeral stream bed located north of Bogenfels, on 15/04/87, after the stream flowed on 4 and 5/04/87. Note that the granule ripples are best developed towards the northern end of the bed. The development of these bed forms is in greater detail in section 6.4.2. Scale 1 m.

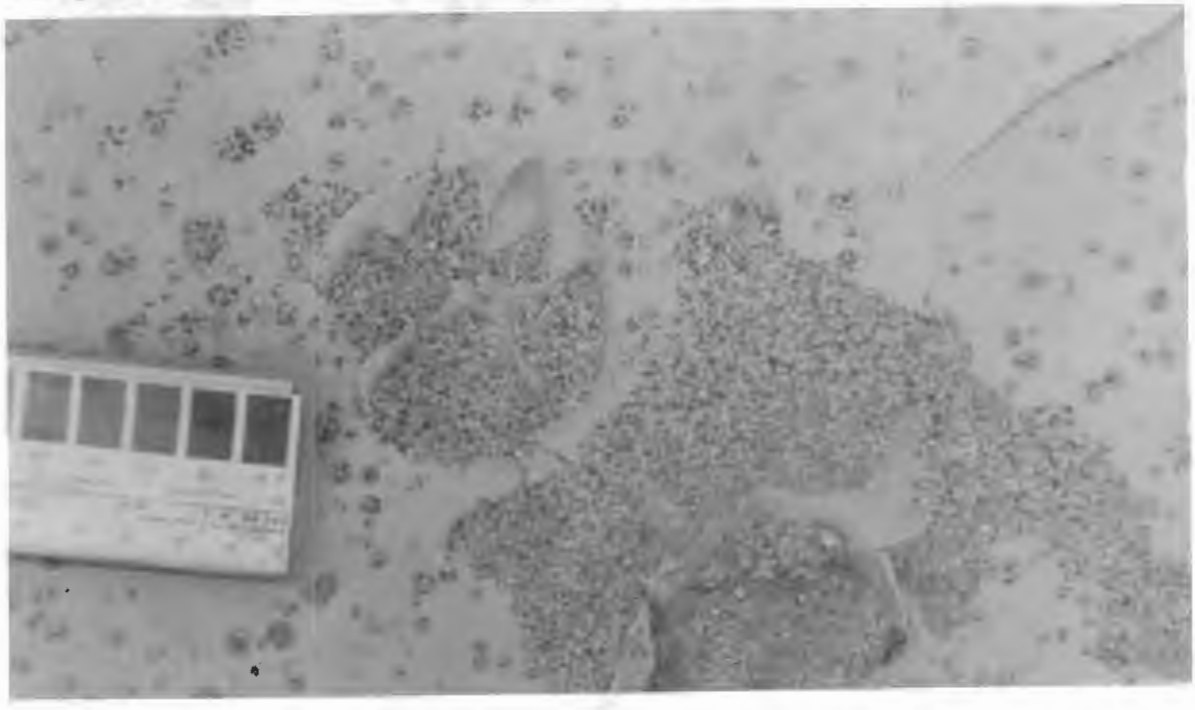

Figure 5.28. Raindrop impact craters which have penetrated through a clay drape which previously covered the floor of a ponded water body. Note also the jackal paw prints, which destroyed the surface carpace. These blemishes form irregularities which are rapidly exploited by aeolian processes, leading to the destruction of the drape and the deflation of the underlying bed. Scale in mm.

5.4. MODEL OF DYNAMIC INTERACTION BETWEEN EPHEMERAL RAINFALL AND THE AEOLIAN SEDIMENT DISPERSAL SYSTEM

5.4.1. EFFECT ON AEOLIAN SANDFLOW

If rainfall is insufficient to generate run-off, the dampening of the ground surface initially reduces the sandflow rate through the basin. The subsequent desiccation proceeds rapidly, and this effect is short-lived. Surface run-off, which leads to ephemeral stream activity, has a much greater effect upon the sandflow through the deflation basin.

Ephemeral stream systems potentially erode large quantities of sand from temporary storage sites within the aeolian system. Once redistributed, these sands are initially out of equilibrium with the southerly wind regime. Consequently, the ephemeral stream deposits provide an additional, widespread source of material for the aeolian system. Therefore, as desiccation proceeds after an ephemeral rainfall event, an initial increase in the sandflow rate throughout the deflation basin is anticipated. Fine-grained sediment is then rapidly deflated from the surface of stream beds, which leads to a reduction in the quantity of fine-grained sediment within the basin (Kaiser, 1926). The interaction of the two current systems therefore provides a mechanism for the lowering of stone pavement surfaces.

The influence of the sandflow pulse upon aeolian transport corridors is likely to be minimal. In other areas, where the sediment supply is normally minimal, this pulse of sandflow will have a significant influence upon aeolian sediment dynamics.

5.4.2. EFFECT ON AEOLIAN CREEP

Kaiser (1926) realised the importance of interaction between the aeolian and ephemeral stream sediment dispersal systems. The south-facing slopes at the northern end of endoreic basins provide natural catchments for the ephemeral system. The aeolian current system transports material to the north, but the ephemeral current system redistributes material to the south. This provides the potential to develop polycyclic deposits through the interaction of these current systems (Kaiser, 1926). The ephemeral stream systems transport aeolian material down the south-facing slopes towards the base-level of the systems. As desiccation proceeds, aeolian processes rework this sediment. The material comprising stream beds

is therefore influenced by aeolian size sorting, during its transport back up the topographic slope. As shown by the garnet creep tracers, the finer-grained creep bedload will be transported more rapidly from the stream beds of the ephemeral system, and the coarser material will remain behind, forming a lag which will eventually stabilise the bed. Any significant change in the sandflow rate through the deflation basin will also influence the creep transport rate, because the frequency of saltation collision will increase. It is therefore anticipated that a brief peak in the creep transport rate will accompany the pulse of sandflow through the basin.

Observations suggest that periods of ephemeral stream activity may be separated by several years or more. Aeolian processes therefore act uninterruptedly over comparatively long periods of time. Within aeolian transport corridors, it is possible that considerable redistribution of the creep bedload can take place over this sort of time-scale. It is thus anticipated that the sediment dispersal pattern within endoreic basins will reflect the combined influence of the aeolian and ephemeral current systems. One or other of the current systems will be dominant, depending upon their ability to redistribute the material, and the periodicity with which ephemeral events occur.

6. HEAVY MINERAL SEGREGATION AND AEOLIAN PLACER DEVELOPMENT

6.1. SEGREGATION BY AEOLIAN PROCESSES

6.1.1. INTRODUCTION

Heavy mineral segregations can be observed in two distinct settings within the aeolian environment:

1) in association with aeolian bedforms;

2) in association with flow transverse obstacles.

A number of early publications drew attention to the existence of low waves or gravel ridges which were attributed to wind action (eg. Merensky, 1909; Krause, 1910; Wagner, 1914). Photographs of the early deposits confirm that these bedforms are analagous to aeolian granule ripples. Mernesky (op. cit.) first recorded that diamonds were preferentially concentrated along the crests of these bedforms. This was subsequently confirmed by Krause (op. cit.), who stated that hornblende and garnet are also segregated behind the crests. These observations confirm that at least some of the economic deposits were the product of aeolian transport processes operating during bedform migration. Although the examples cited by the earlier workers were largely mined-out between 1908 to 1930, some examples of segregation on bedforms have been located during this study. These show that segregation is not restricted to granule ripples, and that aeolian processes during the migration of other bedforms also results in segregation.

A brief account by Wagner (1914) recorded the segregation of heavy minerals at flow transverse obstacles. Kaiser (1926) documented further examples of this type. The processes leading to heavy mineral segregation under these circumstances are governed by a different set of factors.

Comparatively few studies have been made of heavy mineral segregation in the aeolian environment. Those which have been published more commonly examine segregation arising from the transport of sands by saltation (eg. Willets, 1983; Gerety and Slingerland, 1983). Barchan dunes composed almost solely of heavy mineral sand grains occurring east of Swakopmund (Lat. 23°32'S; Long. 14°30'20"E) convincingly demonstrate that particle size-density-shape characteristics lead to segregation by aerodynamic forces and saltation under natural conditions.

In the case of bedload creep examples, the reason for

segregation is not clear, but size-density-shape characteristics of the grains must significantly affect the entrainment potential of particles. Chepil (1950) found that the amount of soil removal (q) by the wind could be expressed by:

$$q = K\ R\ Ou\ (V2-V1)$$ where:

V1 = volume of non-erodible projections existing at surface prior to exposure to wind;
V2 = volume of projections after soil removal by wind has ceased;
Ou = density of projecting units;
R = ratio of erodible to non-erodible fractions;
K = coefficient depending on the shape of projecting units.

V2 varied widely with wind velocity, and with the size, shape and apparent specific gravity of the erodible and non-erodible fractions. Hence particle density is an important variable. It has been shown above, that aeolian size sorting by bedload creep rapidly alters the grain size distribution of garnet bedload creep tracers. The same processes also affect quartz particles on the bed. Theoretically, if a quartz population and a heavy mineral population with similar grain size distributions are mixed to form a heterogeneous size-density sand which aerodynamic forces alone cannot entrain, size-density sorting by aeolian creep and saltation will modify the original grain size distribution.

Observations made during high-energy surface-winds and consideration of wind tunnel and flume studies of flow over obstacles allow a brief theoretical explanation of some segregations to be attempted. The development of heavy mineral segregations in the natural environment is relatively slow, and could not be observed during this study. The processes responsible for their formation will have to be examined under controlled experimental conditions, where the complex patterns of surface airflow across flow transverse obstacles can be measured directly.

6.1.2. SEGREGATION ON THE PLANAR BED OF ENCROACHMENT DEPOSITS

Description

Examples of segregation on a planar bed are located at Eisenkieselklippenbake, and to the north of the Grillental. Minimal evidence of bedform development is seen on the surface of an encroachment deposit situated on a gently inclined south-facing slope. The locality lies on the eastern side of the Chameis Bay aeolian transport corridor. This surface is thus subjected to high sandflow conditions, with the saltation load crossing an extensive alluvial plain immediately south of this locality.

Iron oxide and hydroxide particles form patchy, flow transverse segregations on a surface dominated by quartz granules (Figure 6.1). Better developed segregations of heavy minerals define flow-transverse arcuate lines, with their concave margin pointing into the southerly wind. This is the opposite orientation to granule ripples, which generally exhibit convex crests pointing into the southerly wind. Adjacent edges of the arcuate segregations overlap.

Bedforms of similar arcuate form, with concave crests pointing into the southerly wind occur more extensively within the high wind-energy coastal tract of the deflation basin bordering the western margin of the Namib Sand Sea near Meob Bay (Lat. 24°15'50" S; Long. 14°31'25"E), in Diamond Area Number 2. Although the bedforms do occur on sub-horizontal surfaces, they are more commonly observed on encroachment deposit surfaces covering south-facing slopes (Figure 6.2). Adjacent edges of the arcuate bedforms overlap, and closely resemble the segregations at Eisenkieselklippenbake. In plan-view, they surround planar, undisturbed encroachment deposit surfaces elevated a few centimetres above the surrounding bed (Figure 6.3).

The bedforms are defined by a south-facing slope which rises to the higher elevation of the bed immediately downwind (ie. north). The crest at the top of the south-facing slope, is defined by a ridge of quartz granules a few grain diameters high (Figure 6.4). The internal structure of the bedforms resembles that of an encroachment deposit. Low-angle sandy cross-strata dip at the same angle as or at a slightly greater inclination than the sediment surface. Granular material occurs as lens-shaped concentrations

Figure 6.1. Heavy mineral segregations forming part of an encroachment deposit comprised predominantly of quartz granules, on a gentle south-facing slope north of the Grillental. Arrow on surface points in the direction of the southerly wind flow. Scale 11.5 cm.

Figure 6.2. View north, up a south-facing slope near Meob Bay, showing small, concave crests of bedforms facing into the southerly wind flow. Scale 1 m.

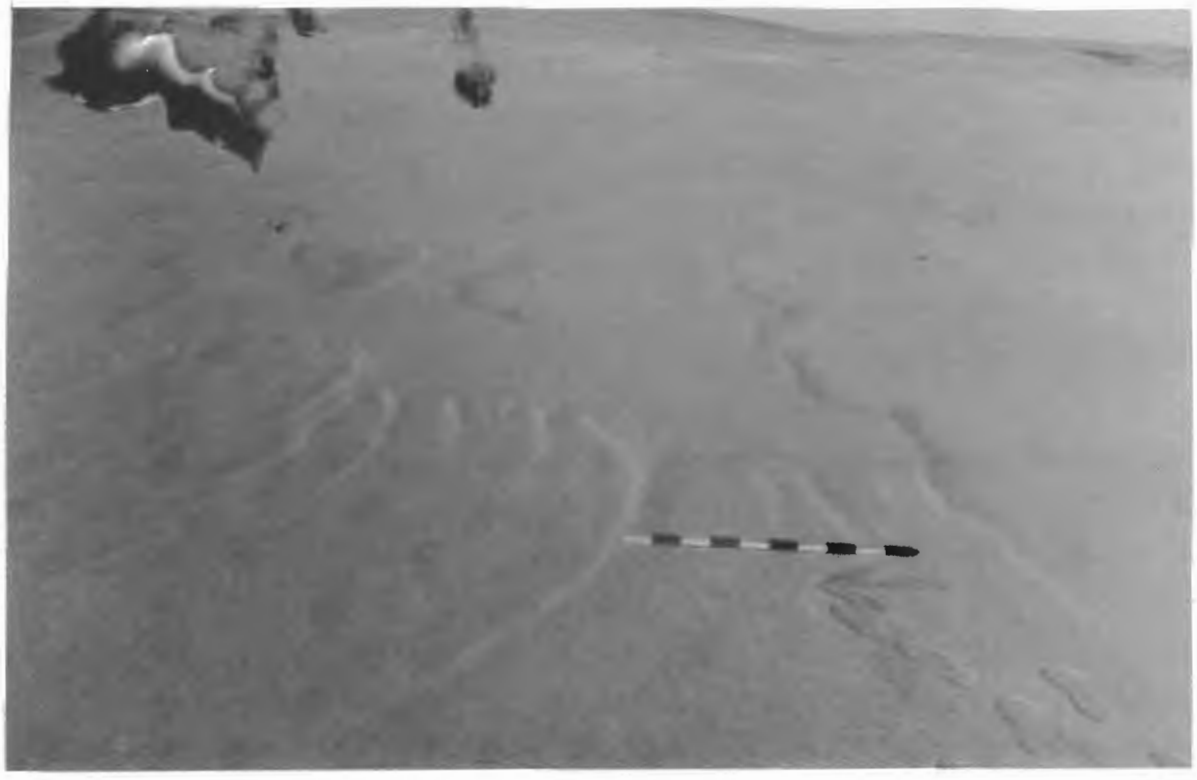

Figure 6.3. An area of planar, undisturbed encroachment deposit composed predominantly of quartz granules, surrounded by sinuous, transverse crests of bedforms on a south-facing slope near Meob Bay. Arrow points in direction of southerly wind flow, scale in 10 cm units.

Figure 6.4. Longitudinal section through the concave crest of a bed form, showing the low-angle stratification of the encroachment deposit, which is mainly composed of quartz sand. Southerly wind flow from right to left, scale in cm.

along well-defined planes.

The bed upwind of concave crests is coarser-grained than the encroachment deposit surface immediately downwind of the crests (Figure 6.5). Angular to sub-rounded, small, quartz pebbles are concentrated at the foot of the slope beneath the crest. Garnet granules are segregated along the concave crestal area of the bedforms (Figure 6.6). These segregations resemble the plan-form of those at Eisenkieselklippenbake.

Interpretation

The examples given above all occur on aeolian encroachment deposits situated on south-facing slopes. This is confirmed by the internal structure of sediments associated with the bedforms exhibiting concave crests at Meob Bay. Lens-shaped concentrations of granular material along bedding planes observed within longitudinal sections reveal that earlier encroachment deposits are partially preserved in a thin sequence of sediments a few tens of centimetres thick.

Planar, undisturbed encroachment deposit surfaces elevated above the surrounding bed between the concave bedforms are interpreted as evidence of surface lowering, indicating that an earlier encroachment deposit is now being reworked, resulting in the generation of a new sediment surface. The concave bedforms are therefore interpreted as erosional fronts. The coarser grain size of material upwind of the crest (ie. south) shows that the erosion fronts are migrating up the south-facing slope to the north. It is suggested that these bedforms be termed "creep erosion ripples". As creep erosion ripples migrate up-slope, the encroachment deposit is reworked to a depth approximately equal to the ripple height. This reintroduces material previously preserved within the sequence back into the aeolian system.

Pebble-sized material remains behind on the new surface together with some of the larger granules. The smaller quartz granules and their entrainment equivalents are apparently incorporated into the advancing ripple crest, and subsequently removed in the downwind direction by creep. A layer of the encroachment deposit is thus effectively being peeled back, as the creep bedload advances north in a series of "waves".

The erosional fronts represented by creep erosion ripples provide

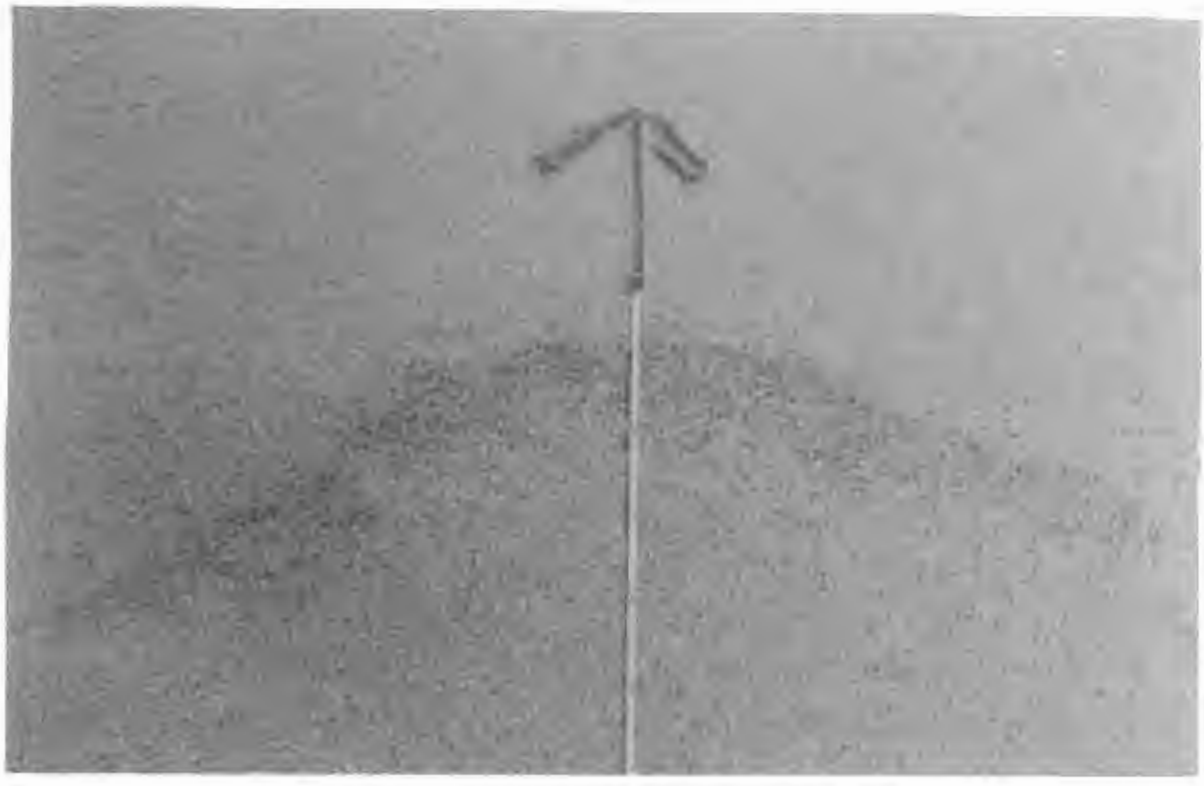

Figure 6.5. Plan-view of concave-crested bedform. Note that the bed upwind of the crest is covered by coarser quartz and feldspar grains than the bed downwind of the crest. The dark specks are garnet grains. Fewer garnets are present on the upwind side of the crest. There is also evidence for the concentration of garnet grains along the crest, relative to that present downwind of the crest. The bed downwind of the crest is interpreted as being undisturbed by the migration of the bedform. The arrow points in the direction of the southerly wind flow, scale in cm.

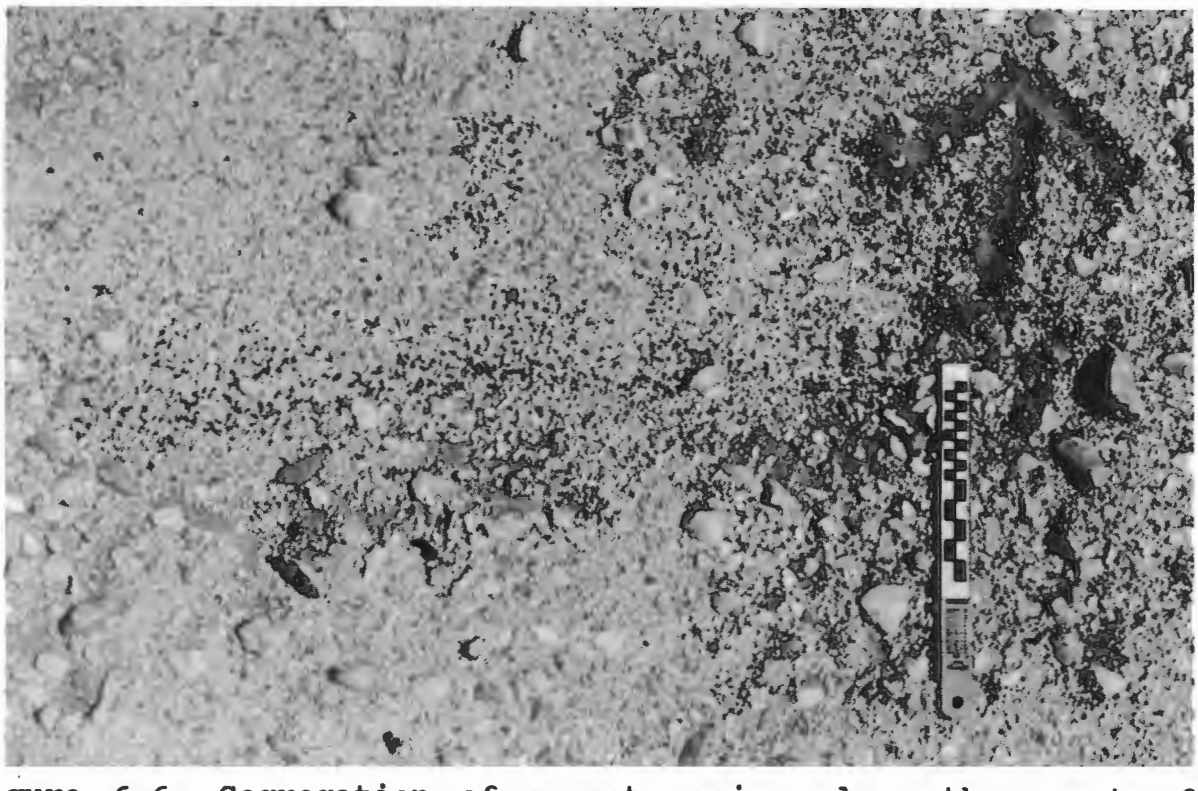

Figure 6.6. Segregation of garnet grains along the crest of a creep erosion ripple. Arrow on bed points in direction of southerly wind flow. Graduated part of scale 10 cm.

sites of optimum reworking of the bed. Newly eroded material from the earlier encroachment deposit continuously supplies garnet and quartz grains to the crest, as the front migrates northwards. The material forming the crest therefore exhibits size-density-shape contrasts. The very coarse sand and small granule fractions are more susceptible to entrainment into saltation and creep. The small pebbles of quartz and feldspar therefore remain behind, and form the new bed. In time, as deflation proceeds, their spatial distribution will alter, and the larger particles become more densely packed. This leads to restabilisation of the bed. Bagnold (1935) considered that larger particles on the bed potentially shield smaller ones from direct saltation impact. The larger quartz grains possibly affect the garnet grains in two ways (Figure 6.7):

1) they potentially shield garnet grains from direct saltation impact;
2) the garnet grains have to overcome a larger pivotting angle than the quartz grains, in order for them to be dislodged.

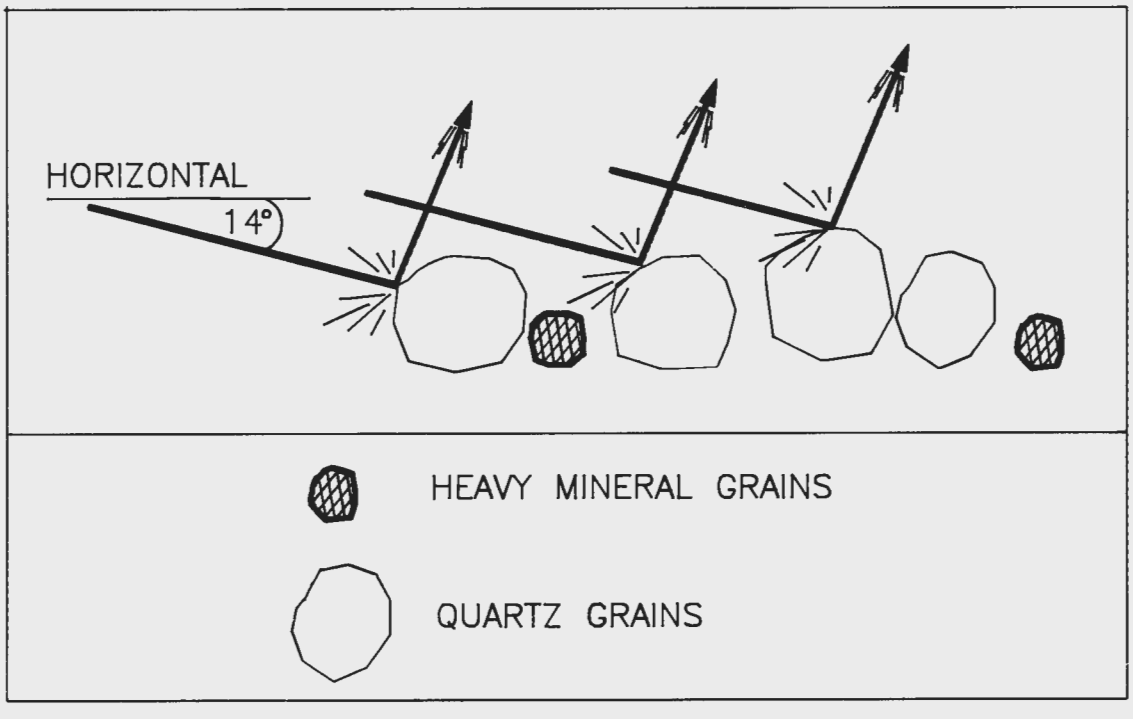

Figure 6.7. Sketch showing the possible influence of large quartz grains upon the entrainment of smaller heavy mineral grains into creep by saltation.

6.1.3. SEGREGATION ON GRANULE RIPPLES

Description

As stated earlier, examples of diamond segregation on granule ripples was recorded in 1909. As with examples from the encroachment deposits, segregations on the stoss slope of granule ripples form discrete bands oriented transverse to surface-wind flow (Figure 6.8).

Interpretation

The dynamics of granule ripples in the Southern Namib deflation basin has been examined during this study. The net migration direction of the bedforms, according to measurement of their advance and their internal geometry, is to the north. This reflects the dominant influence of the southerly surface-wind flow over the direction of sandflow through the basin. Infrequent high-energy northerly surface-winds temporarily reverse the migration direction. Although the reversals are of comparatively brief duration, a wedge of granules develops rapidly at the top of what under normal conditions, is the lee slope of the bedform. Sections through sequences deposited by granule ripples near Bakers Bay are comprised entirely of the basal part of sandy bottomsets (Figure 6.9). Few granules could be seen in any part of the sections excavated, and rare lenses of granules seem likely to indicate former trough positions. The non-preservation of the upper part of stoss and lee-side slopes confirms that the bedforms migrate by erosion on the stoss slope and deposition on or downwind (ie. north) of the lee slope. The stoss slope of granule ripple profiles is therefore interpreted as a dynamic area on the bedform on which the coarse-grained fraction is recycled. This is comparable to the situation observed on the stoss slope of barchan dunes (see section 4.3.3.). It also resembles the recycling observed on the stoss slope of sub-aqueous bedforms (McQuivey and Keefer, 1969). In time, granules from earlier ripples are reworked, providing additional material for the stoss slope. Size-density sorting probably occurs continuously on the stoss slope as material from within the present ripple, together with earlier ones, re-enters the aeolian system through stoss slope erosion.

Detailed observations under controlled conditions are required to observe the size-density sorting process on the stoss slope of the

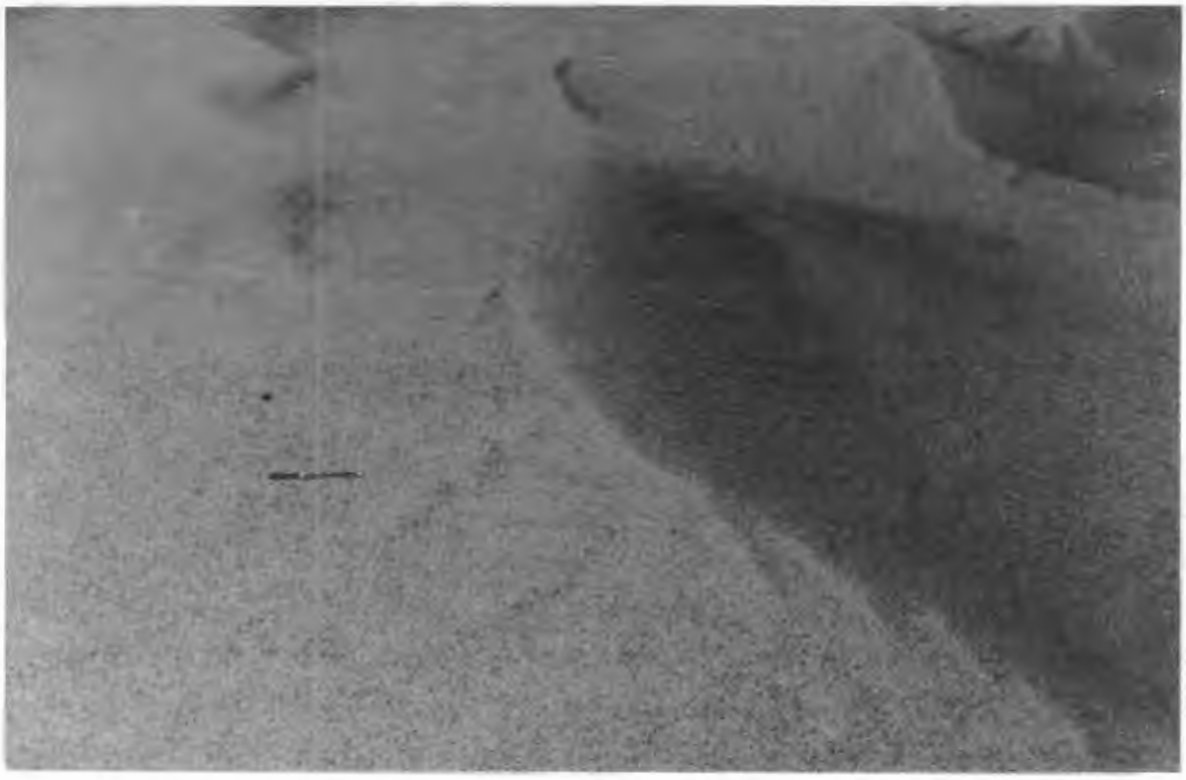

Figure 6.8. Heavy mineral segregation on the stoss slope of a granule ripple north of the Grillental. Note the distinct line of heavy mineral grains slightly upwind of the crest. Southerly wind flow from right to left, scale 1 m.

Figure 6.9. Longitudinal section through a sequence deposited by granule ripples to the east of Bakers Bay. Note the absence of quartz granules from the section, despite the preservation of the bottomsets of the bed forms. Scale 10 cm. Southerly wind flow from left to right.

bedforms before definitive statements about segregation can be made. Ultimately, however, heavy mineral segregation on the stoss slope of granule ripples is probably strongly influenced by aeolian size-density sorting. Variation in the susceptibility of particles of differing size and density into saltation and creep are also probably influenced by other factors. Observations suggest that the larger, quartz granules are theoretically more readily entrained into either saltation or creep by saltation impact of the sand fraction because they protrude a greater height above the bed. Shielding of smaller heavy mineral grains by larger quartz grains from direct saltation bombardment potentially also influences the entrainment potential of grains. In addition, the pivotting angle through which grains have to move is smaller for large grains than it is for the smaller heavy mineral particles in the interstices between them. This highly variable situation is likely to be further complicated by the development of an imbricate shape-fabric by stoss slope surface particles, which also modifies the pivotting angle through which grains must move.

Observations indicate that heavy mineral segregations on aeolian granule ripples are consistently maintained towards the upper part of the stoss slope, slightly upwind of the crest. The segregation of magnetite on sub-aqueous current ripples has been shown to occur preferentially on the stoss slope in response to the surface-flow pattern and the resulting distribution of turbulence intensity and bed shear stress (McQuivey and Keefer, 1969). Grains on the stoss slope of aeolian granule ripples are too large to be entrained solely by aerodynamic forces. For this reason, the factors governing segregation in the aeolian environment probably differ from that of sub-aqueous examples. Controlled experiments are required to assess the role played by the pattern of surface-flow over aeolian granule ripples on creep bedload dynamics. One possibility, for example, is that the surface-flow influences the frequency of saltation impact with the bed towards the the crest of granule ripples, where the flow velocity is predicted to be accelerating (Figure 6.10a). In terms of aeolian size-density sorting, the variation between the creep velocity and the ripple velocity may be an important factor in maintaining segregations on the stoss slope of the bedforms (Figure 6.10b). According to Southard (1986), three classes of size-density fraction can exist

on a ripple surface based on the average particle velocity ((Ugi)av) relative to ripple velocity (Ub) (Figure 6.10b):

1) (Ugi)av > Ub everywhere on the ripple profile (supertractile);
2) (Ugi)av < Ub everywhere on the ripple profile (subtractile);
3) (Ugi)av > Ub on the lower part of the ripple profile, (Ugi)av < Ub on the upper part of the ripple profile, hence (Ugi)av = Ub at some point on the ripple profile (equitractile).

This study has shown that granules are rapidly size sorted on entering the aeolian system and that different particle sizes travel at slightly different velocities. If the ripples were supertractile, the surface concentration of size-density fractions would vary monotonically along the profile with minimal development of sharp local concentrations (Southard, op. cit.). This description does not correspond with field observation of granule ripples, which shows that concentrations are locally much greater. On subtractile ripples, the heavy mineral grains would ultimately be expected to form a lag concentration in the ripple trough (Southard op. cit.). Longitudinal sections through sequences deposited by aeolian granule ripples exhibit no evidence of this type of a lag deposit, which suggests that the segregations on granule ripples are equitractile. Hypothetically, grains re-introduced to the aeolian system near the base of the granule ripple stoss slope are sorted according to size and density by aeolian processes as they migrate towards the crest. If the condition is met whereby (Ugi)av = Ub, for a particular grain size and density at some point on the profile, the grain will effectively occupy a stable surface position to which like grains will be added. Over a long period of time, repeated addition of heavy mineral grains to this point on the ripple profile will lead to the development of a lag concentration as heavy mineral grains are segregated from the lighter quartz component. This type of segregation would occupy a particular location on the bedforms, which appears to conform more closely both to early reports regarding the distribution of diamond on the bedforms and to observations made during this study.

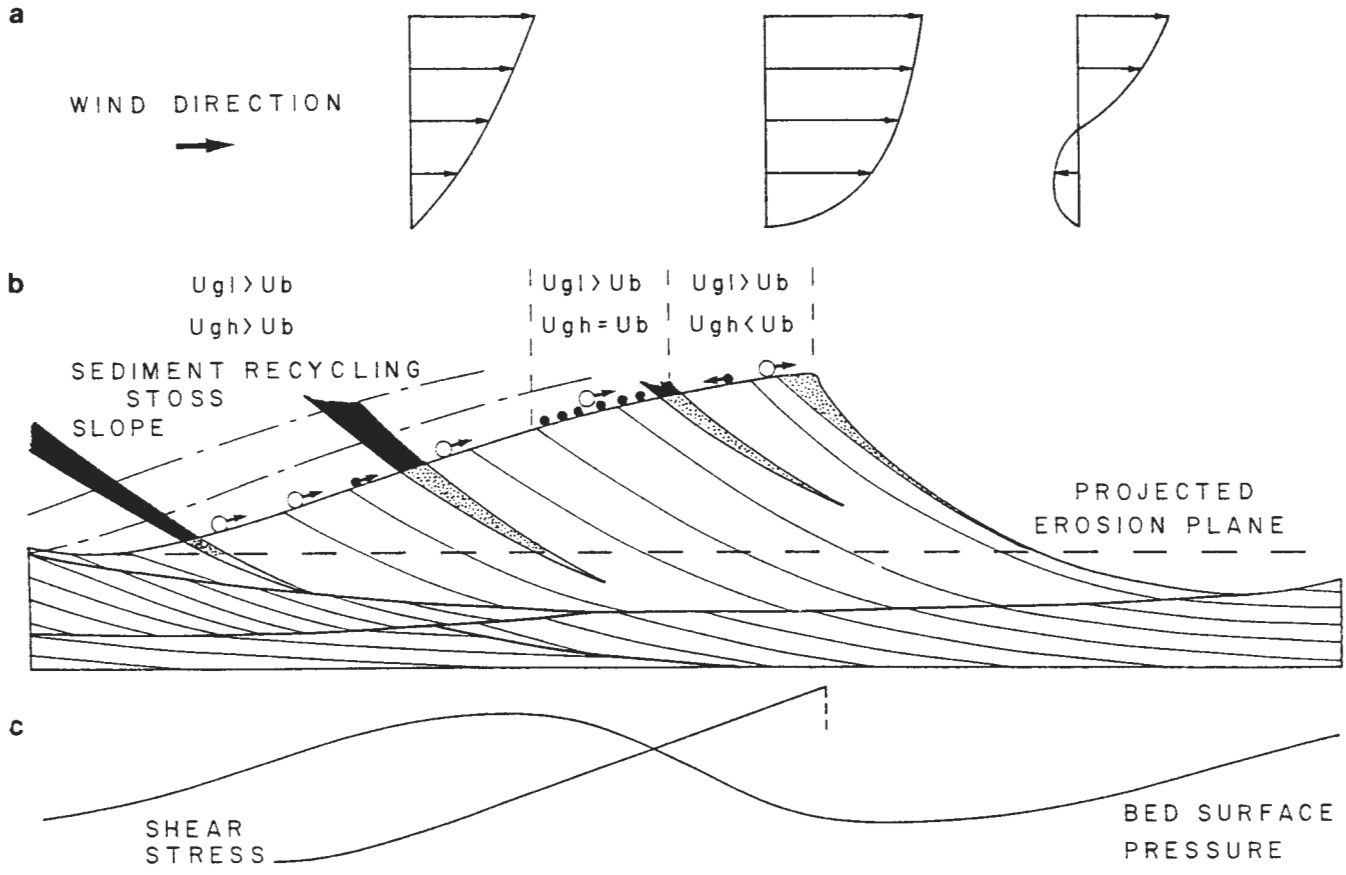

Figure 6.10. (a) The theoretical variation of flow velocity and (c) bed pressure across a granule ripple based upon consideration of the pattern across subaqueous bedforms. (b) The distribution of supertractile, subtractile, and equitractile bedload creep populations on the stoss slope of aeolian granule ripples, and the envisaged cyclical pattern of reworking of the coarse-grained component. Ugl = average light particle velocity, Ugh = average heavy mineral particle velocity, Ub = average granule ripple velocity.

6.1.4. SEGREGATION AT POSITIVE TRANSVERSE STEPS AND WALLS

Introduction

In addition to heavy mineral segregation associated with aeolian bedforms, Wagner (1914) and Kaiser (1926) also record examples associated with obstacles oriented perpendicular to the southerly surface-wind flow. As the earlier workers noted, obstacles formed by resistant dykes creating positive topography on the floor of endoreic basins form effective barriers to the transport of diamonds.

Detailed explanation of these concentrations based upon consideration of sedimentary processes has not previously been attempted. The complex form of many of the barriers probably means that the surface-flow over natural examples would be difficult to measure. Observation under controlled experimental conditions would be required to fully define the pattern. Consequently, explanations presented here are primarily based upon field observation during periods of high wind velocity and sandflow. The general surface-flow pattern has been estimated from the consideration of published flume and wind tunnel studies of flow over steps.

Example of Segregation at Ventifacts on Stone Pavement Surfaces

The smallest examples of segregation at a transverse wall occur towards the eastern end of the Grillental. Obstacles are provided by cobbles of quartzite and phonolite on the surface of a coarse-grained alluvial gravel tentatively correlated with the Gemsboktal Gravel further south. This locality is situated at the northern end of the Bakers Bay aeolian transport corridor which continues along the eastern margin of the Namib Sand Sea prior to entering the depositional basin. Consequently, very high sandflow conditions prevail.

One phonolite cobble, which was probably blade- or disc-shaped originally, was standing on its edge and oriented approximately transverse to the southerly surface-wind (Figure 6.11). The windward face exhibited a stepped profile when viewed perpendicular to the airflow, with a basal 1 to 2 cm high step rising sharply from the bed to an abrupt junction with an almost vertical face rising to a height of about 6.5 cm above the bed. The step was covered by shallow flutes, whilst the steep face had been polished.

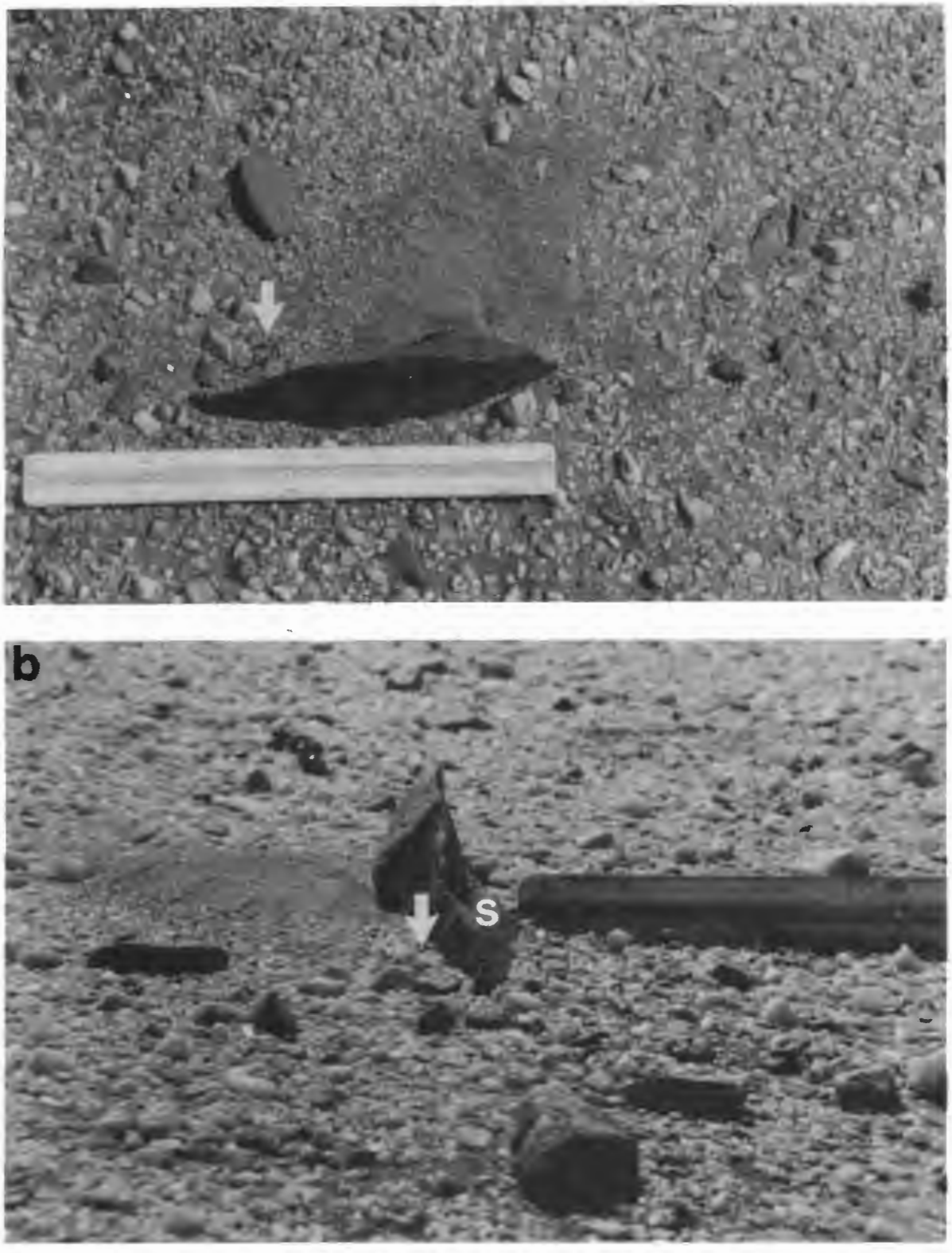

Figure 6.11. (a) Plan-view, showing the phonolite roughness element on the stone pavement surface. Note the aeolian sand current shadow on the north side. The position of the segregated garnet grains is arrowed. Southerly wind flow from bottom to top of frame, scale 30 cm long. (b) Longitudinal view, showing the stepped profile of the windward face of the roughness element formed by aeolian corrasion. Note the fluting on the south-facing riser which forms the step (S), and the imbricate shape-fabric displayed by the creep bedload at the base of the windward slope. The location of the segregated garnet grains is arrowed. Southerly wind flow from right to left, scale in mm.

The lee-face of the phonolite cobble showed no development of a stepped profile and its surface was comparatively unpolished. Quartz granules and pebbles were present at the foot of the windward face, and an aeolian current shadow had formed on the lee side.

Immediately west of the current shadow, a surficial concentration of garnet extended downwind for 1 to 3 cm from the lee face (Figure 6.12). Quartz granules and very coarse sand formed a northward fining tail along the western edge of the sand current shadow, which extended about 20 cm downwind. When the obstacle was excavated from the surface, garnet grains were found to be abundant in zones about 5cm wide on both the windward and leeward sides. The maximum concentration was visually estimated to be along the margins of the obstacle.

Interpretation

The phonolite clast forming the obstacle is a ventifact produced principally by aeolian corrasion of the original clast. The inflection point of the stepped profile of the windward face probably indicates the height at which the kinetic-energy flux of the saltation load (sensu Anderson, 1986) declines near the bed. Much less evidence of aeolian corrasion is seen on the leeward face, strongly suggesting once again that the southerly surface-winds govern the development of aeolian corrasion features in the Southern Namib. Modification of the original roughness element has created a complex shape, which can be viewed more simply as an impermeable vertical wall oriented approximately transverse to flow. The surface-flow over an obstacle of this type is potentially comprised of two separation bubbles (Figure 6.13) according to experimental results (eg. Good and Joubert, 1968; Etheridge and Kemp, 1978). The first is encountered at the base of the windward face as observed in the field by placing a ruler transverse to the flow. The second bubble is developed in the lee of the obstacle. Fluid passing over the leeward face of a wall is upthrust, so that the crest of the roller is about two wall heights above the flow boundary (Allen, 1982). For this reason, the roller formed in the lee of the wall is large compared to that on the windward side, which partially accounts for the large size of the current shadow in the lee of the phonolite ventifact.

Figure 6.12. Close-up showing the patch of segregated garnet grains (outlined in the lee of the phonolite roughness element. Southerly wind flow from bottom to top, lower edge of scale in mm.

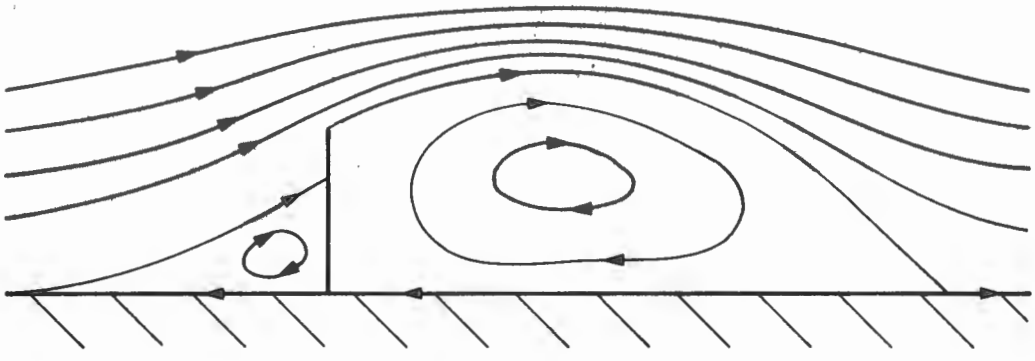

Figure 6.13. Theoretical pattern of surface flow over a transverse wall, which approximates to the cross-sectional form of the roughness element, to show the form of the flow separation bubbles which are anticipated to exist.

encounters an area of increased shear stress along the base of the windward face. Placing a ruler approximately transverse to flow, granules and even small pebbles are found to be transported along the edge during high-velocity winds. Hence scour is likely to occur periodically in this region. Size-density sorting of the creep bedload probably occurs under these conditions, with the result that the heavy mineral component of the creep bedload is progressively concentrated along the obstacle's leading edge. Wind scour at the base of the transverse wall could explain the abundance of garnet grains beneath the surface. Scoured hollows potentially provide sites in which heavy minerals would concentrate due to their lesser susceptibility to entrainment relative to the quartzitic material (eg. Willetts, 1983). Such scours would probably be infilled once more during reduced wind velocities, burying the heavy minerals.

The lee-side concentration of garnet grains is also attributed to the pattern of flow separation. This study has shown that garnet grains are readily moved by aeolian creep. Over a long period of time, many grains have potentially migrated past the fixed point represented by the phonolite clast. Experiments by Tsoar (1983) show that for vertical, windward-facing risers, a large separation bubble develops. As the slope of the riser with the horizontal is decreased, the size of the separation bubble at its base diminishes. At angles less than 38° no flow separation occurs. It is thus probably significant, that at the western end of the transverse wall the riser is not vertical, but inclined at 20° to 30°. Consequently, no separation bubble is anticipated to occur along the windward face at the western end of the ventifact. A notable increase of particles greater than about 2 to 3 mm diameter occurs immediately upwind of the sloping riser, and there is an apparent absence of very coarse sand and small granules. This is seen as evidence that the smaller grains in creep were periodically swept over the riser onto the obstacle's lee-side and incorporated into the western margin of the current shadow. The lee-side pattern of surface-flow at the western end of the obstacle probably also differs considerably from that at the eastern end where the vertical wall rises about 4 cm higher into the airflow. At the western edge, the riser was only 2 to 3 cm above the bed at its

highest point. Consequently, the separation bubble probably extended downwind for a shorter distance. This is possibly confirmed by the surficial distribution of the garnet grains, which were concentrated in a zone extending from the negative step over a much shorter distance downwind compared to the sandy current shadow. Slightly larger granules marking the northern limit of the surficial garnet concentration possibly define the position of the reattachment line of the separation bubble. Coarse particles on the western margin of the sandy current shadow appear to fine downwind from this point, suggesting that flow to the north resumes at this distance downwind of the step. The surficial segregation of garnet grains in the lee of the transverse negative step is most likely to have resulted from size-density sorting as grains were carried across the sloping riser. In the aeolian environment, where the difference between the density of the air and the garnet is so pronounced, segregation is likely to be very marked.

The zone of garnet concentration below the sediment surface along the base of the leeward face possibly developed in a similar manner to that of the windward face. In this instance, however, the scour along the base of the leeward slope is most likely to have occurred during northerly wind reversals. Under these conditions, the ordinarily leeward face briefly becomes the windward one, and significant scour along the base is possible. Segregated garnet from southerly wind conditions is then susceptible to concentration in scour hollows, which were subsequently infilled with the inevitable return to southerly surface-winds.

Heavy mineral segregations associated with ventifacts on the bed provides further evidence of particle cluster development by the creep bedload on stone pavement surfaces. In addition to quartz granule particle clusters, roughness elements situated in localities experiencing sufficient heavy mineral throughput by creep are capable of generating segregated particle clusters in response to the subtleties of aeolian size-density sorting aided by complex patterns of surface-wind flow. Heavy mineral segregations of this type may provide a useful indicator for the presence of stone pavements in the rock record, especially if the surface wind direction can be shown to be at variance with any alluvial system operating during the formation of the deposit.

Segregation Associated with Complex Bedrock Morphology

Complex bedrock morphology resulting from differential weathering occurs throughout the deflation basin. Small-scale examples of south-facing, sloping risers and transverse negative steps varying in height from 10-15 cm to 50-60 cm (Figure 6.14) are formed by Bogenfels Formation dolomite cropping out about 3 km east of Bogenfels. These examples are located a few hundred metres west of the Bakers Bay aeolian transport corridor. Consequently they are only subject to low or moderate sandflow conditions under the present aeolian sediment dispersal system.

The south-facing risers are polished and fluted by aeolian corrasion, but the face of transverse negative steps in their lee are relatively unaffected. Fractures in the dolomite release angular blocks from the edge of the negative steps. In time, sand infiltrates the cracks and the blocks are gradually forced away from the step. This significantly complicates the bedrock morphology.

Heavy mineral segregations are located both at the base of south-facing risers, and in the lee of the transverse negative steps. Segregations at the foot of south-facing risers are patchily distributed along ridge systems. The heavy mineral component comprised of iron oxide and hydroxide minerals, begins to concentrate slightly upwind of the risers, but the main segregation is commonly tightly packed against the base (Figure 6.15). Heavy mineral grains smaller than 2 to 3 mm in diameter are absent from segregations at the windward base of risers, and quartz granules on the bed exhibit a poorly developed imbricate shape-fabric (Figure 6.16).

Heavy mineral segregation at the foot of the transverse negative steps in the lee of risers prove that some heavy mineral grains are transported over the obstacles. Heavy mineral segregations are best developed where clefts occur in the dolomite ridge (Figure 6.17). In some instances wind aligned concentrations of large clasts of weathered dolomite also occur. Where present, the segregations occur on the floor of depressions in the lee-side deposit rather than on inclined planar surfaces of lee-side deposits. In contrast to segregations at the base of risers, those in the lee of transverse negative steps are relatively poorly sorted, and contain a large proportion of sand grade particles (Figure 6.18).

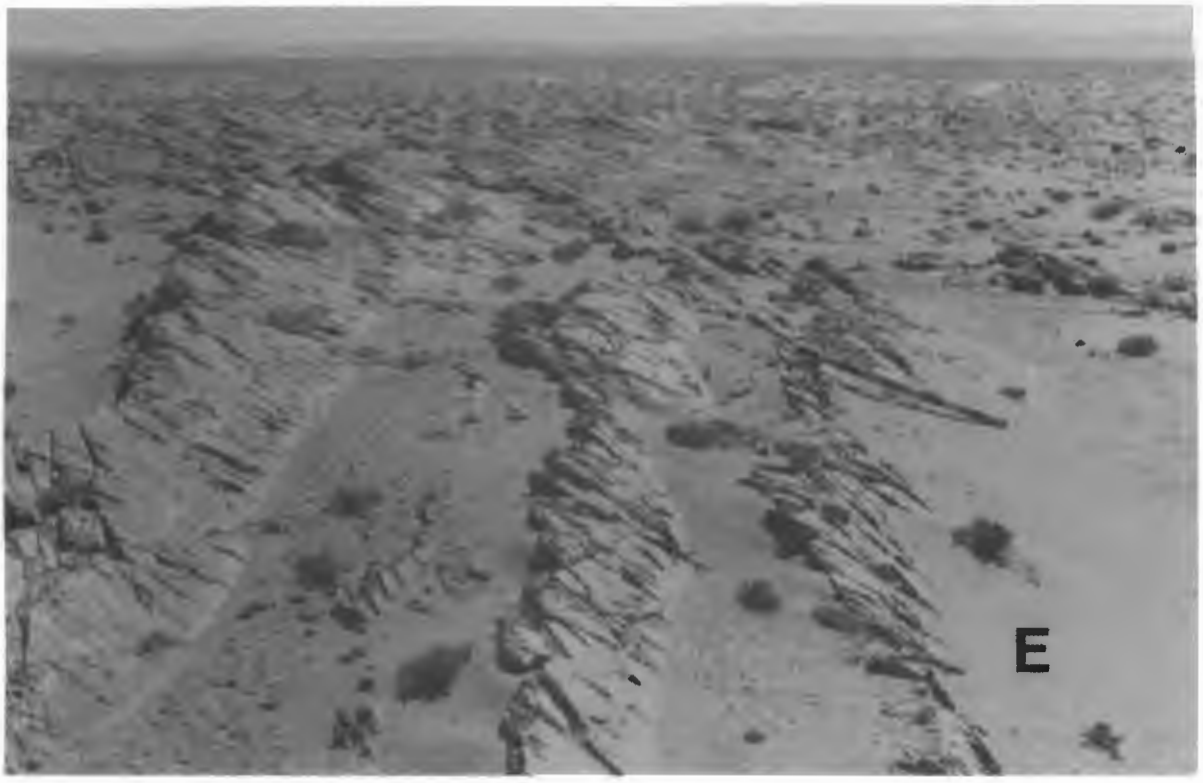

Figure 6.14. South-facing, dolomite risers which have been polished by aeolian processes, and transverse negative steps which form a "baffled", complex bedrock morphology through which the aeolian creep bedload must migrate. Note the encroachment deposit (E) formed at the base of the initial riser. Southerly wind flow from right to left, scale 1 m.

Figure 6.15. Heavy mineral segregation at the base of a south-facing riser, illustrating the wide variation in grain size. Note that in this instance, there is minimal development of an imbricate shape-fabric by the creep bedload. Southerly wind flow from left to right, scale in mm.

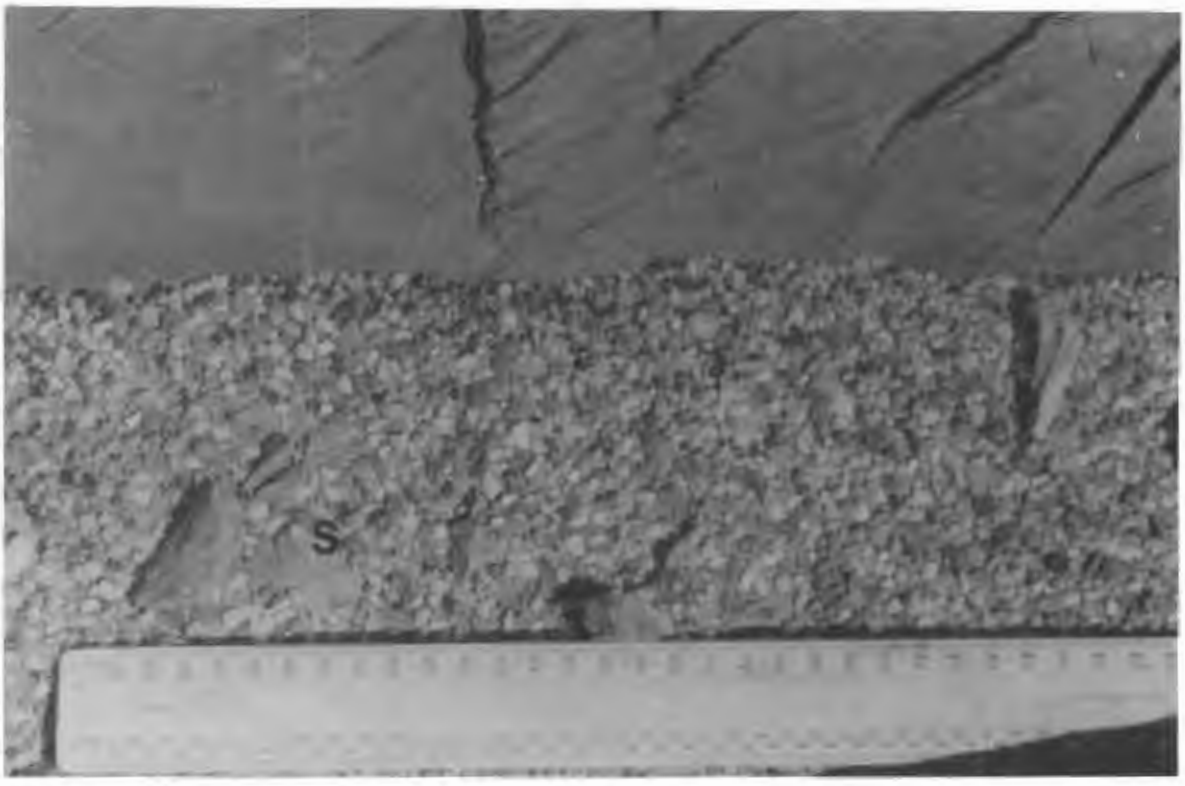

Figure 6.16. Heavy mineral segregation at the base of a polished, south-facing riser. Note the close packing of the creep bedload, which exhibits a poorly developed imbricate shape-fabric. Of interest is the exposed area of the silty soil (S) underlying the encroachment deposit. This soil exhibits a vesicular texture, when excavated. Southerly wind flow from bottom left to top right, scale in mm.

Figure 6.17. Scoured depression in the lee of a transverse negative step formed by dolomite. The scour is located downwind of a cleft in the step, and it is floored by heavy mineral grains. Note the wind-aligned concentration of dolomite fragments in the background at the site of another cleft. Southerly wind flow from left to right, scale in mm.

Interpretation

Summarised experimental data from numerous sources given by Allen (1982) and work by Tsoar (1983) predict the existence of a separation bubble in the lee of transverse negative steps and the possibility of a less developed bubble at the base of south-facing risers (Figure 6.19). The development of the latter is dependent upon the inclination of the riser.

Segregations at the base of risers are characterised by their relatively coarse grain size and very good sorting. The absence of finer-grained heavy mineral particles is interpreted as evidence for the absence or smaller size of the separation bubble formed at the base of risers. Aerodynamic forces probably entrain finer-grained material as the airflow accelerates up the riser, and grains are almost certainly ejected from the bed by saltation impact and carried over the transverse negative step. The very coarse sand and granules of heavy minerals are too large to be entrained by aerodynamic forces alone, and are also less readily entrained into saltation. These grains are interpreted as part of the creep bedload population, and their segregation at the foot of risers is the result of size-density sorting by creep transport. It is evident from the presence of quartz granules in lee side deposits that some of the creep bedload periodically crosses the transverse negative step. Relatively larger, quartz granules are likely to be more susceptible to being moved onto the riser by creep. Once there, it is possible that the accelerating airflow is capable of blowing the grains up the polished surface of the riser and across the step.

Segregations formed in the lee of the transverse negative steps are interpreted as the product of aeolian size-density sorting. Due to their greater settling velocity, heavy mineral grains will be deposited more rapidly in the lee of the step than quartz grains. Observations show that this only partially accounts for their segregation. The dolomite risers shield the surface of the lee-side deposit from direct saltation bombardment during southerly surface-wind conditions. Hence the segregation of heavy mineral grains beneath the transverse negative steps are considered to primarily result from size-density sorting by aerodynamic forces alone. During high velocity southerly surface-winds, gusting at

Figure 6.18. Close-up of the heavy mineral segregation shown in Fig. 6.17. Note the small size of the heavy mineral grains relative to those in Fig. 6.15 and 6.16. The presence of quartz granules, and rare heavy mineral granules suggest that components of the creep bedload periodically migrate across the riser. Southerly wind flow from top to bottom, scale in mm.

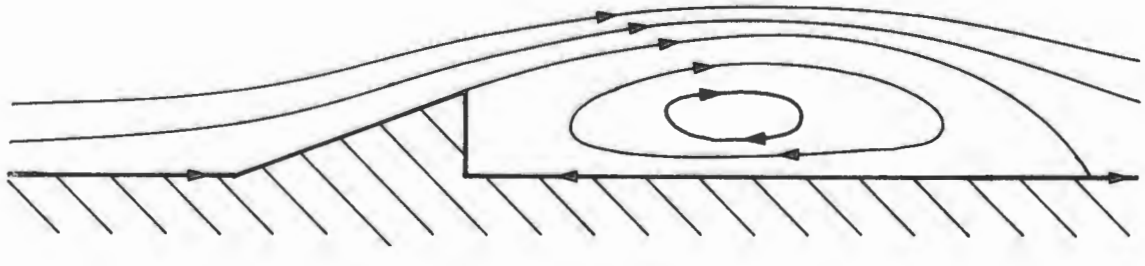

Figure 6.19. The theoretical pattern of surface flow across transverse negative steps combined with upwind, sloping risers based upon a summary of experimental work given by Allen (1982) and experiments by Tsoar (1983), showing the expected pattern of flow separation.

between 20 to 25 m/sec, evidence of the separation bubble in the lee of the negative step is seen. The movement of sediment within the separation bubble is particularly evident at clefts in the negative steps, where heavy mineral segregation has occurred. Viewed over several minutes, powerful turbulent eddies along the reattachment line of the separated flow sweep material from the surface of the surrounding lee side deposit into the wind-scoured pit beneath the separation bubble. The more readily entrained light particles are removed from the scour pit by the powerful eddies, leaving the heavy mineral particles slowly migrating around the floor of the pit. These particles remain trapped within the separation bubble, and the progressive segregation of more heavy mineral grains in time forms a densely packed surficial lag on the floor of the scour pit. The observed pattern of grain movement within the separation bubble resembles that predicted by Allen's (1968) experiments of low-speed flow separation at three-dimensional negative steps of differing plan form (Figure 6.20). Thus the heavy mineral segregation within the scour pit approximately defines the pattern of limiting streamlines for the separated flow, confirming that aerodynamic forces control the development of the lag deposits in the lee of transverse negative steps.

The wind-aligned concentration of angular dolomite fragments on the surface of lee-side deposits is also attributed to aeordynamic forces in the lee of the negative steps. It is suggested that scour by the powerful eddies sweeping the bed within the separation bubbles undermine the margins of the clasts, which subsequently become unstable and slide into the scour pit. As new fragments are weathered from the step, these are added to the debris flooring the pit until a coarse-grained lag deposit develops.

Break-up of the dolomite risers by weathering processes results in more complex bedrock morphologies. Heavy mineral segregations occur at the base of the depressions which approximate to rectangular cavities (Figure 6.21). As with segregations at negative steps, these examples are dominated by heavy mineral sands, suggesting that aerodynamic forces play an important part in their development. Allen (1982) summarises the results of experiments by various researchers examining the pattern of surface-flow across a cavity, and shows that the secondary flow

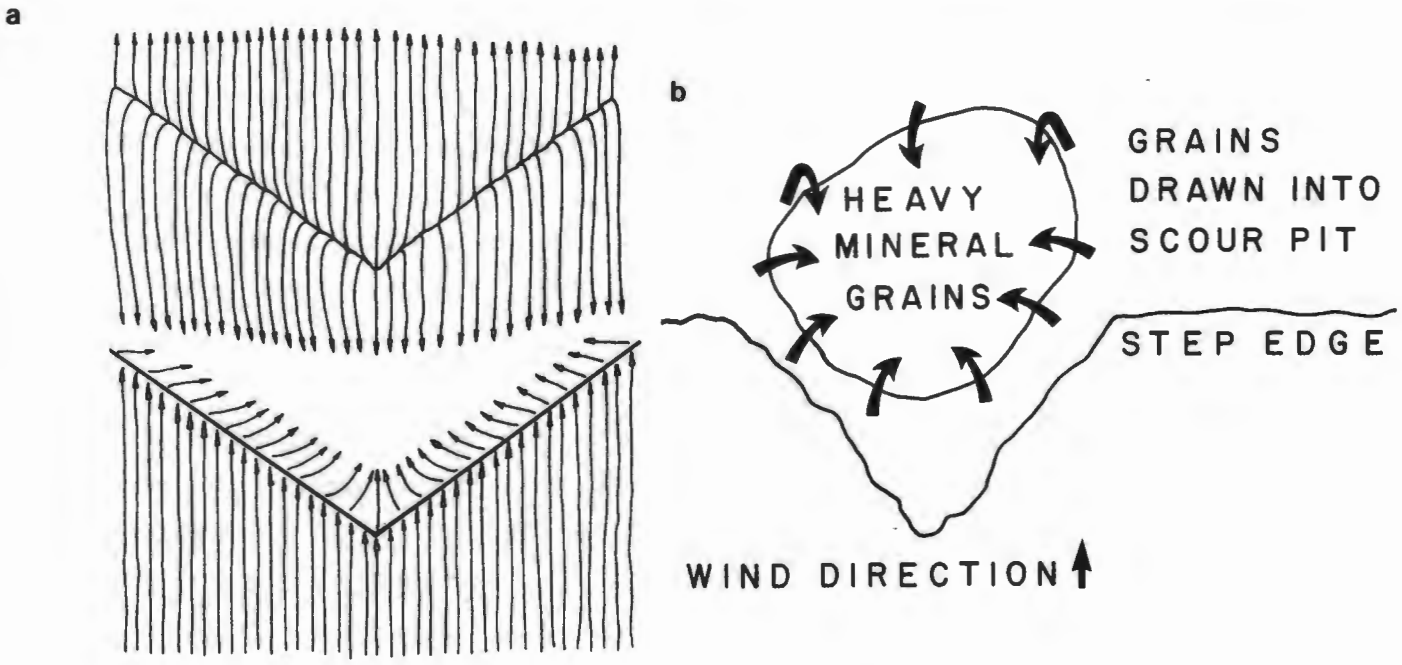

Figure 6.20. a) The theoretical pattern of limiting streamlines associated with the southerly wind flow across the transverse negative step. Based upon the consideration of flume experiments by Allen (1968), the observation of the flow pattern across the step in the field during high-velocity southerly winds, and b) the pattern of sediment movement observed on the floor of the scoured pits.

Figure 6.21. Heavy mineral segregation (arrowed) in the flow separation bubble at the base of a cavity formed by a weathered block of dolomite separated from the main ridge. The small gap on the bed between the heavy mineral segregation and the downwind margin of the cavity probably indicates the presence of a secondary vortex cell at the base of the cavity. Southerly wind flow from bottom to top, scale 30 cm.

consists of a main vortex together with secondary ones depending upon the Reynolds number and depth of the cavity. In the example of heavy mineral segregation shown here, a slight gap exists between the northern margin of the heavy mineral grains and the base of the north wall of the cavity. This implies the existence of a secondary vortex located at the base of the northern wall based upon observations by Tsoar (1983) on the development of echo dunes at cliff faces. The segregation of heavy minerals in this setting is therefore interpreted to be the result of size-density sorting in the separated surface-flow. There is little doubt that the larger settling velocity of the heavy mineral grains plays an important part in this process.

Implications

From the above discussion of the factors governing the development of heavy mineral segregations, it is clear that lag concentrations can develop by creep and/or aerodynamic forces alone. Segregations at the base of south-facing obstacles on the bed prove the dominant influence of the southerly surface-wind flow in maintaining creep transport to the north. Provided that aeolian processes at these sites are not disturbed by ephemeral stream activity or surface run-off to any great extent, surficial lag accumulations of heavy minerals will form. It is therefore extremely significant that marked concentrations of diamond were located on the windward side of dykes running perpendicular to the prevailing wind direction across the floor of endoreic basins (Figure 6.22). As Kaiser (1926) observed, these local concentrations prove that diamonds are transported along the floor of endoreic basins by aeolian processes. They also provide further proof that the palaeowind direction has consistently been dominated by southerly quadrant winds during the development of the placer bodies.

The importance of positive steps is greater still when the bedrock morphology of endoreic basins such as the Idatal and Hexenkessel is more closely examined. Positive features can halt the progress of the heavy minerals being transported by aeolian processes (Kaiser, op. cit.). Those oriented obliquely to the southerly surface-winds locally modify the direction of surface-wind flow, and hence sandflow. Consequently, they also

govern the migration direction of the creep bedload. Evidence for this is seen within the Idatal, where granule ripples encounter bedrock steps obstructing their advance. Instead of continuing along the main axis of the basin, the migration direction of the granule ripples alters and they travel parallel to the oblique positive step (Figure 6.23). On a larger-scale, this means that once material enters an endoreic basin, it is highly unlikely that aeolian processes will transport it into an adjacent basin. Hence it either migrates north under the dominant influence of the southerly surface-wind regime or, more rarely, it migrates south under the influence of relatively infrequent northerly wind reversals.

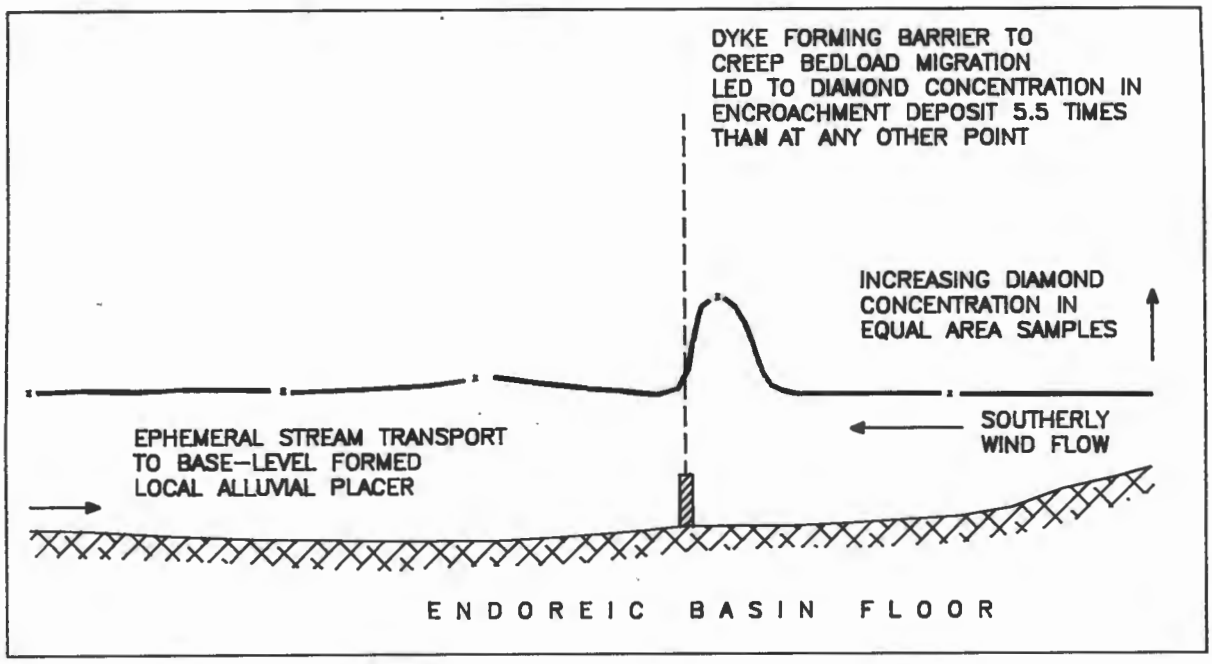

Figure 6.22. Development of a local diamond placer body associated with an encroachment deposit on the upwind side of a phonolite dyke running east-west across the floor of an endoreic basin. Based upon prospecting data belonging to CDM.

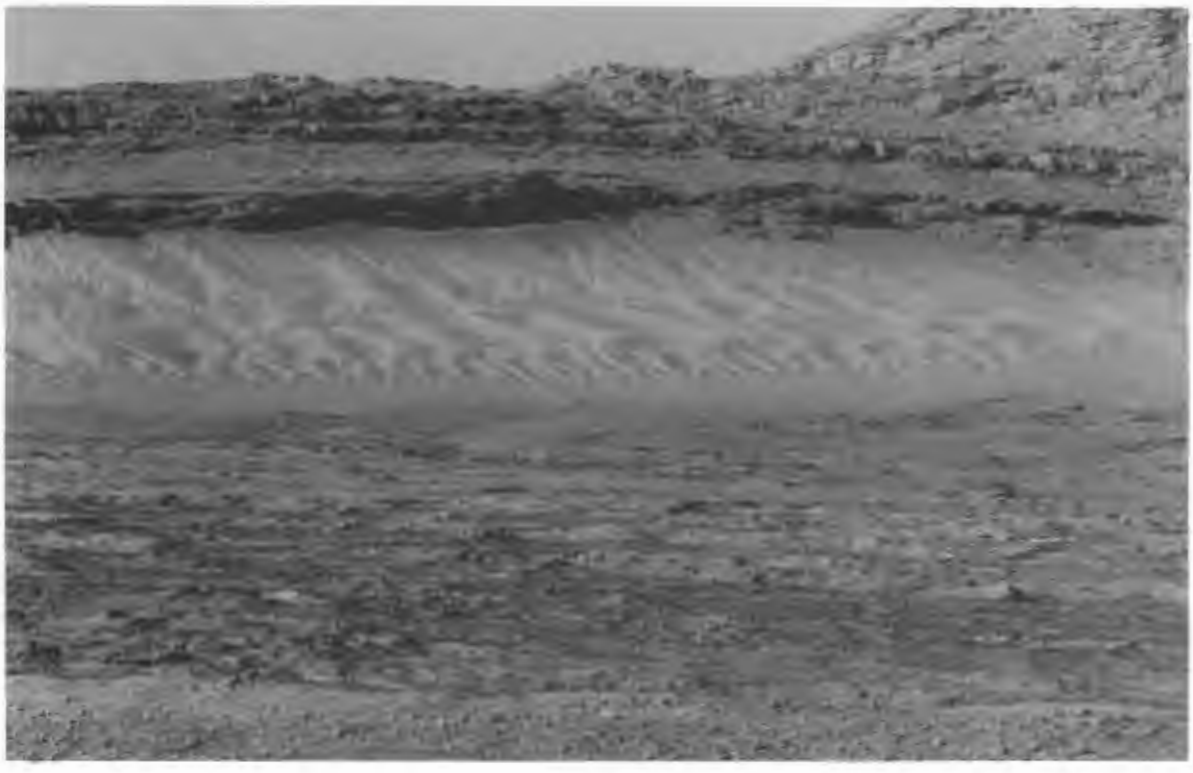

Figure 6.23. Control of the migration direction of granule ripples in the Idatal imposed by the bedrock topography. Southerly wind flow from right to left, scale 1 m.

6.2. SEGREGATION BY EPHEMERAL SURFACE RUN-OFF

6.2.1. THE NATURE AND DIRECTION OF FLOW

The form of endoreic basins severely restricts the potential for ephemeral surface run-off to redistribute material. Alluvial transport can only move material downslope, hence the primary effect is to bring sediment back towards the base-level of the system (Kaiser, 1926). The observation of ephemeral events in the Southern Namib over a four year period has shown that surface run-off is very short-lived. Infiltration of the run-off coupled with the ephemeral nature of the precipitation generating it serve to limit the transport capacity of the ephemeral stream systems.

6.2.2. REDISTRIBUTION OF AEOLIAN MATERIAL

As demonstrated by examination of an encroachment deposit surface near Meob Bay, aeolian transport is not restricted to movement down a topographic slope. All modes of aeolian transport are capable of moving material upslope. Kaiser (1926) realised that due to the dominance of southerly surface-winds, aeolian material is progressively transported northwards, up the topographic slope defining the northern end of endoreic basins. As shown above, ephemeral stream systems within these basins are characterised by a specific pattern. A dendritic tributary channel network generated at the northern end of the endoreic basins, feeds a main channel which subsequently flows into a ponded water body at the system's base-level. In basins with a stepped south-north longitudinal profile, this pattern may be repeated a number of times. Optimum conditions for surface run-off generation are provided where bedrock is exposed, minimising infiltration. During heavy rainfall, run-off is generated in areas of complex bedrock topography which formerly were sites for heavy mineral segregation by aeolian processes. Aeolian sediments are therefore reworked by the dendritic tributary network and transported towards the main channel. The sediment is then transported towards the ponded water body (Kaiser, 1926).

6.2.3. POTENTIAL SITES FOR HEAVY MINERAL SEGREGATION

Channel Confluences

As a result of the dendritic tributary network, ephemeral stream systems within endoreic basins are comprised of numerous stream junctions. Additional confluences exist where the individual channels of braided stream systems join. Mosley and Schumm (1977) drew attention to the role of stream junctions in the genesis of alluvial placer deposits. These authors noted that a scour is formed at the confluence of two channels. Controlled experiments demonstrated that the depth of scour is greatest when:

1) the discharge of the joining channels is half to equal to that of the main channel;
2) the streams have a small bedload transport rate;
3) the channels join at angles between 60° to 90°.

It was also observed that sediment entering the confluence was not transported through the scour, but migrated around its margins. The segregation of magnetite grains occured slightly downstream of the scour, and not within the scour itself. More recently, Best and Brayshaw (1985) have shown that this type of segregation is governed by the pattern of flow separation developed at channel confluences (Figure 6.24a). This is largely controlled by the junction angles and discharges of the confluent channels (Best, 1985, cited in Best and Brayshaw, 1985). On entering the confluence from a tributary channel, Best and Brayshaw (op. cit.) observed that higher density grains are entrained along the shear layer bounding the separation bubble. Sediment transport towards the separation zone results in the deposition and segregation of the heavy mineral fraction in an area of rapidly decreasing shear stress within the separation zone (Figure 6.24b).

The geologists who prospected the Bogenfels area where the braided ephemeral stream system from the Langental enters the basin sketched the distribution of diamonds on a plan. Localised areas of high concentration were surrounded by areas of lower concentration. The pattern of broadly south-north oriented strips closely resembles that of a braided stream network. Significantly, perhaps, some of the areas of greatest diamond concentration appear to be located at what would be the downstream confluences of lower values (Figure 6.25). This strongly suggests that channel confluences within ephemeral stream systems are important sites for the

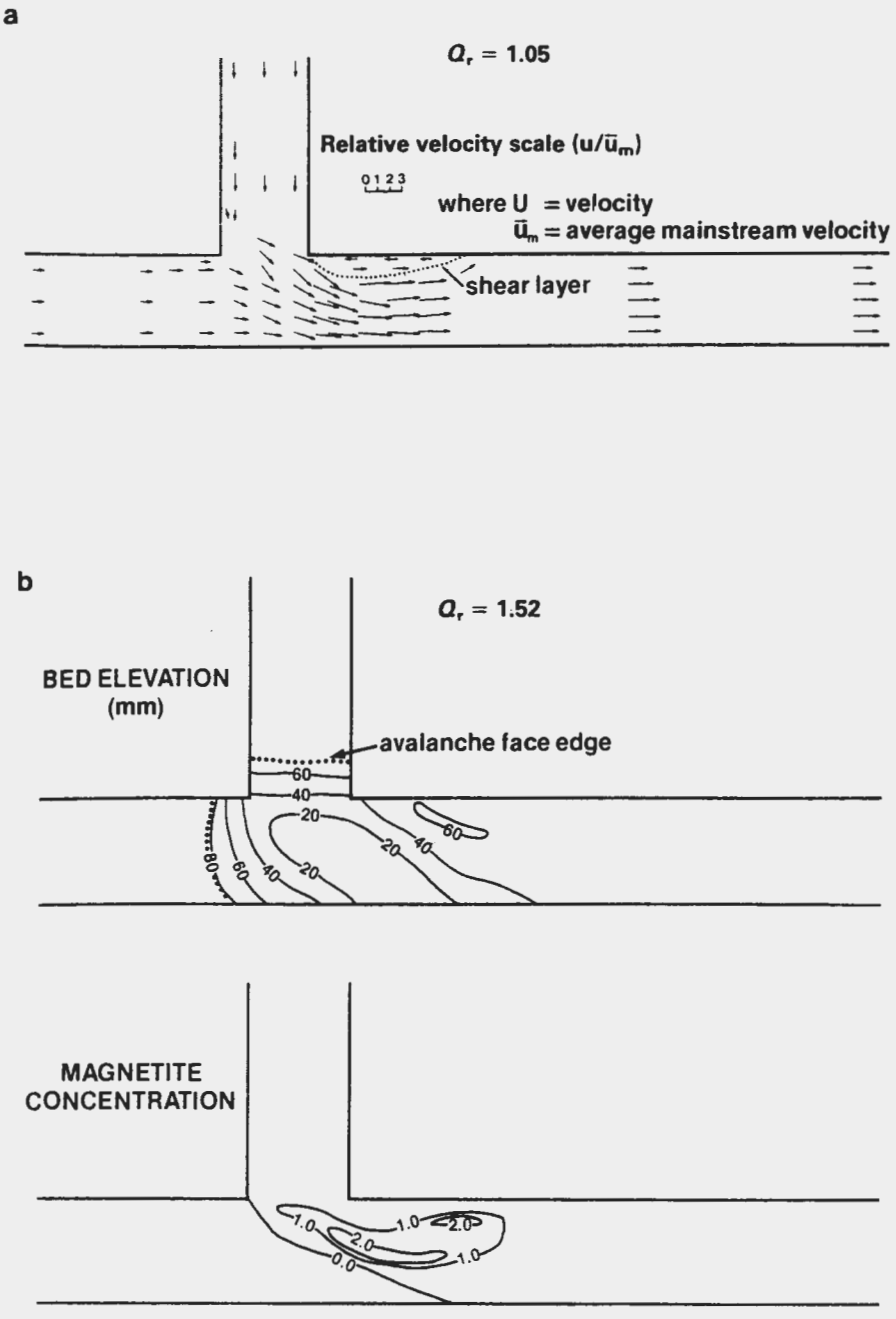

Figure 6.24. (a) The pattern of flow separation developed at a 90° channel confluence. (b) The distribution of sites for heavy mineral segregation arising from the flow pattern through the confluence. After Best and Brayshaw, 1985.

development of very localised placer bodies within the deflation basin. The confluence of a dendritic tributary system, on a south-facing slope, with a larger channel was sampled during this study (Figure 6.26). The main channel was only 10 to 20 cm deep, and the material on the stream bed consisted of locally derived weathered bedrock. Twenty diamonds were recovered from the sample downstream of the confluence. The same sized sample from the adjacent stone pavement only yielded two diamonds.

Implications

Endoreic basins are continuously modified by ongoing salt weathering and aeolian processes today. Weathering and erosion operates to both lower and alter the position of the base-level of the ephemeral stream systems within the endoreic basins. These systems are therefore periodically rejuvenated. Very local-scale concentrations of diamonds are thus hypothetically subjected to polycyclical reworking. A concentration within an earlier confluence may be destroyed by the rejuvenation of the ephemeral stream system, and reform at a new confluence nearer to the new base-level of the basin. As Kaiser (1926) noted, aeolian deflation resulting in the reworking of ephemeral streams deposits removes some of the fine-grained sediment. This, in itself, potentially results in a relative enrichment of the coarser-grained sediment, and resistant heavy minerals forming channel confluence placer bodies are likely to become better concentrated. Theoretically a rather uneven diamond dispersal pattern is likely to result, which is then subjected to the influence of the aeolian system once ephemeral stream beds become desiccated once more. Thus an alluvial dispersal pattern is modified, in time, to show features characteristic of an aeolian dispersal pattern. The degree of modification by aeolian processes will ultimately be dependent upon the periodicity of the ephemeral rainfall events, the energy of the aeolian current system, and the sandflow rate.

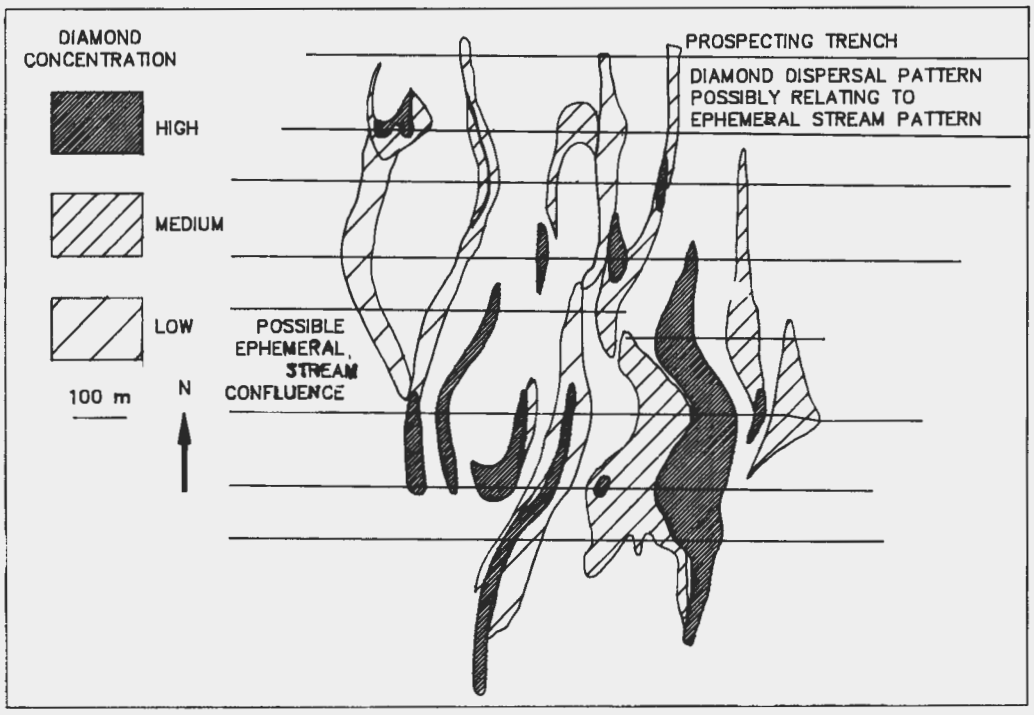

Figure 6.25. Part of the diamond dispersal pattern interpreted by geologists c. 1908 in an area about 1 km north of Bogenfels, where the ephemeral Langental drainage system enters the Bogenfels Basin. Note the resemblance to a braided stream system, and the location of higher values at "confluences".

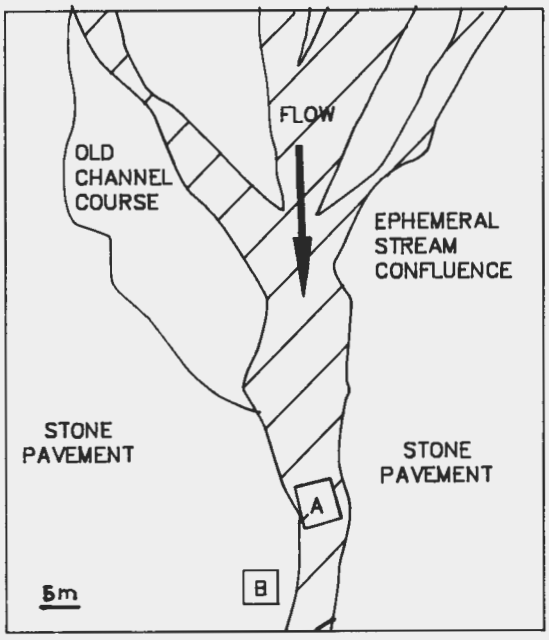

Figure 6.26. Sample sites about 2 km east of Bogenfels. 20 diamonds were recovered from sample (A), downstream of the channel confluence, whilst the stone pavement at site (B) yielded only two diamonds. The difference in diamond concentration is attributed to segregation at the ephemeral stream channel confluence.

6.3. DIAMOND DISPERSAL PATTERNS

6.3.1. INTRODUCTION

Diamond dispersal patterns from endoreic basins have not previously been discussed in detail. Wagner (1914) noted that the payable ground was located along the lowermost parts of basins and on south-facing slopes. He also observed that the diamond concentration was characterised by rapid variation. Greater detail was provided by Kaiser (1926), who was not permitted to publish supporting data. He did, however, make some general comments:

1) diamonds were concentrated in south-north oriented zones;
2) discrete concentrations were located in southern locations, from which northward tails of diamonds were present;
3) diamond size declined from south to north;
4) some basins showed a greater concentration along their western margin;
5) diamonds were not generally present on the divides between succeeding basins;
6) diamond concentration did not occur immediately north of basin divides, but some distance down the north-facing topographic slope.

The data used for the examination of the diamond dispersal patterns have been extracted from original prospecting plans (c. 1912). Prospecting was undertaken using east-west oriented trenches perpendicular to the south-north basin axes. The trenches were excavated in individually treated 20 m sections. The number of diamonds recovered and the total weight of the diamonds per sample was recorded on the plans. Unfortunately details of the size-weight frequency distributions of the samples no longer exist. The data have been examined using the VULCAN interactive computer graphics programme. Diamond dispersal patterns based upon the number of stones and the average size of the stones from each sample were modelled and their position was related to the bedrock topography.

6.3.2. DIAMOND DISPERSAL PATTERNS IN A SOLITARY ENDOREIC BASIN

Basin Morphology

The Idatal endoreic basin is located to the north of the Bogenfels Basin, from which it is separated by Daheimtal, another endoreic basin (Figure 6.27). The Idatal, like the other endoreic basins, has formed by a combination of salt weathering, aeolian deflation and aeolian corrasion. The basin is a linear south-north oriented feature, with the minimum base-level of 1 m below sea-level situated near its southern end (Figure 6.28). From this point, the basin floor rises gradually, to form a south-facing slope, which tapers to an apex in the north, near Pomona. The Idatal has a stepped longitudinal profile and a number of sub-basins exist within it. Only the portion of the basin lying within the original Pomona claim boundary will be discussed here since this was where the main placer body was located before it was mined-out.

Spatial Variation of the Average Diamond Size

The dispersal pattern forms a linear feature running along the floor of the Idatal basin (Figure 6.29). The average diamond size data is very clearly zoned spatially. The largest diamonds were located at base-level along the western margin of the basin. A series of concentric bands on the northern side of the zone containing the largest stones show that there is a reduction of diamond size to the north, up the topographic south-facing slope. The zones representing the large and medium average diamond sizes are relatively narrow, compared to those of the smaller average diamond sizes, which extend to the north.

Spatial Variation of the Diamond Concentration

The maximum number of diamonds was located towards base-level (Figure 6.30). The number of diamonds declines rapidly to the north of the main concentration. A smaller secondary peak occurred north of the main one. This marks the position of a smaller bedrock depression forming a local base-level lying above that in the south. Thus a smaller endoreic feature is present within the main basin. The peak in the number of diamonds coincides with the location of the zones representing large and medium average diamond

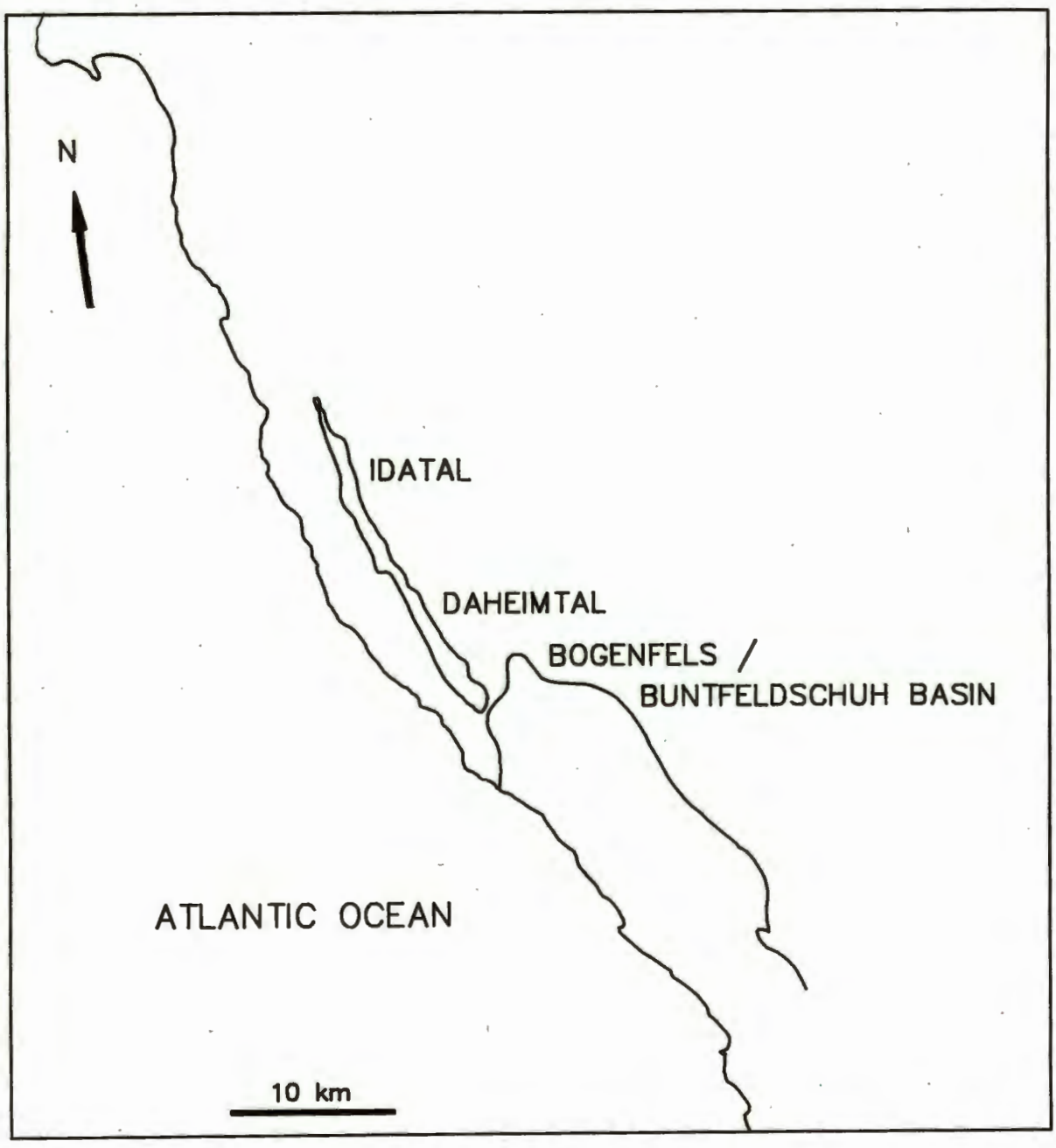

Figure 6.27. Map showing the endoreic basin system between Bogenfels and the Idatal.

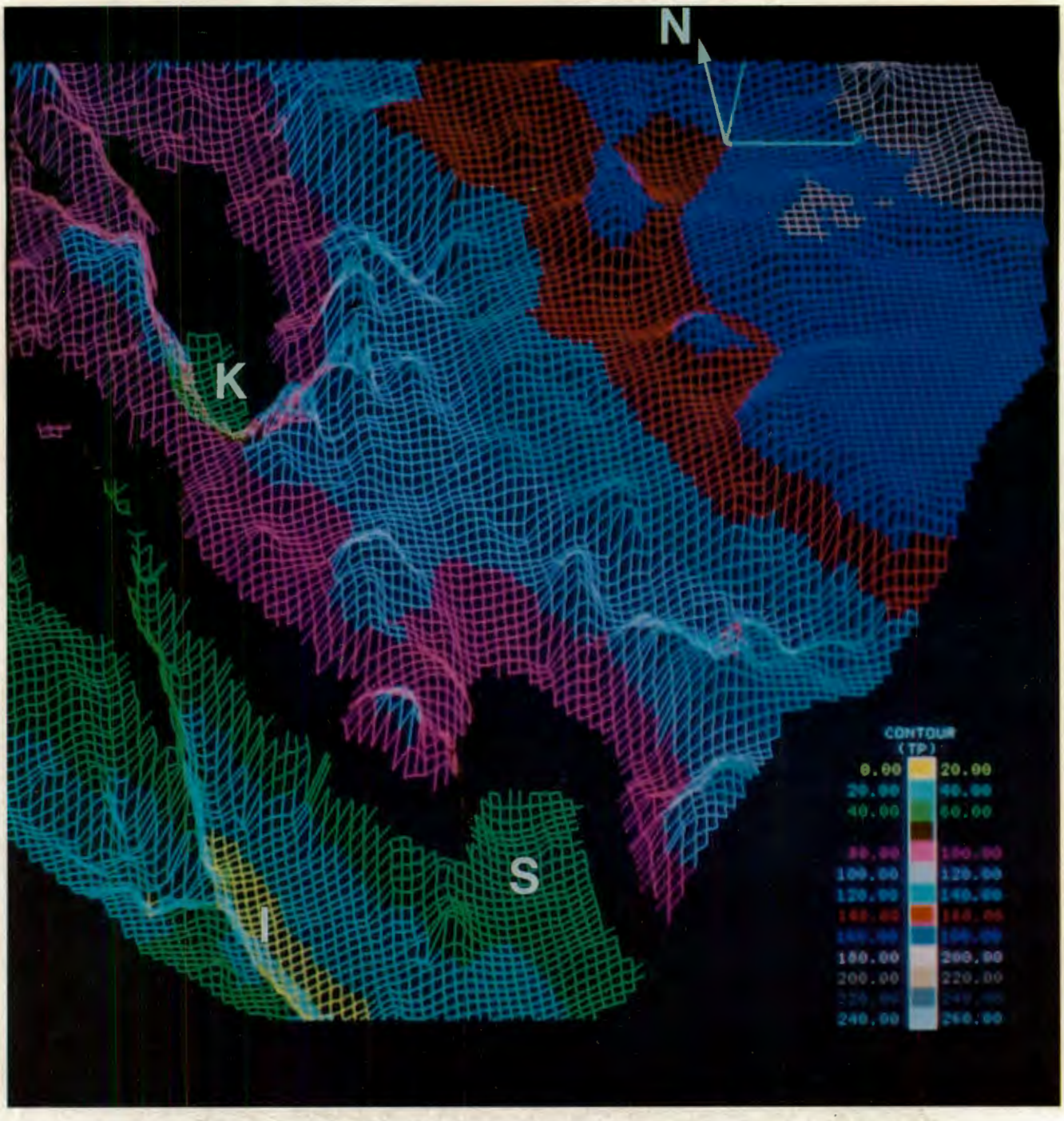

Figure 6.28. Computer generated topographic net of part of the Pomona claim, showing the form of the Idatal (I), Scheibetal (S), and the Kaukausibtal (K). Note that the base-level of the endoreic basins is located towards the southern end in each case. Contour elevations provided on coloured legend.

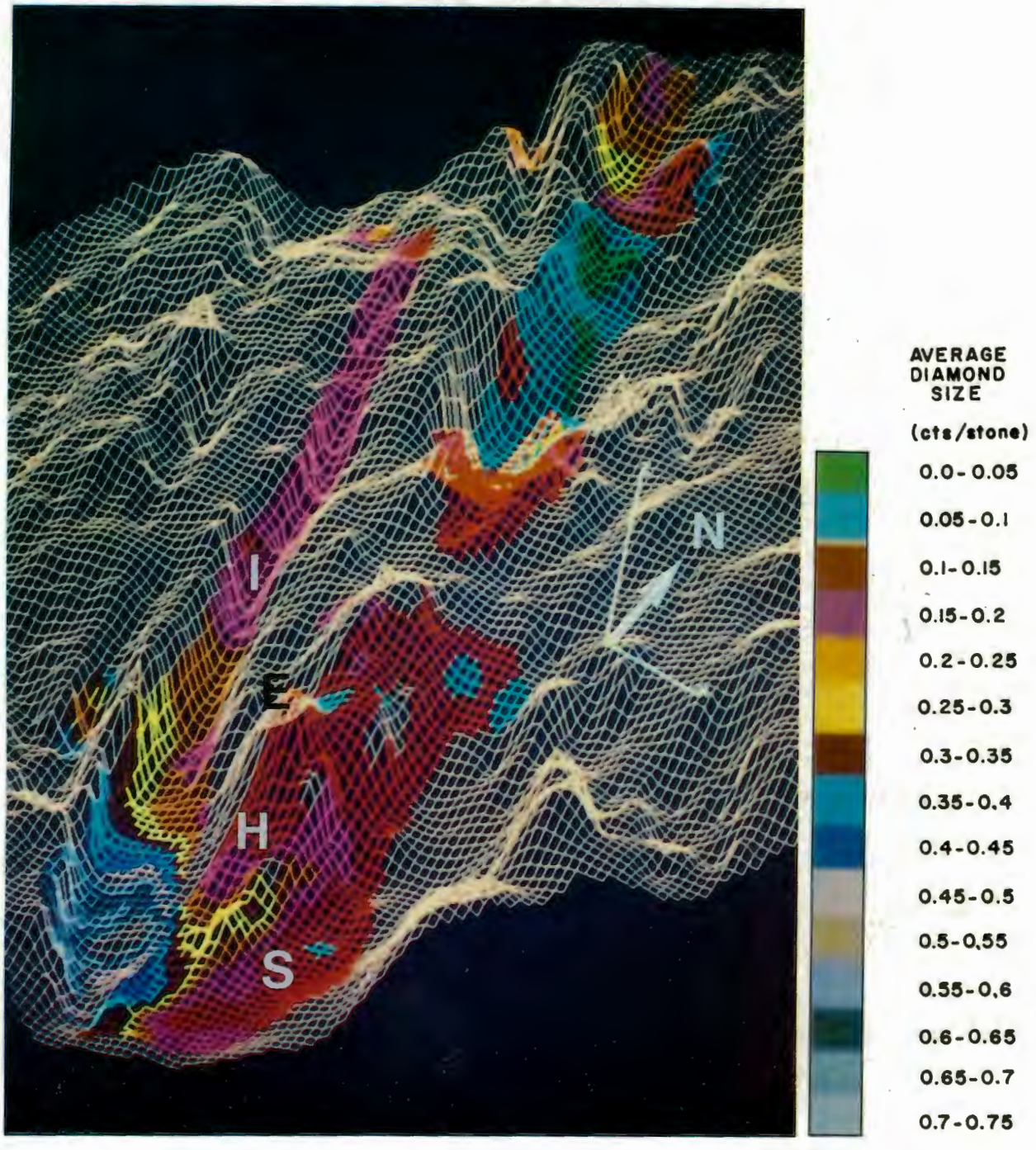

Figure 6.29. Diamond dispersal pattern shown by the variation of average diamond size in the southern part of the Pomona claim. Thecolurs denoting the different class intervals are given in the legend. In the text describing the dispersal pattern, the term small refers to values of 0.05 to 0.2 cts/stone, medium to values of 0.25 to 0.4 cts/stone, and large to values of 0.4 to 0.75 cts/stn. The endoreic basins in which the placer bodies were situated are: Idatal (I), Hexenkessel (H), Scheibetal (S), and the Kaukausibtal (K). The silcrete residual known as Elfertberg (E) separates the Hexenkessel from the Scheibetal. Note the concentric zones of decreasing diamond size extending to the north along the Idatal endoreic basin.

Figure 6.30. Diamond dispersal pattern shown by the variation of diamond concentration in the southern part of the Pomona claim. The variation of concentration is shown graphically, with peaks corresponding to high diamond concentrations. Colour coding of the diamond concentration contours are, shades of:

red, pink, and grey = high concentration;
blue, and white = medium concentration;
brown, green, and orange = low concentration.

The massive peak in the diamond concentration is located within the Hexenkessel. The smaller peak to the west, near the base-level of the Idatal endoreic basin, approximately corresponds with the position of the zones of large and medium average diamond sizes.

sizes. Hence peaks in the concentration of diamonds do not correspond with zones containing small diamonds.

Interpretation

In terms of the present-day sedimentary environment, two dispersal systems influence terrigenous sediment dispersal (Kaiser, 1926). These are the aeolian sediment dispersal system and the ephemeral stream sediment dispersal system, which operate independently of each other.

According to Sternberg's Law, in any alluvial system, sediment transport will result in the downslope reduction of particle size. Examination of the spatial variation of average diamond size data shows that this does not occur within the Idatal. The dispersal pattern clearly shows that the average diamond size fines to the north, up the south-facing topographic slope. This diamond dispersal pattern is therefore not solely the result of alluvial transport.

Garnet tracers deployed during this study prove that the dominant migration direction for both the creep and saltation modes of aeolian transport is to the north. These are the only present-day transport processes operating in the region which are able to account for the up-slope decline in diamond size as Kaiser (op. cit.) realised. Observations made during this study strongly suggest that the small to medium diamonds are probably periodically entrained into saltation. The largest diamond recovered from the Fiskus Sandstone Beds (see section 7.2.10) during CDM prospecting work at Elizabeth Bay weighed 1.2 carats. This diamond would have been transported across a soft dune sand substrate prior to its deposition. The creep transport capacity across the hard substrate of the stone pavements which floored the Idatal endoreic basin would be greater because of reduced dissipation of saltation grain kinetic energy on rebound. The majority of the medium and large diamonds recovered from the Idatal would therefore have been susceptible to aeolian creep transport. This confirms Kaiser's view that diamonds were transported northwards, up the south-facing slopes of the valleys by aeolian processes.

The concentrically zoned pattern of progressively smaller diamond size, which fines to the north, have not been previously defined. This pattern is interpreted as evidence for differential aeolian

transport rates according to particle size. The process has been modelled using the garnet tracers, but the Idatal diamond disperal pattern exemplifies the subtlety with which it occurs. The garnet tracers also confirm that small diamonds should be more frequently entrained into saltation and/or creep. The small diamonds are therefore transported more rapidly than the medium and large diamond sizes, which accounts for the extreme downwind extension of the fine-grained dispersal tail. The decrease in both the diamond concentration and the average diamond size to the north, is not seen as evidence for a deficit of small diamonds in the original size-frequency distribution. This feature of the diamond dispersal pattern is also attributed to the differential transport rate of the particles according to their size. The faster transport rate of small diamonds means that they are likely to migrate through the endoreic basin system by aeolian processes more rapidly than the medium to large diamonds. Thus, if diamond input to the endoreic basin system occurred in pulses, the quantity of small diamonds left will progressively diminish as a function of time spent in the high-energy aeolian environment.

Kaiser (1926) concluded that the diamonds concentrated within endoreic basins represented polycyclic lag placers which were generated by the interaction of the aeolian and ephemeral stream sediment dispersal systems (Figure 6.31). This interpretation depends upon how the diamonds were introduced to the basin. Kaiser favoured the deflation of a pre-existing sediment pile, which resulted in the progressive concentration of diamonds on the basin floor. Provided that this interpretation is correct, the location of the main placer body of larger diamonds near the Idatal's base-level tends to support the lag theory. It has, however, been stated above that although the large to medium sized diamonds were less readily entrained into creep transport, they formed part of a mobile creep bedload population. The larger diamonds would therefore remain within the endoreic basin system for a much longer period of time than the smaller diamonds. Provided that sufficient sandflow occurred through the endoreic basin, creep transport would ultimately also have transported the larger diamonds onto the south-facing slope at the northern end of the basin. They would then become susceptible to ephemeral reworking back towards the basin's base-level by stream systems.

The progressive deepening of base-level due to the continued evolution of the endoreic basin leads to the periodic rejuvenation of the ephemeral stream systems within it. The points at which the aeolian placer bodies on the south-facing slope are reworked by the streams therefore alters with time. Sampling during the course of this study, and the consideration of experimental flume work by Mosley and Schumm (1977) and Best and Brayshaw (1985), demonstrates that channel junctions within dendritic tributary networks provide sites for the local generation of alluvial placer bodies. This substantially modifies the aeolian sediment dispersal pattern.

Comparative photography of sites in the Idatal proves that the alluvially redistributed granule sized material is not locked in the stream bed beyond the influence of the aeolian system. Kaiser (1926) observed aeolian deflation of the ephemeral stream beds. This study illustrates that the aeolian reworking commences with deflation shortly after the flood event, prior to the total desiccation of the stream bed. The time required for the coarse-grained, re-released alluvial material to generate a new stone pavement surface, and the periodicity of rainfall, determines the extent of deflation. The previous aeolian dispersal pattern is

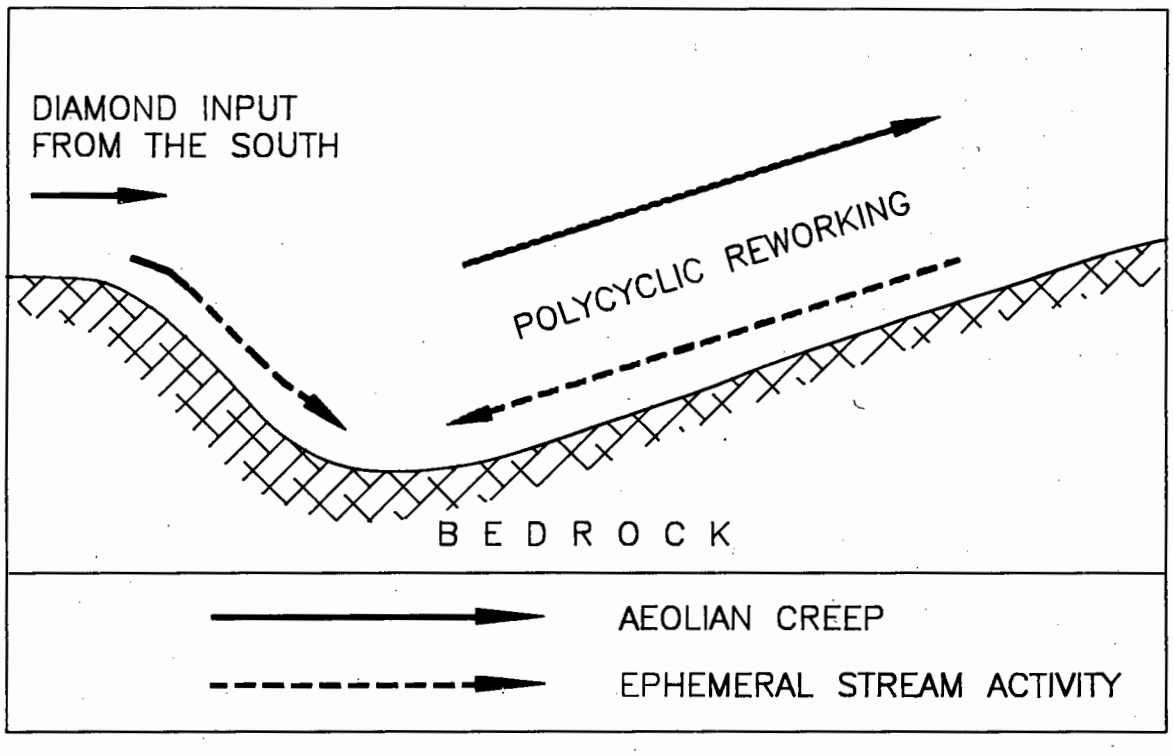

Figure 6.31. Sketch illustrating the polycyclic nature of the diamond placer deposits located within endoreic basins occurring in the vicinity of Pomona. Based upon observations by Kaiser (1926) and this study.

partially destroyed by the alluvial activity. Progressive size-density-shape sorting of the material forming the ephemeral stream beds leads to the removal of the smaller diamonds. Provided that the diamonds remaining on the ephemeral stream bed are too large to be entrained into aeolian creep transport, a lag placer body is then generated.

The floor of the Idatal endoreic basin is not smooth, and complex bedrock morphology also influences the ephemeral stream systems. The basin floor slopes to the west, descending in a series of steps. The rapid breaks in slope create localised areas of flow velocity reduction at which rapid deposition of ephemeral stream sediment occurs. These deposits are also reworked by aeolian processes as desiccation proceeds, and banks of coarse-grained material form encroachment deposits and granule ripples. As discussed previously, the bedrock morphology controls the migration direction of the granule ripples. In the case of the Idatal, the material is transported towards the base-level of the system lying within the Pomona claim boundary. Sediment is therefore funnelled into the area covered by the diamond dispersal patterns shown here. The continued transport of material into this part of the basin is a pre-requisite for the generation of the placer deposit. If polycyclic reworking continuously removes the majority of the diamonds to the north, and no new material entered the basin, the placer body would degenerate in time.

Provided that rainfall events remain infrequent, and the high-energy aeolian system maintains sufficient sandflow, continued size sorting of the sediment ultimately leads to the redevelopment of the aeolian dispersal pattern.

6.3.3. DIAMOND DISPERSAL PATTERNS IN SUCCESSIVE ENDOREIC BASINS

Basin Morphology

A series of mature endoreic basins characterises the geomorphology of the Pomona area (see Figure 6.28). Placer bodies were present in the Idatal, Hexenkessel, Kaukausibtal and Scheibetal. The Idatal, the largest of the basins occurs on the western side of the area, whilst the Hexenkessel is situated south of the Kaukausibtal. The Scheibetal is the large endoreic basin on the eastern side of the area being considered. As with the Idatal,

this basin's base-level occurs along its western margin. Uneven bedrock topography exists between the Hexenkessel and Kaukausibtal basins. The main feature is a steep south-facing slope at the northern end of the Hexenkessel which leads up to the duricrusted residual known as Elfertberg. This sub-horizontal to gently dipping silcrete capping provides evidence for extensive topographic inversion (Kaiser, 1926) by about 120 m of post-silcrete erosion. Each basin is essentially endoreic, and minimal connection by ephemeral stream systems is present.

Spatial Variation of Average Diamond Size

The diamond dispersal pattern of the Hexenkessel closely resembles that of the Idatal (see Figure 6.29), with a clear reduction of the average diamond size from south to north. A slight increase in the diamond size was located on Elfertberg at the northern end of the south-facing slope.

The diamond dispersal pattern within the Scheibetal also shows a general size decline from south to north. There is a noticeable reduction of the average diamond size from west to east across the Idatal, Hexenkessel and Scheibetal.

The Kaukausibtal diamond dispersal pattern is particularly interesting, when viewed in conjunction with the data from the Hexenkessel and Scheibetal. The general trend of a south-north reduction of the average diamond size is found within these basins. Viewed in detail, several deviations from this trend are observed within the Kaukausibtal. The larger stones were concentrated at the base-level of the system, with slightly smaller diamonds at the extreme southern margin. Hence on the north-facing slope at the southern end of the basin, there is evidence of a northward increase in diamond size. To the north of the base-level concentration of diamonds, a tail of small diamonds extends along the gently inclined south-facing slope of the basin floor. At the northern end, on a steeper south-facing slope, the average diamond size increases slightly. A slight increase in the average diamond size was also found to occur at the base-level of the succeeding endoreic basin. Another series of northward fining zones of average diamond size extended to the north of this point.

Spatial Variation of the Diamond Concentration

Viewed overall, the distribution of diamonds from south to north resembles that shown by the Idatal (see Figure 6.30). The main concentration occurs at the southern end of the area, with a marked decline in concentration to the north.

Considered as separate entities, each basin exhibits a distinctive pattern. The classical form is nowhere better demonstrated than the Hexenkessel where fabulously rich deposits, situated at a local base-level, yielded 1693 diamonds from a 40 m sample. The concentration tailed off abruptly both to the south and the north. In the Scheibetal, the main concentration is located along the western margin of the basin, corresponding to the location of the base-level.

The Kaukausibtal exhibits a more complex dispersal pattern. Alternating bands of higher and lower diamond concentration oriented perpendicular to the southerly surface-wind occur along the floor of the basin. A similar pattern occurred towards the northern end of the Idatal basin. Unfortunately, because these deposits have been mined-out, it is no longer possible to determine whether this pattern is the product of the sampling methods or a characteristic of the dispersal pattern. The better concentrations in these bands were associated with more steeply inclined south-facing slopes.

Interpretation

The overall trend of average diamond size reduction from south to north is interpreted as further evidence for the aeolian transport of diamonds. The dispersal pattern exhibited by the Idatal represents that of a discrete, solitary basin. A more complex dispersal pattern is seen on a multi-basin scale.

Kaiser (1926) discussed the possibility that diamonds are transported from one basin to another, but was indefinite about the extent to which this has occurred. The diamond dispersal pattern based upon average diamond size data shown in this study closely resembles the pattern one would predict if this were the case. Each basin examined exhibits a south to north reduction of the average diamond size. Significantly, the most southerly basin examined contains the largest diamond sizes, and successive basins to the north contain smaller diamonds. This indicates that the diamonds

have been transported northwards from a southerly point by aeolian processes. The progressive reduction of average diamond size within successive basins is interpreted as the result of aeolian size sorting of a southerly source. Based upon the garnet tracers, it is concluded that the small to medium sized diamonds migrate more rapidly through the endoreic basin systems than the larger ones. Many of the diamonds in the Kaukausibtal basin are therefore likely to have been introduced from the south by aeolian transport.

Aeolian size sorting is a response to variation of the entrainment potential of particles on the basis of their shape, size and density. Although the smaller diamonds are theoretically shielded from direct saltation bombardment by larger grains, they appear to remain more susceptible to entrainment than the medium and large diamonds. This is probably at least partially because bombardment by larger grains is required to entrain the bigger diamonds. As these grains have been shown by sand trap data to be comparatively rare, larger diamonds are unlikely to be entrained as frequently as smaller ones. Conceptually, this means that diamonds are moving at differing transport rates, which are variably influenced by changes in the bedrock topography. Evidence supporting this concept appears to be present in the diamond dispersal pattern exhibited by the Kaukausibtal basin. Looking north from the Scheibetal, very small average diamond sizes were unstable on the divide between the basins, and only small to medium average diamond sizes are represented. The slight increase in diamond size at base-level is likely to be the result of alluvial transport down both the south- and north-facing slopes together with aeolian size sorting. On reaching the northern end of the basin, the increased complexity of the bedrock morphology together with the presence of a steeper south-facing slope caused a change in the conditions resulting in the deposition of slightly larger diamonds.

The examination of south-facing slopes outside previous mining areas shows that they provide conditions suitable to the formation of encroachment deposits. Kaiser (1926) commented upon the presence of diamonds in amongst neatly placed, spindle-shaped, consistently oriented grains on the surface of deposits. Kaiser attributed the shape and orientation of these grains to aeolian corrasion. Observations from this study indicate that Kaiser's interpretation

was probably incorrect. Whilst aeolian corrasion does produce small ventifacts from the creep bedload population, he was probably referring to the shape-fabric exhibited by the creep bedload. It was shown in section 4.4.4. that the entrainment of the creep bedload, once the imbricate shape-fabric has developed, is likely to become increasingly difficult. Theoretically, increasing the angle that the south-facing slope makes with the approaching saltation load will have a similar effect. In the case of heavy mineral grains, the effect is possibly even more pronounced because a larger impact force is required relative to quartz material, simply to move the grains upslope in the first place. As shown by the distribution of diamonds within the Hexenkessel, if the south-facing slope is steep enough it will form a barrier to the migration of the creep bedload. The transport of the lighter, quartzitic material is possibly maintained, leading to the segregation of diamonds by the aeolian system. The differential transport rates exhibited by the light and heavy mineral components of the population prevented the rapid removal of the diamonds from the basin. The large to medium sized diamonds that did migrate up the slope were periodically reworked by ephemeral streams, and redeposited at the base-level of the system. This explains why the steep part of the slope, leading north from the Hexenkessel was characterised by particularly small diamonds with a high entrainment potential. Inevitably some diamonds, migrating at slower rates, were unaffected by the periodic ephemeral stream activity, and entered the Kaukausibtal. This potentially explains the diamonds of increased average size on the basin floor and south-facing slope at the northern end of the Kaukausibtal basin. Provided the throughput of diamonds by aeolian processes was maintained at a sufficiently high level, it is envisaged that progressive segregation by aeolian size sorting would account for the multi-basin diamond dispersal pattern exhibited by average diamond size data.

6.4. KINEMATIC SHOCK WAVES - IMPLICATIONS FOR PLACER DEVELOPMENT IN ENDOREIC BASINS

According to kinematic wave theory, a bottleneck can affect the creep bedload in two ways. If the oncoming flow of grains does not exceed the bottleneck capacity, the passage of the creep bedload

will merely be slowed down. If, however, the oncoming flow does exceed the capacity of the bottleneck, the shock wave developed will cause the creep bedload to pile up in front of the entrance to the bottleneck and deposition is predicted to occur.

It is suggested that creep erosion ripples near Meob Bay provide evidence for the former case in response to transport up a south-facing slope. Observations indicate that the progress of the creep bedload is hindered by south-facing slopes because:

1) the force required to move the grains upslope is greater than that on a horizontal surface;
2) the angle of saltating grains approaching the bed changes, resulting in a change in the direction in which the impact force acts;
3) of the development of an imbricate shape-fabric and the resulting increase in the pivotting angle which has to be overcome.

Under these conditions, interparticle interference is envisaged to increase, with the result that some mixing of grain sizes occurs due to the closure of the distance separating kinematic waves composed of particles travelling at different speeds. Some grains which were previously part of the creep bedload are probably unable to migrate up the slope at all and come to a standstill. The velocity of the kinematic waves is consequently reduced as they enter the bottleneck. Due to the variation of particle size-shape-density characteristics, some waves are possibly less affected than others. Theoretically, an encroachment deposit will result in response to the increased mutual interference of the grains and the reduction of kinematic wave velocities.

Creep erosion ripples show that the top few centimetres of encroachment deposits can be progressively reworked, and the material removed to the north (ie. downwind). The new surficial deposit is characterised by a low density population. The maximum concentration of grains occurs at the advancing crest of the bedform, in front of which the concentration declines again - this is characteristic of a kinematic wave. The concentration downwind of the crest exceeds that upwind of the crest, confirming that the granules are being removed upslope. This suggests that a specific fraction of the creep bedload is migrating downwind as a kinematic wave, leaving slower kinematic waves composed of coarser grains

downslope. Once the wave reaches the crest of the slope, provided that the topography ahead is flat, it will accelerate and travel more quickly downwind once more until another bottleneck is encountered.

The net result of this kinematic wave effect is theoretically to enhance the segregation of the particles in motion, according to the speed with which they migrate through the system. Coarser particles grouped on slower kinematic waves hypothetically spend longer on south-facing slopes than those composed of more rapidly moving grains. Hence slower kinematic waves would be expected to occur upwind of faster ones on south-facing slopes. This resembles the multi-basin diamond dispersal pattern observed on the basis of the variation of average diamond size.

Dykes crossing basin floors perpendicular to the transport direction, provide a different set of conditions. In this instance, the rate of the oncoming flow of creep bedload clearly exceeds the potential capacity of the transport system. A kinematic shock wave is thus potentially developed, which travels south (ie. upwind). The creep bedload approaching the obstacle is subjected to a rapid reduction of speed, and grains pile up on the upwind side of the bottleneck. Again, differences in the size-shape-density characteristics of the creep bedload might influence the migration of particles beyond the obstacle. For some, rare entrainment into saltation will perhaps carry them across the dyke. For the rest, this is the ultimate point of deposition provided that the aeolian system remains undisturbed. In time, similar grains will be added to the deposit, as long as the oncoming creep bedload is maintained. It is theoretically possible that if deposition continues for long enough, this will lead to the reduction of the obstacle's height, and that its influence upon the aeolian system would ultimately cease.

Additional Considerations

To examine the aeolian system using kinematic wave theory, it is necessary to simplify the sediment dispersal system. Whilst the creep bedload does essentially migrate through the region under the influence of a unidirectional aeolian system, ephemeral stream systems also operate. Polycyclical reworking of deposits on the south-facing slopes of endoreic basins partially destroys the

kinematic waves composed of the aeolian creep bedload. Thus, as the material transported towards the base-level of the endoreic basin systems by ephemeral streams is reworked by aeolian processes, new kinematic waves are developed. Complex interaction between the systems therefore takes place.

The distinct, northward-fining tail of diamonds indicates that the aeolian system governs the overall diamond dispersal pattern at the present time. The interpretation of the placer bodies within endoreic basins using kinematic wave theory applied to the creep bedload, therefore appears to be justified. In this respect, the flow-perpendicular bands exhibited by the diamond dispersal pattern based upon the number of stones, is particularly interesting. The bands define alternating zones of slightly lower and higher concentration. Provided that the diamonds enter the aeolian dispersal system at its southern end, the variation of entrainment potential theoretically results in bunches of like grains composing kinematic waves travelling at variable speeds along the transport path. These bands possibly provide evidence for kinematic waves. Unfortunately the absence of detailed information prevents this hypothesis being proved, and it is impossible to determine whether this pattern is an artefact of the prospecting technique used or not.

7. PALAEO-AEOLIAN SEDIMENT DISPERSAL SYSTEMS IN THE CENOZOIC STRATIGRAPHY

7.1. INTRODUCTION

The preceeding analysis described the processes resulting in sediment dispersal within the present-day, high-energy aeolian environment of the southern Namib deflation basin. The orientation and scale of the aeolian landforms created from crystalline rock within the deflation basin, indicate that southerly quadrant palaeowinds have controlled aeolian processes within the region for some time. Suggested revisions to the Cenozoic lithostratigraphic succession are given in Table 7.1. Brief descriptions of the lithostratigraphic units, starting at the base of the succession, are used to examine the controversial subject of regional palaeoclimatic change, and the aridification of the Namib.

The relative ages of the palaeo-dune systems within the Southern Namib have been reassessed using lithostratigraphic and palaeontological data collected during this study. The knowledge gained from the detailed examination of sediment dynamics within the deflation basin has then been applied to the interpretation of the palaeo-aeolian dispersal systems.

7.1.1. PREVIOUS STUDIES

Detailed geological maps compiled by Kaiser and Beetz, were published by Kaiser (1926). These maps covered the area between the Buntfeldschuh and the Grillental. The main exposures of the palaeo-dune systems between Elizabeth Bay and Luderitz thus lay beyond their limits. Until the present study, the most recent regional stratigraphic review was by Stocken (1978), who provided a stratigraphic framework, but did not discuss the sedimentology of the deposits in detail. Although Ward (1984; 1987) attempted to correlate the palaeodune systems of the Southern Namib within his stratigraphic framework, the sedimentology of the deposits has not previously been described. This study therefore presents the first synthesis of the palaeodune systems within the Southern Namib.

Published sedimentological and palaeontological accounts have essentially been confined to isolated exposures of stratigraphic significance. In mapping a sequence of alluvial and aeolian sediments within the area covered by the Government 1:50 000 topographic map 2615C, to the south of Luderitz, Greenman

(1966,1969) named the Elizabeth Bay Formation (sensu SACS, 1980). The Cretaceous marine deposit in the Bogenfels Basin, which was initially described by Haughton (1931), was named the Wanderfeld IV Beds by Klinger (1977). Siesser (1978) and Siesser and Salmon (1979) have redefined the age of the Upper Eocene Langental Beds using the contained calcareous nannofossils. Hamilton and Van Couvering (1977) recovered vertebrate assemblages from the Lower Miocene alluvial sequences scattered throughout the region, and revised the faunal list.

7.2. THE REGIONAL STRATIGRAPHIC FRAMEWORK

The western passive continental margin of southern Africa has been repeatedly influenced by contrasting depositional environments during the Cenozoic. This variation has occurred in response to sea-level fluctuation and palaeoclimatic change. Laterally continuous sections through the deposits, which would allow lithological contacts to be observed, are therefore scarce because of post-depositional erosion. The construction of a stratigraphic framework is therefore difficult. Fortunately, palaeontological ages, radiometric ages, and laterally extensive duricrusts, provide stratigraphic marker horizons against which field relationships can be tested (Figure 7.1). A summary of the suggested revisions is provided in Table 7.1.

7.2.1. THE POMONA SILCRETE

Stocken (1978) proposed the name Chalcedon Tafelberg Silcrete Formation for the fine-grained silcretes within the region, which are equivalent to the Tafelberg Quartzites of Beetz (1926). The silcrete horizons are generally 1 to 3 m thick, and vary widely in colour, from brown and purple to light grey/green. X-ray fluorescence analyses of samples from different silcrete residuals demonstrate that they differ compositionally (Table 7.2a). The levels of titanium and iron show the most variation, which to some extent is reflected by the silcrete colour. The brown and purple silcretes exhibit the highest iron and titanium contents. In all cases, however, the silcrete horizon is underlain by a kaolinised weathering profile (Table 7.2b), as discussed in section 2.2.2.

The Pomona Beds have previously been interpreted as a locally derived alluvial deposit (Beetz, 1926; Stocken, 1978). The best

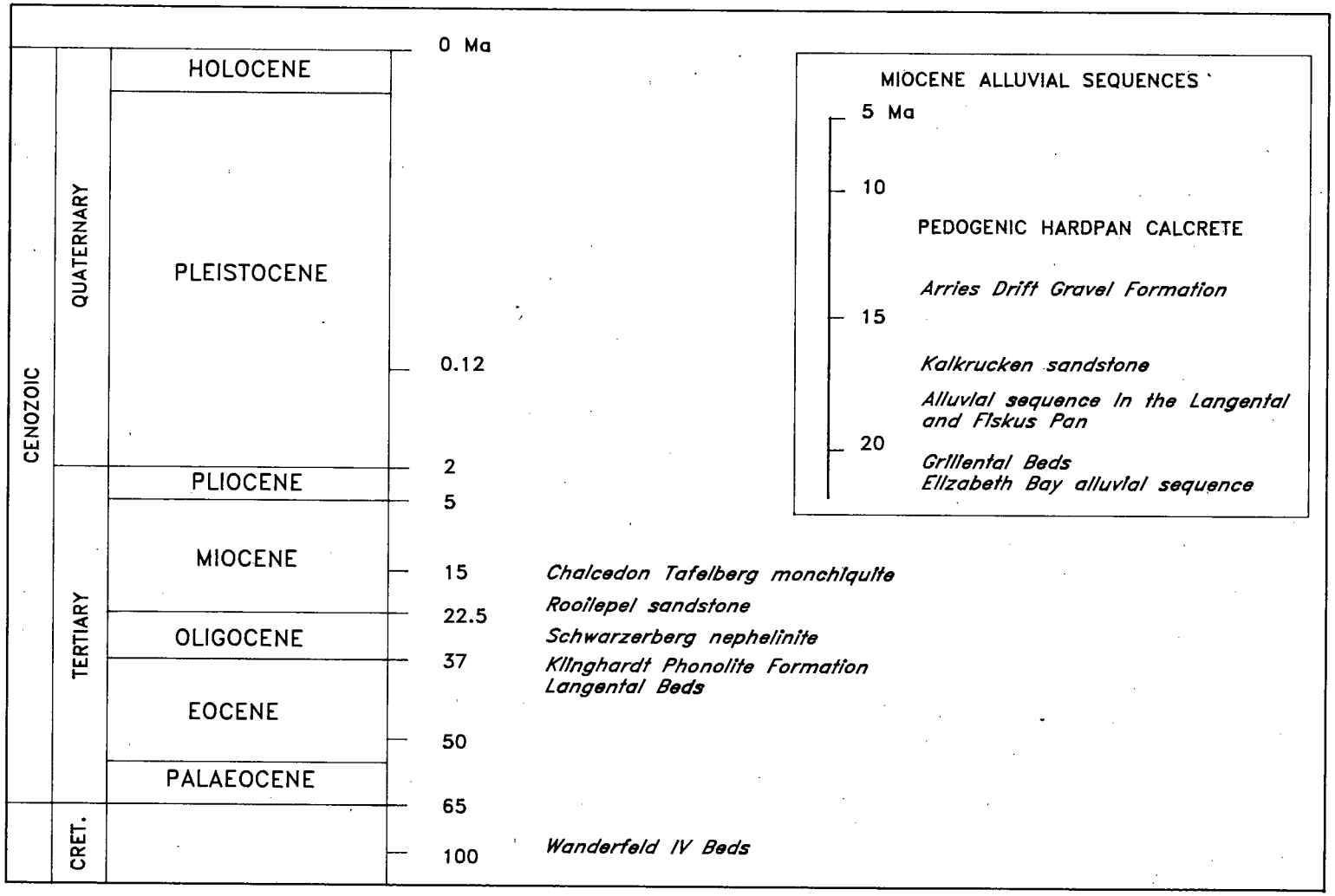

Figure 7.1. Summary of palaeontologically dated sediments and radiometrically dated igneous bodies which provided the basis for the Southern Namib stratigraphic framework of the Cenozoic.

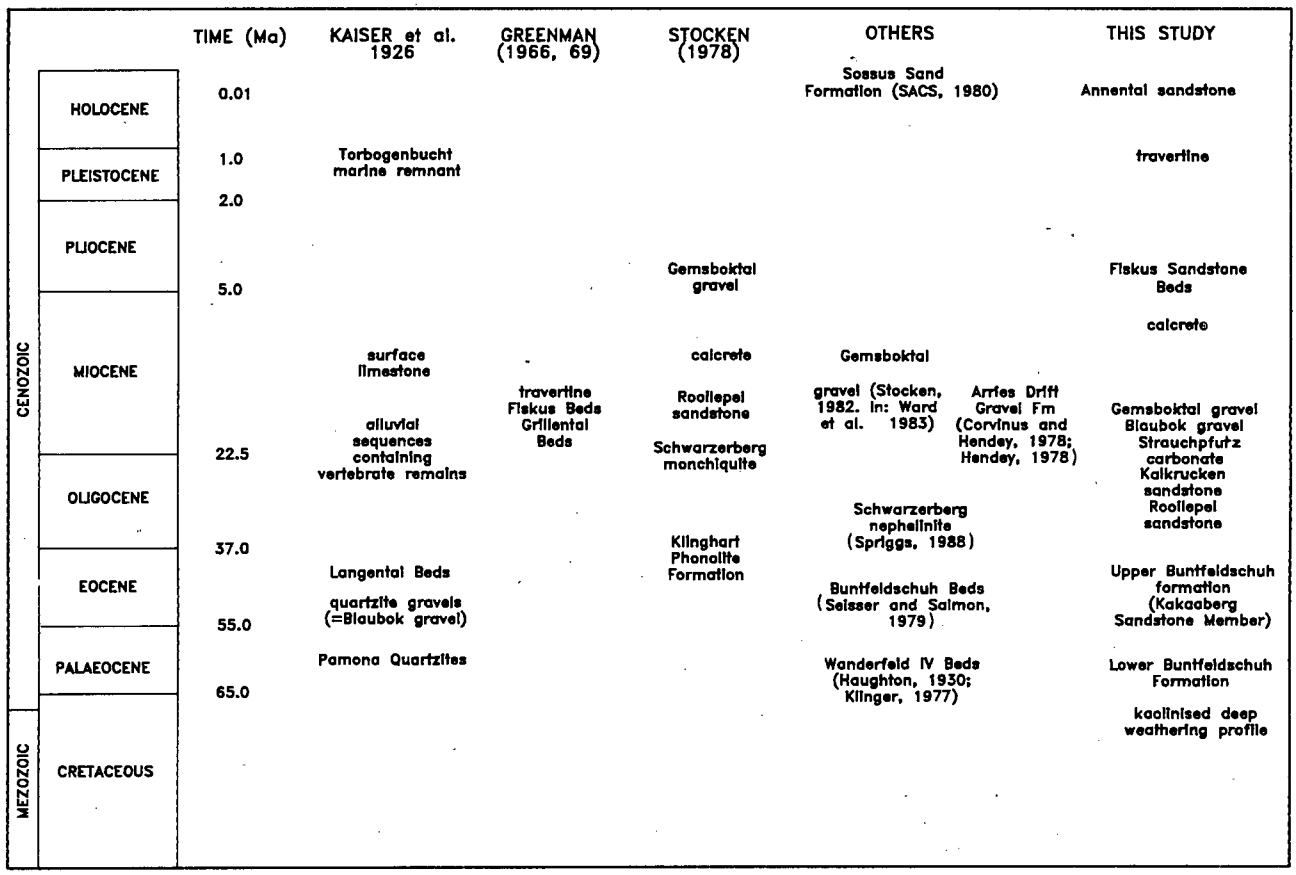

Table 7.1. Suggested stratigraphic revisions of the Cenozoic Era arising from this study.

exposures are found capping an isolated residual to the north of Elfertberg, along the eastern margin of the Katchen Plateau. The exposure lies directly along the strike of the Basal Clastic Member of the Bogenfels Formation, in which relict sedimentary structures

(a)

No	HOST	SiO_2	Al_2O_3	TiO_2	Fe_2O_3	MgO	CaO	K_2O	MnO	P_2O_5
R 1	M	94.66	1.88	1.49	0.78	0.16	0.39	0.16	0.08	0.39
R 2	M	95.37	2.17	0.75	0.75	0.08	0.30	0.15	0.08	0.30
R 7	M/S?	96.81	1.34	0.37	0.89	0.00	0.22	0.07	0.15	0.15
R 8	M	95.56	1.76	1.07	0.84	0.00	0.23	0.08	0.15	0.31
E 1	M	96.20	1.61	0.36	0.73	0.07	0.29	0.15	0.15	0.44
E 5A	M	96.10	1.88	0.45	0.75	0.08	0.38	0.15	0.08	0.15
E 5B	M	96.86	1.15	0.46	0.92	0.08	0.38	0.08	0.08	0.15
E 6	M	94.31	1.92	0.38	2.07	0.08	0.46	0.15	0.15	0.46
E 7	M	94.26	1.81	0.94	1.57	0.08	0.55	0.16	0.16	0.47
E 8	M	89.58	2.40	3.29	3.74	0.09	0.45	0.09	0.18	0.18
E 9	M	94.90	2.06	0.46	0.83	0.08	0.99	0.15	0.15	0.53
K 1A	S/G?	89.77	2.06	0.87	1.19	0.08	2.94	0.24	0.08	2.78
K 1B	S/G?	96.25	1.61	0.77	0.61	0.00	0.31	0.15	0.08	0.23
K 2	S/G?	97.14	1.43	0.38	0.53	0.00	0.23	0.08	0.08	0.15
K 3	S/G?	96.66	1.22	0.68	0.76	0.00	0.23	0.08	0.15	0.23

(b)

SAMPLE LOCALITY	XRD MINERAL ABUNDANCE abundant	common	rare
Roadside quarry 15 km north of Chameis	quartz	kaolin	mica
Mile 70 borrow pit	kaolin		

Table 7.2 a) Major element bulk chemical analyses of silcrete normalized to 100%. Sample position R = Rundekuppe, E = Elfertberg. Host symbol M = clastic metasediment (Bogenfels Formation Basal Clastic Member), M/S = clastic metasediment / reworked silcrete. b) XRD results from analyses of the weathering profile which underlies the silcrete.

can be seen. The Basal Clastic Member would thus have provided another host lithology in which the kaolinised weathering profile might have developed. This would have released quartz pebbles from the metasediment for later incorporation into a silcrete profile. The quartz clasts within silcrete horizons could thus represent a skeletal soil profile developed from material derived from the kaolinised profile, rather than the in situ silicification of an alluvial deposit. This explains why the quartz pebble-rich horizons, which superficially resemble cross-sectional profiles through channels, cannot be traced laterally along sections. Further evidence supporting this interpretation occurs at the base

of the main "channel" feature, where the silcrete enveloped blocks of the metasedimentary bedrock. The incorporation of these large blocks into the base of the skeletal soil then created the impression of a fining-upward sedimentary sequence.

The Chalcedon Tafelberg Silcrete Formation and the Pomona Beds therefore appear to represent lateral facies variations within the silcrete, rather than entirely different stratigraphic units. It is thus suggested that they should be collectively termed the Pomona silcrete.

The radiometric age for phonolite overlying the silcrete at Swartkopp is 37 Ma. SACS (1980) point out that this is probably the minimum possible age for the phonolite. This is supported by the recovery of weathered phonolite clasts during this study from the marine Lower Buntfeldschuh Formation and the tentatively correlated shoreline deposit at Eisenkieselklippenbake. An Upper Palaeocene to Lower Eocene age has been inferred for these deposits by Siesser and Salmon (1979), based upon correlation with the global sea-level curve of Haq, Hardenbol and Vail (1987). The silcrete is thus likely to pre-date the Upper Palaeocene, and probably formed during the late Cretaceous (Partridge and Maud, 1987), which makes them slightly older than Stocken (1978) believed.

The lithostratigraphic relationship of the Pomona silcrete with the kaolinised profile resembles that of the Grahamstown Silcrete Formation, which suggests that they share a common origin. Frankel and Kent (1938) showed that the decomposition of complex alumino-silicates by meteoric water to clay minerals frees silica which can then be dissolved by liberated carbonates in solution:

$$2KAlSi_3O_8+2H_2O+CO_2 \rightarrow H_4Al_2Si_2O_9+4SiO_2+K_2CO_3$$

According to Frankel and Kent (op. cit.), the presence of NaCl within a soil profile, which is a primary feature of arid zone soils, would greatly enhance the precipitation of silica from solution. Partridge and Maud (pers. comm., 1987) have therefore suggested that palaeoclimatic change from humid to arid or semi-arid conditions, after the development of the kaolinised profile, accounts for the development of the silcrete. The atmospheric circulation models of Parrish and Curtis (1982) suggest that this palaeoclimatic event would have coincided with the establishment of the South Atlantic Anticyclonic system.

7.2.2. THE LOWER BUNTFELDSCHUH FORMATION

Lower Marine Unit

The marine Lower Buntfeldschuh Formation is divisible into two parts (Figure 7.2). The lower unit consists of a predominantly structureless, massive, pale green, fine-grained sandstone which contains ferruginous concretions upto 1 m in diameter (Figure 7.3). The base of the structureless sandstone overlies a laterally continuous, sub-horizontal gravel lag, which rests upon Pomona silcrete at the northern end of the escarpment.

Large-scale, tabular-planar cross-bedding, is faintly visible within the generally structureless sandstone of the lower marine unit at the northern end of the Buntfeldschuh escarpment. Compositionally, the structureless sandstone closely resembles the overlying aeolian Kakaoberg Sandstone Member of the Upper Buntfeldschuh Formation (see section 7.2.3).

It has previously been difficult to provide a plausible interpretation for the lower marine unit of the Lower Buntfeldschuh Formation. Eschner and Kocurek (1986) describe massive structureless sandstone horizons up to 12 m thick within marine transgressive deposits of the Upper Jurassic Curtis Formation, in north-eastern Utah. They interpret these horizons as mass flows of aeolian sand generated by the liquefaction of aeolian dunes forming the Entrada Sandstone. It is tempting to speculate that the basal structureless sandstone, which overlies a marine wave-cut platform, represents mass flows generated during a transgression across a more ancient aeolian sand body during the Upper Palaeocene to Lower Eocene.

Upper Marine Unit

The planar erosional contact truncating the lower-most marine unit is overlain by alternating tabular-planar cross-bedded sand horizons and laterally persistent, sub-horizontal pebble bands between 10 to 50 cm thick. Characteristically, the pebble bands contain abundant exotic clasts of agate, chalcedony and jasper. The presence of sharks teeth within the pebble bands, which was initially reported by Böhm (1926) and Stocken (1978) has been confirmed during this study. In addition, delicate shells tentatively identified as the brachiopod Lingula by Pether (pers. comm., 1989) have been recovered from the sequence for the first time.

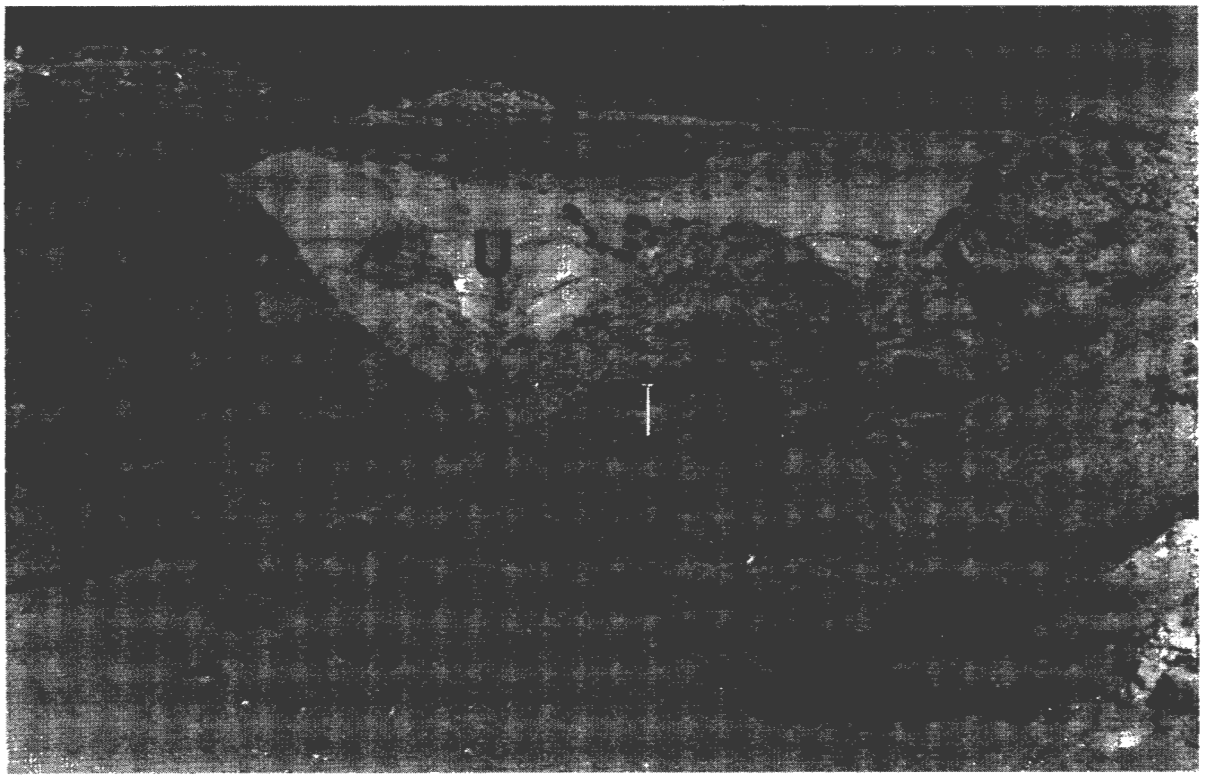

Figure 7.2. Photograph showing the principal lithostratigraphic units identified within the Buntfeldschuh escarpment. Ferruginous concretions within a structureless pale green sandstone comprise the lower marine unit (L) of the Lower Buntfeldschuh Formation, whilst alternating cross-bedded sands and pebble bands form the upper unit (U). The Kakaoberg Sandstone Member (K) of the Upper Buntfeldschuh Formation, overlying the marine sequence, is capped by a regionally extensive pedogenic hardpan calcrete (arrowed). The white pole is 1.5 m tall, and north is to the left.

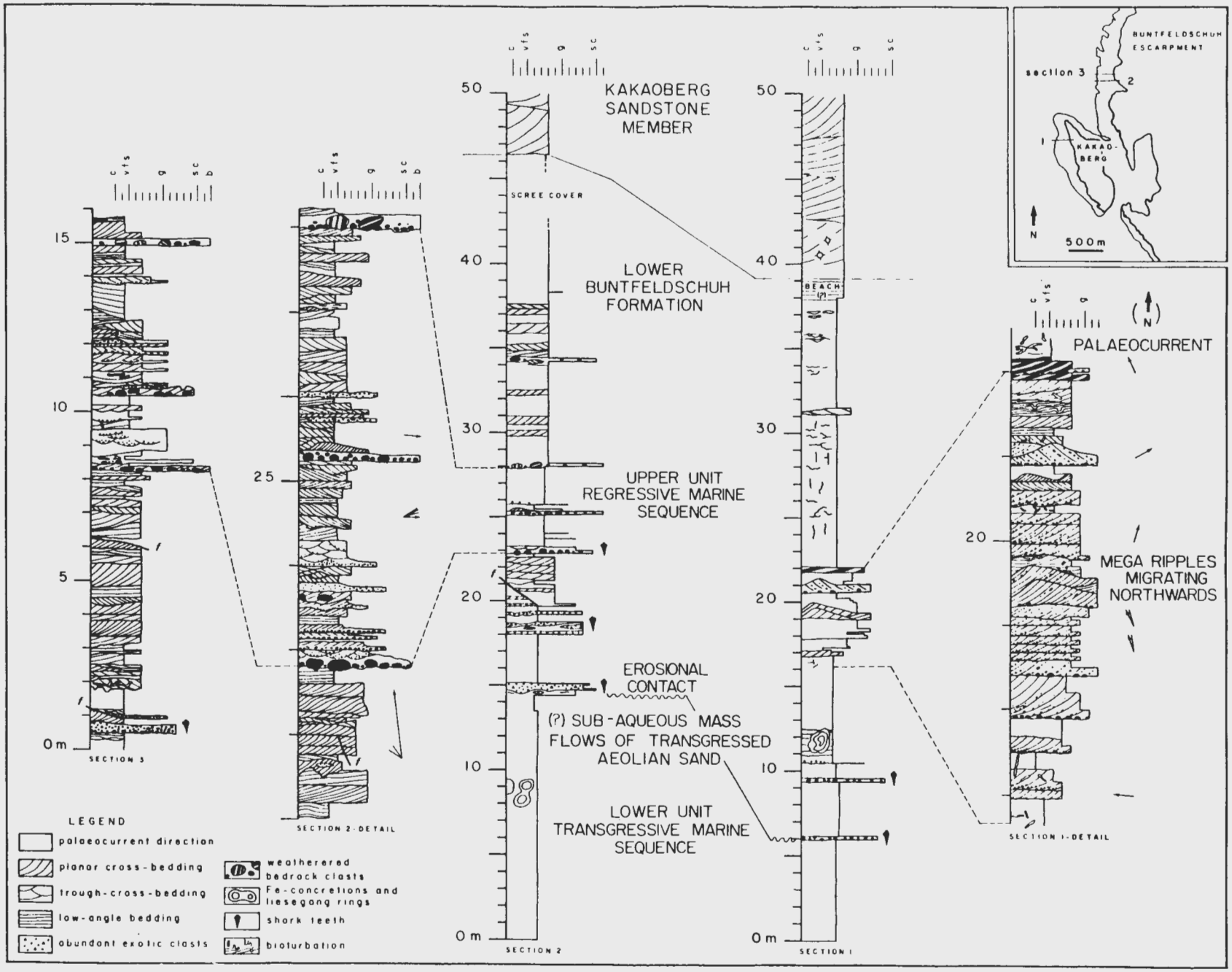

Figure 7.3. Summary of measured sections through the lower and upper units of the marine Lower Buntfeldschuh Formation.

Lingula has a long time range from Silurian to Recent, which negates its usefulness for constraining the age of the Lower Buntfeldschuh Formation.

The upper unit of the Lower Buntfeldschuh Formation exhibits a repetitive succession of laterally extensive pebble bands separated by cross-bedded sands (Figure 7.4). The sandy horizons were probably deposited by megaripples, of which good examples with an amplitude of at least 19cm and wavelength exceeding 0.7 m occur near the base of section 1 in Figure 7.2. This example showed evidence of bedform climbing, which indicates that the rate of deposition periodically exceeded the sediment transport rate. Palaeocurrent data from the cross-bedded sandy sets define a weakly bimodal current direction, but sediment transport was predominantly northwards and offshore (Figure 7.2). Although the megaripples primarily consist of sand and granules, pebbles of 4 to 12 mm diameter are present on some bedding planes. Periodic reworking of the megaripple deposits by shoreward currents, perhaps during storms, led to the development of thin pebble lags which are associated with shoreward migrating low amplitude megaripples.

De Decker (1986) recorded the presence of megaripple fields in water depths of 15 to 25 m along the present-day coastline using sonographs. The crests of the bedforms tend to be approximately coast parallel, but they are influenced by local bedrock topography. According to work off Rhode Island by Cook (1970), megaripples exhibiting a seaward asymmetry, such as those at the Buntfeldschuh, probably form in response to nearshore rip-current activity. In the cases studied by Cook, shallow channels associated with the rip-currents extended seawards from the beach to landward of the breaker zone.

The lowermost pebble bands of the upper marine unit contain a greater proportion of exotic agate, chalcedony, jasper and chrysoprase clasts than the overlying ones, in which locally derived cobbles of weathered bedrock become increasingly common. The pebble bands also coarsen upwards, which is a characteristic of beach profiles (Elliot, 1978). The cyclical repetition of the cross-bedded sand horizons with pebble bands observed in sections (Figure 7.5) resembles the inner rough and inner planar facies of non-barred high-energy coasts, described by Clifton et al. (1971). The upper marine unit of the Buntfeldschuh Formation is

Figure 7.4. View south along the Buntfeldschuh escarpment showing the alternating pebble bands and cross-bedded sand units.

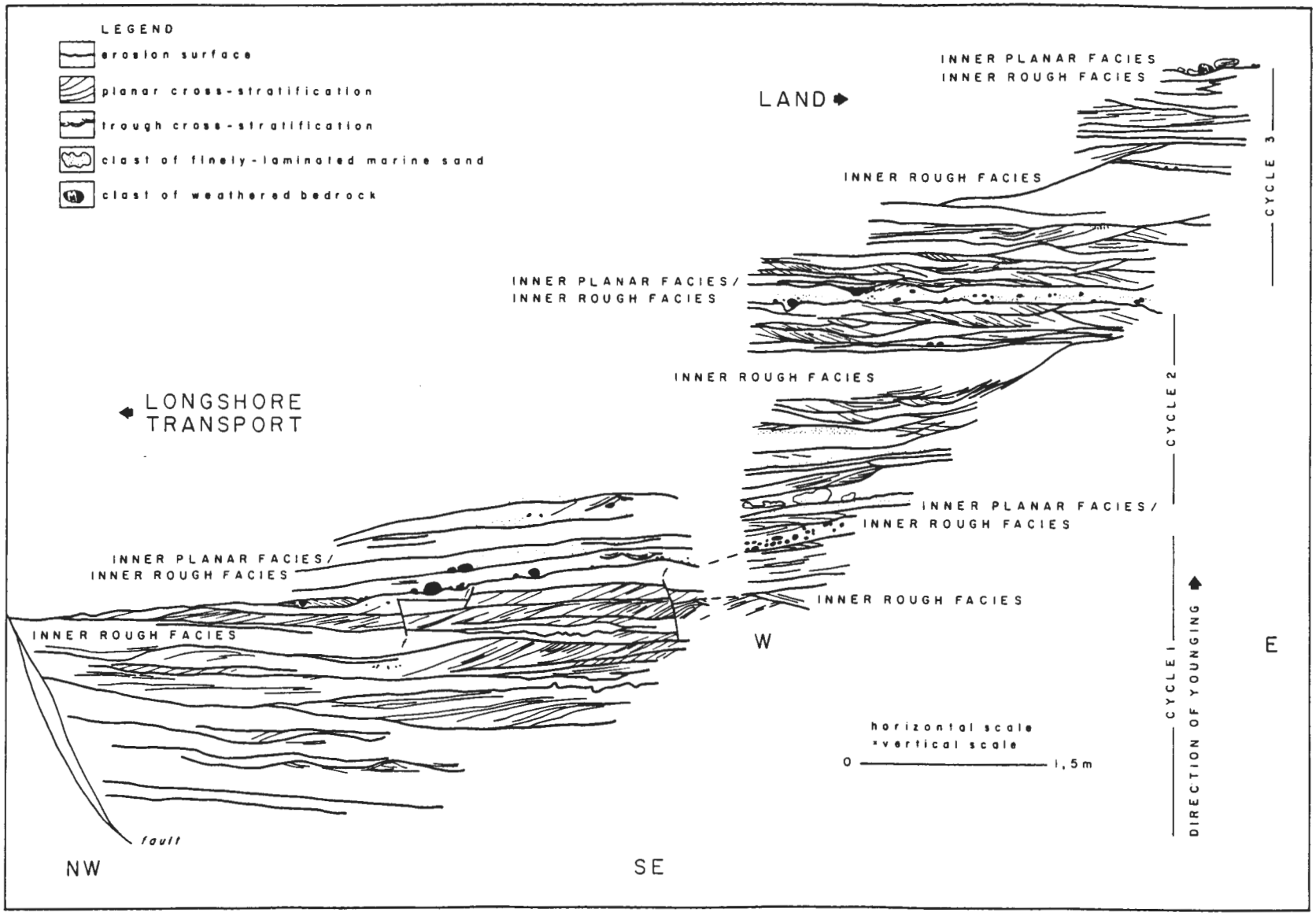

Figure 7.5. Drawing composed from photographs of cleaned faces between 22 and 28 m above the base of section 2. Cyclical alternation of horizons of the upper unit of the Lower Buntfeldschuh Formation exhibiting structures resembling the inner rough and inner planar facies of a non-barred, high-energy coast.

therefore interpreted as a regressive shoreline sequence in which the pebble bands represent the beach toe.

7.2.3. UPPER BUNTFELDSCUH FORMATION - KAKAOBERG SANDSTONE MEMBER

Description

The 50 to 60 m thick Kakaoberg Sandstone Member of the Upper Buntfeldschuh Formation, which overlies the Upper Palaeocene to Lower Eocene Lower Buntfeldschuh Formation (see Figure 7.2 and 7.3), was interpreted as an aeolian deposit by Beetz (1926). At Kakaoberg, near the southern end of the Buntfeldschuh escarpment, a 15 to 20 m thick ferricrete, hosted by the aeolian sandstone, now caps the sequence. Isolated pedogenic hardpan calcrete residuals overlying the ferricrete at the southern end of Kakaoberg prove that the entire sequence was once capped by a regionally extensive hardpan pedogenic calcrete.

The fine to medium sands forming the 60 m thick sequence of pale green sandstone are classified as an arkose. Two notable compositional characteristics of the sands are:

1) the high feldspar content (24.4%);
2) volcanic fragments, including volcanic glass constitute about 16% of the sandstone. Many of the grains have been altered to a clay mineral, which might explain the chlorite and montmorillonite content of the sandstone illustrated by XRD analyses.

The volcanic component is likely to either represent phonolite erosion products input to the system from the east, or input directly by the volcanic activity centred on the Klinghardt Mountains.

Large-scale tabular-planar cross-bedding is exhibited by the sandstone exposed along the south-north oriented Buntfeldschuh escarpment. The sandstone was deposited by southerly to south-westerly palaeowinds (Figure 7.6), which indicates that the pattern of surface wind flow was comparable with that of today. The absence of east-west oriented sections prevents the attitude of the bounding surfaces (sensu Brookfield, 1977) from being measured. Observations indicate that they are variably inclined, which results in wedge-planar cross-bedding being observed in some south-north oriented sections (Figure 7.7). The second-order

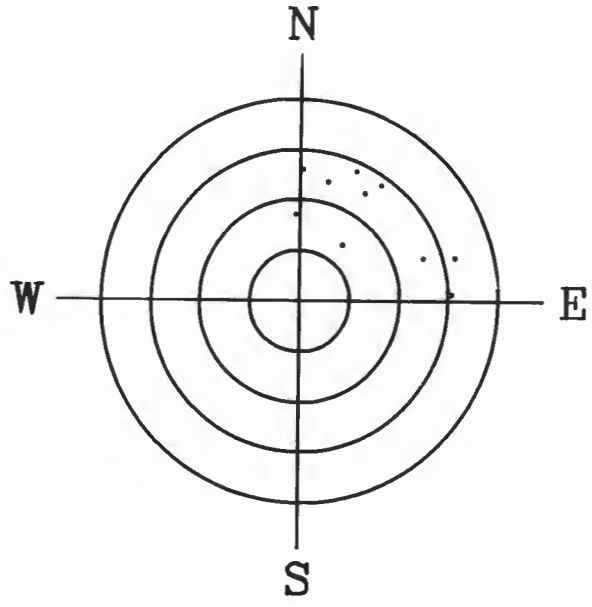

Figure 7.6. Polar plot of cross-bedding dip directions, which demonstrate that the aeolian sequence was deposited by a southerly to south westerly palaeowind regime.

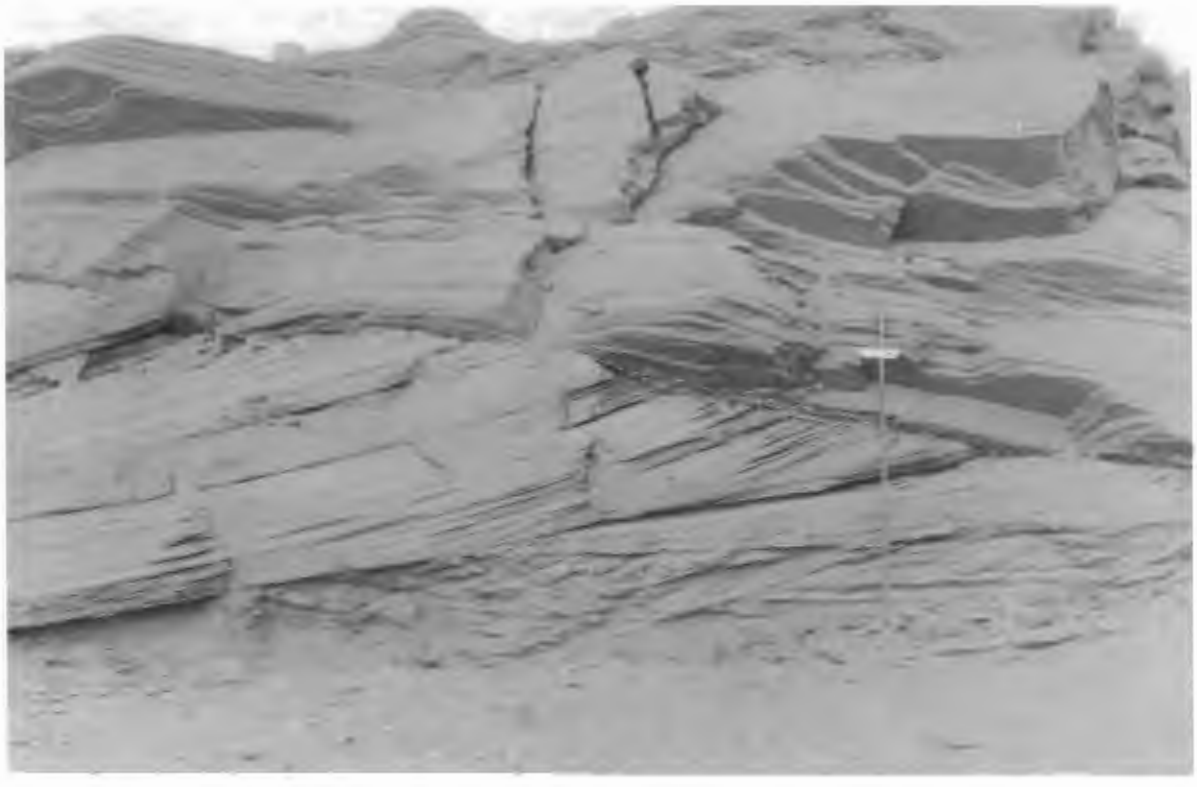

Figure 7.7. Tabular-planar cross-bedding exhibited by the Kakaoberg Sandstone Member. The apparent wedge-planar form of the bedding reflects the attitude of the second order bounding surfaces (S). North is to the left. The white section of the pole is 1.5 m above its base.

bounding surfaces separate grouped, concave-up bottomsets which are up to 5 m thick and extend several metres downwind. The bottomsets are essentially comprised of grainfall laminae (sensu Hunter, 1977). This structure closely resembles the pin stripe lamination of Fryberger and Schenk (1988), which characterise other aeolian deposits. Third-order bounding surfaces are also present. Climbing translatent strata (sensu Hunter, 1977) are preserved in the sequence (Figure 7.8), which represent the migration of small wind ripples under strong southerly wind conditions.

Moulds of vegetation were located within the aeolian sequence in the central part of the Buntfeldschuh escarpment by Ward in 1987. The moulds underlie a gently dipping ferruginous horizon, which probably represents a lateral equivalent of the ferricrete seen at Kakaoberg. The presence of the root systems is marked by a white, fibrous, central core, which is surrounded by a cream to pale green halo (Figure 7.9a). X-ray diffraction analyses show that the plant remains are silicified. Some specimens deflated from the sandstone are hollow. When the centre is preserved the internal structure closely resembles the xylem / phloem vessels of fossilized !Nara roots (Acanthosicyos horrida) recovered from Khommabes Pan in the Central Namib by Ward (1984) (Figure 7.9b). These are the oldest known !Nara-type plant remains which have so far been located within the Namib. No body fossils of animals have yet been recovered from the sandstone, but trace fossils resembling termitaria prove that organisms were present.

Interpretation

The contact of the Kakaoberg Sandstone Member with the underlying, marine Lower Buntfeldschuh Formation shows no evidence of an appreciable time break. Low-angle, parallel laminated marine sands representing beach lamination at the top of the upper marine unit of the Lower Buntfeldschuh Formation are overlain by the aeolian Kakaoberg Sandstone Member, with minimal evidence of a time break. Provided that the inferred date for the underlying marine sequence is correct, aeolian processes were operating within the Namib during the Lower to Middle Eocene regression. This has important palaeoclimatic implications (section 7.3).

Figure 7.8. Climbing translatent strata (T) provide evidence for the depostion of the sandstone by wind ripples. Scale 11.5 cm, southerly to south-westerly palaeowind blew from right to left.

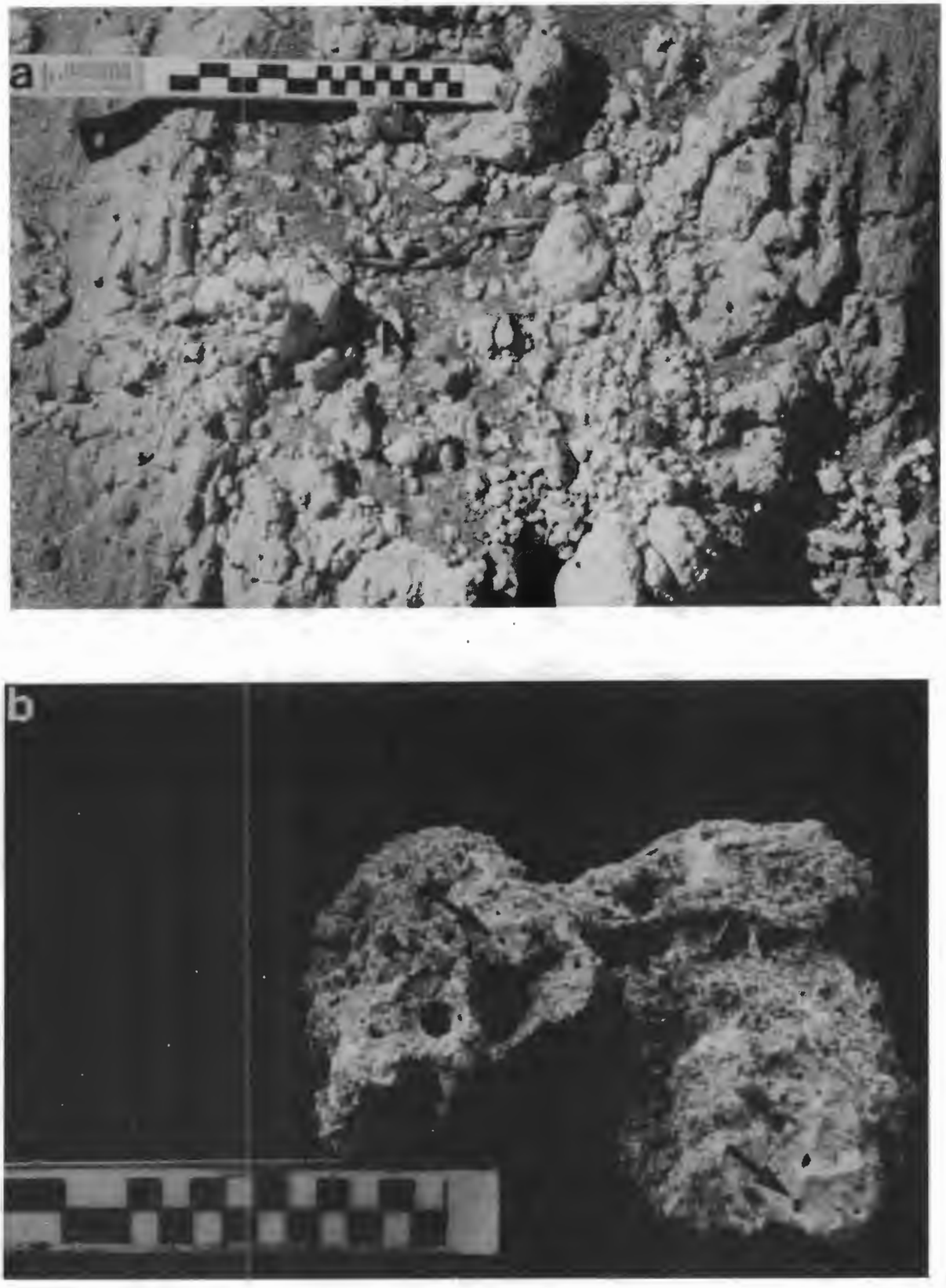

Figure 7.9. (a) In situ Nara-type root (N), surrounded by a light-coloured halo within the sandstone of the Kakaoberg Sandstone Member. (b) Xylem / phloem vessels (arrowed) preserved within a Nara-type root structure. Scale in both frames 10 cm.

The Kakaoberg Sandstone Member has previously been interpreted as a backshore dunefield (Stocken, 1978). The overall thickness of 60 m, together with the size of the cross-bedded sets indicates the migration of large aeolian dunes, which leads to an interpretation of it representing a much larger sand body. The complete absence of interbedded alluvial deposits within the aeolian sequence proves the persistence of a purely aeolian depositional environment throughout the development of the sand body. The portion of the sand body that is now visible along the escarpment is thus considered to represent the coastal margin of a palaeo-erg.

During the deposition of the base of the aeolian sequence, the palaeo-shoreline would have lain close to its present position. As the Oligocene regression to about 500 mbsl proceeded (Siesser and Dingle, 1981), the shoreline would have been displaced some 100 to 200 km futher west. It is therefore possible that the aeolian sands at the top of the sequence were deposited by dune forms which were located far to the east of the Oligocene coastline. Provided that the pattern of surface wind flow across the region resembled that of today, the distribution of aeolian dune forms within the Namib Sand Sea implies that this shift would have manifested itself by a change in dune morphology. Transverse dunes were probably responsible for the deposition of the basal part of the aeolian sequence, but linear, or even star dunes, might be represented by the upper part of the sequence. The variable orientation of the second-order bounding surfaces in the section possibly supports this concept, but the extent to which the aeolian sequence was eroded prior to the formation of the calcrete is not known. The absence of three-dimensional sections along the escarpment prevents confirmation of the above hypothesis.

The Kakaoberg Sandstone Member was probably the provenance for the ephemeral alluvial systems which operated during the deposition of the Kalkrücken sandstone between about 17 to 20 Ma, when the initial phase of aeolian activity was terminated (see section 7.3).

7.2.4. ROOILEPEL SANDSTONE

Description

Dark red, fine- to coarse-grained sandstone is exposed along the 120 m high, north-facing scarp slope of a depression that is currently being re-exhumed by aeolian deflation (Figure 7.10). The base of the sandstone is gritty, with some evidence for periodic alluvial activity. The entire sequence is capped by a mature, regionally extensive, pedogenic hardpan calcrete (Figure 7.11) (Stocken, 1978), which is now degenerating rapidly. Loose sand cover prevents detailed examination of the sand body's sedimentary structure. Faintly visible, very large-scale cross-bedding indicates the presence of second order bounding surfaces (Figure 7.12). Weathered sections exhibit finely laminated bottomsets in which pin stripe lamination can be identified. Cross-bedding dip directions show that the sequence was deposited by a southerly quadrant palaeowind regime (Figure 7.13).

This locality has good potential for future palaeontological work. Part of a rodents upper jaw (Figure 7.14) located in situ within the sandstone at the base of the sequence has tentatively been identified as the pre-maxilla W2 incisors of Paraphiomys pigotti (Pickford, pers. comm., 1988). Specimens of P. pigotti were also recovered from the Arries Drift Gravel Formation, dated at between 17.2 to 14 Ma by Pickford (1987). Hendey (1978) considers P. pigotti to be indistinguishable from Neosciuromys africanus described by Stromer (1926) from alluvial sediments within the Langental, and from sediments at Elizabeth Bay. The sediments at both of these localities were considered by Hamilton (pers. comm., Stocken, 1977) to pre-date the Arries Drift Gravel Formation by several million years. Further collecting is required to obtain better resolution of the sandstone's age, and will be undertaken at a future date.

Low-energy aeolian deflation has delicately exhumed large pieces of eggshell from the sandstone (Figure 7.15). The shell is between 3 to 5 mm thick, and characterized by unusual circular pits with a "granular" basal relief (Figure 7.16). The pit structure differs from that of Struthio (Ostrich) related birds reported by Sauer (1966) from Etosha Pan in Northern Namibia. Eggshell fragments with a similar pit structure to the Rooilepel specimens have been recovered from aeolian sandstones north of Luderitz. Efforts are

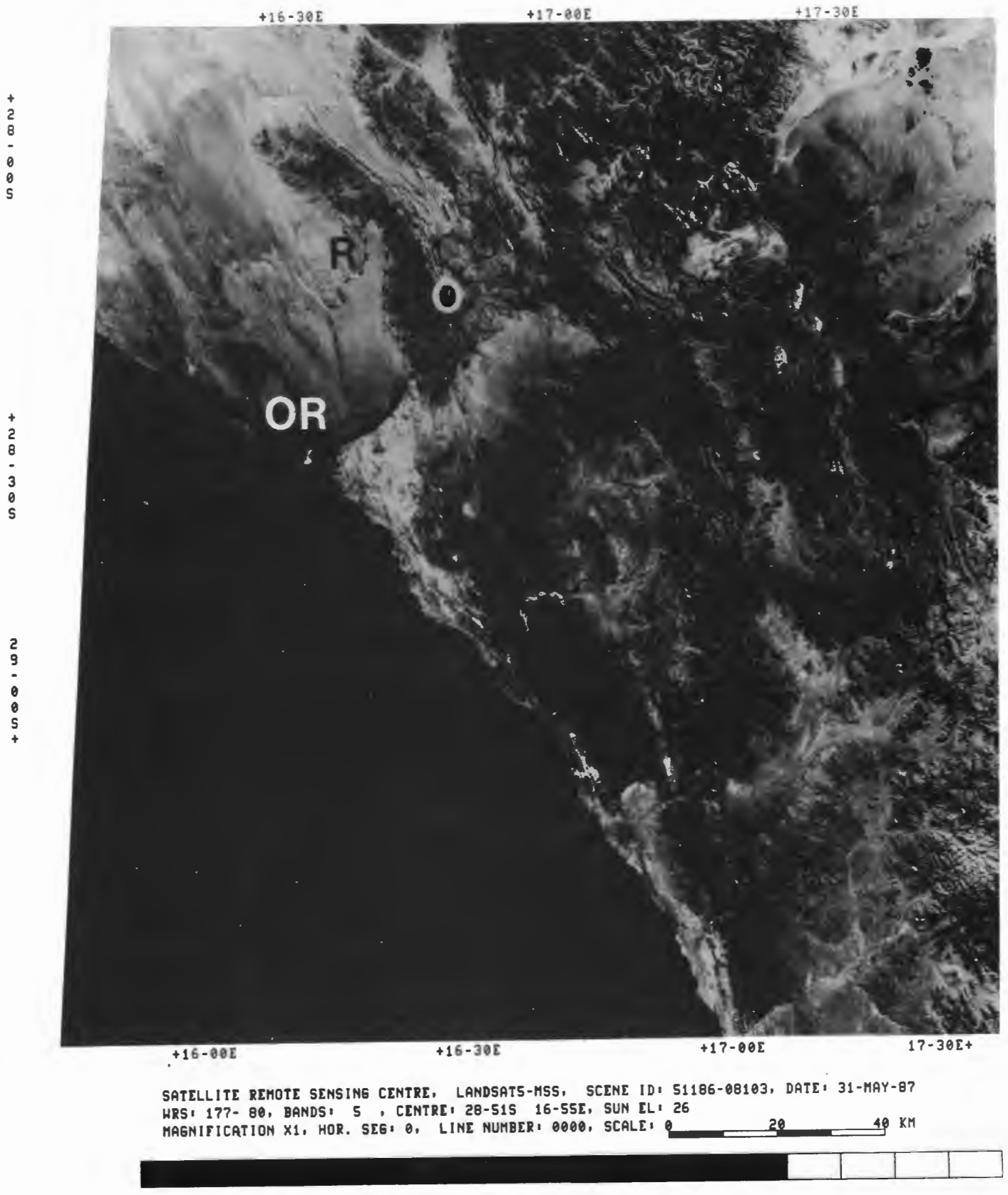

Figure 7.10. Landsat image showing the location of the Rooilepel depression (R) which contains the Rooilepel sandstone. The limit of the hardpan pedogenic calcrete (- -) capping the aeolian sequence is also shown. (O) is the Orange River, and (OR) marks the position of Oranjemund.

Figure 7.11. Degenerating remnant of the once regionally extensive, pedogenic hardpan calcrete capping the Rooilepel sandstone. Scale 1 m.

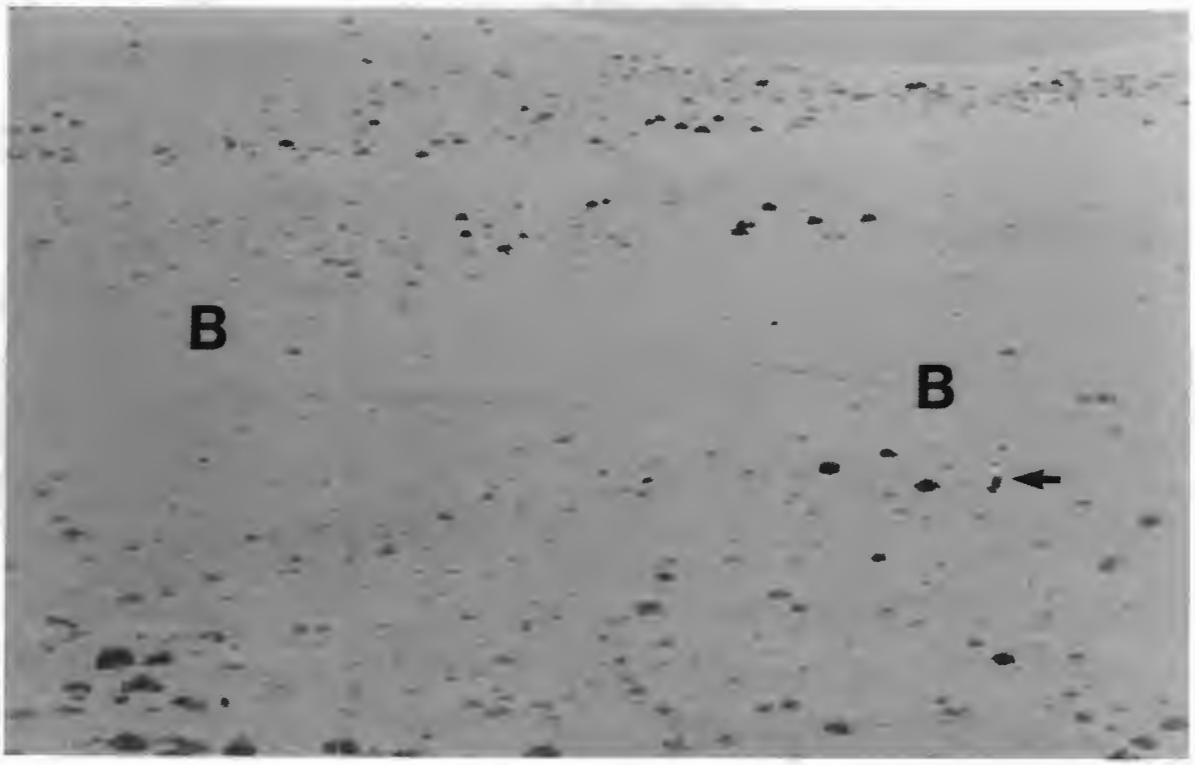

Figure 7.12. Main north-facing slope comprised of the Rooilepel sandstone. Note the very large-scale second-order bounding surfaces (B). Southerly quadrant palaeowind blew from top to bottom of frame. Person (arrowed) for scale.

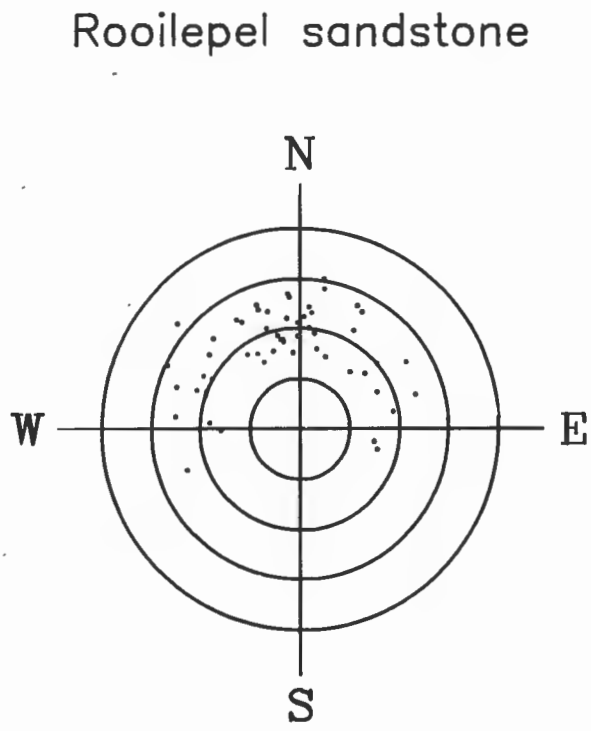

Figure 7.13. Polar plot showing the direction of cross-bedding dip azimuths, which demonstrate that the sand body was deposited by a southerly palaeowind regime.

Figure 7.14. In situ upper jaw fragment at the base of the Rooilepel sandstone, consisting of two incisors identified as being of Paraphiomys pigotti. Scale 10 cm.

presently being made to identify the specimens, which provide an exciting possibility of differentiating some of the ancient aeolian sand bodies within the Namib.

Shells and internal moulds of Trigonephrus sp., are abundant within the Rooilepel sandstone. This is possibly palaeoclimatically significant, because Trigonephrus presently appears to be restricted to the winter rainfall region of the Namib. The modern snails burrow below the ground surface during dry conditions and come to the surface only after rainfall or heavy fog. The recovery of a specimen in what appears to be a preferentially calcified burrow (Figure 7.38) suggests that the earlier forms might have lived under comparable palaeoclimatic conditions, and behaved similarly. Other trace fossils etched from the sandstone by deflation closely resemble those of Psammotermes described by Coaton and Sheasby (1973).

Interpretation

The recovery of Paraphiomys pigotti from the base of the aeolian sequence indicates that the Rooilepel sandstone is of Lower Miocene age. The magnitude of the cross-bedding is interpreted as evidence of a palaeo-erg, which infilled pre-existing topography. Isolated remnants of Pomona silcrete in the vicinity of the Rooilepel depression indicate that considerable incision of the silcrete had commenced prior to the Miocene. As shown in section 7.2.6., further evidence of early incision of the silcrete is provided by the Grillental Beds. Southern Namib field evidence therefore implies that this incision occurred prior to the Mid-Miocene, as envisaged by Partridge and Maud (1987) on geomorphological grounds.

The deposition of the sandstone was possibly initiated during the Oligocene. The scale of the cross-bedding is indicative of very large dune forms. The scatter of dip azimuths from the tabular-planar cross-bedding are typical of linear dunes, which implies an easterly location within the palaeo-erg.

The stratigraphic relationship of the Rooilepel sandstone with the Kakaoberg Sandstone Member of the Upper Buntfeldschuh Formation is not proven at this stage. Deposition of the Kakaoberg Sandstone Member probably commenced during the Lower to Middle Eocene. The deposition of the Rooilepel sandstone therefore appears to have commenced somewhat later, but both aeolian sequences pre-date the

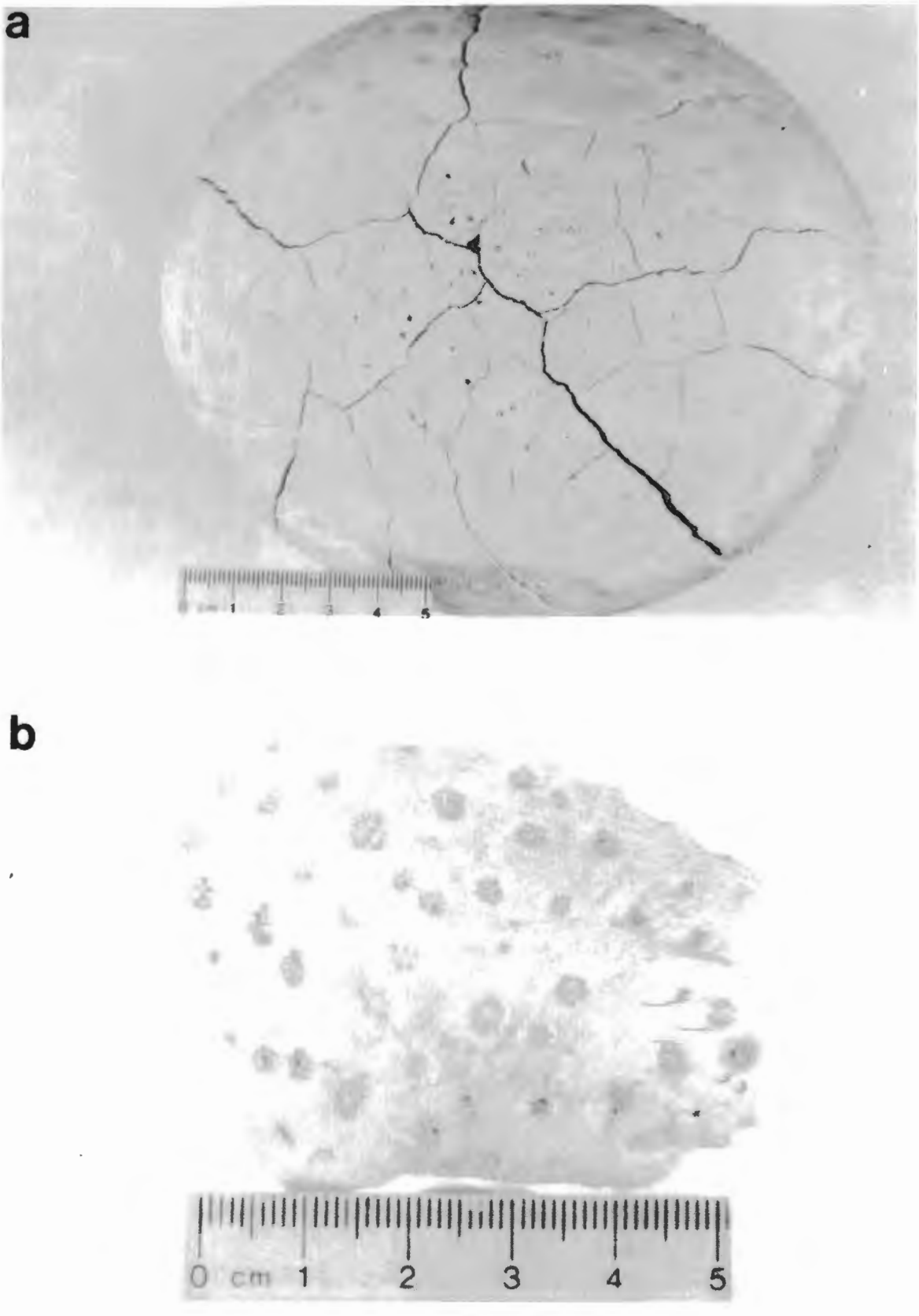

Figure 7.15. (a) Approximately half a complete eggshell deflated from the Rooilepel sandstone. Note the large pits visible on the surface. Scale 10 cm. (b) Close-up of the pits, to show the granular relief on their floor. Scale in cm.

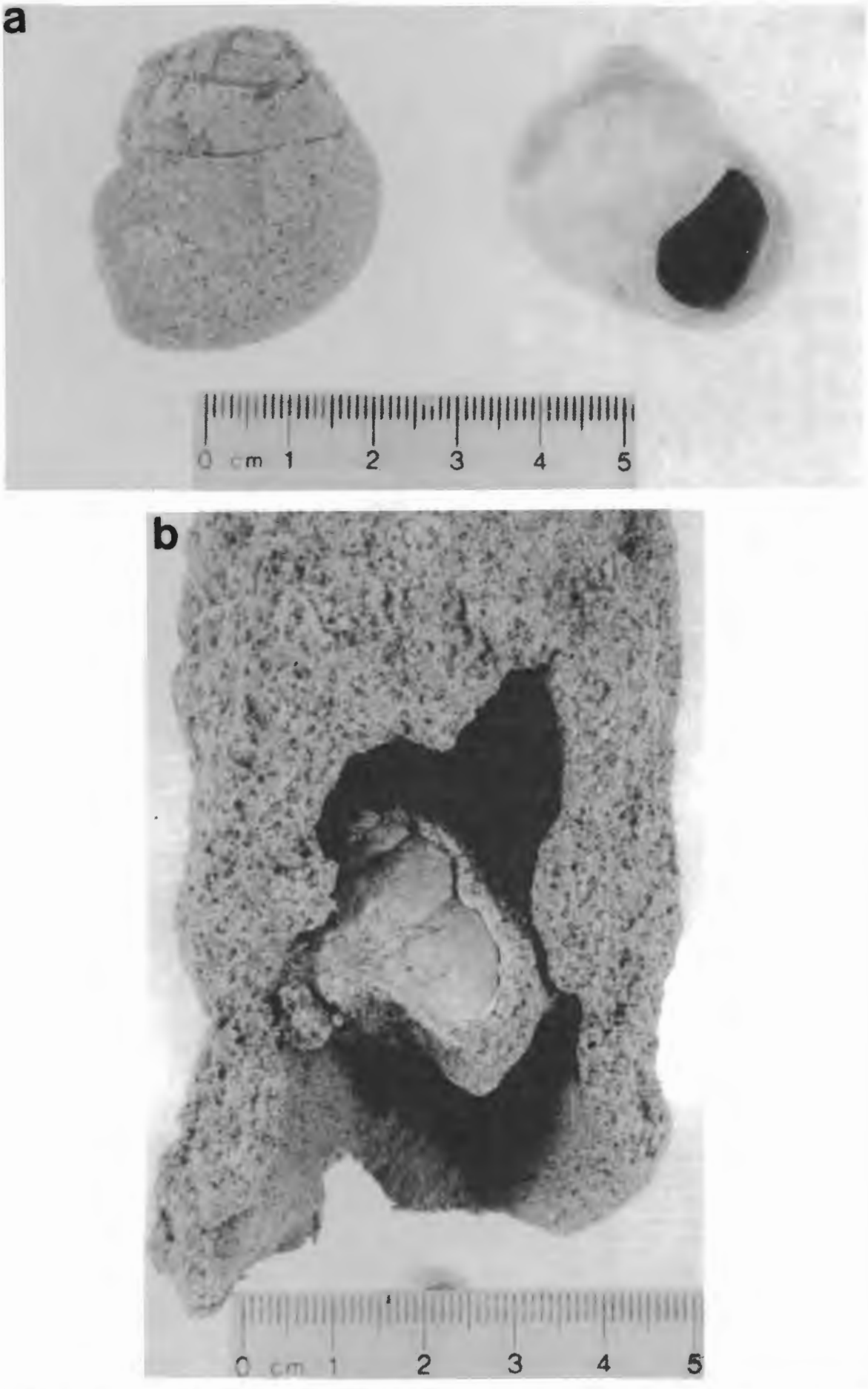

Figure 7.16 (a) An internal mould (left) and a complete Trigonephrus from the Rooilepel sandstone. (b) A Trigonephrus shell within a preferentially calcified cylindrical tube of Rooilepel sandstone which is interpreted as a burrow.

point at which Siesser considers that aridification of the Namib occurred.

Both the Kakaoberg Sandstone Member and the Rooilepel sandstone are capped by the mature, regionally extensive pedogenic hardpan calcrete. The possibility therefore exists that these two aeolian sand bodies, which represent the initial phase of aeolian sedimentation within the Southern Namib, might have been active contemporaneously for at least part of their development. On a regional scale, these sandstone bodies are tentatively correlated with the Tsondab Sandstone Formation of the Central Namib. This supports the earlier view expressed by Ward (1984, 1987).

7.2.5. KOLMANSKOP SANDSTONE

Description

Only one clearly identifiable exposure of this sandstone has so far been located south of Luderitz (Lat. 26°45'30"S; Long. 15°15'E) on the eastern side of the Kolmanskop valley (Figure 7.17). Shallow pits in the surrounding area, however, suggest that this deposit might extend laterally for some distance.

The orange to red sandstone, comprised of fine to medium sand, is noticeably finer-grained than the surrounding exposures of the Fiskus Sandstone Beds. The sandstones differ compositionally (Table 7.3). The principal distinguishing feature of the Kolmanskop sandstone is that it does not contain agate and chalcedony grains, which are characteristic of the Fikus Sandstone Beds. In addition, the feldspar content of the Kolmanskop sandstone greatly exceeds that of the Fiskus Sandstone Beds.

The Kolmanskop sandstone exposure is cross-bedded, and exhibits pin stripe lamination (Figure 7.18). Ripples of fine-grained sand occur along some bedding planes. The crestal grains are distinctly coarser-grained, which is a feature of wind ripples, according to observations in the Kelso Dunefield by Sharp (1963).

Table 7.3. Point-counting results illustrating the compositional differences of the sandstones south of Fiskus Pan.

SANDSTONE BODY	% QUARTZ	% FELDSPAR	% OTHER	NOTES
Fiskus	59.0	25.6	15.4	Agate & chalcedony granules.
Kolmansop	26.6	64.8	7.6	Agate and chalcedony absent.
500 grains counted in each slide.				

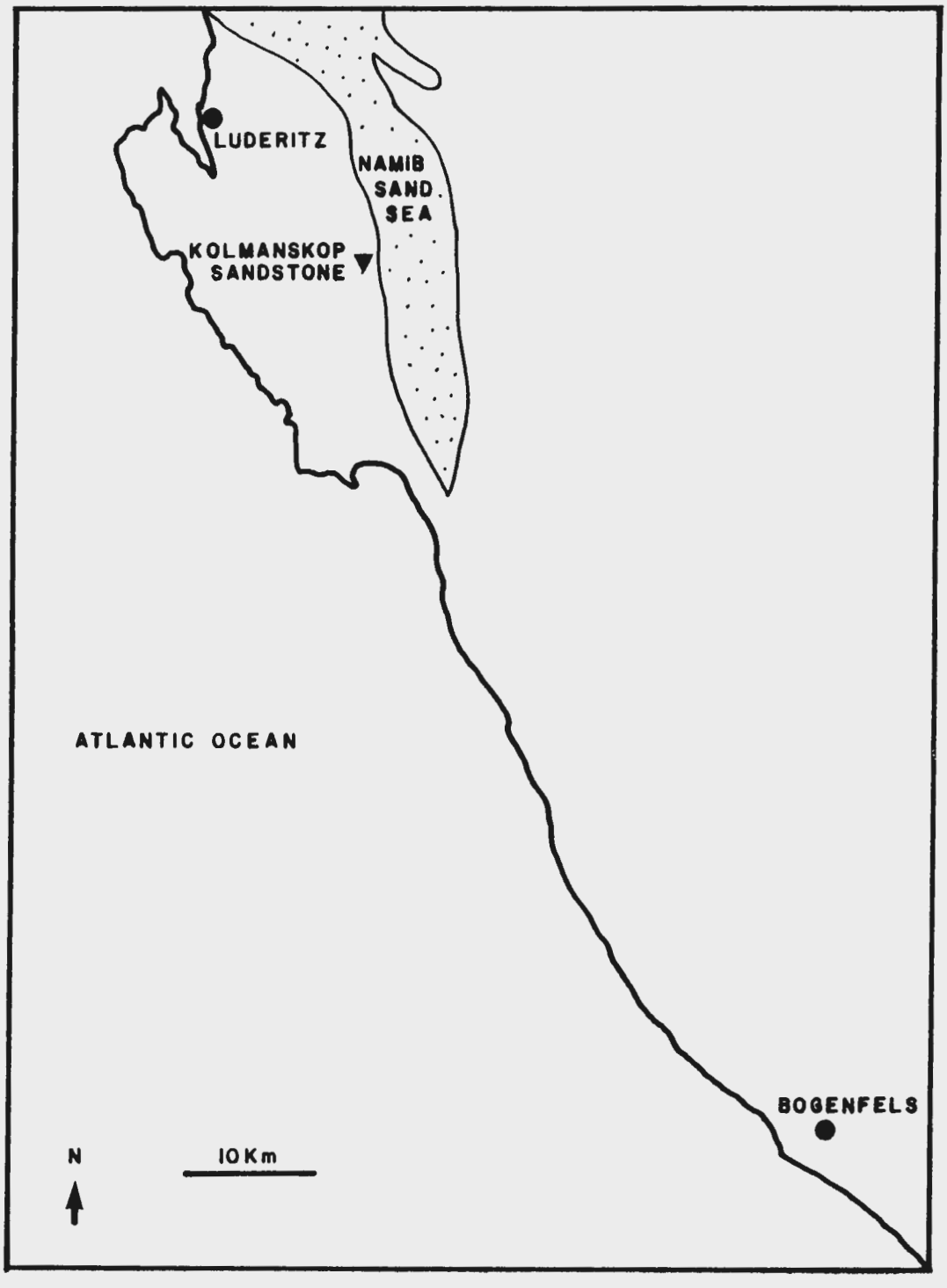

Figure 7.17. Map showing the location of the single exposure of the Kolmanskop sandstone in relation to the present-day Namib Sand Sea.

Figure 7.18. View of the single exposure of the Kolmanskop sandstone. Note the erosive contact with the overlying arkosic alluvial deposit. Scale 1 m. b) Close-up of the exposure, showing pin stripe lamination (P), and wind ripples (R) preserved along bedding planes. Note the darker crestal area, which indicates a slight increase in the grain size. These ripples resemble the form of those described by Sharp (1963).

Poorly cemented feldspathic alluvial sediments erosively overlying the Kolmanskop sandstone are also reddened. It is uncertain whether this upper contact represents a significant time break or not.

No fossils have been recovered from the exposure described above but red aeolian sandstone cropping out along the western margin of the Namib Sand Sea at Schmidtfeld (Lat. 26°30'30"S; Long. 15°10'E), to the north of Luderitz, contains eggshell fragments about 3.6 mm thick. The pit structures resemble those in the specimens from the Rooilepel sandstone.

Interpretation

The compositional variation of the sandstones outcropping near the Fiskus Pan indicate that two sandstone provenances are represented. The cross-stratification styles of the sandstones also differ. Although both are typical of aeolian dunes, it is concluded that two different sand bodies might be present. The small size of the Kolmanskop sandstone exposure prevents thorough examination of the dune form which is represented. The preservation of wind ripples overlying slip-face grainfall deposits suggest deposition by a strong, but relatively gentle palaeowind regime compared to that responsible for the deposition of the much coarser-grained Fiskus Sandstone Beds.

It may be significant that the upper surface of the isolated remnant of the Kolmanskop sandstone was eroded by alluvial, arkosic gravel derived from the local gneissic bedrock. Although the alluvial sediments have not been dated, they possibly correlate with the early Miocene phase of alluvial deposition, which infilled the present-day Fiskus Pan depression (see section 7.2.10). Supporting evidence for this is possibly found at Schmidtfeld, where eggshell fragments within sandstones closely resemble those recovered from the Rooilepel sandstone. If the tentative correlation with the Tsondab Sandstone Formation of the Central Namib can be proved, the existence of a very extensive palaeo-erg is implied.

7.2.6. THE GRILLENTAL BEDS

Description

The Grillental is an east-west oriented valley which cuts across the regional structural trend of the Precambrian basement (Figure 7.19a). The valley is thus perpendicular to the trend of the south-north oriented endoreic basins which result from the combined action of salt weathering and deflation. A 1 to 2 km-wide valley extends about 12 km west southwest from the seaward end of the Grillental to a depth of about 130 mbsl. (Murray et al., 1970; O'Shea, 1971).

The eastern and central parts of the Grillental are floored by the different sedimentary facies which comprise the Grillental Beds (Figure 7.19b). Although Stromer (1926) considered that the sediments within the Grillental are alluvial, Greenman (1966) provided the first description when he included the sequence within the Elizabeth Bay Formation (sensu SACS, 1980), along with the aeolian Fiskus Beds at the western end of the valley (see section 7.2.10. Fiskus Sandstone Beds).

Channel facies

Fining-upward units of white, calcified, angular, arkosic grits from 1 to 2 m thick crop out over large areas of the valley floor. Occasionally, sediments of the channel facies are seen to erosively overlie the pale green fine sand, silt and clay units of the floodplain facies (Figure 7.19c) in shallow sections through the sequence. Remnants of calcified grit along the margins of the Grillental demonstrate that erosion of at least 10 to 15 m of the sequence has taken place and that the valley is currently being re-exhumed.

The calcified arkosic grits exhibit two forms of large-scale cross-bedding. The commonest type consists of compound tabular-planar cross-bedded sets. Viewed in plan, sinuous edges of the 1 to 2 m thick cosets can be seen covering the sub-horizontal planes which have subsequently been eroded through the facies (Figure 7.20). Although the orientation of the sinuous cosets varies widely, the palaeocurrent direction was from east to west. A poorly developed basal lag gravel consisting of sub-angular to poorly rounded feldspar and quartz pebbles marks the erosive

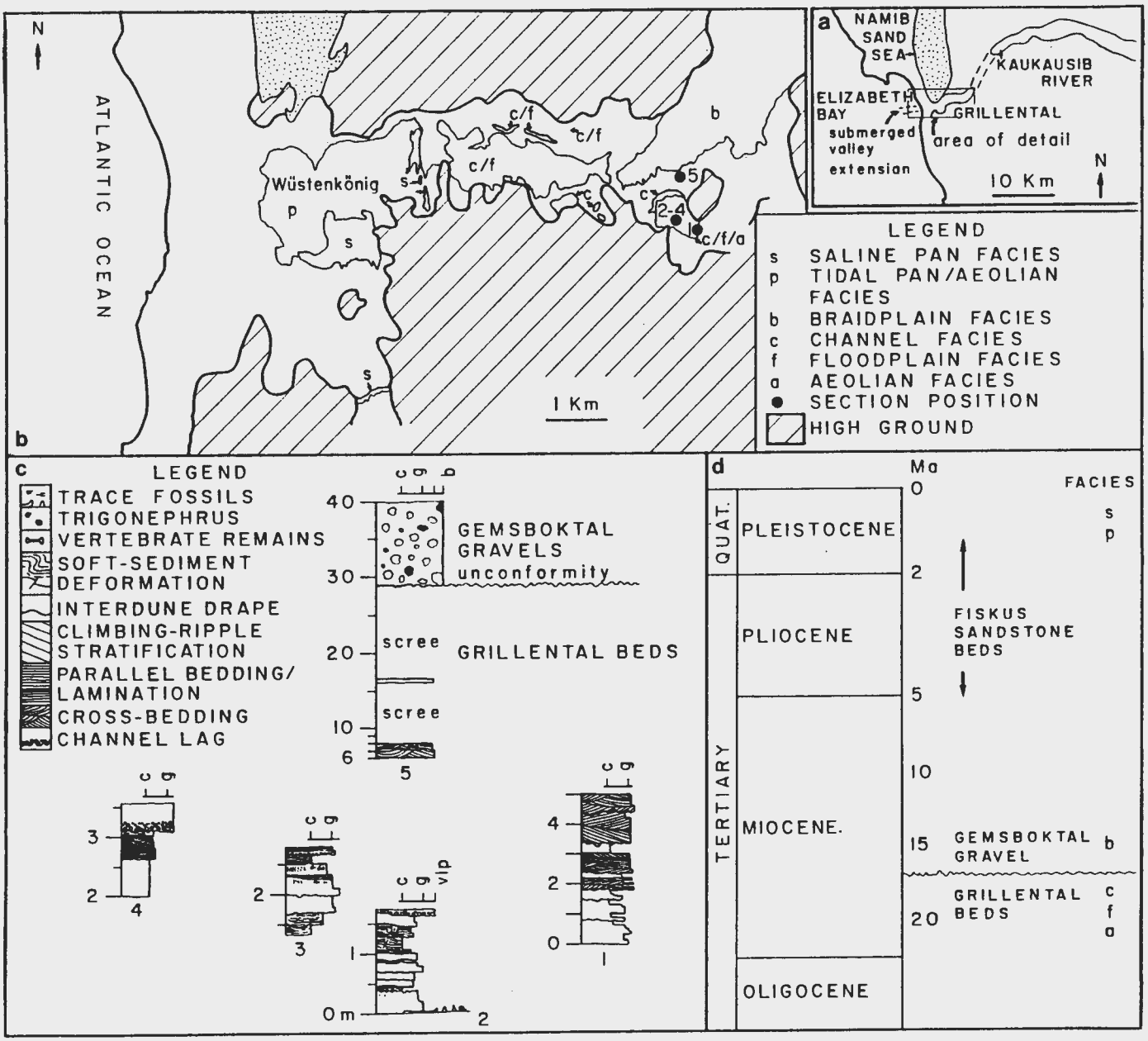

Figure 7.19. (a) Locality plan for the Grillental. (b) Map showing the spatial variation of the facies comprising the different lithostratigraphic units within the Grillental. (c) Vertical section through the Grillental Beds exposed in the deflation hollow at the south eastern end of the Grillental. (d) Revised stratigraphic relationship of the Grillental Beds.

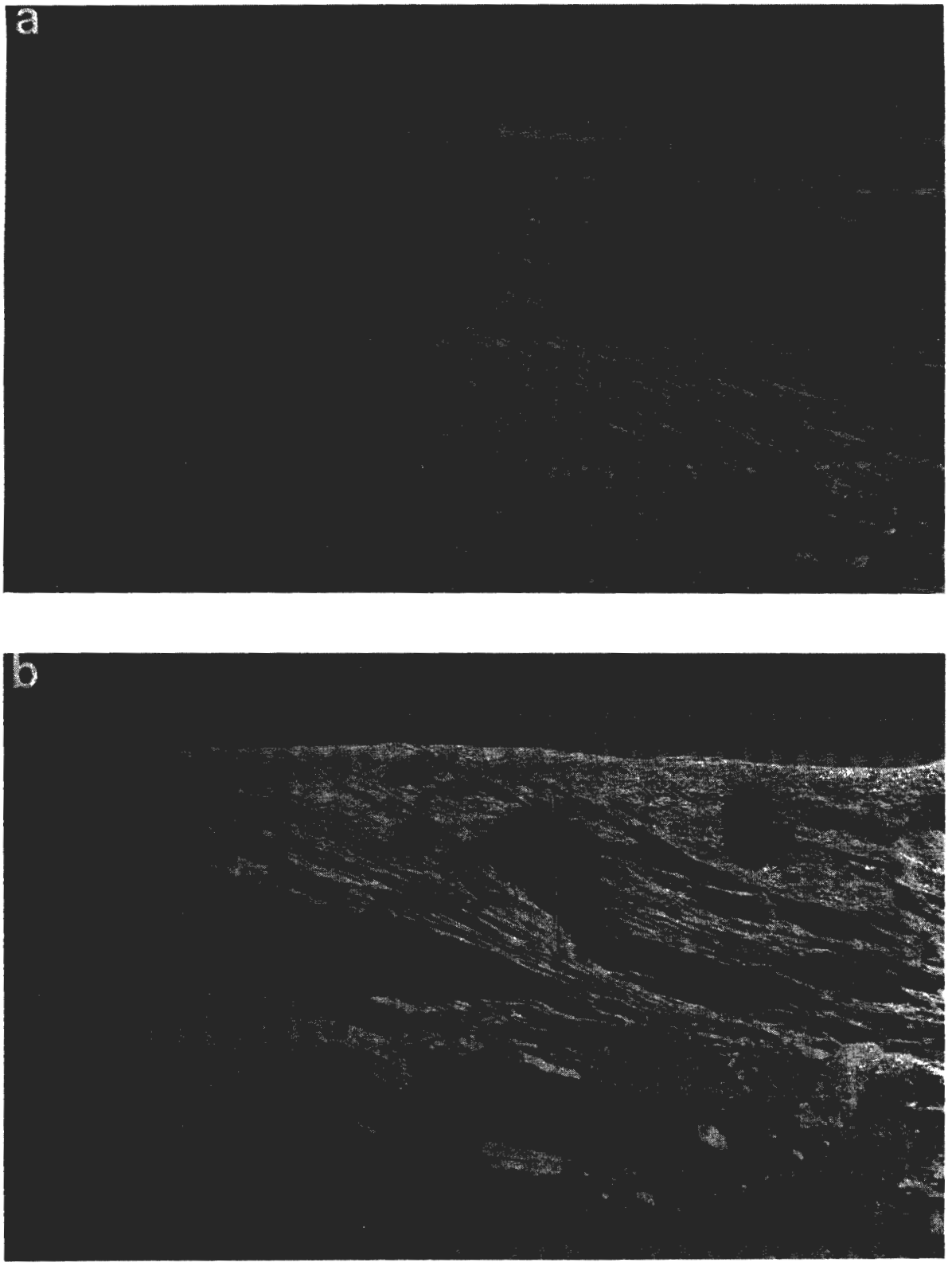

Figure 7.20. (a) A sub-horizontal erosion surface through compound tabular-planar cross-bedding. The largest bar form can be traced for more than 50 m downstream, and indicates the large size of the bar forms. Flow was from left to right. (b) Section through the large tabular-planar cross-bedded set forming part of the bar in (a). Flow from left to right, scale 1 m.

contact of tabular-planar cross-bedded units with the underlying pale green fine sands and silts. Intraclasts eroded from the pale green to light brown fine-grained sediments are commonly incorporated into these basal lags. Viewed as a whole, the tabular-planar cross-bedded units therefore fine upwards from the basal lag gravel.

Grouped and solitary trough cross-bedded sets varying in breadth from 1 to 3 m form the second type of large-scale cross-bedding (Figure 7.21). The grouped trough cross-bedded sets create a rib and furrow pattern. Palaeocurrent measurements of the grouped and solitary sets both indicate palaeoflow to the west (TN 284°E to TN 312°E). Areas of backflow did, however, occur towards the eastern end of the Grillental in the vicinity of complex bedrock morphology. The solitary trough cross-bedded sets were erosively scoured into the barforms comprised of compound tabular-planar cross-bedding, and some troughs can be traced westwards over 30 m.

Floodplain and aeolian facies

At the south-eastern end of the Grillental, erosion of the calcified grits has exposed the underlying fine-grained sediments in which subsequent aeolian erosion has produced a deflation hollow. In places, isolated pedestals of pale green sands and silts are separated from the overlying coarser-grained channel facies by a scoured, erosive contact.

The silt and sand units of the floodplain facies are interbedded with sub-horizontal clay horizons, and commonly exhibit climbing ripple cross-stratification (Figure 7.22). The clay horizons vary from a few centimetres to tens of centimetres thick. Trace fossils of burrow systems are abundantly preserved within the fine-grained horizons. The deflation of the uncemented fine-grained matrix surrounding the preferentially calcified burrow systems has led to the development of residual lags covering the ground surface (Figure 7.23).

Within the main deflation hollow at the south eastern end of the Grillental, horizons of silt and clay are interbedded with structureless sands. The comparatively fine-grained horizons are separated from the overlying channel facies by erosive, scoured contacts.

Unusual, large concave-up bedding planes of silt and clay are

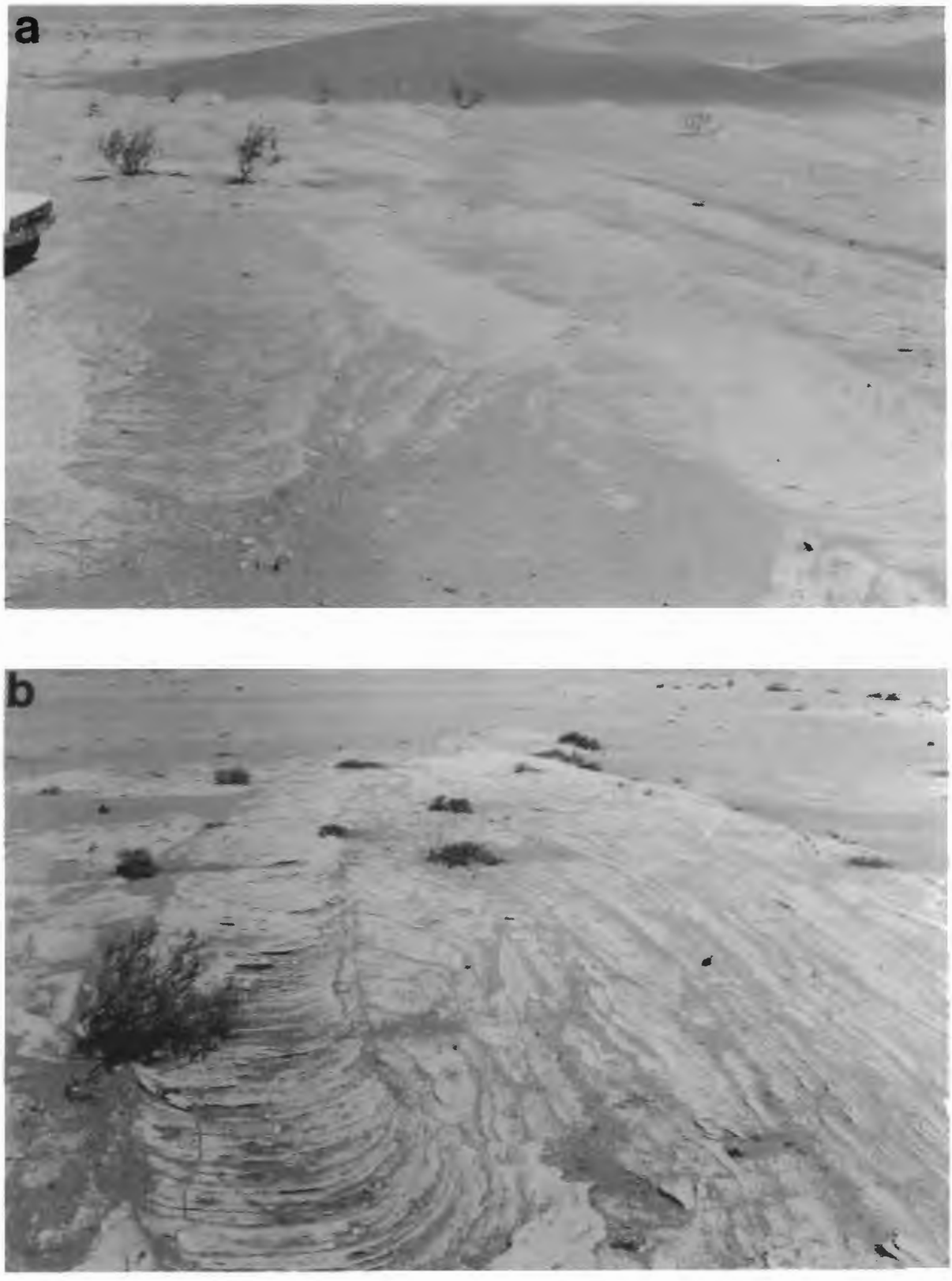

Figure 7.21.(a) Large, grouped, trough cross-bedded sets of calcified, arkosic grits. Flow from bottom right to top left. (b) Solitary, 2.5 m wide trough that has eroded into arkosic grits exhibiting tabular-planar cross-bedding. Flow from bottom to top of frame.

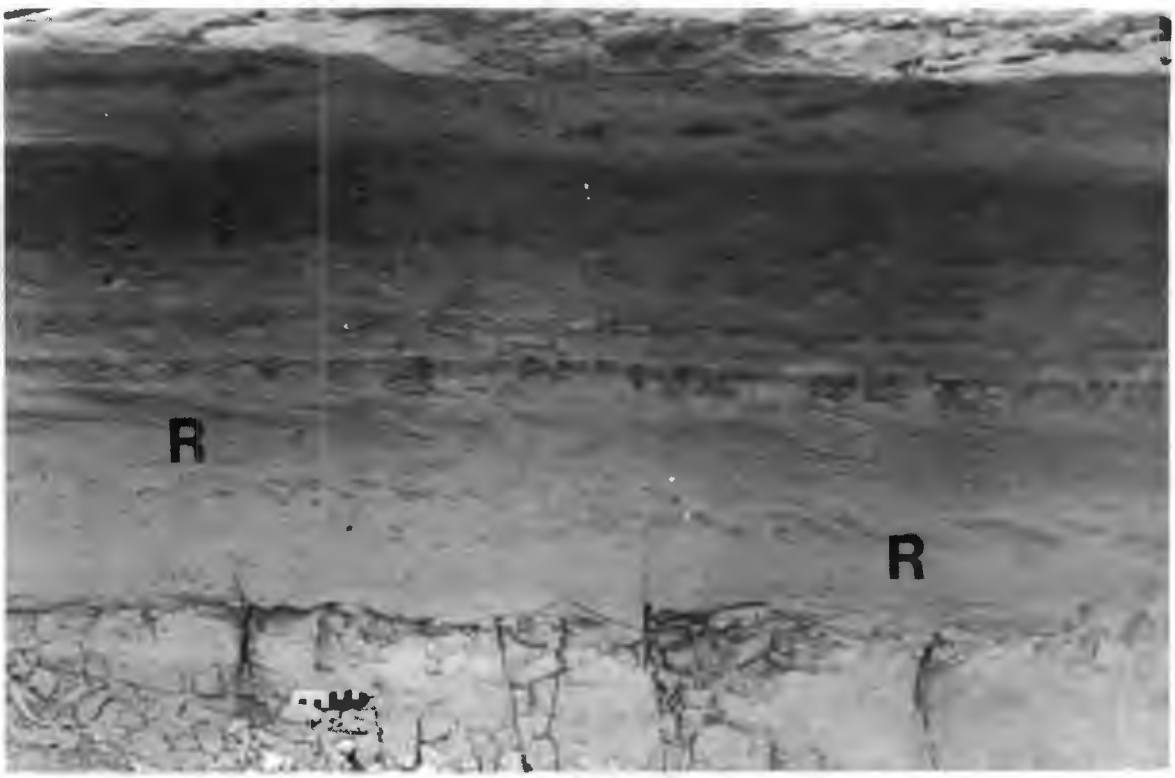

Figure 7.22. Alternating sub-horizontal, parallel laminated clay and silt (C) with fine sand horizons exhibiting ripple drift lamination (R), interpreted as evidence of floodplain deposition. Note the sharp, erosive base of the overlying fining-upward, calcified grit unit. The top sandy horizon has been burrowed intensively. Palaeo-flow from right to left, scale 10 cm.

Figure 7.23. A lag of preferentially calcified burrow systems created by aeolian deflation of the surrounding fine-grained sediment. Note the encroachment deposit by the scale along the margin of the exposure. Southerly wind flow from bottom to top, scale 15 cm.

defined by inclined, arcuate margins which dip towards the centre of the depressions (Figure 7.24). The arcuate margins are seen to truncate one another in plan view. Large pebble and cobble sized clay intraclasts, which occur abundantly within some of the sandy horizons (Figure 7.25), are draped by laminae of fine to medium sand which progressively covered the surface irregularities created by the intraclasts.

To the west of the concave-up arcuate features, aeolian erosion of pale yellow to orange, fine- to medium-grained sands on the depression floor have formed yardangs from 0.5 to 1.0 m high and a few metres long, parallel to the southerly surface-wind flow. Some of these landforms are capped by calcified grits of the channel facies. The toeset laminae and gently dipping bedding planes exhibited by the sands have been enhanced by iron staining (Figure 7.26a). In places, stratification resembling the pin-stripe lamination described from aeolian sandstones by Fryberger and Schenk (1988) has been etched out by weathering (Figure 7.26b). Petrographic examination of the finely laminated sands proves that they contain a much greater proportion of quartz than the calcified grits which characterise the channel facies (Table 7.4). The grains of the quartz-rich sands are also better rounded and sorted than those of the channel facies.

Table 7.4. Compositional variation of the calcified sands and the quartzitic cross-bedded sands associated with the concave arcuate features at the south-eastern end of the Grillental.

DEPOSIT TYPE	% QUARTZ	% FELDSPAR	% OTHER
Trough cross-bedded calcified sands.	37.2	61.8	1.0
Cross-bedded sands underlying calcified grits.	57.4	36.0	6.6
500 grains counted in each thin-section			

Figure 7.24. Variably inclined, "domed" arcuate bedding planes of alternating units of parallel laminated clay and sand units at the south-eastern end of the Grillental. Some sand horizons exhibit current ripple lamination. Flow from top left to bottom right. Scale bar is 1 m long.

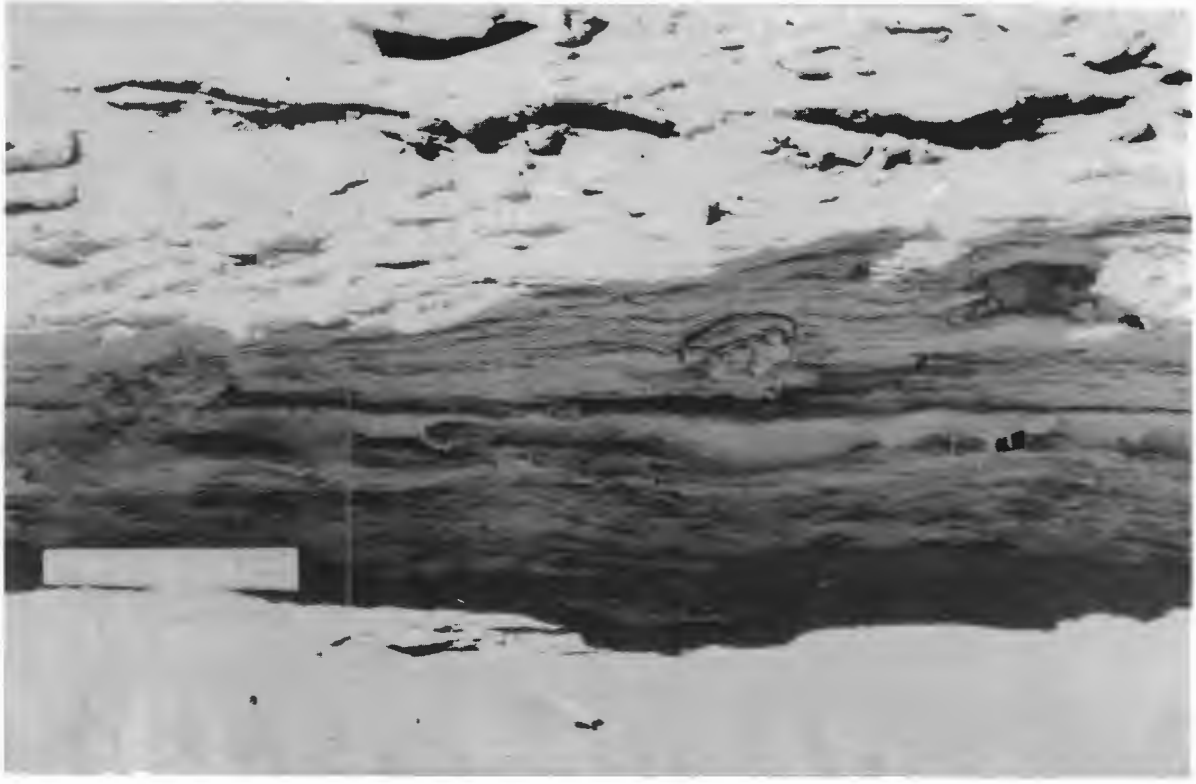

Figure 7.25. Section through sands underlying the margin of a concave-up, arcuate feature showing clay intraclasts draped by fine sand laminae. Flow from right to left, scale 16 cm long.

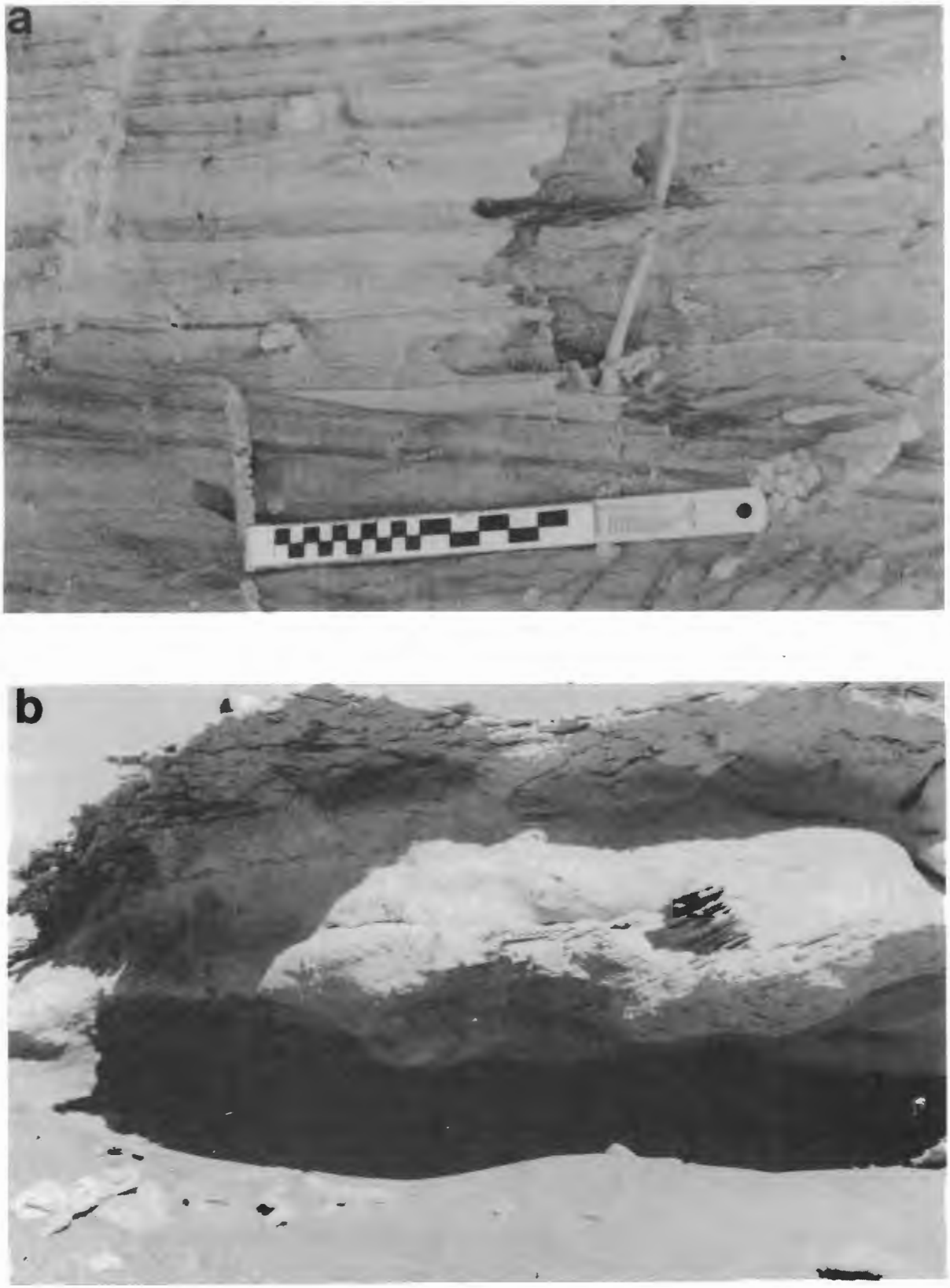

Figure 7.26. (a) Iron-staining along bedding planes in the fine to medium-grained quartz-rich sands. (b) Finely laminated exposure of yellow to orange, fine- to medium-grained quartz sand, etched by weathering processes, which resembles pin stripe lamination typical of aeolian sands. Note the scouring along the contact with the overlying white, calcified arkosic grits of the channel facies. Graduated portion of scale 10 cm long.

Fossils

Greenman (1966) recovered bone fragments from both the channel and the floodplain facies of the Grillental Beds. Prior to this, Stromer (1926) and Hopwood (1929) constructed a faunal list of Lower Miocene mammals from specimens collected at Elizabeth Bay. Specimens of vertebrates deflated from the Grillental Beds confirmed that they are also of Lower Miocene age (Hamilton and Van Couvering, 1977), and led to the revision of the previous faunal list. Observations during this study have shown that trace fossils are abundant within the Grillental Beds, and that previously unrecorded body fossils of invertebrates are also present.

At the southern side of the deflation hollow, erosion has left cones of white, preferentially calcified arkosic grits, which continue beneath the sediment surface as periodically branching cylindrical tubes about 6 cm in diameter (Figure 7.27a). Although no evidence of back-filling has been seen in any tubes, they are possibly the burrows of a small vertebrate. In the same locality, ferruginous concretions have been deflated from the fine-grained sediments. Gastropod shells appear to have acted as nuclei for the formation of some of the concretions, and some specimens closely resemble Trigonephrus sp. (Figure 7.27b). This land snail had previously been considered to be absent from the Lower Miocene deposits (Stromer, 1926).

Thin-walled eggshell fragments have been recovered from the silt horizons of the floodplain facies of the Grillental Beds. The fragments neither resemble examples of Struthio sp. (ostrich) eggshell fragments from Southern Namib aeolian sequences nor those recorded by Sauer (1966, 1968) from northern Namibia. Bone fragments of very large tortoises (Testudinae), which probably exceeded 1 m in height, are characteristic of the early Miocene vertebrate fauna of Elizabeth Bay, Grillental and the Langental to the south (Stromer, 1926; Hamilton and Van Couvering, 1977). Additional remains have been located during this study, and it is tentatively suggested that the eggshell fragments from the Grillental Beds represent fragments of tortoise eggs. Remains of the frog Xenopus stromerei, were recovered from boreholes east north east of Elizabeth Bay and west-northwest of the Kaukausib drainage tract at depths of between 13 to 22 m below the surface (Stromer, 1926).

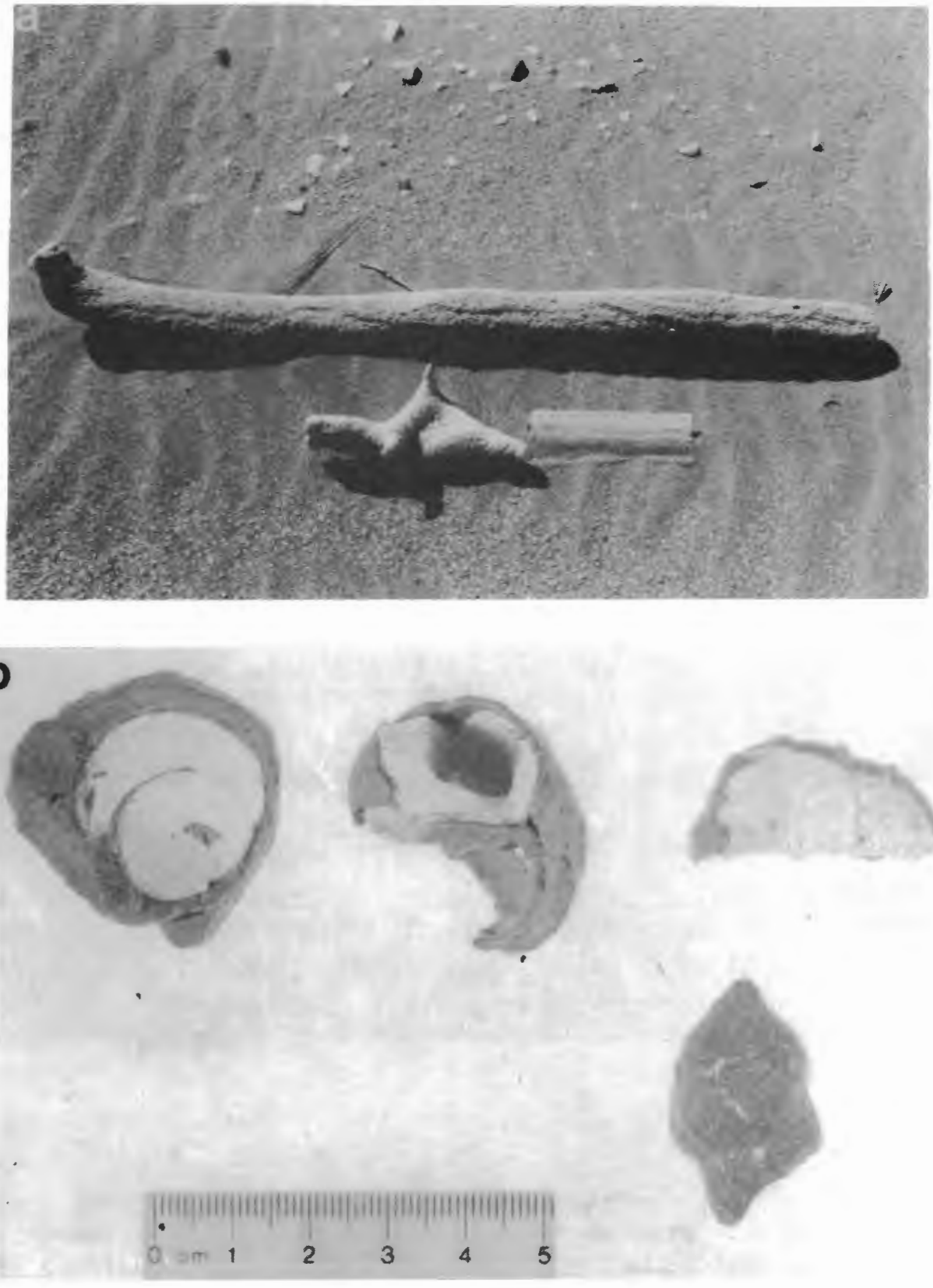

Figure 7.27. Fossils associated with the concave-up arcuate features. (a) Long, cylindrical trace interpreted as a burrow system about 6 cm in diameter. The curved end probably formed the entrance to the system from the sediment surface. Some evidence for the branching of these burrows is present. Scale 15 cm. (b) Internal moulds of the land snail Trigonephrus from ferruginous concretions. The lower right specimen is probably a freshwater gastropod. Scale in cm.

A preferentially calcified termitaria, resembling that of the present-day Hodotermes, has been exposed by deflation of the well-sorted, quartz-rich cross-bedded sands forming the depression floor to the west of the concave, arcuate features (Figure 7.28).

Figure 7.28. A preferentially calcified termitaria resembling that of Hodotermes, exposed on the surface of the Grillental Beds by aeolian deflation. Note the +20 m high barchan migrating to the north in the background, which is part of the Bakers Bay aeolian transport corridor. Southerly wind flow from bottom to top. Scale 10 cm.

Interpretation

The vertical facies variation exhibited by the Grillental Beds defines a series of stacked, fining-upward units typical of alluvial deposits, which are separated by erosive, scoured contacts. The sediments are confined to a ribbon-shaped valley which cuts across the regional tectonic strike. The majority of the sediments within the Grillental are interpreted as having been deposited by an alluvial system which flowed from east to west.

The tabular-planar cross-bedding exhibited by the channel facies is characteristic of linguoid and transverse bar forms (eg. Miall, 1977), and provides evidence for the migration of large bars along the channels in the Lower Miocene alluvial system. Collinson (1970) suggested that linguoid bars are generated during flood events within present-day fluvial systems. Personal observation of bar forms near the Orange River mouth, after the floods during March 1988, confirm this to be the case, but as Smith (1971) observed, such bars also undergo modification during non-flood conditions.

Allen (1982) considers that grouped sets of trough cross-bedding indicate the migration of subaqueous dune trains. The grouped, trough cross-bedded sets within the Grillental either represent the passage of dunes across bar surfaces as flood activity waned, or the migration of dune trains along the floor of active channels which subsequently cut through previously deposited bars. Although the solitary trough cross-bedded sets of the Grillental Beds resemble the elliptical scours described by Harms and Fahnestock (1965), personal observation of emergent bar surfaces after flooding of the Orange River suggest an alternative origin. Excavations showed that the large, mid-channel bars were comprised of tabular-planar cross-bedded sands. Flow-parallel troughs were eroded into the bars in the lee of trees and large vegetation-bound aeolian current shadows, established during a previous period(s) of bar emergence. The infilling of the scours by cross-bedded sands, as the flood subsided, left solitary trough cross-bedded features, which closely resembled those seen within the Grillental Beds.

The presence of termitaria, which indicate sub-aerial conditions, are particularly important to the interpretation of the Grillental Beds. In contrast to the sands which comprise the channel facies, the cross-bedded, well-sorted sands in which the termitaria occur are more quartzitic, which indicates that two different provenances

are represented. The pin stripe lamination of the quartz-rich sands provide evidence for their deposition by aeolian processes. Further evidence of aeolian activity during the deposition of the Lower Miocene alluvial sequence is given by the concave depressions defined by sand, silt and clay units. Ponding of the Kuiseb River, in the Central Namib, today occurs some 10 to 20 km inland from the coast, at the distal end of the drainage system. The interaction of fluvial and aeolian depositional systems creates a distinctive sequence of interbedded fluvial and aeolian sediments (Ward, 1984, 1987). The distal end of the drainage system lies within the coastal tract which is influenced by high-energy southerly surface-winds. The infiltration of flood water into the porous, sandy stream beds, together with the viscous nature of the flood water due to its saturation with the suspended load, minimises erosion of the sandy aeolian substrate during ephemeral flood events (Ward, pers. comm., 1987). Ponded water bodies are therefore created within the transient interdune depressions that form between the transverse dunes and the semi-stabilised coppice dunes, and block the seaward exit of the fluvial system. The drapes formed by clays and silts settling from suspension onto the floor of these water bodies within concave interdune depressions floored by aeolian sands provide a modern analogue for the features observed within the Grillental Beds (Figure 7.29). Changes in the location of the interdunes leads to the erosion of the aeolian sand underlying the concave clay and silt drapes, and the release of loose blocks of clay and silt which tumble onto the margins of former interdune depression. It is envisaged that a similar mechanism, together with the incorporation of rip-up clasts generated by successive flood pulses during rainy seasons, probably accounts for the abundance of intraclasts within the Grillental Beds. The quartz sands interbedded with the arkosic channel and floodplain facies of the Grillental Beds therefore prove that aeolian activity occurred contemporaneously with the deposition of the Lower Miocene alluvial sequence. Trace fossils of vegetation, which would provide evidence for semi-stabilised coppice dunes have not yet been found within the Grillental, which suggests that the aeolian sands were deposited by small transverse aeolian dunes.

Figure 7.29. An example of a concave-up clay drape overlying aeolian sands within the distal reaches of the present-day Kuiseb River. The drape marks the former position of an interdune depression between aeolian bedforms within a former channel of the Kuiseb River. Note the truncation of arcuate margins delineating previous drapes on the floor of the present depression near the person. The sand mound overlying the main drape is maintained by the growth of a !Nara plant (Acanthosicyos horrida). Southerly wind-flow from top right to bottom left. Kuiseb River flow from top left to bottom right.

Siesser and Dingle (1981) documented evidence of a major Oligocene regression to about 500 mbsl. At the time that the Grillental Beds were being deposited around 20 Ma, sea-level would still have been recovering from this event. Thus, by implication, the Lower Miocene coastline would have been located to the west of its present position.

The arkosic alluvial sediments comprising the majority of Grillental Beds exposures were probably derived from the reworking of an older alluvial sequence which is preserved beneath a capping of the Klinghardt Phonolite Formation. The complete absence of exotic clasts from the Grillental Beds supports this concept of a local provenance.

The recognition of aeolian sands interbedded with the alluvial deposits indicates that the drainage system was not perennial. This interpretation is supported by the presence of termitaria, which suggest prolonged periods of bar emergence and sub-aerial exposure. The sequence is therefore re-interpreted as an ephemeral alluvial system which was periodically affected by very high discharge and flood conditions which generated the large-scale bar forms. Along the eastern margin of the present-day Namib, large-scale alluvial fans are prograding westwards from catchments along the Great Escarpment (Figure 7.30). These systems possibly provide a modern analogue for the Lower Miocene ephemeral system, which is believed to have operated under semi-arid palaeoclimatic conditions. It is reasoned that rather than providing evidence for savannah conditions, the Grillental Beds indicate a reduction in the periodicity of catastrophic rainfall events along the escarpment.

The Grillental valley is also geomorphologically important. Partridge and Maud (1987) have stated that the incision of the Late Cretaceaous African palaeo-surface only commenced during the Miocene. The deposits flooring the Grillental are, however, known to be of Early Miocene age (Hamilton and Van Couvering (1977). The incision of the valley must therefore have commenced by the latter part of the Oligocene, when sea-level was still well below its present level, in order to account for the depth of the submerged valley extension. Field evidence thus demonstrates that the post-African geomorphological evolution of the Namib probably began well before 20 Ma. In some respects, it is surprising to find an aggradational alluvial sequence within such a major valley which

cuts across the regional structural trend. It is suggested that the drainage system was funnelled by pre-existing relief. Speculatively, this might have been provided by the re-occupation of a valley which had originally developed during the Dwyka glaciation although to-date, no Dwyka clasts have been recovered from the Grillental Beds. If this hypothesis is correct, it would extend the distribution of glacial, Dwyka valleys which are known to occur within northern Namibia (Martin, 1953; Martin and Schalk, 1957).

The upper contact of the Grillental Beds with the overlying cobble and boulder alluvial gravel which contains phonolite clasts is important from the regional context. A similar upward-coarsening sequence is described in section 7.2.9.

Figure 7.30. Landsat image showing the catchment of a major alluvial system (A) along the present-day Great Escarpment. It is postulated that a system of this type, with a large catchment, might provide a modern analogue for the Lower Miocene palaeo-system which deposited the Grillental Beds.

7.2.7. LOWER MIOCENE SEDIMENTS IN THE LANGENTAL

Description

The Langental is an ancient, broad, shallow, ribbon-shaped valley at the northern end of the Bogenfels/Buntfeldschuh Basin (Figure 7.31a). Remnants of Cretaceous and Eocene marine deposits are preserved within the valley, together with a sequence from which Lower Miocene vertebrates were recovered (Stromer, 1926; Hopwood, 1929; Hamilton and Van Couvering, 1977).

The Lower Miocene deposits primarily consist of pale green, uncemented arkosic sands and grits (Figure 7.31b), in which white, carbonate rich horizons are interbedded. In one of the few available sections, large wedge-shaped vertical cracks from 10 to 15 cm wide taper downwards into the underlying sediments to depths of 1 to 1.5 m (Figure 7.32). The cracks have been displaced at depth in some instances, and they are infilled by deep red, fine-grained sands containing scattered exotic pebbles of agate and chalcedony.

A sharp contact at the top of the sequence separates the sands containing the deep vertical cracks from an overlying deposit of very large pebble and cobble gravel. This coarse-grained deposit also contains abundant exotic clasts of agate, chalcedony and jasper, which were derived by alluvial reworking of the Lower to Upper Eocene marine shorelines which lay to the east up the palaeo-slope.

Stromer (1926) recorded a faunal assemblage which included large tortoises (Testudinae) and a rhinoceratid, which Heissig (1971) has subsequently identified as Brachypotherium heinzelini. An incisor of B. heinzelini was recovered during this study, along with scutes of a large tortoise. Numerous rodents and ruminants (Artiodactyla), of which Propalaeoryx austroafricanus appears to be particularly well represented, suids, Prohyrax tertiarus (Hyracoidea) and the elephant shrew Myohyrax oswaldi (Macroscelidea) have also been recovered. Stromer (op. cit.) also recorded the presence of the frog Xenopus stromerei in the Langental sequence.

Interpretation

Beetz (1926) first interpreted the Lower Miocene sediments within the Langental as being fluvial. Stromer (1926) supported this conclusion on the basis of the faunal assemblage which was

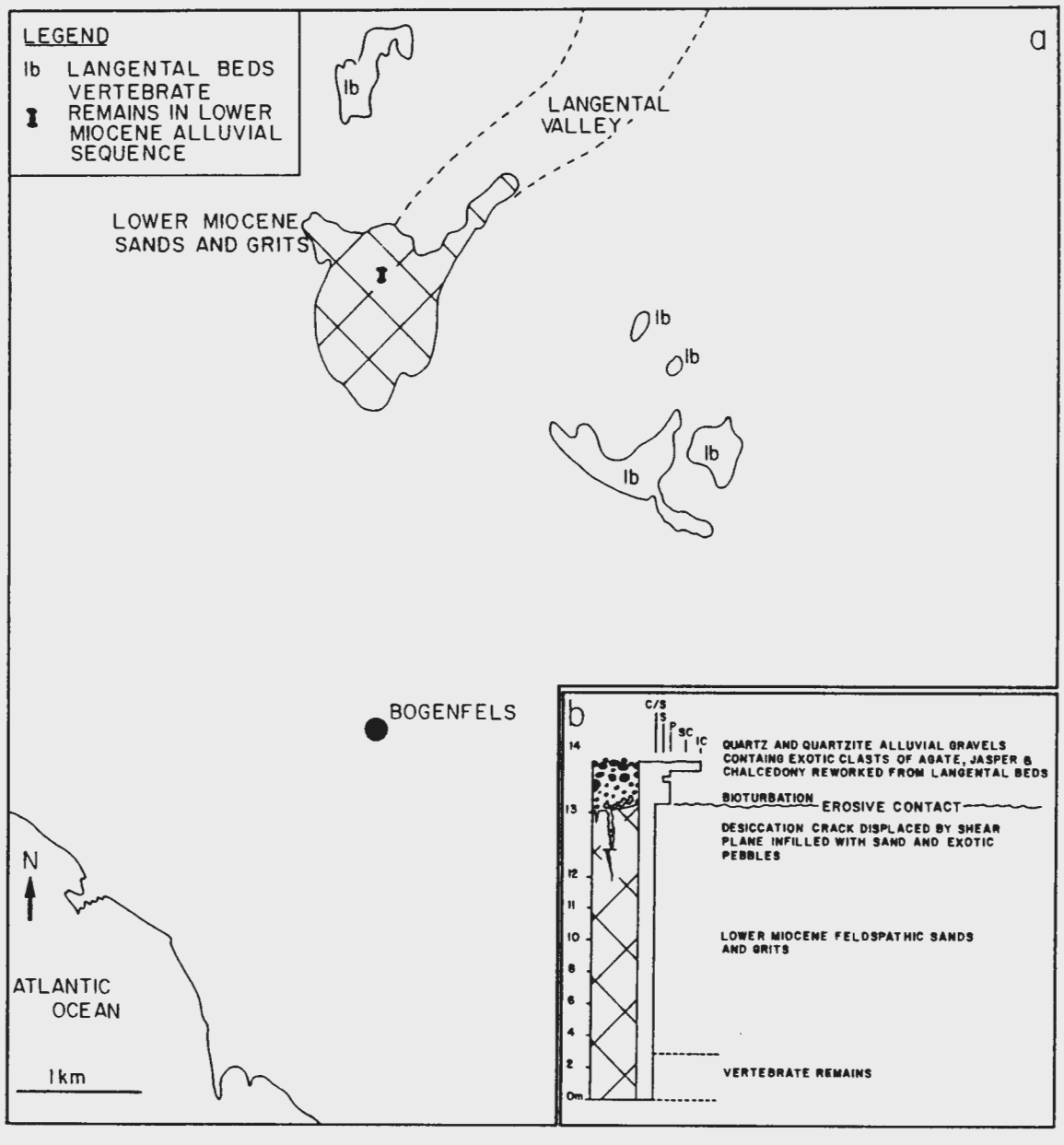

Figure 7.31. a) Locality plan showing the Langental valley and the distribution of the marine, Upper Eocene Langental Beds and the Lower Miocene alluvial sediments. b) Sketch section through the Lower Miocene sequence within the Langental.

Figure 7.32. Section through the top of the Lower Miocene sequence within the Langental, showing a deep vertical crack. Note that the crack is displaced (arrowed) at depth. The crack is infilled by red, iron-stained sands, and less common exotic clasts of agate, chalcedony and jasper. Note the coarsening upward nature of the sequence. The cobbles at the surface are possibly related to the deposition of the Blaubok gravel (see section 7.2.9). Scale 1 m.

recovered. The sequence of sediments closely resembles the fine-grained, arkosic horizons of the Grillental Beds, and as with the Grillental, the sequence coarsens upwards. No primary sedimentary structures are visible within the sandy horizons, but the ribbon-shaped geometry of the sediment body supports the earlier interpretation. A palaeocurrent direction from east to west is inferred by the recovery of Turritella sp. from the sediments during the early mining operations (Stromer, 1926), which indicate that the alluvial system reworked the Upper Eocene Langental Beds which lie to the east, up-slope of the deposit.

The large vertical cracks at the top of the sequence provide evidence for sub-aerial exposure and desiccation. The displacement of individual cracks along what appear to be shear planes, possibly resulted from lateral movement within the profile in response to alternate swelling and shrinkage during wetting and drying. The material infilling the cracks is interpreted as a combination of aeolian sand and surface wash from run-off. The exotic clasts of agate and chalcedony were probably derived from the reworking of Eocene marine deposits lying up-slope to the east.

The arkosic composition of the Lower Miocene alluvial sediments within the Langental, and their resemblance with the Grillental Beds suggests that both systems originated from a Klinghardt Mountain provenance. The relative lack of coarse sediment within the Langental possibly reflects a smaller catchment, or more simply means that coarse material was unavailable for input to the system.

7.2.8. THE KALKRÜCKEN SANDSTONE AND THE STRAUCHPFÜTZ CARBONATE

Introduction

A stratigraphically important sequence of sediments is preserved at the northern end of the Buntfeldschuh escarpment (Figure 7.33). A carbonate cemented red sandstone is interbedded with calcified, white, cross-bedded feldspathic grits. It is suggested that these sediments be termed the Kalkrücken sandstone, which is equivalent to the Kalksandsteine in Revierinnen of Beetz (1926). A unit comprised of interbedded clay and carbonate horizons, termed here the Strauchpfütz carbonate, which is closely associated with the Kalkrücken sandstone was previously identified as freshwater limestone by Beetz (1926).

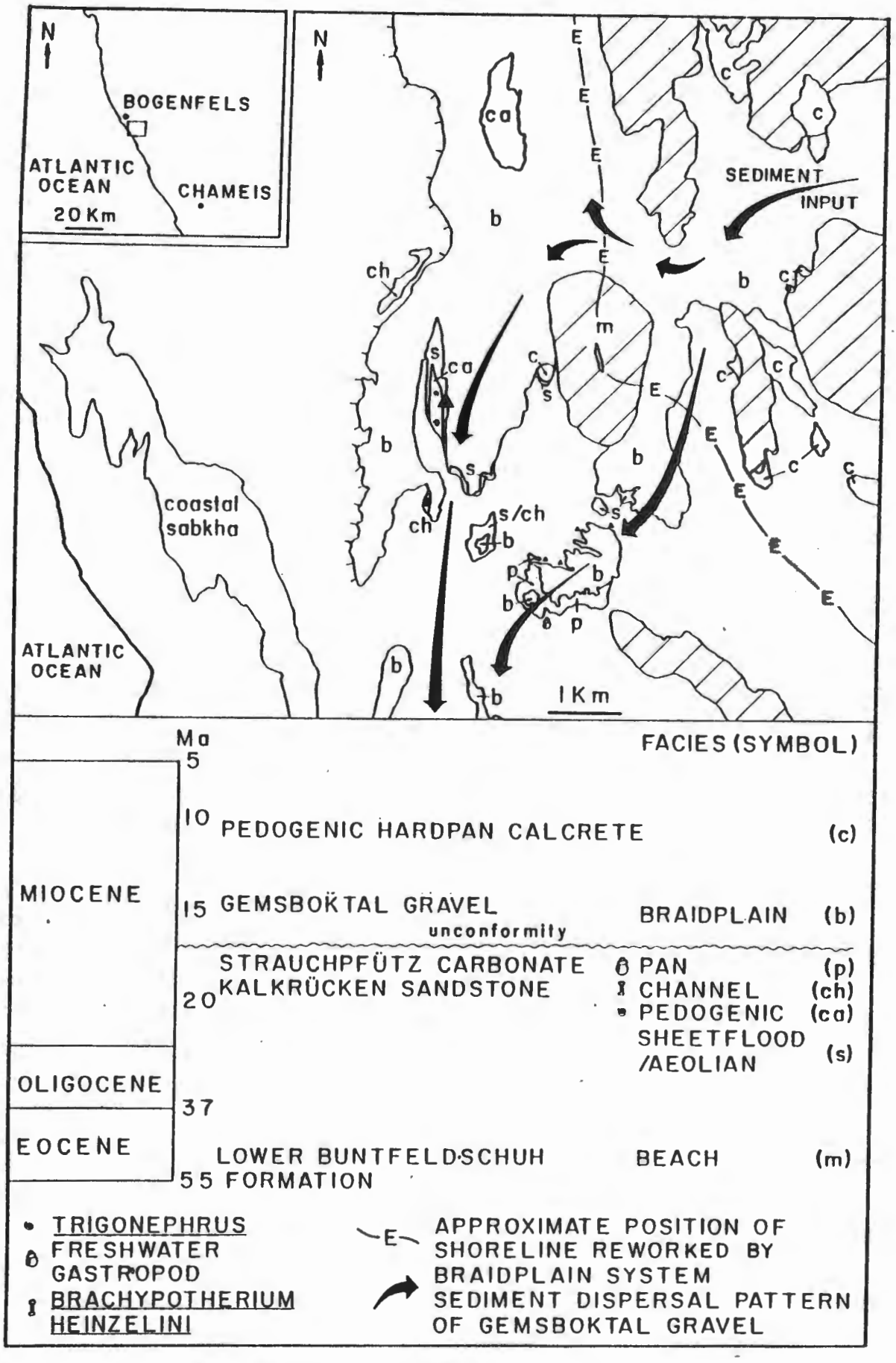

Figure 7.33. Map showing the distribution of the Kalkrücken sandstone, the Strauchpfütz carbonate, and the Gemsboktal gravels. (▲) denotes position of section in Fig. 7.34.

The Kalkrücken sandstone, as defined here, was previously divided into two stratigraphic units by geologists of the CDM (Pty) Ltd. The term Kalkrücken sandstone formerly referred solely to the basal red, carbonate cemented sandstone, and the white, cross-bedded, calcified arkosic grits were named the Glastal grits. Detailed examination during this study has shown that the two facies are interbedded, although the red sandstone eventually gives way to the calcified arkosic grits higher up in the sequence. The two units are thus probably better interpreted as differing facies of a coarsening upward sequence, which is ultimately overlain by a coarse deposit of cobbles and boulders termed the Gemsboktal gravels (Figure 7.34).

Description of the Kalkrücken sandstone

The Kalkrücken sandstone consists predominantly of red, well-sorted fine to medium quartz sand. In thin-section, the well-rounded grains are seen to be surrounded by a thin, iron-rich clay pellicle, and cemented by calcite.

The basal part of the sequence is dominated by sandstone, but the grain size varies widely. Angular quartz and feldspar granules occur along low-angle to sub-horizontal, laterally extensive bedding planes, in horizons a few centimetres thick. These gritty horizons become more common higher in the sequence. Occasional channel features, eroded into the underlying sandstone, contain fining-upward channel-fill sequences comprised of angular to well-rounded pebbles and cobbles. A nodular carbonate, which is probably of groundwater origin, cements a channel-fill sequence at one locality. Trough cross-bedding observed within the channel-fill deposits indicates that the palaeo-flow direction during the deposition of the lower part of the sequence was southerly to south westerly. This agrees with the direction indicated by the isolated exposures of cross-bedded, calcified, arkosic grit about 2 km due east of Bogenfels. These isolated exposures at the base of a small scarp slope marking the western edge of the Gemsboktal gravels closely resemble the channel facies of the Grillental Beds. Prior to erosion, they would also have formed part of a coarsening upward sequence.

Sedimentary structure is rarely observed within the sandstone. Large-scale, poorly preserved trough cross-bedding occurs at a

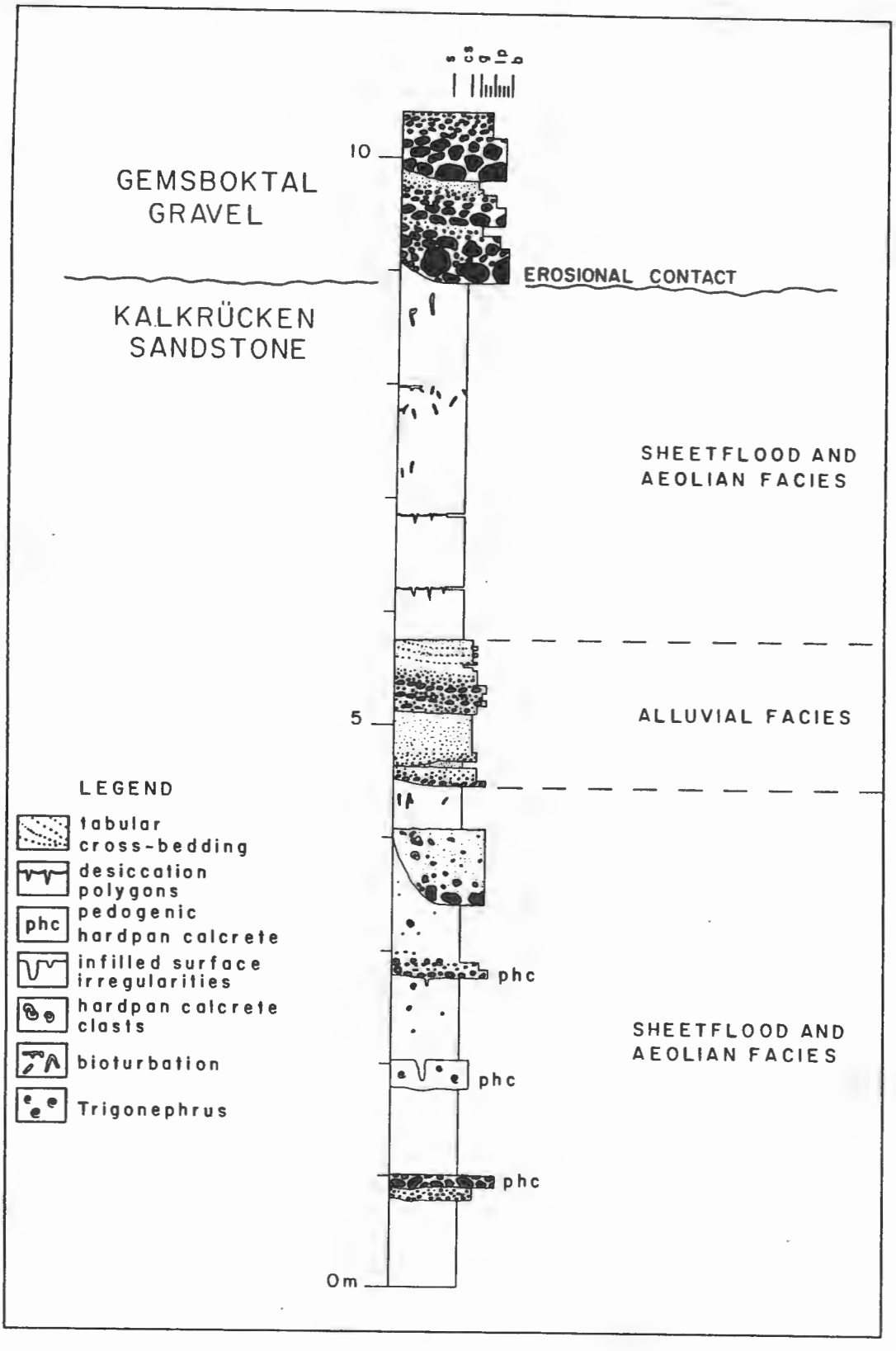

Figure 7.34. Sketch section summarizing the Kalkrücken sandstone succession, showing the position of the pedogenic calcrete profiles within the sequence. Location of section shown in Fig. 7.33.

locality north-northwest of the Strauchpfütz carbonate. The concave bottomsets dip gently northwards, up the palaeoslope. Thus the sands were deposited by a north flowing current system, in contrast to the coarse-grained channel-fill deposits, which were deposited by south and westerly flowing palaeocurrents down the palaeoslope.

Fawn coloured, sub-horizontal marl horizons, up to a few tens of centimetres thick, form lens-shaped bodies devoid of primary structure. Polygonal patterns of cracks commonly cross their upper surfaces, and the margins of individual polygonal blocks are curled upwards. The cracks taper with depth, and in many cases the spaces are infilled by red sandstone.

Erosion of the red, carbonate cemented sandstone separating stacked, laterally extensive pedogenic calcrete horizons has formed a stepped profile along the margins of the Glastal drainage tract. The better developed calcrete profiles are a few tens of centimetres thick. An immature hardpan calcrete commonly caps a nodular basal calcrete horizon formed in the red sandstone host.

Beetz (1926) located abundant Trigonephrus sp. shells cemented in the upper part of the more mature calcrete profiles (Figure 7.35), along with rare bone fragments. At the north eastern margin of the Strauchpfütz carbonate, preferentially calcified traces resembling the modern termitaria of Psammotermes and Hodotermes described by Coaton and Sheasby (1973, 1975) have weathered from the sandstone. Significantly, an in situ metatarsal III, tentatively identified by Hendey as being of Brachypotherium heinzelini (pers. comm. Schneider, 1982), was recovered from the Kalkrücken sandstone, beneath the contact with the overlying Gemsboktal gravel. This suggests that the sandstone was deposited between 17 to 20 Ma. Hendey considered that the sequence might be of about the same age as the alluvial sequence within the Langental, which he puts at about 17 Ma.

Interpretation

Although the nodular carbonate horizons within the channel-fill sequences are probably of groundwater origin, the calcretes containing Trigonephrus sp. are pedogenic. Netterberg (1969) and Goudie (1973) concluded that the present-day distribution of calcretes in Southern Africa coincides with Thornwaites semi-arid warm to arid warm climatic zone. Yaalon and Ward (1982) consider

Figure 7.35. Trigonephrus shells in a more mature pedogenic hardpan calcrete, which has been polished by aeolian processes. Southerly wind flow from bottom to top, scale 10 cm.

that the rainfall during the main pedogenic phase of calcrete development within the Central Namib was about 350 to 450 mm/year. The pedogenic calcrete horizons interbedded with the Kalkrücken sandstone thus indicate a semi-arid palaeoclimate during the deposition of the sandstone, when temperatures were probably warmer than today. The polished pavements of more mature calcrete containing Trigonephrus sp. compare favourably with modern examples of T. shell lags produced by the deflation of sandy surfaces in lightly vegetated areas of the Southern Namib. These semi-stabilized, present-day surfaces, are also sites of incipient soil formation under the present climate. Trigonephrus presently appears to be restricted to the winter rainfall areas of the Southern Namib. The apparent similarity between their palaeo-distribution and that of the present-day, is possibly palaeoclimatically significant. It implies that the rainfall pattern about 17 to 20 Ma resembled that of today.

Studies by Garvie (1983) for Anglo American Corp. of SA. Ltd. demonstrated that the quartz grains of the red carbonate sands exhibit surface textures representative of beach and aeolian depositional environments. Some evidence of fluvial features was also present.

The relatively coarse-grained, calcified, arkosic grits are interpreted as evidence for alluvial activity. They closely resemble the coarse-grained facies of the Grillental Beds, which suggests that they were also reworked from an older arkosic deposit within the Klinghardt Mountain area. This is supported by the presence of phonolite clasts within alluvial horizons. The increasing frequency of gritty, alluvial horizons, towards the top of the sequence is interpreted as evidence for an increase in the rainfall, which resulted in more widespread alluvial deposition.

Poorly preserved outcrops exhibiting large-scale trough cross-bedding indicate that large bedforms resembling dunes were actively migrating within an alluvial system in which bars were also present. Erosive channel margins within the sandstone dominated sequence are rare, and poorly sorted planar horizons of quartz and feldspar granules are more common. These horizons are interpreted as evidence for periodic surface run-off, resulting in sheet-like activity during the more major events. Ponding of the surface run-off led to the formation of mud drapes, as marls were

deposited from suspension within standing water bodies in shallow depressions. The polygonal patterns on the surface of marly horizons are interpreted as desiccation cracks which developed when the ponded water bodies dried out. These cracks were subsequently filled by aeolian sand or surface run-off events.

The scarcity of primary structure makes the interpretation of the sandstone difficult. The identification of crescentic bedforms, comprised of well-sorted and rounded sand grains, that migrated up the palaeoslope suggests that aeolian dunes are represented. The sub-horizontal, laterally extensive, gritty horizons interbedded with the sandstones become more common higher in the succession. Together with the evidence of ponded water bodies, this implies that alluvial systems gradually became dominant over the aeolian system with time. Due to the well-sorted and well-rounded nature of the sand grains comprising the sandstone, it is suggested that some of the alluvial material was derived from the reworking of an older aeolian sand body.

The presence of Lower Miocene vertebrates along the main fluvial channels, which are best interpreted as ephemeral stream systems operating under semi-arid conditions, suggests that this was a time of palaeoclimatic change. Sedimentological evidence demonstrates that although the palaeoclimate remained semi-arid, the depositional environment altered. The deposition of the aeolian Kakaoberg Sandstone Member of the Upper Buntfeldschuh Formation appears to have been terminated in response to ephemeral rainfall events becoming more frequent. The resulting increase in surface run-off would have allowed alluvial processes to rework the aeolian sand body, which might account for the deposition of some of the Kalkrücken sandstone. With continued palaeoclimatic change, headward erosion by the ephemeral stream systems appears to have reworked older arkosic alluvial sequences in the vicinity of the Klinghardt Mountains. The westward progradation of these alluvial systems resulted in the deposition of a coarsening upward sequence capped by arkosic grits.

Description of the Strauchpfütz Carbonate

The main exposure is about 5 m thick, and consists of a number of nested 1 to 2 m thick, off-white carbonate horizons with green and pink mottling, which are interbedded with olive green clays. The

carbonate horizons delineate an almost circular feature, with the margins dipping in towards the centre of a concave-up depression (Figure 7.33). At Eisenkiesselklippenbake, north east of the main exposure, a similar carbonate horizon forms a rim around the bedrock which defines the Upper Palaeocene to Lower Eocene marine embayment. This suggests that the main exposure was either more extensive or that other similar bodies existed in the area prior to erosion by later alluvial systems.

Neither the clay nor the carbonate horizons exhibit any primary sedimentary structure. Subtle variation between carbonate horizons due to changes in the quantity of sand grains present or differences in the shade and degree of mottling can be seen. Basal, gritty horizons along the north eastern margin of the main exposure contain rare exotic clasts of agate, jasper and chalcedony.

A 1 m deep trench on the southern side of the main exposure revealed that the olive green clays are being pervasively calcified. This results in the formation of pale green, calcified clay nodules surrounded by a partially altered halo. The density of the nodules increases with depth until a calcified horizon is formed. This possibly accounts for the lack of sedimentary structure and provides one mechanism whereby the nested series of saucer-shaped carbonate horizons might have formed. The incorporation of carbonate clasts in the Gemsboktal gravel (see section 7.2.9), however, proves that present-day diagenesis does not entirely account for the development of the carbonate horizons.

The only fossil material found to date was located by Ward in 1986 under an overhang on the southern side of the exposure. This consisted of a solitary gastropod shell (Figure 7.36) which is probably a freshwater type.

Interpretation

Erosion of the surrounding sediment has left nested carbonate horizons dipping towards the centre of a circular depression, as defined by their inclined margins. The fine-grained sediments infilling the depression are most likely to have been deposited from suspension in a large ponded water body, at the distal end of an ephemeral alluvial system. The preservation of Kalkrücken sandstone along the north-eastern margin of the main exposure suggests that the deposition of the two deposits was possibly

contemporaneous. The Kalkrücken sandstone is believed to be at least partially of aeolian origin. Within the present-day Namib, the interaction of aeolian and coarse-grained alluvial systems is seen at Sossusvlei (Figure 7.37). This area possibly provides a modern analogue for the deposition of the Strauchpfütz carbonate.

Gritty horizons containing exotic clasts of agate and chalcedony at the base of the Strauchpfütz carbonate demonstrate that initially, alluvial processes reworked the Upper Palaeocene to Lower Eocene marine shoreline which once existed at about 160 masl. The higher carbonate horizons do not contain exotic clasts, and coarse clastics are absent. It is therefore suggested that the water body later became more distally located within the alluvial system. The increase in ephemeral activity indicated by calcified arkosic grits capping the Kalkrücken sandstone, later led to the rejuvenation of the alluvial system, and the deposition of the very coarse-grained Gemsboktal gravels, which completely covered the Strauchpfütz carbonate.

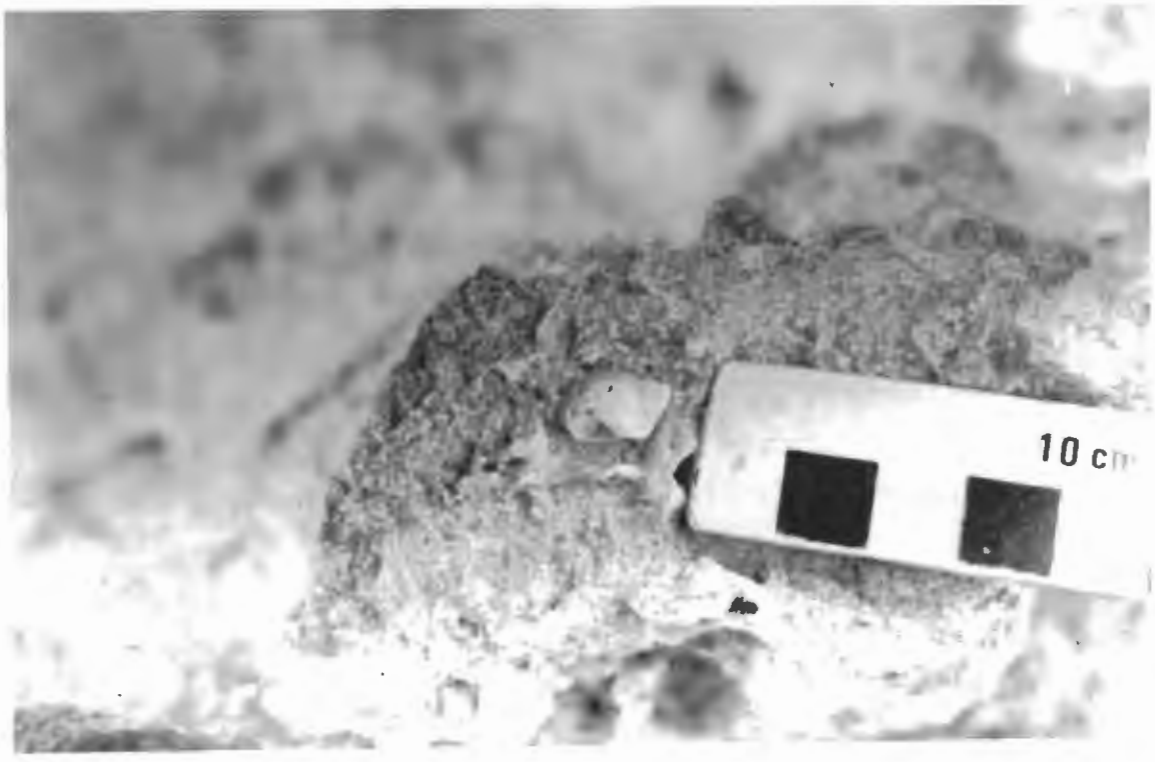

Figure 7.36. A shell, probably of a freshwater gastropod, in the Strauchpfütz carbonate. Photo by J.D. Ward.

Figure 7.37. Aerial view of Sossusvlei. Note the large pan area in the foreground at the distal end of the drainage tract. This type of environment is seen as a possible modern analogue for the Strauchpfütz carbonate. Photo by J.D. Ward.

7.2.9. BLAUBOK AND GEMSBOKTAL GRAVELS

Distribution and Stratigraphic Relationships

Both the Kalkrücken sandstone and the Strauchpfütz carbonate are unconformably overlain by the Gemsboktal gravel (equivalent to the post-Eocene "young river gravels" of Beetz, 1926). The Gemsboktal gravel forms an extensive, gently undulating sheet-like body within the Bogenfels area (Figure 7.38). A similar coarse-grained gravel overlies the Grillental Beds. The clast assemblage in the Bogenfels area is dominated by quartz, quartzite, silcrete and phonolite. Boulders and cobbles of phonolite are a distinctive feature at both localities, and serve to differentiate the Gemsboktal gravels from the Blaubok gravels (equivalent to the pre-Eocene "quartzite river gravels" of Beetz, 1926), in which phonolite clasts are either absent or comparatively rare. In the vicinity of the Strauchpfütz carbonate exposure, the Gemsboktal gravel also contains clasts eroded from the carbonate, together with clasts of calcrete from the Kalkrücken sandstone.

The quartz dominated Blaubok gravels were previously considered to pre-date the Upper Eocene Langental Beds that are preserved within the Bogenfels area (Stocken, 1978). Examination of the field relationships of these two lithostratigraphic units throughout the area suggest that this is unlikely to be the case. The Upper Eocene shoreline cannot be traced laterally for any distance before it is distorted by isolated remnants of Blaubok gravel. When traced up-slope, exotic clasts of agate, chalcedony and jasper within the Eocene marine deposits stop abruptly where the contact with Blaubok gravels is intersected. This implies that the gravels probably post-date the Upper Eocene deposits. The excavation of pits is planned to test the relationship more thoroughly. Isolated remnants of a similar quartz gravel, capping hills between Bakers Bay and Chameis strongly suggest that the distribution of the Blaubok gravels was once far more extensive than previously believed.

Description

Primary sedimentary structures are not readily observed in either the Blaubok or Gemsboktal gravels. Sections through the Gemsboktal gravel shows that the deposit is about 3 to 5 m thick. The gravels are generally crudely stratified. Planar cross-bedding indicates that transport was approximately towards the south and west, which

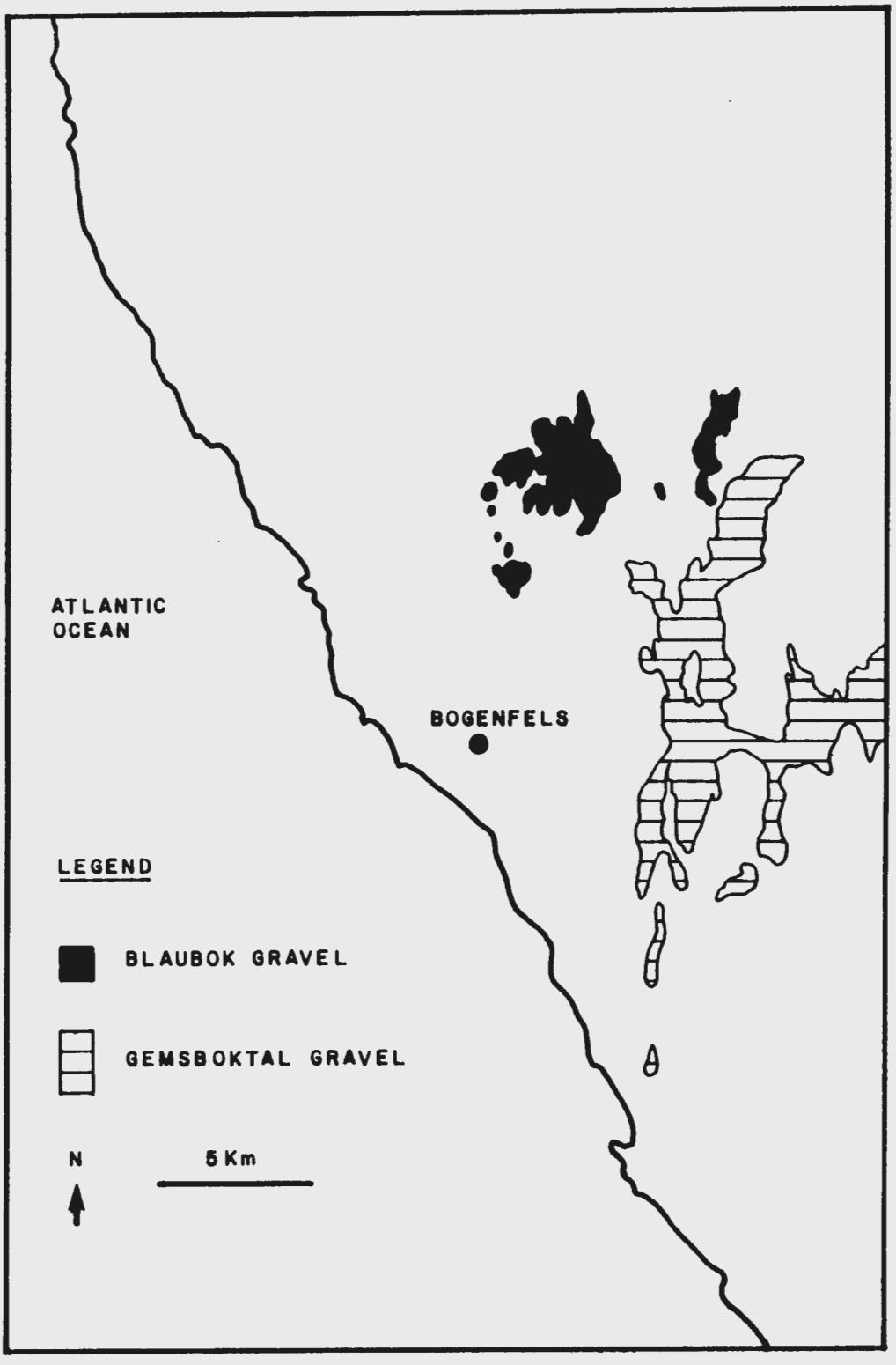

Figure 7.38. Map showing the distribution of the Blaubok and Gemsboktal gravels.

is confirmed by the orientation of imbricate clasts.

Little fossil material has been recovered from either of the gravels. The internal mould of a gastropod shell resembling Trigonephrus sp. was located in the Gemsboktal gravel by Ward in 1987. Clasts of silicified wood have been recovered principally from the Blaubok gravel, but some have previously been located within the Gemsboktal gravel by other geologists. Samples of the wood have been identified as angiosperms by Scholtz (pers. comm., 1988). Scholtz suggests that on this basis, the woods are younger than the mid-Cretaceous, and probably date from the Late Cretaceous to Early Tertiary. More recently, Shaw (pers. comm., 1988) located a number of fragmented tree trunks on the surface of the Blaubok gravel. The largest trunk represents a tree which was probably at least 20 m high, and about 1 m in diameter. Interestingly, borings, presumably by insects, have also been preserved in some of the specimens. The size and preservation of the trunks suggests that they have undergone minimal transport by the alluvial system.

The contact between the Gemsboktal gravel and the Kalkrücken sandstone can be observed near Eisenkieselklippenbake. Both deposits are cemented by a mature pedogenic hardpan calcrete. A few kilometres to the north, the Blaubok gravels are also cemented by the same calcrete. Traced laterally, there is no doubt that this is equivalent to the calcrete horizon which caps the Kakaoberg Sandstone Member of the Upper Buntfeldschuh Formation and the Rooilepel sandstone.

Interpretation

Beetz (1926) originally interpreted the Blaubok gravel as an alluvial fan which prograded from the Klinghardt Mountains under arid conditions. He considered that these gravels were subsequently partially eroded and incorporated into the alluvial system represented by the Gemsboktal gravels. Stocken (1978) also concluded that both the Blaubok and Gemsboktal gravels were deposited by sheetflood activity under arid conditions.

The absence of obvious channel margins and the crude stratification of the laterally extensive, relatively thin gravel bodies supports Beetz's interpretation. Calcretes within the Kalkrücken sandstone beneath the Gemsboktal gravel, and the mature pedogenic hardpan calcrete cementing both of the gravels, supports

the interpretation that the alluvial fans were deposited under semi-arid palaeoclimatic conditions.

Phonolite bearing gravels closely resembling the Gemsboktal gravel also occur within Grillental, where they occupy a similar stratigraphic position, above the Lower Miocene Grillental Beds. A regional pattern of alluvial sedimentation is therefore recognised, with channelised Lower Miocene alluvial sediments containing a vertebrate fauna being overlain by coarse-grained alluvial braidplain deposits. As the alluvial braidplains prograded across the region, the underlying Lower Miocene sediments together with the Upper Palaeocene to Upper Eocene shorelines were partially reworked and the material was incorporated into the systems.

The incorporation of Kalkrücken sandstone clasts in the Gemsboktal gravel suggests that a time break separated the deposition of the two sequences. Consequently, the contact of the Gemsboktal and Blaubok gravels with the underlying Lower Miocene alluvial sequences is considered to be erosional. The difference in the style of sedimentation supports this conclusion, because the coarseness of the gravel sequences increases markedly across the contact. The current system that deposited the regional alluvial braidplains represented by the Blaubok and Gemsboktal gravels, was therefore much larger than those responsible for the deposition of the channelised alluvial deposits underlying them. This implies that the rainfall became less sporadic, and that major surface run-off was more frequent, even though the palaeoclimate remained semi-arid.

The most westerly occurrence of the Gemsboktal gravel is located on a bedrock pedestal 20 to 30 masl., about 1 km inland of the present coastline. The presence of quartzite and phonolite boulders at this point suggests the location of a reasonably proximal position within the braidplain system. Examination of Orange River flood deposits shows that comparatively little coarse bedload material presently reaches the coast. Most of the cobble and boulder gravel is deposited considerable distances upstream. If the Lower to Middle Miocene coastline had been close to that of today it seems probable that the alluvial system would also have deposited the coarse bedload further east. The presence of boulders at the present-day coast thus implies that the shoreline was

further west when the Gemsboktal gravel was deposited. The maximum age of the Gemsboktal gravel is about 17 Ma, based upon the age of the Kalkrücken sandstone beneath it. A lateral equivalent of the mature pedogenic calcrete cementing the Gemsboktal gravel overlies the Chalcedon Tafelberg monchiquite. This body has been radiometrically dated at 15 Ma., which is probably the minimum age because weathered material is likely to have been dated. Despite this, it confines the age of both the Blaubok and the Gemsboktal alluvial braidplain sequences to a period when sea-level was rising after the major Oligocene regression.

The Kamberg Calcrete Formation appears to occupy a similar position within the lithostratigraphic framework of the Central Namib (Ward, 1984, 1987). It has been suggested by Ward (1984, 1987) and Ward and Corbett (in press) that correlation between this calcrete, and the regionally extensive hardpan pedogenic calcrete within the Southern Namib is possible. Yaalon and Ward (1982) concluded that rainfall in the order of 350 to 450 mm/yr prevailed during the development of the Kamberg Calcrete Formation, which far exceeds the rainfall experienced by the coastal tract of the Southern Namib today. The frequency of sporadic rainfall therefore appears to have decreased again at about the time Siesser (1978) considers that the Benguela Current became fully established. Conceivably, this sets the minimum age for the mature pedogenic hardpan calcrete within the Southern Namib to between 10 to 12 Ma, during the early late-Miocene.

7.2.10. FISKUS SANDSTONE BEDS

Introduction

Greenman (1966, 1969) originally interpreted the aeolian Fiskus Sandstone Beds as a member of the Lower Miocene Elizabeth Bay Formation (SACS, 1980). Stocken interpreted the Miocene pan carbonate rim about 6 km south of Kolmanskop to be mature pedogenic hardpan calcrete overlying the Fiskus Sandstone. This was taken as proof of a Miocene age for the aeolian sand body.

Greenman (1969) suggested that the "aeolian" sandstone at Wüstenkönig in the western part of the Grillental was possibly estuarine. Stocken (1978), however, envisaged it to be an aeolian sequence damming the Lower Miocene drainage tract, which subsequently developed into a lacustrinal environment, in which

travertines were deposited.

The characteristics of the Fiskus Sandstone Beds will first be described and interpreted prior to the presentation of evidence for revision of the age of the sand body.

Distribution

The main exposures of the red to brown coarse-grained sandstone comprising the Fiskus Sandstone Beds occur along the eastern margin of the Fiskus Pan some 6 km south of Kolmanskop, about 10 km east of Luderitz (Figure 7.39). The sandstone also crops out along the northern and eastern margin of Elizabeth Bay, where it underlies an extensive aeolian sand sheet. It can also be seen beneath the present-day Namib Sand Sea (Sossus Sand Formation, SACS, 1980).

Isolated exposures of cross-bedded sandstone resembling the Fiskus Sandstone Beds have also been located south of Bogenfels during this study, along the sidewall of an ephemeral stream near Frohe Hoffnüng (Lat. 27°33'S; Long. 15°33'30"E). Recent excavations into the Bogenfels sand sheet uncovered a similar cross-bedded sandstone (Shaw, pers. comm., 1988). This suggests that the areal distribution of the Fiskus Sandstone Beds is much greater than previously envisaged. Unfortunately, the poor preservation potential of the sandstone once exposed, means that better resolution of its distribution will be difficult to achieve. At both Fiskus Pan and Elizabeth Bay, the Fiskus Sandstone Beds overlie palaeontologically dated Lower Miocene alluvial sequences. It therefore represents a much younger phase of aeolian sedimentation than the Kakaoberg Sandstone Member and the Rooilepel sandstone.

Description

The presence of exotic, well-rounded granules of agate, chalcedony and jasper form a very distinctive component of the sandstone. In thin-section, sand grains are surrounded by an iron-rich clay pellicle. The degree of cementation by calcite varies considerably. In some areas the sandstone is not cemented at all.

At both of the main localities, the Fiskus Sandstone Beds exhibit well-preserved large-scale tabular-planar bottomsets. In plan, arcuate, grouped, trough cross-bedded sets are visible, with

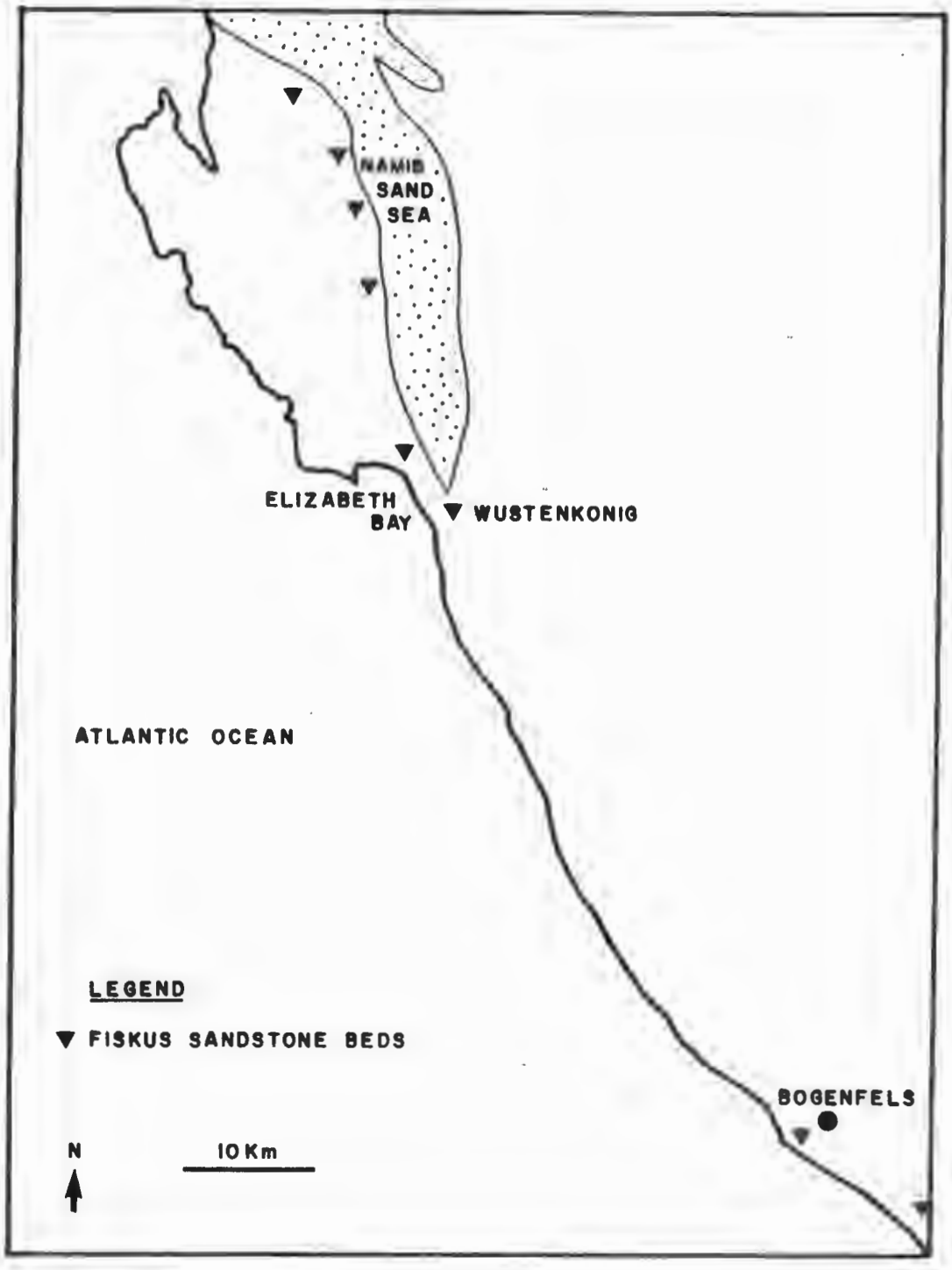

Figure 7.39. Map showing the distribution of the Fiskus Sandstone Beds.

individual sets 70 m or more in breadth (Figure 7.40). Within the bottomsets, exotic granules of agate, chalcedony and jasper comprise grainflow deposits (sensu Hunter, 1977) forming arcuate wedges between finer-grained grainfall cross-strata (Figure 7.41). At the Fiskus Pan, tabular-planar cross-bedded sandstone is both underlain and overlain by sub-horizontal, planar surfaces dominated by 1 to 2 cm thick lens-shaped concentrations of granules a few tens of centimetres long (Figure 7.42).

Body fossils have not yet been recovered from the Fiskus Sandstone Beds. In situ eggshell fragments from Kolmanskop exhibit the typical pit structure of Struthio sp. (ostich) reported by Sauer (1966). On average the shells are about 2.3 mm thick (Figure 7.43). These specimens differ from Rooilepel specimens, and from those recovered in situ from an aeolian sandstone cropping out at Schmidtfeld, to the north of Luderitz. As discussed above, this indicates that more than one aeolian sand body is represented in the Luderitz area.

Trace fossils are common within the Fiskus Sandstone Beds. Small back-filled burrows about 1 cm in diameter closely resemble the traces of present-day dune dwelling beetles such as the tenebrionid beetles Onymacris sp. and Lepidochora sp. (Ward, pers. comm., 1987). Evidence of termite activity is widespread, with examples resembling the present-day dwellings of both Hodotermes and Psammotermes (eg. Coaton and Sheasby, 1973,1975) present (Figure 7.44). Of particular interest are ellipsoidal back-filled burrow systems about 2 to 6 cm in diameter (Figure 7.45). These traces typically follow a meandering path across sub-horizontal sandstone surfaces. Ward (pers. comm., 1987) identified these traces as those of the golden mole (Eremetalpa granti namibensis). The faunal assemblage represented by trace fossils thus indicates that dune dwelling organisms, similar to those found today, were present during the deposition of this sand body.

Interpretation

Applying the criteria of Kocurek and Dott (1981, Fig. 14), individual grainflow cross-strata from 4 to 6 cm thick within the Fiskus Sandstone Beds are indicative of aeolian dune forms in excess of 20 m high. The measurement of cross-bedding dip attitudes confirms that the sandstone was deposited by a southerly wind

Figure 7.40. Very large sets of tabular-planar cross-bedding about 70 m in breadth exhibited by the Fiskus Sandstone Beds near Kolmanskop. Southerly quadrant palaeowind blew from left to right.

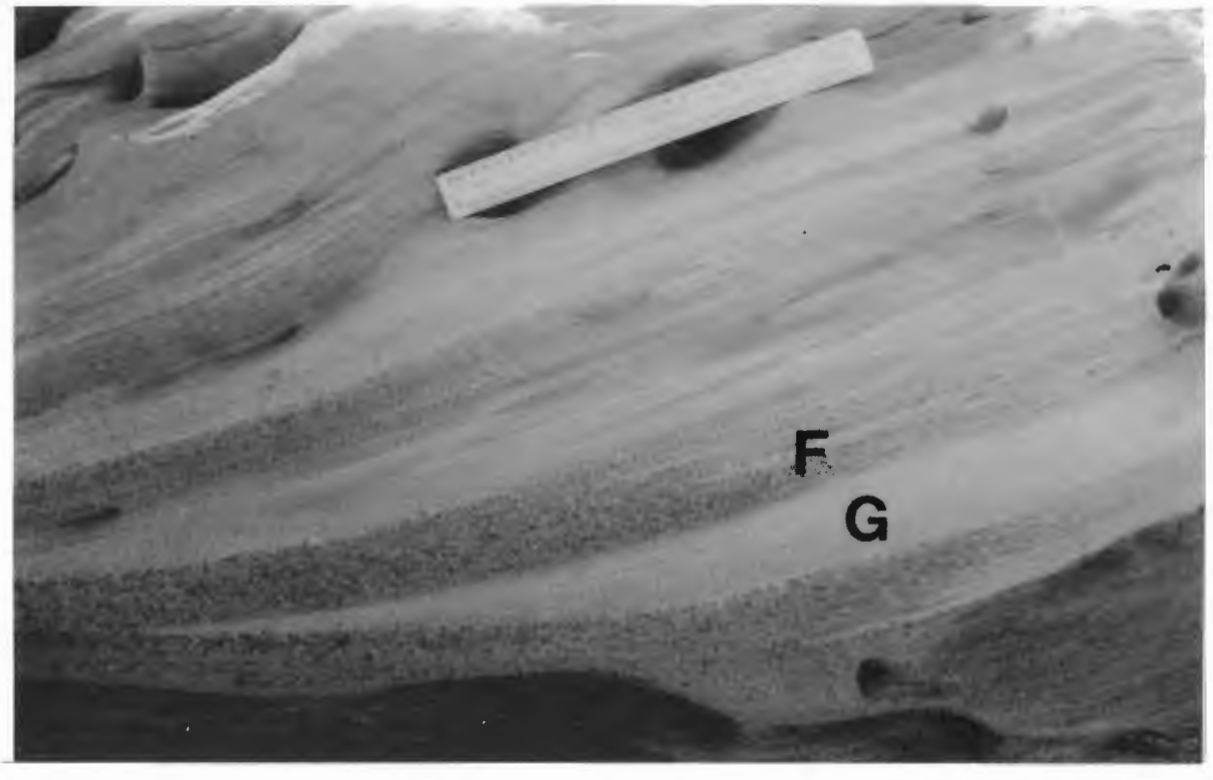

Figure 7.41. Grainflow strata (F), composed of granules and very coarse sand, within large aeolian toesets of the Fiskus Sandstone Beds. Fine-grained grainfall strata (G) separate the grainflow strata. Southerly quadrant palaeowind blew from right to left. Scale in cm.

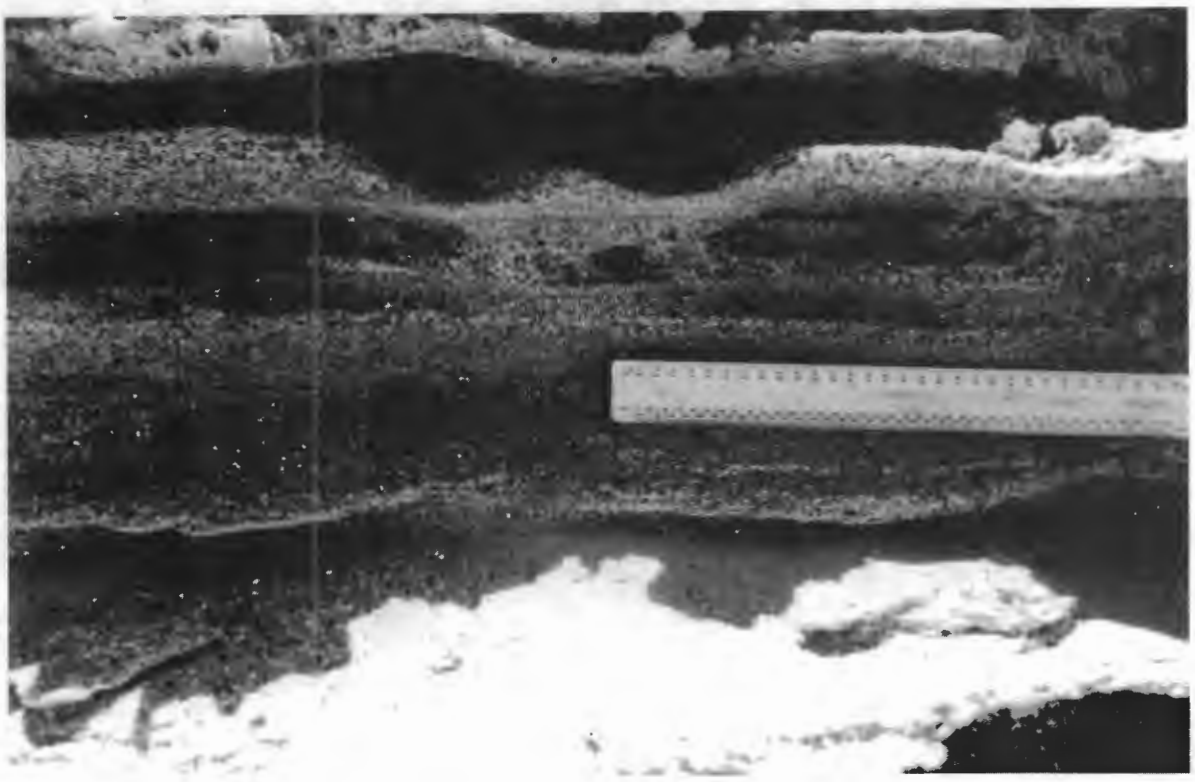

Figure 7.42. Lens-shaped concentrations of granules within the Fiskus Sandstone Beds, at the Fiskus Pan, which were probably deposited by granule ripples. Southerly wind flow from right to left, scale 30 cm long.

Figure 7.43. Struthio sp. (ostrich) eggshell fragments from the Fiskus Sandstone Beds at Kolmanskop. Scale 11.5 cm.

Figure 7.44. A termitaria, resembling that of Hodotermes, in the foreground, with tabular-planar cross-bedded Fiskus Sandstone Beds in the background. Note the coarse granule ripples surrounding the termitaria, which are composed of granules weathered from the Fiskus Sandstone Beds. This material is currently being transported to the north by creep. The southerly wind blows from left to right. Scale 10 cm. long.

regime comparable with that of today (Figure 7.46). According to Hunter (1977), tabular-planar grainflow cross-strata indicate the migration of transverse aeolian dune forms. This interpretation of the dune forms responsible for the deposition of the Fiskus Sandstone Beds is supported by the concave, crescentic plan-form of the bottomsets.

The sub-horizontal, lensoid accumulations of granules underlying the tabular-planar cross-bedded sandstone probably represent sheet deposition. The structures closely resemble those seen within the sand sheet at Elizabeth Bay formed by aeolian transport of the Fiskus Sandstone Beds weathering products (see Figure 4.51).

Within the present Namib Sand Sea, transverse dune forms are restricted to the coastal zone influenced by the high-energy southerly surface-wind regime. By inference, the exposures of the Fiskus Sandstone Beds described above were probably deposited in a similar position within a palaeo-erg. The sand sheet deposition at the base of the aeolian sequence is interpreted as evidence of fore-erg deposition (sensu Porter, 1986, 1988) prior to the build-up of the main sand body.

The Age of the Fiskus Sandstone Beds

The evidence presented above indicates that the aeolian sandstones preserved in the vicinity of Luderitz are stratigraphically more complex than was previously realised. The examination of the white, sub-horizontal carbonate rim along the eastern margin of the Kolmanskop valley supports this view. Thin-section and X-ray diffraction examination of the mature pedogenic hardpan calcrete show that it is composed of clastic grains in a calcite cement. Samples from the carbonate rim at Kolmanskop analysed by X-ray diffraction (Ward, pers. comm. CDM, 1983) show that while calcite is the dominant constituent, dolomite is also present, as confirmed by analyses made during this study (Table 7.5). Thin-sections of specimens from the carbonate rim do not exhibit the "floating texture", which is typically exhibited by clastic grains in calcrete.

Figure 7.45. Meandering trace crossing a sub-horizontal surface of Fiskus Sandstone Beds, which resembles that of the present-day dune dwelling golden mole.

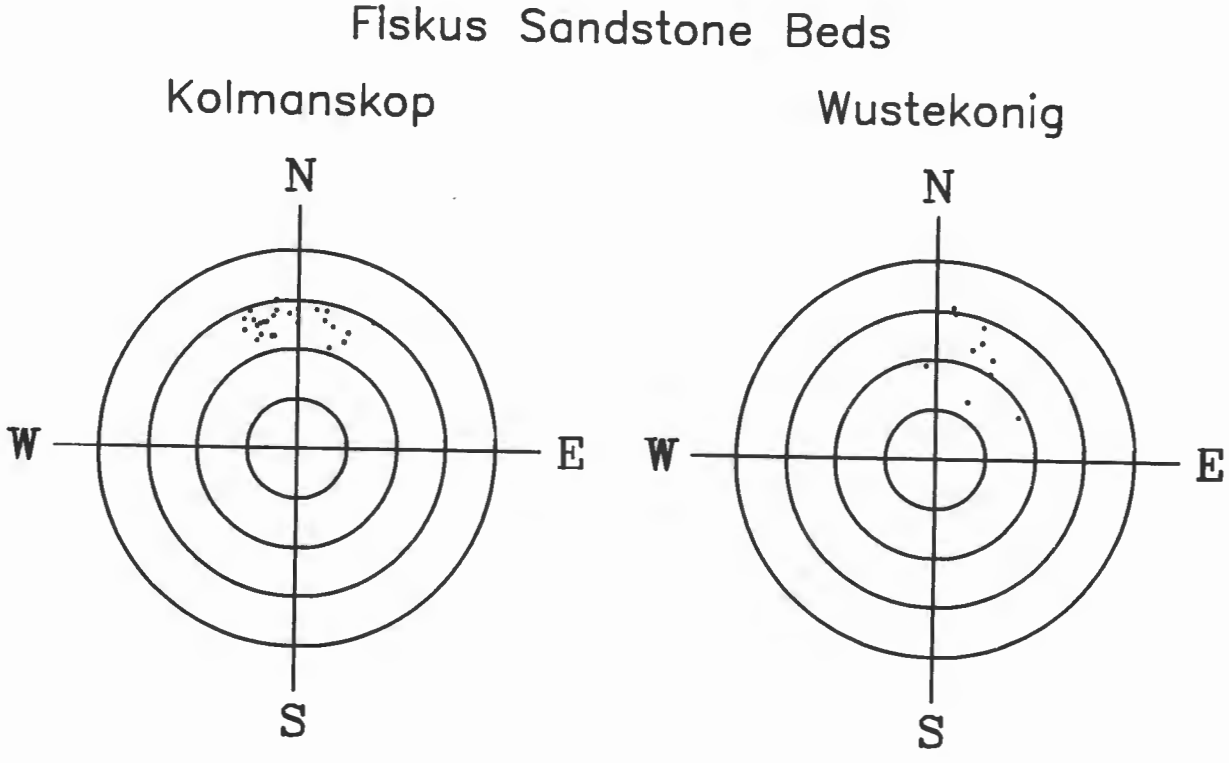

Figure 7.46. Polar plot of cross-bedding dip azimuths showing that the Fiskus Sandstone Beds were deposited by a southerly palaeowind regime.

Table 7.5. XRD analyses of samples from the carbonate forming a resistant rim around the top of the eastern side of the Fiskus Pan depression.

LOCALITY	MINERALOGICAL CONSTITUENTS (in decreasing order of abundance)
(1) Rim carbonate at the top of the eastern margin of Fiskus Pan depression	calcite quartz chlorite
(2) Gritty unit beneath the carbonate rim	quartz calcite dolomite plagioclase feldspar mica

The presence of dolomite suggests that the deposit is likely to represent a pan environment. To some extent this is supported by the impression that the rim feature was once part of an extensive sheet covering the present Kolmanskop valley in which the Fiskus Pan is currently situated. The presence of back-filled burrows in the thin carbonate horizons cropping out beneath the main rim is also inconsistent with its interpretation as a calcrete. A Lower Miocene alluvial sequence is exposed along the eastern side of the present-day Fiskus Pan, at the base of the depression. During the late seventies, Corvinus recovered a number of in situ bone fragments from the carbonate horizons beneath the main carbonate rim. This indicates that the Lower Miocene alluvial sequence probably infilled the entire Kolmanskop valley. The carbonate rim is interpreted as representing the top of this sequence.

At the base of the Fiskus Sandstone Beds, aeolian sediments overlie and are interbedded with red, poorly stratified horizons of pebble gravel composed of locally derived, gneissic weathering products from surrounding topographic highs. Carbonate clasts derived from the erosion of the Miocene pan carbonate are also present. The poorly sorted, crudely stratified, matrix-supported horizons appear to represent sheet-like units a few tens of centimetres thick. They cannot be traced laterally due to poor exposure, and may be restricted to localized input points. Towards the contact with the overlying aeolian sequence, polygonal carbonate features are visible on bedding planes. X-ray diffraction

analyses show that dolomite is the major constituent of the carbonate.

The matrix-supported, poorly sorted sediments are typical of present-day deposits formed by alluvial slope processes. Dolomitic, polygonal features are interpreted as evidence of periodic desiccation of ponded water bodies. The association of these sediments with aeolian horizons almost certainly indicates the existence of palaeo-stone pavements within the sequence.

The incorporation of Miocene pan carbonate clasts, in the basal part of the Fiskus Sandstone Beds, which is interpreted as a mixed aeolian and sheetflood facies, is significant. It proves that the aeolian sandstone post-dates the deposition of the Miocene pan carbonate. Its stratigraphic correlation with the Lower Miocene Grillental Beds is therefore incorrect.

Sediment input to the transverse dune system represented by the Fiskus Sandstone Beds at Elizabeth Bay could only have occurred during a regression, when the shoreline would have been further west. Offshore evidence for a westward shift of the Benguela Current during the late Miocene to early Pliocene has been interpreted as indication of a brief regression (Siesser and Rogers, 1976). This event probably coincided with the rapid expansion of the Antarctic ice sheet between about 4.7 and 4.3 Ma (Shackleton and Kennet, 1975, cited by Siesser and Dingle, 1981). It is postulated that the deposition of the Fiskus Sandstone Beds commenced at about this time. The contact of the Fiskus Sandstone Beds with the underlying Lower Miocene alluvial deposits is therefore considered to be unconformable. Field evidence indicates that the Miocene pan carbonate formed part of the Miocene alluvial sequence, which probably infilled the entire Kolmanskop valley. A period of erosion, which preceeded the deposition of the Fiskus Sandstone Beds, is believed to have partially re-exhumed the depression in which the Lower Miocene alluvial sequence was deposited. This depression was then infilled during the development of the palaeo-erg represented by the Fiskus Sandstone Beds. Subsequent erosion has probably removed much of the Fiskus Sandstone Beds, and re-exhumed the valley once more. The exposures of the Fiskus Sandstone Beds along the valley walls are therefore interpreted as being a thin veneer, which drapes the valley sides (Figure 7.47). This conclusion can be confirmed only if drilling is

undertaken at a future date.

Greenman (1966) originally assigned the Fiskus Sandstone Beds (equivalent to his Fiskus Beds) to the Lower Miocene on the assumption that they are interbedded with the alluvial Lower Miocene Grillental Beds. This view was supported by Stocken (1978) who suggested that exposures at Wüstenkönig, at the western end of the Grillental, represent an early Miocene dune dam complex. Fieldwork during this study has failed to prove that Lower Miocene alluvial sediments are interbedded with the aeolian sandstone. The significance of the cross-bedded sandstone capped by travertine at Wüstenkönig (Figure 7.48), between 25 to 30 masl has therefore been re-assessed.

Along the eastern end of the south-facing scarp slope at Wüstenkönig red, locally derived, poorly sorted and crudely stratified sediments are interbedded with pale green cross-bedded sandstone horizons (Figure 7.49). Further west, the scarp is entirely composed of fine- to coarse-grained, pale green sandstone. In north-south sections, sandy bottomsets dipping predominantly towards the north are interbedded with parallel laminated sub-horizontal to gently dipping units (Figure 7.50). In plan view, the bottomsets define large-scale, sinuous, concave sets, with a breadth of about 10 m (Figure 7.51). The upper surfaces of cross-bedded, tabular-planar grouped sets, are mostly planed sub-horizontal. Sandstone exhibiting low-angle lamination, and containing distinctive soft-sediment deformation structures (Figure 7.52), separates tabular-planar cross-bedded units. The entire sequence is overlain by red sandstones resembling the Fiskus Sandstone Beds, and capped by travertine.

Greenman (1969) interpreted the pale green sandstones as an estuarine deposit. Failure to locate evidence of interbedded Lower Miocene Grillental Beds indicate that this is incorrect. The structures within the pale green cross-bedded sandstone at Wüstenkönig closely resemble Stoke's surfaces associated with soft-sediment deformation in the tidally flooded, coastal dunefield at Guerrero Negro, Mexico, described by Fryberger, Schenk and Krystinik (1988). The cross-bedded sandstone horizons at Wüstenkönig are therefore interpreted as the foresets of transverse aeolian dunes which have been truncated by Stoke's surfaces. The soft-sediment deformation structures, which are commonly overlain

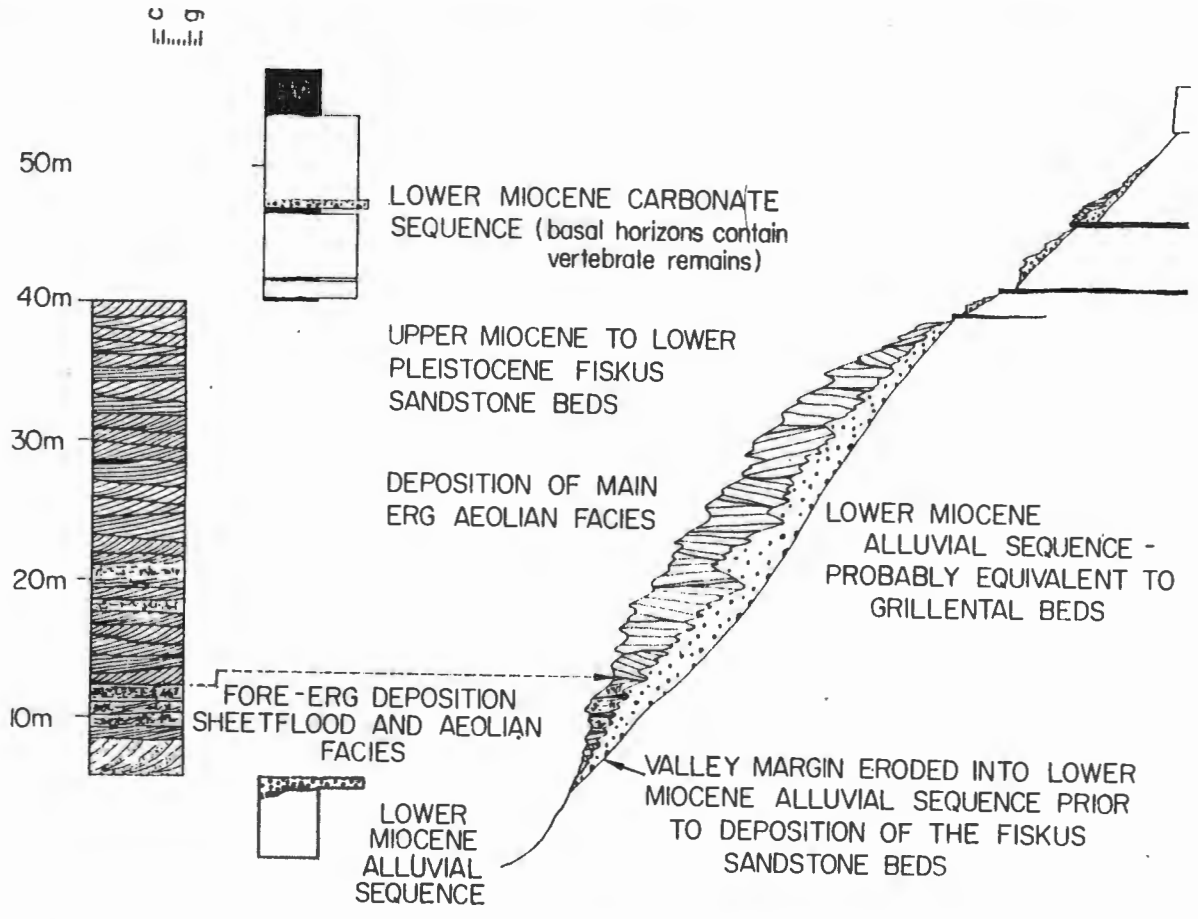

Figure 7.47. Sketch section through the Fiskus Pan illustrating the suggested relationship between the Fiskus Sandstone Beds and the Lower Miocene alluvial sequence.

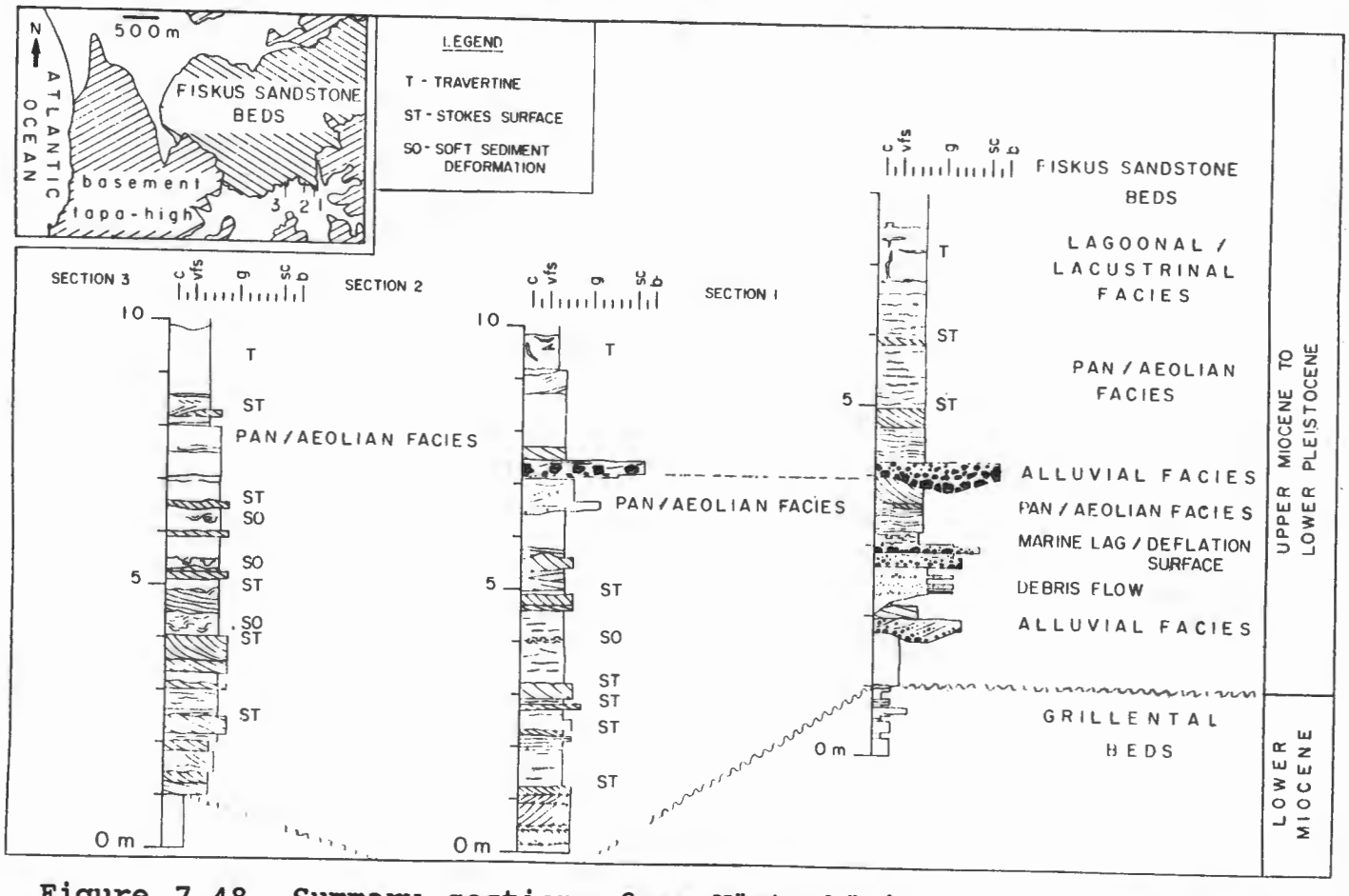

Figure 7.48. Summary sections from Wüstenkönig showing east-west variation along the south-facing scarp slope.

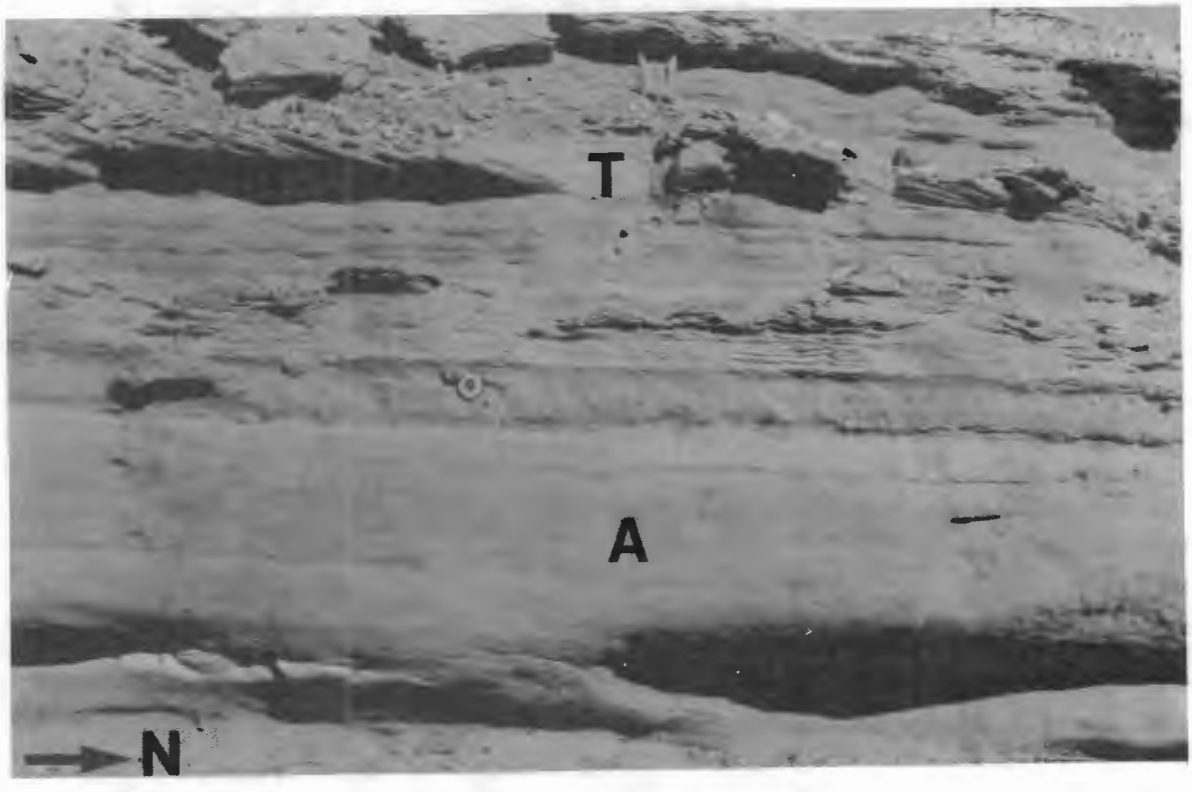

Figure 7.49. Section at the eastern end of the Wüstenkönig scarp slope, showing alluvial sediments (A) interbedded with tabular-planar cross-bedded sandstones (T), and low-angle strata. Circular tape 9 cm diameter.

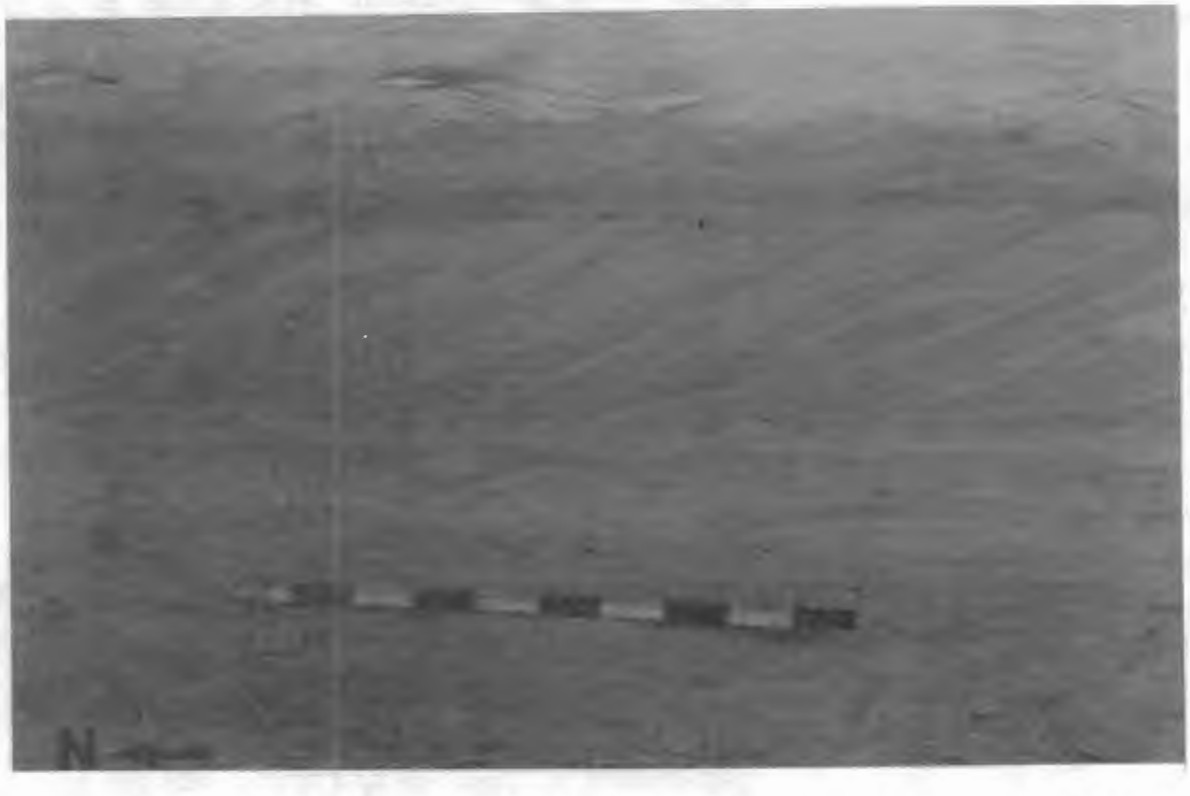

Figure 7.50. Section west of that in Fig. 7.49. Sub-horizontally truncated tabular-planar cross-bedded horizons of grainfall and grainflow cross-strata composed of fine to medium sands are interbedded with units dominated by low-angle strata. Note the soft-sediment deformation structures. Scale is 1 m.

Figure 7.51. Plan view of tabular-planar cross-bedded sets of sandstone, showing the crescentic form of the foresets, which are about 10 to 15 m in breadth. Southerly wind flow is from right to left, scale in centre of frame is 1 m.

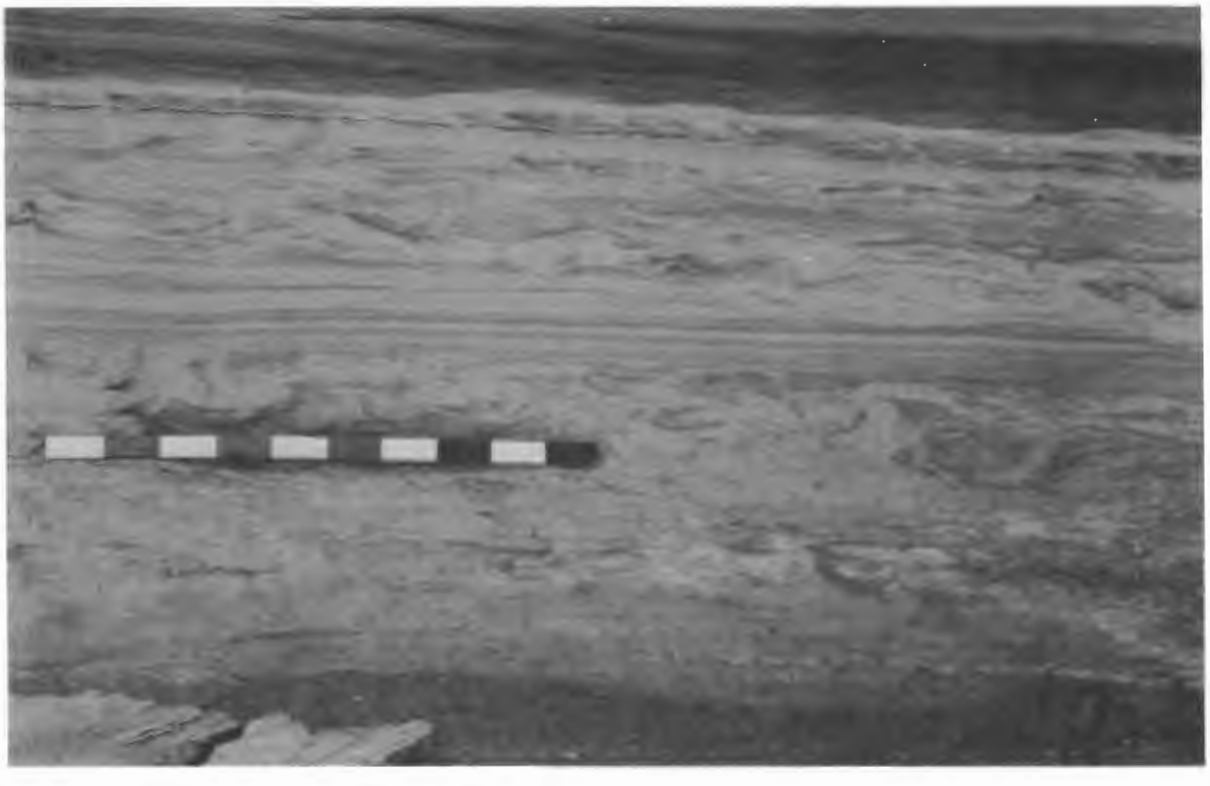

Figure 7.52. Close-up of soft-sediment deformation exhibited by the fine to medium sand units at the western end of the scarp slope. Note that the upper unit displaying soft-sediment deformation is overlain by toesets of tabular-planar cross-bedded foresets which dip to the right (north). Scale 1 m.

by undeformed aeolian bottomsets, probably resulted from pressure loading of tidally flooded sediments by migrating transverse dunes. Modern analogues for the sediments at Wüstenkönig are present within the Southern Namib today, where endoreic basins have been transgressed by the Atlantic Ocean. Beach deflation from the resulting log-spiral or south-facing embayments lead to the development of transverse aeolian dunes in the backshore area. These dunes subsequently migrate across a periodically flooded pan environment (Figure 7.53).

The red, poorly sorted, matrix supported sediments at the eastern end of the scarp are interpreted as a small alluvial fan prograding westwards across the pan margin. The travertine interbedded with the pan sediments at the top of the sequence forms extensive sheets which are overlain by aeolian sands containing granules of agate and chalcedony characteristic of the Fiskus Sandstone Beds. Polygonal features formed by fragmented travertine, on sub-horizontal bedding plane surfaces (Figure 7.54), are similar to examples described by Kocurek and Hunter (1986). These features resemble overthrusting tepees described by Kendall and Warren (1988) from the strandline of an ephemeral lake in the Coorong, South Australia. The travertine at Wüstenkönig probably either formed within a saline, backshore lagoonal environment, or alternatively, formed by evaporation after storm surge and upwelling across coastally situated deflation flats. The latter process has been observed by Handford et al. (1983, 1984, cited by Kendall and Warren, 1987).

It is concluded that the Wüstenkönig sequence was deposited during a transgression. The sequence is tentatively correlated with with the marine Plio-Pleistocene 30 m Complex at Hondeklip Bay, described by Pether (1986). This can be confirmed only if Donax rogersi is located in the Wüstenkönig sequence. At the present time, no body fossils have been found. If this interpretation is proved correct, scattered agate gravels situated 40 masl. at Torbogenbucht (Lat. 27°24'40"S; Long. 15°24' 40"E), recorded by Beetz (1926), may provide further evidence of Plio-Pleistocene transgressive elevations within the Sperrgebiet. Coupled with the Rooikop Gravels, near Walvis Bay (Miller and Seely, 1976; SACS, 1980; Ward, 1987), this implies that Plio-Pleistocene transgressive deposits at elevations exceeding 40 masl., were once present along

Figure 7.53. Oblique aerial view showing compound barchan dunes propagated at a south-facing embayment migrating across a backshore pan environment which is periodically flooded by high tides. This is thought to be a modern analogue for the sequence of the Fiskus Sandstone Beds exposed at Wüstekönig.

the entire west coast. The validity of the crustal warping theory invoked to explain apparent differences in the elevation of the "F" Beach at CDM, and the transgressive elevations between Alexander Bay and CDM generally is thus brought into question.

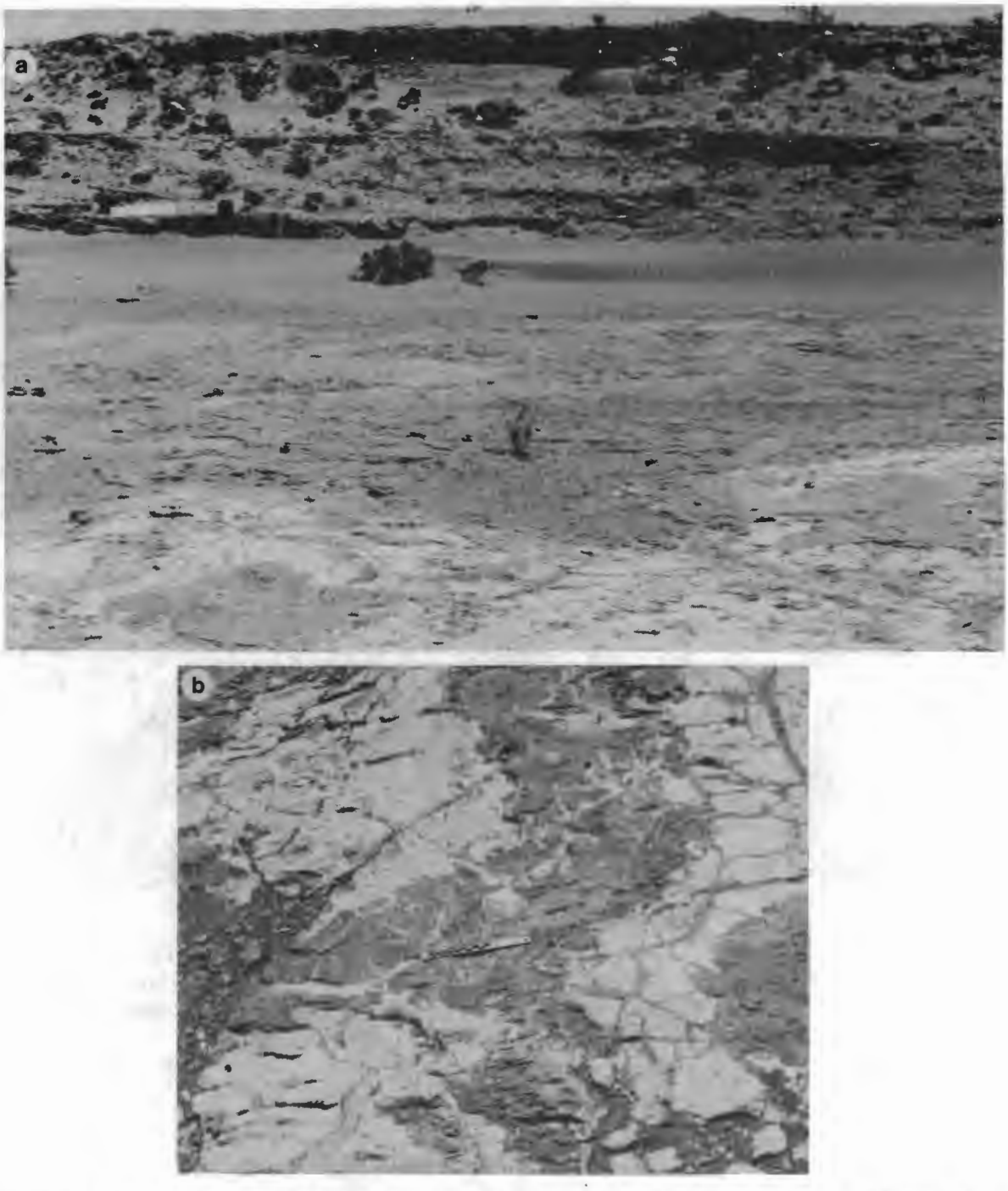

Figure 7.54. a) Aeolian dune toesets of the tidally flooded pan facies overlying a sub-horizontal surface covered by polygonal overthrust tepees of fragmented travertine. Southerly wind from left to right, white scale bar 1 m. b) Fragmented travertine overthrust tepee with fractures infilled by sand. Similar features are formed by halite crusts along the strandline of the present-day coastal sabkhas within the Southern Namib. Graduated scale 10 cm.

7.2.11. ANNENTAL SANDSTONE

The best exposures of this pale yellow, cross-bedded, poorly cemented fine- to medium-grained sandstone occur in the vicinity of Unverhoft (Lat. 27°26'45"S; Long. 15°24'E) (see Figure 7.56), south of Luderitz, within an ancient ephemeral stream course. More commonly, exposures consist of isolated remnants preserved within deep, east-west oriented coastal gulleys. The most southerly remnants occur along the coast to the west of Pomona.

The internal structure of the cross-bedded sandstone at Unverhoft is indicative of deposition by transverse aeolian dune forms. Grainfall lamination within toesets preserved in gullies represent the initial stages of palaeo-erg development when bedrock depressions were infilled. Pebbles and cobbles of angular bedrock occasionally lie on bedding planes within the sandstone. The angular bedrock clasts represent minor rock falls, which released weathered bedrock fragments onto dune surfaces.

The Annental sandstone represents the youngest extension of the Namib Sand Sea (Sossus Sand Formation) and was probably deposited during the last glacial maximum c.18 000 to 20 000 years ago, which was a time of global aeolian sand body expansion (eg. Sarnthein and Diester-Haas, 1977).

7.2.12. SUMMARY OF STRATIGRAPHIC FRAMEWORK

The revised lithostratigraphic framework for the Cenozoic sediments preserved within the Southern Namib deflation basin is shown in Figure 7.55. The palaeoenvironmental implications of the information discussed above are outlined in section 7.3.

7.2.13. SUMMARY OF EVIDENCE FOR PALAEO-ERG DEVELOPMENT AND ITS RELATIONSHIP TO SEA-LEVEL

Exposures of aeolian sequences of various ages are widely distributed to the north of the Orange River throughout the Southern Namib (Figure 7.56a). Their preservation is generally poor to the south of the Grillental, with the exception of the Buntfeldschuh and Rooilepel localities, where an extensive calcrete capping provides partial protection. Within the deflation basin, the poorly cemented aeolian sandstones have little chance of survival once exposed, but remnants occur locally within steep-walled gullies which run east-west. Preservation within

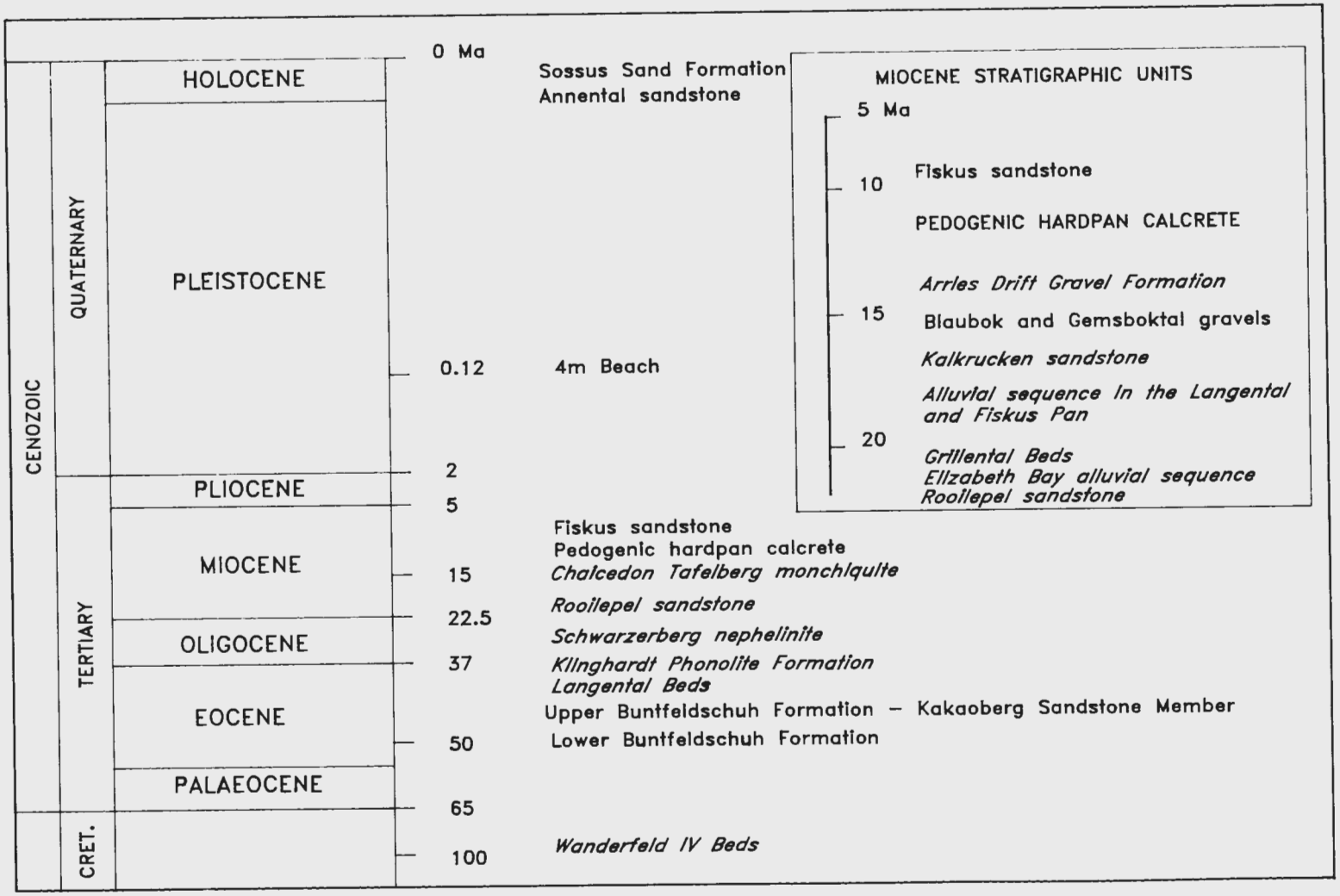

Figure 7.55. Summary of the lithostratigraphic framework for the Southern Namib deflation basin.

pre-existing bedrock depressions improves to the north of the Grillental as the margin of the present-day Namib Sand Sea is approached. This is probably a function of the variable sand cover afforded to earlier sand bodies by the expansion and contraction of palaeo-ergs across the area.

Based upon the broadly defined time constraints provided by the stratigraphic framework, it has been possible to examine the approximate relationship between phases of palaeo-erg development and sea-level movement along the west coast during the Cenozoic (Figure 7.56b). As described above, all of the aeolian sand bodies appear to indicate phases of palaeo-erg expansion.

Deposition of the initial phase of aeolian activity represented by the Kakaoberg Sandstone Member, is now known to have commenced during, or shortly after, the deposition of a regressive marine sequence. Provided that the inferred age of the marine Lower Buntfeldschuh Formation is correct, aeolian activity therefore occurred before the deposition of the marine Langental Beds during the Upper Eocene.

On the basis of fossils recovered from the base of the aeolian sand body represented by the Rooilepel sandstone, this palaeo-erg had developed by the Lower Miocene, or possibly even earlier in the Upper Oligocene. Based upon the available evidence, it is suggested that this sand body was active when the shoreline was situated west of its present position. This might have coincided with the start of the major Oligocene regression documented by Siesser and Dingle (1981) or, as is more likely, towards the end of this event when sea-level was rising.

The deposition of the Fiskus Sandstone Beds occurred after the full development of the Benguela Current, and is likely to have commenced at an as yet undetermined point during the Late Miocene to Early Pliocene regression. Based upon the facies represented at Wüstenkönig, the development of this sand body continued through the Late Pliocene into the Early Pleistocene. The recognition of a mixed tidally influenced pan and aeolian facies at about 25 masl indicates that this sand body was influenced by the series of Pliocene to Early Pleistocene transgressions.

The most recent evidence of palaeo-erg expansion is provided by the Annental sandstone. This phase of palaeo-erg expansion is likely to correlate with the global expansion of aeolian sand

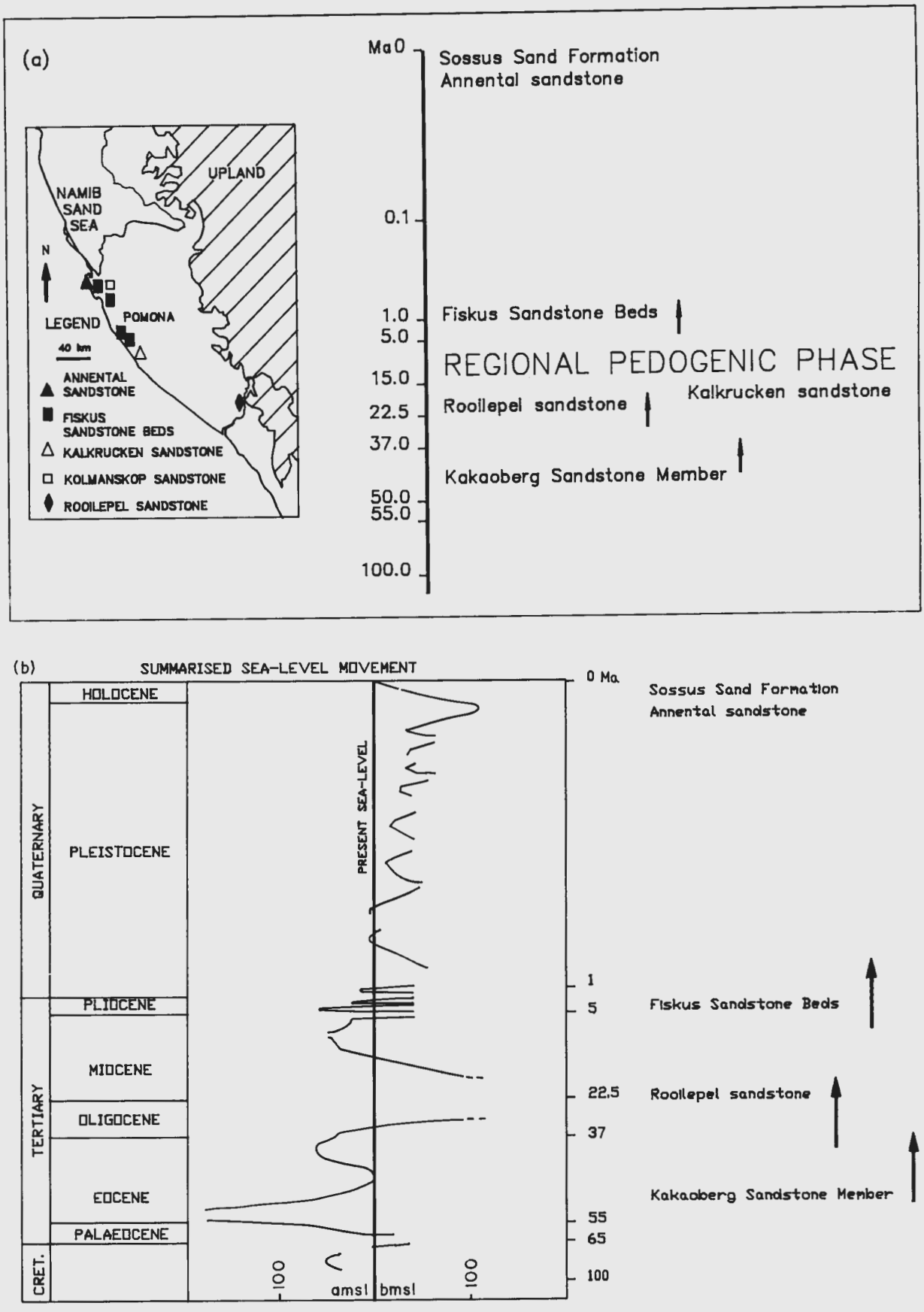

7.56. a) Map summarising the distribution of palaeo-dune systems within the Southern Namib. b) Approximate correlation of the palaeo-erg systems represented within the Southern Namib with sea-level movement influencing the west coast. Sea-level curve based upon field relationships determined during this study, and Siesser and Dingle (1981), Tankard et al. (1982) and De Decker (1986).

bodies during the regression which accompanied the last glacial maximum, between 18 000 and 20 000 BP.

Direct evidence for the distribution of ancient aeolian sand bodies within the Southern Namib suggests that phases of aeolian system expansion are a feature of regressions. As discussed below, however, there are circumstances under which expansion might occur during a transgression. This is presently a difficult point to prove, and could be established only if the sand bodies are comprehensively dated and their distribution mapped on a regional-scale.

7.3. PALAEOENVIRONMENTAL CONDITIONS IN THE SOUTHERN NAMIB

7.3.1. INTRODUCTION

Palaeoclimatic variation within the Southern Namib has influenced the nature of the sediment dispersal systems that have contributed to the development of the deflation basin and the sediments that it contains. The nature of the Cenozoic palaeoclimates influencing the west coast of southern Africa is a controversial topic (eg. Ward, Seely and Lancaster, 1983). The timing of the initial onset of aridity within the region is central to the problem. Van Zinderen Bakker (1975) believes that aridity could have existed along the west coast since the Early Oligocene, approximately 35 My. ago, when the temperature of high-southern-latitude bottom water dropped markedly (Shackleton and Kennett, 1975), and the northward movement of cold Antarctic water became possible. On the basis of microfossil abundances and sedimentation rates in deep sea sediment cores Siesser (1977), however, has postulated that the Benguela Current only became fully established about 10 My. ago. Two contrasting theories have consequently evolved regarding the antiquity of the Namib:

1) Based on lithostratigraphic evidence, Ward et al. (1983) and Ward (1984, 1987) have reasoned that arid conditions have prevailed within the Namib for much of the Tertiary and through to the present-day;
2) The opposing view, expressed by Endrody-Younga (1981) and Tankard and Rogers (1978), is that the Namib is a comparatively young Plio-Pleistocene feature. This view has

been supported by Partridge (1985), who claims that the Tertiary Tsondab Sandstone Formation rests upon a mid-Miocene planation surface.

Both Siesser, and Tankard and Rogers, used the presence of Lower to early Middle Miocene vertebrate remains within the Southern Namib to support their conclusions. These remains were recovered from widely distributed alluvial sequences of varying age within the deflation basin (Figure 7.57). Those located in Elizabeth Bay, Kolmanskop and the Grillental being the oldest according to Stromer (1926) and Hamilton (pers. comm. to Stocken 1977). The faunal assemblage includes hares and artyodactylid ruminants. It was the presence of Myohyrax cf. oswaldi, which also occurs within early Miocene sediments of northern Egypt, which led Stromer (1926) to conclude that the palaeoclimate was wet. The recovery of the frog (anuren) Xenopus stromerei appeared to confirm this conclusion, and the concept of savanna or grassland conditions in the Namib during the Miocene was formulated. The recovery of a vertebrate assemblage (dated at 17,2 to 14 Ma by Pickford, 1987) from Arries Drift by Corvinus and Hendey (1978), interpreted as evidence of an extensive, wooded grassland habitat (Hendey, 1978), has been used as further support by advocates of a wet Miocene and relatively youthful Namib. Stocken (1978) considered that this assemblage was more readily explained as a riparian community.

Ward et al. (1983) show that the Namib is an unusual desert biome. The present-day deflation basin is no exception. Animals which do not usually inhabit hyper-arid areas are found. A troop of Chacma babboons (Papio ursinus), inhabiting the Klinghardt Mountains, regularly visit the Buntfeldschuh escarpment to drink at a freshwater seepage. Their preservation as fossils in this environment in the rock record would be difficult to interpret. Hares in the fossil assemblage were used as evidence supporting the existence of savannah conditions during the early Miocene. Personal observation, however, shows that the Cape hare (Lepus capensis), presently occurs throughout the deflation basin, from the Atlantic coast into the Klinghardt Mountains. Even the recovery of frog remains identified as Xenopus stromeri (Stromer, 1926) is not necessarily conclusive proof that the Grillental drainage tract was part of a perennial system (Channing, pers. comm, 1988). Channing (1976) records the presence of Xenopus laevis in permanent pools

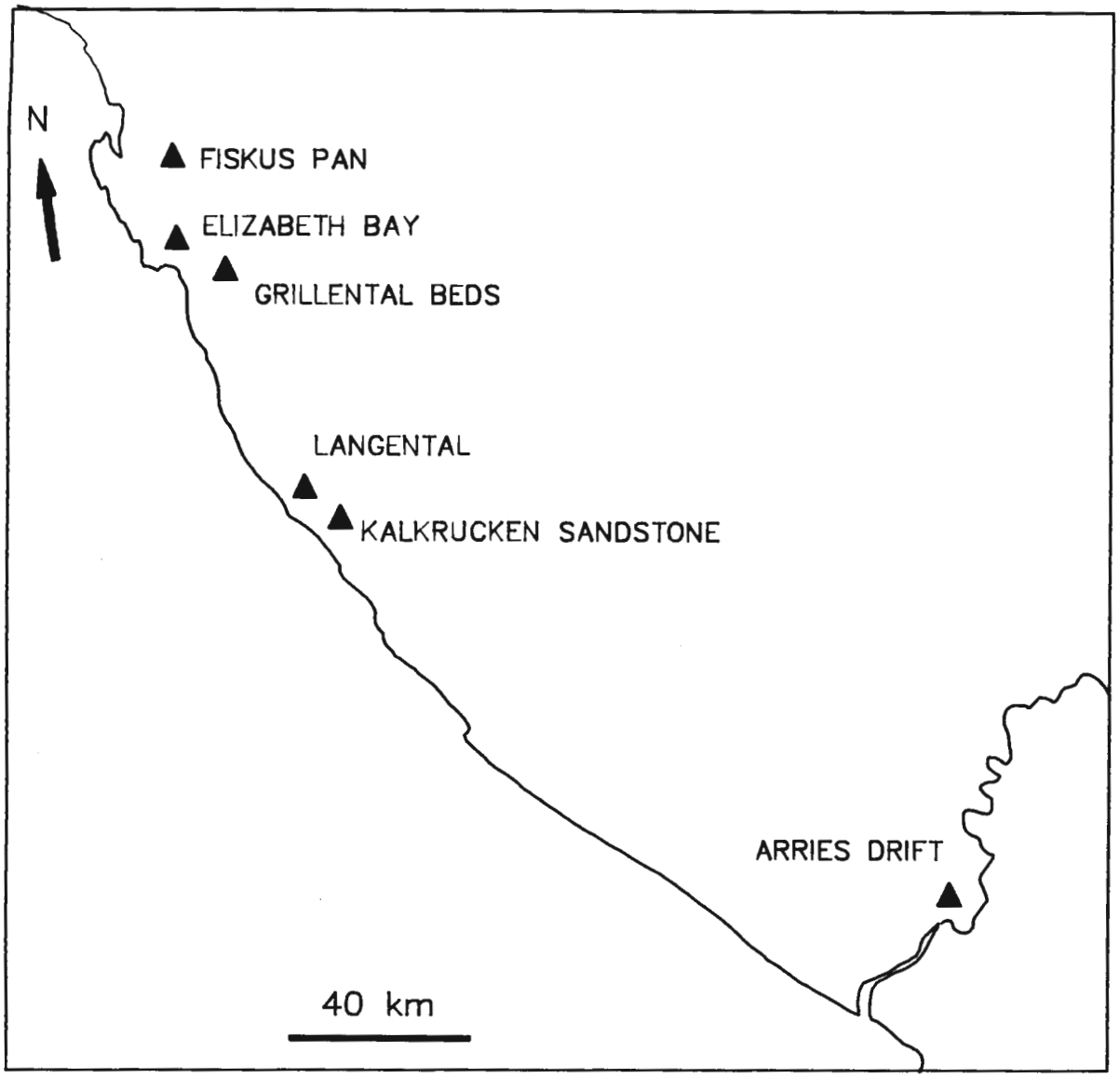

Figure 7.57. Map showing the distribution of the Lower to Middle Miocene localities to the north of the Orange River, where alluvial sequences containing vertebrate remains occur within the Southern Namib.

within the present-day Kuiseb Canyon. He considers it probable that ephemeral floods carry adults and larvae downstream to temporary pools west of their permanent range, where survival for some months prior to the desiccation of ponded water bodies is possible. A breeding population in such an environment is capable of creating an unrealistically large death assemblage of frogs which would have excellent preservation potential (Channing, pers. comm., 1988).

Examined in isolation, the faunal assemblages recovered from the early Miocene deposits could be interpreted as evidence of less arid palaeoclimatic conditions. In many instances a similar conclusion might be drawn if today's faunal assemblages were examined out of context of the depositional environment.

7.3.2. SUMMARY OF PALAEOCLIMATIC CONDITIONS WITHIN THE SOUTHERN NAMIB DURING THE CENOZOIC

The reinterpretation of lithostratigraphic units within the Southern Namib, together with the examination of their regional relationships, allows clearly defined phases in the deflation basin's development to be identified (Figure 7.58). A Lower to Middle Miocene alluvial phase of sedimentation is identified, which is sandwiched between two periods dominated by aeolian sedimentation.

Partridge (1985) has questioned the possibility that the Tsondab Sandstone Formation within the Central Namib could represent Early Tertiary aeolian activity on geomorphological grounds. He believes that the aeolian Tsondab Sandstone Formation rests upon the Mid-Miocene Post-African 1 surface (sensu Partridge and Maud, 1987). Facies analysis of dated exposures prove that aeolian activity occurred within the Southern Namib prior to 10 to 12 My. ago. The Grillental Beds and the Rooilepel sandstone provide the earliest palaeontologically dated evidence of aeolian activity, but the nature of the Kalkrücken sandstone, which is older than 17 My., is more significant. Reinterpretation of this sandstone body indicates that the Kakaoberg Sandstone Member of the Upper Buntfeldschuh Formation probably acted as the provenance for much of the alluvially deposited material at the base of the sequence, which supports the inferred Lower to Middle Eocene age for the ancient aeolian sand body. This early phase of aeolian sedimentation is believed to correlate with the Tsondab Sandstone

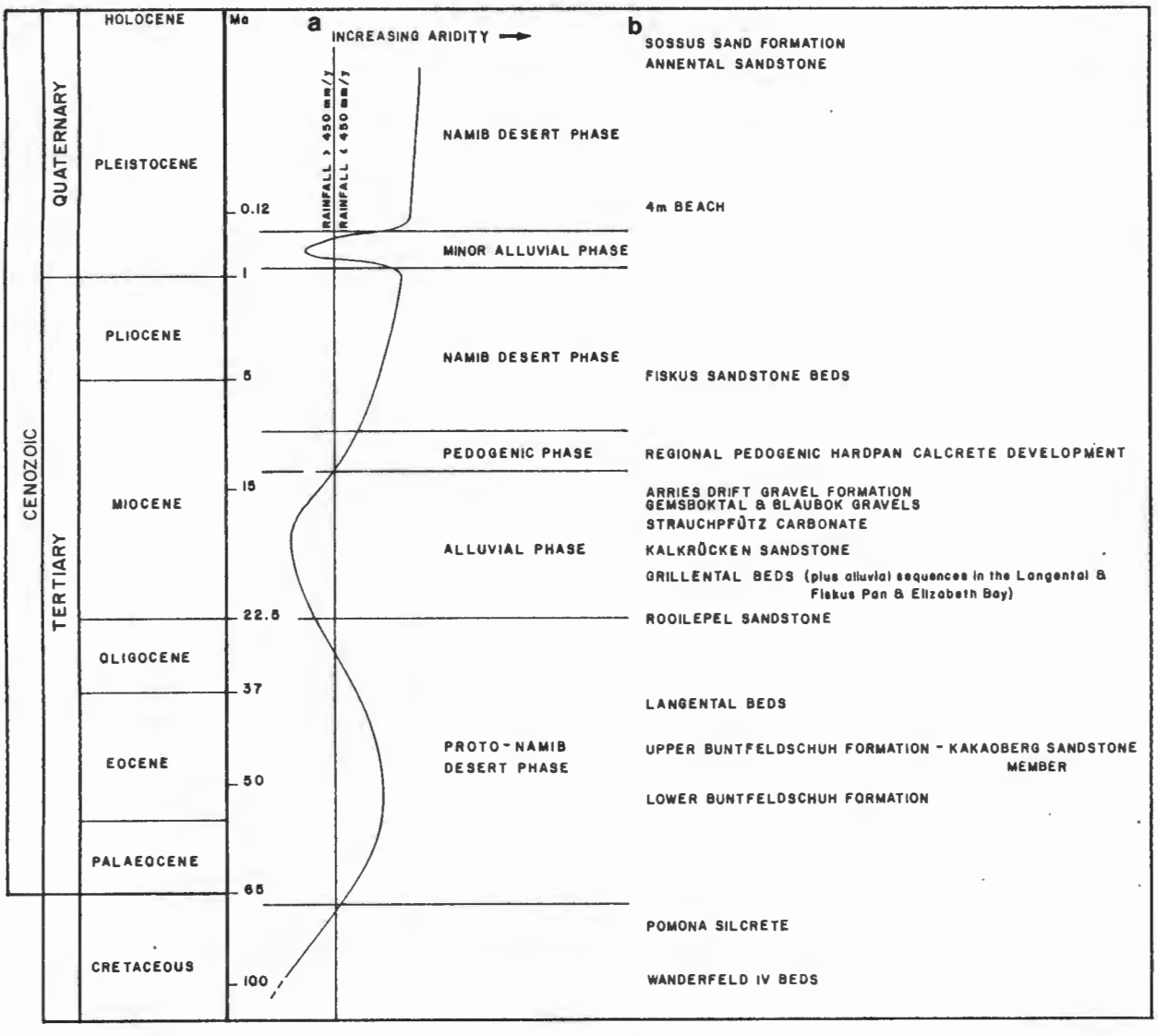

Figure 7.58. a) Summary of Cenozoic palaeoclimatic variation within the Southern Namib based upon sedimentological evidence from this study. b) Summary of Cenozoic stratigraphy.

Formation (Ward, 1984, 1987; Ward and Corbett, in press), which places the start of the Proto-Namib Desert Phase of west coast aridification at least as far back as the Middle Eocene. As pointed out in section 7.2.2., the possibility exists that the initial Upper Palaeocene to Lower Eocene transgression took place across a palaeo-erg.

The early phase of aeolian deposition was succeeded by a period of alluvial activity during the Lower to Middle Miocene, which signifies palaeoclimatic change. An increase in the frequency of sporadic rainfall is believed to have led to the deposition of regionally extensive, coarsening-upward, alluvial sequences. Initially, there was some interaction between the ephemeral alluvial systems and the aeolian system, as shown by the Grillental Beds and the Kalkrücken sandstone, in which the Lower Miocene vertebrate remains occur. Sedimentological evidence thus contradicts previous palaeoclimatic interpretations based primarily upon the vertebrate assemblages. The interbedded pedogenic calcrete horizons within the Kalkrücken sandstone show that semi-arid warm to arid warm conditions prevailed within the Southern Namib between 20 to 17 My. ago. The continued coarsening-upward trend of the alluvial sequences implies that continued palaeoclimatic change was probably reflected in the ability of the later alluvial systems to transport much coarser bedload material. Despite this, the palaeoclimate within the Southern Namib is envisaged to have remained semi-arid to arid during the deposition of the regionally extensive alluvial braidplains. The mechanism responsible for initiating the progradation of the extensive braidplain systems is not known at present. An increase in the frequency of major sporadic rainfall events within the catchments which were probably located along the Great Escarpment is, however, likely to at least partially account for the change in the nature of the systems. The Gemsboktal gravel is known to be youger than 17 My. old because it is underlain by the Kalkrücken sandstone. The Arries Drift Gravel Formation is presently the best dated alluvial sequence, which Pickford (1987) considers to have been deposited between 17 to 14.2 My. ago. It is possible that this sequence represents the culmination of the Lower to Middle Miocene alluvial phase. The extensive alluvial braidplains of the Namib were therefore conceivably deposited at about the same time. The Karpfenkliff

Conglomerate Formation of the Central Namib is seen as being equivalent to the period of alluvial braidplain deposition within the Southern Namib.

The alluvial sequences within the Grillental and Langental valleys are also geomorphologically important. According to Partridge (1985) and Partridge and Maud (1987) the deflation basin floor, where not covered by Pomona silcrete, should represent the Mid-Miocene to Late Pliocene Post-African 1 surface. In order for the Grillental valley to be infilled with the aggradational Grillental Beds sequence the incision of the African surface (sensu Partridge and Maud, 1987) must, however, have occurred before or during the Upper Oligocene. The concept of the Post-African 1 surface also breaks down at Rooilepel, where the depression contains the Rooilepel sandstone which has been tentatively dated as being Upper Oligocene to Lower Miocene in age. Remnants of the Pomona silcrete in the vicinity of the scarp slope prove that the African surface was initially present, but the incision to 120 m below this surface must have occurred prior to the Lower Miocene at this locality.

One of the most notable similarities in the pattern of sedimentation between the Southern and Central Namib is that sediments of both the Proto-Namib Desert and Alluvial Phases acted as hosts for the regional development of a mature, pedogenic hardpan calcrete. This calcrete has been termed the Kamberg Calcrete Formation in the Central Namib (Ward, 1984, 1987). It is presently difficult to accurately establish the age of the calcrete, but it is likely to have developed between 14 to 10 My. ago, when the full establishment of the Benguela Current possibly marked the resurgence of aridification along the west coast. The transition from semi-aridity was possibly characterised by a period of widespread geomorphic stability which would have allowed the calcrete to develop. Calcretes are generally taken to indicate warm semi-arid to arid conditions. It is therefore postulated that with the full development of the Benguela Current came a further palaeoclimatic change. The Southern Namib became a relatively cool desert.

The Timing of the Initial Aridification

As Ward et al. (1983) and Ward (1984, 1987) conclude, there is stratigraphic evidence which demonstrates that a cold Benguela Current is not a prerequisite for aridity within the Namib. This study has established that the Proto-Namib Desert Phase probably influenced the region from the Middle Eocene to the Upper Oligocene. The mechanism causing aridification prior to the Benguela Current is presently unclear. It is, however, likely that the establishment of the South Atlantic Anticyclonic system during the Late Cretaceous (Parrish and Curtis, 1982) played an important role. This high pressure cell creates conditions of atmospheric subsidence, and would have allowed the establishment of an inversion layer which would prevent the occurrence of convective rainfall. The palaeo-rainfall distribution for the Cenomanian by Parrish et al. (1982) consequently indicates that the west coast has been a long-standing region of reduced rainfall (Figure 7.59).

The oldest terrigenous deposit currently known within the deflation basin is represented by the Pomona silcrete. The identification of a deeply weathered kaolinised profile beneath the silcrete horizon indicates that correlation with the African surface (sensu Partridge and Maud, 1987) is feasible. This kaolinised weathering profile probably developed during the Middle Cretaceous, when the global climate is believed to have been both warmer and more humid (eg. Barron, 1986).

The Pomona silcrete is known to pre-date the Klinghardt Phonolite Formation for which a minimum age of 37 Ma. has been obtained. Weathered, discoidal phonolite clasts occur in remnants of a marine beach at Eisenkieselklippenbake, and within laterally extensive pebble beds within the marine Lower Buntfeldschuh Formation. Both of these deposits have tentatively been assigned an Upper Palaeocene to Lower Eocene age by Siesser and Salmon (1979). At the northern end of the Buntfeldschuh escarpment, the marine sequence overlies the silcrete horizon. Frankel and Kent (1938) showed that the decomposition of complex alumino-silicates by meteoric water to clay minerals potentially frees silica which can then be dissolved by liberated carbonates in solution. According to Frankel and Kent, the presence of NaCl, which is characteristic of arid zone soils, greatly enhances silica precipitation from solution. Partridge and Maud (pers. comm., 1987) have therefore suggested that the

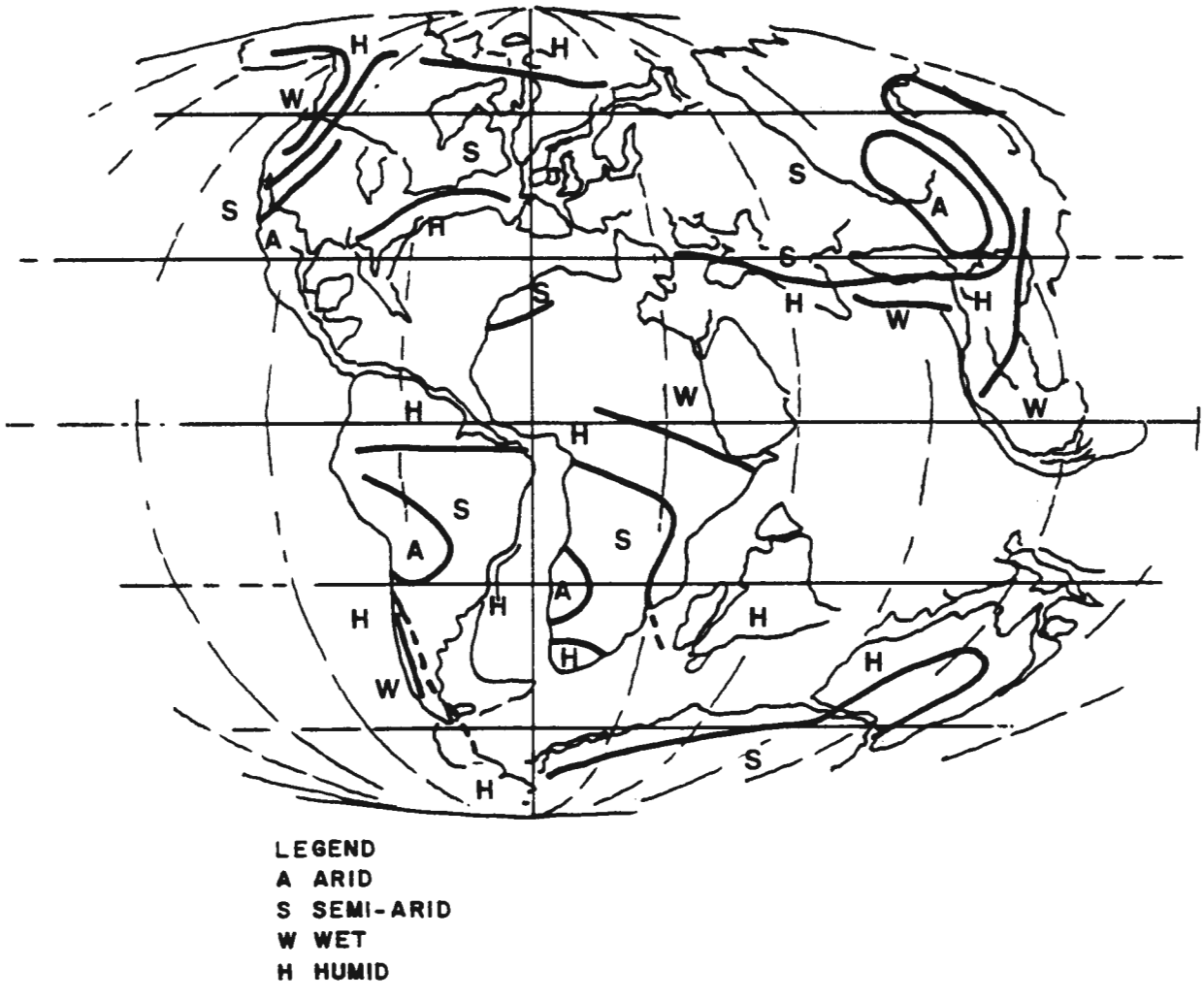

Figure 7.59. Map illustrating the global distribution of arid zones predicted by the rainfall distribution models of climatic models of Parrish et al. (1982). Note the predicted area of aridity along the west coast of southern Africa. After Barron (1986).

development of the silcrete indicates palaeoclimatic change from humid to arid or semi-arid conditions. The Pomona silcrete is believed to have developed during the Late Cretaceous (Beetz, 1926; Stocken, 1978; Partridge and Maud, 1987). This broadly coincides with the time at which the South Atlantic Anticyclonic system is predicted to have been established. This leads to the suggestion that the Pomona silcrete might signify the beginning of the Proto-Namib Desert Phase along the west coast.

7.4. DYNAMICS OF THE PALAEO-AEOLIAN SEDIMENT DISPERSAL SYSTEM

7.4.1. THE PRESENT-DAY SURFACE-WIND REGIME, DUNE FORMS AND SANDFLOW

The distribution, age and character of the palaeo-aeolian deposits within the deflation basin indicate that the dispersal system has varied during the Cenozoic. The palaeowind regime responsible for the deposition of the different sand bodies has consistently been from the south, closely resembling that of today. Since the development of palaeo-ergs is likely to have occurred within a similar coastal geographical setting, it is reasonable to examine their palaeo-dynamics using the present-day system as a modern analogue. In this way, the effects of Cenozoic sea-level movement on the aeolian system can be examined.

Measurement of the surface-wind flow (Ward, 1983; Lancaster, 1983; Ward, 1984) along the Kuiseb River at the northern end of the main Namib Sand Sea has proved the spatial relationship between aeolian dune form and surface-wind regime observed by Fryberger and Dean (1979). Crescentic dunes occur within the 10 to 20 km wide coastal high-energy tract which is dominated by the southerly unimodal regime. Complex linear dunes occur east of this belt, where a low- to intermediate-energy, complex bimodal surface-wind regime governs aeolian dispersal.

A similar spatial zonation of the surface-wind regime governs the aeolian sediment dispersal system at the southern end of the depositional basin (Lancaster, 1985), resulting in a similar distribution of dune forms.

Observations and data collected during this study show that the same coast parallel zonation of the surface-wind regime exists to the south of the depositional basin. The main deflation basin is confined to the 10 to 15 km wide, high-energy coastal tract. Areas to the east experience a lower-energy surface-wind regime of greater complexity.

Empirical data from the northern end of the main Namib Sand Sea proves that the crescentic dunes in the high-energy coastal tract migrate faster than the complex linear dunes influenced by a low- to intermediate-energy complex bimodal wind regime (Ward, 1984). Ward (1984) also demonstrated that the rate of aeolian sand accretion within the coastal tract is appreciably greater than that

associated with the complex linear dunes. As the zonation of the surface-wind pattern into coast-parallel, linear belts, influences the entire aeolian system, it is postulated that the sandflow is higher within the coastal tract than at any other point within the Namib Sand Sea. This hypothesis is supported to some extent by the regional pattern of resultant sandflow calculated by Lancaster (1985). Additional empirical sandflow and wind data are required before more definitive statements can be made, because of the influence of sediment supply on the spatial distribution of sandflow.

7.4.2. AEOLIAN SEDIMENT DISPERSAL FROM DEFLATION TO DEPOSITIONAL BASIN

This study demonstrates that the sediment supply to the present aeolian system is principally generated along the coast of the main deflation basin. Localised entry points are found within log-spiral and south-facing embayments. The sand deflated from these beaches enters aeolian transport corridors, along which it is transported northwards to the depositional basin.

The southern margin of the Namib Sand Sea is presently located slightly east of Elizabeth Bay, about 30 km south of Luderitz (Figure 7.60). The coastal morphology between Prinzenbucht, a log-spiral embayment, and Elizabeth Bay, a south-facing embayment, is presently important for the generation of sandflow. The surface-wind flow locally approaches saturation point immediately north of Prinzenbucht, resulting in the development of crescentic dunes in a narrow coast-parallel belt. Another dunefield of triangular ground-plan, with the apex pointing upwind, occurs at the seaward end of the Grillental (Figure 7.60). Development of this small dunefield also indicates local saturation of the surface-wind flow, and the plan-form resembles that produced by Southard and Dingler (1971) during bedform initiation studies on a granular flume bed. Despite the locally saturated surface-wind conditions, the southern margin of the Namib Sand Sea is displaced slightly east of the coast. This sand therefore does not enter the depositional system immediately. Instead, it seems to be transported northwards, along the western margin of the sand sea into the Kolmanskop valley before finally entering the depositional system due east of Luderitz. The main aeolian transport corridors

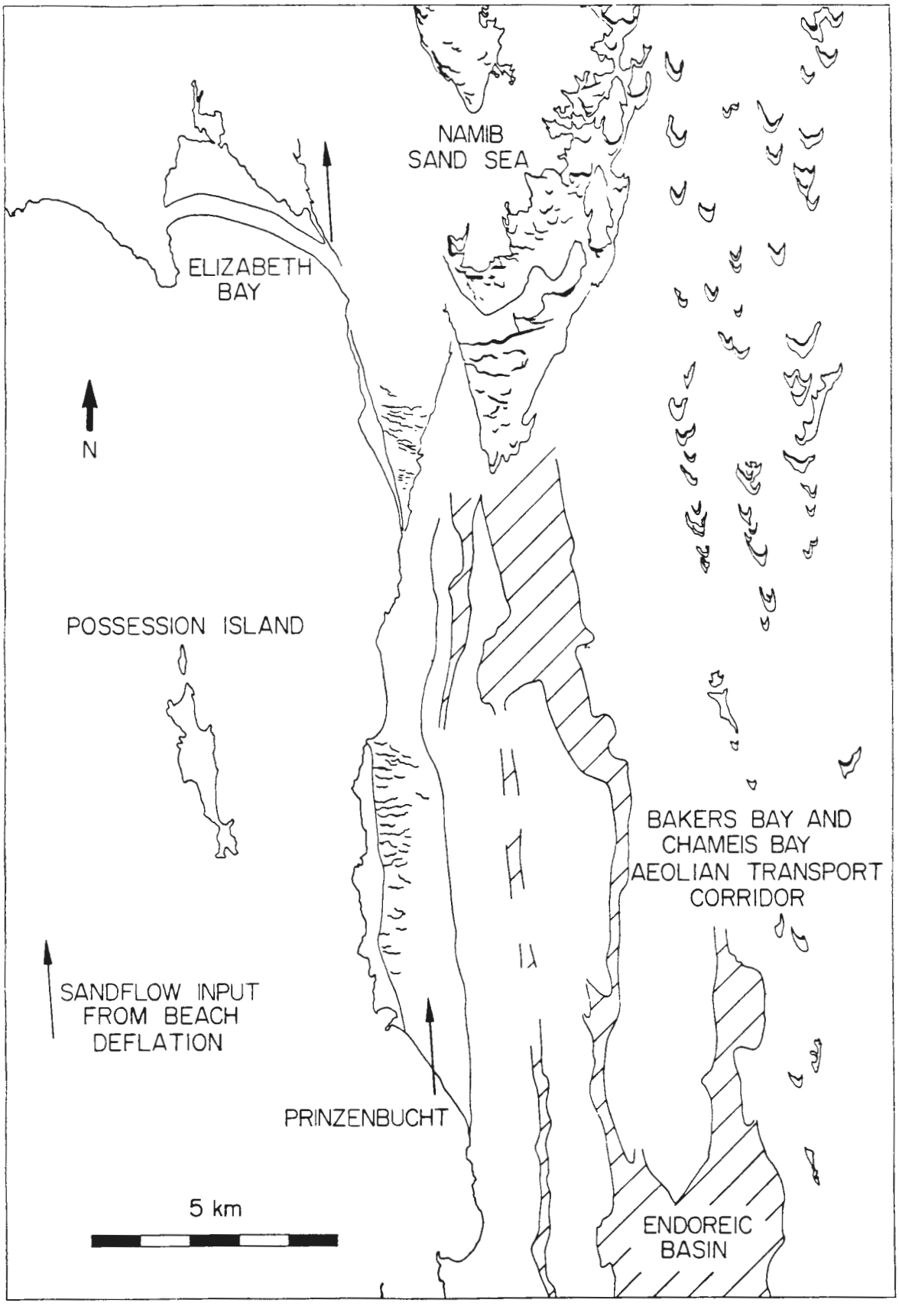

Figure 7.60. Summary of aeolian system sediment dynamics at the southern end of the Namib Sand Sea, to show the role played by the log-spiral embayment at Prinzenbucht and the south-facing re-entrant at Elizabeth Bay, and aeolian transport corridors arriving from the deflation basin.

enter the depositional system on the eastern side of the southern margin, about 20 km north of the Grillental (see section 7.2.6). This is surprising because it appears logical that the majority of sandflow should enter the southernmost point of the sand sea. Instead, the large barchanoid draas at this point appear to be maintained by sandflow emerging from the complex topography to the south of the Grillental. On crossing the Grillental tract, deceleration of the surface-wind flow appears to result in the saturation of the surface-wind. As Wilson (1971) demonstrated in the Sahara, this condition leads to the development of ergs.

Sandflow generated within the deflation basin therefore does not enter the depositional basin at one point. Whilst some sandflow undoubtedly enters the linear dune systems, the majority is likely to remain within the high-energy coastal tract. This material then maintains the rapidly migrating compound crescentic dunes, and the coastal sand sea plinth, which is periodically reworked by storms waves arriving at the coast. On this basis, the depositional system consists of two parts, with a dynamic coastal zone characterised by high sand throughput bordering a more stable eastern zone across which sandflow diminishes (Figure 7.61).

The coastal belt of crescentic dunes is thus envisaged to be a highly mobile, linear tract of sand moving around the less dynamic part of the sand body lying to the east. Any change in the spatial distribution of sandflow generation sites is liable to substantially alter the sediment dispersal pattern of the deflation basin. Modification of the aeolian system in this way is thought to result in alteration of the depositional system.

7.4.3. THE PALAEOWIND REGIME

The models of the atmospheric circulation pattern by Totman Parrish and Curtis (1982) indicate that the South Atlantic Anticyclone may have begun to influence the west coast surface-wind pattern during the Cenomanian. The theoretical models suggest that the anticyclonic system would have been more established towards the end of the Cretaceous. Kennett (1982), considers that the anticyclonic gyre was well established by the Eocene, in reasonable agreement with the model.

Field evidence from the aeolian sequences within the Southern Namib demonstrates that all of the palaeo-aeolian systems were

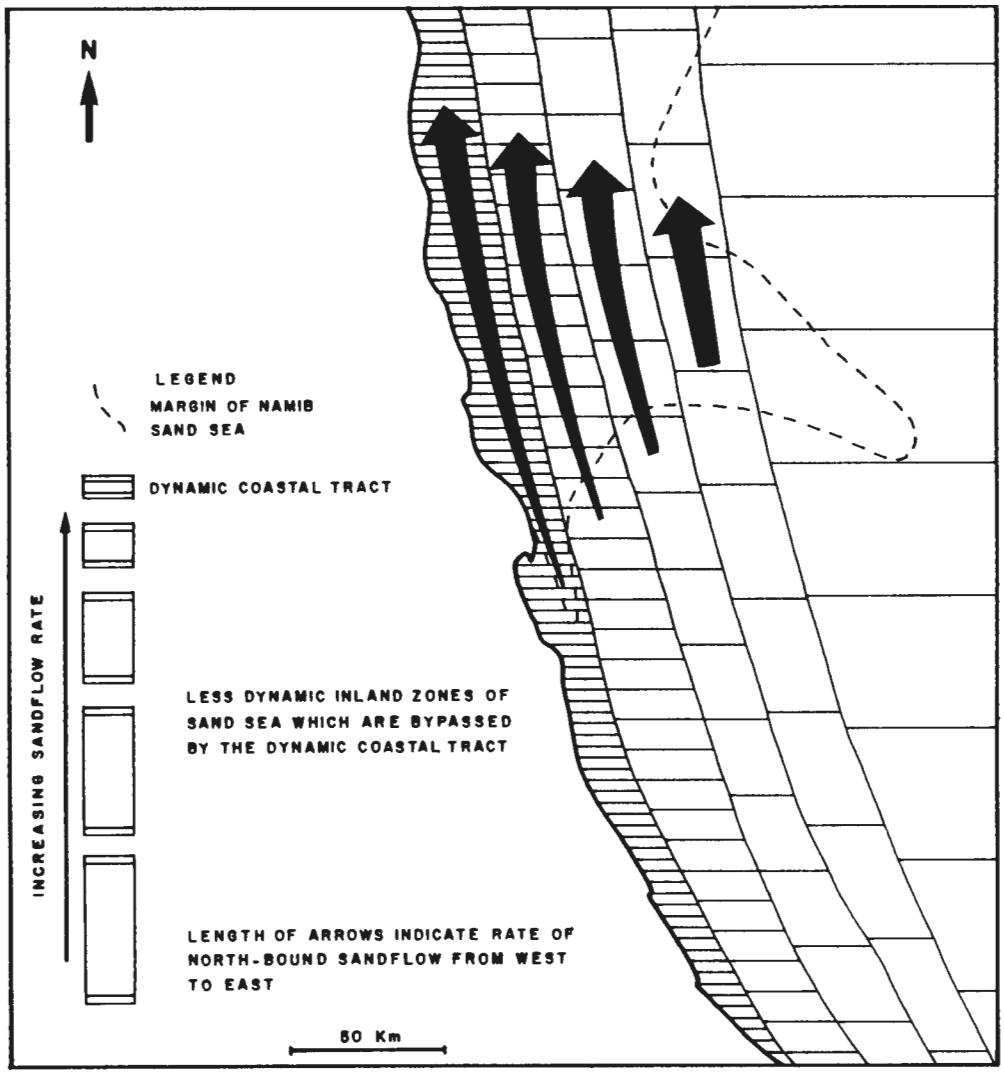

Figure 7.61. Conceptual division of the aeolian depositional system into a highly dynamic coastal belt influenced by the high-energy unimodal wind regime and a more stable eastern zone which is influenced by a lower-energy bimodal wind regime.

governed by a southerly quadrant wind regime. A similar conclusion has been reached in the Central Namib by Ward (1984; 1987). No evidence for a sustained switch to a dominant northerly quadrant regime, and the breakdown of the zonal atmospheric circulation pattern, has been found in any of the aeolian exposures examined. It is therefore concluded that the palaeo-aeolian systems were governed by surface-wind regimes comparable with those of today. There is, however, evidence for variation of the surface-wind speeds influencing the region. For instance, the extremely coarse-grained nature of the Fiskus Sandstone Beds is strongly indicative of deposition by surface-wind speeds greatly exceeding those of today. The palaeo-erg represented by the Fiskus Sandstone Beds probably began developing during the Late Miocene to Early Pliocene regression, and possibly remained active during the Late Pliocene to Early Pleistocene regression to 200 mbsl. Siesser and Dingle (1981) suggest that the former regression coincided with the rapid expansion of the Antarctic Ice Sheet 4.7 to 4.3 Ma recorded by Shackleton and Kennett (1975). Sarnthein (1977) has postulated that an increase in the equator-to-poles thermal gradient results in higher wind speeds. It is suggested that a similar mechanism might account for the conditions that prevailed during the deposition of the Fiskus Sandstone Beds.

The south-north velocity gradient exhibited by the present-day surface-wind system along the west coast significantly influences the dynamics of the aeolian system. The surface-wind speed variation has not been properly defined with a complete set of contemporaneous recordings. As Rogers (1977) has pointed out, however, the reduction of surface-wind velocity north of Pomona, in the vicinity of Luderitz, must influence the point at which the depositional system commences. It is uncertain what effect sea-level movement, resulting in shifts of the coastline, might have had on the location of this gradient, which might also have varied in response to changes in the equator-to-poles thermal gradient. Shifts of the peak in southerly wind-energy to the north or south, theoretically alter the point at which the aeolian depositional system becomes saturated, and consequently the location of erg development. In addition, Ward (1984) has shown that the south to north gradient is quite complex, with one peak in the vicinity of Pomona, and one further north, near Toscannini.

Changes in the latitudinal distribution of wind velocity gradients of this type are likely to further complicate the aeolian system response to change.

7.4.4. GEOMORPHIC EVIDENCE FOR AEOLIAN TRANSPORT CORRIDOR DISPLACEMENT

Yardangs are widely distributed throughout the deflation basin. To some extent, their occurrence is controlled by the susceptibility of different bedrock lithologies to salt weathering. Sperling and Cooke (1984) have shown that dolostone is particularly resistant, which probably explains why many areas of positive relief in which yardangs have formed are comprised of Bogenfels Formation Dolomite. The tectonic structure of upstanding areas of steeply dipping dolomite also influences yardang development. Where the beds strike east-west and dip to the south, across the southerly surface-wind flow, sub-horizontal polished and fluted surfaces develop. Gradational change from poor- to well-developed yardangs occurs as the strike changes from north-south to east-west with beds dipping to the north.

Concept of Active and Non-Active Yardangs

There are three main localities in which yardangs are found (Figure 7.62). Two of the localities lie outside the influence of present-day sandflow based upon the distribution of aeolian transport corridors. One locality is located on the coast at Bogenfels, and the other lies east of the present deflation basin margin.

In the main yardang field lying within the path of present-day aeolian transport corridors, the yardangs exhibit the following characteristics:

1) windward surfaces show evidence of aeolian corrasion and are polished (Figure 7.63a);
2) convex sidewalls are fluted towards the downwind apex (Figure 7.63b), providing evidence of flow convergence along the centre-line of the long axis. This convergence of flow has been reported from other studies of aeolian landforms and from snow drifts by Whitney (1983);
3) deep, polished flutes develop along the basal part of sidewalls at the junction with the bedrock floor which is

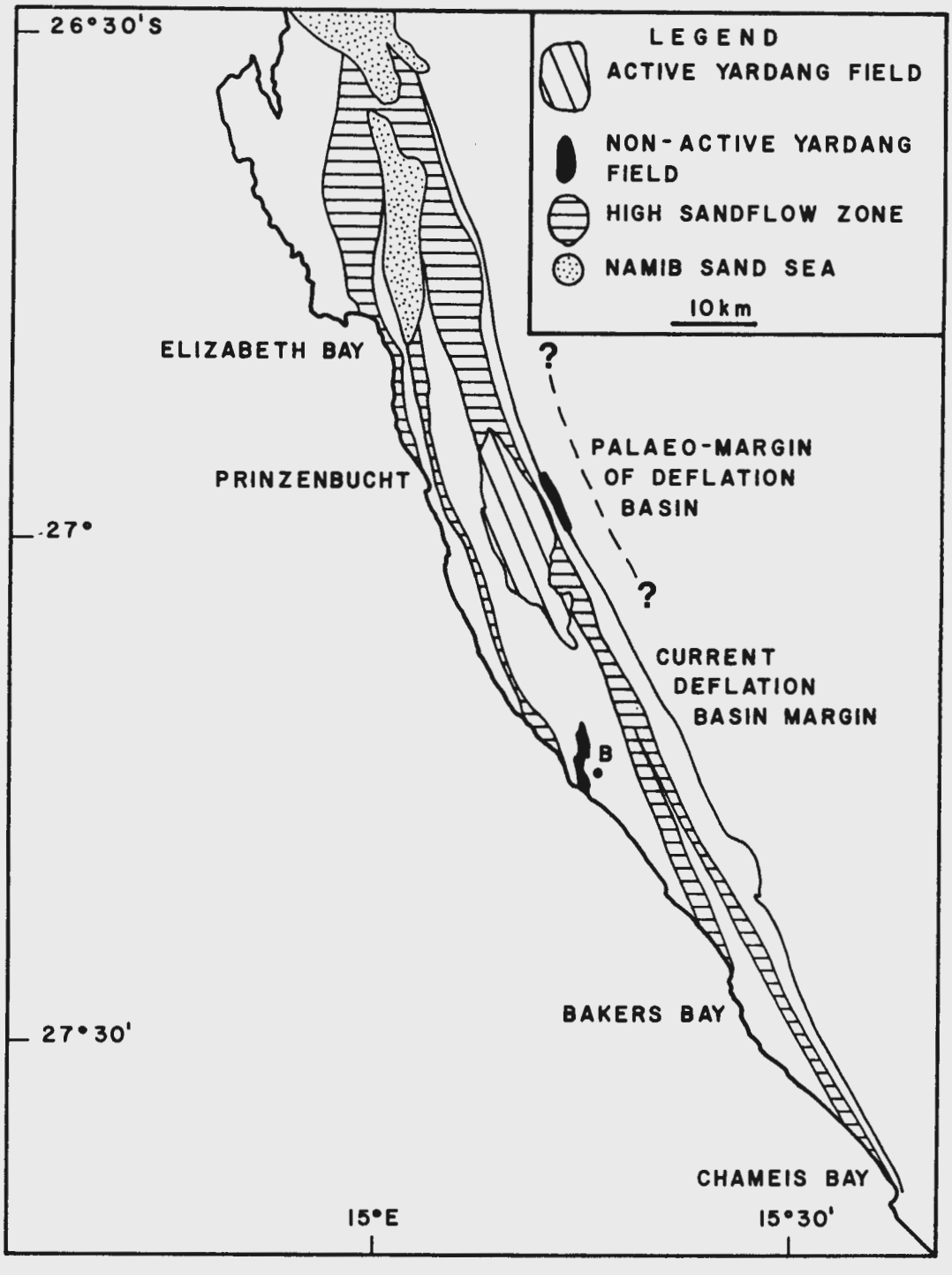

Figure 7.62. The distribution of yardangs within the Southern Namib to the north of the Orange River, shown in relation to the spatial distribution of high sandflow zones, which principally correlate with the position of aeolian transport corridors. The concept of "active" and "non-active" yardangs is discussed below.

Figure 7.63. a) Windward face of a dolomite yardang to the south of Chalcedon Tafelberg. Note that the surface is highly abraded and polished by aeolian corrasion, and that there is very little weathered debris at the base of the landform. Southerly wind flow is into the frame. Scale 1 m. b) Western side of the same yardang. Note the very deeply scoured flutes along the side of the landform (arrowed). Further flute development can be seen at the junction with the bed, near the scale resting on a polished dolomite pavement. The flutes define a pattern of flow convergence along the centre-line, where the absence of sandflow permits weathered debris to collect and vegetation to become established.

planed and polished. These flutes also define the pattern of flow convergence.

Experimental studies by Ward and Greeley (1984) show that model yardangs evolve through a series of stages:

1) erosion of windward corners;
2) erosion of the front slope and upper surface;
3) erosion of the rear flanks;
4) erosion of the downwind upper surface.

The flute orientation of Southern Namib examples formed from dolomite suggests that the features develop by progressive aeolian erosion of the planed and fluted floor towards the downwind apex of the landform (Figure 7.64). A characteristic feature of the dolomite surfaces is the polishing which takes place in the present-day high-energy aeolian environment. Minimal evidence for other forms of weathering occurs on these dolomite surfaces, although some spalling is seen. Yardangs of this type are termed "active".

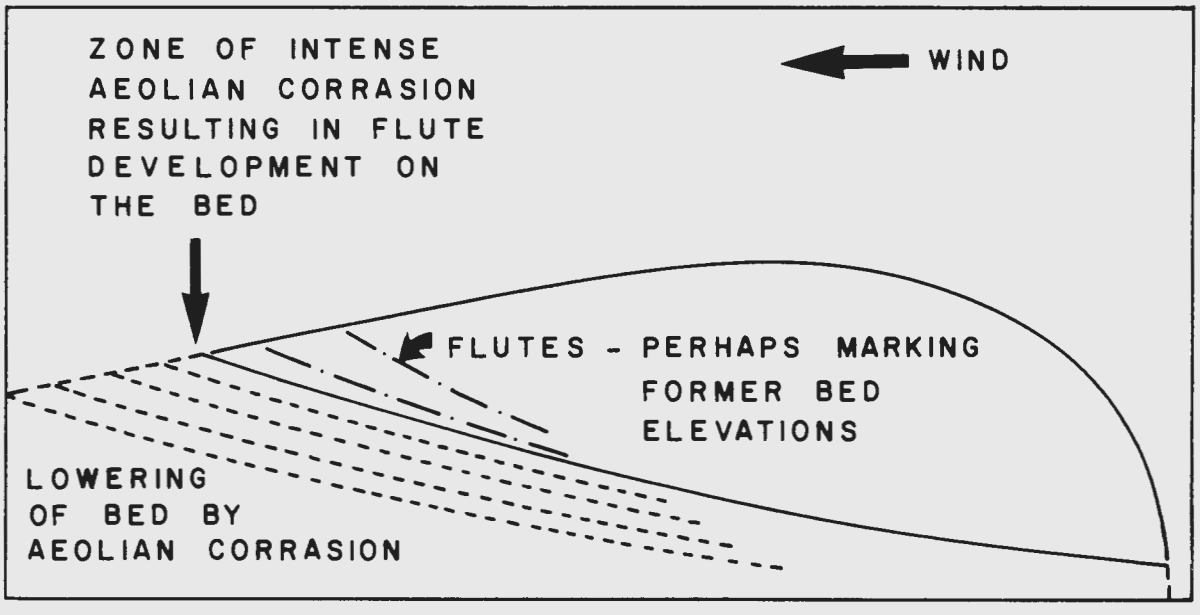

Figure 7.64. Sketch illustrating the envisaged pattern of aeolian corrasion at the apex of the yardangs, based upon the orientation of fluting. Progressive corrasion of the bed at the apex probably leads to the lowering of the bed, resulting in an increase in the dimensions of the landform.

The surfaces of yardangs at Bogenfels are not polished like those of active examples. The windward surfaces show evidence of gross modification by solution weathering, and sidewall flutes which were once highly polished have now been severley modified (Figure 7.65). Solution weathering now dominates on these features, modifying the surface morphology and forming solution pipes surrounded by rillenkarren along the central crests of some yardangs. In addition, weathered debris is more common than on the surfaces of active yardangs in the main field east of Pomona, through which aeolian transport corridors presently disperse sediment. This demonstrates that the present-day sandflow through the yardang field at Bogenfels is too small to maintain the domination of aeolian processes responsible for their formation. This interpretation is supported by the growth of lichens on yardang sidewalls and within flutes, where sandflow normally does not permit colonisation. The establishment of vegetation upwind of the yardang field provides further proof of low sandflow conditions, which is probably further reduced by the vegetation itself (eg. Buckley, 1987). These features are therefore termed "non-active", and are out of equilibrium with the present-day sandflow. Sand trap results prove that no aeolian transport corridor is presently generated from deflation of the Bogenfels Beach. It is concluded that the pattern of sandflow through the basin has not remained constant through time, and that aeolian transport corridors generated during periods of marine regression probably accounted for the formation of the yardangs at Bogenfels.

Further evidence supporting the variation in the spatial distribution of sandflow through time is provided by small dolomite yardangs lying east of the present-day deflation basin margin (Figure 7.66). These yardangs occur within the transition zone between the deflation basin and the eastern plains, where the ground surface is covered by relatively dense vegetation. This both reduces the sandflow and is also an indicator of low sandflow conditions. The yardang surfaces have been greatly modified by solution weathering, and perfect rillenkarren form intricate patterns on surfaces exposed to the southerly wind flow. Angular blocks of loose, weathered debris form gravity cones on some sidewalls, which are also frequently covered by vegetation. These yardangs are also interpreted as being "non-active", and lie

Figure 7.65. Chemical solution, modifying flutes on dolomite yardangs which were previously formed by aeolian corrasion, and are now located within a non-active yardang field at Bogenfels. Note also the lichens (L) on the dolomite surface. These are normally prohibited from growing by high sandflow conditions. Southerly wind flow from left to right. Scale 10 cm.

Figure 7.66. Small dolomite yardang on the eastern margin of the current deflation basin. Note the dense vegetation surrounding the feature, indicating that low sandflow conditions prevail. A large amount of weathered debris lies on and around the yardang. This is not seen in areas of high sandflow. The dolomite surface is covered with rillenkarren. Southerly wind flow from left to right. Scale 1 m.

outside the influence of the present aeolian dispersal system of the deflation basin.

Implications of Active and Non-Active Yardang Fields

The identification of active and non-active yardang fields proves that the present spatial distribution of aeolian sandflow is currently unable to maintain the characteristics of some of the aeolian landforms within the present-day deflation basin. Hence the spatial distribution of sandflow has not been constant through time. It also supports the definition of aeolian transport corridors on the basis of sand trap results, since it proves that sandflow under the present regime is not evenly distributed throughout the deflation basin.

The Bogenfels yardang field is presently situated on the coast, where deflation of the straight, steep, high-energy beach provides minimal input to the aeolian system. Sandflow through this area is only possible if a southern source is located to the west of the present coastline. This yardang field must therefore have developed during a regression. The location of aeolian transport corridors is governed by the geographic position of coastal sediment input points to the aeolian system. Modification of the coastal morphology during a regression would theoretically alter the distribution of log-spiral and south-facing embayments. As a consequence, aeolian transport corridors would shift to the west of their former position.

Non-active yardangs east of the present deflation basin margin also indicate the displacement of aeolian transport corridors. In this case, a relative shift to the east is implied, which suggests that the margin of the deflation basin was east of its present position. The position of the margin is set by the width of the coastal tract dominated by high-energy southerly surface-wind flow. For the palaeo-margin to be displaced to the east, either the width of the coastal tract must be increased or the position of the coastal high-energy tract itself changed.

Non-active yardang fields therefore not only provide evidence for the east-west displacement of aeolian transport corridors, but also the eastern displacement of the deflation basin's eastern margin.

7.4.5. CONCEPTUAL MODEL OF THE AEOLIAN SYSTEM RESPONSE TO PAST REGRESSIONS

A number of marine regressions have influenced the west coast of the southern African sub-continent during the Cenozoic (eg. Siesser and Dingle, 1981). Evidence presented in this study indicates that the development of much larger aeolian sand bodies than the present-day Namib Sand Sea probably occurred during marine regressions, as discussed in section 7.3.4.

Previous concepts of aeolian system response to a regression have emphasized the quantity of sediment exposed on the shelf as sea-level drops. This material is theoretically available for incorporation into an expanding sand sea. Whilst this is likely to result in a certain amount of expansion, the consideration of the present-day aeolian system suggests that this model is too simplistic. In order to maintain the erg at the coast, a more permanent coastal supply is necessary.

The Concept of Climatic Zonal Shifts During Regressions

The available theoretical and empirical data suggests that the present-day pattern of atmospheric circulation influencing the west coast has existed since the Eocene, and probably earlier. The rock record in the Southern and Central Namib also indicates that the palaeoclimate has been arid to semi-arid for much of the Cenozoic. The assumption is therefore also made that the spatial distribution of rainfall over the region has also been broadly similar to todays, excluding the conditions during the Miocene alluvial phase. This assumption is supported by global palaeo-rainfall distribution patterns modelled by Parrish et al. (1982), which indicates that an area of low rainfall has probably existed over Namibia since the Cenomanian. It is important to consider the potential influence a westward shift of the coastline might have had on the surface-wind regime.

The active and non-active yardangs in the Southern Namib show that the coastal tract, dominated by the high-energy unimodal southerly surface-wind regime, has not occupied a constant geographic position throughout the Cenozoic. It has been shown that regression(s) resulted in the westward shift in the position of the coastline, and there is some evidence that the Benguela Current would also have been similarly displaced (eg. Siesser and Rogers,

1976). It is postulated that the coast-parallel surface-wind zones would also have been displaced, in order to maintain their position relative to the new coastline. As a result, the area which was previously situated within the coastal high-energy tract was subsequently influenced by the lower-energy surface-wind zone which previously lay to the east. An accompanying change in the rainfall pattern is also likely to have occurred, resulting in a westward shift of the coastal zone of hyper-aridity.

Influence of Regression on Aeolian Transport Corridors

The coastal morphology governs the distribution of points where aeolian transport corridors are generated. The present distribution corresponds with the location of transgressed endoreic basins and south-north oriented valley systems. Since these zones of high sandflow largely maintain the present-day Namib Sand Sea, alteration of their distribution is liable to alter the dynamics of the depositional basin.

The westward shift of the coastline exposes the shelf, and the coastal morphology consequently must change, altering the distribution of suitable sites for bay formation. As a consequence of both the theoretical westward shift of the surface-wind zones, and the coastline, aeolian transport corridors will lie west of their previous position. This concept is supported by the non-active yardangs at Bogenfels.

Influence of Regression on the Depositional Basin

In response to the westward shift of aeolian transport corridors, their entry point to the depositional basin is also theoretically displaced west of its previous position. It is postulated that an accretionary wedge of material forms within the new coast-parallel high-energy tract, dominated by transverse dunes between the earlier sand sea plinth and the regressed shoreline (Figure 7.67). With this, the former belt of transverse dunes is subsequently situated to the east of the coastal tract. It is then influenced by low- to intermediate-energy surface-winds, and the transverse dune forms are likely to be modified into linear dunes by the new surface-wind conditions.

The net effect of continued sea-level lowering is thus predicted to be the westward progradation of the sand sea by the aggradation

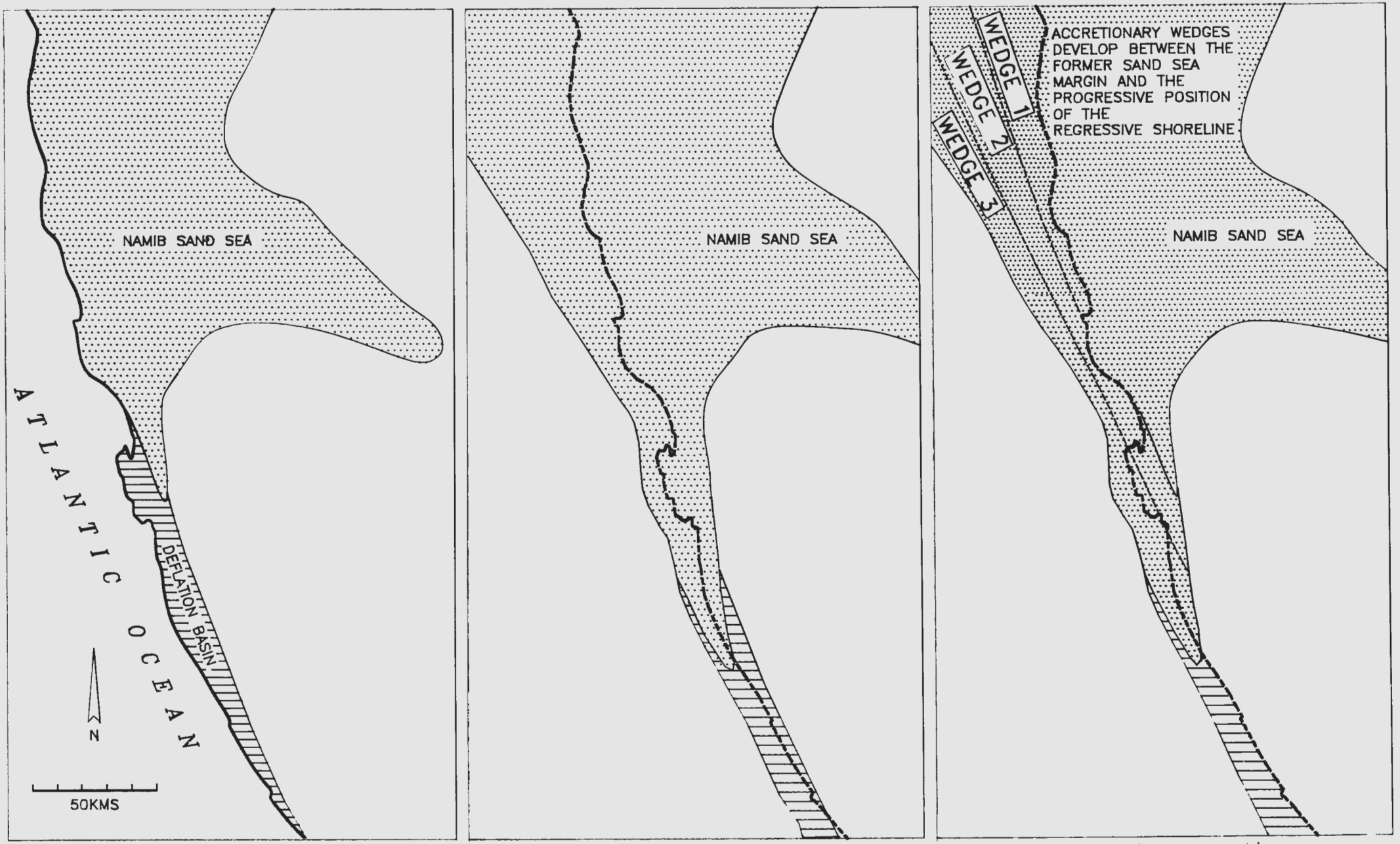

Figure 7.67. Sketch illustrating the concept of the addition of accretionary wedges to the western margin of the sand sea during regression, in response to the creation of new coastal dynamic tracts of high sandflow.

of a series of accretionary wedges. Consequently, the area of less active linear dune forms, to the east of the coastal tract, theoretically expands westwards as well.

7.4.6. CONCEPTUAL MODEL OF THE AEOLIAN SYSTEM RESPONSE TO PAST TRANSGRESSIONS

Transgressions have also influenced the west coast during the Cenozoic, resulting in changes in the coastal morphology. This must also have modified the aeolian system. The development of endoreic basins has resulted in very complex geomorphology. As the present coastline shows, this is ideal for the development of bays suitable for aeolian transport corridor generation.

The Concept of Climatic Zonal Shifts During Transgressions

The coastline is displaced to the east during a transgression. It is postulated that the surface-wind zones also shift in order to maintain their position relative to the new coastline. The zone influenced by coastal high-energy surface-winds therefore occupies a more easterly position than it did formerly, and the low- to intermediate-energy surface-wind zone moves accordingly.

Influence of Transgression on Aeolian Transport Corridors

When endoreic basins are transgressed, log-spiral and south-facing embayments are generated in a more easterly position. This results in an eastward shift of the aeolian transport corridors migrating through the deflation basin.

The Bogenfels Basin, which has been in existence since the Cenomanian, provides the ideal location for the generation of a major south-facing embayment. This is significant because the exposures of the Fiskus Sandstone Beds at Wustekonig indicate that Plio-Pleistocene transgressions between 90 to 20 masl which occur south of the Orange River (eg. Pether, 1986), have also influenced the deflation basin. Computer modelling of the coastline using VULCAN, shows the potential form of the embayment for transgressions between 25 to 30 masl., 35 to 40 masl., and 50 to 60 masl., and 80 to 90 masl (Figure 7.68). The close resemblance of the embayment within the Bogenfels Basin to the present-day coastal morphology between Prinzenbucht and Elizabeth Bay is striking. Consideration of the present-day system leads to the conclusion

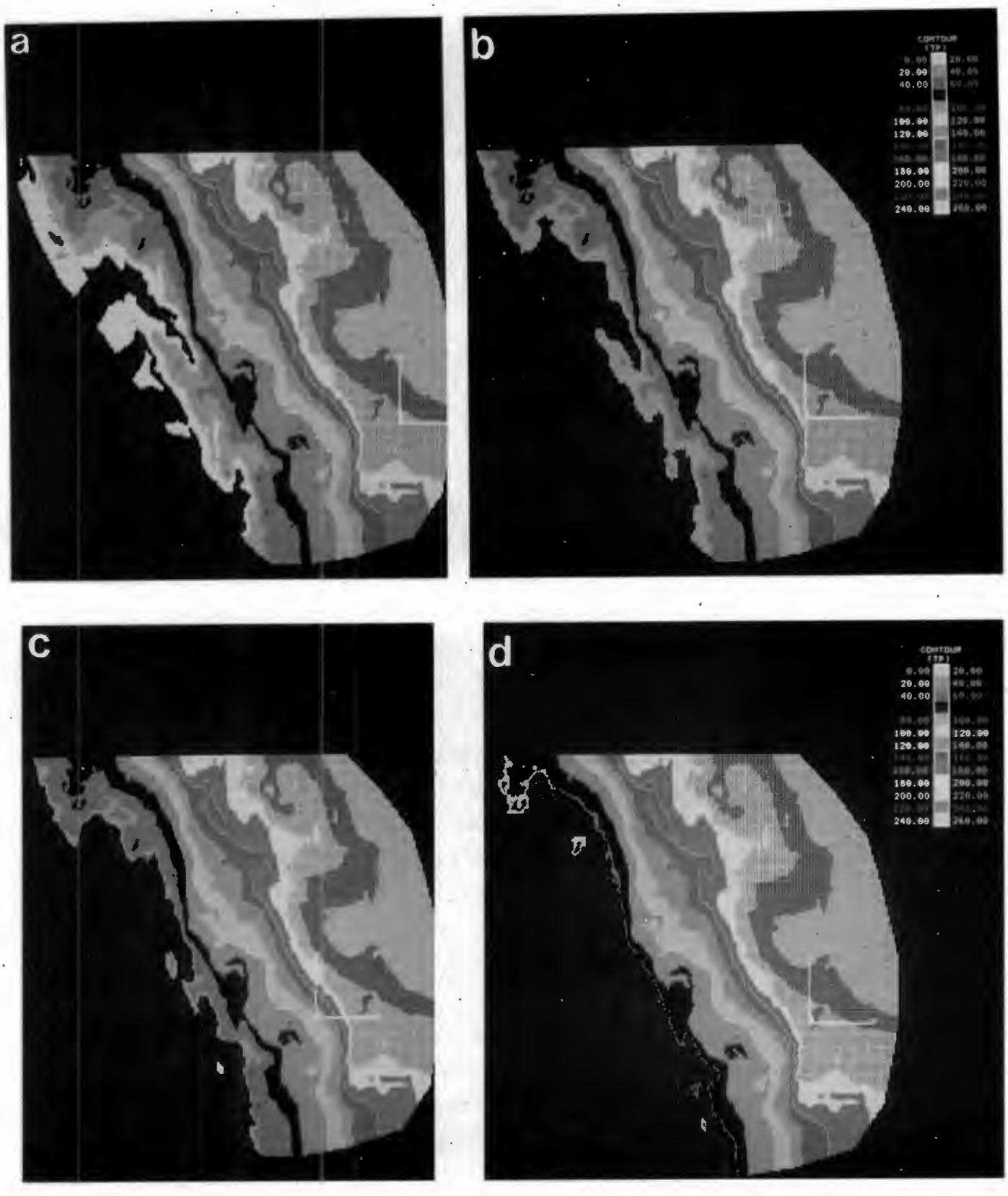

Figure 7.68. Computer model showing the changes in coastal morphology within the Bogenfels basin during transgressions to: 5 to 15 masl, 20 to 30 masl, 35 to 40 masl, and 55 to 60 masl. Note the similarlity of the predicted coastline with that between Prinzenbucht and Elizabeth Bay today.

that the south-facing embayment at Bogenfels would significantly modify the aeolian sediment dynamics of the deflation basin. Provided that sufficient sandflow was generated, it is possible that the southerly surface-wind flow would become saturated to the south of its present position.

Influence of Transgression on the Depositional System

During a transgression, the western margin of the depositional system is reworked by marine processes. The east-west extent of any aeolian sand body will therefore diminish. The coastal high-energy tract progressively shifts across areas which were formerly influenced by the low- to intermediate-energy wind regime. Linear dune systems developed under the influence of this regime are then liable to modification by the new higher-energy conditions, and a new coastal belt of transverse dunes develops. This leads to the gradual contraction of the sand body (Figure 7.69), which is confined in the east by the Great Escarpment.

Depending upon the number and distribution of suitable log-spiral and south-facing embayments, the degree and point at which the surface-wind becomes sand saturated will probably also change. As studies by Wilson (1971) in the Sahara demonstrated, aeolian depositional systems are sensitive to this factor. If the system is saturated deposition will take place. If the system subsequently becomes undersaturated, the equilibrium between the rate of deflation from the bedform and the input of new material will become unbalanced. If this imbalance continues for long enough, the aeolian deposit will ultimately be reworked. In terms of the Namib Sand Sea, if the aeolian current system becomes saturated further south, the potential exists for the southward extension of the sand body. If, however, the aeolian current system becomes undersaturated the sand sea will be destroyed. Dune systems at the southern (ie. upwind) margin of the depositional basin will then be subjected to aeolian erosion, and the southern margin will progressively migrate northwards. This is possibly the situation influencing the present Namib Sand Sea, where this form of adjustment might explain why the sandflow from the deflation basin does not directly enter the depositional system at its southern extremity.

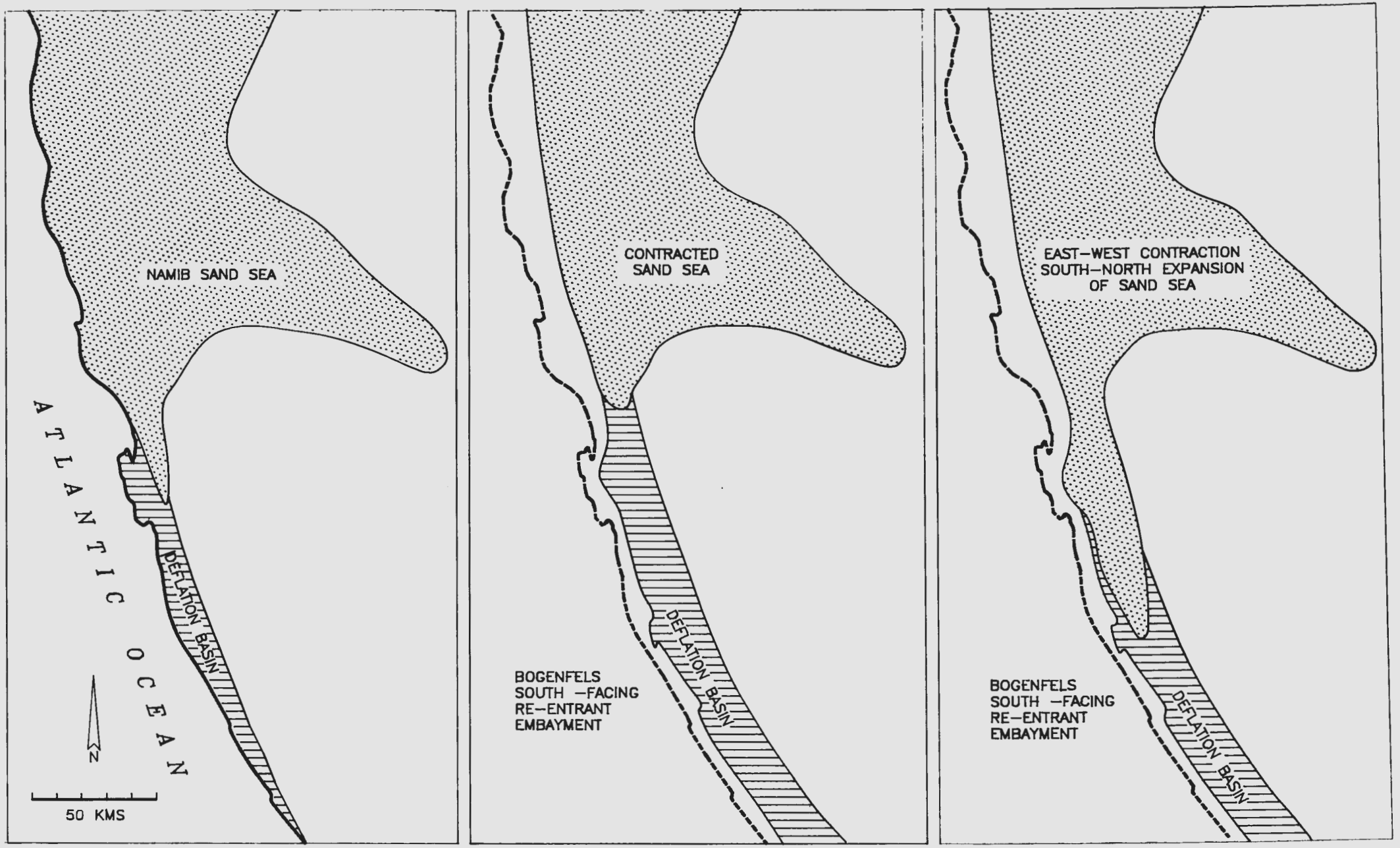

Figure 7.69. Sketch showing hypothetical sand sea contraction during transgression. (a) The situation as it is now. (b) Northward migration of the erg margin due to reduction in sand supply to the systm (c) West-east contraction could be accompanied by southward expansion if the aeolian system becomes saturated further south due to sediment supply from Bogenfels.

Interpretation of Regional Bounding Surfaces

The alternation of aeolian response to regressions and transgressions over a long period will generate a complex sedimentary sequence. Due to the poor preservation potential of aeolian sandstones within the deflation basin environment, scant evidence of this sequence is found to the south of the Grillental. The Kolmanskop area at the southern end of the present-day sand sea does show evidence for the multiple development of palaeo-ergs.

Four sand bodies are represented, the oldest being the Kolmanskop sandstone. The Fiskus Sandstone Beds are the most extensively preserved palaeo-erg, and the Annental sandstone is restricted to very localized occurrences in old ephemeral drainage tracts. The fourth sand body is the present-day Namib Sand Sea (Sossus Sand Formation).

The Fiskus Sandstone Beds were deposited by transverse dunes during a regression. This sand body was subsequently overlain by the Annental sandstone, and the present-day Namib Sand Sea represents an aeolian sand body developed during a later transgression across both of these sand bodies. The coastal morphology and the location of the coast-parallel surface-wind zones of the aeolian current system have therefore altered a number of times during the deposition of the different palaeo-ergs.

As shown by exposures at Elizabeth Bay, the Fiskus palaeo-erg extended south and west of the present-day sand sea. The same is probably true for the Annental sandstone. The aeolian current system thus presently becomes sand saturated at a point located to the north and east of that at which the palaeo-aeolian systems were. Hence the palaeo-ergs are out of equilibrium with the present-day aeolian system, because the relative position of the deflation basin has changed. The palaeo-ergs, which once occupied a position within the depositional basin, are therefore now located within the deflation basin, and they are thus being subjected to aeolian erosion.

Despite the increased preservation potential of the Fiskus sand body due to its partial cementation by calcite, and its very coarse-grained texture, it is progressively being reworked by the present-day aeolian system. Aeolian processes remove weathering products, and truncate the palaeo-erg to produce a regional bounding surface. Exposures of this surface occur along the eastern

margin of the Elizabeth Bay depression (Figure 7.70) and in windows through the present-day Namib Sand Sea. As demonstrated by the Fiskus Pan depression to the south of Kolmanskop, aeolian erosion proceeds more rapidly in some localities than others. The majority of the Fiskus sand body has been completely eroded, and a gap in the bounding surface has developed, through which Lower Miocene deposits have been exposed. The depression containing the Fiskus Pan, thus pre-dates the Lower Miocene, and is presently being re-exhumed.

Thus the regional bounding surfaces confirm that the aeolian sediment dispersal system, which has operated on the west coast throughout much of the Cenozoic, has undergone substantial modification. Many of the changes are apparently attributable to the influence of sea-level movement on the generation of sand for the aeolian system, and the regional spatial zonation of the surface-wind regime. The modification of the coastline, and consequently the position of aeolian transport corridors, is likely to greatly influence the aeolian system. At the present time, the number of embayments along the coast principally controls the availability of sand for the aeolian system. If fewer embayments were present, aeolian transport corridor generation would be reduced, and saturation of the surface-wind will be difficult to achieve. If numerous log-spiral and south-facing embayments are present, saturation will be achieved more rapidly. Conditions during regressions appear to favour the expansion of sand bodies. Subsequent modification of the aeolian system during a transgression appears to result in the development of extensive regional bounding surfaces by aeolian erosion of the palaeo-erg. Bounding surfaces within the aeolian sequence of the Southern Namib probably span considerable time gaps, during which substantial changes to the depositional environment have occurred. The highly erosional nature of the environment severely restricts the preservation potential of the sand bodies. With continued erosion and modification of these extensive bounding surfaces, it will become progressively more difficult to fully appreciate the nature of these changes in the rock record.

Figure 7.70. A regional bounding surface produced by aeolian erosion of the Fiskus Sandstone Beds along the eastern margin of Elizabeth Bay. Note the arcuate form of the tabular-planar cross-bedded sets of the palaeo-erg in the foreground. Large barchanoid draas, which provide a modern analogue for the interpretation of these features are faintly visible in the background, (arrowed). This photograph demonstrates the similarlity between the palaeo- and present-day aeolian current system within the Namib.

8. SUMMARY OF PLACER FORMATION WITHIN ENDOREIC BASINS

8.1. PHASES OF DIAMOND INPUT TO THE WEST COAST

Beetz (1926) proved the presence of diamonds in the marine deposits at Eisenkieselklippenbake, 160 masl. The inferred age of these sediments based on the presence of exotic clasts of agate, chalcedony, jasper and chrysoprase is Upper Palaeocene to Lower Eocene (Siesser and Salmon, 1979). According to Beetz (1926), Reuning recovered a diamond of 2.5 cts from the marine Lower Buntfeldschuh Formation. This sequence of sediments has been tentatively correlated with the Eisenkieselklippenbake deposit by Siesser and Salmon (1979). The association of exotic clasts of agate, chalcedony, jasper and chrysoprase with placer deposits led to the concept that many of the diamonds within the region were derived from the reworking of these palaeo-shorelines (eg. Lotz, 1909 (cited by Krause, 1910); Range, 1909 (cited by Krause, 1910); Kaiser,1926).

Kaiser (1926) also considered it likely that diamonds had been introduced by the Pomona Beds, which he interpreted as a silicified alluvial deposit pre-dating the Chalcedon Tafelberg Silcrete Formation (sensu SACS, 1980). Prospecting at the time failed to prove this. In addition, diamonds were recovered from the extensive, coarse-grained alluvial braidplain deposits represented by the Gemsboktal and Blaubok Gravels.

It is now known that diamonds were also introduced to the west coast during the Miocene, via the Orange River, on the basis of the Arrisdrift vertebrate assemblage. Lateral equivalents of these deposits have effectively been worked for diamonds at Ochta (now known as Reuning), about 100 km inland on the Orange River (eg. Van Wyk and Pienaar, 1986) and at a number of other localities on the south bank. The CDM (Pty) Ltd., is currently in the process of establishing its own mining facility on the north bank.

8.2. PREVIOUS MODELS

Early workers such as Blake (1904), studying desert environments, concluded that the removal of fine-grained sediment by aeolian processes (deflation) resulted in surface lowering. Brüggen (1951, cited by Cooke, 1970) summarised this concept (Figure 8.1), which leads to stone pavement formation by the progressive accumulation

of immobile roughness elements at the surface of the bed. This study has proved that surfaces of this type are present within the Southern Namib deflation basin (section 4.4.2 and 5.3).

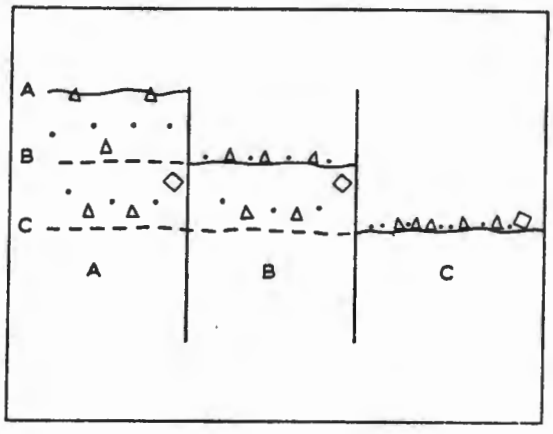

Figure 8.1. The concept of residual gravel lag stone pavements resulting from deflation. After Brüggen (1951).

Merensky (1909) originally expressed the view that the placer bodies were deflation residues primarily derived from Cretaceous marine deposits, but Kaiser (1926) noted that this conclusion was not substantiated by thorough investigation.

Kaiser (op. cit.) concluded that the Eocene marine sediments, and the Miocene alluvial gravels once completely infilled the area comprised of endoreic basins within the Southern Namib. Kaiser (op. cit.) refined the "residual lag" theory, and determined that cyclical reworking by the aeolian and ephemeral stream current systems was responsible for the formation of the placer bodies within endoreic basins. Although he realized that aeolian processes had, and continue to transport diamonds northwards from one basin to another, he retained the initial concept that the placer bodies resulted from surface lowering by deflation (Figure 8.2).

More recently, Sutherland (1985), has reiterated that the placer bodies within the deflation basin were of a residual or lag nature. This opinion was based on Macdonald's (1983) concept that aeolian processes are less efficient than sub-aqueous processes in the sorting of sediment.

The evidence presented in this study, however, does not support this concept. Within the aeolian environment of the Namib, barchan dunes composed entirely of heavy mineral grains can be seen, along with examples of segregation-associated aeolian bedforms migrating under the influence of creep. These observations lead to the conclusion that the aeolian system is perfectly capable of subtle size, density, shape sorting, as demonstrated by the creep tracer experiment in section 4.3.2.

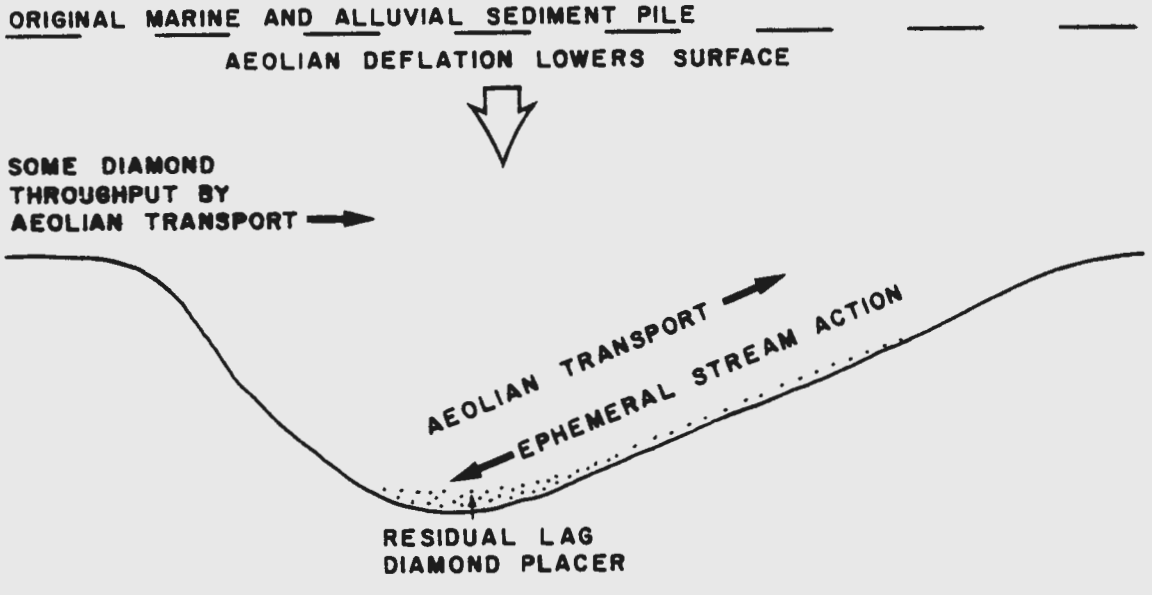

Figure 8.2. Summary of the concept of placer development envisaged by Kaiser (1926).

8.2.1. PROBLEMS WITH THE PREVIOUS MODEL

The recovery of diamonds from Upper Palaeocene to Lower Eocene marine sequences containing agate, chalcedony, jasper and chrysoprase led to the widespread belief that the presence of these exotics in stone pavement surfaces was indicative of placer formation. The examination of the exotic clast distribution (Figure 8.3) shows that exotic pebbles are confined to localised patches. The largest concentrations occur in the vicinity of the

Buntfeldschuh escarpment and Bogenfels, within the Bogenfels-Buntfeldschuh Basin. Additional, small, isolated localities are also present to the north of Bogenfels. In most cases, the exotic clasts are likely to have been derived from the reworking of the Upper Palaeocene to Eocene shorelines.

Significantly, to the north of Bogenfels, there is little evidence of any correlation between the presence of exotic clasts and the distribution of mining. This field evidence is confirmed by Kaiser (1926), who recorded that a number of the larger placer bodies did not contain agate, chalcedony, jasper and chrysoprase clasts. This contradicts the theory that the placer bodies represented residual deflation lags of material derived from the Eocene transgressive sequences. If this interpretation was correct, the main placer bodies would have been located in the vicinity of the Buntfeldschuh, and/or Bogenfels. Prospecting data confirm that minimal economic potential existed in the vicinity of the Buntfeldschuh. Placer deposits were associated with remnants of the Eocene shoreline at Bogenfels, within the re-entrant embayment, and in ephemeral drainage tracts. These were not as well developed as those within the endoreic basins around Pomona.

Implications of the Miocene and Post-Miocene Alluvial Phases for Placer Formation

The deposition of extensive alluvial braidplain deposits across the region during the Miocene highlights a major problem with the deflation residue hypothesis. Braidplain progradation was towards the west. The Eocene marine shorelines formed linear, south-north oriented sediment bodies similar to today. These would have been susceptible to reworking by the alluvial systems, as confirmed by the distribution of remnants of the Eocene shorelines within the Bogenfels-Buntfeldschuh Basin. At Eisenkieselklippenbake, remnants are preserved on the west-facing slope of a topographic high, within a bedrock depression. The dolomite ridge therefore prevented the alluvial system from reworking this part of the palaeo-shoreline. To the north and south, this remnant is surrounded by the Gemsboktal gravels, which extensively reworked the Eocene shoreline at 160 masl. The preservation of the Lower and Upper Buntfeldschuh Formation is probably due to the location of this sequence on an interfluve. Evidence that alluvial braidplain

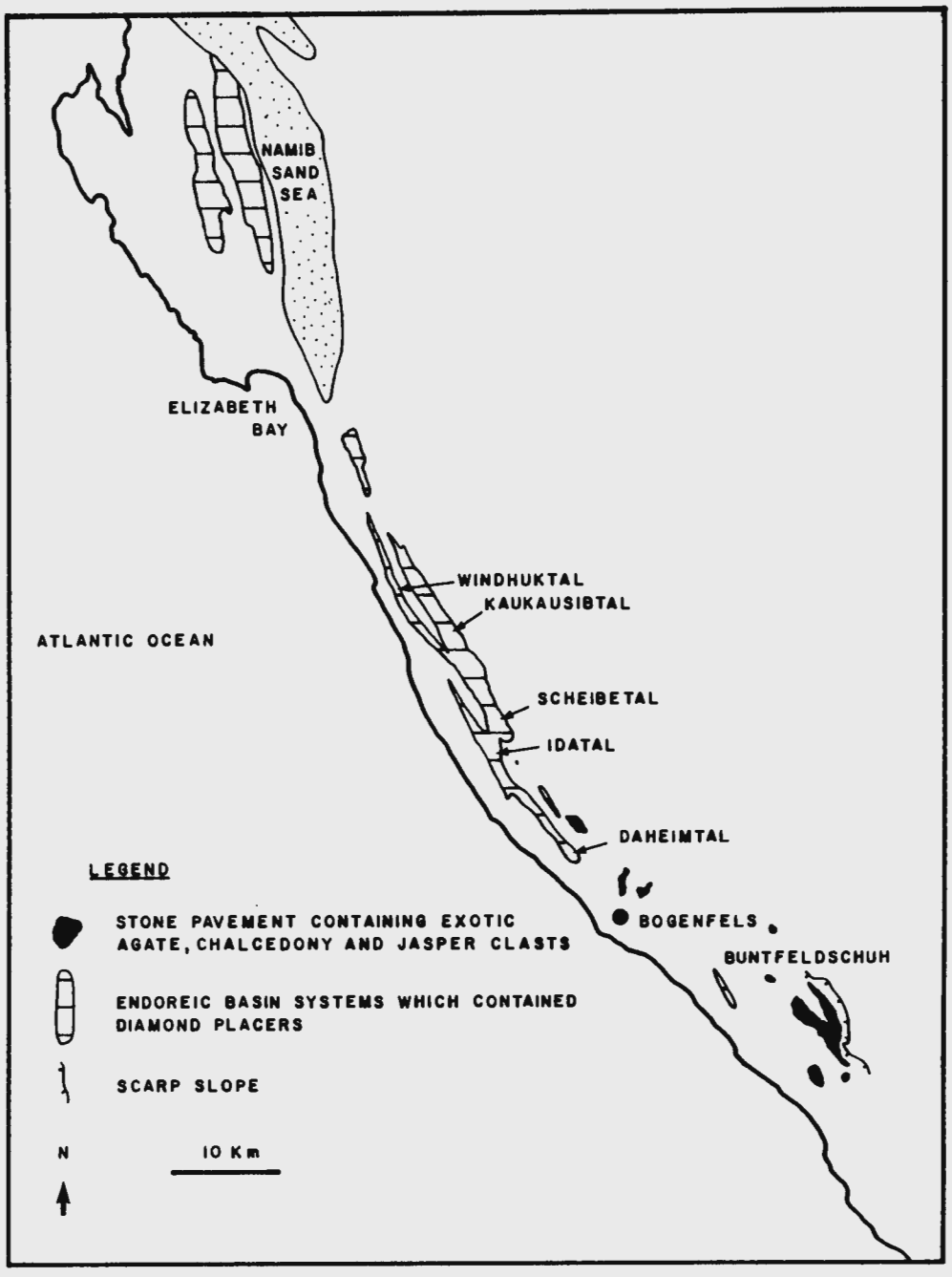

Figure 8.3. Map showing the distribution of exotic clasts within the deflation basin.

deposition occurred is present both to the north and south of the escarpment.

In other areas, the incorporation of agate, chalcedony and jasper clasts within the alluvial gravels is interpreted as confirmation that unprotected parts of the palaeo-shorelines were redistributed towards the west. The Miocene shoreline probably lay to the west of its present position during the progradation of the alluvial braidplains. The reworked material from the palaeo-shorelines was therefore potentially transported onto the sub-aerially exposed continental shelf, explaining the scarcity of preserved Eocene shoreline deposits.

Alluvial gravels containing clasts of the regionally extensive pedogenic hardpan calcrete dated at about 12 to 10 Ma, located during this study at Chameis, prove that post-Miocene alluvial systems have operated. In the Kuiseb Valley, of the Central Namib, the alluvial history is more completely preserved. This evidence suggests that some alluvial activity probably occurred between about 5 to 2 Ma, and then at later points during the Pleistocene. At the present time it is difficult to prove the exact timing of these events, but they probably also resulted in the transport of diamonds from the deflation basin, onto the continental shelf.

Any alluvially reworked material that did not reach the continental shelf is likely to have been incorporated into comparatively thick alluvial sequences, causing dilution of the original placer bodies. The deflation residue hypothesis therefore appears to be unsatisfactory, and it is unlikely to explain the diamond placer bodies contained within the endoreic basins.

A further failing of the deflation hypothesis is that it does not provide a mechanism whereby the transport of a heavy mineral component through the endoreic basin systems was/is maintained. Any model should fulfill this criterion for the progressive concentration of the resistant heavy mineral component to proceed. It is highly unlikely that diamonds were mainly deposited in sequences located above the underlying endoreic basins, which possibly were not developed by the Eocene.

8.3. A NEW MODEL FOR PLACER FORMATION WITHIN ENDOREIC BASINS

The theory that longshore drift within the nearshore marine environment has played an important role in the generation of the placer bodies along the west coast to the north of the Orange River, has existed since the deposits were initially discovered (eg. Merensky, 1909; Lotz, 1909).

Information which became available after Kaiser had completed his work in 1926 considerably altered the interpretation of the deposits. Of primary importance were the discoveries of the marine placer bodies at Alexander Bay, Oranjemund and Kleinzee in the late 1920's. These deposits proved that Kaiser had been incorrect in considering that diamond input had occurred only during the Eocene transgressions.

Prior to this study, Plio-Pleistocene transgressive deposits were thought to have been absent along the coastal margin of the deflation basin. A backshore mixed pan and aeolian facies of the Fiskus Sandstone Beds, which was tidally influenced, is interpreted as evidence of the 30 m transgression. That others have not been recognised may well be a function of preservation potential. Provided that a heavy mineral component was present, placer bodies resembling the CDM raised beach deposits could have been generated along the deflation basin's coastal margin. This supports the concept that the heavy mineral component was either derived from the reworking of earlier deposits or introduced to the marine environment by a palaeo-fluvial system (eg. Lotz, 1909, Range, 1909).

8.3.1. THE ABILITY OF THE AEOLIAN SEDIMENT DISPERSAL SYSTEM TO REWORK MARINE PLACER BODIES AND CREATE AEOLIAN PLACERS

Kaiser (1926) noted that a significant increase in diamond concentration occurred in the vicinity of aeolian barchan dunes. The examination of this diamond dispersal pattern using the concept of aeolian transport corridors, independently maintained by secondary helical vortices in the planetary boundary layer, provides the basis for the new placer model.

Empirical sandflow data collected using sand traps, proves that the position of barchan dune trains define the maximum areal

concentration of sandflow within aeolian transport corridors. As a result, the creep transport rate, driven by the collision of saltating grains with the bed, is also greater within aeolian transport corridors. These zones are therefore highly dynamic tracts in which aeolian sediment is transported from its coastal generation point, to the southern margin of the depositional basin.

The present-day location of aeolian transport corridors within the deflation basin is dependent upon the location of log-spiral and south-facing re-entrant embayments along the coast. This location varies in response to sea-level movement. Geomorphological evidence presented in section 7.4.3. shows that the western margin of the south-facing Bogenfels re-entrant embayment has previously been traversed by an aeolian transport corridor during marine regression(s). Computer modelling shows that this re-entrant would provide conditions suitable for the generation of a major aeolian transport corridor during transgression(s) (section 7.4.5). It is therefore postulated that an aeolian transport corridor has periodically been located within Daheimtal, from which it has entered the Idatal, prior to passing north via Pomona (Figure 8.4).

In the discussion of stone pavement surface morphology (section 4.4.6.) it was demonstrated that weathering, both by aeolian processes and by salt weathering, profoundly modify exposures of raised beaches, such as the 55 masl. Upper Eocene deposit at Bogenfels. Weathering breaks down the coarse-grained clastics, rendering the fragments susceptible to removal by both aeolian saltation and creep transport. During periods when aeolian transport corridors have traversed the position of the Bogenfels re-entrant embayment, the potential has thus existed for the weathering products to be transported north by the aeolian sediment dispersal system. The resulting surface lowering would have released resistant heavy mineral grains from marine placer bodies and incorporated them into the aeolian bedload creep population. Theoretically, during regressions, aeolian transport corridors traversing previously submerged marine placers have also transported weathering products, including heavy minerals, into the endoreic basin systems via the Bogenfels area. The mining of the aeolian Fiskus Sandstone Beds at Elizabeth Bay and Kolmanskop for diamonds earlier this century is interpreted as confirmation that this has taken place.

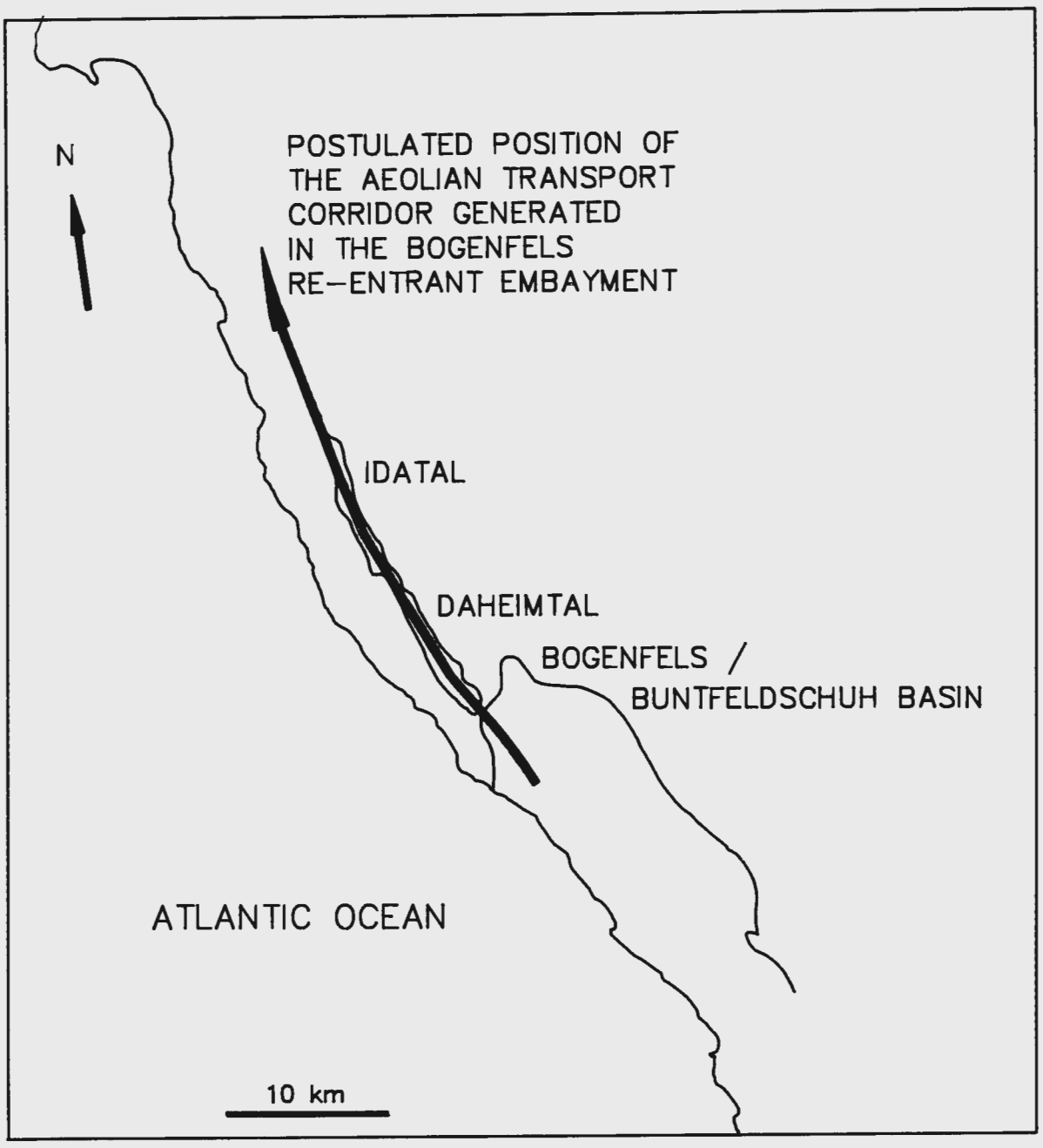

Figure 8.4. Sketch map showing the location of the Bogenfels re-entrant embayment and the path of the aeolian transport corridor which has periodically traversed it.

Although Kaiser (1926) realised that the placer bodies within the endoreic basins at least partially resulted from aeolian transport, and that diamonds have been transported from one basin to another by aeolian processes, he did not fully appreciate the extent to which this has probably occurred. This is clearly revealed by the computer generated diamond dispersal patterns in section 6.3. The examination of aeolian size-sorting within aeolian transport corridors (section 4.3.3) indicates that creep transport along these wind-aligned zones is very fast compared to that in other parts of the deflation basin. It is thus envisaged that the aeolian transport corridors, periodically located within the Bogenfels-Daheimtal-Idatal conduit, were narrow tracts along which creep bedload rapidly migrated north into the Pomona area. It is even conceivable that diamonds were transported onto the stoss slope of the barchan dunes by creep. The measurement of present-day barchan migration suggests that diamonds might then have moved through the deflation basin system at between 35 to 60 m/year. The new model therefore fulfills the condition that the resistant, heavy mineral component has progressively been transported into and through the endoreic basin system, thus permitting the formation of the placer bodies to proceed.

Fluctuations of sea-level during the development of the placer bodies would have resulted in periodic shifts in the position of the aeolian transport corridors. It it therefore unlikely that the creep transport rate was maintained at a continuously high level within the Bogenfels-Daheimtal-Idatal conduit. Hypothetically, pulses of diamond transport by aeolian creep thus progressed along the conduit. These pulses were punctuated by periods dominated by weathering processes, when the creep transport rate was reduced in response to reduced sandflow conditions.

During pulses of increased sandflow, when creep transport rates were high, diamonds would be subjected to aeolian size-shape sorting. Kinematic wave theory suggests that slightly different size fractions of the population would become incorporated into kinematic waves travelling at different speeds. It is probable that any increase or decrease in the sandflow rate, in response to changing coastal morphology, would modify the speed with which the kinematic waves progressed through the endoreic basin system. The present-day coastal morphology does not appear to be conducive to

rapid creep transport along the conduit, because no major aeolian transport corridor is located within it. The minor corridor generated at Van Reenen Bay does, however, influence aeolian sediment dispersal within the Idatal. It is therefore concluded that the northward migration of the aeolian creep bedload component of the placer body within the Idatal was comparatively slow when the deposit was discovered. Had the placer body remained intact, it is predicted that at some point in the future another aeolian transport corridor would have traversed the Bogenfels south-facing re-entrant, and migrated along the Daheimtal-Idatal conduit. A new pulse of aeolian creep transport would then have occurred, and the rapid migration of the kinematic waves to the north would have been resumed.

A variety of bottlenecks of various scales, leading to the generation of kinematic shock waves, would have been encountered by the kinematic waves as they progressed through the endoreic basin system. This study has demonstrated that stone pavements within aeolian transport corridors are not comprised of immobile particles forming residual lag accumulations on the bed. Roughness elements provide nuclei for the development of particle clusters by the creep bedload. Observations presented above conclusively show that provided the transport of the heavy mineral component of the creep bedload is maintained past these nuclei, particle clusters dominated by heavy mineral grains will result (Figure 8.5). Stone pavement surface micro-topography also creates small-scale bottlenecks formed by gaps between roughness elements on these dynamic substrates within aeolian transport corridors. It is therefore probable that diamonds forming the placer deposit were incorporated into particle clusters. As previous workers have noted, granule ripples also provide sites for heavy mineral segregation by aeolian processes. Repeated cycling of the creep bedload component associated with granule ripples has been shown to provide one mechanism by which the segregation of heavy minerals can occur on the stoss slope. This is probably in response to subtle variation in the creep transport rate on the stoss slope with respect to the migration rate of the bed form itself. The south-facing slopes at the northern ends of the endoreic basins appear to act as large-scale bottlenecks. The advance of the creep bedload on reaching these topographic obstacles appears to

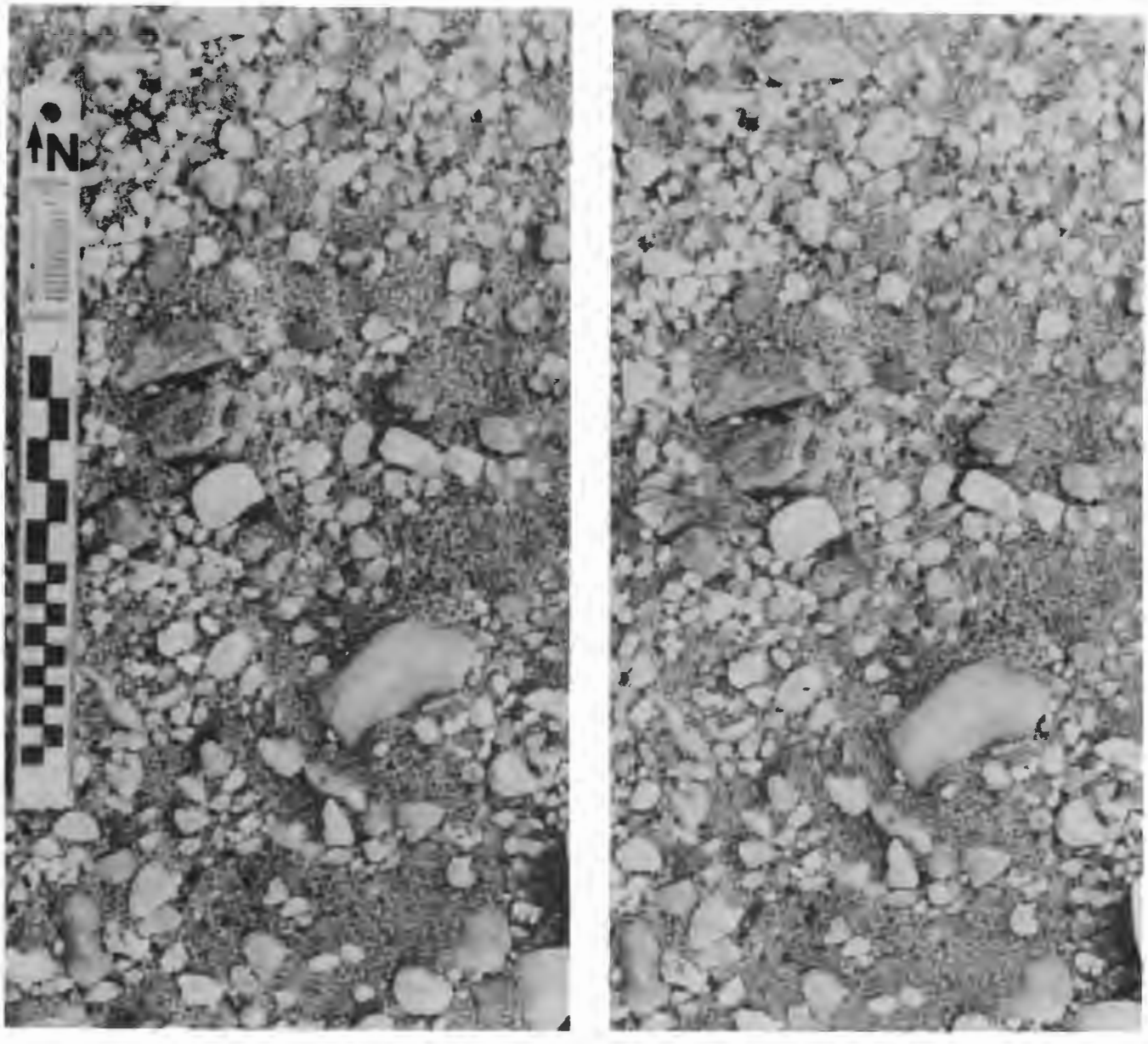

Figure 8.5. Stereo-pair taken on 23/11/88, showing part of the garnet creep experiment. Note the particle clusters of garnet in the split between fragments of a quartzite roughness element, and between and against quartz roughness elements on the stone pavement surface. Scale 10 cm.

decrease, resulting in the formation of encroachment deposits. It has been shown above that the surficial grains comprising encroachment deposits exhibit an imbricate shape-fabric. Kaiser (1926) records that diamonds were recovered from stone pavements of this type. Changes in the pivotting angle, and the direction in which the collision force due to saltation impact acts on particles theoretically increase bed stability, and reduce the entrainment potential from these surfaces. With the continued transport of diamonds across such a surface, the relative concentration of the heavy mineral component would potentially increase, in response to aeolian size-density-shape sorting. Once incorporated into the imbricate shape-fabric, the entrainment potential of the diamonds into creep theoretically decreases, creating conditions suitable for aeolian placer deposit formation. It is postulated that this explains the frequent occurrence of placer bodies on the south-facing slopes of endoreic basins.

To what extent palaeoclimatic changes resulting in increased rainfall, and more frequent alluvial activity, influenced placer deposit formation once the endoreic basin system had fully developed is difficult to assess. This is primarily because the point at which the endoreic basins developed is not yet clear. Once formed, the possibility for alluvial transport from one basin to another was severely reduced. Ephemeral alluvial current systems operating within the Luderitzfelder area did rework deposits within basins located on the eastern side of the main deflation basin. These systems transported diamonds, and undoubtedly introduced material to the southern end of the Idatal which was derived from raised shorelines which lay to the east (Figure 8.6). No evidence for these shorelines now exists. In time, the resumption of aeolian processes progressively reworked the channel floors of the ephemeral stream systems. The material was reintroduced to the aeolian sediment dispersal system, and the resistant heavy minerals were ultimately incorporated into placer bodies within the Idatal, Hexenkessel, Scheibetal and Kaukausibtal.

Aeolian transport potentially removed many diamonds from these basins, and transported them northwards. In response to aeolian size, density, shape sorting, the smaller diamonds were preferentially removed by more rapid transport. The coarser material forming part of the dynamic creep bedload followed at a

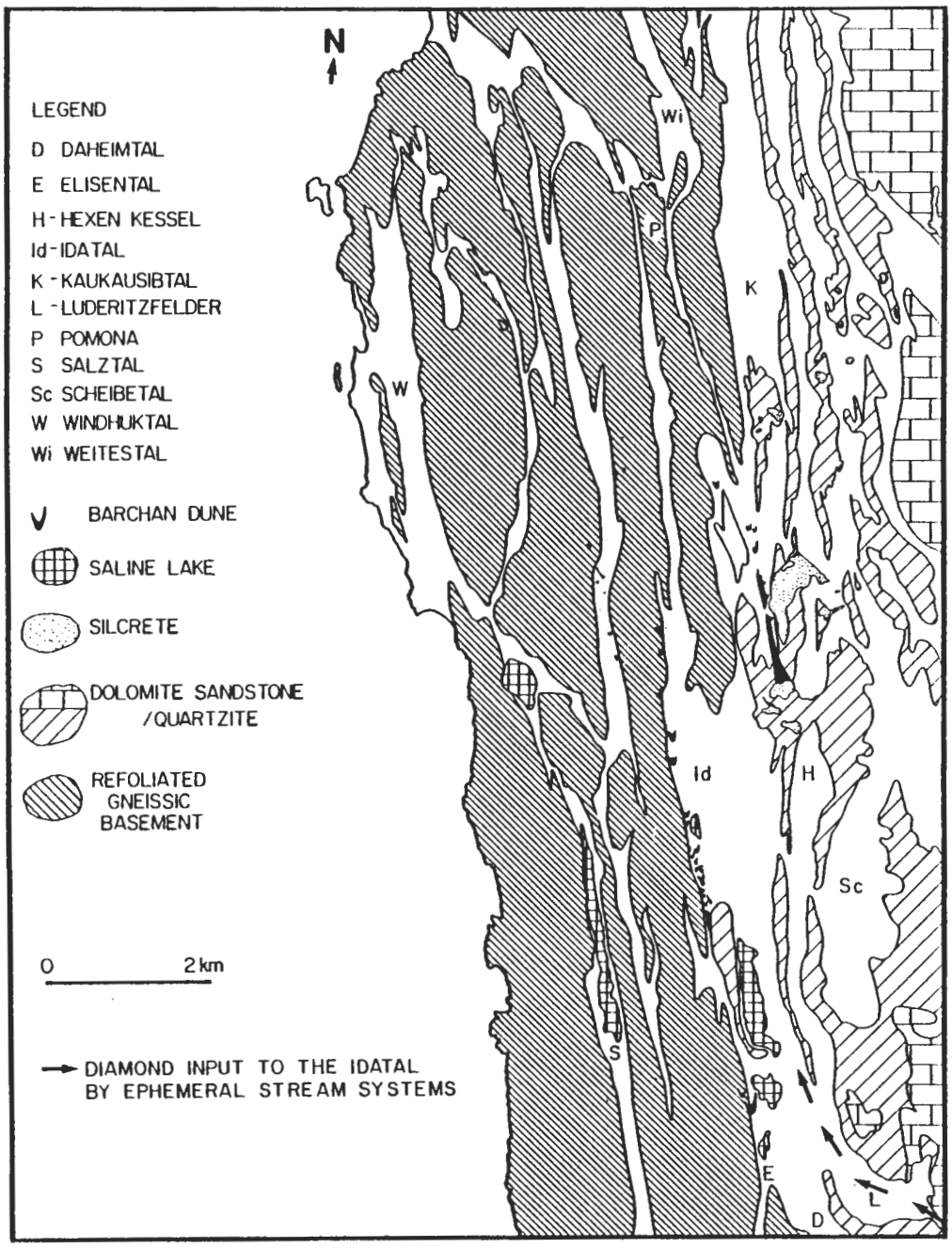

Figure 8.6. Map showing the location of the Luderitzfelder drainage tract by which diamonds entered the Idatal and Hexenkessel endoreic basins. The diamonds were probably derived from ephemeral stream reworking of palaeo-shorelines and aeolian placer bodies which lay to the east.

slower transport rate. It is concluded that only the diamonds that were too large to be transported by aeolian creep can be interpreted to be residual lag deposits resulting from deflation and aeolian removal processes (Figure 8.7).

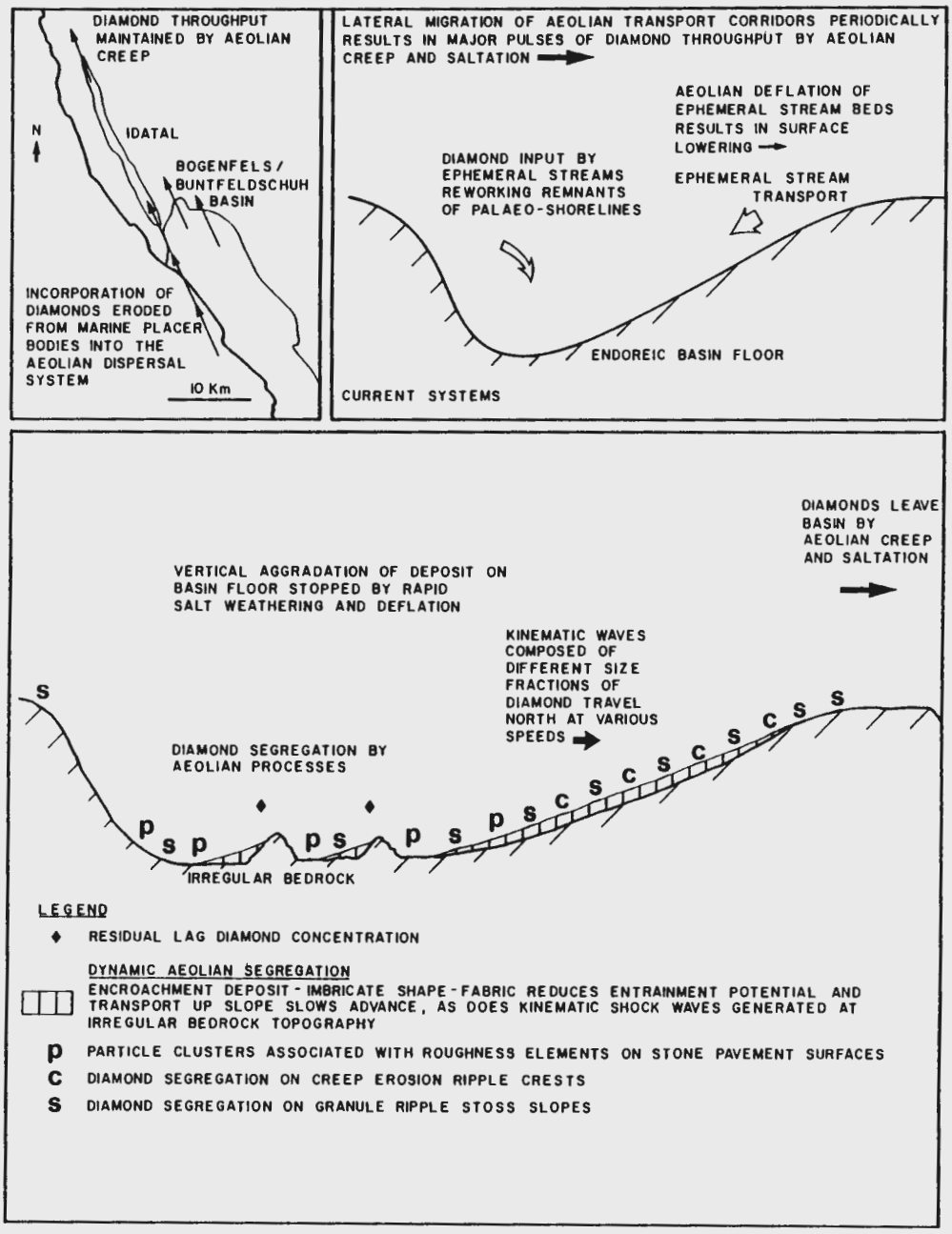

Figure 8.7. Conceptualised summary of placer body development within endoreic basins by aeolian transport processes influencing the bed.

REFERENCES

Allen, J.R.L. (1968a). Current Ripples. North Holland, Amsterdam, 433p.

Allen, J.R.L. (1982). Sedimentary Structures: their character and physical basis Vol. 1, 593p. Elsevier, Amsterdam. Developments in Sedimentology 30 A.

Allen, J.R.L. (1982). Sedimentary Structures: their character and physical basis Vol. 2, 663p. Elsevier, Amsterdam. Developments in Sedimentology 30 B.

Anderson R.S. (1986). Erosion Profiles due to particles entrained by wind: Application of an eolian sediment-transport model. Geol.Soc.Am. Bull.,97 ,1270-1278.

Arie, M. & Rouse, H. (1956). Experiments on two-dimensional flow over a normal wall. J.Fluid Mech., 1, 129-141.

Ashmore, G.P. (1911). The Occurrence of Diamonds in German South West Africa. S.A. Mine Journal, 440.

Bagnold, R.A. (1935). The transport of sand by wind. Geog. Jour., 85, 342-369.

Bagnold, R.A. (1954, first edition 1941). The Physics of Blown Sand and Desert Dunes. Methuen, London, 265p.

Bascom, W.H. (1951). The relationship between sand size and beach slope. Trans. Am. Geohys. Union, 32, 866-874.

Beetz, W. (1926). Die Tertiärablagerungen der Küstenwüsternamib. In: Kaiser, E., (Ed.), Die Diamantenwüste Südwestafrikas, 2, 1-54. Dietrich Reimer (Ernst Vohsen), Berlin.

Best, J.L. (1985). Sediment transport and bed morphology at river channel confluences. Sedimentology, 35, 481-498.

Best, J.L., Brayshaw, A.C., (1985). Flow separation - a physical process for the concentration of heavy minerals within alluvial channels. Geol.Soc., 142, 747-756.

Blake,W.P. (1904). Origin of pebble-covered plains in desert regions. Trans. Am. Inst. Min. Eng., 34, 161-162.

Böhm, Von J. (1926). Uber tertiare Versteinerungen von den Bogenfelser Diamanfeldern. In: Kaiser,E., Die Diamantenwüste Südwestafrikas, 2, 55-87. Dietrich Reimer (Ernst Vohsen), Berlin.

Bosworth, T.O. (1922). Desert conditions and processes in the desert of Tumbes, Peru. In: Geology of the Tertiary and Quartenary periods in the north western part of Peru. Macmillan and Co., London, p. 269-309.

Brayshaw, A.C., Frostick, L.E., Reid, I. (1983). The hydrodynamics of particle clusters and sediment entrainment in coarse alluvial channels. Sedimentology, 30, 137-143.

Brookfield, M.E. (1977). The origin of bounding surfaces in ancient aeolian sandstones. Sedimentology, 24, 409-414.

Brown, R.A. (1983). The flow in the planetary boundary layer. In: Brookfield, M.E. & Ahlbrandt, T.S., (Eds) Eolian sediments and processes. Elsevier, Amsterdam, pp. 291-310. Developments in sedimentology 38.

Brüggen, J. (1951). Las costras de proteccion en los desiertos, Revista Universitaria (Chile), 36, 101-104.

Buckley, R. (1987). The effect of sparse vegetation on the transport of dune sand by wind. Nature, 325, 426-428.

Channing, A., (1976). Life histories of frogs in the Namib Desert. Zoologica Africana, 11, 299-312.

Chepil, W.S. (1945). Properties of soil which influence wind erosion: the governing principle of surface roughness. Soil Sci., 69, 149-62.

Chepil, W.S. (1945). Dynamics of wind erosion: 1. Nature of movement of soil by wind. Soil Sci., 60, 305-319.
Chepil, W.S. (1945). Dynamics of wind erosion: 2. Initiation of soil movement. Soil Sci., 60, 397-411.
Chepil, W.S. (1945). Dynamics of wind erosion: 3. The transport capacity of wind. Soil Sci., 60, 475-480.
Clifton, H.E., Hunter, R.E. & Phillips, R.L. (1971). Depositional structures and processes in the non-barred high-energy nearshore. J. Sedim. Petrol., 41, 651-670.
Clifton, R.E. (1977). Rain-Impact Ripples. Jour. Sedim. Petrol., 47, 678-679.
Coaton, W.G.H. & Sheasby, J.L. (1973). National survey of the Isoptera of Southern Africa. 3. The genus Psammotermes Desneux. Cimbebasia, Ser. A, 3, 19-28.
Coaton, W.G.H. & Sheasby, J.L. (1975). National survey of the Isoptera of Southern Africa 10. The genus Hodotermes Hagan (Hodotermitidae). Cimbebasia, Ser. A, 3, 105-138.
Collinson, J.D. (1970). Bed forms of the Tana River, Norway. Geogr. Ann., 52A, 31-55.
Cook, D.O. (1970). The occurrence and geologic work of rip currents off southern California. Mar. Geol., 9, 173-186.
Cooke, R.U. (1970). Stone pavements in deserts. Ann. Ass. Am. Geogr., 60, 560-577.
Cooke, R.U. (1981). Salt weathering in deserts. Proc Geol.Soc. (Lond)., 92, 1-16.
Corvinus, G. & Hendey, Q.B. (1978). A new Miocene vertebrate locality at Arrisdrift in South West Africa (Namibia). N. Jb. Geol. Palaeont. Mh., 4, 193-205.
Dal Cin, R. (1968). Pebble clusters: their origin and utilisation in the study of palaeocurrents. Sedim. Geol., 2, 233-241.
De Decker, R.H. (1986). The geological setting of diamondiferous deposits on the inner shelf between the Orange River and Wreck Point, Namaqualand. Joint Geol. Surv./Univ. Cape Town Tech. Bull., 16, 230p.
Dingle, R.V., Siesser, W.G. & Newton, A.R. (1983). Mesozoic and Tertiary Geology of Southern Africa. Balkema, Rotterdam, 375p.
De Wit, M.C.J. (1988). Aspects of the geomorphology of the north-western Cape, South Africa. In: Dardis, G.F. & Moon, B.P., (Eds.) Geomorphical Studies in Southern Africa. Balkema, Rotterdam.
Elliot, T. (1978). Clastic shorelines. In: Reading, H.G., (Ed.), Sedimentary environments and facies. Blackwell, Oxford, pp.147-177.
Endrody-Younga, S. (1981). Dispersion and translocation of dune specialist Tenebrionids in the Namib area. Cimbebasia, 5, 257-271.
Eschner, T.B. & Kocurek, G. (1986). Marine Destruction of Eolian Sand Seas: Origin of Mass Flows. Jour. Sedim. Petrol., 56, 401-411.
Etheridge, D.W. & Kemp, P.H. (1978). Measurements of turbulent flow downstream of a rearward-facing step. Jour. Fluid Mech., 86, 545-566.
Fahnestock, R.K. & Haushild, W.L. (1962). Flume studies of the transport of pebbles and cobbles on a sand bed. Geol. Soc. Am. Bull., 73, 1431-1436.

Folk, R.L. (1971). Longitudinal dines of the northwestern edge of the Simpson Desert, Northern territory, Australia. 1: Geomorphology and grain size relationships. Sedimentology, 16, 5-54.
Folk, R.L. & WARD, W.C. (1957). Brazos River Bar: a study in the significance of grain size parameters. Jour. Sediment. Petrol., 27, 3-26.
Frankel, J.J. & Kent, L.E. (1938). Grahamstown surface quartzites (silcretes). Trans. Geol. Soc. S. Africa, 40, 1-42.
Free, E.E. (1911). Desert pavements and analagous phenomena. Science, 33, 355.
Fryberger, S.G. & Dean, G. (1979). Dune forms and wind regime. In: Mckee, E.D.,(Ed.) A Study of Global Sand Seas. U.S. Geol. Surv. Prof. Pap., 1052, pp. 136-169.
Fryberger, S.G., Ahlbrandt, T.S. & Andrews, S. (1979). Origin, sedimentary features, and significance of low-angle eolian "sand sheet" deposits, Great Sand Dunes National Monument and vicinity, Colorado. J. Sedim. Petrol., 49, 733-746.
Fryberger, S.G. & Schenk, C.J. (1988). Pin stripe lamination: A distinctive feature of modern eolian sediments. Sedimentary Geology, 55, 1-16.
Fryberger, S.G., Schenk, C.J. & Krystinik, L.F. (1988). Stokes surfaces and the effects of near-surface groundwater-table on aeolian deposition. Sedimentology,35, 21-42.
Garvie, O. (1983). Grading analysis and surface textures of six sand samples from the Bogenfels area, Namibia/South West Africa. Unpubl. Anglo American Res. Lab. Rep., No.486.
Gerety, K.M. & Slingerland, R. (1983). Nature of the saltating population in wind tunnel experiments with hetergeneous size-density sands. In: Brookfield, M.E., and Ahlbrandt, T.S.,(Eds.) Eolian sediments and processes, Elsevier, Amsterdam, pp. 115-132. Developments in Sedimentology 38.
Gilbert, G.K. (1914). The transportation of debris by running water. U.S. Geol. Surv., Prof. Pap., 86, 263p.
Gillette, D.A., Adams, J., Mutts, D. & Kihl, R. (1982). The threshold friction velocities and rupture moduli for crusted desert soils for the input of soil particles into the air. J. Geophys. Res., 87, 9003-9015.
Glennie, K.W. (1970). Desert Sedimentary Environments. Elsevier, Amsterdam 222p. Developments in Sedimentology 14.
Good, M.C. & Joubert, P.N. (1968). The form drag of two-dimensional bluff-plates immersed in turbulent boundary layers. Jour. Fluid Mech., 31, 547-582.
Goudie, A.S., Cooke, R.U. & Doornkamp, J.C. (1979). The formation of silt from quartz dune sand by salt-weathering processes in deserts. Jour. Arid Env., 2, 105-112.
Goudie, A. (1972). Climate, weathering crust formation, dunes and fluvial features of the Central Namib Desert, near Gobabeb, South West Africa. Madoqua, 4, 54-62.
Goudie, A., Cooke, R.U. & Evans, I. (1970). Experimental investigation of rock weathering by salts. Area, 4, 42-48.
Goudie, A.S. & Day, M.J. (1980). The disintegration of fan sediments in Death Valley, California, by salt weathering. Physical Geogrraphy, 1, 126-137.
Greeley, R. (1986). Aeolian landforms: laboratory simulations and field studies. In: Nickling, W.G., (Ed), Aeolian Geomorphology. Proc. 17th. Annual Binghampton Geomorph. Symp., pp. 195-211. Allen & Unwin.

Greeley, R. & Iversen, J.D. (1985). Wind as a geological process. Cambridge Univ. Press, England, 333p.
Greeley, R., Williams, S.H. & Marshall, J.R. (1983). Velocities of wind-blown particles in saltation: preliminary laboratory and field measurements. In: Brookfield, M.E. & Ahlbrandt, T.S., (Eds) Eolian sediments and processes. Elsevier, Amsterdam, pp. 133-148. Developments in Sedimentology 38.
Greenman, L. (1966). The geology of area 2615C Lüderitz, South West Africa. Unpubl. MSc. thesis, Univ. Cape Town, South Africa.
Greenman, L. (1969). The Elizabeth Bay Formation, Luderitz, and its bearing on the genesis of dolomite. Trans. geol. Soc. S.Afr., 72, 115-121.
Grolier, M.J., Ericksen, C.E., McCauley, J.F. & MORRIS, E.C. (1974). The desert landforms of Peru: A preliminary photographic atlas. U.S. Geol. Surv. Interagency Rep., Astrogeology, 57, 146p.
Hallam, C.D. (1964). The geology of the coastal diamond deposits of Southern Africa (1959). In: Haughton, S.H., (Ed.) The geology of some ore deposits in Southern Africa. Geol. Soc. S. Afr., pp. 671-728.
Hamilton, W.R. & van Couvering, A.W. (1977). Lower Miocene Mammals from South West Africa. Namib Bull. Suppl. 2, Transv. Mus. Bull., 9-11.
Handford, C.R., Kendall, L.A.C., Dunham, J.B. & Logan, B.W. (1983). Aragonitic crusts and pisolites beneath dolomitic tepees, Lake MacCleod Evaporite Basin, Western Australia (abstr). Bull. Am. Ass/ Petrol. Geol., 67, 478.
Handford, C.R., Kendall, L.A.C., Prezbindowski, D.R. & Dunham, J.B. (1984). Salina-margin tepees, pisoliths and argonitic cements, Lake MacCleod, Western Austalia: their significance in interpreting ancient analogs. Geology, 12, 523-527.
Hanna, S.R. (1969). The formation of longitudinal sand dunes by large helical eddies in the atmosphere. Jour. Applied Meteorol., 8, 874-883.
Haq, B.U., Hardenbol, J., & Vail, P.R. (1987). Chronology of fluctuating sea levels since the Triassic. Science, 235, 1156-1167.
Harger, H.S. (1914). Some features associated with the denundation of the South african continent. Proc. Geol Soc. SA., 16, 22-41.
Harms, J.C. & Fahnestock, R.K. (1965). Stratification, bedforms, and flow phenomena (with an example from the Rio Grande) Soc. Econ. Paleontologists & Mineralogists Spec. Pub. 12.
Haughton, S.H. (1931). The late Tertiary and Recent deposits of the west coast of South Africa. Trans. Geol. Soc. S. Afr., 34, 19-58.
Heissig, K. (1971). Brachypotherium aus dem Miozan von Südwestafrikas. Mitt. Bayer. Sttatssammel. Palaont. hist. Geol., 11, 125-128.
Hendey, Q.B. (1978). Miocene Vertebrates from Arrisdrift, South West Africa. Ann. S. Afr. Mus., 76, 1-41.
Hopwood, A.T. (1929). New and little known mammals from the Miocene of Africa. Am. Mus. Novitt, 344, 1-9.
Horikawa, K. & Shen, H.W. (1960). Sand movement by wind action - on the characteristics of sand traps. Beach Erosion Board Tech. Mem., 119, 51p.
Horikawa, K., Shintaro, H., Kubota, S. & Katori, S. (1983). On the sand transport rate by wind on a beach. Coastal Eng. Japan, 26, 101-120.

Hunter, R.E. (1977). Terminology of cross-stratified sedimentary layers and climbing ripple structures. Jour. Sedim. Petrol., 47, 697-706.
Illenberger, W.K. & Rust, I.C. (1986). Venturi-compensated Eolian Sand Trap for Field Use. Jour. Sedim. Petrol., 56, 541-542.
Iversen, J.D. & Greeley, R. (1978). Atmospheric and wind tunnel experiments of the Amboy Crater sand-covered lava flow. Iowa State Univ. Eng. Res. Inst. Rep., ERI-78235, 79p.
Jeffreys, H. (1928). Some cases of instability in fluid motion. Proc. R. Soc. London, Ser.A, 118, 195-208.
Jury, M.R. (1985). Case studies of alongshore variations in wind-driven upwelling in the southern Benguela region. In: Shannon, L.V., (Ed.) South African ocean colour and upwelling experiment. Sea Fisheries Res. Inst., Cape Town, 270p.
Kaiser, E. (1926). Die jungen sedimentären neubildungen om extrem-ariden klima der Namibwüste. In: Die Diamantenwüste Südwestafrikas, 2, 317-380. Dietrich Reimer (Ernst Vohsen), Berlin.
Kamstra, F. (1985). Environmental Features of the Southern Benguela with Special Reference to Wind Stress. In: Shannon, L.V., (Ed.) South African ocean colour and upwelling experiment. Sea Fisheries Res. Inst., Cape Town, 270p.
Karcz, I. (1966). Secondary currents and the configuration of a natural stream bed. Jour. Geophys. Res., 71, 3109-3112.
Karcz, I. (1967). Harrow marks, current aligned sedimentary structures. Jour. Geol., 75, 113-121.
Kendall, C.G.St. C. & Warren, J.P. (1987). A review of the origin and setting of tepees and their associated fabrics. Sedimentology, 34, 1007-1028.
Kennett, J.P. (1982). Marine Geology. Prentice-Hall, New Jersey, 813p.
King, C.A.M. (1953). The relationship between wave incidence, wave direction, and beach changes at Marsden Bay, Co. Durham. Trans Brit. Geogr., 19, 13-23.
Klinger, H.C. (1977). Cretaceous deposits near Bogenfels, South West Africa. Ann. S. Afr. Mus., 73, 81-92.
Kocurek, G. & Dott Jr., R.H. (1981). Distinction and uses of stratification types in the interpretation of eolian sand. Jour. Sedim. Petrol., 51, 579-595.
Kocurek, G. & Hunter, R.E. (1986). Origin of Polygonal Fractures in Sand, Uppermost Navajo and Page Sandstones, Page Arizona. Jour. Sedim. Petrol., 56, 895-904.
Krause, C. (1910). Notes on the German South-West African Diamonds. Trans. Geol. Soc. S. Afr., 13, 61-64.
Kröner, A. (1974). The Gariep Group, Part 1: Late Precambrian formations in the western Richtesveld, Northern Cape Province. Precambrian Res. Unit Univ. Cape Town Bull. No. 13.
Lancaster, N. (1983). Linear dunes of the Namib sand sea. Z. Geomorph. Suppl., 45, 27-49.
Lancaster, N. (1985). Winds and sand movements in the Namib Sand Sea. Earth Surf. Proc. & Landforms, 10, 607-609.
Langbein, W.B. & Leopold, L.B. (1968). River channel bars and dunes - Theory of kinematic waves. U.S. Geol. Surv. Prof. Pap., 422-L, 20p.
Laronne, J.B. & Carson, M.A. (1976). Inter-relationships between bed morphology and bed transport for a small gravel bed. Sedimentology, 23, 67-85.

Li, Z. & Komar, P.D. (1986). Laboratory measurements of pivoting angles for applications to selective entrainment of gravel in a current. Sedimentology, 33, 413-423.
Lighthill, M.J. & Whitham, G.B. (1955a). On kinematic waves. 1. Flood movement in long rivers. Proc. Roy. Soc. Lond. Ser.A., 229, 281-316.
Lighthill, M.J. & Whitham, G.B. (1955b). On kinematic waves. 2. A theory of traffic flow on long crowded roads. Proc. Roy. Soc. Lond. Ser.A., 229, 317-345.
Lotz, H. (1909). Über die Luderitzbuchter diamantvorkommen. Zeitschr. F. Prakt. Geol. 17. S. 142. Cited in: Kaiser, E., Die Diamantenwüste Südwestafrikas, Dieter Reimer, Berlin.
Lyle L., Schrandt, R.L. & Schneidler, N.F. (1974). How aerodynamic roughness elements control sand movement. Trans. Am. Soc. Agr. Eng., 17, 134-139.
Mabutt, J.A., Wooding,R.A. & Jennings,J.N. (1969). The asymmetry of Australin desert sand ridges. Austalian Jour. Sci., 32, 159-160.
MacDonald, E.H. (1983). Alluvial mining. Chapman-Hall, London. Cited in: Sutherland, D.G. (1985). Geomorphological controls on the distribution of placer deposits. J. geol. Soc. London, 142, 727-737.
Maegley, W.J. (1976). Saltation and Martian sandstorms. Rev. Geophys. Space Phys., 14, 135-142.
Marshall, J.K. (1971). Drag measurements in roughness arrays of varying density and distribution. Agr. Meteorol., 8(4/5), 269-292.
Martin, H. (1953). Notes on the Dwyka succession and on some pre-Dwyka valleys in South West Africa. Trans. Geol. Soc. S. Afr., 56, 37-41.
Martin, H. & Schalk, K. (1957). Gletscherschliffe an der Wand eines U-Tales im nördlichen Kaokoveld, Südwestafrika. Geol. Rdsch., 46, 571-575.
McCauley, J.F., Breed, C.S., El Baz, F., Whitney, M.I., Grolier, M.J. & Ward, A.W. (1979). Pitted and fluted rocks in the Western Desert of Egypt: Viking Comparisons. Jour. Geophys. Res., 84, B14, 8222-8232.
McCauley, J.F., Grolier, M.J. & Breed, C.S. (1977). Yardangs of Peru and other desert regions. U.S. Geol. Surv. Interagency Rep., Astrogeology, 81, 177p.
McCauley, J.F., Grolier, M.J. & Breed, C.S. (1980). Yardangs. In: Doehring D.O., (Ed.), Geomorphology in arid regions. Proc. 8th Geomorphology Symposium, State University of New York, Binghampton, pp. 233-269. Allen & Unwin.
McFadden, L.D., Wells, S.G. & Jercinovich, M.J. (1987). Influences of aeolian and pedogenic processes on the origin and evolution of desert stone pavements. Geology, 15, 504-508.
McQuivey, R.S. & Keefer, T.N. (1969). The relation of turbulence to deposition of magnetite over ripples. U.S. Geol. Surv. Prof. Paper, 650-D, 244-247.
Meigs, P. (1953). World distribution of arid and semi-arid homoclimates. In: Reviews of Research on Arid Zone Hydrology. Arid Zone Prog. 1., UNESCO, Paris, pp. 203-209.
Meigs, P. (1966). Geography of coastal deserts. UNESCO, Arid Zone Res., 28, 1-40.
Merensky, H. (1909). The Diamond Deposits of Luderitzland, German South West Africa. Trans. Geol. Soc. S. Africa, 12, 13-23.

Meylan, P. & Auffenberg, W. (1986). New land tortoises (Testudines: Testudinae) from the Miocene of Africa. Zool. Jour. Linnean Soc., 86, 279-307.
Miall, A.D. (1977). A Review of the braided-river depositional environment. Earth Sci. Rev., 13, 1-62.
Middleton, G.V. & Southard, J.B. (1984). Mechanics of sediment movement (2nd. ed.). Soc. Econ. Pal. & Mineral., Short Course 3.
Miller, R. McG. & Seely, M.K. (1976). Fluvio-marine deposits south-east of Swakopmund, South West Afica. Madoqua, 9, 23-26.
Mosely, M.P. & Schumm, S.A. (1977). Stream Junctions - a probable location for bedrock placers. Economic Geology, 72, 691-697.
Moulden, J.C. (1905). Origin of pebble-covered plains in desert regions. Trans. Am. Inst. Mining Eng., 35, 963-964.
Murray, L.G., Joynt, R.H., O'Shea, D.O'c., Foster, R.W., & Kleinjan, L. (1971). The geological environment of some diamond deposits off the coast of South West Africa. In: Delany, F.M., (Ed.), The geology of the East Atlantic continental margin. Rep. Inst. geol. Sci., 70, 119-141.
Nelson, G. & Hutchings, L. (1983). The Benguela upwelling area. Progr. Oceanogr., 12, 333-356.
Netterberg, F. (1969). The interpretation of some basic calcrete types. S. Afr. Archaeol. Bull., 24, 117-122
Nickling, W.G. & Ecclestone, M. (1981). The effects of soluble salts on the threshold shear velocity of fine sand. Sedimentology, 28, 505-510.
O'Brien, R.F. (1972). The barchans of the southern Namibia: grain size analysis. Proc. 4th S.Afr. Univ. geogr. conf., pp. 22-31.
Ollier, C.D. (1977). Outline geological and geomorphological history of the Central Namib Desert. Madoqua, 10, 207-212.
O'Shea, D.O'c. (1971). An outline of the inshore submarine geology of the southern South West Africa and Namaqualand. Unpubl. MSc. thesis, Univ. Cape Town, South Africa. 101p.
Parrish, J.T. (1986). Palaeoclimatic reconstructions and qualitative models. In: Parrish, J.T. & Barron, E.J., Paleoclimates and economic geology. Soc. Econ. Mineral. Palaeont., Short Course No. 18, pp. 17-30.
Parrish, J.T. & Curtis, R.L. (1982). Atmospheric circulation, upwelling, and organic-rich rocks in the Mesozoic and Cenozoic Eras. Palaeogeog, Palaeoclim. & Palaeoecol., 140, 31-66.
Parrish, J.T., Ziegler, A.M. & Scotese, C.R. (1982). Rainfall patterns and the distribution of coals and evaporites in the Mesozioc and Cenozoic. Palaeogeog,. Palaeoclim. & Palaeoecol., 40, 67-101.
Partridge, T.C. (1985). Tertiary to Recent coastal deposits. In: Brink, A.B.A. (Ed.), Engineering Geology of Southern Africa. Building Publications, Pretoria, pp. 57-87.
Partridge, T.C. & Maud, R.R. (1987). Geomorphic evolution of Southern Africa since the Mesozoic. S. Afr. Jour. Geol., 90, 179-208.
Pether, J. (1986). Late Tertiary and early Quaternary marine deposits of the Namaqualand coast, Cape Province: new perspectives. S. Afr. Jour. Sci., 82, 464-470.
Phillips, A.C. & Walker R.G. (1932) ???
Q.J.R. Meteorol. Soc., 58, 23-30.
Pickford, M. (1987). Miocene Suidiae from Arris Drift, South West Africa/Namibia. Ann. S. Afr. Mus., 97(10), 283-295.
Pietruszka, R.D. & Seely, M.K. (1985). Predictability of two moisture sources in the Namib Desert. S. Afr. Jour. Sci., 81, 682-685.

Porter, M.L. (1986). Sedimentary record of erg migration. Geology, 14, 497-500.
Porter, M.L. (1988). Sedimentology of an ancient erg margin: Lower Jurassic Aztec Sandstone, southern Nevada and southern California. Sedimentology, 34, 661-680.
Range, P. (1909). Die Diamantfelder bei Lüderitzbucht. Deutsches Kolonialblatt, No. 22, 1039-1048.
Reid, I. & Frostick, L.E. (1987). Toward a better understanding of bedload transport. Soc. Econ. Palaeont. Mineral. Spec. Publ., 39.
Rogers, J. (1977). Sedimentation on the continental margin off the Orange River and the Namib Desert. Joint Geol Surv./Univ. Cape Town Mar. Geosci. Unit Rep, 7.
Sarnthein, M. (1977). Neogene sand layers off Northwest Africa: composition and source environment. In: Lancelot, Y., Seibold, L., et al., Init. Rep. Deep Sea Drill Proj. 41 Suppl., pp. 939-959.
Sarnthein, M. & Diester-Haas, L. (1977). Eolian-sand turbidites. Jour. Sediment. Petrol., 47, 868-890.
Sauer, E.G.F. (1966). Fossil eggshell fragments of a giant Struthious bird (Struthio oshanai, sp. nov.) from Etosha Pan, South West Africa. Cimbebasia, 14, 2-51.
Sauer, E.G.F. (1968). Calculations of Struthios egg sizes from measurements of shell fragments and their phylogenetic aspects. Cimbebasia, Ser. A, 1, 27-55.
Schell, I.I. (1968). On the relation between winds off South West Africa and the Benguela Current, and Agulhas Current pentration in the South Atlantic. Deutsche Hydrographische Zeitschrift, 21, 109-117.
Schulze, B.R. (1972). South Africa. In: Griffiths, J.F. (Ed.), Climates of Africa, pp. 501-586. Elsevier, Amsterdam.
Shackleton, J.N. & Kennett, J.P. (1975). Paleotemperature history of the Conozoic and the initiation of Antarctic glaciation: oxygen and carbon isotope analyses in DSDP sites 277, 279, and 281. In: Kennett, J.P., et al., Initial Rep. Deep Sea Drilling Project, 29, 743-755. U.S. Government Printing Office, Washington.
Shannon, L.V. (1985). The Benguela ecosystem. 1. Evolution of the Benguela, physical features and processes. Barnes, M. (Ed.), Oceanography and Marine Biology. Oceanogr. Mar. Biol. Ann. Review, 23, 105-182. Aberdeen University Press.
Sharp, R.P. (1963). Wind ripples. J. Geol., 71, 617-636.
Sharp, R.P. (1964). Wind-driven sand in Coachella Valley, California. Geol. Soc. Am. Bull., 75, 785-804.
Shepard, F.P. & Lafond, E.C. (1940). Sand movements near the beach in relation to tides and waves. Am. J. Sci., 238, 272-285.
Siesser, W.G. (1978). Aridification of the Namib Desert: Evidence from oceanic cores. In: van Zinderen Bakker, E.M., (Ed.), Antarctic glacial history and world palaeoenvironments, Balkema, Rotterdam, pp. 105-113.
Siesser, W.G. & Dingle, R.V. (1981). Tertiary sea-level movements around southern Africa. Jour. Geol., 89, 83-96.
Siesser, W.G. & Rogers, J. (1976). Authighenic pyrite and gypsum in South West African continental slope sediments. Sedimentology, 23, 567-577.
Siesser, W.G. & Salmon, D. (1979). Eocene marine sediments in the Sperrgebiet, South West Africa. Ann. S. Afr. Mus., 79, 9-34.

Smith, N.D. (1970). The braided stream depositional environment: Comparison of the Platte River with some Silurian clastic rocks, North-Central Appalachians. Geol. Soc. Am. Bull., 81, 2993-3014.
Smith, N.D. (1971). Transverse bars and braiding in the lower Platte River, Nebraska. Geol. Soc. Am. Bull., 82, 3407-3420.
South African Committee for Stratigraphy (SACS). (1980). Kent, L.E. (Comp.); Part 1. Lithostratigraphy for the Republic of South Africa, South West Africa/Namibia, and the Republics of Boputhatswana, Transkei and Venda. Handb. geol. Surv. S. Afr., 8, 690p.
Southard, J.B. & Dingler, J.R. (1971). Flume study of ripple propagation behind mounds on flat sand beds. Sedimentology, 16, 251-263.
Sperling, C.H.B. & Cooke, R.U. (1984). Laboratory simulation of rock weathering by salt crystalization and hydration processes in hot, arid environments. Earth surf. proc. & Landforms, 10, 541-555.
Spriggs, A.J. (1988). An isotopic and Geochemical study of kimberlites and associated alkaline rocks from Namibia. Unpubl. PhD. thesis, Univ. Leeds. 268p.
Stocken, C.G. (1978). A review of the later Mesozoic and Cenozoic deposits of the Sperrgebiet. Unpubl. Rep. Geol. Dep. Consolidated Diamond Mines of Namibia.
Stromer, Von E. (1926). Reste Land und Sußasser bewohnender Wirbeltiere aus den Diamantfeldern Deutsch-Südwestafrikas, Kaiser, E., Die Diamantenwüste Südwestafrikas, 2, pp.107-153. Dietrich Reimer (Ernst Vohsen), Berlin.
Sutherland, D.G. (1985). Geomorphological controls on the distribution of placer deposits. J. geol. Soc. London, 142, 727-737
Svasek, J.N. & Terwindt, J.H.J. (1974). Measurement of sand transport by wind on a natural beach. Sedimentology, 21, 311-322.
Swart, D.H. (1983). Physical aspects of sandy beaches - a review. In McLachlan, A. & Erasmus, T. (Eds.) Sandy beaches as ecosystems. Junk, the Hague.
Taljaard, J.J., Schmidt, W. & Van Loon, H. (1961). Frontal analyses with application to the Southern Hemisphere. Notos, 10, 25-58.
Taniguchi, S., Sakamoto, H. & Arie, M. (1982). Interference between two circular cylinders of finite height vertically immersed in a turbulent boundary layer. J. Fluids Eng., 104, 529-536.
Tankard, A.J., Jackson, M.P.A., Eriksson, K.A., Hobday, D.K., Hunter, F.T. & Minter, W.E.L. (1982). Crystal Evolution of Southern Africa. 3.8 Billion Years of Earth History. Springer-Verlag, Berlin, 523p.
Tankard, A.F. & Rogers, J. (1978). Late Cenozoic palaeoenvironments on the west coast of Southern Africa. J. Biogeogr., 5, 319-337.
Tsoar, H. (1983). Wind tunnel modelling of echo and climbing dunes. In: Brookfield, M.E. & Ahlbrandt, T.S., (Eds.), Eolian sediments and processes. Elsevier, Amsterdam, pp. 247-259. Developments in Sedimentology 38.
Tyson, P.D. (1969). Atmospheric circulation and precipitation over South Africa. Envir. Studies, 2, 1-22.
Van Loon, H. (1972). Cloudiness and precipitation in the Southern Hemisphere. In: Newton, C.R., (Ed.), Meteorology of the Southern Hemisphere. Am. Met. Soc. Meteorological Monograph, 13, 101-111.

Van Loon, H. (1972). Wind in the Southern Hemisphere. Newton, C.W., Meteorology of the Southern Hemisphere. Am. Met. Soc. Meteorological Monograph, 13, 87-100.
Van Zinderen Bakker, E.M. (1975). The origin and palaeoenvironment of the Namib Desert biome. J. Biogeogr., 2, 65-73.
Wagner, P.A. (1910). The origin of the German South West African diamonds. Proc. Geol. Soc. S. Arf., 13, XLVI-XLVII.
Wagner, P.A. (1914). The diamond fields of Southern Africa. The Transvaal Leader, 347p.
Ward, A.W. & Greeley, R. (1984). Evolution of the yardangs at Rogers Lake, California. Geol. Soc. Am. Bull., 95, 829-837.
Ward, J.D. (1984). Aspects of the Cenozoic geology in the Kuiseb Valley, Central Namib Desert. Unpubl. PhD. thesis, Univ. Natal, Pietermaritzburg, 310p.
Ward, J.D. (1987). The Cenozoic succession in the Kuiseb Valley, Central Namib Desert. Geol. Surv. South West Africa/Namibia Memoir, 9, 124p.
Ward, J.D. & Corbett, I.B. (In press). Towards an age for the Namib. Transvaal Museum Monograph.
Ward, J.D., Seely, M.K. & Lancaster, N. (1983). On the antiquity of the Namib. S. Afr. Jour. Sci., 79, 175-183.
Ward, J.D., Teller, J.T., Rutter, N.W. & Lancaster, N. (1987). Quaternary lacustrine deposits in the Central Namib. INQUA Prg. with Abs., p.284.
Watson, A. (1985). Structure, chemistry and origins of gypsum crusts in southern Tunisia and the Central Namib Desert. Sedimentology, 32, 855-870.
Watson, A., 1983. Gypsum crusts. In: Goudie, A.S. & Pye, K.(Eds.), Chemical sediments and geomorphology: Precipitates and residues in the near-surface environment, Academic Press, London, pp. 163-186.
Weissermel, W. (1926). Neues über Tabulaten, Hydrozoen und eine Hexakoralle aus dem Tertiarder Bogenfelser Diamantfelder. In: Kaiser, E. (Ed.), Die Diamantenwüste Südwestafrikas, 2, pp. 88-153. Dietrich Reimer (Ernst Vohsen), Berlin
Wellman, H.W. & Wilson, A.T. (1965). Salt weathering, a neglected erosive agent in coastal and arid environments. Nature, 205, 1097-1098.
White, B.R. & Schultz, J.C. (1977). Magnus effect on saltation. Jour. Fluid Mech., 81, 497-512.
Whitney, M.I., (1978). The role of vorticity in developing lineation by wind erosion. Bull. Geol. Soc. Am., 89, 1-18.
Whitney, M.I. (1983). Eolian features shaped by aerodynamic and vorticity processes. Brookfield, M.E. & Ahlbrandt, T.S., (Eds.), Eolian sediments and processes, Elsevier, Amsterdam, pp.223-246. Developments in sedimentology 38.
Willetts, B. (1983). Transport by wind of granular materials of different grain shapes and densities. Sedimentology, 30, 669-679.
Willetts, B. & Rice M.A. (1986). Collision in aeolian transport: the saltation/creep link. In: Nickling, W.G., (Ed.), Aeolian geomorphology. Proc. 17th Ann. Binghampton Geomorph. Symp., pp. 1-17. Allen & Unwin.
Williams, G. (1964). Some aspects of the eolian saltation load. Sedimentology, 3, 257-287.
Wilson, I.G. (1971). Aeolian bedforms - their development and origins. Sedimentology, 19, 173-210.

Yaalon, D.H. & Ward, J.D. (1982). Observations on calcrete and recent calcic horizons in relation to landforms, Central Namib Desert. In: Coetzee, J.A. & Van Zinderen Bakker, E.M., (Eds.), Palaeoecology of Africa, 15, Balkema, Rotterdam.

Zingg, A.W. (1953). Wind tunnel studies of the movement of sedimentry material. Proc. 5th Hydraulic Conf. Bull., 34, 111-135.

APPENDIX 1

METHOD FOR TAKING POSITIVE PLASTER CASTS OF A GRANULAR BED

This technique was devised to make a positive plaster cast of a loose granular bed. The casts obtained accurately portray medium sand grains, as well as larger particles. The technique allows complex features with undercuts to be accurately, and easily cast.

Fixing the Surface

Equipment Required

1) Hand pump with a fine spray nozzle;
2) Acetone (industrial quality);
3) Cellulose acetate beads.

Method

1) Dissolve 1 part cellulose acetate in 15 to 20 parts acetone by volume. This has to be done well in advance, and takes several days for all of the acetate to dissolve if large quantities are mixed.
2) Prepare the hand pump with some of the dissolved cellulose acetate. Adjust the nozzle to a fine spray.
3) Holding the nozzle about 30 cm above the bed, lightly spray the surface. Care should be taken not to produce any "run-off" as this results in surface modification. If working in a windy area subjected to sandflow, avoid windy days. The cellulose acetate traps the saltation load and the bed configuration is destroyed by the adhesion of the sand.
4) Allow a few minutes for the acetone to evaporate and the cellulose acetate to harden. The surface should now be lightly fixed.

Making the Mould

Equipment Required

1) Perspex frame to "mask-off" the area intended for casting;
2) "Pink Zelgan" - a dental impression material available from dental suppliers;
3) Mixing bowl and spoon, spatula or palette knife for mixing;
4) 5 litres of very cold water;
5) Builder's plaster of paris.

Method

1) Mask of the area of fixed surface of which the mould is to be taken.
2) Mix a bowl of pink zelgan powder with cold water until it has a consistency which is slightly runnier than stiffly whipped cream. The use of very cold water increases the setting time to about 3 to 5 minutes. One therefore has to proceed rapidly after this step.
3) Starting in one corner of the masked area, pour the mixture onto the fixed bed. If it is the correct consistency, it will very slowly spread across the bed. This action effectively expels air and the production of bubbles is minimal. The layer should cover the largest particles if possible. If a large area is to be covered, it is advisable to have a helper who mixes the next batch of zelgan whilst the other is pouring. Succeeding pourings should start at the margin of the former. If applied quickly, the two batches form a better "join". Continue until the entire masked area is covered. It is difficult to handle areas larger than 50 cm by 30 cm.
4) Allow the zelgan to set.
5) Mix plaster of paris to a creamy consistency.
6) Pour the plaster of paris onto the upper surface of the zelgan covering the bed. Build the thickness of the plaster upto about 1.5 to 2 cm. This provides a rigid back for the rubbery mould and ensures that the mould is an accurate reproduction of the original bed. Draw the compass orientation on the plaster once it is set.
7) Carefully turn the mould over. Pick up and transport back to camp / office. The sediment will adhere to the zelgan.
8) Gently ease the particles from the surface of the zelgan. Care at this stage ensures the accuracy of the cast. A dental probe, or a blunt needle is best for this. For clasts with large undercuts ease the clast out slowly, allowing the zelgan to "give", rather than tear. The zelgan accurately retains the bed configuration for 1 to 2 hours. After this it starts to deform due to dehydration. If necessary, wrap the mould in a damp towel and keep moist. Avoid too great a delay if possible.

9) Wash the surface of the mould lightly with a shower to remove loose sand.

Making the Cast

Equipment Required

1) Vibrating table (if possible);
2) Mixture of 1 part plaster of paris and 1 part dental stone;
3) Mixing bowl.

Method

1) Place cleaned mould, resting upon its plaster backing, on the vibrating table.
2) Mix plaster / stone mixture to a "runny cream" consistency.
3) Whilst the table is vibrating, pour the mixture onto the surface of the mould. Ensure that all cavities are filled. Allow the vibration of the table to expel air, and add some more plaster / stone mix.
4) Mix further quantities of the plaster / stone mix to the consistency of whipped cream.
5) Apply the plaster / stone mix onto the surface of the initial plaster / stone. Build-up the cast to a thickness of 1 to 2 cm, and smmoth off the base. Allow the cast to set hard.
6) Orientate the cast, and then remove the plaster backing from the zelgan mould. Carefully peel the zelgan from the surface of the cast.

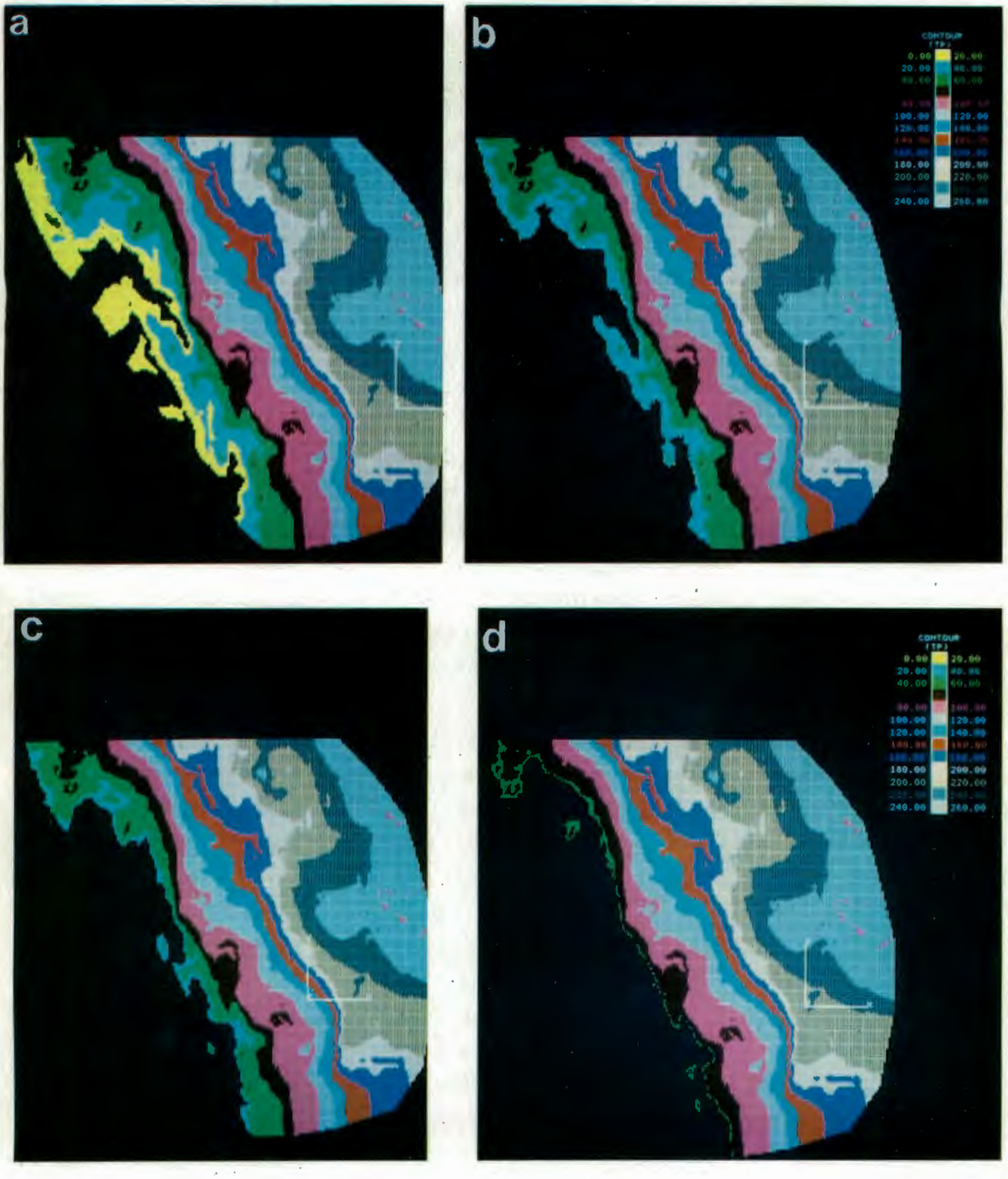

Figure 7.68. Computer model showing the changes in coastal morphology within the Bogenfels basin during transgressions to: 5 to 15 masl, 20 to 30 masl, 35 to 40 masl, and 55 to 60 masl. Note the similarlity of the predicted coastline with that between Prinzenbucht and Elizabeth Bay today.